MEMOIR OF THE
GEOLOGICAL SURVEY OF NAMIBIA

# THE GEOLOGY OF THE KAMANJAB INLIER, NORTHERN NAMIBIA

MINISTRY OF MINES AND ENERGY

MEMOIR 23
2023

**GEOLOGICAL SURVEY OF NAMIBIA**

MINISTRY OF MINES AND ENERGY

Deputy Permanent Secretary: Gloria Simubali

# MEMOIR 23

# THE GEOLOGY OF THE KAMANJAB INLIER, NORTHERN NAMIBIA

Editor: M. Pickford

Manuscript reviewed by: M. Pickford

Obtainable from
Geological Survey of Namibia
Private Bag 13297, Windhoek, Namibia
and
https://www.mme.gov.na/publications/?designation=gsn

ISSN 2026-8262 (Online)
ISSN 2026-8270 (CD-ROM)

ISBN 978-99945-0-093-2 (Online)

# CONTENTS


Introduction....2
Regional Geology....3
Kamanjab Inlier (KI)....5
Huab Metamorphic Complex (HMC)....5
Khoabendus Group (KG)....6
Fransfontein Granitic Suite (FFG)....8
Geochronology of the Kamanjab Inlier....9
Problems of stratigraphy, tectonics and metamorphism in the Kamanjab Inlier....9
Analytical Methods and Laboratories....11
Whole rock geochemistry....11
Sr-Rb, Sm-Nd whole rock isotope analysis....11
U-Pb single zircon age dating....12
SHRIMP method....12
LA-ICP-MS method....12
K-Ar muscovite age dating....12
$^{40}Ar/^{39}Ar$ muscovite/hornblende age dating....13
Sample preparation and neutron irradation....13
$^{40}Ar/^{39}Ar$ isotope dating....13
Mineral geochemistry....13
Geological Mapping....14
Kamanjab-Grootberg area....14
Khoabendus Group (KG)....14
West End Formation (MWs)....14
Ombonde Member (MWsOm)....19
Bruno Member (MWsBr)....19
Eendrag Member (MWsEe)....19
Otjovasandu Formation (MOv)....20
Voorspoed Member (MOvVs)....21
Doorslaan Member (MOvDo)....21
Arendsnes Member (MOvAd)....21
Fransfontein Granitic Suite (FFG)....22
Huab area....26
Huab Metamorphic Complex (HMC)....26
Rooikop-Lofdal Subdomain (SD)....29
Suiderkruis-Aandgloed Subdomain (SD)....30
Ehobib Subdomain (SD)....35
Magmatic rocks....38
Tectonics....41
Kamanjab-Grootberg area – Khoabendus East and West domains....41
Kinematics....42
Transition Zone....42
Huab Metamorphic Complex (HMC)....43
Ehobib Subdomain (SD)....45
Suiderkruis-Aandgloed Subdomain (SD)....47
Kinematics....54
Rooikop-Lofdal Subdomain (SD)....54
Post-$D_2$ / pre-Damara deformation....56
Pan-African deformation....57
Geochemistry and Sm-Nd systematics....57

Felsic rocks....57
Geochemical classification....59
REE-normalised and trace element multi-element diagrams (spidergrams)....60
Sm-Nd (Rb-Sr) isotope systematics....61
Mafic and intermediate rocks ($SiO_2$ < 60%)....63
Geochemical classification....67
Plate tectonic setting....69
Normalised REE and trace elements diagrams (spidergrams)....70
Sm-Nd (Rb-Sr) isotope systematics....72
Metamorphism....74
Petrography....76
231104-1 (Suiderkruis SD)....76
260406-14 (Suiderkruis SD)....76
290709-3 (Suiderkruis SD)....77
290709-8 (Suiderkruis SD)....77
200900-1 (Aandgloed SD)....78
260406-10 (Aandgloed SD)....78
101203-2 (Transition Aandgloed-Rooikop SD)....79
101203-1 (Rooikop SD)....79
260406-4 (Rooikop SD)....80
020809-3 (Lofdal SD)....80
020809-4 (Lofdal SD)....81
Mineral chemistry....81
Garnet....81
Amphibole....85
Biotite....86
Feldspar....86
Geothermobarometry....87
Conventional thermometry....87
Suiderkruis Subdomain (SD)....88
Aandgloed Subdomain (SD)....88
Transition Aandgloed-Rooikop subdomains....88
Lofdal Subdomain (SD)....88
Conventional barometry....90
Suiderkruis Subdomain (SD)....90
Aandgloed Subdomain (SD)....90
Rooikop-Aandgloed Transition....90
Lofdal Subdomain (SD)....90
P/T diagrams....90
Suiderkruis Subdomain (SD)....92
Aandgloed Subdomain (SD)....92
Transition Zone Aandgloed-Rooikop....92
Rooikop Subdomain (SD)....92
Lofdal Subdomain (SD)....92
P/T pseudosection modelling....92
Geochronology....95
LA-ICP-MS U-Pb single zircon analysis....95
Fransfontein Granitic Suite (FFG)....98
Kamdescha Granite (sample 260205-4)....98
Franken Granodiorite (sample 280205-6)....99

Kaross Granite (sample 170405-6)....101
Huab Metamorphic Complex (HMC)....103
Mylonitic Red Granite Orthogneiss (ROG, sample 210900-2/HU0....103
Gneissic K-feldspar porphyry (sample 130503-1)....105
K-feldspar porphyritic granodiorite (augen) gneiss (POGD, Sample 100900/HU-03)....107
SHRIMP U-Pb zircon analysis....110
Fransfontein Granitic Suite (FFG)....111
Kamdescha Granite (sample 081203-2)....111
Huab Metamorphic Complex (HMC)....111
Metarhyolite (sample 270802-1)....111
Fault breccia (sample NA101-2)....112
K-Ar muscovite geochronology....114
$^{40}Ar/^{39}Ar$ hornblende geochronology....115
Discussion....117
Depositional environment, magmatism, plate tectonic setting....117
Huab Metamorphic Complex....117
Khoabendus Group....118
Mafic magmatism....119
Fransfontein Granitic Suite – HMC orthogneiss – Felsic volcanism Khoabendus Group....119
Tectonics and metamorphism....120
$M_1$ tectono-metamorphic event....120
$M_2$ tectono-metamorphic event....121
Mesoproterozoic thermal event....126
Post-$M_2$ / pre-Damara deformation....126
Pan-African deformation....126
Regional context....127
Palaeoproterozoic era....129
Magmatism and sedimentation....129
Metamorphism....130
Mesoproterozoic era....130
Magmatism....130
Metamorphism....131
Conclusions....132
Open questions....135
Acknowledgments....136
References....136
Annexes
I - Kamanjab Inlier - sample locations, geochemistry and isotope analyses
II - Mineral analyses, Depiné (2008)
III - Mineral analyses, Nolte (2012)
IV - 1: 100 000 Geological Map of the Khoabendus Area
V - 1: 100 000 Geological Map of the Huab Metamorphic Complex
VI - Abbreviations
VII -Toponymics

**Cover image**: Sunset on farm Aandgloed – view of the Huab valley (photo: T. Becker)

# The Geology of the Kamanjab Inlier, Northern Namibia

**Thomas Becker[1], Nicole Nolte[2], Franziska Wilsky[2], Marc Depiné[3], Ilka Kleinhanns[4], Reiner Klemd[3], Kombada Mhopjeni[5], Ewereth Muvangua[5], Bettina Wiegand[6], Klaus Wemmer[6], Sergei Sergeev[7] & Masafumi Sudo[8]**

*[1]Geological Survey of France (BRGM), Orléans, France*
*[2]MASA Institute, Göttingen, Germany*
*[3]University of Erlangen, Germany*
*[4]University of Tübingen, Germany*
*[5]Geological Survey of Namibia*
*[6]University of Göttingen, Germany*
*[7]Centre of Isotopic Research, St Petersburg, Russia*
*[8]University of Potsdam, Germany*

Corresponding author: T. Becker (Fullgraf) <*t.fullgraf@brgm.fr*>

**Abstract** :- The Kamanjab Inlier (KI) in northern Namibia exposes the southern margin of the Archaean to Palaeoproterozoic Angola Shield. It consists of Palaeoproterozoic low-grade volcaniclastic rocks of the Khoabendus Group (KG), medium to high-grade gneisses, schist and quartzite of the Huab Metamorphic Complex (HMC), and the Fransfontein Granite Suite (FFG). 1:50k geological mapping in two key areas west of Kamanjab and Khorixas, combined with petrography, isotope analysis and geochemistry (rocks and minerals) provides a wealth of new data contributing to the reconstruction of the inlier's geological history.

Geological mapping in the Kamanjab area yielded details of the stratigraphy of the KG comprising the lower West End and upper Otjovazandu formations dominated by volcanic and sedimentary rocks, respectively. The volcanics and sediments were deposited mainly in local basins under shallow marine conditions. However, in the upper part of the Otjovazanadu Formation, regional transgression is recorded in the Arendsnes Member. The base of the KG is obscured by massive, layer-parallel megasills of the FFG, digesting the basal rocks of the West End Formation and concealing the base of the KG.

The FFG is marked by great variation in composition and petrography. Geological mapping combined with interpretation of airborne geophysics data and petrography reveals 10 different types, which were emplaced into the KG as sheet-like intrusions and plutons. Geochemistry and geochronology of the FFG and the mostly felsic volcanic rocks of the KG show their coeval evolution between 1.88 and 1.82 Ga within an active continental margin setting. Nd-isotope analyses of FFG rocks $T_{DM}$ yielded model ages of 2.3-2.7 Ga and mostly negative $\varepsilon Nd_{1.85\ Ga}$ values (-6.2 to -2.2) indicating mixing of mantle derived magmas with crustal country rocks of predominantly Palaeoproterozoic provenance.

Geological mapping of the HMC shows the subdivision into (i) southern migmatitic Rooikop/Lofdal subdomains (SD) (ii) central non-migmatitic Suiderkruis-Aandgloed SD and (iii) northeastern low-grade Ehobib SD comprising Khoabendus rocks intruded by the FFG Suite. This constrains a normal geothermal gradient from the bottom to the top of the structural pile and excludes nappe tectonics to explain the observed thrusted contacts between the Suiderkruis-Aandgloed and Ehobib SD.

The HMC was intruded by voluminous mafic magmas prior to a first phase of regional medium to high-grade metamorphism and deformation (M1). Their geochemical composition and geochronology indicate a continental arc/backarc system between 1.96 Ga (the youngest $NdT_{DM}$ age) and 1.88 Ga (the oldest FFG granite) and mixing of a juvenile mantle source with Palaeoproterozoic to Archaean crustal components.

Metamorphic petrology yields preliminary results for M1 metamorphic conditions in the high-grade domains, since M1 mineral paragenesis were reset during M2. In the northern, non-migmatitic part of the HMC, M1 metamorphic conditions are estimated at 10.5-11.3 kb and 650-700 °C.

The continuation of subduction after M1 suggests that metamorphism and deformation were associated with magmatic underplating under extensional conditions and not to classical collision tectonics.

Migmatitic paragneisses of the HMC were intruded after M1 by sheeted bodies of granitoids that were subsequently transformed into orthogneiss. The magmas coincide in age (1.84-1.82 Ga), Nd-isotope and geochemical composition with those of the FFG Suite, therefore representing their deeper-level equivalents.

The M2 tectono-thermal event is characterised in the northern study area (KG and FFG) by generally weak, mostly steep NE-SW trending foliations, down-dip stretching lineations with a small sinistral component and irregularly spaced, upright, tight folds that are often bound by normal faults. Outside these zones, the rocks are almost undeformed and foliations/lineations are missing. Metamorphism reaches greenschist facies conditions.

In the HMC, M2 metamorphic conditions are estimated at 5.6-6.9 kb and 520-560°C. M2 deformation records non-cylindrical folds and dome-and-basin structures defining the present map scale geometry. D1 structures were generally transposed into the new penetrative D2 foliation. In the Rooikop SD, concentric sheath folds up to km-scale with steep axes attest to highly ductile conditions and predominantly vertical movements in the southern part of the HMC. In the north and NE, near the sheared contact with the overlying low-grade Khoabendus Fm and FFG granites, all rocks are transformed into mylonite. These features argue for the interpretation of the HMC as M2 mantled gneissic dome, or metamorphic core complex, which developed again in an extensional setting either at ca 1.8 Ga (the time of local granite emplaced into a syn- to post-D2 fault) or at ca 1.4-1.3 Ga within Mesoproterozoic rifting of the Kibaran event. Thermal overprinting of the HMC during this period is indicated by Ar-Ar and K-Ar hornblende and muscovite mineral ages from 1.45 to 1.32 Ga coinciding with the emplacement age of the Kunene Igneous Complex.

**Key words** :- Namibia, Kamanjab Inlier, Palaeoproterozoic, Mesoproterozoic, magmatism, metamorphism, geochemistry, geochronology, extension tectonics, mantled gneissic dome.

**To cite this paper** :- Becker, T., Nolte, N., Wilsky, F., Depiné, M., Kleinhanns, I., Klemd, R., Mhopjeni, K., Muvangua, E., Wiegand, B., Wemmer, K., Sergeev, S. & Sudo, M. 2023. The Geology of the Kamanjab Inlier, Northern Namibia. *Memoir of the Geological Survey of Namibia*, **23**, 1-146 + Annexes 49 pp. and 2 Geological Maps.

## Introduction

Despite its considerable economic potential for base metals and gold the Palaeoproterozoic Kamanjab Inlier (KI) of northern Namibia has, in the past, attracted minor interest in geological research (Geological Survey of Namibia, 1992; Steven, 2000; Steven & Armstrong, 2001; Anonymous, 2005): Geological mapping has been carried out only in parts of the region and at 1: 100,000 scale (Frets, 1969; Porada, 1974). The study of the tectono-metamorphic history was previously limited to field observations and petrography, supplemented by a few conventional U-Pb multigrain zircon ages (Burger & Coertze, 1973, 1975; Tegtmeyer & Kröner, 1985) and whole rock analyses (Clifford *et al*. 1969). The state of knowledge was summarised by Miller (2008) who concluded an active continental margin setting as the most probable scenario for the evolution of the KI.

In 2000, the Geological Survey of Namibia initiated a research program comprising geological mapping of nine 1:50,000 scale sheets of two key areas (Becker, 2004a-c, 2005a-c, 2006a-c). Geochemical and isotope analyses carried out during associated studies suggest evolution of the Kamanjab Inlier from 1.86-1.83 Ga within the context of an active continental margin setting (Muvangua, 2006; Mhopjeni, 2006; Wilsky, 2010; Nolte, 2012; Kleinhanns *et al*. 2013). Here, we present the results of field mapping, structural analysis and geothermobarometry which, together with additional geochronological data, allow the establishment of the principal crustal architecture of the region which prompt us to propose a first model for the orogenic processes leading to the present configuration of coeval low-grade and high-grade metamorphic rocks (Fig. 1).


**Figure 1**. A) View into the Huab Valley and surrounding rugged hills exposing the Huab gneisses; B) sheared low-grade amygdaloidal metabasalt rocks of the Khoabendus Group in the Ehobib Subdomain; C) polyphasely folded anatectic amphibolite of the Aandgloed Subdomain.

## Regional Geology

The Kamanjab Inlier together with the Epupa Complex (EC) to the west and the Grootfontein Inlier (GI) to the east in northern Namibia expose Palaeoproterozoic crust representing the southernmost portion the Archaean to Palaeoproterozoic Angola Shield (Fig. 2). The origin of rocks from these inliers is related to a period of major global crustal growth between 2.3-1.8 Ga (Condie, 2000; Condie *et al*. 2009) leading to the formation of a hypothetical supercontinent Columbia (Rogers & Santosh, 2002; Zhao *et al*. 2002, 2004).

Isotope and geochemical analysis of the EC and KI suggest a diachronous continental active margin setting as the main mechanism for crustal accretion with supposed younging from the GI in the east (2.0 Ga; Hoal *et al*. 2000) through the central KI (1.86-1.83 Ga; Wilsky, 2010; Nolte, 2012; Kleinhanns *et al*. 2013) to the western EC (ca 1.86-1.73; Seth *et al*. 1998, 2003, 2005; Kröner *et al*. 2004, 2010). At the regional scale these inliers constitute the

western part of the proposed Kamanjab-Bangweulu magmatic arc (Rainaud *et al*. 2005; Kleinhanns *et al*. 2013). Late Palaeoproterozoic regional HT-LP metamorphism between 1740 and 1720 Ma constitutes the oldest metamorphic event that was followed by Early Mesoproterozoic (1530 Ma) HT-LP metamorphism culminating at granulite facies peak-conditions of 830°C and 2 kb in the northern part of the Epupa Complex (Brandt *et al*. 2021). Mesoproterozoic 1.5-1.3 Ga ultrahigh granulite facies metamorphism marked by P/T conditions of 960°C and 9.5 kb and younger upper amphibolite facies metamorphism from 1370 to 1310 Ma are recorded in the southern part of the EC (Seth *et al*. 1998, 2003, 2005; Brandt *et al*. 2003, 2007; Brandt & Klemd, 2008) and were accompanied by the two-stage emplacement of the Kunene layered anorthosite.

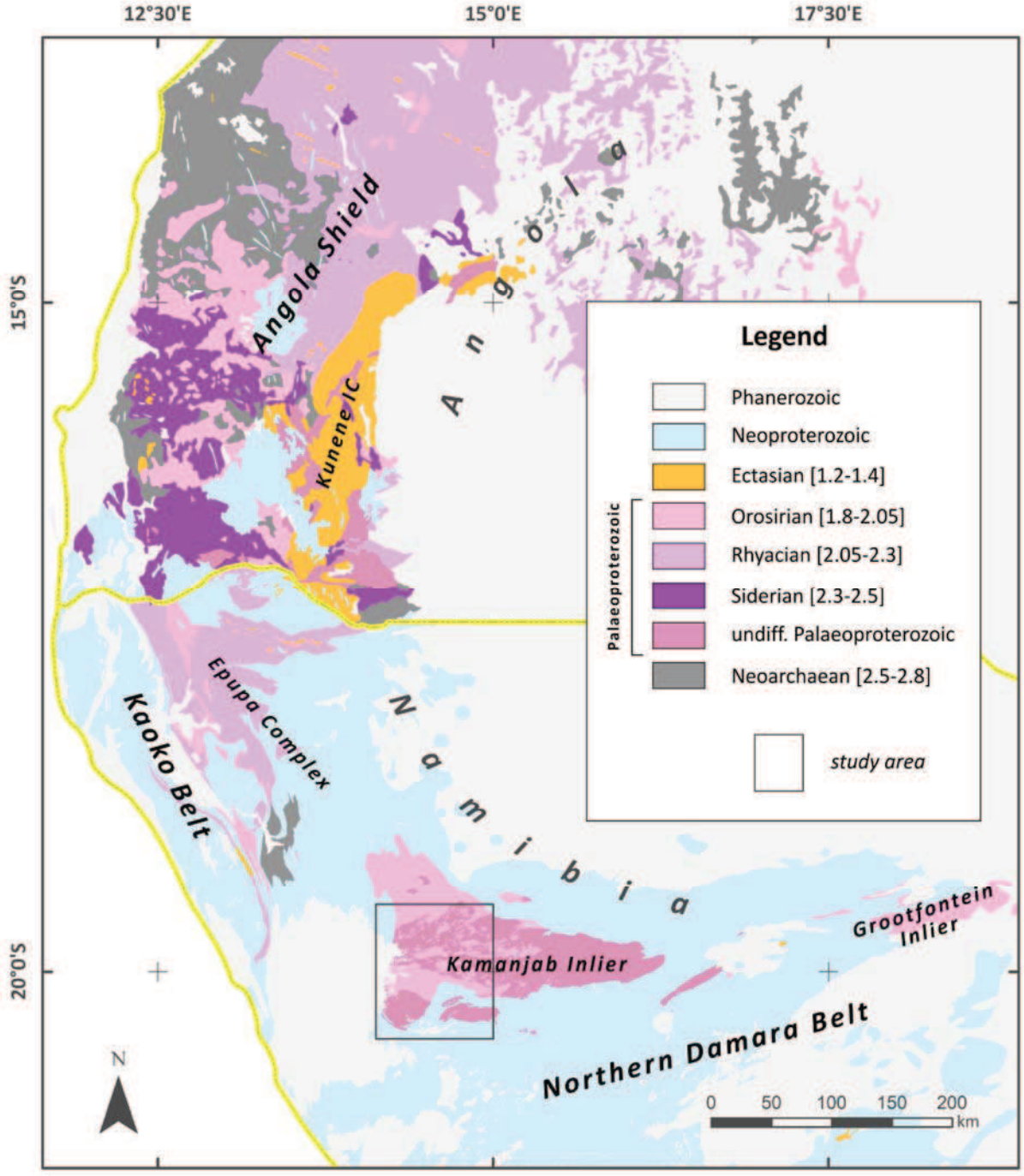


**Figure 2**. Overview geological map of southern and central Africa, illustrating the Archaean to Mesoproterozoic units. Simplified and modified extract from BRGM SIG-Afrique (unpublished); ages in [Ga].

## The Kamanjab Inlier (KI)

The KI is exposed in northern Namibia over an area of approximately 13,000 km$^2$. Quaternary aeolian sediments cover most of the eastern portion whereas to the south and west it is concealed below Neoproterozoic rocks of the Damara and Kaoko orogenic belts (Fig. 2). Rocks of the KI are well exposed in a 60 km wide, 80 km long strip from the Huab River in the south, to farm Hobatere west of the Etosha Pan in the north. The unit has been subdivided by SACS (1980) into three major geological units, which are the Huab Metamorphic Complex (HMC), the Khoabendus Group (KG) and the Fransfontein Granitic Suite (FFG).

### Huab Metamorphic Complex (HMC)

The HMC was mapped and described by Frets (1969). He considered the HMC to be a collective term comprising rocks of different parentage and age; they include metapsammitic and pelitic sediments, amphibolite, granitic orthogneiss and minor metapyroxenite. The metasediments identified comprise white orthoquartzite, conglomerate, schist and mixed paragneiss. Granitic gneiss comprises about 35-45 % of the HMC and according to the author, all transitions from banded gneiss to granitic gneiss occur, arguing for the metasomatic origin of the igneous rocks. The HMC was subdivided by Frets (1969) into three lithostructural units separated from each other by major faults (Fig. 3).

Firstly, the Rooikop Domain is composed of granitic gneiss, amphibolite gneiss, amphibolite and quartzite invaded by two generations of pegmatite forming layer parallel quartz-feldspar veins and massive cross-cutting dykes. The overall structure of the domain is a large dome with steep dips (70-80°) in the north, moderate dips in the south (30-40°) and a horizontal attitude in the central part. Apart from a Pan-African steep schistosity in the southern part, the absence of any other schistosity in this domain is quite striking. However a few isoclinal mesoscopic folds were observed in the central part the axial plane of which is parallel to the banding and foliation in the adjacent rocks.

Secondly, the Soutput-Boesmanpan Domain comprises the same rock types as the Rooikop Domain and again two generations of pegmatites have been observed, which are, however, rare. Most of the rocks display pronounced foliations and often record mylonitic fabrics in discrete horizons. The three main fold structures are the NNW-SSE trending Soutput Synform, the Mesepotamie Antiform and the Soutput Dome. A major recumbent isoclinal fold has been mapped on Soutput 505, which is refolded into the NNW-SSE Mesepotamie Antiform. Mineral and intersection lineations are subhorizontal to shallow N-NE plunging and are interpreted to be related to the NNW-SSE folding. Subsequent mylonite zones are N-S trending and associated with a steep E-dipping schistosity.

Thirdly, the Huab-Suiderkruis Domain is marked lithologically by a thick sequence of white quartzite, schist, amphibolite of both intrusive and volcanic origin, and a few metaconglomerate bands. It is intruded by massive sills of granodiorite transformed into augengneiss and medium-grained equigranular granite gneiss. A few thick pegmatites are limited to the southern part where they cross-cut the gneissic compositional banding. Well-developed gneissic layering in the north is overprinted by younger schistosities. The regional trend recorded by orthogneisses and metasediments consists of early NNW-SSE D1 folds that correspond to the D1 structures in the Rooikop and Soutput-Boesmanpan domains. In the north, they were refolded around subhorizontal W to moderately NW plunging D2 axes into E-W and NE-SW trending tight and isoclinal folds. Two schistosities S1 and S2 have been observed in places and attributed to either fold phase. S2 commonly varies in orientation from moderate (45°) N to NE dip. In the NE of the domain the S2 structures change to a steep (60-70°) NE dip.

A late NE-SW striking subvertical crenulation cleavage appears limited to this domain.

ESE-WNW trending subvertical orthogneiss and metasediments within a belt of ca six km width limit the HMC to the NE against the Fransfontein Suite and undifferentiated

Kamanjab basement rocks. They were included by Frets (1969) in the HMC due to the presence of amphibolite, metaquartzite and granitic gneiss indicating amphibolite facies conditions. This contrasts with the interpretations of Stahl (1940), Martin (1965), Guj (1970) and Miller (2008) who classified these rocks together with the Huab-Suiderkruis SD of Frets (1969) as part of the Khoabendus Group.

In conclusion, the first gneissic event is characterised by Barrovian type metamorphism (almandine-hornblende) and associated with mesoscopic tight to isoclinal folding F0 (Frets, 1969). It was followed by folding around N-S axes (F1, S1), tight to isoclinal folding around E-W axes (D2, S2) and a late crenulation cleavage with a constant NE-SW orientation (S3). Thereby, D2 and D3 are limited to the northern part of the HMC whereas D1 is recorded throughout the study area. All tectono-metamorphic fabrics were considered to pre-date intrusion of the Fransfontein granites.

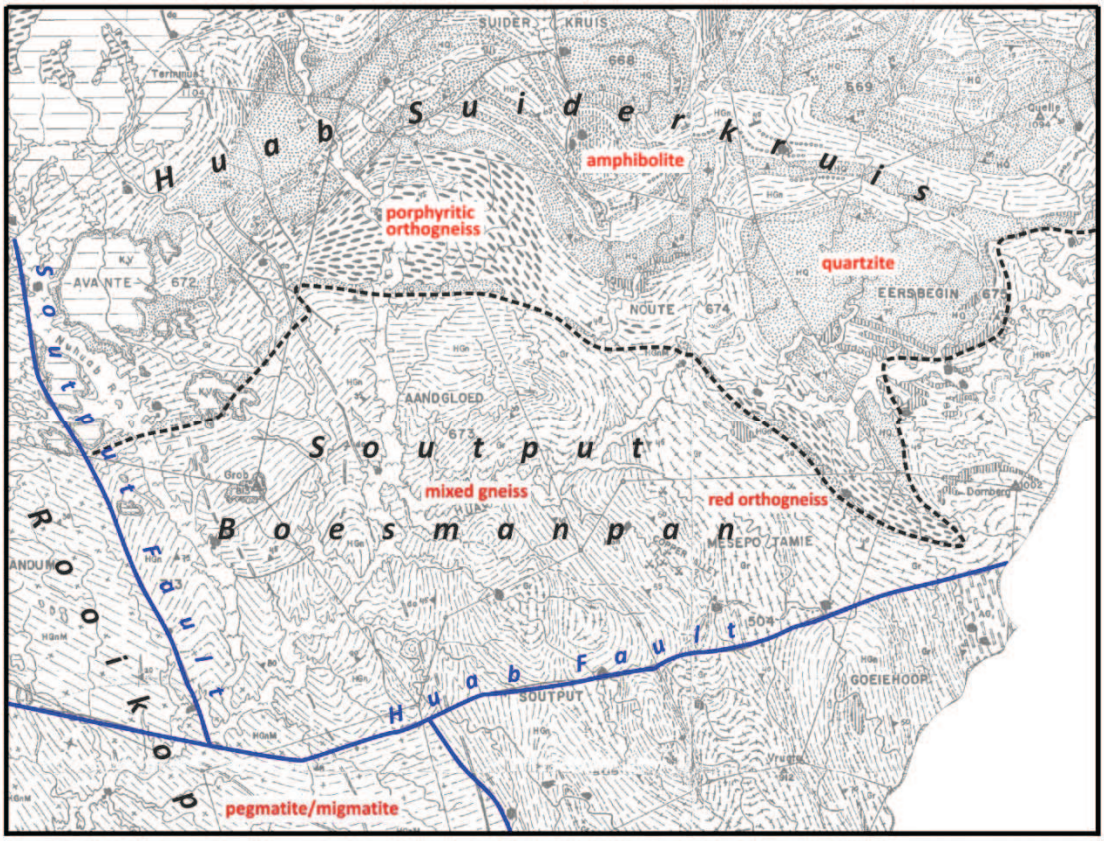


**Figure 3**. Geological map of the Huab area (Frets, 1969). The stippled line marks the approximate boundary between the southern Soutput-Boesmanpan and Suiderkruis domains, indicated by the first occurrence of white quartzite. The Rooikop Domain is characterised by abundant pegmatite and migmatite.

**Khoabendus Group**

The Khoabendus Group crops out in two areas northwest of Kamanjab and west of Fransfontein; they were mapped and described by Porada (1974, Kamanjab-Otjovazandu) and Hugo (1974, Fransfontein). The synthesis of the stratigraphy, geochemistry, deformation and age as well as the depositional model of the group was published by Miller (2008, Table 1). The basal West End Formation in the north and its southern equivalent, the Tweelingskop Formation are comprised of porphyritic ignimbrite overlain by rhyodacitic to dacitic lava. They are overlain along an unconformity by andesitic tuff and lava (Smallruggens Formation) and a succession of flow-banded rhyolite interbedded with quartzite, pebbly quartzite, lithic quartzite, quartz-feldspar porphyry and layers of andesite (Blyerus Formation). The upper Otjovazandu Formation disconformably overlies these rocks. A prominent basal white quartzite, the Voorspoed Member (600 m) grades into overlying massive felsite and rhyolite with interbedded quartzite, tuff and agglomerate (Robyn Member, 300 m).

**Table 1.** Stratigraphy of the Khoabendus Group (Miller, 2008).

| Fransfontein area (Hugo, 1974; SACS, 1980) | | Kamanjab-Otjovazandu area (Porada, 1974) | | Miller, 2008 | |
|---|---|---|---|---|---|
| Formation | Lithology | Formation | Lithology | Formation (Maximum thickness, m) | Member |
| | | Otjovazandu | Strongly altered andesitic to basic lavas | Otjovazandu in north | Dinteri Carbonate (200) |
| | | | Upper, more massively bedded, pink limestone and grey dolomite with a few layers of chert | | |
| | | | Lower thin bedded limestone and dolomite with layers of chert, schist and sandstone; tuff lenses; white marble in west with interbedded quartzite, schist, purple slate and chlorite-actinolite schist | | |
| | | | Basal siliceous iron formation with siderite and hematite (up to 50 m thick), grades into ferruginous quartzite or chert | | |
| | | | Local red, gritty quartzite up to 300 m thick in SE | Aub in south | Arendsnes Pelite (500) |
| | | | Grey to black shale, phyllite and schist; interbedded grey to purple chert, purple siltstone, grey and white quartzite, black and purple dolomite, purple, grey and black bedded or oolitic chert, lithic sandstones, iron formation, chlorite-actinolite schist; layers of felsite, flow-banded rhyolite and acid tuff | | |
| | | | Local schist, mainly greenish grey | | |
| Aub | West - tuff and andesite | | Massive felsite and rhyolite; few or no phenocrysts; flow banding rare; interbedded quartzite, tuff, agglomeratic rocks | | Robyn Felsite (300) |
| | East- tuff and quartz-feldspar porphyry | | Contact to underlying quartzite sharp in east but gradational in west through decreasing number of quartzite beds, increasing number of layers of acid volcanic rocks | | |
| | Voorspoed Quartzite Member - massive white quartzite; interbedded andesite at base and phyllite throughout | | Massive, white, upwards-fining orthoquartzite ("Khoabendus quartzite"); thin local interbedded grey lithic quartzite, chlorite-actinolite schist, sericitic schist, iron formation; thick interbedded acid lavas and tuff in NW which increase in abundance upwards | | Voorspoed Quartzite (600) |
| | | | Basal, red, feldspathic, pebbly quartzite or conglomerate | | |
| | | DISCONFORMITY | | | |
| | | | Interbedded, massive felsite and flow-banded rhyolite with small scattered phenocrysts of quartz, potash feldspar and plagioclase; interbedded grey to reddish quartzite, pebbly quartzite, lithic quartzite, quartz-feldspar porphyry and layers of Smalruggens Andesite | Blyerus Rhyolite (2000?) | |
| | Andesitic tuff and lava | | Green, massive to well stratified, andesitic tuff, locally cross-bedded, phenocrysts of hornblende and quartz; green andesitic lava, phenocrysts of hyperthene, diopside, plagioclase and local hornblende; both rock types generally sheared | Smalruggens Andesite (200) | |
| UNCONFORMITY | | | | | |
| Tweelingskop | North | West End | Rhyodacitic to dacitic lava as below | West End in north | (± 500) |
| | Feldspar porphyry | | | | |
| | Tuff, rhyolite, layers of agglomerate, quartzite near | | Porphyritic ignimbrite- variably sheared and foliated, grey where least sheared but greenish grey top to green in colour where sheared due to saussuritisation and greenschist facies metamorphism, fragment grain sizes decreases upwards and tuffs become the dominant pyroclastic rock type in the upper part; quartz , potash feldspar and plagioclase phenocrysts, feldspars up to 20 mm in size in the lower part, decreasing to 2- 6 mm higher up; local graded bedding; interbedded, fine-grained , porphyritic to non-porphyritic, grey, dacitic to rhyodacitic Javas, flows 10 to 15 m thick, become more abundant upwards and towards the west, quartz, potash feldspar, plagioclase, biotite and hornblende phenocrysts | | |
| | Quartz and quartz-feldspar porphyry | | | Tweelingskop in south | |
| | South | | | | |
| | Thin phyllitic tuff, interbedded amphibolite, rhyolite | | | | |
| | Dacitic to rhyodacitic feldspar porphyry which displays local intrusive relationships; leptite layers in the upper portion | | | | |
| | Local basal quartzite | | | | |

The Arendnes Member (500 m) is characterised by a great variety of sedimentary rocks (shale, phyllite, schist, chert, quartzite, dolomite, lithic sandstone, iron formation with minor proportions of interbedded volcanic rocks (chlorite actinolite schist, rhyolite and acid tuff)). The uppermost Dinteri Member comprises basal siliceous iron formation overlain by a heterogeneous succession of limestone and dolomite with interbedded quartzite, schist, slate and chlorite actinolite schist. These rocks are capped by massively bedded, pink limestone and grey dolomite with few layers of chert. Miller (2008) suggested that the depositional environment was a gradually subsiding terrain made up of one large or several smaller depositional basins with large proportions of the volcanic rocks deposited under subaqueous conditions. Sediment structures record relatively quiet, shallow water deposition with occasional transgressions or regressions. Abundant intermediate volcanic rocks (andesite) are taken as an indicator for an active continental margin environment.

Low-grade regional metamorphism of the KG is characterised in intermediate volcanic rocks by strong saussuritisation of plagioclase, alteration of hornblende to epidote, chlorite and magnetite, hypersthene to bastite and diopside to uralite. The groundmass of andesitic tuffs and lavas consists of fine-grained sericite, epidote, quartz, albite, uralite, chlorite, opaque minerals and calcite with ubiquitous epidote (Miller, 2008). Contact metamorphism in an aureole several metres wide around the Kamdescha Granite resulted in strong recrystallisation of carbonate whereas quartzite and tuffs became splintery and glassy hornfels.

The tectonic style is characterised by regional NE trending, open to tight, slightly SE-overturned, folds of pre-Damaran age that are associated with an axial planar cleavage. In the west they are overprinted by NW trending Damara folds and reverse faults.

**Fransfontein Suite (FFG)**

The Fransfontein Suite has been mapped by Frets (1969) and Porada (1974) and descriptions of the intrusive rocks were published by Miller (2008). The granites occur throughout the Kamanjab Inlier where they intruded the Khoabendus Group and the Huab Metamorphic Complex. Rocks range in modal composition from granite to granodiorite and in geochemistry from alkaline to calc-alkaline. The main facies, classified as Kamdescha Granite, is a grey coarse-grained to porphyritic rock, which consists of centimetric microcline and minor plagioclase (albite to oligoclase) set in a medium-grained, equigranular groundmass of quartz, microcline and plagioclase. Biotite and more rarely green hornblende occur in variable amounts. Muscovite forms a minor component in all but the granodioritic rocks. Very minor minerals include apatite, epidote, calcite, rutile, zircon and opaque minerals.

Porada (1974) recognised an additional older red to greenish-red “Kaross type” granite, which varies from fine to coarse-grained and is sometimes porphyritic with feldspar phenocrysts set in a medium-grained matrix of quartz, microcline, perthite and plagioclase with minor amounts of biotite, muscovite and accessory chlorite and ore. A granophyric texture is present in places.

Most of the intrusions are weakly foliated and some microgranites have a strong lineation. In thin section, all rocks show signs of cataclasis. Frets (1974) noted the transition between these granites and the Huab red orthogneiss. The intrusive nature of the contact between ortho- and paragneiss was observed in the NW of the Huab-Suiderkruis SD.

Whole rock geochemistry combined with Sm-Nd / Rb-Sr-isotope systematics of the FFG and the HMC by Kleinhanns *et al*. (2013) reveal the monzogranite to alkali feldspar granite composition of Cordilleran I-type defining a calc-alkaline trend in a late- to post-orogenic setting related to an active continental margin. Trace element ratios indicate their origin as juvenile magma within an active margin setting. The absence of residual garnet excludes major assimilation or melting of lower crust influencing the distribution of REE and Y. Granodioritic orthogneiss from the HMC displays similar features documenting the geochemical affinity with the FFG Suite. Highly differentiated, A-type red orthogneiss that has no equivalent in the FFG, is interpreted as a late stage anatectic melt.

Sm-Nd and Rb-Sr isotope signatures of several samples of the HMC and all FFG granitoids indicate mixing between juvenile mantle source and non-radiogenic crustal component, whereas the other HMC samples record the contribution of high-radiogenic crust. Most Nd $T_{DM}$ model ages vary from 2.1 to 2.4

Ga (15/17 samples) corresponding to the Eburnian crust-forming event.

**Geochronology of the Kamanjab Inlier**

Table 2 and Fig. 4 summarise the geochronological data concerning the Kamanjab Inlier. U-Pb multigrain zircon ages from 2124-1749 Ma do not discriminate between the HMC, the KG and the FFG (Clifford *et al*. 1962, 1969; Burger & Coertze, 1973-75; Burger *et al*. 1976; Tegtmeyer & Kröner, 1985).

U-Pb single zircon ages constrain the age of the FFG between 1841±15 and 1834±14 Ma whereas gneisses of the HMC display slightly younger ages of 1830±17 Ma (granodioritic gneiss), 1826±30 Ma (metarhyolite) and 1801±27 Ma (late stage A-type granite gneiss) (Wilsky, 2010; Nolte, 2012; Kleinhanns *et al*. 2013).

The age of the Khoabendus rhyolite (Blyerus Formation) has been determined by the SHRIMP method to be 1862±6 Ma (Steven & Armstrong, 2002).

A low-grade Pan-African thermal overprint (or cooling during uplift) at 481-503 Ma was identified by the K-Ar whole rock method (Ahrendt *et al*. 1983b).

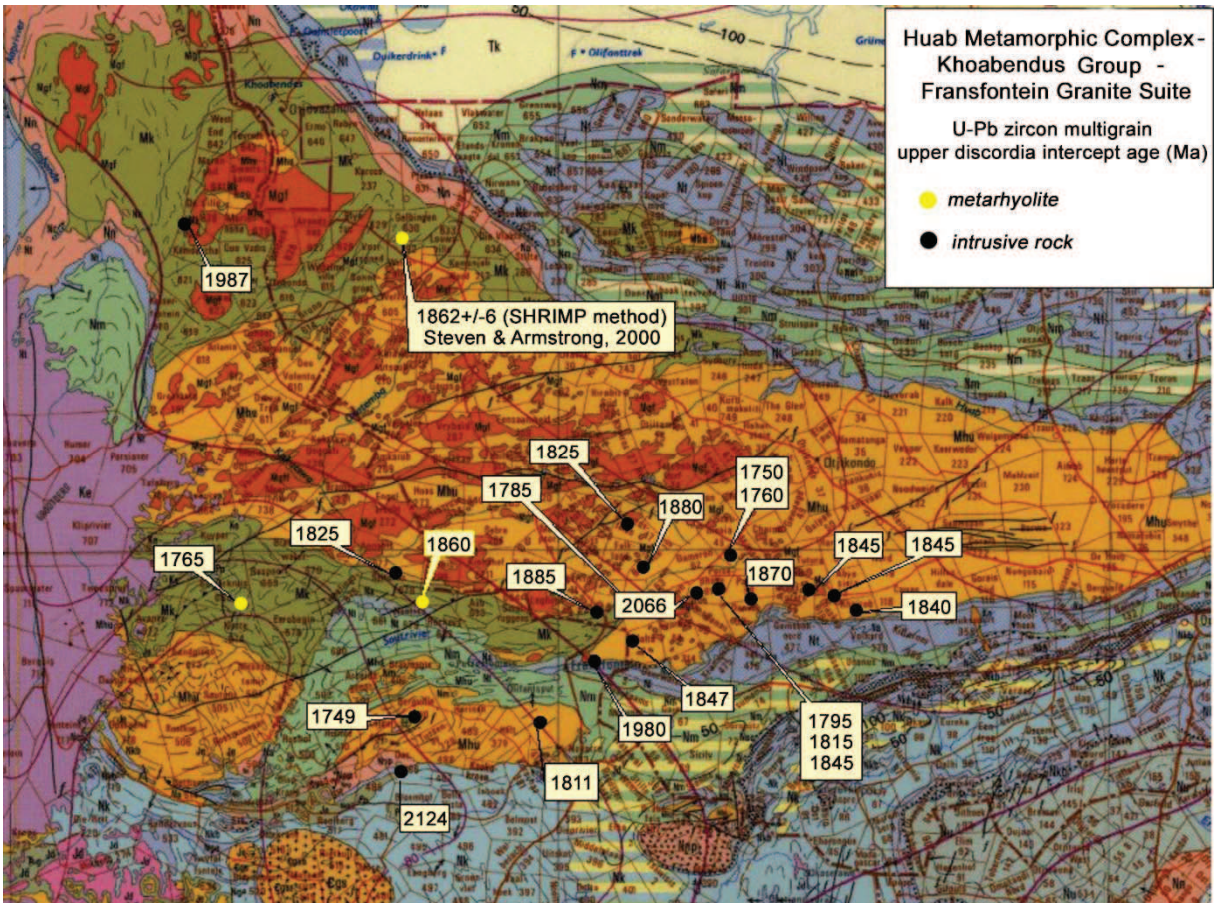


**Figure 4.** U-Pb multigrain zircon ages of the Kamanjab Inlier (except one U-Pb single zircon SHRIMP age by Steven & Armstrong, 2000) with the 1:1,000,000 geological map of Namiba as background.

**Problems of stratigraphy, tectonics and metamorphism in the Kamanjab Inlier**

The spatial, temporal and structural relationships between the HMC, the FFG and the KG has been always unclear and even the classification of rocks in each unit in the Huab area has been the subject of debate. Included in the HMC by Frets (1969) were white orthoquartzite, conglomerate, schist, mixed paragneisses, amphibolite, orthogneiss and, in the southwest, migmatitic rocks. In his model, the emplacement of the Fransfontein Granitic Suite occurred after rocks of the HMC had become metamorphosed and deformed. Subsequent

reconnaissance mapping by Guj (1970) showed that the northeastern portion of the HMC comprises low metamorphic sedimentary and volcanic rocks; these were classified as southern equivalent of the Khoabendus Group (Table 1a). The particular, white orthoquartzite was taken as a marker defining the boundary between the HMC *sensu stricto* and the Khoabendus Group. This assumption found its expression on the 1:1,000,000 map of Namibia (1980) and was repeated by Miller (2008) thereby reducing the surface of the HMC to the southern part (Fig. 4).

Similar problems of "stratigraphic" classification exist in the northern part of the study area mapped by Porada (1974). Again, orthogneisses identified as part of the HMC have been separated from less gneissic or undeformed granitic rocks grouped into the FFG, the latter being further subdivided into the Kaross and Kamdescha types. The contact of the West End Formation with the underlying granitic rocks of the basement complex has been observed in a few localities and has been described as indistinct due to palaeo-weathering. This does not exclude an intrusive relationship.

**Table 2.** Geochronological data base of Kamanjab Inlier; zr = zircon, WR = whole rock, fs = feldspar, bt = biotite, gr = granite, eva = evaporation.

| Sample | Easting | Northing | Rock type | Unit | Method | Age [Ma] | Interpretation | Reference |
|---|---|---|---|---|---|---|---|---|
| FGS19A | 526944 | 7737608 | qtz-monzonitic orthogneiss | Fransfontein S | U-Pb multigrain zircon | 1316 | emplacement | Burger *et al.* 1976 |
| FGS19B | 526944 | 7737608 | | | | 1335 | | |
| FGS19C | 526944 | 7737608 | | | | 1498 | | |
| FGS20 | 526944 | 7737608 | | | | 1585 | | |
| FGS21 | 526944 | 7737608 | | | | 1620 | | |
| NN | 503483 | 7768231 | alkali (& calc-alkali) granite | | | 1650±80 | partial reset | Clifford *et al.* 1969 |
| No 66 | 503483 | 7768231 | | | | 1680±60 | | Clifford *et al* . 1962 |
| FGS1 | 502554 | 7767554 | | | | 1720 | emplacement | Burger *et al* . 1976 |
| FGS19-21 | 526944 | 7737608 | | | | 1725±25 | | |
| FGS1 | 502554 | 7767554 | | | | 1730 | | |
| FGS1 | 502554 | 7767554 | | | | 1730±30 | | |
| FGS1 | 502554 | 7767554 | | | | 1735 | | |
| PRU141 | 472213 | 7757665 | orthogneiss | | | 1749±78 | | Tegtmeyer & Kröner, 1985 |
| FGS15 | 532660 | 7788335 | granodiorite | | | 1750 | | Burger *et al.* 1976 |
| FGS1 | 502554 | 7767554 | alkali granite | | | 1760 | | |
| FGS15 | 532660 | 7788335 | granodiorite | | | 1760 | | |
| FGS8 | 515304 | 7778245 | alkali granite | | | 1785 | | |
| FGS7 | 530208 | 7781761 | granodiorite | | | 1795 | | |
| FGS12 | 526673 | 7768641 | granite | | | 1800 | | |
| FGS12 | 526673 | 7768641 | granite | | | 1805 | | |
| FGS7 | 530208 | 7781761 | granodiorite | | | 1815 | | |
| FGS12 | 526673 | 7768641 | granite | | | 1815 | | |
| FGS11 | 512935 | 7794182 | alkali granite | | | 1825 | | |
| PH13 | 468625 | 7784802 | granite | | | 1825±40 | | Burger & Coertze, 1975 |
| FGS12 | 526673 | 7768641 | granite | | | 1830 | | Burger *et al* . 1976 |
| FGS6 | 534233 | 7767951 | granodiorite | | | 1830 | | |
| FGS16 | 556482 | 7777853 | alkali granite | | | 1840 | | |
| FGS6 | 534233 | 7767951 | granodiorite | | | 1843 | | |
| FGS7 | 530208 | 7781761 | | | | 1845 | | |
| FGS18 | 547461 | 7781569 | | | | 1845 | | |
| FGS17 | 552367 | 7780602 | | | | 1845 | | |
| No 67 | 513934 | 7771914 | calcalkali gr | | | 1847±60 | | Burger & Coertze, 1973 |
| FGS3,10,11,14, | 536391 | 7779997 | granodiorite | | | 1870±30 | | Burger *et al.* 1976 |
| FGS6,13,7 | 534134 | 7769519 | | | | 1870±30 | | |
| FGS2,12 | 527165 | 7767748 | granite | | | 1870±30 | | |
| No 68 | 533090 | 7770044 | calcalkali gr | | | 1874±55 | | Burger & Coertze, 1973 |
| FGS2 | 527961 | 7766671 | granite | | | 1870 | | Burger *et al* . 1976 |
| FGS6 | 534233 | 7767951 | granodiorite | | | 1875 | | |
| FGS10 | 516008 | 7785991 | | | | 1880 | | |
| FGS13 | 535322 | 7768625 | | | | 1880 | | |
| FGS14 | 507173 | 7777451 | | | | 1885 | | |
| FGS3 | 533440 | 7770689 | calc-alkali gr | | | 1890 | | |
| No 69 | 526121 | 7768211 | alkali & calcalkali gr | | | 1905±55 | | Burger & Coertze, 1973 |
| No 70 | 506559 | 7768260 | | | | 1980±60 | | |
| No 71 | 526140 | 7781122 | | | | 2066±60 | | |
| 170405-6 | 463750 | 7833320 | granite | | LA-ICP-MS single zircon | 1834±14 | | Kleinhanns *et al* . 2013 |
| 260205-4 | 461861 | 7825462 | granite | | | 1836±17 | | |
| 280205-6 | 482717 | 7833268 | granodiorite | | | 1841±14 | | |
| A451 | 508708 | 7770073 | granite | | Rb-Sr bt | 494±5 | cooling | Hawkesworth *et al.* 1983 |
| No 41 | 503483 | 7768231 | | | | 570±20 | partial reset | Clifford *et al.* 1962 |
| No 38 | 503483 | 7768231 | | | | 545±20 | | |
| No57 | 503483 | 7768231 | | | Rb-Sr fs | 960±50 | | |
| No 61 | 503483 | 7768231 | | | Rb-Sr WR | 1260±70 | | |
| No 65 | 503483 | 7768231 | calcalkali gr | | | 1580±20 | | Clifford *et al.* 1969 |
| NN | 429284 | 7851854 | rhyolite | Khoabendus G | Pb-Pb eva zr | 1987±4 | min emplacement | Kroener, unpubl. in Seth *et al* . 1998 |
| NN | | | | | SHRIMP zr | 1862±6 | emplacement | Steven & Armstrong, 2002 |
| No 57 | 447438 | 7876967 | slate | | K-Ar WR | 445±20 | cooling or deformation | Ahrendt *et al* . 1983a |
| 233/1 | 466765 | 7847505 | metatuff | | | 481±15 | | Ahrendt *et al.* 1983b |
| No 235 | 458010 | 7851175 | | | | 483±11 | | |
| 235A | 458010 | 7851175 | | | | 494±11 | | |
| No 233 | 466765 | 7847505 | | | | 503±11 | | |
| HU-1 | 437903 | 7785386 | anatectic orthogneiss (ROG) | Huab MC | LA-ICP-MS single zircon | 1801±27 | emplacement | Kleinhanns *et al* . 2013 |
| 130503-1 | 450066 | 7772045 | metarhyolite | | | 1826±30 | | |
| HU-3 | 442645 | 7762399 | granodioritic orthogneiss (POGD) | | | 1830±17 | | |

Geochronological data suggest more or less coeval evolution of the HMC, the KG and the FFG. If correct, this requires a model explaining the remarkable difference in metamorphism and structural fabrics in the HMC and the adjacent KG/FFG and a mechanism for the juxtaposition of the two domains.

The age(s) of one or several metamorphic and deformation event(s) recorded by rocks of the HMC, the reconstruction of the respective P/T path(s) as well as the interpretation within a plate tectonic (?) context have never been addressed prior to the present study.

The possible correlation of the HMC with the Epupa Complex (EC) needs to be investigated. The northern EC is characterised by Late Palaeoproterozoic regional HT-LP metamorphism that was followed by Early Mesoproterozoic HT-LP metamorphism culminating at granulite facies peak conditions of 830°C and 2 kb in the northern part of the Epupa Complex (Brandt *et al*. 2021). Meso-proterozoic 1.5-1.3 Ga ultrahigh granulite facies metamorphism and younger upper amphibolite facies metamorphism are recorded in the southern part of the EC (Seth *et al*. 1998, 2003, 2005; Brandt *et al*. 2003, 2007; Brandt & Klemd, 2008), accompanied by the two-stage emplacement of the Kunene layered anorthosite complex within the geodynamic context of a continental rift setting attributed to the Kibaran event (Ernst *et al*. 2013).

## Analytical Methods and Laboratories

The production of this memoir was achieved with the collaboration of scientists based at several international laboratories and universities, and included training of Namibian MSc and PhD students. The following colleagues contributed largely to the realisation of the project.

Project coordination: Becker, T.; PhD and MSc supervision: Kleinhanns, I., Klemd, R., Becker, T.; Writing: Becker, T.; Geological mapping: Becker, T., Mhopjeni, K., Muvangua, E.; Structural analysis: Becker, T.; Mineral analysis, metamorphic petrology: Nolte, N., Depiné, M.; Whole rock geochemistry: Nolte, N., Wilsky, F. Mhopjeni, K., Muvangua, E.; Sm-Nd isotope analysis: Nolte, N.; U-Pb geochronology: Wilsky, F., Wiegand, B., Sergeev, S.; K-Ar geochronology: Wemmer, K.; Ar-Ar geochronology: Sudo, M.

### Whole rock geochemistry

Samples weighing 5-10 kg were cleaned and, where present, weathered rims were removed. Whole rock aliquots of ca 100 g and < 40 µm grain size were prepared by using a rock crusher, riffle splitter, and planetary agate disc mill. Sample powders were dried overnight at 100°C. For XRF analysis 600 mg of the sample powder were mixed with 3.600 mg $LiBO_2$ - $Li_2B_4O_7$ Spektromelt and ~ 1.000 Milligramm $NH_4NO_3$, and fused into a glass disc. For ICP-AES approximately 0.9 g of the powdered unknown was fused into glass discs, and subsequently dissolved in $HNO_3$–HCl. Major and trace elements were analysed by using X-ray fluorescence (XRF) on a Philips PW 1480 spectrometer and a VG Plasma Quad 2+ inductively coupled plasma mass spectrometer (ICP-MS) at the Geoscience Centre of Georg-August University Göttingen, Germany.

### Sr-Rb, Sm-Nd whole rock isotope analysis

Rb-Sr and Sm-Nd isotope analysis was carried out at the Isotope Geology Department at the Geoscience Centre of Georg-August University Göttingen, Germany. Prior to digestion, samples were mixed with spikes enriched in $^{87}$Rb-$^{84}$Sr and $^{149}$Sm-$^{150}$Nd isotopes, respectively. Rb, Sr and rare earth elements were separated from dissolved aliquot powders of whole rock samples by standard cation exchange procedures. The separation of Sm and Nd was done through reverse ion chromatography in hydrogen-diethylhexyl-phosphate (HDEHP) resin. Mass spectrometry of lead and uranium was done on Triton thermal ionisation mass spectrometer (TIMS). International standards were measured at regular intervals between the samples. Long-term reproducibility for National Bureau of Standards Standard Reference Material (NBS SRM) 987 (n = 16) are 0.71026±13 (2σ) and 0.056473±7 (2σ) for $^{87}$Sr/$^{86}$Sr and $^{84}$Sr/$^{86}$Sr, respectively. Analytical mass bias was corrected with an $^{88}$Sr/$^{86}$Sr of 0.1194 using exponential law. Analytical mass bias correction for Rb measurements was achieved via repeated analyses of NBS SRM 984,

yielding a $^{85}Rb/^{87}Rb_{raw}$ of 2.5952±13 (2σ; n = 7), resulting in an exponential mass bias of 0.4‰/a.m.u. Sample measurements were performed under the same conditions and corrected with the exponential mass bias derived from the standard measurements. Long-term reproducibility for the Nd in-house standard (n = 18) are 0.511790±5 (2σ) and 0.348389±3 (2σ) for $^{143}Nd/^{144}Nd$ and $^{145}Nd/^{144}Nd$, respectively. This $^{143}Nd/^{144}Nd$ value agrees with the value of 0.511830 for $^{143}Nd/^{144}Nd$ for the La Jolla solution (Nolte, 2012). Analytical mass bias was corrected with a $^{146}Nd/^{144}Nd$ of 0.7219 using exponential law.

**U-Pb single zircon age dating**

***SHRIMP method***

Centre for Isotopic Research (VSEGEI, St. Petersburg, Russia)

Zircon grains were hand selected and mounted in epoxy resin, together with chips of the TEMORA (Middledale Gabbroic Diorite, New South Wales, Australia, age = 417 Ma, Black & Kamo, 2003) and 91500 (Geostandard zircon, age = 1065 Ma, Wiedenbeck *et al*. 1995) reference zircons. The grains were sectioned approximately in half and polished. The analysis was performed on a SHRIMP-II ion microprobe. Each analysis consisted of five scans through the mass range; the spot diameter was about 18 μm and the primary beam intensity about 4 nA. The data were reduced in a manner similar to that described by Williams (1998) and references therein, using the SQUID Excel Macro of Ludwig (2000). The Pb/U ratios were normalised relative to a value of 0.0668 for the $^{206}Pb/^{238}U$ ratio of the TEMORA zircon, equivalent to an age of 416.75 Ma (Black & Kamo, 2003). Uncertainties given for individual analyses (ratios and ages) are at the one T-level, whereas uncertainties in calculated Concordia ages are reported at the 2 σ level.

Harvard University, USA

Zircon U–Pb ages and trace element compositions were obtained using the sensitive high resolution ion microprobe with reverse geometry (SHRIMP-RG) jointly operated by the U.S. Geological Survey and Stanford University. Operating procedure included an O2– primary ion beam focused to a ∼14 × 18 μm diameter spot for trace element analyses and a ∼30 × 40 μm diameter spot for U–Pb isotopes. Zircon U-Pb analyses were calibrated using zircon standard Temora-2 ($^{206}Pb/^{238}U$ age = 416.8 Ma; Black *et al*. 2004) and trace element concentrations standardised relative to MAD-559 (Coble *et al*. 2018). Data were reduced using Squid 2.51 (Ludwig, 2009) and Isoplot 3.76 software (Ludwig, 2012). Measured $^{206}Pb/^{238}U$ was corrected for common Pb (Pbc) using measured $^{207}Pb$ based on a model Pb composition from Stacey & Kramers (1975) and corrected for $^{230}Th$ disequilibrium using the method of Schärer (1984) and an initial assumed ($^{230}Th/^{238}U$) melt value based on whole rock Th/U values (Th/U = 4.7 for IESn1 and IESn2; Th/U = 3.7 for IESn3 based on values from the same units sampled by Hards (1995). The magnitude of the correction was typically 85–90 kyr.

***LA-ICP-MS method***

University Bergen, Norway

Backscattered (BSE) and cathode-luminescence (CL) images were produced using a Jeol JXA-8900 R Microprobe at the GZG - Department of Geochemistry (Georg-August University/Göttingen, Germany). These images were used for optical inspection of the grains for mechanical damage during the preparation procedure, but more importantly the internal structures of the zircon grains. Laser-ablation ICPMS (LA-ICP-MS) measurements were done at the Department of Earth Science, University of Bergen (Norway), on a Thermo FinniganTM Element 2. The following description is based on the technique described in Košler *et al*. (2002). A 213 nm Nd-YAG laser (New Wave, UP213) connected to an Element2 Thermo FinniganTM single collector was used for the ablation of the zircon samples. Firing was done at 10 Hz repetition rate, with a fluence energy of 1.4 J/cm², a laser beam diameter of 30 μm, and line length from 50 to 100 μm depending on size and condition of the zircon grain. Blanks were measured before each analysis. For mass bias correction simultaneous measurement of a tracer solution was performed. To assess the degree of U and Pb fractionation and to ensure high quality data the 91500-, GJ-1- and the Plešovice-standard zircons were analysed after about every 15 unknown zircon grains (i.e. one run) (91500: Wiedenbeck *et al*. 1995; GJ-1: Jackson *et al*. 2004; Plešovice: Sláma *et al*. 2008).

**K-Ar muscovite age dating**

K-Ar muscovite age dating was carried out at the Isotope Geology Department at the

Geoscience Centre of Georg-August University Göttingen, Germany. Samples included pegmatitic mica of several cm size and coarse-grained metamorphic mica from paragneiss where coarse-grained muscovite was hand-picked from the crushed rocks. Potassium was determined by using the classic AES method. The argon isotopic composition was measured in a Pyrex glass extraction and purification line coupled to a VG 1200 C noble gas mass spectrometer operating in static mode. The amount of radiogenic $^{40}Ar$ was determined by the isotope dilution method using a highly enriched $^{38}Ar$ spike from Schumacher, Bern (Schumacher, 1975). The spike is calibrated against the biotite standard HD-B1 (Fuhrmann *et al*. 1987). The age calculations are based on the constants recommended by the IUGS, quoted in Steiger & Jäger (1977).

**$^{40}Ar/^{39}Ar$ muscovite, hornblende age dating**

***Sample preparation and neutron irradiation***

Mineral separates of hornblende with 300 microns diameter and of muscovite with 100-200 microns were prepared from the rocks by the standard methods for mineral separation. Neutron irradiation of those mineral separates was performed at CLICIT (Cadmium-Lined In-Core Irradiation Tube) facility in the nuclear reactor OSTR (Oregon State TRIGA Reactor), Oregon State University, USA. The six unknown samples were wrapped in commercial grade Al foil and subsequently loaded into a sample container (22.7 mm in diameter and 101.5 mm in height) made of 99.999% pure Al. All samples were irradiated for 4 hours with the fast neutrons of the flux of $2.47 \times 10^{13}$ n/cm$^2$/s for inducing the reactions of $^{39}K(n,p)^{39}Ar$ in the samples. The $^{40}Ar/^{39}Ar$ ages were obtained as the relative ages against the neutron flux monitoring mineral age standard, which was irradiated together with the unknown samples. The age standard used was Fish Canyon Tuff sanidine, FC3, which was prepared at the Geological Survey of Japan and its age was determined as 27.5 Ma (Ishizuka, 1998; Uto *et al*. 1997). This age is consistent with that obtained by Lanphere & Baadsgaard (2001). Additionally, crystals of $K_2SO_4$ and $CaF_2$ were also irradiated for correcting the interference of Ar isotopes produced by the reactions of K and Ca in the samples during neutron irradiation. After the irradiation the samples were stored for a few weeks at OSTR to cool down their radioactivity before they were delivered to the University of Potsdam.

***$^{40}Ar/^{39}Ar$ isotope dating***

Argon isotope analyses were performed at the $^{40}Ar/^{39}Ar$ geochronology laboratory of the University of Potsdam. The common procedure usually conducted for the $^{40}Ar/^{39}Ar$ dating at Potsdam has been described in the literature (Wilke *et al*. 2010; Halama *et al*. 2014), but the summary of the present system is as follows. The Ar isotopic analytical system in the laboratory consists of, (1) a New Wave Gantry Dual Wave laser ablation system including a 50W $CO_2$ laser (wavelength 10.6 micrometer) for heating samples and extracting sample gases, (2) an ultra-high vacuum purification line equipped with SAES getters and the cold stainless finger-trap cooled at -90˚C through ethanol, and (3) the high-sensitivity Micromass 5400 noble gas mass spectrometer equipped with an electron multiplier. The extracted gas with $CO_2$ laser from a single white mica grain was introduced into the ultra-high vacuum purification-line and was held for 10 minutes for purifying the gas to pure Ar, then the Argon isotopic ratios were determined with the noble gas mass spectrometer. All Ar isotope ratios from the samples were finally obtained after blank, mass discrimination, interference and decay corrections of the analysed results. Each J value at one location was obtained as a weighted or arithmetic average by the four single grain total fusion analyses of the Fish Canyon Tuff sanidine grains, then the J values at the unknown samples were interpolated from those directly obtained J values. The $^{40}Ar/^{39}Ar$ age calculation was conducted following the method of Uto *et al*. (1997) and the isochrons calculation follows York (1969). The $^{40}Ar/^{36}Ar$ ratio of the atmosphere and the decay constants for $^{40}K$ used were those recommended in Steiger & Jäger (1977) as 295.5, $\lambda_\beta = 4.962 \times 10^{-10}$ /yr and $\lambda_e = 0.581 \times 10^{-10}$ /yr. Our used interference correction parameters are: $(^{39}Ar/^{37}Ar)_{Ca}$ = (6.638±0.263) x $10^{-4}$, $(^{36}Ar/^{37}Ar)_{Ca}$ = (2.730±0.032) x $10^{-4}$, $(^{40}Ar/^{39}Ar)_K$ = (50.97±24.35) x $10^{-4}$ and $(^{38}Ar/^{39}Ar)_K$ = (1.182±0.003) x $10^{-2}$. Conditions of plateau follow Fleck *et al*. (1977). All errors (in the figures and tables) indicate 1 sigma error.

**Mineral geochemistry**

Normal 30 μm thick polished thin sections were made of each sample and first

studied under an optical microscope. Mineral composition was determined by using JEOL JXA-8200 microprobe at the GeoZentrum Nordbayern of the University of Erlangen. Analysis was done using wavelength dispersive spectrometers with an accelerating voltage of 15 kV, a current of 15 nA and a beam diameter of ca 1 µm. Matrix corrections and data reduction were done by matrix correction software supplied by the manufacturer. All iron was calculated as $Fe^{2}$+. The relative errors are ±1 % for major elements and ±5 % for minor and trace elements. Calibration was done at regular intervals by using mineral standards orthoclase (K), albite (Na), barite (Ba), andradite (Ca, Si); corundum (Al), MgO (Mg), $Fe_2O_3$ (Fe), $Cr_2O_3$ (Cr), and $MnTiO_3$ (Mn, Ti).

## Geological mapping

Geological field mapping at a scale of 1:50,000 was carried out intermittently from 2000-2005 in (i) the area from Khorixas to the Grootberg Pass and (ii) the Huab Region (Fig. 6). This covered the previously unmapped portion of the KG and the FFG in the north (3 sheets) and the entire HMC that was mapped by Frets (1974) at a scale of 1:100.000 (6 sheets; Fig. 7) including the part that was subsequently distinguished as southern Khoabendus Group (Hugo & Schalk, 1974). Geological mapping was complemented by two profiles (in the following sections named the "Transition Zone") between these areas for additional structural information. The field data base of the area includes about 5500 georeferenced entries providing information on rock type, sedimentary and tectonic structures, metamorphism, contacts, samples, photos, etc.

### Kamanjab-Grootberg Area

Geological mapping in the northern Kamanjab-Grootberg area was supported by interpretation of high resolution airborne radiometric and magnetic data combined with remote sensing of Landsat TM7 scenes. The new geological map shows refinement of the stratigraphy of the KG, the new subdivision of the Fransfontein Suite into ten igneous rock types and their geometry and illustrates the overall structural architecture.

#### *Khoabendus Group (KG)*

Detailed geological mapping was carried out in the southwestern part of sheets 1914 CB and DA which exposes the West End and Otjovazandu formations. All formations are extensively invaded by the FFG into which they continue forming large slivers that are progressively assimilated by the surrounding magma. Three profiles through the Bruno, Oortrek and Honib synclines resulted in the detailed stratigraphy of the West End, Blyerus and Otjovazandu formations (Fig. 5, Table 3).

The stratigraphic terms Robin and Smalruggens Member have been omitted, because rhyolitic and andesitic volcanic rocks occur within the Voerspoet quartzite both locally at the base and as intercalations higher up and it is unclear which specific horizons correspond to the units in the type locality in the Huab area.

#### ***West End Formation (MWs)***

The West End Formation starts with a clastic to volcaniclastic succession that higher up grades into the classic porphyritic ignimbrite and rhyodacite, which was formerly considered to be the base of the formation (Porada, 1974). This succession is here distinguished as the Ombonde Member, whereas the ignimbrites are classified as the Bruno Member, with both names derived from the farms of the respective type localities (Fig. 5). However, the Ombonde Member probably does not represent the base of the Khoabendus Group. The basal sediments of the unit are intruded by foliated Kamdescha Granite that was formerly classified as part of the HMC (Porada, 1974). The geological map clearly reveals the discordant nature of the contact with the granite intruding towards the south successively into higher stratigraphic levels. Slivers of fine-grained sandstone and quartz-sericite schist up to several deccametre size occur within the Kamdescha Granite near the contact demonstrating the continuation of the KG into underlying older units.

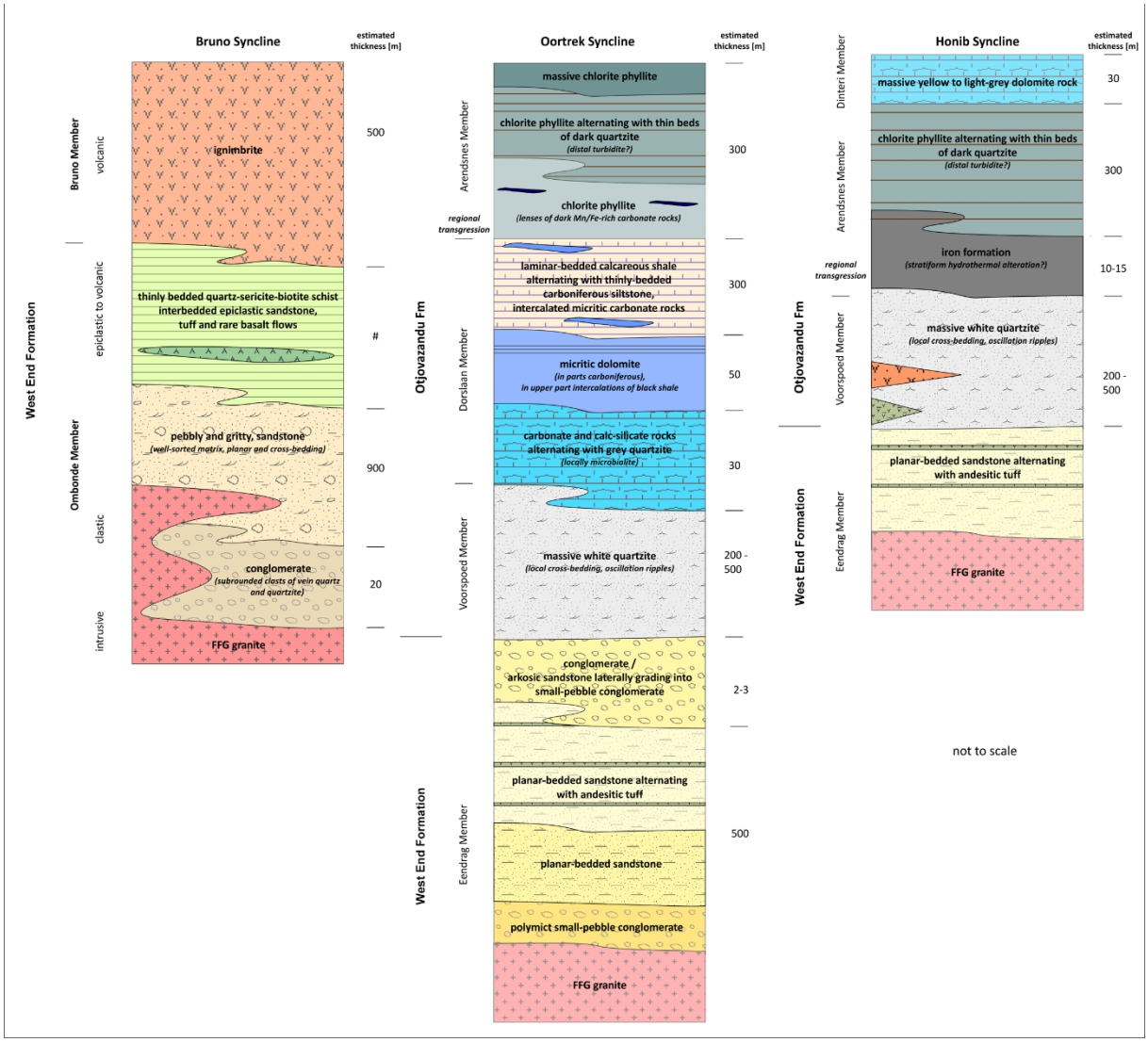


**Figure 5.** Stratigraphic profiles of the Bruno, Oortrek and Honib synclines in the Kamanjab-Grootberg area.

**Table 3.** Revised stratigraphy of the Khoabendus Group in the northern area.

| Northern Kamanjab area | Revised stratigraphy | |
|---|---|---|
| Lithology | Formation | Member |
| | (Maximum thickness, m) | |
| Strongly altered andesitic to basaltic lavas | Otjovazandu (1700) | Dinteri (200) |
| Upper, more massively bedded, pink limestone and grey dolomite with a few layers of chert | | |
| Lower thin bedded limestone and dolomite with layers of chert, schist and sandstone; tuff lenses; white marble in west with interbedded quartzite, schist, purple slate and chlorite-actinolite schist | | |
| Basal siliceous iron formation with siderite and hematite (up to 50 m thick), grades into ferruginous quartzite or chert | | |
| Local red, gritty quartzite up to 300 m thick in SE | | Arendsnes (500) |
| Grey to black shale, phyllite and schist; interbedded grey to purple chert, purple siltstone, grey and white quartzite, black and purple dolomite, purple, grey and black bedded or oolitic chert, lithic sandstones, iron formation, chlorite-actinolite schist; layers of felsite, flow-banded rhyolite and acid tuff | | |
| Local schist, mainly greenish grey | | |
| Carbonate and calc-silicate rocks alternating with grey quartzite (locally microbialite), micritic dolomite, laminar-bedded calcareous shale alternating with thinly-bedded carboniferous siltstone, intercalated micritic carbonate rocks | | Doorslaan (400) |
| Massive, white, upwards-fining orthoquartzite ("Khoabendus quartzite"); thin local interbedded grey lithic quartzite, chlorite-actinolite schist, sericitic schist, thick interbedded acid lavas and tuff in NW which increase in abundance upwards, intercalated beds of andesite | | Voorspoed (600) |
| Local basal, red, feldspathic, pebbly quartzite or conglomerate | | |
| DISCONFORMITY | | |
| Base not exposed. Polymict small-pebble conglomerate grading into overlying planar-bedded sandstone with important volcano-clastic component alternating higher up with andesitic and rhyolitic tuff beds. Top is comprised of conglomerate and arkosic sandstone laterally grading into small-pebble conglomerate. | West End (1900) | Eendrag (500) |
| Porphyritic ignimbrite- variably sheared and foliated, grain size decreases upwards and tuffs become the dominant pyroclastic rock type in the upper part; local graded bedding; interbedded, fine-grained , porphyritic to non-porphyritic, grey, dacitic to rhyodacitic lavas, flows 10 to 15 m thick, become more abundant upwards and towards the west, quartz, potash feldspar, plagioclase, biotite and hornblende phenocrysts | | Bruno (500) |
| Thinly bedded quartz-sericite-biotite schist, interbedded epiclastic sandstone, tuff and rare basalt flows | | Ombonde (900) |
| Pebbly- to gritty sandstone with local cross and planar bedding, heavy mineral seams | | |
| Oligomict conglomerate intruded by Fransfontein Suite granite | | |

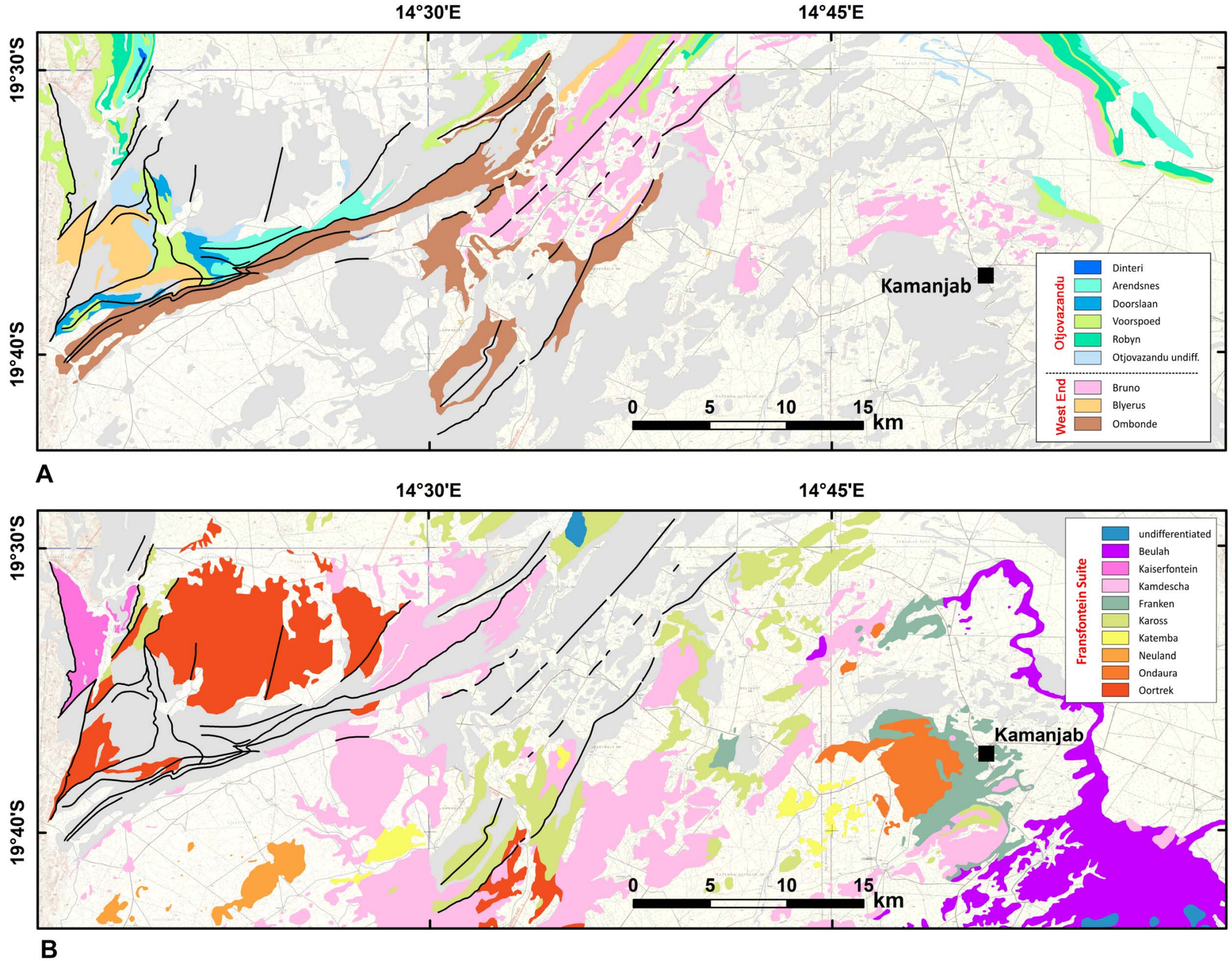


**Figure 6.** Revised geological maps of the northern KI (Kamanjab-Grootberg area). A) West End and Otjovazandu formations in detail; B) Fransfontein Suite in detail.

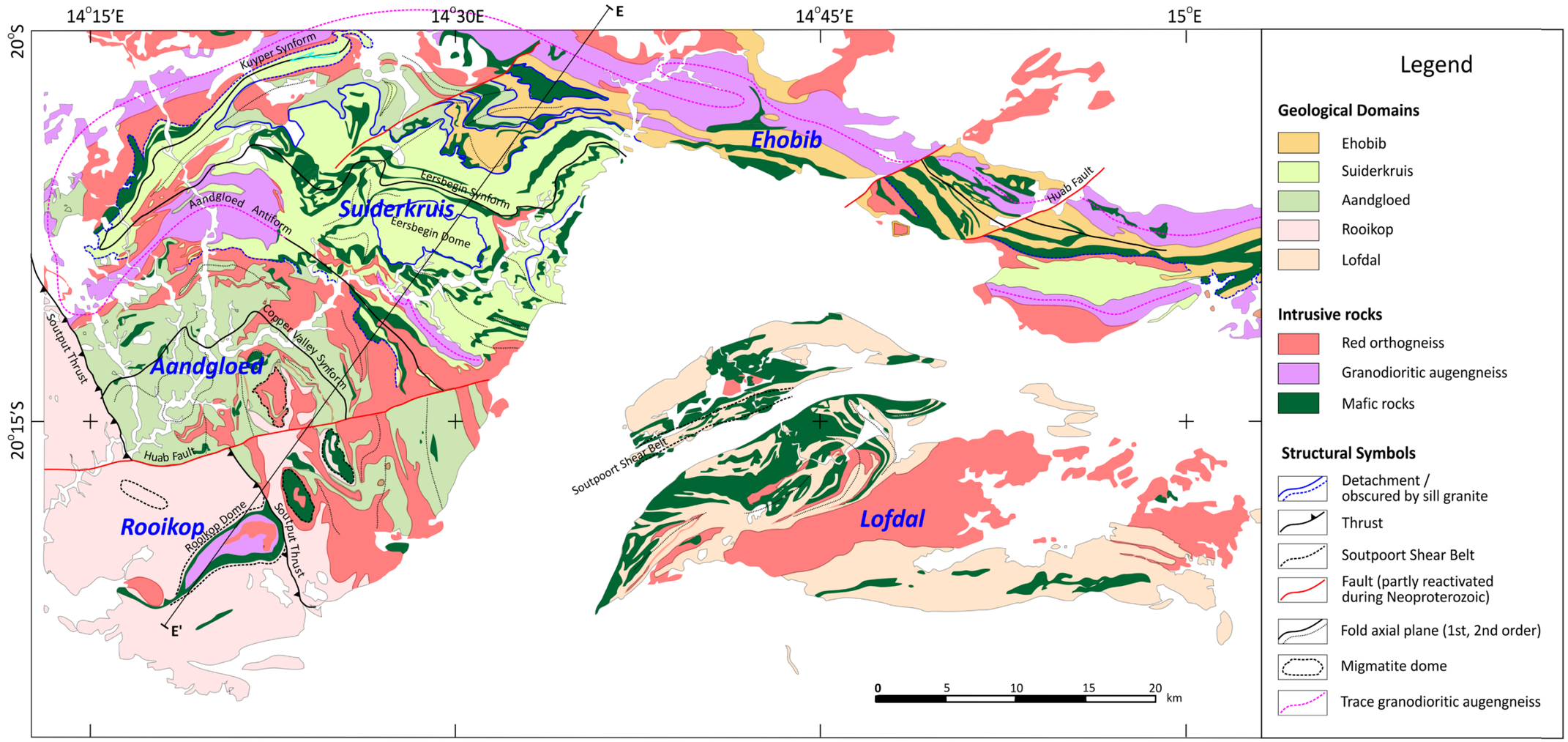


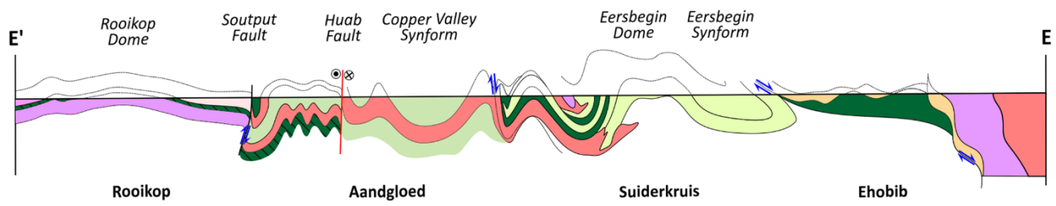


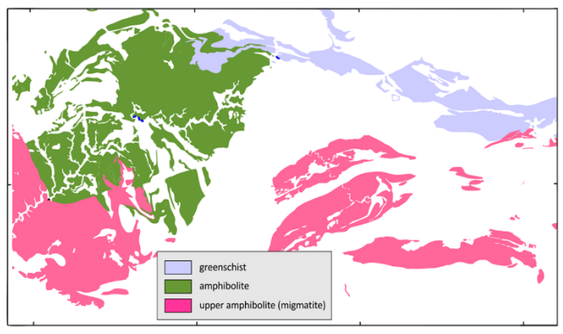


**Figure 7**. Revised simplified geological map of the HMC and overlying Damara rocks (Huab Region).

*Ombonde Member (MWsOm)*

The Ombonde Member is characterised by overall normal grading coinciding with the change from clastic to volcaniclastic deposition (Fig. 5). Locally preserved conglomerate (20 m) at the base comprises sub-rounded to rounded clasts of vein quartz and quartzite of 2- 50 cm size set in a coarse sand quartz-feldspar matrix with abundant magnetite. Tectonic deformation results in both flattening and stretching of the clasts (Fig. 8a). The conglomerate grades into pebbly sandstone that further up turns into pink-to-grey, well-sorted gritty quartz-feldspar sandstone (900 m). Sedimentary structures comprise both planar bedding at cm-scale and more rarely cross-bedding of 15-40 cm size indicative of fluviatile deposition. Sedimentary structures are often outlined by heavy mineral seams of magnetite (Fig. 8b) and in the airborne magnetic data the unit represents a prominent marker. The upper portion of the Ombonde Member comprises thinly bedded quartz sericite biotite schist interbedded with volcanic fragment-bearing quartz sandstone, felsic to intermediate tuffs and rare basalt (<120 m). These rocks are exposed in the south and north of the study area. On Bruno 614 the transition from clastic to volcaniclastic deposition is marked by pale-green andesitic tuff alternating with gritty sandstone. One intercalated, massive basalt flow about 30 metres thick, locally contains amygdales filled with calcite and epidote. The quartz sericite is intruded in the south by sills of Fransfontein Granite and finally forms major slivers within that intrusion.


**Figure 8.** Ombonde Member. A) metaconglomerate alternating with sandstone overprinted by steep foliation transposing the clasts; B) cross-bedded sandstone; the cross bedding is outlined by heavy mineral seams.

*Bruno Member (MWsBr)*

The Bruno Member corresponds to the classic porphyritic ignimbrite sequence of the West End Fm documented in detail by Porada (1974) and Miller (2008; Table 1).

*Eendrag Member (MWsEe)*

Clastic and volcaniclastic rocks that are now classified in this member occur on farms Kaiserfontein and Eendrag 619 in the SW corner of the study area and on Farm Wilhelmsville 615 in its central northern part. To the south they are in faulted contact with the Ombonde Member of the West End Formation. To the east and north quartzite of the Voorspoed Member overlies it and in the west basal conglomerate and sandstone of the Neoproterozoic Nosib Group. In the NW the unit is bound by a fault with the FFG suite which, in addition, intrudes the formation in various places. Due to the mostly tectonic or intrusive nature of contacts between Khoabendus rocks, the stratigraphic position of the volcaniclastic succession remains uncertain. The base of the formation is not exposed and the stratigraphically lowest horizon consists of a polymict small-pebble conglomerate, which is exposed in the core of an anticline (Fig. 5). It is overlain by a succession of clastic, epiclastic and pyroclastic rocks at least 500 m thick. Its lower part is dominated by immature medium-grained planar-bedded quartz-feldspar sandstone with alternating grey and red-brown beds between 3 and 50 cm thick. Higher up these

rocks grade into cream planar-bedded quartz sandstone alternating with green, up to 5 cm thick beds of fine-grained epiclastic or pyroclastic rocks (Fig. 9). The latter are marked by an abundance of volcanic fragments and interpreted as metatuff or tuffite of andesitic to dacitic composition. In the Honib Syncline, andesitic rocks at the top of the Blyerus Fm are up to 200 m thick and are distinguished as the Smallruggen Member. The formation is overlain disconformably by the Voorspoed quartzite.

**Figure 9**. Lower Eendrag Member; pale sandstone alternating with pale-green fine-grained pyroclastic rocks.

A second isolated volcaniclastic succession on Farm Wilhelmsville 615 documents the great variation in volcanic and volcaniclastic facies; the base of the unit is intruded by granite and at the top it is unconformably overlain by quartzite of the Otjovasandu Formation. The lowermost rocks are sheared metabasalts or mafic tuffs transformed into chlorite schist. They are overlain by a succession of quartz-sericite-biotite schist with intercalated, grey, occasionally banded chert (Fig. 10a). Petrography reveals fine-grained crystals of quartz, K-feldspar and plagioclase in a microcrystalline matrix suggesting their interpretation as former ash beds. Higher up these rocks grade into immature tuffaceous sandstone and quartz sandstone that contains dark grey angular volcanic fragments 0.5-1 cm in diameter with a second series of quartz-sericite-biotite schist terminating the succession (Fig. 10b).

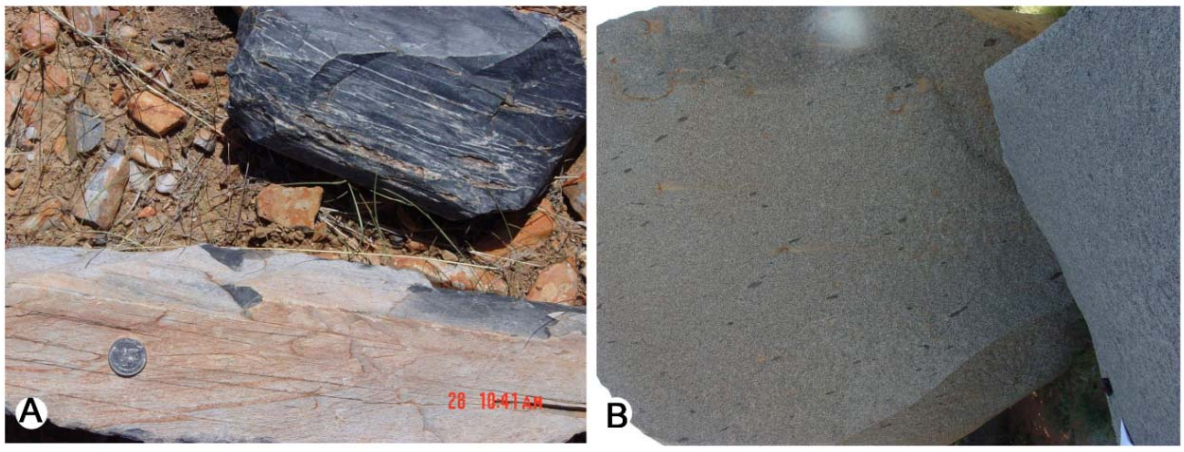


**Figure 10**. Eendrag Member. A) black banded chert of volcanic origin; B) arkosic sandstone with disseminated angular volcanic fragments.

***Otjovasandu Formation (MOv)***

Most of the MOv outcrops north of the study area and the initial stratigraphy is derived from mapping by Porada (1974) in that area. Later the MOv was subdivided from the base to the top into Voorspoed Quartzite, Robyn Felsite, Arendsnes Pelite and Dinteri Carbonate Members (Miller, 2008). In the study area, the MOv crops out in the northern half of sheet 1914CB and in the NW corner of sheet

1914DA. The predominantly sedimentary rocks were deposited unconformably on the West End and Blyerus formations and were intruded by FFG granites. Some of the facies can be correlated with those known from the north, but important changes render such correlations tenuous. Two profiles across the Ootrek and Honib synclines are described in the following section, documenting the considerable facies variation over less than 3 km along strike.

Oortrek Syncline

*Voorspoed Member (MOvVs)*

The unit starts with a basal conglomerate which is overlain by the characteristic white orthoquartzite. On Kaiserfontein 619, a continuous, about 70 m thick conglomerate horizon was mapped over more than 5 km along strike. The clast-supported and oligomictic conglomerate comprises rounded to subrounded clasts, 1-20 cm in diameter, of vein quartz and quartzite. The matrix is fine-grained and is pervasively altered by hydrothermal chert-epidote, transforming the rock into a breccia (Fig. 11).

**Figure 11**. Hydrothermal breccia at the base of the Voorspoed Quartzite Member.

On Wilhelmsville 615, white orthoquartzite overlies arkosic sandstone, less than 2-3 m thick, that grades laterally into gritty sandstone and a small-pebble conglomerate. The contacts of these rocks with the underlying volcaniclastic rocks is also gradational. The white massive quartzite forms a prominent horizon 200-500 m thick. The medium- to fine-grained recrystallised rock is commonly devoid of any sedimentary structures, however bedding at decimetre-scale is suggested by the preferred layer-parallel wide cleavage that probably traces altered laminae of interbedded fine-grained sediments or pyroclastic rocks. Oscillation ripples locally occur in beds less 2-3 cm thick and in other places cross-bedding is outlined by heavy mineral seams. The sedimentary structures document a very shallow marine depositional environment.

*Dorslaan Member (MOvDo)*

A first cycle of carbonate deposition recorded in the Oortrek syncline identified during the present mapping programme is classified as the Dorslaan Member; the contact with the underlying Voorspoed quartzite is transitional. Up to 2 m thick carbonate and calc-silicate layers alternate with grey quartzite and locally record microbialite structures (clotted thrombolite; Fig. 12a). The overlying, ca 30 m thick, carbonate sequence starts with light grey limestone, which occasionally displays microbial mat structures (Fig. 12b) attesting to very shallow marine deposition. It is overlain by brown micritic occasionally carbonaceous dolomite that in the upper part alternates with thin beds of black shale. The overlying graphite-bearing laminated calcareous shale, up to 300 m thick, alternates with grey thinly bedded carbonaceous siltstone. Intercalated are up to 2 m thick beds of cream brown micritic carbonate rocks.

*Arendsnes Member (MOvAd)*

The MOvAd overlies the Dorslaan Member in the Oortrek Syncline along a sharp sedimentary contact. The unit starts with a 10-15 m thick horizon of dark iron-rich rocks

grading into overlying laminar bedded chlorite phyllite with dark lenses of Mn and Fe-rich carbonate rocks. Higher up, these facies grade into rhythmic sequences of 10 cm thick phyllite beds alternating with thin beds (0.5 cm) of dark quartzite. In the upper part of the sequence, quartzite beds become less and less abundant until only massive phyllite remains in the uppermost portion of the unit.

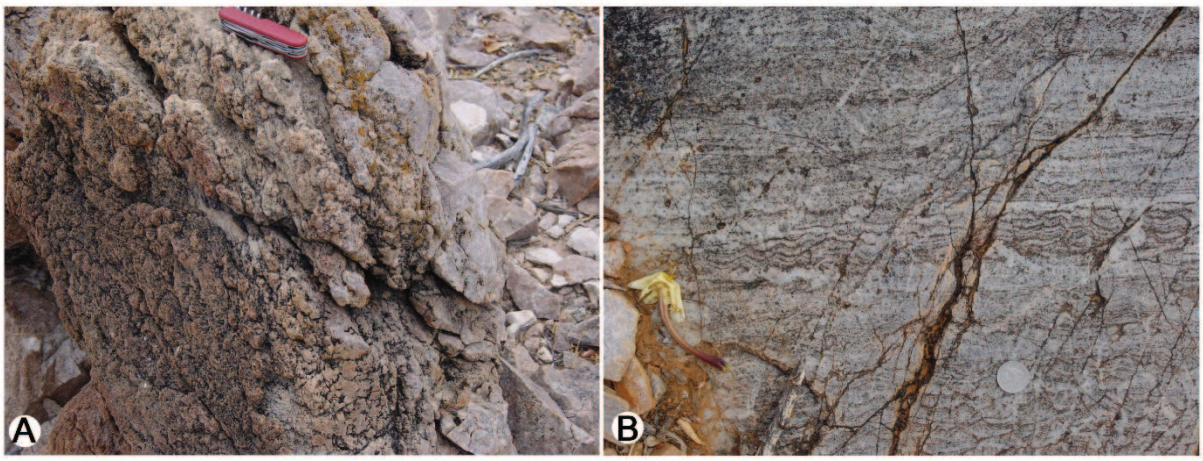


**Figure 12**. Limestone of the Doorslaan Member displaying undeformed sedimentary microstructures. A) microbialite (clotted thrombolite, B) microbial mats (stromatolite).

Honib Syncline

In the Oortrek syncline, quartzite of the Voorspoed Member overlies volcaniclastic rocks of the Blyerus Formation comprising quartzite with intercalated horizons of andesite and rhyolite in the lower part. The succession is overlain by phyllite that towards the contact grades into highly altered iron-rich rocks, which are interpreted to result from hydrothermal fluids following the barrier. The ca 300 m thick phyllite sequence resembles the one in the Ootrek Syncline. As in that unit, it starts with rhythmic sequences of thin dark quartzite beds alternating with thick beds of phyllite that higher up grade into massive phyllite. These rocks are capped along a sharp sedimentary contact by massive yellow to light grey dolomitic rocks 30 m thick, classified as the Dinteri Member. The rocks record marine regression and the change from deep water deposition into a restricted lagoon environment.

***Fransfontein Granitic Suite (FFG)***

Geological mapping and airborne radiometric data (K, Th, and U) reveal the high variation in texture, composition and geometry of the FFG intrusions that allows eleven phases to be distinguished (Fig. 6, Fig. 14). Table 4 shows the main properties of each facies (outcropping surface area, field description, the intrusion mode, radiometric properties and where available petrography, geochemical classification and age).

Outcrop areas of individual phases vary in area from more than 400 $km^2$ to less than 15 $km^2$ representing their minimum size. Phases less than 100 $km^2$ in outcrop are commonly restricted to only one locality whereas the larger ones either form major sills (Beulah, Kamdescha) or distinct circular bodies (Kaross). Only a few relative age constraints were established by field observation: the Oortrek granite forms the central part of the Waterbron granodiorite body and therefore is younger whereas xenoliths of Kaross facies within the Kamdescha granite indicate the greater age of the red granite. FFG granites are not cross cut by mafic dykes or sills which are ubiquitous in the HMC attesting to their greater age.

Petrography shows that FFG granitoids are mostly undeformed coarse-grained to megacrystic rocks with equigranular, seriate and porphyritic textures. Rapakivi textures have been observed in two facies (Franken and Tevrede, the latter forming a small pluton north of the study area). Disseminated biotite is present in all facies but varies in modal proportion from 15-20% (Franken, Beulah) to less than 5% in leucocratic rocks (Katemba, Kaross, Tevrede). Dark green amphibole is associated with nests of biotite but is absent in the leucocratic facies. Angular xenoliths of andesite, red granite and mafic rocks are characteristic of a number of intrusions. Rounded mafic magmatic enclaves and

sometimes diffuse contacts attesting to magma mixing were found only in the Neuland Intrusion.

A weak metamorphic foliation is developed in most granitoids of the FFG and commonly increases with the proportion of biotite in the rocks. Leucocratic granitoids therefore appear to be almost undeformed whereas the biotite-rich Beulah and Franken granodiorites are marked by a penetrative foliation and in places turn into augengneiss.

**Table 4.** Properties of Fransfontein Suite phases. The two lowest and highest values for each element are marked in blue and red, respectively. Values for K are in [%], for U, Th in [ppm]

| Intrusion | Outcrop area | Field description | Intrusion mode | Airborne radiometry statistics | | | | | | Q-ANOR classification | Age |
|---|---|---|---|---|---|---|---|---|---|---|---|
| | [km2] | | | Element | min | max | range | mean | std | (Kleinhanns *et al*. 2013) | |
| Beulah | 156 | Fine- to medium grained equigranular biotite- (amphibole) rich granodiorite, occasionally transition into ignimbritic rocks, often sheared, | major sill | K | 0,4 | 5,6 | 5,2 | 3,3 | 0,7 | | |
| | | | | Th | 2,3 | 22,1 | 19,8 | 12,7 | 2,7 | | |
| | | | | U | 1,2 | 6,4 | 5,3 | 3,8 | 0,7 | | |
| | | | | Ternary | 22,9 | 135 | 112 | 95,9 | 17,6 | | |
| Neuland | 16 | Medium- to coarse-grained, seriate, biotite-rich granodiorite, numerous mafic enclaves (xenoliths) | oval shaped body 16 x 3 km late stage | K | 1,4 | 4,1 | 2,7 | 2,9 | 0,5 | | |
| | | | | Th | 4,7 | 31,8 | 27,0 | 14,8 | 5,5 | | |
| | | | | U | 1,6 | 9,7 | 8,1 | 4,3 | 1,1 | | |
| | | | | Ternary | 41,4 | 162 | 120 | 96,4 | 22,2 | | |
| Waterbron | 73 | Medium-grained equigranular biotite-bearing granodiorite | 2 circular intrusions of 15 and 4 km size, one dyke | K | 0,4 | 4,7 | 4,3 | 3,1 | 0,6 | | |
| | | | | Th | 2,0 | 35,7 | 33,7 | 15,1 | 3,3 | | |
| | | | | U | 1,3 | 8,3 | 7,0 | 4,3 | 0,9 | | |
| | | | | Ternary | 20,4 | 162 | 142 | 98,2 | 17,2 | | |
| Franken | 36 | Coarse - to megacrystic porphyritic biotite-bearing granodiorite | medium sill | K | 1,8 | 5,1 | 3,3 | 3,6 | 0,4 | Monzo to Alkali-feldspar granite | 1841 +/- 14 Ma |
| | | | | Th | 7,2 | 23,0 | 15,8 | 14,4 | 2,5 | | |
| | | | | U | 1,8 | 6,7 | 4,9 | 4,0 | 0,7 | | |
| | | | | Ternary | 53,6 | 142 | 88,2 | 105 | 12,4 | | |
| Kamdescha | 417 | Medium- to coarse grained, equigranular to porphyritic biotite-bearing granite, abundant enclaves of intermediate andesitic composition | major sill | K | 0,5 | 7,4 | 6,9 | 3,5 | 0,8 | Syenogranite | 1836 +/- 17 Ma |
| | | | | Th | 2,6 | 52,5 | 50,0 | 17,6 | 6,4 | | |
| | | | | U | 0,9 | 11,4 | 10,5 | 4,2 | 1,1 | | |
| | | | | Ternary | 18,7 | 233 | 214 | 111 | 27,8 | | |
| Katemba | 14 | Medium-grained equigranular biotite bearing feldspar-rich granite, few mafic enclaves up to 30 cm size | one circular intrusion of 5 km diameter, 2 smaller intrusions of 1 and 2 km size, respectively (deformed into oval body) | K | 1,2 | 5,3 | 4,0 | 3,5 | 0,7 | | |
| | | | | Th | 9,8 | 24,9 | 15,1 | 17,5 | 2,9 | | |
| | | | | U | 2,3 | 6,9 | 4,6 | 4,4 | 0,6 | | |
| | | | | Ternary | 60,1 | 150,6 | 90,5 | 111,7 | 16,7 | | |
| Kaiserfontein | 16 | Medium-grained equigranular biotite-bearing subvolcanic granodiorite, occasionally volcanic fragments | probably sill, overlain to the west by Damara sedimentary rocks | K | 0,9 | 6,3 | 5,4 | 3,7 | 0,8 | | |
| | | | | Th | 5,3 | 43,1 | 37,8 | 15,3 | 3,0 | | |
| | | | | U | 1,6 | 9,9 | 8,3 | 4,7 | 1,0 | | |
| | | | | Ternary | 32,4 | 200 | 167 | 110 | 18,3 | | |
| Kaross | 249 | Red biotite-poor fine to medium-grained equigranular potassic granite | 3 circular plutons with diameters between10 and 22 km | K | 0,6 | 5,8 | 5,2 | 3,6 | 0,6 | Monzo- to Syenogranite | 1834 +/-14 Ma |
| | | | | Th | 2,2 | 54,0 | 51,8 | 19,5 | 10,7 | | |
| | | | | U | 0,0 | 14,6 | 14,6 | 4,1 | 2,0 | | |
| | | | | Ternary | 23,6 | 250 | 227 | 115 | 38,2 | | |
| Oortrek | 44 | Late-stage medium-to coarse-grained equigranular high K, Th, U amphibole and biotite-bearing granite | central part of Waterbron body; 6 km diameter | K | 2,2 | 5,0 | 2,8 | 4,1 | 0,3 | Syenogranite | |
| | | | | Th | 10,0 | 33,5 | 23,6 | 19,9 | 3,8 | | |
| | | | | U | 1,2 | 7,0 | 5,8 | 4,2 | 0,7 | | |
| | | | | Ternary | 72,6 | 169 | 96,4 | 123 | 13,5 | | |
| Ondaura | 27 | Red to pinkish biotite-bearing fine- to medium-grained equigranular potassic granite | one circular intrusion of 6 km diameter, two smaller plugs | K | 2,5 | 5,6 | 3,1 | 4,3 | 0,3 | | |
| | | | | Th | 12,4 | 42,8 | 30,4 | 22,7 | 3,3 | | |
| | | | | U | 1,8 | 9,0 | 7,2 | 5,0 | 0,8 | | |
| | | | | Ternary | 100 | 201 | 101 | 140 | 12,1 | | |

Airborne geophysics data document considerable variation in geochemical whole rock composition coinciding with the mineralogy of the rocks. Less fractionated granodiorite (Beulah Neuland, Waterbron and Franken intrusions) is characterised by relative low mean values of K, Th and U and total count, whereas the more fractionated Ondaura and Oortrek intrusions show high concentrations of the radio elements. High standard deviations in radio elements mark the Kamdescha and Kaross phases forming the largest intrusions, which indicates that they could be possibly subdivided into further, more homogeneous, phases.

Hierarchical classification analysis (HCA) of the 10 FFG phases based on mean values of K, Th, U and total count using Euclidean distance and single linkage method results in the tree diagram given in Fig. 13. The phases are arranged by the HCA according to their fractionation degree. Less fractionated phases with low radio-elements (e.g. granodiorite, Table 4) occur to the left of the x-axis whereas the highly-fractionated Ondaura and Oortrek phases, marked by elevated radio-elements have been placed to the right. Low Euclidean distances corresponding to similar geochemical characteristics classify six intrusions into two groups comprising the Kamdescha-Katemba-Kaiserfontein granite and Neuland-Waterbron-Beula granodiorite. The fractionated Oortrek and Ondaura intrusions show the greatest distances to the other phases, indicating their special composition.

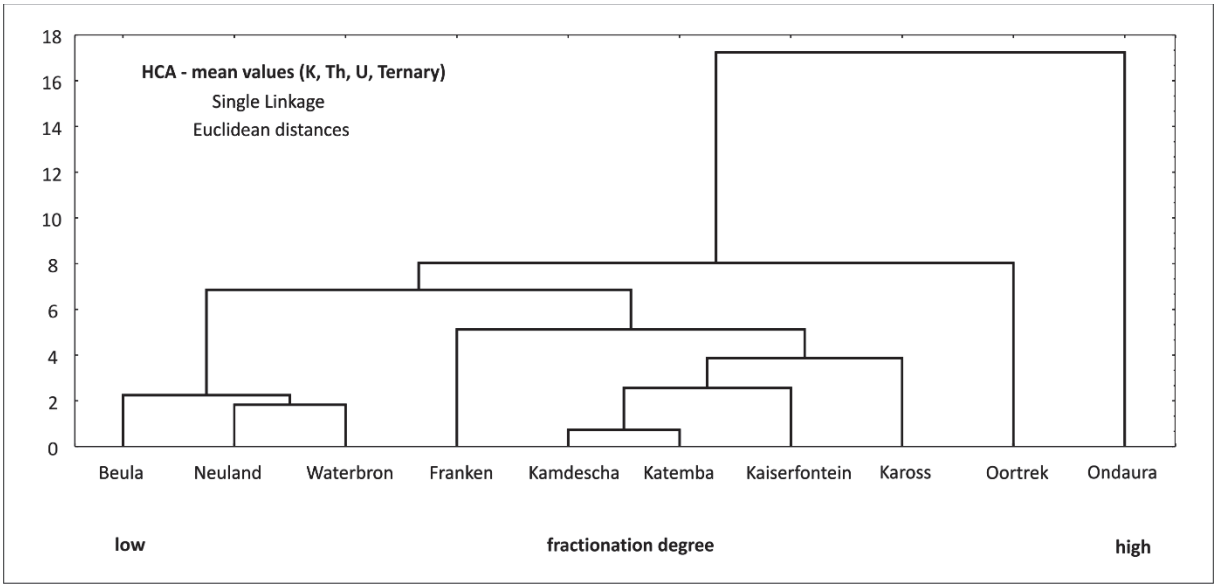


**Figure 13**. Hierarchical classification analysis of the FFG phases based on the mean values of K, Th, U and Total count.Transition Zone

Two cross sections over the Transition Zone between the northern and southern study areas show predominantly medium-grained, equigranular red orthogneiss, which is intruded by coarse FFG granites (Kamdescha type) and, more rarely, by mafic amphibolite dykes. An exception to this are two parallel ENE-WSW trending discontinuous bands of supracrustal rocks between 50-200 m wide, about 3 km from each other, which can be traced along strike on the Landsat image over more than 90 km and appear to join in an eastern fold closure. To the west these bands widen and, in the area north of Suiderkruis the Landsat image shows numerous folded amphibolite dykes suggesting that this domain already forms part of the HMC s.s. The metasediments comprise highly deformed conglomerate, metaarenite, quartzite, chert and schist described in detail.

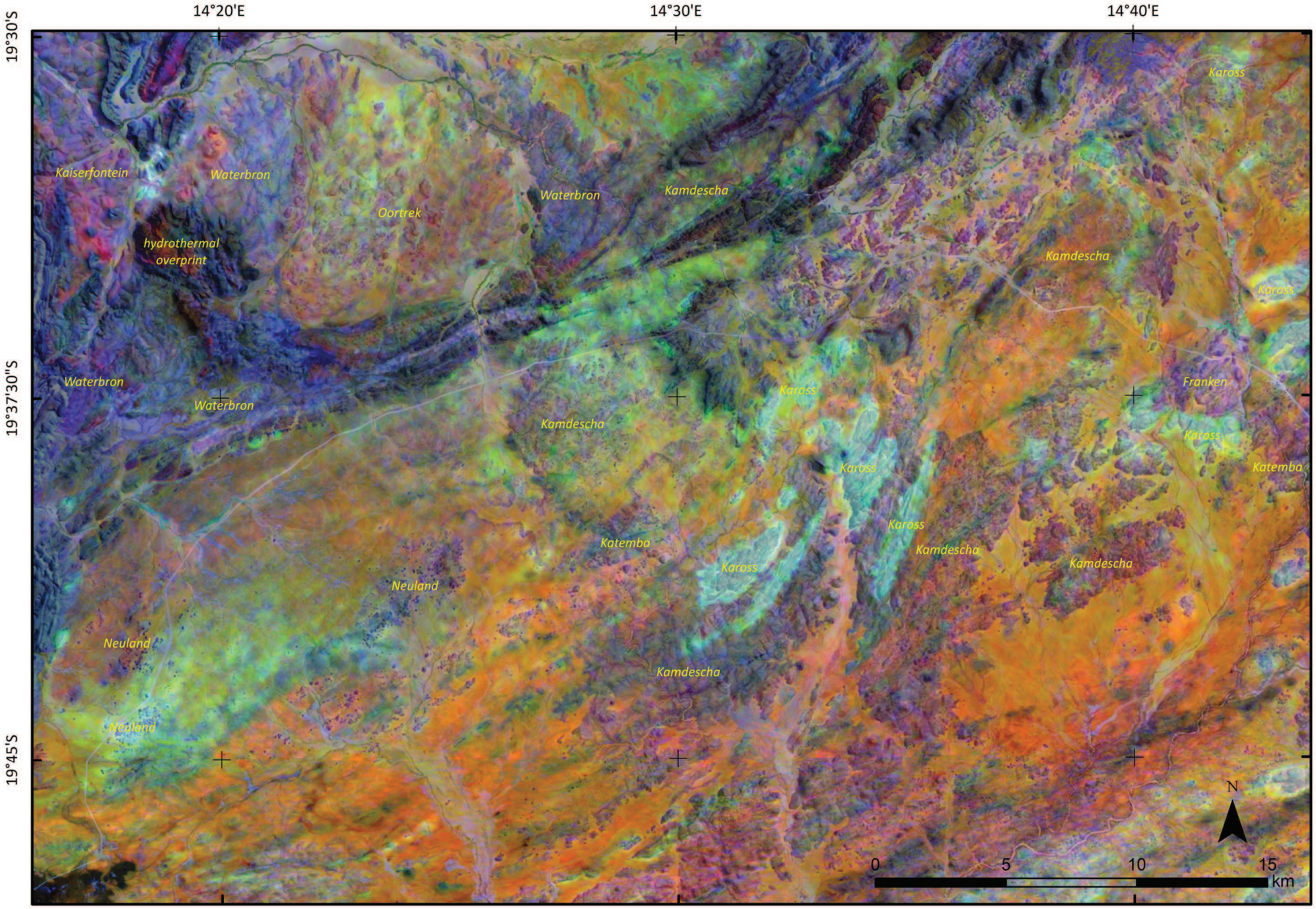


**Figure 14**. Ternary data draped over Landsat 741 imagery illustrates the variation of radio-element concentrations with the Fransfontein Granite Suite.

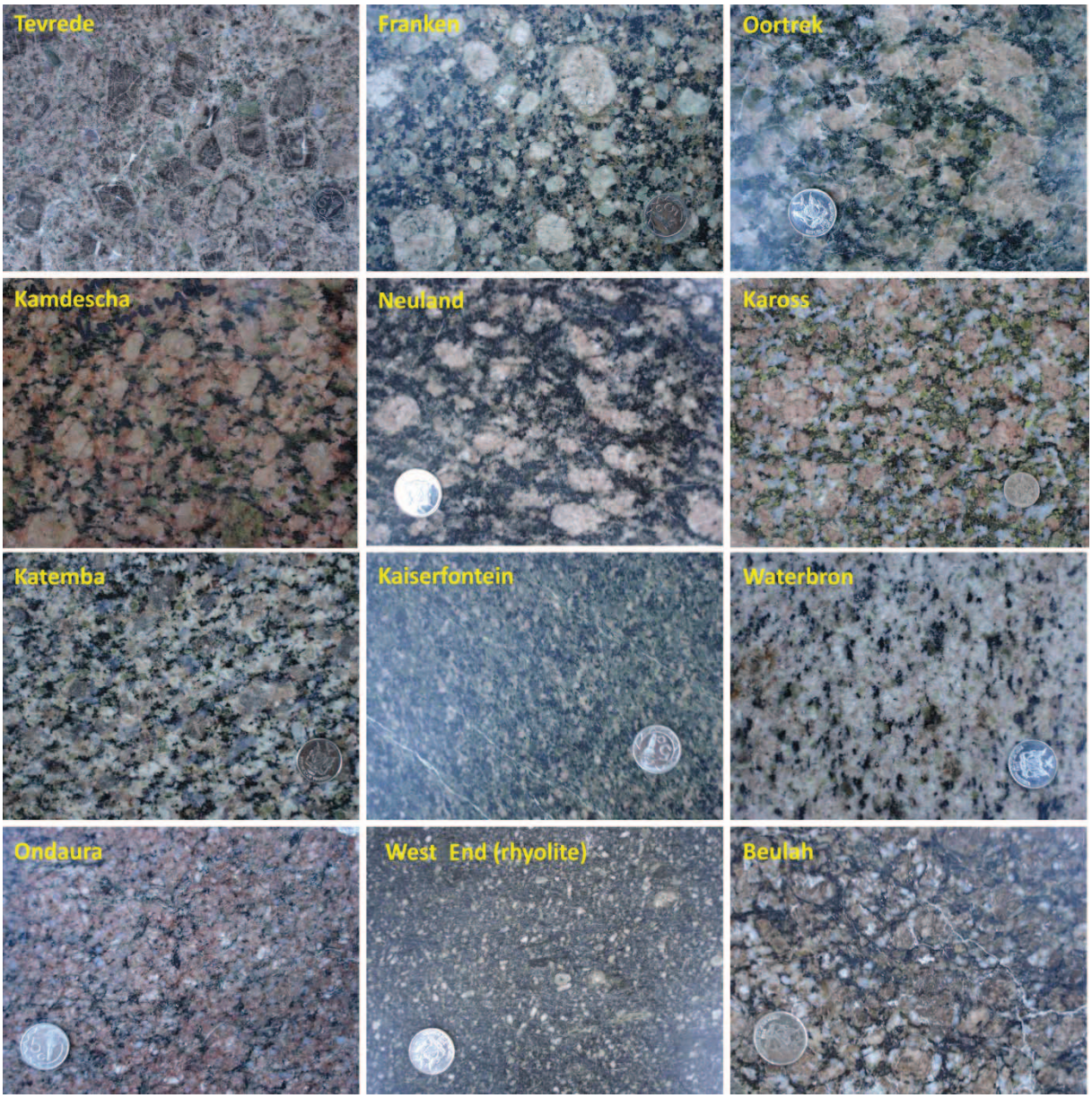


**Figure 15**. Fransfontein Suite granitoids show considerable variation in composition and texture allowing subdivision into eleven subtypes. Beulah subvolcanic granite grades into West End rhyolite.

## Huab area

### *Huab Metamorphic Complex (HMC)*

Geological mapping shows that the HMC can be subdivided into three subdomains marked by distinct rock types and/or metamorphic conditions (Fig. 16), which are separated from each other by first-order shear zones. These domains partly coincide with those already outlined by Frets (1969), which have, however, been re-interpreted in terms of metamorphism and structures. In the following section they are referred to as the Rooikop-Lofdal (southwest and south), Suiderkruis-Aandgloed (central and north) and Ehobib (northeast) subdomains. Several schematic cross sections illustrate the regional deformation style (Fig. 17). Detailed descriptions of most rocks are given by Frets (1969).

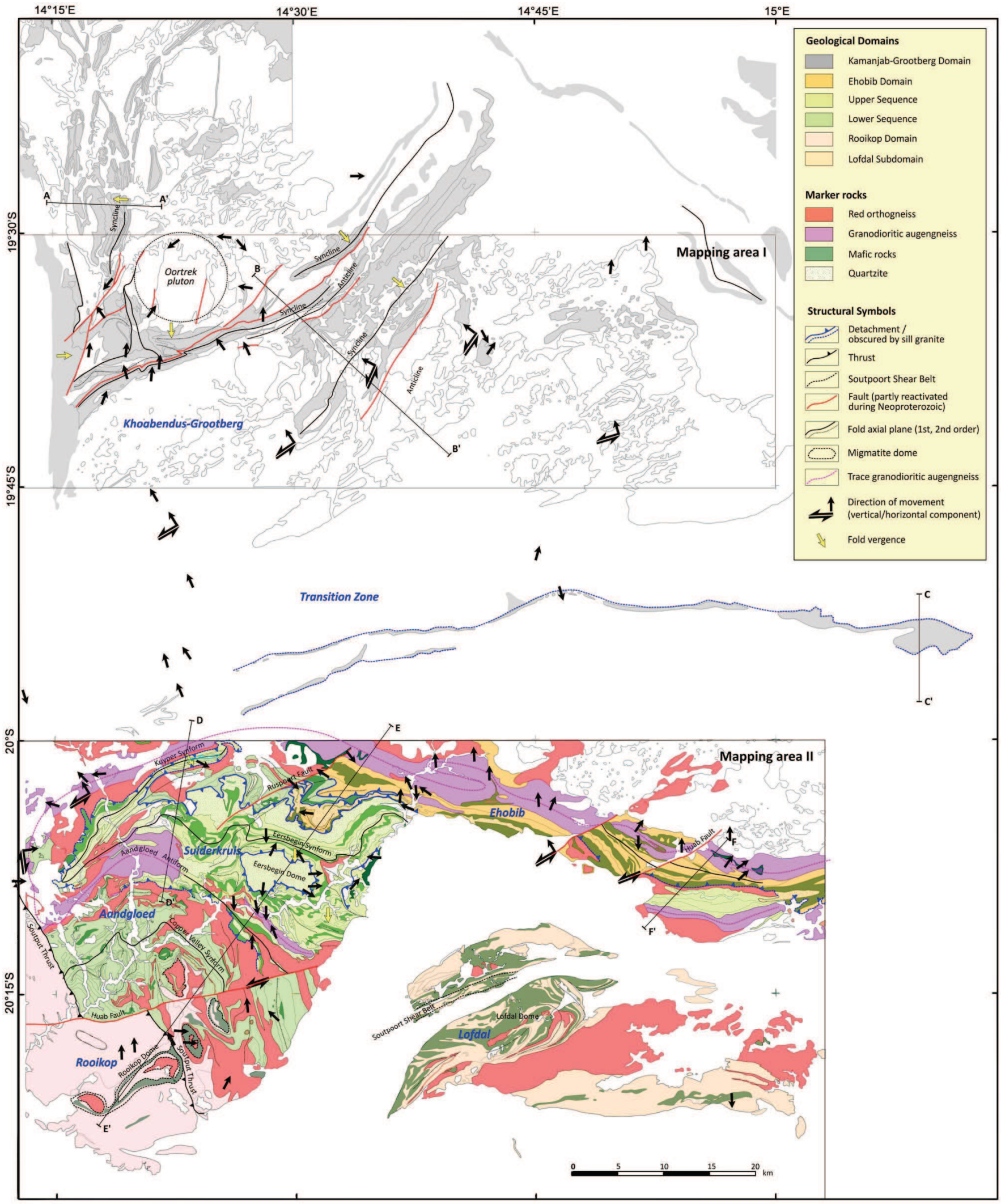


**Figure 16**. Simplified geological and structural map of the Huab Metamorphic Complex showing the main units, structures and relative movements. The names of syn- and antiforms have been adopted from Frets (1969).

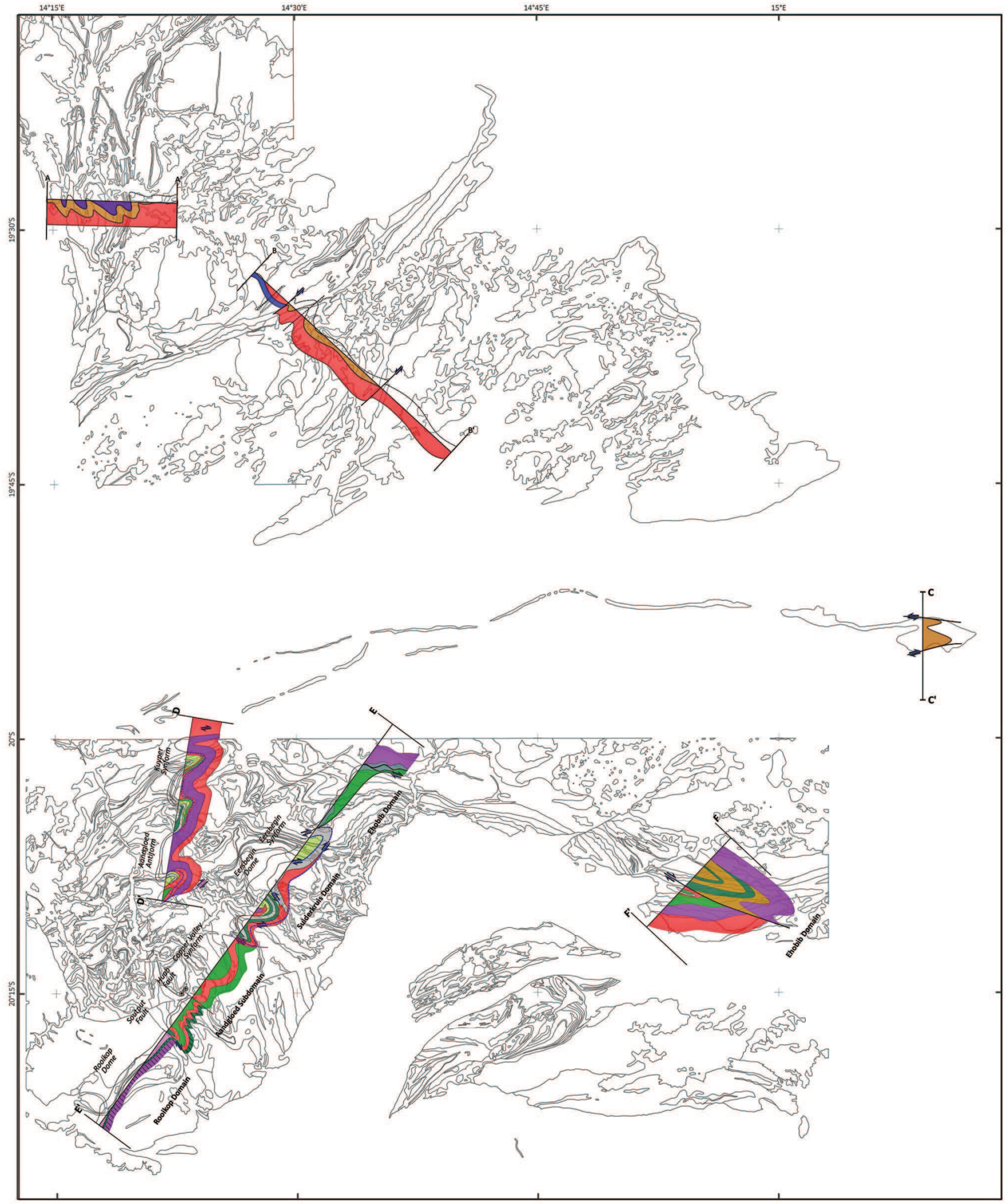


**Figure 17**. Schematic cross sections illustrating the regional deformation style in the northern and southern study areas.

***Rooikop/Lofdal SD***

The domain in the south of the HMC is characterised by the highest metamorphic conditions resulting in regional migmatisation of the gneissic rock with the leucosome commonly forming stromatic and phlebitic structures (Fig. 19a). The main supracrustal and intrusive rock types are (i) massive medium to coarse-grained, equigranular, grey quartz-feldspar-biotite gneiss derived from greywacke or granodiorite (Fig. 18a), (ii) light grey to white banded, fine to medium-grained equigranular leucogneiss (Fig. 18b), (iii) quartz-muscovite schist (Fig. 18C), (iv) medium-grained, equigranular massive garnet-biotite gneiss (Fig. 19b), (v) abundant layers of (garnet-bearing) amphibolite of volcanic and/or intrusive origin that locally predominates over other facies (Fig 19c) and (vi) minor coarse-grained, equi-granular, grey-bluish quartzite forming discontinuous layers up to several metres thick. Ubiquitous anatectic pegmatite and aplite form two generations of early stage transposed bodies with irregular outlines (Fig. 18d) and late stage cross-cutting dykes. The highest metamorphic conditions are indicated in the Lofdal Subdomain by nebulitic structures developed in amphibolite classifying the rock as diatexite (Fig. 19d).

All rocks are intruded lit par lit by massive medium-grained equigranular, garnet-bearing granite whereas granodioritic biotite-hb augengneiss (POGD) and medium-grained, equigranular, red biotite-poor granitic orthogneiss (ROG) form a few transposed sheet-like bodies up to 40 km long following and outlining the regional gneissic trend. The high degree of deformation, the absence of distinct marker horizons and regional anatexis of the rocks do not allow establishment of the lithodemic pile in this domain.

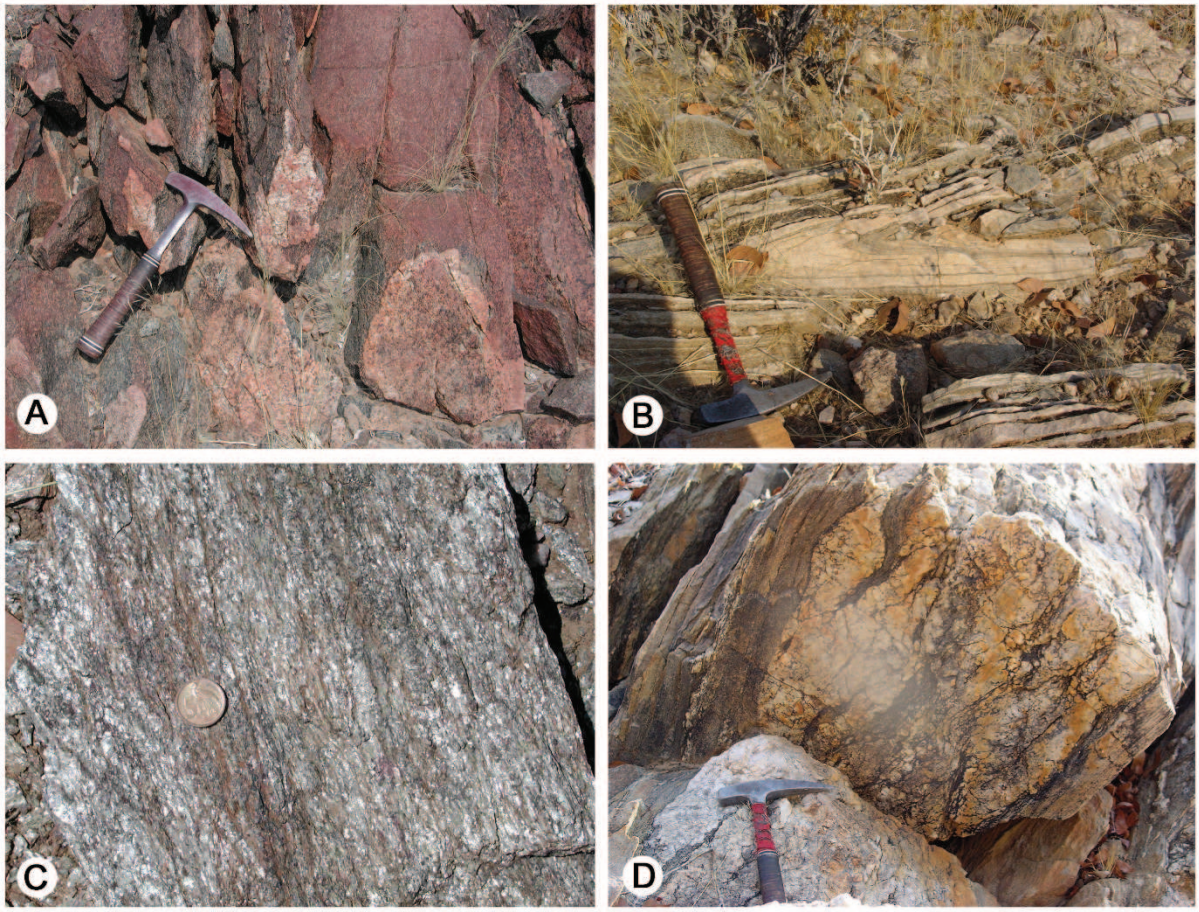


**Figure 18**. Characteristic rock types of the Rooikop SD (Rooikop 506).

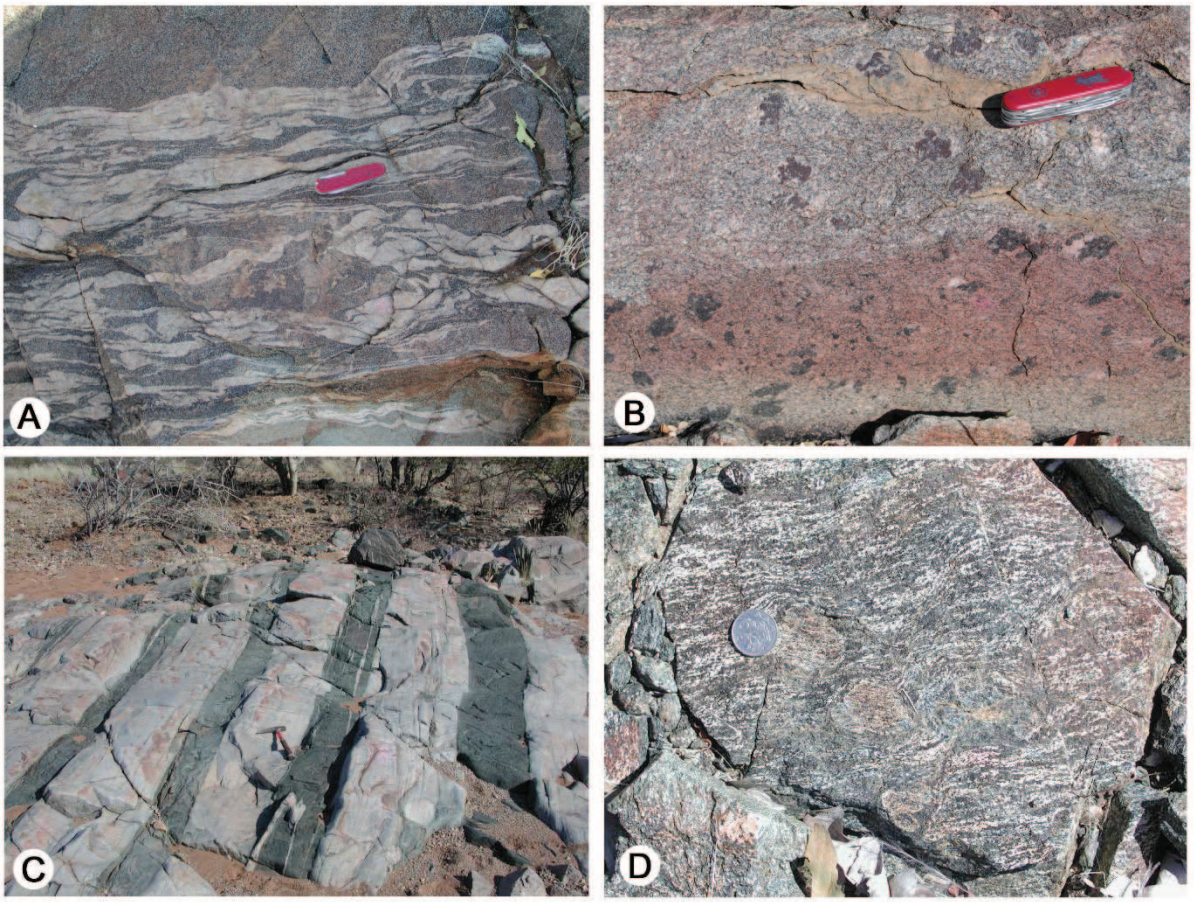


**Figure 19**. Characteristic rock types of the Lofdal SD (Farm Lofdal).

***Suiderkruis-Aandgloed SD***

The subdomain is juxtaposed with the Rooikop/Lofdal SD along the moderate to steeply W to SW dipping Soutput Thrust (Fig. 16). In the NW, pegmatite veins have been observed immediately west of the thrust but away from the boundary their quantity decreases soon and 300 m further east they are absent. Similarly, migmatitic gneisses appear limited to the Aandgloed Subdomain. However, on Soutput 505, pegmatite and migmatite occur on both sides of the structure documenting the transitional nature of the contact between the Rooikop and Aandgloed SD: Migmatitic gneisses occur in the Suiderkruis SD up to 6 km east of the fault demonstrating only limited offset across the structure, thereby excluding the interpretation of the Rooikop SD as a nappe.

The paragenesis muscovite-garnet-hornblende-biotite indicates regional Barrovian type amphibolite facies metamorphism. The absence of sillimanite, cordierite and staurolite is noteworthy.

Careful remapping reveals subdivision of the Suiderkruis-Aandgloed SD into a lower and upper sequence characterised by different rock assemblages (Fig. 16, Fig. 17, 20 and Table 5). The principal organisation of the lithodemic pile and the younging direction is shown in Fig. 20.

The Lower Sequence comprises similar rock types to the Rooikop/Lofdal SD including migmatitic gneiss (Fig. 21a), grey biotite-paragneiss (metagreywacke), banded leucogneiss and quartz-muscovite schist. The migmatitic rocks appear limited to the south at the probable base of the unit. In the Copper Valley on Mesepotamie 504, a pile of predominantly metapsammitic rocks, comprises banded leucogneiss alternating with thick layers of megacrystic biotite-garnet leucogneiss and quartz-muscovite schist (Fig. 21b-c). Amphibolite is intercalated frequently in this series forming generally < 1m thick layers (Fig. 21d). Further north, towards the top of the sequence, semipelitic quartz-mica schist and garnet-muscovite schist alternate with cm to dm thick layers of metaarenite indicating overall fining-upward deposition (Fig. 21f-g). Rare meta-pyroxenite sills intruded the sequence and on Suiderkruis 668, together with intercalated

(garnet-bearing) amphibolite, form a small layered intrusion ca 2 km in diameter.

The supracrustal rocks described above are mixed at all scales, but are presented on the geological map as single lithologies indicating the predominant facies in the respective area. This suggests a lithodemic pile with predominance of metagraywacke at the base of the Lower Sequence overlain by garnet-mica schist, banded (garnet-bearing) leucogneiss, and towards the top, quartz-muscovite schist with intercalated metaarenite and grey quartzite.


**Figure 20**. Geological map of the northwestern HMC (Suiderkruis-Aandgloed SD) illustrating the principal organisation of the lithodemic pile.

The Upper Sequence is exposed mainly in the Kuyper Synform on Suiderkruis and here less deformed units allow the establishment of a more detailed lithodemic pile. Massive white to light grey quartzite forms the base of the unit. It has been formerly correlated with the Voorspoed quartzite of the Khoabendus Group (SACS, 1980; Miller, 2008). However, sedimentary transition into the overlying semipelitic gneisses and schist is shown by intercalated dm- to m-thick layers of grey quartzite at the base of the metapelitic pile. Sedimentary structures comprise rare cross-beds of dm-size and symmetric oscillation ripples in the steeply dipping outer part of the Eersbegin Dome, indicating shallow marine sedimentation of mature sediments (Fig. 22a-b). The quartzite overlain by the mixed series of gneiss and schist along a major extensional thrust are interpreted as a detachment. The more than 30 m wide structure has been mapped at the eastern flank of the Eersbegin Dome but probably envelops the entire structure. It consists of green garnet-bearing chlorite-phyllonite with abundant boudins and slivers of quartzite up to 50 m long (Fig. 31f). The phyllite is overlain by a thick pile of quartz-feldspar-muscovite schist that in its lower part alternates with dm to m thick layers of grey quartzite and quartz-feldspar metaarenite (Fig. 22c-d). One intercalated exotic 1-2 m thick marker horizon of a biotite-garnet leucogneiss, ca 50 m above the basal white quartzite, comprises disseminated megacrysts of garnet up to 3 cm in diameter surrounded by bleached reaction rims (Fig. 22e). Another conspicuous, up to 5 m thick, red mylonite derived from a felsic igneous precursor has been mapped over a distance of more than 15 km in the upper part of the quartz-muscovite schist series and both an

intrusive (granite sill) or volcanic (quartz-feldspar porphyry) origin are possible (Fig. 22f). It is overlain by another sequence of monotonous quartz-muscovite schist followed by a 10-15 m thick succession of amygdaloidal metabasalts transformed into amphibolite (Fig. 22g). Additional intercalated (garnet-bearing) amphibolite horizons are probably of intrusive origin.

The metabasalts are overlain by rudaceous, clast-supported, monomict conglomerate consisting of rounded quartzite pebbles ranging in diameter from 5-30 cm with reddish-stained quartz grains in the interstices (Fig. 22i). It is overlain by quartz-muscovite schist with intercalated metachert probably derived from rhyolitic tuffs. The uppermost portion of the Upper Sequence crops out in the SE corner of the Eersbegin Syncline consisting of > 50 m of graphite schists alternating with amphibolite (Fig. 22j).

Metarhyolite in the western part of Suiderkruis 668 has been mapped as part of the Upper Sequence, but could be also an isolated remnant of the Ehobib SD.

In summary, the precursors of the gneisses and schist are of similar composition as those of the Khoabendus Group but are of higher metamorphic grade and deformation. Calcareous rocks have not been identified in the HMC though

**Table 5.** Lithodemic pile of the Aandgloed -Suiderkruis SD.

| **Suiderkruis Domain** | **Rocks** |
|---|---|
| **Upper Sequence (Suiderkruis 668)** | graphite schist |
| | qz-ms schist alternating with metapsammite |
| | metachert or very fine-grained quartzite |
| | monomict metaconglomerate |
| | amygdaloidal metabasalt (amphibolite) |
| | qz-ms schist, (gt) amphibolite |
| | **Mixed series**: qz-fs-ms schist, grey quartzite, metapsammite, intercalated bt-gt-bt-leucogneiss, qz-fs porphyry (possibly Ehobib SD), sill granite (or metaporphyry), (gt-bearing) amphibolite |
| | gt-bearing chl phyllonite, gt-mica schist (gt generally transformed into chl) |
| | white quartzite (rare cross bedding, oscillation ripples) |
| **Lower Sequence (Aandgloed 673)** | **Upper part** : banded leucogneiss, gneiss, (gt-bearing) qz-mica schist, gt-ms schist alternating with metapsammite, amphibolite, |
| | **Lower part**: migmatitic grey bt gneiss and gt-bt gneiss (metagreywacke), banded leucogneiss, qz-ms schist, amphibolite |

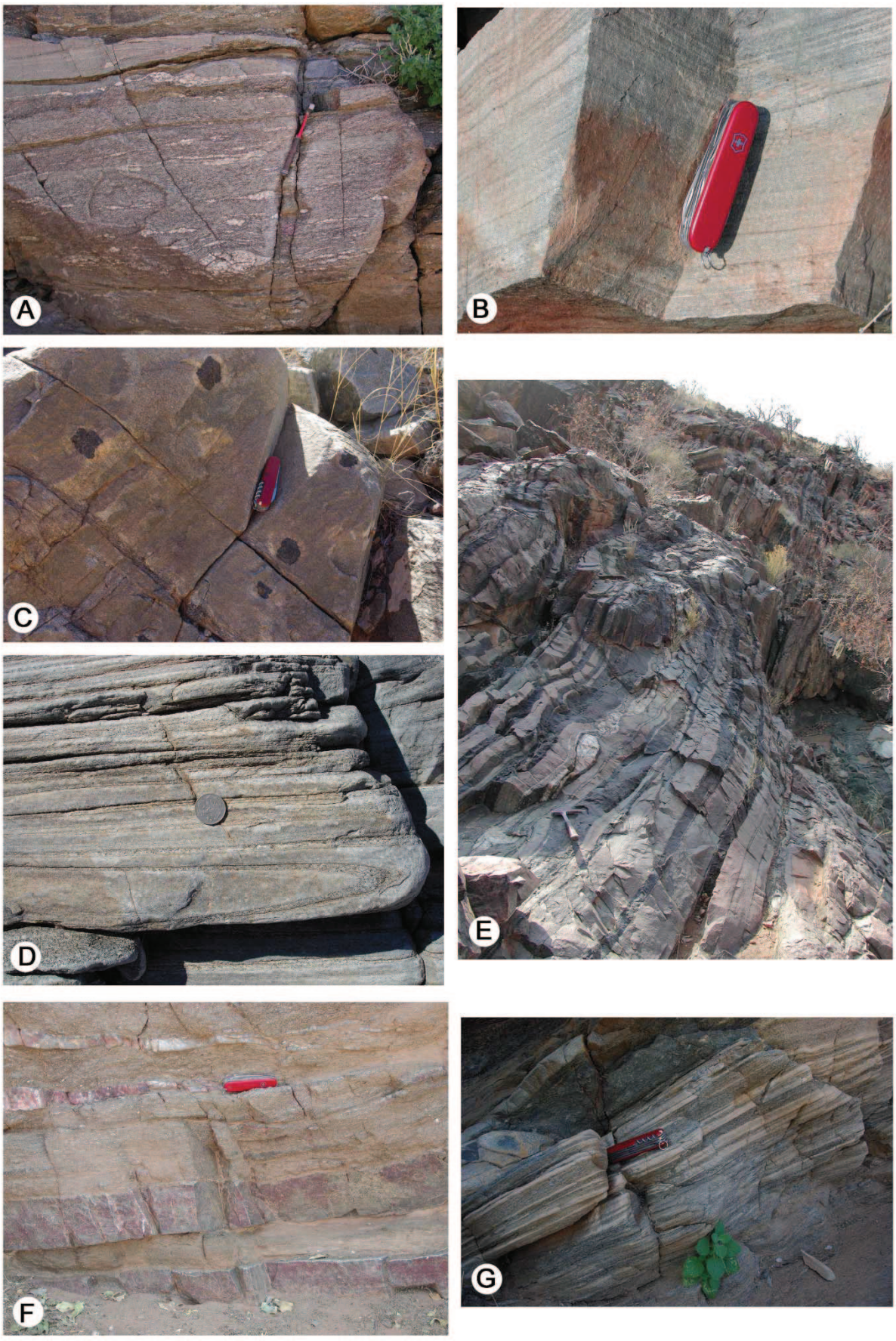


**Figure 21**. Characteristic rock types of the Aandgloed Subdomain (Lower Sequence).


**Figure 22 (part 1).** Characteristic rock types of the Suiderkruis-Aandgloed SD (Upper Sequence)

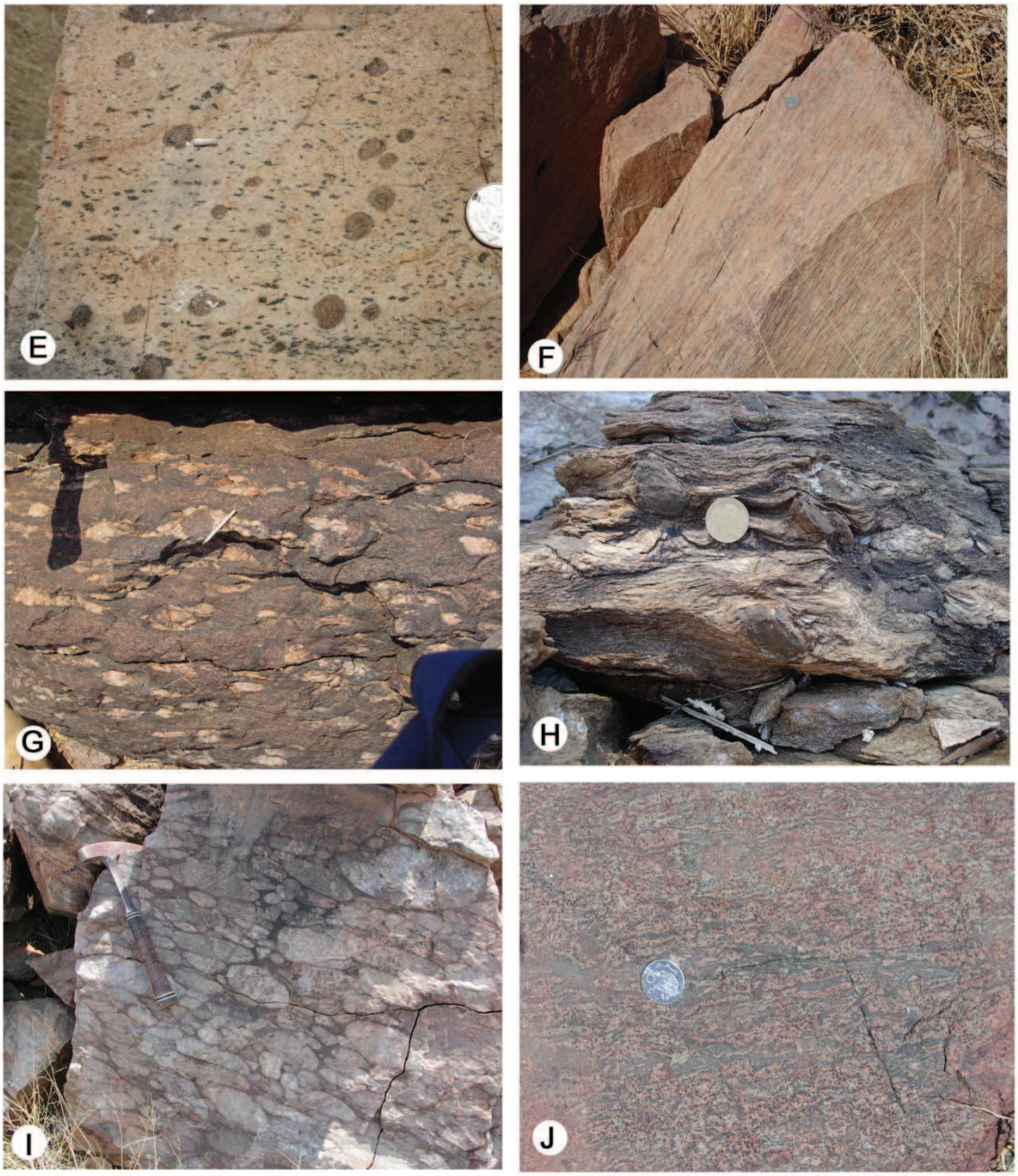


**Figure 22 (part 2)**. Characteristic rock types of the Suiderkruis-Aandgloed SD (Upper Sequence).

***Ehobib SD***

The Ehobib SD is exposed in the north-eastern part of the study zone and limits the HMC with undifferentiated Kamanjab basement intruded by FFG granites (i.e. the "transition zone"). The domain comprises mainly low-grade metamorphic rocks of sedimentary, pyroclastic and intrusive origin that were classified by Miller (2008) as a southern equivalent of the Khoabendus Group into the basal Tweelingskop, central Smalruggen and upper Aub formations (Table 1). However, intercalated thrust slivers of gneiss and amphibolite are frequent, forming a tectonic mélange with the low-grade rocks. The Ehobib SD is bound with the adjoining units by WNW-ESE trending shear zones that change from a subvertical position in the E to a folded low angle thrust in the W. The orientation of all rock units follows these structures changing from a vertical dip in the east to a low to moderate dip in the west. The geological map further indicates as principal structures two NNW-SSE trending synforms that are in thrust contact with each other. The Ehobib SD is juxtaposed to the

NW with the Suiderkruis SD along the NE-SW striking Ruspoort fault.

Intense vertical shearing hinders the reconstruction of the former stratigraphy. The most likely succession starts with basal, often pebbly, white and grey gritty poorly recrystallised quartzite about 200 m thick (Fig. 23a). Pebbles up to 10 cm in diameter are comprised chiefly of quartzite with minor mafic rocks and phyllite, while gneisses and granitoids are absent. Heavy mineral seams are locally developed and outline both plane-parallel and cross-bedding. The presence of pebbles and the lower metamorphic grade distinguish this unit from the white quartzite of the Suiderkruis SD. The quartzite is overlain by a sequence of fine-grained quartz-feldspar sandstone (Fig. 23b) alternating with beds of green andesitic metatuff and tuffitic sandstone. They grade into a series of overlying pyroclastic and epiclastic rocks, comprising green to cream ash and lapilli tuff of andesitic and dacitic composition (Fig. 23c-e), mafic and silicified rhyolitic tuffs metamorphosed into chlorite schist, quartz-feldspar-muscovite schist, dark chert, agglomerate, small-pebble conglomerate composed of felsic fine-grained pyroclastic clasts and quartzite (Fig. 23f). In addition, a few amygdaloidal basalts flows 2-3 m thick are intercalated in the series which show grading. The unit attains a tectonic thickness of up to 700 m (Fig. 23g). The top of the volcanic succession in the core of the syncline is comprised of voluminous quartz-feldspar porphyries, which could be correlated either with the ignimbrite of the West End Formation or the Blyerus Rhyolite Formation in the north (Fig. 23h).

An important element of the Ehobib SD is the coarse-grained to megacrystic biotite-bearing equigranular granodiorite of the FFG which is classified as Kamdescha facies. It forms a sill about one km thick that is folded around WNW-ESE axes into the northern syncline of the Ehobib SD. The transition of almost undeformed granodiorite into the augengneiss that is part of the Suiderkruis SD has been observed in several places thereby demonstrating that the FFG Suite is also emplaced into the HMC and transposed into parallelism with the gneissic host rock.

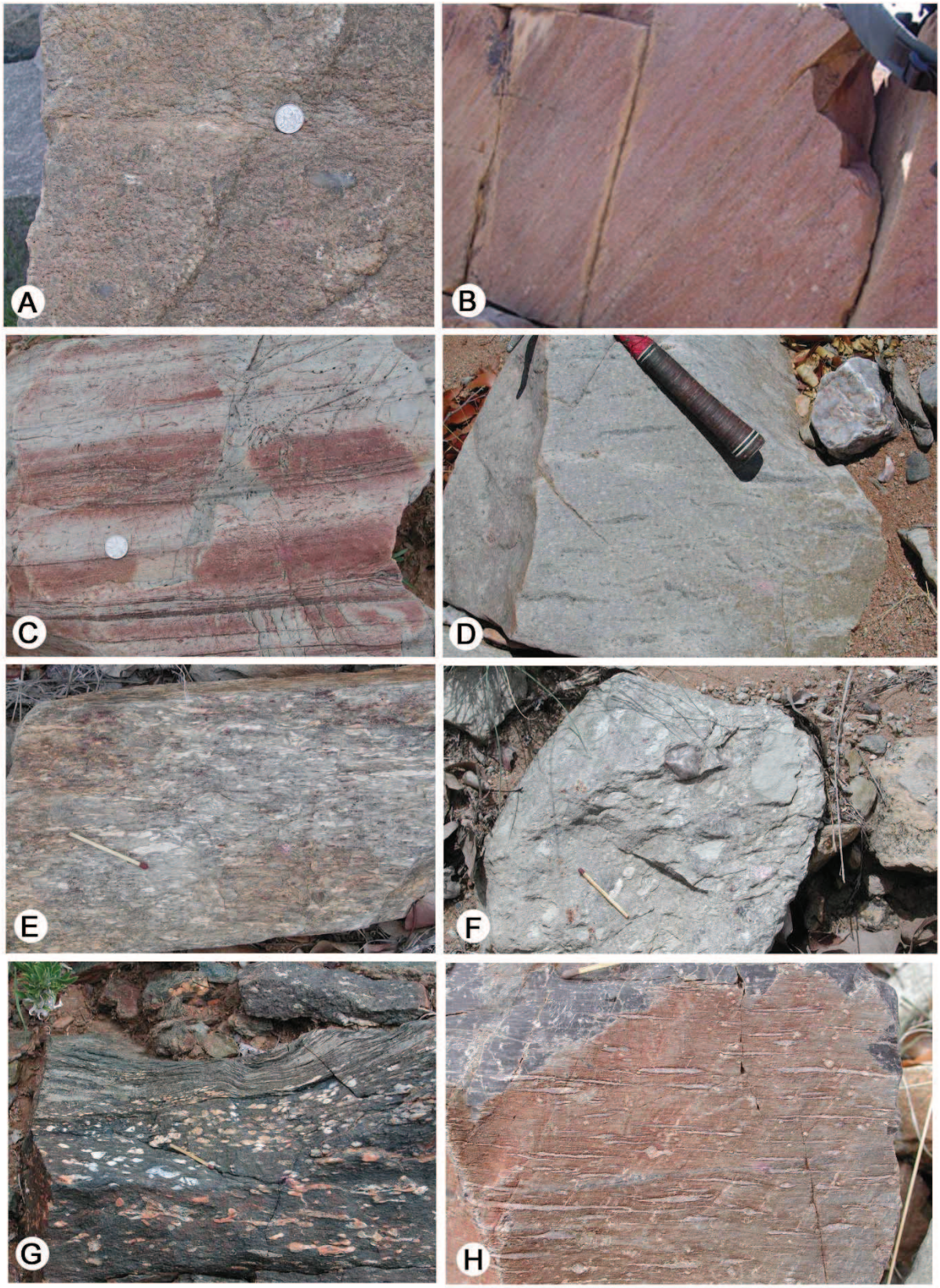


**Figure 23**. Low-grade metamorphic clastic, epiclastic and volcanic rocks of the Ehobib SD. A) pebbly quartzite, B) red sandstone, C) andesitic tuff D-E) lapilll tuff(ite)?, small pebble conglomerate, G) amygdaloidal basalt, H) quartz-feldspar porphyry (ignimbrite).

***Magmatic rocks***

Fig. 24 shows the main intrusive facies of the HMC, which underlies ca 55 % of the exposed surface with paragneiss, schist and quartzite comprising the remainder (45 %). They comprise amphibolite and metagabbro (10%), medium-grained, equigranular red orthogneiss of granitic composition (ROG, 28 %, Fig. 25a-b), non-migmatitic biotite K-feldspar augengneiss of granodioritic composition (POGD, 10 %, Fig. 25c-f) and undeformed very coarse-grained biotite granite of the Fransfontein Suite in the NE corner of the study area (FFG, 4%).

Amphibolite is abundant in the Suiderkruis, Lofdal and Ehobib subdomains where they represent up to 50% of the rocks but are of minor amount in the Aandgloed-Rooikop SD. The rocks form layers mostly less than two metres thick commonly transposed into the gneissic foliation of the host rock. Migmatitic and non-migmatitic amphibolite occurs in the Suiderkruis and Lofdal subdomains whereas elsewhere the rock is non-migmatitic. Garnet up to cm size is often present but commonly transformed into chlorite indicating pervasive retrograde overprinting. A small layered intrusion about 2-3 km in diameter has been mapped on Suiderkruis 668. It comprises a central part of unaltered gabbro with minor pyroxenite and a marginal zone of metadioritic rocks overprinted by hydrothermal epidote. Another isolated ultramafic plug on Arbeidsgenoet 501 has been transformed into amphibole fels.

In some localities, thin bands of amphibolite alternating with leucogneiss suggest their interpretation as a bimodal volcanic sequence. Other layers intercalated between metaquartzite are marked by vesicles with diameters between 2-5 mm, filled by quartz-epidote-feldspar, attesting to the volcanic origin of the rocks.

Migmatitic orthogneiss is relatively rare in the northwestern and central part of the Huab area. A 5-10 m thick, massive sheet-like body was emplaced in the Suiderkruis SD into migmatitic paragneiss and was in turn intruded by non-migmatitic ROG (Fig. 27a). The medium-grained biotite-quartz-feldspar orthogneiss displays planar fabrics with grain-flattening parallel to oriented biotite. The stromatic to phlebitic leucosome is rimmed by biotite selvages (Fig. 27b). In the Rooikop SD migmatitic orthogneiss appears more abundant but the area is largely covered by regolith. The domain is intruded massively by pegmatite associated to the pervasive anataxis in that area.

The POGD and ROG form regional-scale sheet-like bodies that follow the main lithological contacts of supracrustal rocks, thereby outlining late stage regional interference fold geometries. Fig. 25c-e illustrate the change from almost undeformed POGD with K-feldspar porphyroblasts up to 3 cm size set in a grey medium- to coarse-grained, equigranular biotite-quartz-feldspar matrix to augengeiss with a prominent stretching lineation. More equigranular coarse- to very coarse-grained facies of the POGD have been mapped on Suiderkruis 668 grading into Kamdescha type facies of the Fransfontein Suite. In hand specimen the ROG resembles the Kaross type of the FFG.

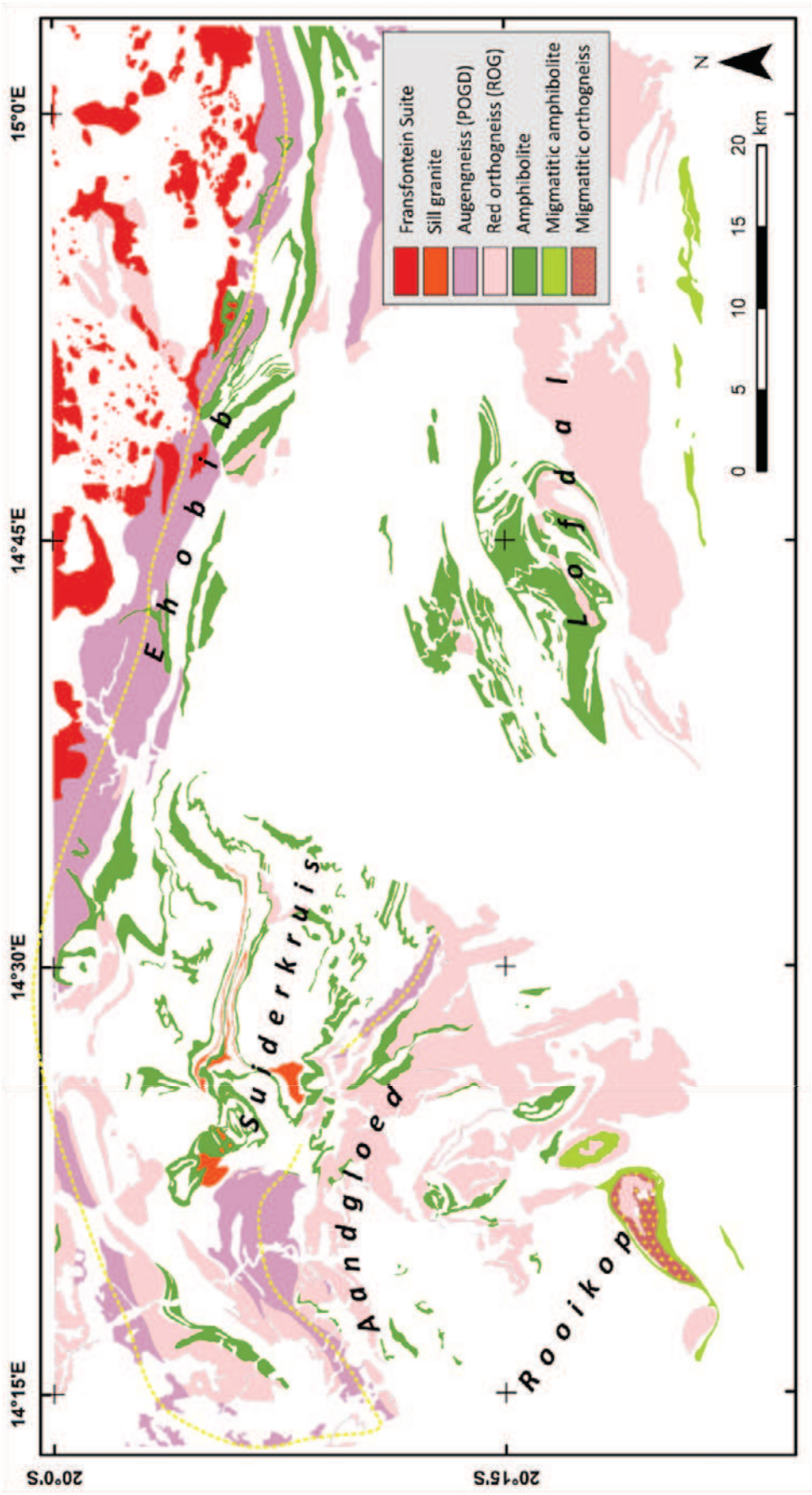


**Figure 24**. Intrusive rocks of the Huab area represent about 55% of the rocks. Two megasills of red orthogneiss and granodioritic augengneiss outline late stage regional deformation; fold axial plane traces are indicated by black and yellow stippled lines.

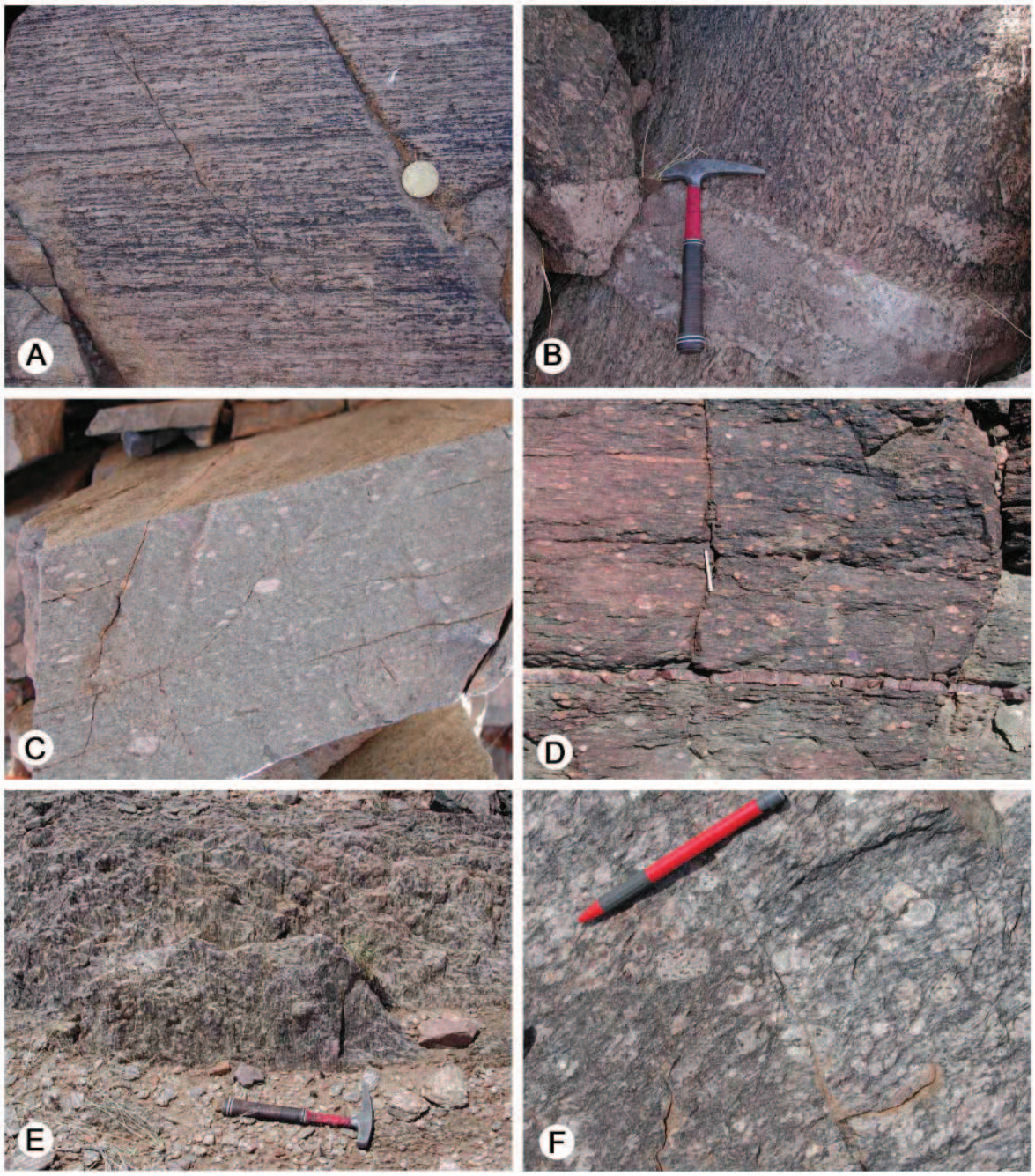


**Figure 25**. Two main granite types forming folded sheet-like bodies of regional scale. A) Massive, non-migmatitic medium to coarse-grained equigranular red orthogneiss (ROG); B-E) progressively deformed non-migmatitic, very coarse-grained, biotite-bearing K-feldspar augengneiss of granodioritic composition (POGD); very coarse-grained biotite-bearing variety of the POGD orthogneiss resembling Kamdescha granite of the Fransfontein Suite. (A, B, F – Suiderkruis 668; C, D, E – Rooikop 506).

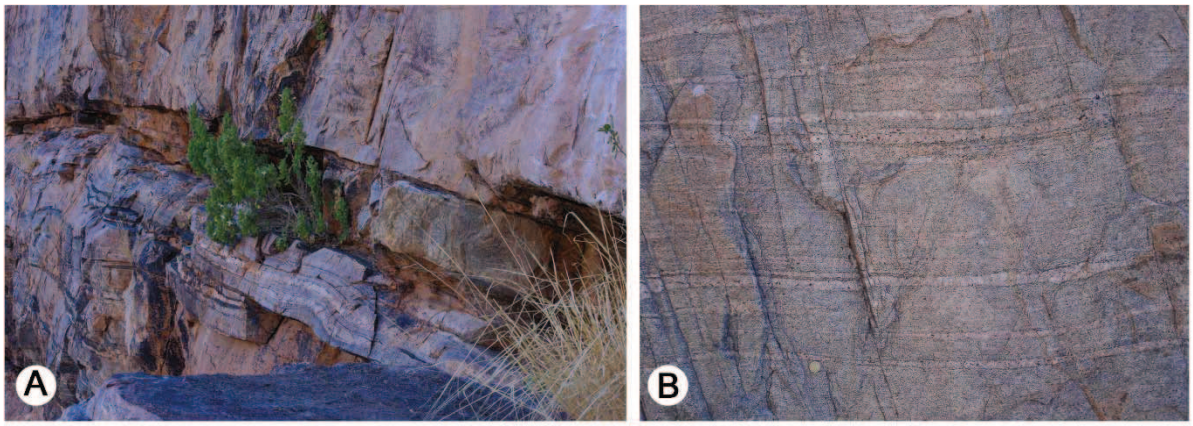


**Figure 26**. A) Migmatitic gneiss of possibly intrusive origin emplaced into migmatitic host rocks and intruded by non-migmatitic ROG (upper part); B) close-up view. (Soutput 505).

## Tectonics

The revised structural map (Fig. 16), cross sections (Fig. 17), stereograms of lineations and foliations (Fig. 28, Fig. 29) and key outcrop descriptions illustrate similarities and differences in tectonic style between the Kamanjab and Huab areas. The following nomenclature was applied: S0 = bedding, S01 bedding parallel foliation, S1 foliation oblique to bedding/layering, S2 younger foliation etc. The relative succession of events refers to the local observations at the individual outcrop; S1 observed in a specific outcrop can be at regional scale S2 or S3.

### Kamanjab-Grootberg area - Khoabendus East and West domains

The Kamanjab area is dominated by two major NE-SW trending synclinoria of pre-Damara age (Miller, 2008). The southern structure is exposed in the study area from farms Bergvalley 609 to Kamanjab North 212 in the Khoabendus East domain and characterised by disharmonic open to tight fold, steeply NW dipping fold axial planes and moderately NE plunging fold axes (Fig. 16, Fig. 19). Important subvertical faulting takes place in the hinges of folds parallel to the fold axial planes coinciding with the change from tight fold geometries in the vicinity of the faults to open and gentle ones further away (Fig. 17). Stretching lineations outside the faults are generally moderately SW to S plunging whereas in the thrusts they are subvertical. Shear sense indicators (sc-fabrics, sigma clasts) within the faults suggest top to the NW down thrusting resulting in the juxtaposition of the Otjovazandu and West End formations. All features indicate that folding and normal faulting are associated and took place in an overall NW-SE extensional setting.

The stereogram of S0, S1 poles illustrates wide scatter but mainly steep dips; the maximum density at 315/06 corresponds to a subvertical SW-NE striking plane (135/84) (Fig. 28). Linear structures (intersection, fold axis, stretching and crenulation) show similar scatter in orientation (Fig. 29). Moderate SW to a shallow NE plunges define a wide girdle parallel to the average S1 plane. The density maximum is a steep NE plunge (050/72), while two smaller ones define moderate S to SW plunges (191/48 and 215/63). The systematic variation in the orientation of linear structures within the S1 plane demonstrates a transtensional or transpressional setting resulting in the progressive rotation of structures into the transport direction.

In the NW part of the Khoabendus West Domain, axial planes of major folds turn into a N-S trend (Fig. 6, Fig. 16, Fig. 19). The circular Oortrek intrusion in the centre of this area appears rather undeformed but is enveloped by NS and NE-SW trending folds and therefore played an important role in the variation of the local stress field (Fig. 16). The fold style in the western area is marked by open to closed slightly west-verging asymmetric folds with steep western and overturned eastern limbs.

The scatter of S0 and S01 poles from the NW to the SW quadrants of the stereogram defines the NE-plunging fold axis (045/51), whereas the maximum at 284/21 corresponds to a steeply east-dipping plane (104/69) (Fig. 28). The few recorded linear structures plot in the NE-SW girdle of structures from the

Khoabendus East domain. The wide variation of linear and planar directions document again non-coaxial deformation associated to transpression or transtension. The adjacent western Damara rocks record similar fold geometries but folds are east-verging.

Several west-directed reverse faults offset rocks of the Otjovazandu Fm and FFG. They are limited by regional Pan-African NE-SW folds and faults. A major subvertical N-S fault of Pan-African age offsets both Damara and Khoabendus rocks in the western part of the domain.

East of the study area, a series of tight NW trending, SW-overturned folds are superimposed on the Khoabendus folds (Porada, 1974). They have produced a rather abrupt change in strike direction along the northern edge of the Kamanjab Inlier (Miller, 2008). These structures are associated with a crenulation cleavage and have been variously classified as Damara (Porada, 1974) and pre-Damara (Miller, 2008). Their orientation parallel to folded Otavi rocks further east and similar geometry argues for the Damara age, which implies concentration of the deformation in discrete couloirs leaving the central part of the Khoabendus rocks unaffected by deformation.

***Kinematics***

Shear sense indicators reveal complex deformation in the Khoabendus domain (Fig. 16). Top to the S, N, NW and NE normal shear sense was identified mostly in steep ductile shear zones associated with faulting. Top to the SW and SE reverse shear sense was analysed in few moderate to steeply dipping structures. The orientation of lineations shows high but systematic variation (Fig. 16).

Outcrop NA059 demonstrates some aspects of the deformation history. The main rock type is a coarse-grained quartz-porphyritic granite (Kamdescha type), which alternates with biotite schist. It displays a penetrative moderately west-dipping mylonitic sc fabric (265/45) associated with pronounced oblique NW-plunging stretching lineations (301/35). Sigma porphyroclasts, en-echelon vein quartz and sc-fabrics indicate top to the SE-movements with a reverse and left-lateral component. The continuum of deformation is demonstrated by the moderately W-dipping crenulation cleavage (273/65) and crenulation lineation parallel to the stretching lineation. The mylonitic rocks were subsequently offset by ESE (115/80) and WNW (280/70) dipping normal faults. Within the fault planes biotite schist and granite boudins form a tectonic breccia.

**Transition Zone**

This domain forms a belt ca 20 km wide between the northern and southern study areas (Fig. 16). Two N-S cross sections at a distance of 40 km from each other show mainly coarse-grained to porphyritic granitoids of the FFG and orthogneiss of the HMC with minor intercalations of amphibolite and paragneiss. An exception is a thin band of folded Khoabendus rocks in the southern part of the transition zone that can be traced on the Landsat image over a distance of more than 100 km. It changes from a NE strike in the west to an E-strike in the east, thus enveloping the HMC. It comprises a subvertical series of clastic and volcanic rocks that is in thrust contact with surrounding granite and gneiss. It starts in the south with a polymict rudaceous conglomerate about 20-30 m thick comprising clasts up to 10 cm in diameter composed of granite, quartzite and mafic rocks (Fig. 27a). Further north it grades into coarse-grained metaarenite followed by a 5-10 m thick horizon of microcrystalline often brecciated white chert or quartzite soaked by veinlets of vein quartz. It alternates with a 10 m thick horizon of microporphyritic K-feldspar sericite schist and a second 2-5 m thick horizon of completely recrystallised chert or quartzite. The series is limited to the north by mylonitic rocks of granitic or volcanic origin that consist of quartz porphyroclasts set in a fine-grained muscovite-rich matrix. The foliated coarse-grained Kamdescha granite further north is cross cut by several discrete mylonite zones in which the rocks are often silicified, too.

Two outcrop descriptions illustrate the tectonic style in the Transition Zone. The first locality on Farm Grootberg 191 exposes coarse-grained foliated Kamdescha type granite alternating with sheeted medium-grained red orthogneiss comprising rare K-feldspar porphyroclasts that could represent deformed Kaross type granite. The former intrusive contacts are sheared and transposed into parallelism with the subvertical E-W striking gneissic foliations. The rocks record prominent WSW plunging stretching lineations (250/20) in a several metre-wide zone around the contacts. In the Kamdescha granite they give way gradually over a distance of 50 m to the

common regional flattening. The features suggests pervasive transformation of Kaross granite into orthogneiss whereas the more competent Kamdescha granite turned into a foliated granite. Shearing is localised at the contact between these rocks and probably results in boudinage of Kamdescha sheet-like bodies. However, all these rocks underwent the same metamorphic evolution and tectonic overprint.

Four km south of this locality another steeply N-dipping shear zone displays down-dip stretching lineations that combined with oriented asymmetric K-feldspar sigma porphyroclasts constrains N-directed normal movements. The same kinematics have been observed in several other outcrops over 20 km to the south into the Huab area.

An exception to this general trend is the second locality at Farm Blydskap 268 on the northern limb of the folded Khoabendus rocks described above (NA052-58). Tectonic structures are characterised by subvertical E-W foliation (350/85, 190/82), often well-developed sc-fabrics and a pronounced down-dip stretching lineation (Fig. 27b). Kinematic indicators (sc-fabrics, sigma clasts) suggest top to the south down-dip movements. Combined with satellite imagery this indicates an upright narrow syncline, similar to the one that preserved Khoabendus rocks in the Ehobib SD of the HMC. The bounding shear zones indicate that folding and down-thrusting were contemporaneous taking place in an extensional setting

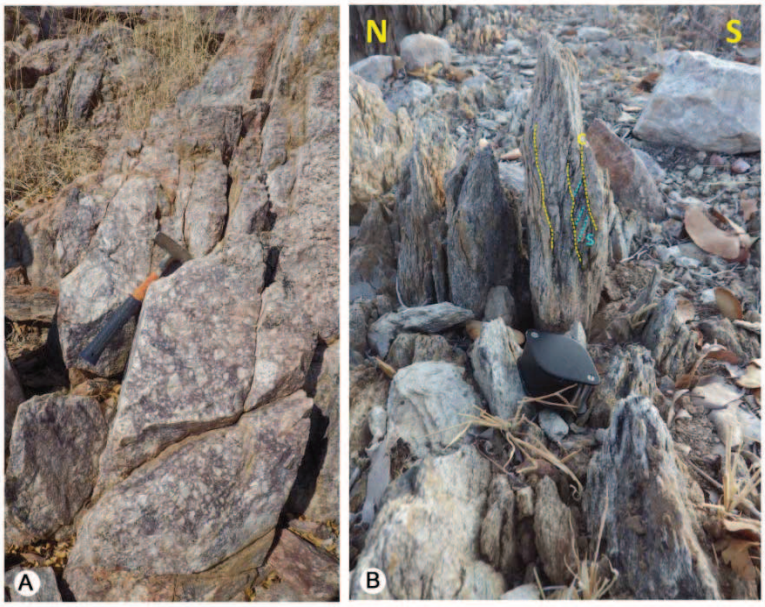


**Figure 27**. A) Rudaceous polymict conglomerate with flattened clasts (Farm Blydskap 268); B) sc-fabrics in sheared Fransfontein granite indicating top-to-the-north movements (N left, S right). (A - NA 053; B - NA052).

The stereograms (Fig. 28, Fig. 29) of the Transition Zone show similar orientation of linear and planar structures as in the Khoabendus East subdomain, however, less variation (which may be due to the small data set collected mainly in one locality, NA052-58). Lineations mainly plunge SWS with the maximum of 207/57 comparable to the average orientation in the north. The poles of S1 and gneissic fabrics scatter in the NW with the maximum at 330/18 corresponding to a steep SE-dipping S1 plane (150/72). The small obliquity between the direction of stretching lineations and the foliation dip implies major vertical and minor sinistral components.

***Huab Metamorphic Complex (HMC)***

The HMC has been subdivided into three tectono-metamorphic subdomains comprising the NE low-grade Ehobib SD, the central medium-grade Suiderkruis-Aandgloed SD, and the southern high-grade Rooikop-Lofdal SD (Fig. 28, Fig. 29). The structural map (Fig. 16) illustrates the main folds and thrusts, the principal directions of foliations and lineations, and the outlines of the metamorphic domains thereby integrating information from previous studies (i.e. Frets, 1969).

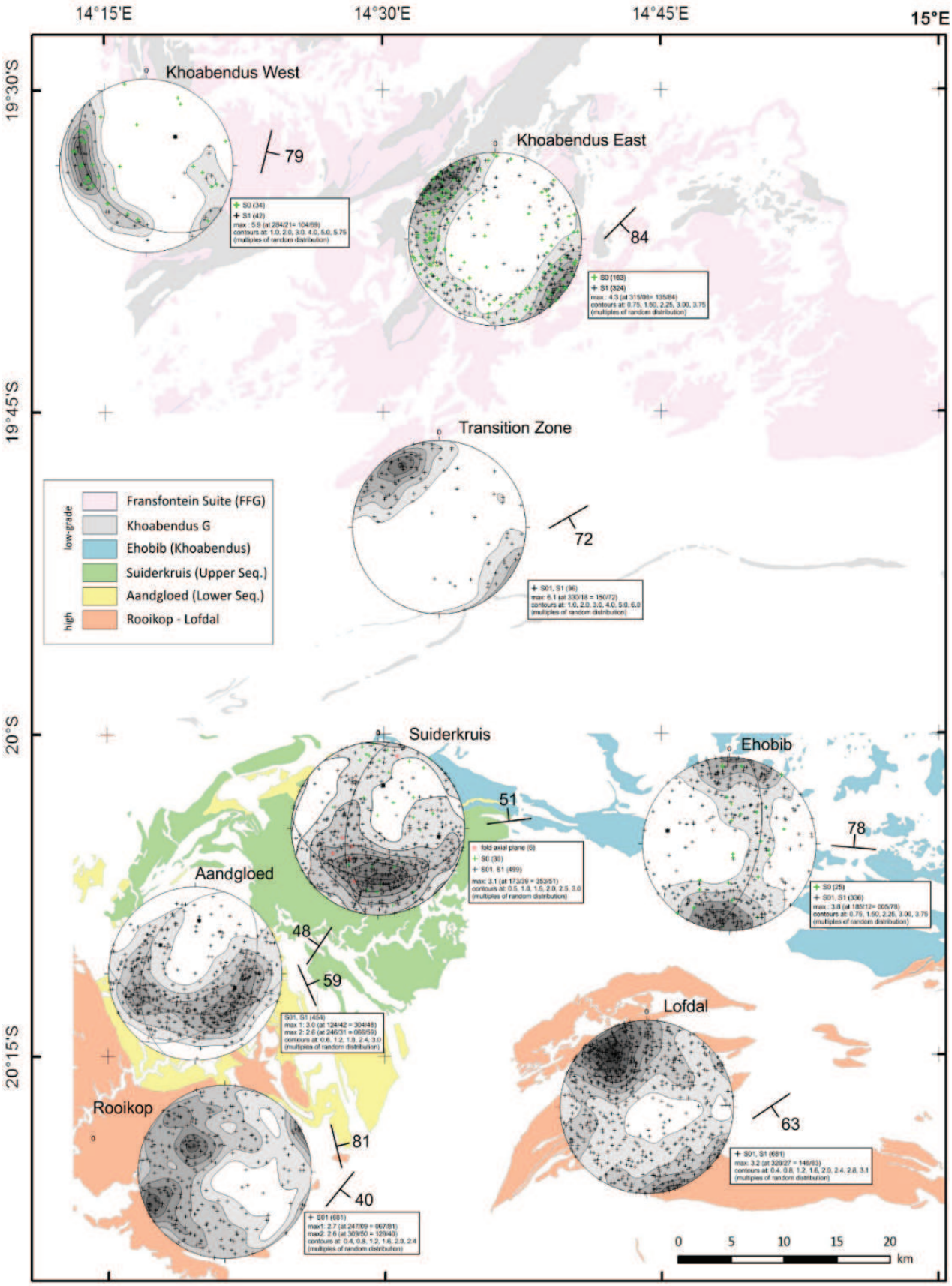


**Figure 28**. Stereograms of planar structures S0, S01, S1 constructed for the subdomains of the study area; (grey = Khoabendus Group, pink = Fransfontein Suite (not shown in Transition Zone and Huab area), light blue = Ehobib SD, green = Suiderkruis SD, yellow = Aandgloed SD, orange = Rooikop/Lofdal SD).

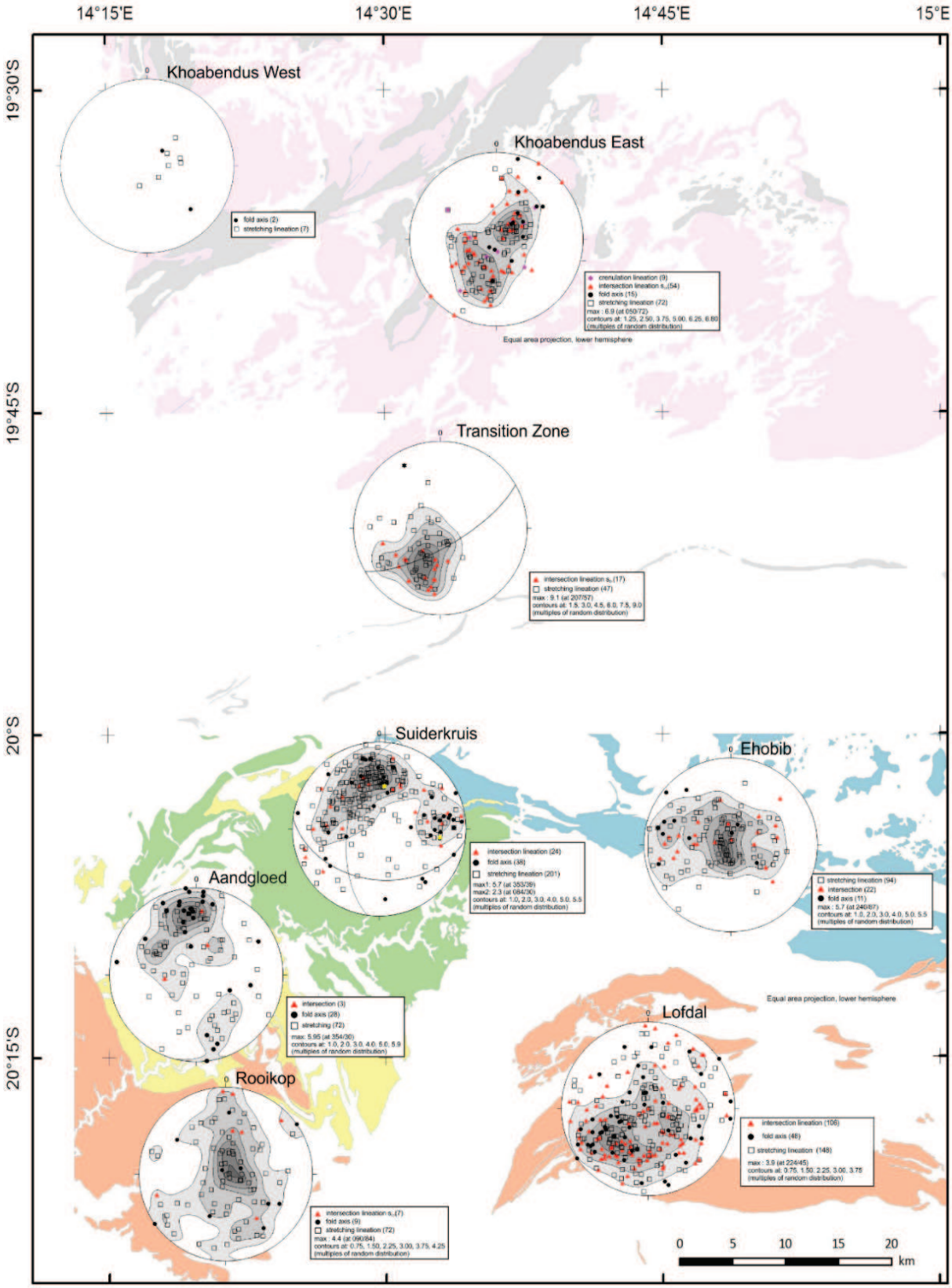


**Figure 29**. Stereograms of linear structures (stretching, intersection, fold axis).

***Ehobib SD***

The Ehobib SD is juxtaposed with the adjacent units by regional WNW-ESE trending shear zones that change from a subvertical position in the SE (Farm Smalruggens 684) to a folded low-angle thrust in the NW (Farm Ruspoort 669). The orientation of adjacent rock units follows these structures indicating their

transposition during transport (Fig. 16). Fransfontein granites were progressively transformed into augengneiss towards the HMC. Thrusting and contemporaneous folding resulted in juxtaposition of the low-grade Khoabendus rocks with high-grade gneisses of the HMC and their preservation in deep-reaching upright synforms.

The geological map illustrates that most of the subdomain is dominated by two NNW-SSE trending upright synforms, which are in steep thrusted contact. Further NW, the Ehobib and Suiderkruis subdomains are juxtaposed along the NE-SW striking Ruspoort fault (Fig. 16, Fig. 17). South of this structure, complex structural relationships with the Suiderkruis SD are characterised by (i) tectonic mélange of low-grade Khoabendus volcanic and sedimentary rocks with higher grade HMC quartzite, amphibolite, paragneiss, red orthogneiss, (ii) development of retrograde garnet phyllite and biotite schist within shear zones, (iii) presence of isoclinal folds, (iv) locally developed mylonites parallel to the intensely folded thrust plane and (v) locally refolding of the mylonitic fabrics into disharmonic upright to N- and E-verging folds associated with a D2 foliation parallel to the axial plane. About 20 m away from the thrust, low-metamorphic rocks are hardly deformed; elongated clasts of pebbly quartzite thus are rotated into a vertical position parallel to the NW-dipping S2 schistosity.

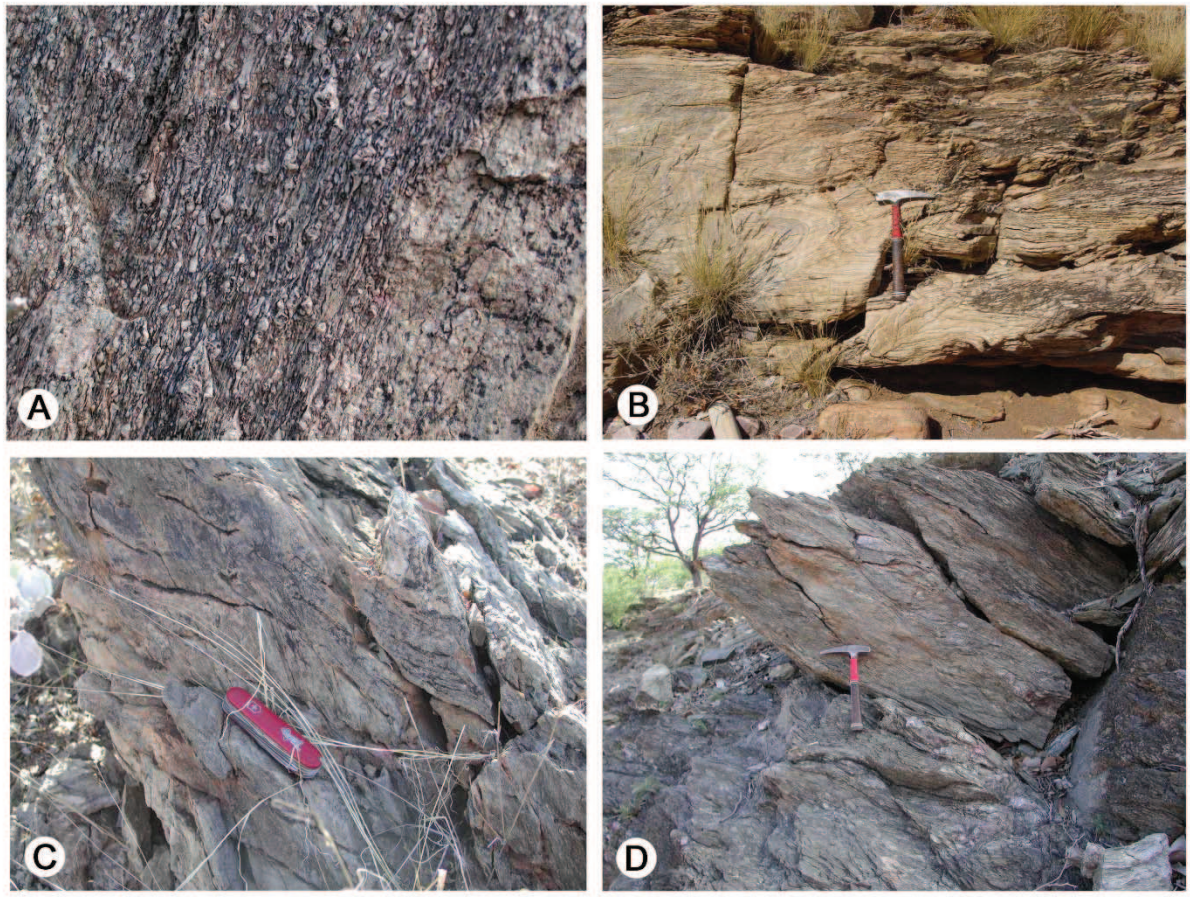


**Figure 30**. Small scale structures recorded in the Ehobib SD. A) mylonitic quartz-feldspar porphyries, B) intense tight folding, C) S1, S2 foliations D) low-grade low-angle shear zone at the base of the Khoabendus Fm in the NW termination of the Ehobib SD on Ruspoort 669 may represent a detachment. (A – Tweelingskop 676; B – Spitskop 678; C, D – Ruspoort 669).

A small outlier of the Ehobib SD is preserved about 10 km west of the main occurrence and overlies the Suiderkruis SD. It comprises low-metamorphic mylonitic meta-rhyolite, chert, muscovite schist and chlorite schist. The underlying quartzite of the Suiderkruis SD is deformed into boudins suggesting thrusted contacts.

Very prominent stretching lineations are developed in the eastern Ehobib SD in steeply dipping massive K-feldspar porphyries of the Khoabendus Group. Kinematic indicators

document north-directed down-dip movements implying uplift of the HMC. Here, the strong gradient in deformation is demonstrated by megaboudins of Kamdescha type granitoids with weakly deformed granitic textures in the cores changing into augengneiss and protomylonite in the outer parts.

The stereogram of planar structures illustrates generally steep N and S dips of the S0, S1 and S01 planes; the maximum at 185/12 corresponds to a steep N-dip (005/78). The poles of the constructed AC plane constrains WNW low-angle plunging D2 fold axes (282/28).

Widely varying lineation directions define a broad E-W girdle. The maximum of all lineations (mainly stretching) is near vertical (240/87). Fold axes and intersection lineations plunge at low to moderate angles to the west in accordance with the constructed fold axis; however, a few vertical fold axes were observed, too.

Crenulation cleavages dip in northern directions (not shown); the maximum of poles at 171/27 corresponds to a moderate northerly dip (009/63). A few crenulation lineations plot within this plane but vary again widely in direction and plunge (not shown).

***Suiderkruis - Aandgloed SD***

The domain is in thrusted contact with the eastern Ehobib and western Rooikop subdomains whereas in the north it terminates in the Kuyper synform and is bounded by a folded thrust with the underlying red orthogneiss. In the Lofdal Inlier, the Aandgled SD is possibly juxtaposed by the NE-SW striking Soutpoort Shear Belt with the southern Lofdal SD (Fig. 16). The regional fold style is characterised by a series of prominent curvilinear folds whose axial planes change from a NE dip in the south to a NW dip in the north, defining a synform about 30 km in diameter (Fig. 16, Fig. 20). However, the simple (late stage) first order structure is marked in the central part by complex interference fold geometries that are outlined by marker horizons such as the white quartzite and the two regional megasills (ROG, POGD). The traces of fold axial planes of map-scale curvilinear folds swing from a general NE trend in the north (Kuyper Synform) into a SSE trend in the south (Copper Valley Synform). The Eersbegin Dome in the central part of the domain is another prominent structure about 5 km across, which is surrounded by complexly folded paragneisses of the Upper Sequence.

The profile from the northern Kuyper Syncline through the Huab into the Copper Valley displays the main structural elements of the domain in a number of key outcrops and yields insight into the nature of the contacts (Fig. 16, Fig. 17 profile E).

Localities NA037 and NA075 at the southern limb of the Kuyper Syncline expose a subhorizontal series of rocks. In the lower part it starts with alternating finely bedded quartz-muscovite schist, quartz-feldspar-muscovite-garnet schist, quartz-feldspar-garnet gneiss with minor intercalated garnet-bearing amphibolite and quartzite that higher up becomes the predominant facies forming massive layers. The series is intruded at the base by a megasill of red orthogneiss. All rocks are mylonitic and are marked by a pronounced NW plunging stretching lineation (305/15; Fig. 31a-b). Asymmetric pressure shadows around pre-tectonic garnet indicate D1 top to the ESE transports. Small scale isoclinal folding associated with this deformation stage was observed in a few places. The mylonites were subsequently refolded around shallow W-plunging D2-axes (293/25) into tight folds of all scales and associated with the main shallow W-dipping S2 foliation (279/28). D1 kinematic indicators were rotated during D2 and therefore cannot be used to constrain the D1 transport directions (Fig. 16). A steep east dipping crenulation cleavage (099/68) is associated with late stage small scale open folding.

The contact between the Lower and Upper Sequence is exposed in two localities (NA038, NA078) at the northern limb of the Eersbegin Synform. Subhorizontal massive white quartzite at the base of the Upper Sequence is in thrust contact with underlying amphibolite and metagreywacke of the Lower Sequence. The quartzite is transformed in the ca 1 m wide thrust zone into an ultramylonite with pronounced W-plunging stretching lineation and abundant refolded small scale isoclinal folds with fold axes slightly oblique to the stretching (Fig. 31c). 100 metres south of this outcrop, isoclinally folded quartzite is refolded into tight asymmetric, disharmonic N-verging folds of metre-scale that are associated with a local steeply S-dipping S2 schistosity (195/75). The crenulation cleavage in this place dips moderately to the SWS (208/40). A late high angle fault in the front of the D2 anticline

indicates reverse transport to the N; the tectonic breccia in the thrust documents the change from ductile to brittle conditions during this stage of deformation (Fig. 31d).

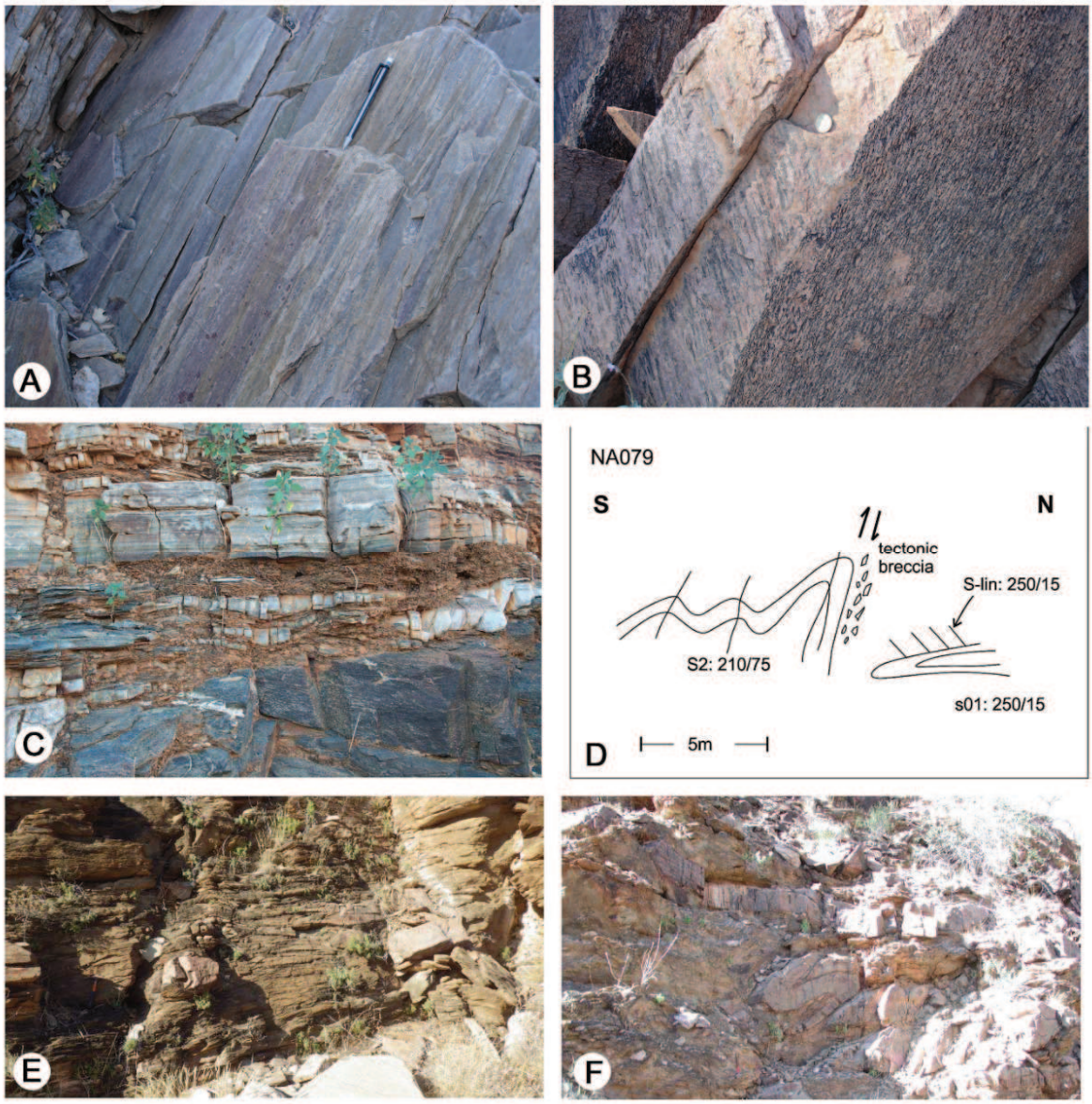


**Figure 31**. Key outcrops exposing the contact between the Lower and Upper Sequence of the Suiderkruis-Aandgloed SD. (Suiderkruis 668) (A and B - NA037; C - NA038; D - NA079; E - NA083; F - NA084).

Numerous outcrops over 3 km along the NE flank of the Eersbegin Dome display boudins of quartz-feldspar gneiss and amphibolite up to 20 m in diameter in a matrix of quartz-mica schist. Together with the shallow east plunging stretching lineations this documents pronounced layer-parallel extension (Fig. 31e). At the contact with underlying white quartzite, an up to 20 m wide horizon of low-grade phyllonite with slivers of chaotically folded quartzite up to 50 m across marks another important shear zone (Fig. 31f). Drag folds and sc-fabrics within a discrete ductile shear zone (057/50) indicate top to the NE down-dip movements.

At NA040 isoclinal folds in gneissic amphibolite refold an older gneissic fabric of oriented amphibole minerals (Fig. 32c-d). The isoclinal folds are in turn refolded around shallow SW-plunging fold axes (235/30) into tight D2 folds; the moderately SE dipping D2 schistosity (135/60) is the predominant fabric. In the adjoining quartz-mica schist all older structures are completely transposed into the new S2 fabrics (Fig. 32 a-b). Late asymmetric W-verging small scale folds are associated with

steeply E-dipping D3 crenulation cleavage (075/82). Ca 5 km west of this locality muscovite-garnet schist in contact with steeply S-dipping white quartzite (179/70) is folded around moderately E-plunging axes into asymmetric disharmonic S-verging folds. Interbedded quartz-feldspar gneiss is again boudinaged. Together with observations from other places this demonstrates radial down-dip movements off the dome.

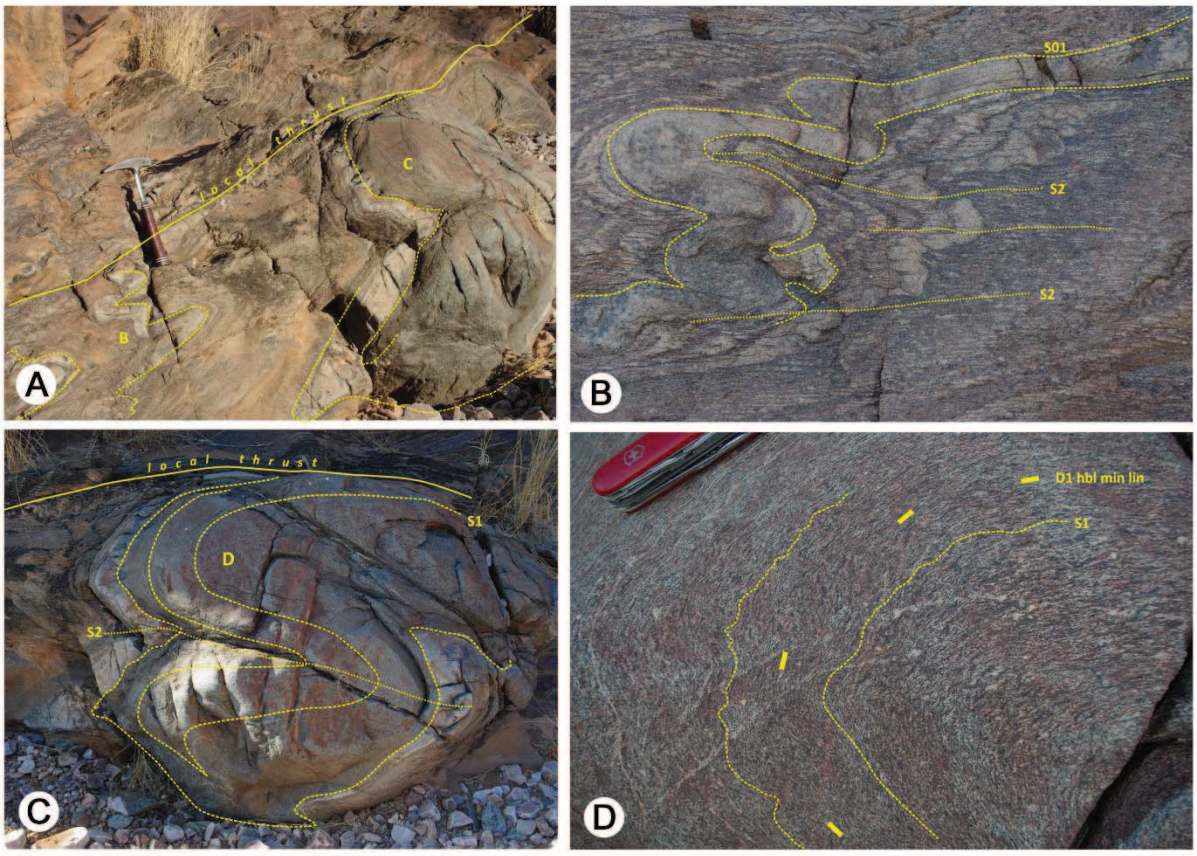


**Figure 32**. Locality NA040 at the NE flank of the Eersbegin Dome. (NA040).

Locality NA101 exposes a moderately NNE-dipping steep shear zone that was intruded by three generations of magma. Early mesocratic biotite-hornblende diorite orthogneiss records a prominent north-plunging stretching lineation (355/52). The second main phase of fine-grained, equigranular garnet-bearing granite is barely deformed and forms a stockwork within the fault and the adjacent country rocks. It comprises abundant angular amphibolite xenoliths and rounded gabbro enclaves (Fig. 33c-d). The third igneous minor phase consists of undeformed gabbro.

Voluminous contemporaneous hydrothermal fluid activity is recorded in this place by zoned garnet-hornblende-epidote mineralisation at the contact between the magmatic breccia and the mylonitic country rock (Fig. 33a-b). The zoned body comprises a core of giant garnet, which is surrounded by a rim of epidote and hornblende. Pre- to syntectonic crystallisation is indicated by the adjacent mylonitic country rock whose fabric wraps around the garnet. Zoned garnet-epidote inclusions within the granite constrain the older age of hydrothermal alteration (Fig. 33d).

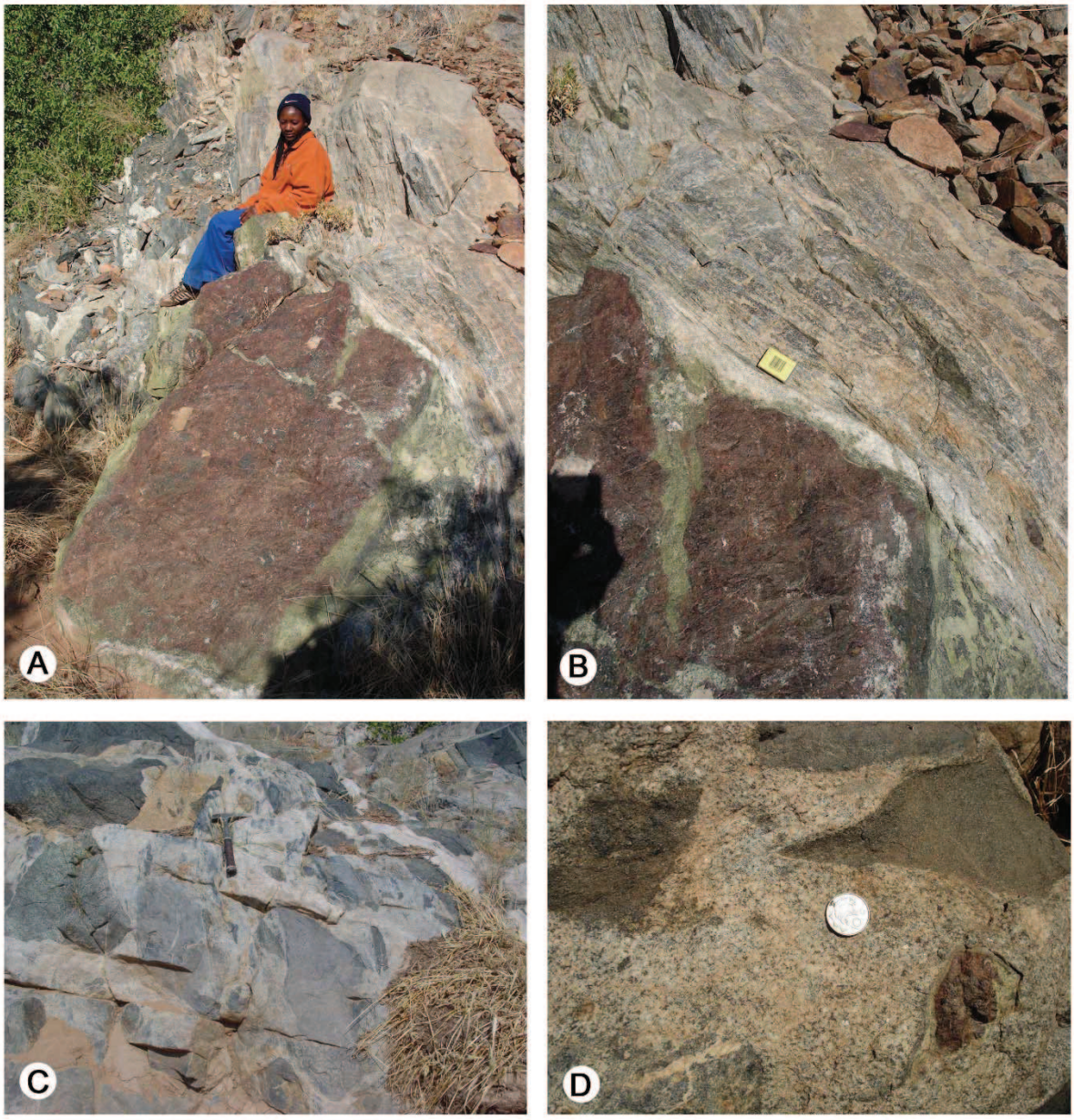


**Figure 33**. Major shear zone intruded by three generations of magma and overprinted by hydrothermal fluids (locality NA101). A-B) Giant garnet-epidote-hornblende mineralisation; C) shear zone hosted granite with abundant xenoliths D) close-up showing polygenetic xenoliths including garnet-epidote mineralisation. (NA101).

The fault-associated magma phases, which are variably affected by deformation demonstrate the longevity and crustal-scale of this structure. It represents a unique feature in the study area and coincides in this place with the boundary to the Aandgloed SD. The fault has been mapped for about 5 km along strike but probably continues in both directions; an elongated tonalite body about 800 m long is distinguished on the geological map at its north-western tip. The map further shows no offset of adjacent lithologies across the fault thereby indicating only minor lateral movements. The reverse or normal shear sense could not be determined, however, moderate to vertical N-dipping flat and ramp structures (001/65, 345/87) in the gneissic tonalite and the presence of magmas, emplaced favourably into extensional systems argue for at least one phase of N-directed normal down-dip movements.

Granite and gabbro were sampled for geochronological analysis in order to constrain the minimum age of regional tectono-metamorphism in the HMC (see chapter on Geochronology NA101-2).

The transition from non-migmatitic to migmatitic rocks occurs in the south of the

Aandgloed Subdomain. Locality NA045 near Mesepotamie settlement exposes folded migmatitic biotite-bearing amphibole gneiss of tonalite to dioritic composition with intercalated non-migmatitic amphibolite layers (Fig. 34). The anatectic melts evolve into up to 20 cm thick stromatic veins of biotite-bearing leuco-gneiss. The rocks record a first gneissic foliation outlined by oriented biotite and flattened quartz-feldspar aggregates parallel to the stromatic structures. It is folded into small scale isoclinal folds, which are in turn refolded around shallow N-plunging axes (015/22) into medium scale upright tight folds that are associated with the regional gneissic fabric (here steeply E-dipping: 101/70) and a pronounced hornblende mineral lineation parallel to the fold axis. The fabric is overprinted by a penetrative crenulation cleavage dipping again steeply to the east (111/87) and associated with symmetric open small scale folds. A second NE-dipping (063/60) crenulation cleavage is less pronounced and is associated with asymmetric SW-verging folds whose axes plunge again shallowly to the N (355/30).

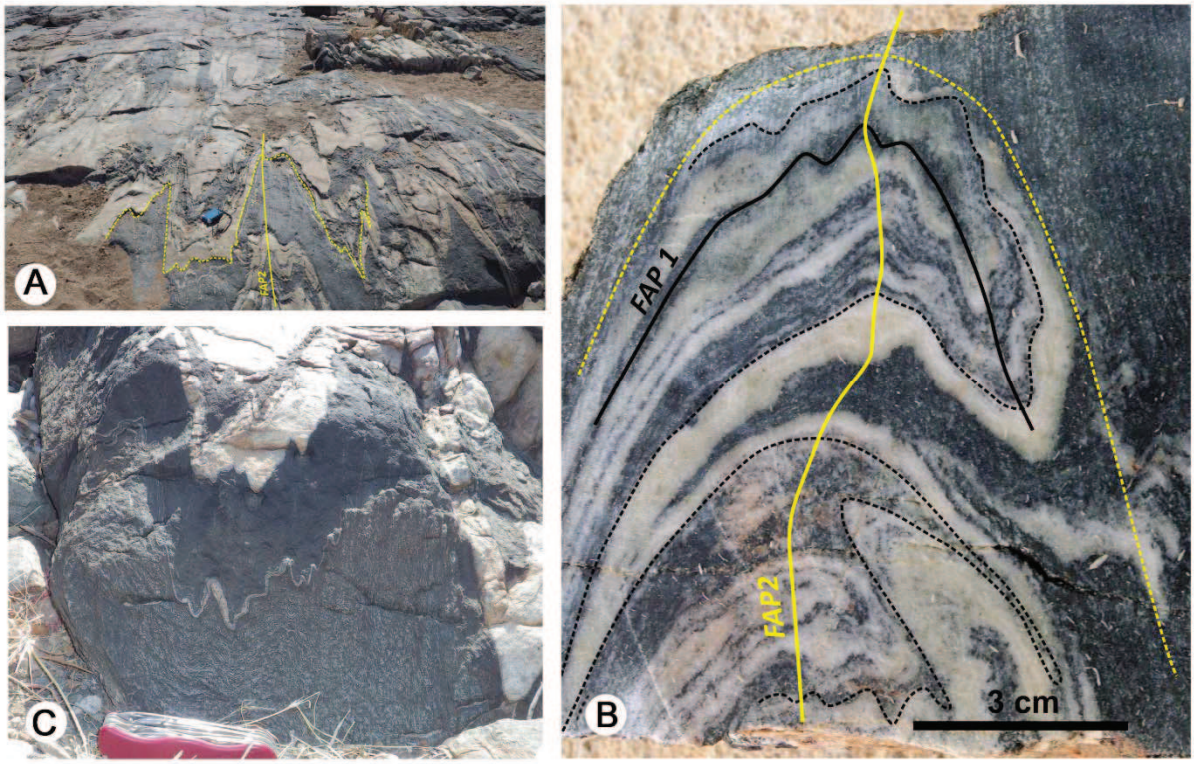


**Figure 34**. Key outcrop NA109 near Mesepotamie settlement is situated in the transition from non-migmatitic to migmatitic gneisses of the Aandgloed SD.

Paragneisses at locality NA044, 3 km further NW, record a similar deformation history. Alternating quartz-feldspar-muscovite schist, amphibolite and biotite-garnet gneiss display a pronounced S01 layering which is folded isoclinally (D1) (Fig. 35a). The isoclinal folds are refolded by tight D2 folds (Fig. 35b). The adjacent quartz-muscovite schist only records D2 deformation while any older structures are transposed. Massive layers of leuco- to mesocratic garnet biotite-quartz-feldspar paragneiss comprises disseminated isometric megacrystic garnet surrounded by bleached reaction rims. The crystals and rims are almost undeformed suggesting post-kinematic crystallisation or very rigid behaviour of the host rocks during deformation (Fig. 35c). First occurrences of the massive pegmatite which is ubiquitous in the Rooikop SD form bodies up to 5 x 30 m in dimensions that are progressively transposed into the D2 plane, smaller intrusions are disrupted into boudins (Fig. 35d).

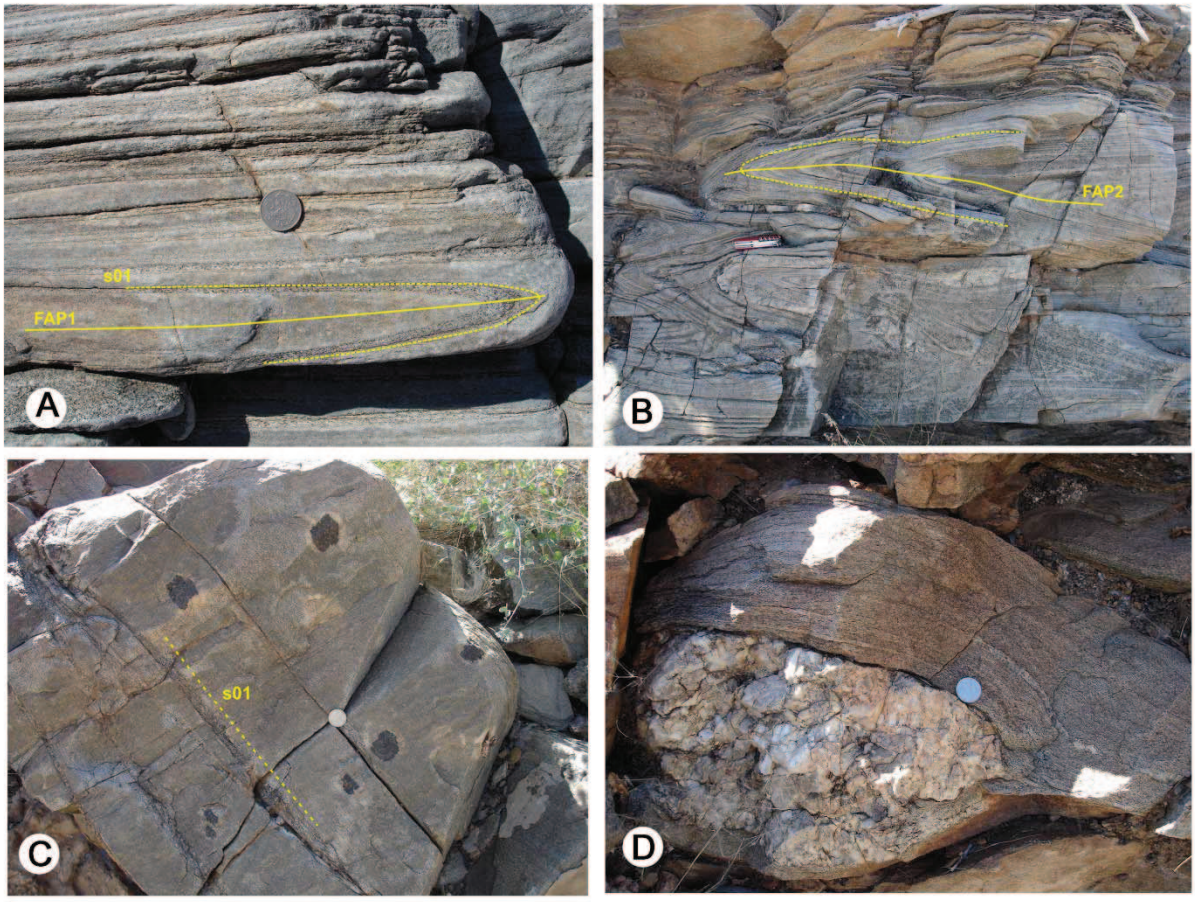


**Figure 35.** Small scale structures in the Copper Valley. A) layer parallel D1 isoclinal folding; B) tight D2 folding with moderately E-dipping axial planes; C) undeformed isometric megacrystic garnet with bleached reaction rims; D) boudinaged pegmatite.

A final key locality demonstrating deformation and metamorphism in the Aandgloed subdomain is situated in the apex of a small migmatitic dome (NA049) exposing subhorizontal to shallow NW-dipping (339/25) gneisses (Fig. 36-37). The main rock is a mesocratic medium-grained layered biotite-quartz-feldspar gneiss that changes laterally into stromatic migmatite marked by coarse-grained quartz-feldspar leucosome with prominent thin biotite selvedge. The rocks are isoclinally to tightly folded but lack any associated foliation. An older generation of anataxis-related quartz-feldspar veinlets parallels the stromatic structures whereas it crosscuts pervasively interlayered amphibolite transforming the rock into injection migmatite. A second generation of more massive pegmatite dykes cross-cuts the folded sequence. The chaotic, highly deformed rock association is intruded along sharp planar contacts by an about 20 m thick sill of massive non-migmatitic red orthogneiss (ROG); faint metamorphic layering in the ROG is defined by medium to coarse grain size variation.

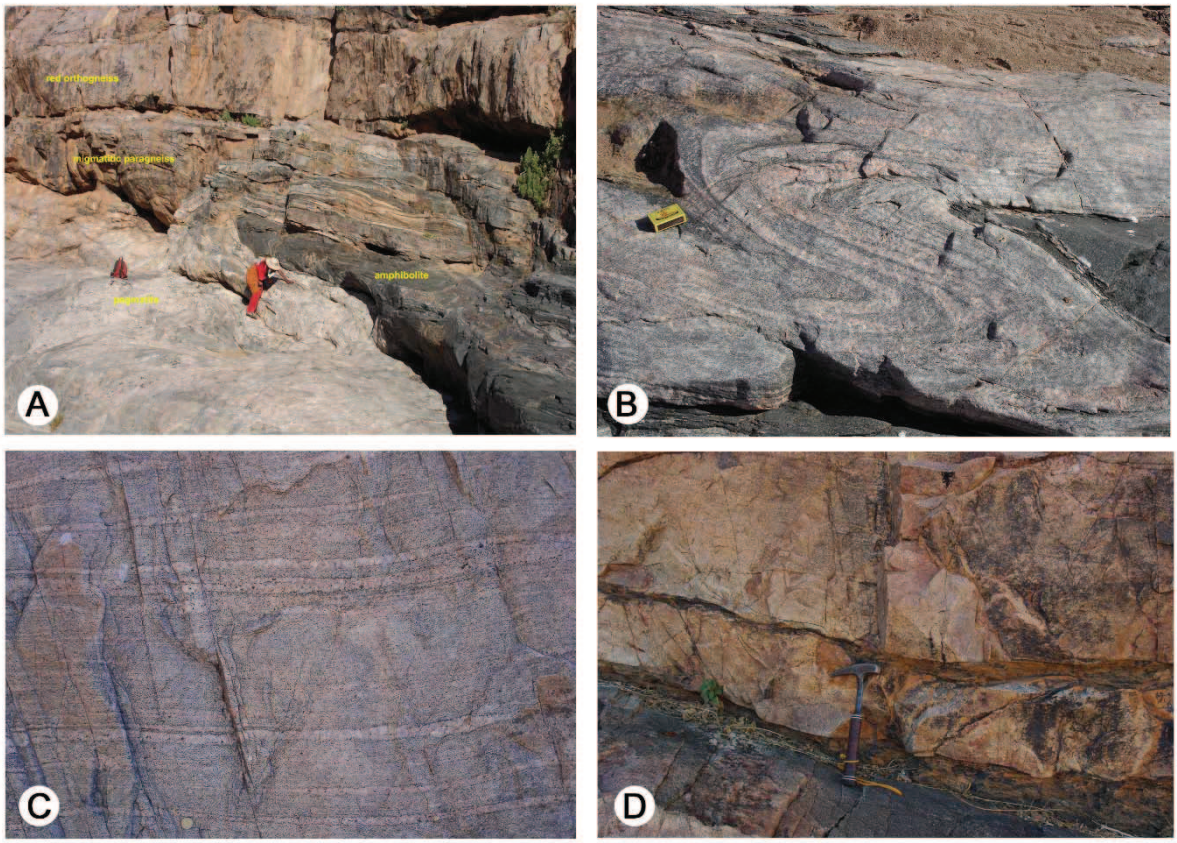


**Figure 36**. A) Migmatitic paragneiss soaked by pegmatite is intruded by a sill of ROG; B) tight to isoclinal folding of migmatite; C) stromatic layering characterised by coarse-grained leucosome veins with biotite selvedge; D) close-up view illustrating the sharp contact between non-migmatitic ROG and underlying amphibolite. (NA049).

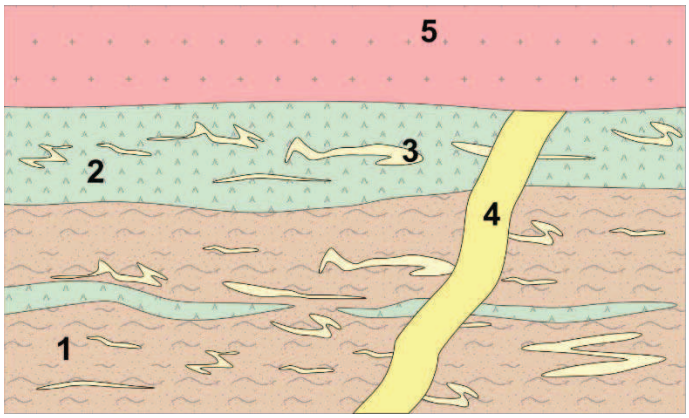


**Figure 37**. Sketch of key outcrop NA049 illustrating the main rock types and structural features. 1) migmatitic paragneiss, 2) migmatitic amphibolite (boudinaged), 3) folded stromatic and phlebitic leucosome, 4) late pegmatite, 5) transposed non-migmatitic red orthogneiss (deformed equivalent of Kaross type FFG) cross-cutting late pegmatite.

The stereograms of planar structures illustrate wide variation in their orientation within the Suiderkruis and Aandgloed subdomains (Fig. 28). In the Suiderkruis Subdomain, most of the poles plot in the SE and SW quadrants corresponding to moderate and steeply NW and NE dipping planes. The pole of the AC-plane defines the general north-plunging fold axis (007/49). A smaller part of the poles defines a second AC-plane corresponding to an east-plunging fold axis (097/30). Many other poles in the eastern hemisphere (off the two AC planes) correspond to westward dipping planes and therefore only the NW and NE quadrants are almost devoid of any data. The poorly defined maximum of poles at 173/39

corresponds to a moderate N-dipping plane (353/51). Structural data from the Aandgloed Subdomain displays a similar pattern, however document a major shift of the maxima and AC-planes. Here, most of the poles plot in the SE quadrant around a poorly defined maximum at 124/42 corresponding to a moderately NW dipping plane (304/48) whereas a second local maximum at 246/31 documents frequent NE-dipping planes. The poles of three AC-planes plunge into northern (004/39), eastern (110/40) and northwestern (309/47) directions implying great variation of the fold axes and interference folding. However, all data also define a small circle with a vertical axis in the centre of the stereogram, being typical for dome and basins structures. Only a few poles are recorded in the NE and northern sectors of the stereogram.

Linear structures are presented in Fig. 29. Most of the lineations plunge in both subdomains at moderate angle to the N and NW, thereby defining a maximum at 353/39. In the Suiderkruis SD a smaller group of E-plunging fold axes and stretching lineations defines a second local maximum at 084/30. Both maxima coincide with poles of AC-planes defined by the planar fabrics suggesting subsequent rotation of the N-plunging D1 fold-axes and stretching lineations around the E-plunging D2 axes. In the Aandgloed Subdomain E-plunging axes are absent, stretching lineations scatter over the entire stereogram, whereas fold axes plunge with low variation principally NNE. The maximum at 354/30 coincides with the pole of the principal AC-plane. The features suggests that D2 folding is less developed or absent in this subdomain.

Shear zones of the Aandgloed and Suiderkruis SD are mostly steeply dipping but vary widely in direction. The maximum of poles at 166/12 corresponds to a steeply N-dipping plane (346/78).

Crenulation cleavages and S2 foliations plot all over the stereogram with the pole maximum at 166/12 corresponding to a steep NNW-dip (348/78). The same holds true for few measured crenulation lineations (26), which do not define any maximum (not shown).

***Kinematics***

Relative movements have been mainly determined by analysis of asymmetric pressures shadows around K-feldspar and garnet porphyroclasts. The structural map illustrates movements in all directions but with systematic changes across the Suiderkruis-Aandgloed SD:

- NW-directed down-dip movements off the HMC are recorded in augengneiss in the NW corner of the Suiderkruis SD.
- Mainly E and NE-directed movements characterise the rocks in the vicinity of the Soutput Thrust.
- Rocks around the Eersbegin Dome record radial down-dip movements away from the structure.
- North and NW directed down-dip movements are recorded in the SE part of the Aandgloed SD in rocks unaffected by the Soutput Thrust.
- East and north-directed movements are indicated in the SE part of the Suiderkruis SD.
- Shear sense indicators in all rocks of the Eersbegin and the Kuyper Syncline suggest S, N, NW and SE-directed transports. Field observation shows rotation of the clasts during subsequent deformation resulting in erroneous opposite shear indicators.

***Rooikop/Lofdal SD***

Paragneisses are transformed through-out the Rooikop SD into migmatite and are intruded massively by pegmatite. Structurally the subdomain is characterised by dome and basin structures up to several km scale, the largest of which has a size of 8 x4 km and is shown on the geological map. It is marked by concentric layering of steeply dipping meta-greywacke, banded leucogneiss, amphibolite, granodioritic augengneiss and red orthogneiss in the core of the structure. Another of these structures is outlined by ring-shaped horizon of quartzite. The structures are repeated at outcrop-scale by metre-size vertical sheath folds (Fig. 39a) with steeply dipping associated foliations and lineations. Other small scale structures include isoclinal and tight folds. Vertical stretching lineations and the shape of the sheath folds suggest predominantly vertical movements post-dating isoclinal folding and anataxis of the rocks.

A prominent feature on farms Nil Desperandum 713 and Soutput 505 is the Soutput Thrust, which juxtaposes the Rooikop and Aandgloed Subdomains. The sharp contact between the two subdomains is perfectly visible on Landsat imagery and is marked by a high-

angle structural unconformity and completely different rock types on either side of the structure (Fig. 38). At locality NA131 in the NW part of the structure, granodioritic augengneiss (POGD) of the Aandgloed SD changes progressively towards the thrust into proto-mylonite marked by prominent WNW (299/45) down-dip stretching lineations and sc-fabrics (Fig. 39). K-feldspar sigma clasts and sc-fabrics indicate ESE-directed reverse transport of the Rooikop over the Aandgloed SD. Massive undeformed veins of late stage pegmatite intrude the mylonitic rocks at a high-angle and constrain the minimum age of thrusting as pre-Damara. The southern part of the Soutput Thrust has been reactivated during Damara deformation; this is demonstrated by Neoproterozoic sedimentary rocks of the Mulden Group that are offset in the continuation of the fault and by the retrograde greenschist facies metamorphism. The gneisses and amphibolites of the HMC are thus transformed over several km along the structure in an approximately 100 m wide zone into schist and/or tectonic breccia

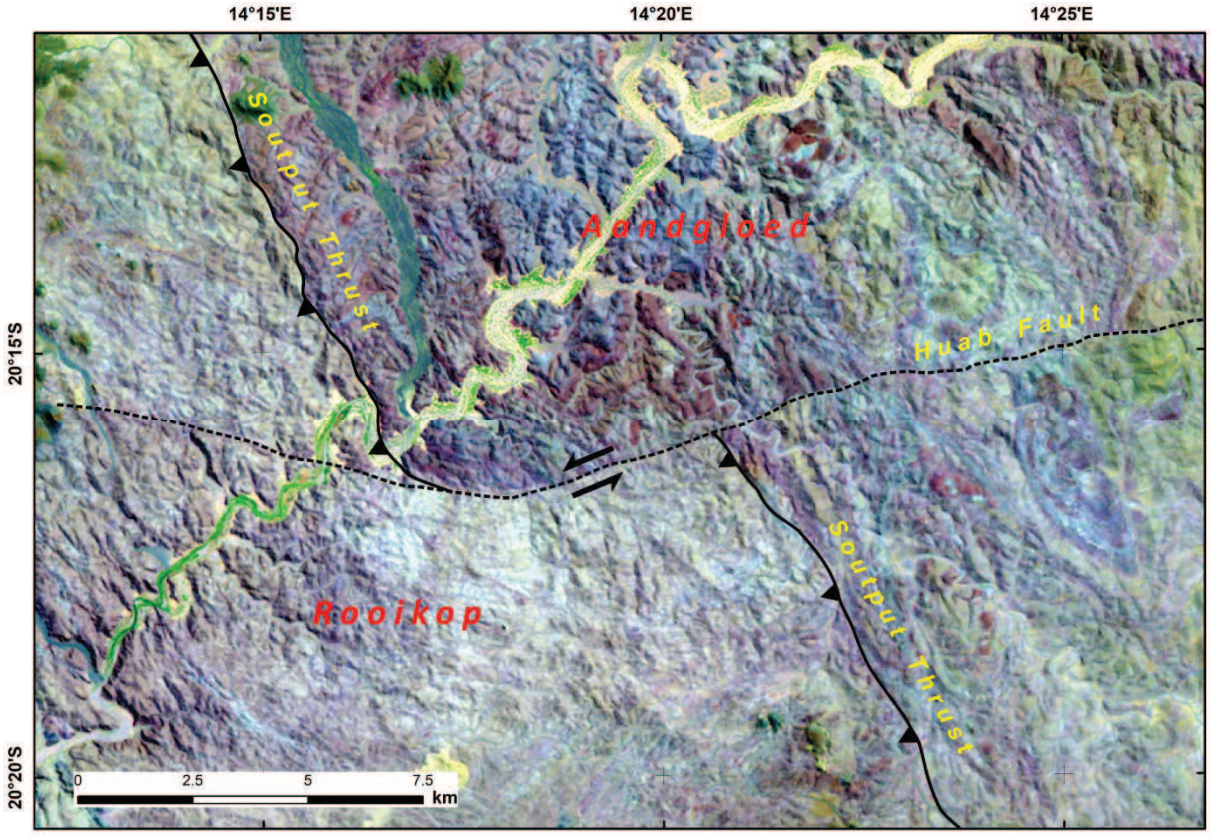


**Figure 38**. Landsat 741 imagery of the SW study area illustrating major differences in rock type and structural orientation between the Rooikop and Aandgloed subdomains.

The Lofdal Subdomain forms two small basement inliers in the Neoproterozoic Mulden Group, measuring 20 x 5 km and 40 x 15 km, respectively. It is comprised of (i) a northern dome with a core of amphibolite and a rim of migmatitic paragneiss intruded by small sills of red orthogneiss, (ii) a central batholith or megasill of red orthogneiss and (iii) a southern E-W striking belt of migmatitic paragneiss with slivers of amphibolite (Fig. 7, Fig. 16). Metamorphic grade and structural style are comparable to the Rooikop SD, however the geological map shows additional large scale folding around ENE axes resulting in complex fold interference structures that can also be observed at small scale (Fig. 39c). In other places only isoclinal folding is documented (Fig. 39D). Localised retrograde metamorphism, probably associated with shearing, is indicated in the northern window by chlorite-feldspar schist grading into massive amphibolite. Similar shearing and massive retrograde

low-grade metamorphism defines the ca 500 m wide E-W striking Soutpoort Shear Belt pre-dating deposition of the Mulden sediments.

Locality NA124 at the Khorixas Rest Camp exposes migmatitic orthogneiss and amphibolite in sharp folded contact with red orthogneiss. The amphibolite is invaded pervasively by strongly deformed pegmatite veins but shows no evidence of anatexis. In contrast, the adjacent orthogneiss displays stromatic structures. Both facies record the same moderate to steep S-dipping gneissic foliation, associated with asymmetric down-dip facing folds with WSW-plunging axes (237/25). As in the Rooikop Subdomain a second generation of undeformed pegmatite dykes crosscuts these structures.

The red orthogneiss (ROG) is again unaffected by anatexis and post-dates the pegmatite of the first generation. The homogeneous silica-rich rock is generally medium-grained but sometimes alternates with more coarse-grained m-thick layers of the same composition and minor intercalated discontinuous amphibolite slivers that may be transposed boudinaged dykes, sills or xenoliths. The rocks are commonly steeply north dipping and record shallow W-plunging stretching lineations.

Locality NA125 at the SE limit of the Lofdal Dome exposes migmatitic layered paragneiss and amphibolite that are overprinted by pronounced shearing. The E-W striking shear zone is marked by subvertical s- and steep c-planes (170/78) that in combination with the W-plunging stretching lineation (266/45) implies oblique movements with reverse top to the N and left-lateral components. The presence of sheath folds documents high deformation gradient. The structure is possibly part of the Soutpoort Shear Belt. It shows the same orientation and lateral shear sense as the Huab Fault 15 km to the north, suggesting that the E-W structures are part of the same system, which is bracketed in time between the deposition of the Otavi and Mulden groups.

Stereograms of planar and linear data (Fig. 28, Fig. 29) of the Rooikop and Lofdal SD are similar but show significant changes with the northern subdomains. Gneissic foliations of the Rooikop SD scatter evenly in the western hemisphere but almost no poles are located in the SE quadrant. The poles define two ill-defined maxima at 247/09 and 309/50 corresponding to subvertical ENE (067/81) and moderate SE (129/40) dips. Two poorly defined AC-planes indicate moderately SE (148/38) and steeply north (008/72) plunging fold axes. Lineations vary considerably in plunge within a ca 30° wide N-S girdle but many of them are steeply plunging. The maximum defines a subvertical axis (090/84) coinciding with the pole of the first AC-plane.

In the Lofdal SD gneissic foliations plot at moderate to steep angles in all directions whereas horizontal to shallowly dipping planes are absent. The well-defined maximum at 326/27 corresponds to a moderate SE-dip (146/63). The data do not allow construction of an AC-plane. Linear structures plot evenly over the stereogram except in the NW and SE. The maximum density at 224/45 corresponds to moderate SE plunge whose direction coincides with the plane axial traces of km-scale folds that characterise the geological map in this area (Fig. 16). The diagrams resemble those of the Transition Zone and Khoabendus East SD.

Crenulation cleavage and S2 foliations (52 data) are moderate to steeply NW and SE dipping; their distribution resembles those of the s01 planes. The planar structures are associated with ENE-plunging crenulation lineation (072/30) (not shown). Shear zones (58) are mostly steep SE dipping (157/78), parallel to the Soutpoort Shear Belt.

***Post-D2 / pre-Damara deformation***

The geometric relations between Post-D2/pre-Damara shear zones and thrusts and their host rocks implies the following succession of events:

- Soutput Thrust: the structure postdates D2 and predates emplacement of late stage pegmatite. The Rooikop SD was transported along the reverse structure towards the ESE over the Aandgloed SD. Rocks in vicinity of the thrust turned into protomylonite and schist (Fig. 39b). The southern part of the structure was reactivated probably twice during Damara rifting and the Pan-African event
- Huab Fault: the oblique fault with an important left-lateral component offsets the Soutput Thrust for about 7 km which constrains the younger age. On Tweelingskop 676 in the eastern part of the study area it affects Otavi G. carbonates, which are preserved only

north of the fault but is concealed below folded Mulden Group rocks. This documents pre-Mulden N-directed normal movements resulting in the uplift of the southern footwall.

- Soutpoort Shear Belt: the steep shear zone runs parallel to the Huab Fault and may be part of the same deformation event. The structure is concealed below folded Mulden Group rocks.

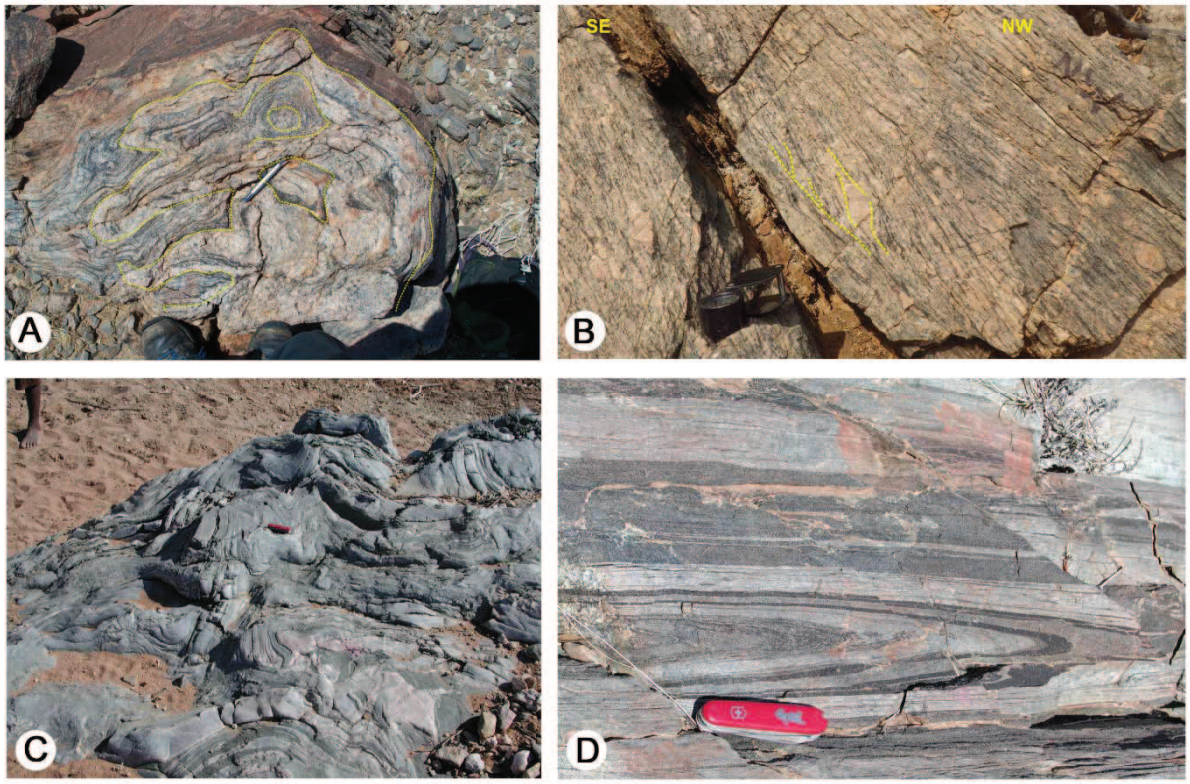


**Figure 39**. Small scale structures in the Rooikop-Lofdal SD. A) Small scale vertical sheath folds (bird's eye view); B) SC-fabrics indicating ESE-directed transports in the post-D2 Soutput Thrust; C) complex interference fold pattern; D) simple isoclinal fold refolding older compositional layering (A, B – Rooikop 506; C, D – Lofdal 491).

***Pan-African deformation***

The deformation overprinting the Damara rocks in the Huab area displays widely varying geometry, orientation and plunge of different folds, which have been described in detail by Frets (1974). Based on geometric considerations, the author subdivided four fold phases of (1) gentle to open E-W trending folds with wavelength of several km, (2) refolding of F1 folds into NNW-SSE to WNW-ESE trending similar style folds associated with a penetrative cleavage, (3) local folding into N-S trending subvertical folds and (4) local WSW-ESE open to close SW-verging (back)folding.

## Geochemistry and Sm-Nd systematics

Analysis of whole rock geochemistry and Sm-Nd isotope systematics was carried out on mafic and felsic igneous rocks of the Khoabendus Fm (KF), the Fransfontein Granite Suite (FFG) and the Huab MC (HMC). The data are presented in Tables 6 - 8.

**Felsic rocks**

The results for felsic igneous rocks are given in Kleinhanns *et al*. (2013) but for completeness are presented again. The relatively few data are insufficient to exclude or to confirm genetic relationships between the FFG and HMC intrusive rocks. The rocks are geochemically slightly different but evolved in the same arc-related plate tectonic setting.

Table 6. Whole rock geochemistry data of FFG Suite granites and HMC orthogneiss

| Unit | HMC-ROG | HMC-ROG | HMC-ROG | HMC-porphyry | HMC-porphyry | | HMC-POGD | HMC-POGD | HMC-orthogneiss | HMC-orthogneiss | HMC-orthogneiss | HMC-orthogneiss | HMC-orthogneiss | FFG undiff | Oortrek | Kamdescha | Kaross | Franken | Franken | Kaross |
|---|---|---|---|---|---|---|---|---|---|---|---|---|---|---|---|---|---|---|---|---|
| Sample ID | 210900-2 | 220802-12 | 220802-13 | 270802-1 | 280802-2 | 090606-1 | 090606-5 | HU-03 | 220802-3 | 260406-14 | 101203-5 | 010305-1 | 101203-1 | 081203-2 | 151104-1 | 260205-4 | 280205-3 | 280205-6 | 280205-7 | 170405-6 |
| **Major elements [%]** | | | | | | | | | | | | | | | | | | | | |
| SiO2 | 77.6 | 77.8 | 77.4 | 75.6 | 76.3 | 75.1 | 64.9 | 72.7 | 70.5 | 70.7 | 72.4 | 73.4 | 62.0 | 69.2 | 68.9 | 68.4 | 65.6 | 65.0 | 67.9 | 78.0 |
| TiO2 | 0.09 | 0.14 | 0.18 | 0.42 | 0.13 | 0.3 | 0.93 | 0.40 | 0.50 | 0.49 | 0.59 | 0.22 | 0.65 | 0.41 | 0.58 | 0.45 | 0.74 | 0.73 | 0.59 | 0.20 |
| Al2O3 | 12.0 | 11.0 | 11.1 | 11.9 | 13.0 | 12.5 | 13.8 | 12.8 | 14.0 | 12.5 | 13.1 | 11.0 | 14.4 | 15.3 | 13.5 | 13.0 | 15.4 | 15.2 | 14.2 | 11.6 |
| Fe2O3 | 1.79 | 1.59 | 2.59 | 2.54 | 0.88 | 1.12 | 6.71 | 3.40 | 3.77 | 6.36 | 3.65 | 0.90 | 9.70 | 2.68 | 3.02 | 2.52 | 4.46 | 4.61 | 3.6 | 1.01 |
| MnO | 0.01 | 0.02 | 0.02 | 0.02 | 0.03 | 0.02 | 0.11 | 0.05 | 0.05 | 0.1 | 0.06 | 0.03 | 0.26 | 0.08 | 0.06 | 0.06 | 0.10 | 0.17 | 0.10 | 0.04 |
| MgO | <0.01 | 0.03 | 0.11 | 0.11 | 0.10 | 0.47 | 1.18 | 0.34 | 1.5 | 0.36 | 0.86 | 0.1 | 3.39 | 0.79 | 0.67 | 0.56 | 1.18 | 1.34 | 0.96 | 0.16 |
| CaO | 0.29 | 1.71 | 1.21 | 0.46 | 0.89 | 2.09 | 3.19 | 1.27 | 2.21 | 2.48 | 3.02 | 0.1 | 4.79 | 2.50 | 1.40 | 1.53 | 3.20 | 2.02 | 2.30 | 0.21 |
| Na2O | 5.44 | 5.39 | 5.85 | 2.93 | 4.29 | 4.68 | 2.94 | 3.12 | 3.83 | 2.47 | 3.46 | 2.81 | 2.24 | 4.38 | 3.53 | 3.33 | 3.66 | 4.56 | 3.71 | 3.33 |
| K2O | 2.13 | 0.54 | 0.23 | 5.11 | 3.42 | 0.94 | 3.88 | 4.80 | 1.99 | 3.46 | 0.89 | 5.27 | 1.47 | 3.64 | 4.91 | 4.94 | 4.30 | 4.08 | 4.24 | 4.61 |
| P2O5 | 0.02 | 0.01 | 0.01 | 0.08 | 0.02 | 0.04 | 0.28 | 0.06 | 0.07 | 0.16 | 0.15 | 0.02 | 0.09 | 0.13 | 0.17 | 0.12 | 0.22 | 0.22 | 0.17 | 0.03 |
| Sum | 99.4 | 98.3 | 98.7 | 99.1 | 99.1 | 97.3 | 97.9 | 98.9 | 98.4 | 99.1 | 98.1 | 93.8 | 99.1 | 99.1 | 96.7 | 94.9 | 98.8 | 97.9 | 97.8 | 99.2 |
| **Trace elements [ppm]** | | | | | | | | | | | | | | | | | | | | |
| Li | 0.20 | 0.46 | 0.88 | 2.40 | 1.57 | 1.65 | 32.1 | 6.57 | 8.71 | 16.2 | 10.4 | 6.72 | 22.8 | 27.4 | 23.4 | 22.2 | 18.4 | 22.4 | 13.0 | 5.89 |
| Be | 2.80 | 2.42 | 1.89 | 3.02 | 2.09 | 1.92 | 2.73 | 5.83 | 2.27 | 3.35 | 3.67 | 3.67 | 1.51 | 3.03 | 3.70 | 3.53 | 3.07 | 3.28 | 3.09 | 3.89 |
| Sc | 2.54 | 2.58 | 2.79 | 12.7 | 5.40 | 6.67 | 15.5 | 6.90 | 7.71 | 19.10 | 23.97 | 4.10 | 21.40 | 8.72 | 9.04 | 6.79 | 11.7 | 11.4 | 9.17 | 3.20 |
| V | 10.7 | 18.6 | 16.5 | 12.9 | 11.8 | 57.2 | 64.7 | 17.2 | 17.9 | 19.1 | 37.2 | 10.7 | 131 | 42.1 | 45.3 | 36.4 | 64.3 | 65.5 | 49.1 | 12.8 |
| *Cr | 38.2 | | | | 0.52 | 4 | 6 | | | | | | | 2 | 7 | 7 | 7 | 12 | 5 | 5 |
| Co | 0.52 | 0.73 | 2.30 | | | 4.8 | 11.8 | 2.76 | 7.1 | 60.9 | 97 | 1.94 | 65.6 | 3.86 | 5.69 | 5.48 | 8.38 | 8.14 | 6.7 | 2.11 |
| Ni | 1.18 | 1.08 | 2.38 | 24.8 | 1.07 | 2.49 | 5.72 | 2.51 | 2.01 | 27.7 | 39.5 | 1.35 | 31.6 | 2.44 | 3.28 | 3.21 | 5.94 | 5.31 | 4.12 | 1.30 |
| Y | 43.6 | 60.0 | 40.0 | 71.2 | 45.2 | 44.8 | 53.0 | 99.5 | 36.3 | 126 | 111 | 37.8 | 108 | 22.2 | 38.4 | 36.7 | 32.1 | 32.0 | 30.5 | 31.0 |
| Zr | 263 | 241 | 495 | 505 | 309 | 245 | 343 | 403 | 407 | 389 | 455 | 162 | 215 | 108 | 130 | 180 | 162 | 161 | 163 | 133 |
| Nb | 24.0 | 20.7 | 21.8 | 32.2 | 15.3 | 14.5 | 23.3 | 29.6 | 15.6 | 35.4 | 30.2 | 21.8 | 11.4 | 10.1 | 19.7 | 17.6 | 14.9 | 14.7 | 14.1 | 19.7 |
| Rb | 45.4 | 10.0 | 2.97 | 201 | 45.1 | 18.0 | 117 | 196 | 39.4 | 155 | 39.7 | 253 | 97.7 | 105 | 176 | 187 | 144 | 125 | 119 | 175 |
| Sr | 117 | 112 | 86.8 | 90.0 | 153 | 219 | 173 | 56.9 | 277 | 129 | 312 | 16.4 | 147 | 351 | 157 | 192 | 393 | 290 | 268 | 43.1 |
| Cs | 0.18 | 0.14 | 0.08 | 0.62 | 0.46 | 0.16 | 1.56 | 6.41 | 0.75 | 3.38 | 0.61 | 1.23 | 6.08 | 2.92 | 1.70 | 3.86 | 7.88 | 20.7 | 1.36 | 0.6 |
| Ba | 925 | 183 | 322 | 1688 | 1387 | 622 | 1390 | 1190 | 1640 | 1083 | 703 | 226 | 438 | 1710 | 1220 | 1220 | 1970 | 1980 | 1760 | 291 |
| La | 64.1 | 114 | 82.2 | 80.3 | 63.3 | 62.7 | 85.1 | 125 | 55.8 | 92.5 | 99 | 44.1 | 38.4 | 55.4 | 76.4 | 80.6 | 71.5 | 72.9 | 70.2 | 53.6 |
| Ce | 114 | 197 | 148 | 145 | 120 | 110 | 151 | 212 | 105 | 169 | 179 | 113 | 68.5 | 93.7 | 140 | 140 | 126 | 124 | 121 | 87.8 |
| Pr | 12.8 | 21.8 | 15.9 | 17.4 | 13.1 | 13.2 | 17.2 | 22.3 | 11.7 | 20.9 | 21.8 | 9.68 | 8.01 | 10.7 | 15.9 | 15.3 | 14.0 | 14.1 | 13.6 | 9.66 |
| Nd | 46.4 | 82.7 | 59.2 | 69.1 | 50.6 | 51.6 | 65.0 | 83.9 | 45.4 | 85.3 | 89.1 | 34.8 | 31.3 | 40.9 | 61.3 | 56.2 | 54.1 | 55.2 | 51.3 | 33.5 |
| Sm | 10.2 | 16.2 | 10.7 | 13.6 | 8.88 | 9.50 | 11.8 | 15.7 | 8.7 | 17.1 | 16.6 | 7.05 | 6.64 | 7.25 | 11.3 | 9.64 | 9.66 | 9.79 | 9.00 | 5.86 |
| Eu | 0.42 | 1.91 | 1.23 | 2.36 | 1.30 | 1.60 | 2.48 | 2.16 | 1.15 | 3.04 | 2.4 | 0.53 | 1.02 | 1.50 | 2.10 | 1.48 | 2.17 | 2.19 | 1.84 | 0.57 |
| Gd | 8.91 | 15.9 | 10.2 | 12.4 | 8.47 | 7.96 | 13.4 | 16.2 | 7.83 | 16.2 | 15 | 7.44 | 7.18 | 7.08 | 11.4 | 9.77 | 9.86 | 9.76 | 9.05 | 5.98 |
| Tb | 1.42 | 2.39 | 1.46 | 2.29 | 1.25 | 1.21 | 1.78 | 2.56 | 1.13 | 3.46 | 2.96 | 1.08 | 1.6 | 0.83 | 1.43 | 1.21 | 1.17 | 1.18 | 1.09 | 0.82 |
| Dy | 9.07 | 15.0 | 9.09 | 14.4 | 8.24 | 7.56 | 11.7 | 17.1 | 6.97 | 25 | 21.3 | 7.39 | 13.8 | 4.90 | 8.66 | 7.57 | 7.15 | 7.26 | 6.58 | 5.59 |
| Ho | 1.78 | 2.87 | 1.81 | 3.02 | 1.67 | 1.58 | 2.44 | 3.52 | 1.47 | 5.74 | 4.82 | 1.55 | 3.62 | 0.96 | 1.70 | 1.54 | 1.41 | 1.44 | 1.32 | 1.20 |
| Er | 5.61 | 8.42 | 5.47 | 9.63 | 5.42 | 5.19 | 7.96 | 11.4 | 4.68 | 19.8 | 15.5 | 5.23 | 13.1 | 3.06 | 5.30 | 5.03 | 4.53 | 4.58 | 4.22 | 4.18 |
| Tm | 0.76 | 1.09 | 0.74 | 1.31 | 0.77 | 0.72 | 1.10 | 1.59 | 0.67 | 2.99 | 2.14 | 0.78 | 2.01 | 0.40 | 0.69 | 0.68 | 0.59 | 0.60 | 0.56 | 0.63 |
| Yb | 5.14 | 7.16 | 5.22 | 9.50 | 5.37 | 5.02 | 7.87 | 10.8 | 4.77 | 23.2 | 15.1 | 5.8 | 15 | 2.84 | 4.70 | 4.80 | 4.08 | 4.16 | 3.89 | 4.72 |
| Lu | 0.75 | 0.97 | 0.81 | 1.36 | 0.80 | 0.74 | 1.16 | 1.56 | 0.74 | 3.41 | 2.16 | 0.85 | 2.22 | 0.43 | 0.66 | 0.71 | 0.60 | 0.61 | 0.57 | 0.71 |
| Hf | 9.52 | 7.48 | 12.1 | 14.2 | 8.9 | 6.51 | 8.01 | 12.0 | 9.6 | 11.7 | 12.9 | 5.5 | 6.2 | 3.12 | 4.00 | 5.30 | 4.35 | 4.48 | 4.63 | 4.81 |
| Ta | 1.51 | 1.02 | 0.93 | 1.86 | 0.95 | 0.91 | 1.31 | 1.93 | 0.79 | 2.24 | 1.87 | 1.52 | 1.34 | 0.64 | 1.28 | 1.17 | 0.89 | 0.89 | 0.91 | 1.46 |
| W | 0.37 | 0.24 | 0.48 | 0.89 | 0.82 | 14.2 | 7.77 | 0.60 | 0.74 | 373 | 511 | 10.9 | 423 | 0.48 | 10.8 | 13.0 | 8.26 | 6.13 | 9.68 | 9.9 |
| Pb | 10.1 | 5.42 | 4.95 | 9.03 | 18.7 | 7.56 | 19.8 | 29.8 | 7.44 | 6.37 | 10.1 | 25 | 7.57 | 18.6 | 20.9 | 26.0 | 25.5 | 22.1 | 16.6 | 23.8 |
| Th | 19.1 | 14.3 | 15.4 | 27.3 | 14.4 | 9.14 | 8.64 | 34.4 | 10.4 | 24.2 | 34.5 | 25.2 | 12.2 | 9.40 | 15.3 | 21.3 | 13.7 | 13.1 | 14.7 | 29.6 |
| U | 5.33 | 1.37 | 2.82 | 7.80 | 2.23 | 1.98 | 1.94 | 8.40 | 2.44 | 3.99 | 7.71 | 4.16 | 2.94 | 2.71 | 2.96 | 2.50 | 3.02 | 2.79 | 3.79 | 5.89 |

Table 6. Suite

| Unit | FFG undiff | FFG undiff | FFG undiff | FFG undiff | FFG undiff | FFG undiff | FFG undiff | FFG undiff | Khoabendus | Khoabendus | FFG undiff | FFG undiff | FFG undiff | FFG undiff | FFG undiff | FFG undiff | FFG undiff | FFG undiff | FFG undiff | FFG undiff | FFG undiff |
|---|---|---|---|---|---|---|---|---|---|---|---|---|---|---|---|---|---|---|---|---|---|
| Sample ID | JM01-CC10 | JM01-CC11 | JM01-CC12 | JM01-CC16 | JM01-CC18 | TBE1 | TBE3 | TBE4 | ETM5 | ETM8 | Franzfontein I | Cypress | Schönau | Schönau | Schönau | Kranzpoort | Persephone | Dante | Franzfontein II | Beatrice | Eduardsfelde |
| **Major elements [%]** | | | | | | | | | | | | | | | | | | | | | |
| SiO2 | 68.9 | 67.1 | 70.8 | 73.1 | 75.2 | 69.4 | 70.7 | 66.4 | 80.5 | 73.9 | 74.0 | 69.7 | 68.9 | 73.6 | 75.4 | 66.1 | 69.3 | 73.9 | 73.3 | 68.6 | 78.8 |
| TiO2 | 0.49 | 0.44 | 0.37 | 0.36 | 0.19 | 0.27 | 0.36 | 0.59 | 0.24 | 0.34 | 0.27 | 0.68 | 0.67 | 0.33 | 0.27 | 0.69 | 0.47 | 0.33 | 0.32 | 0.49 | 0.29 |
| Al2O3 | 15.2 | 15.6 | 14.8 | 13.2 | 12.8 | 12.8 | 12.8 | 13.3 | 7.7 | 12.5 | 12.7 | 14.2 | 15.4 | 14.2 | 13.2 | 14.6 | 14.6 | 13.9 | 13.2 | 15.0 | 10.8 |
| Fe2O3 | 3.21 | 3.27 | 2.45 | 1.87 | 1.48 | 1.84 | 1.61 | 3.43 | 0.18 | 1.8 | 2.66 | 3.26 | 2.77 | 1.37 | 1.3 | 4.78 | 3.29 | 1.11 | 3.41 | 3.06 | 1.22 |
| MnO | 0.07 | 0.06 | 0.05 | 0.03 | 0.03 | 0.08 | 0.1 | 0.06 | 0.03 | 0.04 | 0.05 | 0.04 | 0.1 | 0.02 | 0.03 | 0.09 | 0.06 | 0.03 | 0.01 | 0.08 | 0.03 |
| MgO | 0.7 | 0.65 | 0.51 | 0.2 | 0.23 | 1.18 | 0.8 | 1.76 | 0.31 | 1.31 | 0.31 | 0.84 | 0.51 | | | 1.81 | 1.19 | 0.18 | 0 | 1.22 | 0.09 |
| CaO | 2.08 | 2.43 | 1.92 | 0.92 | 1.05 | 1.73 | 0.71 | 1.54 | 0.32 | 0.07 | 0.48 | 0.82 | 1.99 | 0.5 | 0.62 | 2.54 | 2.83 | 0.26 | 0.24 | 2.74 | 0.60 |
| Na2O | 3.93 | 3.74 | 3.94 | 3.30 | 3.37 | 4.11 | 4.13 | 5.24 | 1.85 | 0.89 | 3.67 | 4.10 | 4.50 | 3.14 | 3.15 | 3.25 | 3.33 | 4.05 | 3.46 | 4.41 | 2.94 |
| K2O | 5.33 | 5.70 | 4.95 | 6.08 | 4.65 | 4.22 | 4.73 | 3.74 | 3.91 | 4.57 | 5.09 | 5.30 | 4.42 | 6.35 | 5.50 | 4.71 | 4.40 | 5.93 | 5.67 | 3.60 | 5.20 |
| P2O5 | 0.13 | 0.13 | 0.09 | 0.06 | 0.04 | 0.11 | 0.06 | 0.2 | 0.05 | 0.03 | 0.05 | 0.27 | 0.18 | 0.07 | 0.05 | 0.28 | 0.17 | 0.09 | 0.07 | 0.2 | 0.06 |
| Sum | 100.1 | 99.2 | 99.9 | 99.2 | 99.1 | 95.7 | 96.1 | 96.3 | 95.1 | 95.5 | 99.3 | 99.2 | 99.5 | 99.6 | 99.5 | 98.8 | 99.6 | 99.7 | 99.7 | 99.4 | 100.1 |
| **Trace elements [ppm]** | | | | | | | | | | | | | | | | | | | | | |
| Li | | | | | | | | | | | | | | | | | | | | | |
| Be | | | | | | | | | | | | | | | | | | | | | |
| Sc | 6.4 | 6.53 | 5.52 | 4.54 | 3.95 | | | | n.d | n.d | | | | | | | | | | | |
| V | 31.5 | 29.8 | 24.4 | 12.5 | 9.91 | 23 | 13 | 52 | 5 | 6 | | | | | | | | | | | |
| *Cr | | | | | | 6 | 7 | 13 | 9 | 7 | | | | | | | | | | | |
| Co | 9.52 | 10.8 | 8.61 | 10.6 | 10 | 118 | 154 | 162 | 113 | 41 | | | | | | | | | | | |
| Ni | 6.39 | 6.93 | 4.8 | | | 20 | 16 | 21 | 26 | 11 | | | | | | | | | | | |
| Y | 4.09 | 4.47 | 3.31 | 2.94 | 2.52 | 15 | 32 | 35 | 21 | 34 | | | | | | | | | | | |
| Zr | 33.7 | 25.3 | 22.6 | 25.4 | 11 | 107 | 206 | 255 | 125 | 275 | | | | | | | | | | | |
| Nb | 274.6 | 281 | 217 | 302 | 94.9 | 4 | 10 | 11 | 3 | 13 | | | | | | | | | | | |
| Rb | 16.3 | 13.5 | 13.2 | 27.5 | 9.2 | 179 | 163 | 114 | 44 | 178 | | | | | | | | | | | |
| Sr | 160 | 176 | 139 | 184 | 156 | 228 | 178 | 165 | 48 | 10 | | | | | | | | | | | |
| Cs | 237 | 280 | 222 | 60.1 | 137 | | | | | | | | | | | | | | | | |
| Ba | | | | | | | | | | | | | | | | | | | | | |
| La | | | | | | | | | | | | | | | | | | | | | |
| Ce | | | | | | | | | | | | | | | | | | | | | |
| Pr | | | | | | | | | | | | | | | | | | | | | |
| Nd | | | | | | | | | | | | | | | | | | | | | |
| Sm | | | | | | | | | | | | | | | | | | | | | |
| Eu | | | | | | | | | | | | | | | | | | | | | |
| Gd | | | | | | | | | | | | | | | | | | | | | |
| Tb | | | | | | | | | | | | | | | | | | | | | |
| Dy | | | | | | | | | | | | | | | | | | | | | |
| Ho | | | | | | | | | | | | | | | | | | | | | |
| Er | | | | | | | | | | | | | | | | | | | | | |
| Tm | | | | | | | | | | | | | | | | | | | | | |
| Yb | | | | | | | | | | | | | | | | | | | | | |
| Lu | 3.29 | 2.73 | 2.54 | 2.81 | 1.2 | | | | | | | | | | | | | | | | |
| Hf | | | | | | | | | | | | | | | | | | | | | |
| Ta | | | | | | 0.03 | 0.68 | 0.52 | | | | | | | | | | | | | |
| W | 1.02 | 0.78 | 0.87 | 1.66 | 0.63 | | | | | | | | | | | | | | | | |
| Pb | | | | | | 26 | 22 | 10 | 85 | 2 | | | | | | | | | | | |
| Th | 24.2 | 29.2 | 11.2 | 16.2 | 19.6 | 32 | 27 | 33 | 28 | 8 | | | | | | | | | | | |
| U | 18.4 | 15.6 | 17.1 | 21.2 | 8.8 | | | | | | | | | | | | | | | | |

***Geochemical classification***

The Q'/ANOR diagram classifies the HMC and FFG igneous rocks as monzogranite, syenogranite and alkali feldspar granite, however HMC samples are marked by higher normative quartz (Fig. 40a). One sample of the HMC (out of six) plots in the granodiorite field close to the boundary with the monzogranite field.

A/CNK values < 1.1 define for most samples a meta- or peraluminous composition (Fig. 40b), whereas ratios of Fe, Mg and Si yield Cordilleran granite signatures typical of I-type igneous rocks evolving in an active continental margin setting (Fig. 41a). Samples of the HMC display higher $FeO_T/(FeO_T + MgO)$ ratios, which can be explained by the higher amount of residual plagioclase and amphibole (Kleinhanns *et al*. 2015). In the AFM diagram (Irvine &

Baragar, 1971), the rocks follow the calc-alkaline trend (Fig. 41b) and tectonic discrimination diagrams (Batchelor & Bowden 1985; Maniar & Piccoli 1989, not shown) indicate late- to post-orogenic settings or evolution in an active continental margin setting (Barbarin, 1999).

***REE-normalised and trace element multi-element diagrams (spidergrams)***

Trace element patterns display subduction zone signatures, which are, however, more pronounced in the FFG samples (Fig. 42). Higher LILE/HFSE ratios in the FFG probably reflect their higher degree of fractionation.

Higher $SiO_2$, lower MgO and pronounced negative Sr-anomalies in the HMC red orthogneiss (3 samples) are attributed to magmatic fractionation. Trace element signatures are similar to those of the other felsic HMC and FFG igneous rocks but enrichment in Zr, Hf and HREE results in lower LILE/HFSE ratios.

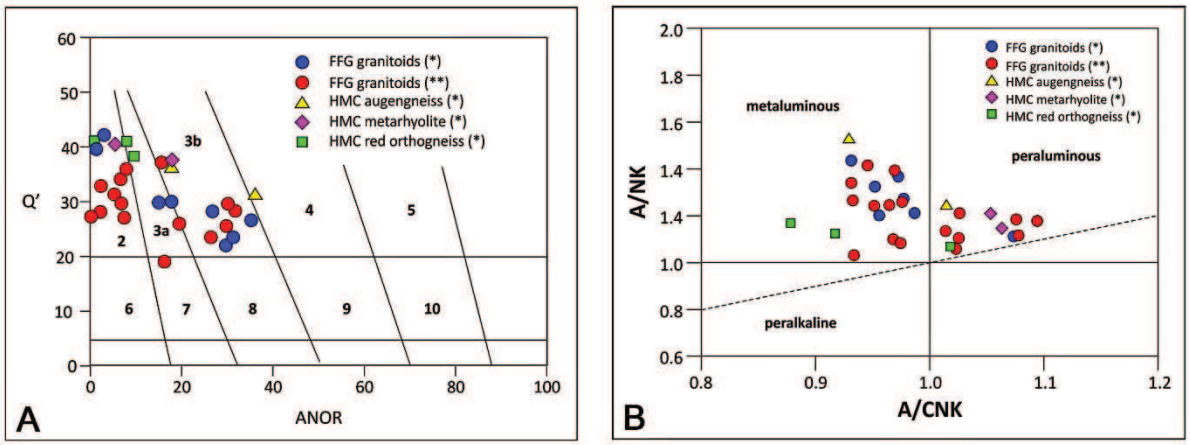


**Figure 40.** A) Classification of FFG and HMC samples based on normative mineral abundance (from Kleinhanns *et al*. 2015, calculated with the MesoNorm using the Geochemical DataKit of Janousek *et al*. (2006) and plotted in the Q-ANOR diagram of Streckeisen & Le Maître (1979)); Q′ ¼ Quartz/(Quartz + Orthoclase + Albite + Anorthite) and ANOR ¼ 100* Anorthite/(Orthoclase + Anorthite)). (*) = Kleinhanns *et al*. 2015; (**) =. Clifford *et al*. 1969; Muvangua, 2006. Fields: 2 = alkali feldspar granite; 3a = syenogranite; 3b = monzogranite; 4 = granodiorite; 5 = tonalite; 6 = qtz-alkalisyenite; 7 = qtz-syenite; 8 = qtz-monzonite; 9 = qtz-monzodiorite; 10 = qtz-diorite; B**)** A/NK vs. A/CNK diagram illustrating the aluminium saturation (Shand index)

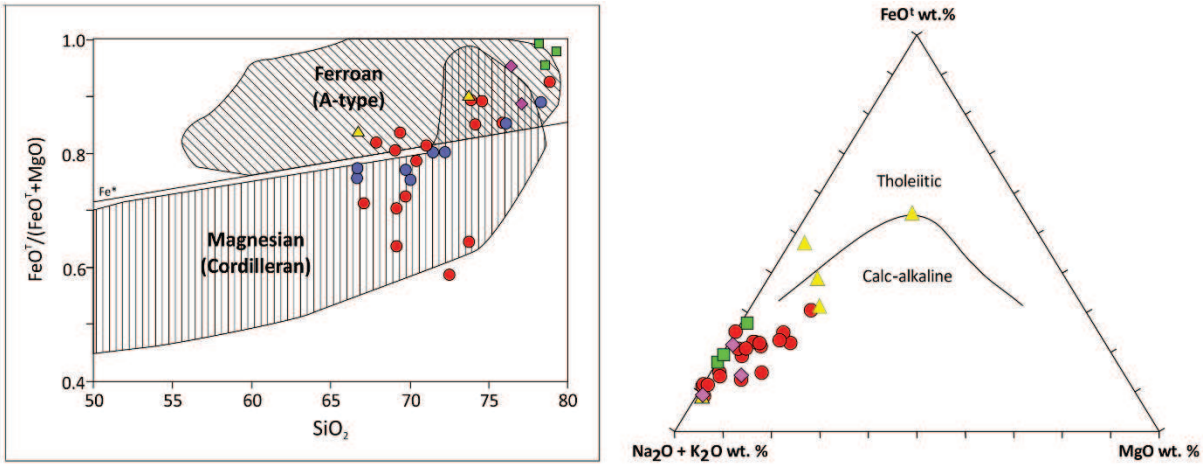


**Figure 41**. A) $FeO^T/(FeO^T + MgO)$ vs. $SiO_2$ discrimination diagram (Frost *et al*. 2001); B) AFM diagram.

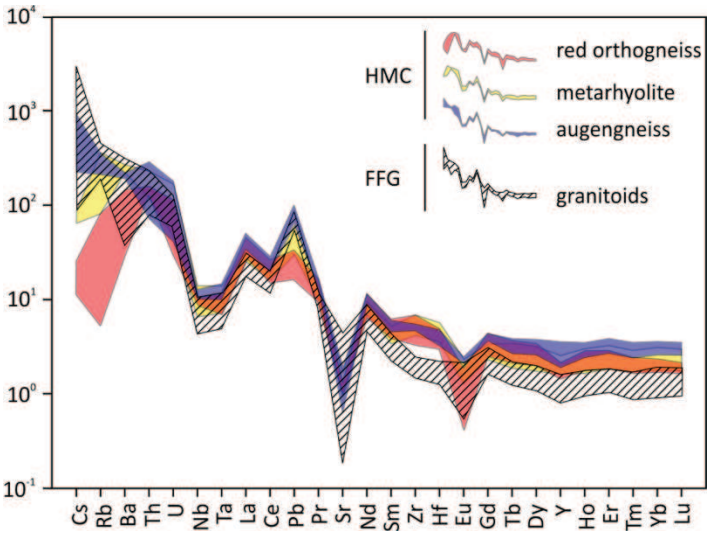


**Figure 42**. N-MORB normalised spider diagram of sample groups from the HMC and FFG.

***Sm-Nd (Rb-Sr) isotope systematics.***

$T_{DM}$ ages (using the model of Nägler & Kramers (1998) and λ [$^{147}$Sm] of $6.5\times10^{-12}$ $a^{-1}$) vary from 2.3-2.7 Ga for FFG rocks (7/8 data) and from 2.1-2.2 Ga for HMC gneisses (4 data), respectively. The generally older model ages of the FFG are interpreted to result from mixing of juvenile 1.85 Ga subduction magma with Palaeoproterozoic country rock during ascent into the upper crust whereas mid-crustal HMC orthogneisses were less affected by this mechanism. This is also reflected by the significantly lower $\varepsilon Nd_{1.85\ Ga}$ values in the FFG (-6.2 to -2.2; 7/8 data) compared to the HMC (-0.9 to 0.1; 4 data).

$T_{DM}$ ages of the red orthogneiss vary from 2.0-2.4 Ga and $\varepsilon Nd_{1.85\ Ga}$ values from -2.1-2.6 Ga. Two samples from a regional sheet-like intrusion of Kaross type granite yielded low $T_{DM}$ ages of 2.0 Ga and high $\varepsilon(Nd)_{1.85Ga}$ values of 2.3 and 2.6 Ga classifying them as juvenile A-type granitoids evolving in a subduction setting. Sample 210900-2 from (mylonitic) sill granite, dated by U-Pb single zircon method at 1829 Ma, yields a $T_{DM}$ age of 2.43 Ga and $\varepsilon(Nd)_{1.85\ Ga}$ value of -2.3, similar to the values of the other FFG and HMC granitoids.

**Table 7.** Rb-Sr isotope data of FFG Suite granites and HMC orthogneiss.

| Sample | Domain | Unit | Rb [µg/g] | Sr [µg/g] | $^{87}Rb/^{86}Sr$ | 87Sr/86Sr [fc] | $^{87}Sr/^{86}Sr$(@t1) | $T_{DM}$ [Ga] Sr | [t1] |
|---|---|---|---|---|---|---|---|---|---|
| 210900-2 | HMC | 1 | 37,5 | 78,9 | 1,37 | 0.73661 ± 71 | 0,70114 | 1,76 | 1829 |
| 220802-12 | | 1 | 9,58 | 111 | 0,25 | 0.72073 ± 2 | 0,71431 | 5,46 | 1830 |
| 220802-13 | | 1 | 2,79 | 85,0 | 0,09 | 0.71348 ± 2 | 0,71103 | 9,94 | 1830 |
| 110503-1 | | 1 | 76,6 | 73,7 | 2,99 | 0.77041 ± 3 | 0,69295 | 1,59 | 1830 |
| 090606-5 | | 2 | 112 | 167 | 1,93 | 0.75461 ± 3 | 0,70470 | 1,90 | 1830 |
| HU-03 | | 2 | 176 | 62,4 | 8,12 | 0.95424 ± 4 | 0,74404 | 2,16 | 1841 |
| 090606-1 | | 3 | 16,5 | 211 | 0,22 | 0.71249 ± 2 | 0,70667 | 3,38 | 1830 |
| 130503-1 | | 4 | na | na | na | na | | nd | 1831 |
| 270802-1 | | 5 | 165 | 73,6 | 6,45 | 0.86226 ± 3 | 0,69532 | 1,17 | |
| 280802-2 | KF | 5 | 43,0 | 136 | 0,91 | 0.72798 ± 2 | 0,70436 | 1,99 | 1830 |
| 081203-2 | FFG | 6 | 102 | 342 | 0,86 | 0.72653 ± 2 | 0,70417 | 1,98 | 1879 |
| 280205-6 | | 7 | 121 | 281 | 1,24 | 0.73651 ± 3 | 0,70433 | 1,93 | 1841 |
| 280205-7 | | 7 | 109 | 264 | 1,19 | 0.73920 ± 3 | 0,70837 | 2,18 | 1830 |
| 260205-4 | | 8 | 182 | 191 | 2,74 | 0.77454 ± 4 | 0,70355 | 1,84 | 1826 |
| 280205-3 | | 9 | 140 | 382 | 1,05 | 0.73047 ± 3 | 0,70318 | 1,88 | 1830 |
| 170405-6 | | 9 | 161 | 44,1 | 10,5 | 0.95277 ± 3 | 0,68067 | 1,66 | 1831 |
| 151104-1 | | 10 | 167 | 154 | 3,11 | 0.78755 ± 3 | 0,70706 | 1,91 | 1830 |

**Units:** (1) red orthogneiss; (2) granodioritic gneiss; (3) injection melt in amphibolite; (4) feldspar porphyry; (5) rhyolite (6) undifferentiated FFG; (7) Franken granodiorite; (8) Kamdescha granite; (9) Kaross granite; (10) Oortrek granite

**Table 8**. Sm-Nd isotope data of FFG Suite granites and HMC orthogneiss. Ages marked in red: emplacement age determined by U-Pb single zircon age dating (see below); * model age by using Nägler & Kramers (1998); + model age by using Goldstein *et al*. (1984).

| Sample | Domain | Unit | Sm (ppm) | Nd (ppm) | $^{147}Sm/^{144}Nd$ | $^{143}Nd/^{144}Nd$ | ±2σ abs | $T_{DM+}$ [Ga] | $T_{DM*}$ [Ga] | ε(t=0) | ε(t1) | t1 [Ma] |
|---|---|---|---|---|---|---|---|---|---|---|---|---|
| 210900-2 | HMC | 1 | 9.12 | 41.0 | 0.1344886 | 0.51177 | 2.3E-05 | 2.63 | 2.43 | -16.9 | -2.3 | 1829 |
| 220802-12 | | 1 | 13.5 | 69.6 | 0.1168240 | 0.51178 | 2.4E-05 | 2.14 | 2.00 | -16.7 | 2.1 | 1830 |
| 220802-13 | | 1 | 9.13 | 52.2 | 0.1056511 | 0.51166 | 2.4E-05 | 2.09 | 1.97 | -19.1 | 2.3 | 1830 |
| 110503-1 | | 1 | 9.59 | 51.3 | 0.1130616 | 0.51167 | 5.4E-06 | 2.23 | 2.09 | -18.9 | 0.7 | 1830 |
| 090606-5 | | 2 | 10.5 | 60.0 | 0.1062474 | 0.51149 | 8.8E-06 | 2.35 | 2.21 | -22.4 | -1.2 | 1830 |
| HU-03 | | 2 | 16.2 | 86.4 | 0.1133417 | 0.51161 | 2.3E-05 | 2.32 | 2.17 | -20.0 | -0.3 | 1841 |
| 090606-1 | | 3 | 9.53 | 51.6 | 0.1116400 | 0.51171 | 1.2E-05 | 2.14 | 2.00 | -18.0 | 1.9 | 1830 |
| 130503-1 | | 4 | 15.6 | 74.6 | 0.1265224 | 0.51190 | 1.1E-05 | 2.18 | 2.02 | -14.4 | 2.1 | 1831 |
| 270802-1 | | 5 | *not analysed* | | | | | | | | | |
| 280802-2 | KF | 5 | 8.41 | 46.6 | 0.1090450 | 0.51158 | 1.6E-05 | 2.28 | 2.14 | -20.7 | -0.1 | 1830 |
| 081203-2 | FFG | 6 | 7.44 | 43.0 | 0.1046851 | 0.51137 | 6.2E-06 | 2.48 | 2.34 | -24.8 | -2.6 | 1879 |
| 280205-6 | | 7 | 8.79 | 51.1 | 0.1040265 | 0.51139 | 6.3E-06 | 2.43 | 2.29 | -24.3 | -2.4 | 1841 |
| 280205-7 | | 7 | 8.22 | 48.4 | 0.1026719 | 0.51138 | 9.5E-06 | 2.42 | 2.28 | -24.5 | -2.5 | 1830 |
| 260205-4 | | 8 | 8.94 | 53.3 | 0.1013232 | 0.51135 | 9.6E-06 | 2.43 | 2.29 | -25.1 | -2.7 | 1826 |
| 280205-3 | | 9 | 8.98 | 49.1 | 0.1105776 | 0.51166 | 5.4E-04 | 2.19 | 2.05 | -19.0 | 1.2 | 1830 |
| 170405-6 | | 9 | 5.31 | 31.0 | 0.1034639 | 0.51139 | 7.2E-06 | 2.43 | 2.29 | -24.4 | -2.5 | 1831 |
| 151104-1 | | 10 | 10.4 | 59.0 | 0.1070523 | 0.51126 | 8.5E-06 | 2.69 | 2.54 | -26.9 | -5.9 | 1830 |

**Units**: (1) red orthogneiss; (2) granodioritic gneiss; (3) injection melt in amphibolite; (4) feldspar porphyry; (5) rhyolite (6) undifferentiated FFG; (7) Franken granodiorite; (8) Kamdescha granite; (9) Kaross granite; (10) Oortrek granite

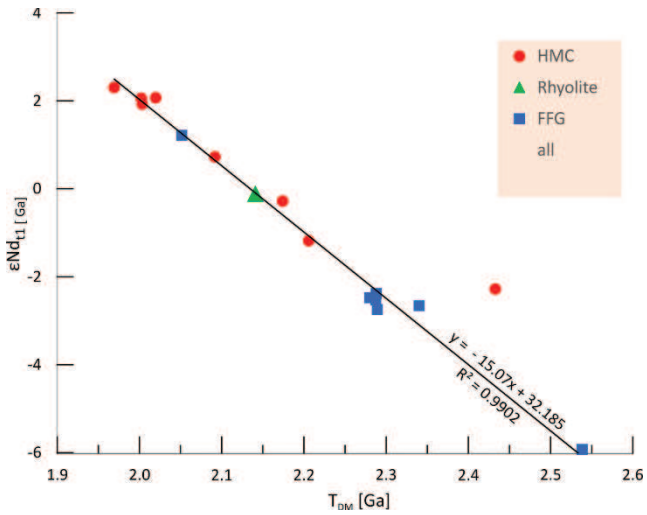


**Figure 43**. In the $\varepsilon Nd_{(1.85\ Ga)}$ vs. $T_{DM}$ diagram the felsic magmatic rocks of the HMC and FFG show a negative correlation of the two variables. Samples of the HMC are marked by younger $T_{DM}$ ages and higher $\varepsilon Nd_{t1\ Ga}$ values demonstrating their more juvenile character. Where available, t1 (the emplacement age) is taken from U-Pb zircon age dating and elsewhere set at 1.83 Ga (the average age of the FFG). Increasing model age and negative epsilon values in the FFG are attributed to assimilation of country rock of Archaean to Palaeoproterozoic provenance.

**Mafic and intermediate rocks ($SiO_2$ <60%)**

Mafic magmatism predates emplacement of the FFG Suite, which is almost void of any cross-cutting dykes. Field observation shows that most of the mafic magmas in the HMC form dykes or sills a few metres thick, which are transposed into the main gneissic fabric. A volcanic origin is suspected in a few places where thin layers of amphibolite alternate at regular intervals with felsic gneisses, possibly constituting a bimodal volcanic sequence. Few amygdaloidal metabasalts were observed in the upper sequence of the Suiderkruis SD and one flow was mapped in the Khoabendus Group.

The dykes/sills are affected by regional deformation and metamorphism ranging from greenschist facies conditions in the area north of Ehobib SD to probably higher amphibolite facies in the Rooikop/Lofdal SD resulting locally in incipient anataxis of the amphibolites. Only rocks without migmatitic textures were sampled for whole rock analysis.

31 samples were taken from the Rooikop/Lofdal (6), Aandgloed (7), Suiderkruis (14), and the area north of the Ehobib (4) subdomains (Fig. 44). In the Suiderkruis SD, 12 out of 14 samples were taken from a small mafic/ultramafic layered complex (UMC) that laterally grades into massive amphibolite layers of several tens of km in length. The geochemical compositions of the analysed samples are given in Table 9.

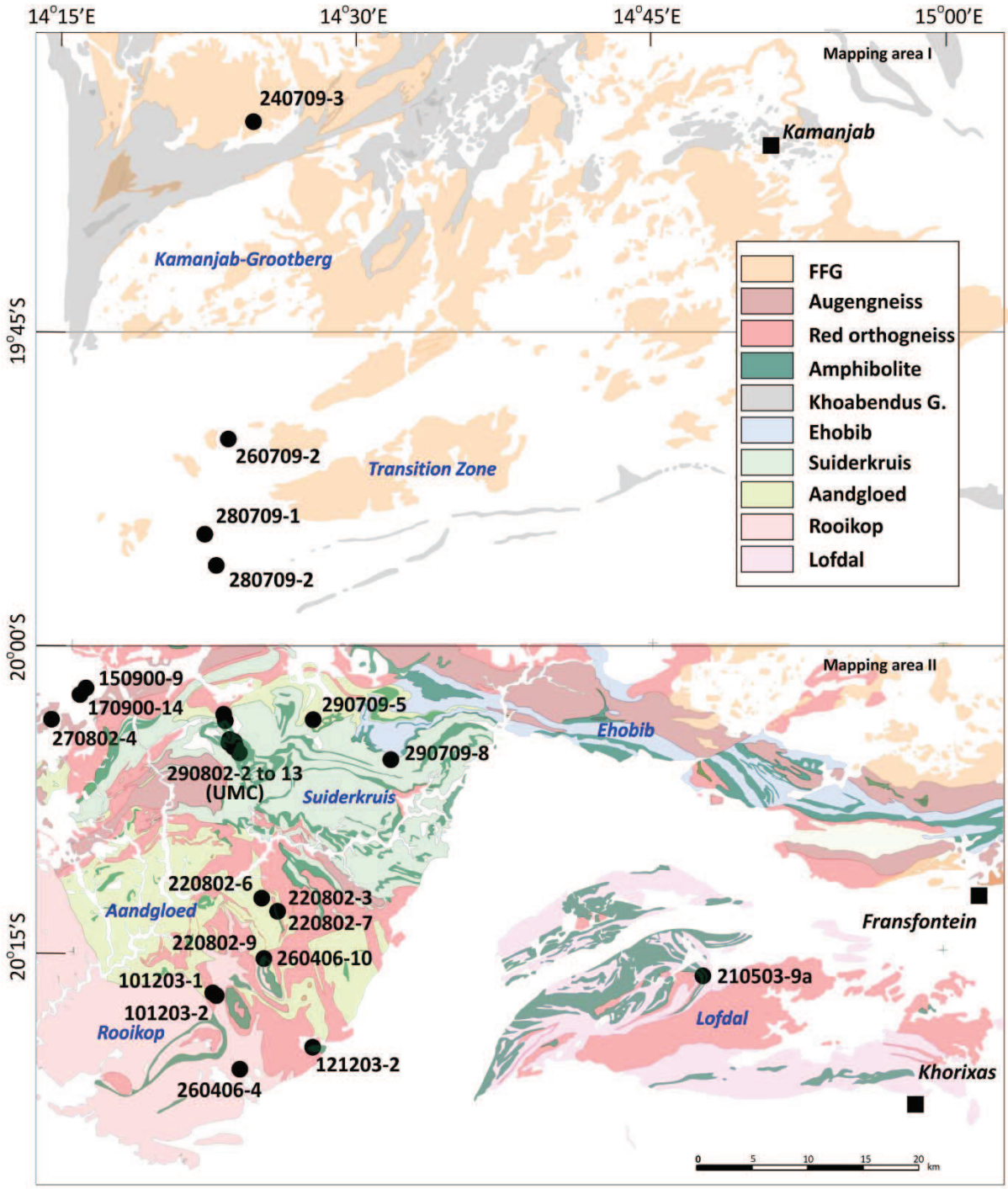


**Figure 44**. Sample positions of mafic rocks for whole rock geochemistry and Sm-Nd isotope analysis.

**Table 9** (part 1). Whole rock geochemistry data of mafic rocks from HMC and KF.

| Unit | Ehobib + TZ | Ehobib + TZ | Ehobib + TZ | Ehobib + TZ | Suiderkruis | Suiderkruis | Suiderkruis | Suiderkruis | Suiderkruis | Suiderkruis | Suiderkruis | Suiderkruis | Suiderkruis | Suiderkruis | Suiderkruis | Suiderkruis | Suiderkruis | Suiderkruis |
|---|---|---|---|---|---|---|---|---|---|---|---|---|---|---|---|---|---|---|
| **Sample ID** | 240709-3 | 260709-2 | 280709-1 | 280709-2 | 270802-4 | 290709-8 | 290802-1 | 290802-10 | 290802-11 | 290802-12 | 290802-13 | 290802-2 | 290802-3 | 290802-4 | 290802-5 | 290802-6 | 290802-7 | 290802-9 |
| **Major element [wt.%]** | | | | | | | | | | | | | | | | | | |
| $SiO_2$ | 52,0 | 45,3 | 50,3 | 47,9 | 45,7 | 52,0 | 51,1 | 55,4 | 47,6 | 47,8 | 47,6 | 46,4 | 57,1 | 46,1 | 46,1 | 48,8 | 42,6 | 49,7 |
| $TiO_2$ | 0,81 | 1,65 | 0,88 | 2,07 | 2,19 | 2,47 | 2,07 | 0,53 | 1,18 | 1,35 | 0,91 | 1,51 | 1,66 | 1,91 | 1,97 | 0,79 | 0,41 | 0,80 |
| $Al_2O_3$ | 16,1 | 15,9 | 14,7 | 12,3 | 14,8 | 13,2 | 15,7 | 21,7 | 14,6 | 16,8 | 13,4 | 18,5 | 14,7 | 16,8 | 16,2 | 10,3 | 5,78 | 13,6 |
| $Fe_2O_3$ | 9,73 | 13,8 | 11,2 | 16,1 | 14,8 | 13,6 | 13,2 | 4,43 | 14,8 | 13,9 | 11,2 | 12,2 | 9,73 | 13,7 | 14,7 | 9,47 | 12,5 | 11,3 |
| MnO | 0,20 | 0,18 | 0,20 | 0,23 | 0,21 | 0,75 | 0,26 | 0,07 | 0,38 | 0,36 | 0,18 | 0,23 | 0,14 | 0,24 | 0,22 | 0,16 | 0,15 | 0,18 |
| MgO | 7,11 | 7,41 | 7,28 | 5,56 | 7,54 | 2,85 | 3,92 | 2,08 | 9,58 | 7,62 | 10,8 | 4,98 | 2,39 | 6,77 | 7,09 | 12,7 | 23,17 | 9,07 |
| CaO | 7,11 | 8,09 | 8,97 | 8,73 | 10,1 | 7,46 | 7,96 | 6,93 | 11,2 | 11,8 | 12,4 | 11,1 | 6,61 | 9,48 | 9,42 | 14,3 | 8,49 | 12,7 |
| $Na_2O$ | 4,37 | 2,12 | 3,49 | 2,37 | 1,90 | 2,88 | 3,93 | 5,01 | 1,36 | 1,60 | 1,66 | 2,72 | 6,76 | 2,92 | 2,34 | 1,46 | 0,42 | 1,23 |
| $K_2O$ | 0,85 | 1,05 | 0,93 | 0,71 | 0,31 | 0,78 | 0,47 | 0,89 | 0,27 | 0,13 | 0,38 | 0,74 | 0,23 | 0,34 | 0,34 | 0,40 | 0,12 | 0,32 |
| $P_2O_5$ | 0,10 | 0,19 | 0,12 | 0,32 | 0,24 | 0,62 | 0,22 | 0,17 | 0,11 | 0,14 | 0,07 | 0,17 | 0,17 | 0,21 | 0,22 | 0,08 | 0,05 | 0,04 |
| LOI | | | | | 0,62 | | 0,93 | | | 0,68 | | 0,09 | 0,98 | 0,96 | 0,69 | 5,19 | 0,38 | |
| Sum | 98,3 | 95,7 | 98,1 | 96,3 | 97,9 | 96,5 | 98,8 | 97,2 | 101,1 | 101,6 | 98,6 | 98,5 | 99,5 | 98,4 | 98,5 | 98,5 | 93,7 | 98,9 |
| **Trace elements [ppm]** | | | | | | | | | | | | | | | | | | |
| Li | 15,8 | 13,5 | 8,98 | 7,19 | 6,37 | 9,72 | 9,67 | 8,06 | 2,57 | 2,38 | 2,67 | 8,16 | 3,92 | 12,9 | 13,8 | 6,31 | 1,41 | 5,04 |
| Be | | | | | 0,92 | | 2,27 | 1,49 | 0,69 | 0,63 | 0,34 | 1,03 | 1,28 | 1,71 | 0,69 | 0,37 | 0,11 | 0,84 |
| Sc | | | | | 33,5 | | 48,9 | 7,76 | 36,7 | 32,3 | 45,4 | 24,6 | 26,3 | 27,6 | 28,4 | 63,5 | 36,2 | 45,5 |
| V | | | | | 206 | | 318 | 121 | 274 | 297 | 239 | 274 | 267 | 264 | 267 | 261 | 157 | 243 |
| Co | | | | | 55,1 | | 44,2 | 14,7 | 46,9 | 45,2 | 50,4 | 42,0 | 31,4 | 51,7 | 53,1 | 46,2 | 80,7 | 45,9 |
| Ni | 135 | 187 | 92,2 | 151 | 153 | 127 | 34,3 | 17,6 | 83,8 | 52,3 | 127 | 62,9 | 37,7 | 89,1 | 85,1 | 153 | 501 | 79,0 |
| Y | 17,3 | 21,7 | 16,6 | 31,5 | 31,2 | 59,8 | 39,7 | 10,6 | 18,2 | 14,4 | 16,1 | 21,4 | 29,3 | 22,0 | 22,5 | 11,9 | 6,03 | 22,4 |
| Zr | 38,6 | 57,2 | 43,3 | 126 | 160 | 300 | 216 | 26,4 | 42,4 | 32,4 | 35,6 | 35,6 | 80,0 | 44,3 | 44,5 | 37,2 | 18,5 | 35,4 |
| Nb | 2,78 | 5,95 | 2,21 | 6,06 | 12,2 | 24,6 | 13,3 | 3,55 | 2,77 | 2,16 | 2,40 | 5,69 | 8,43 | 5,97 | 6,23 | 1,52 | 0,79 | 3,16 |
| Rb | 41,9 | 64,7 | 62,4 | 25,6 | 15,1 | 31,5 | 9,4 | 34,6 | 3,37 | 1,91 | 4,96 | 25,8 | 1,23 | 11,0 | 9,67 | 8,95 | 2,40 | 14,0 |
| Sr | 428 | 343 | 355 | 363 | 174 | 205 | 401 | 673 | 324 | 435 | 269 | 254 | 189 | 225 | 249 | 230 | 51,0 | 307 |
| Cs | 1,28 | 0,66 | 0,31 | 0,44 | 1,06 | 3,11 | 18,27 | 0,50 | 4,31 | 3,86 | 0,45 | 0,53 | 0,03 | 0,15 | 4,22 | 0,46 | 0,10 | 1,93 |
| Ba | 118 | 318 | 364 | 457 | 84,9 | 509 | 459 | 596 | 148 | 85,8 | 154 | 188 | 41,5 | 359 | 738 | 202 | 162 | 181 |
| La | 11,2 | 12,6 | 11,1 | 26,8 | 15,4 | 66,4 | 35,4 | 17,2 | 10,2 | 8,53 | 7,77 | 15,3 | 27,5 | 11,5 | 11,9 | 7,97 | 3,45 | 11,1 |
| Ce | 20,4 | 24,9 | 20,5 | 50,0 | 31,1 | 122 | 67,5 | 27,7 | 21,3 | 17,0 | 14,4 | 29,4 | 48,4 | 25,6 | 27,9 | 14,3 | 6,39 | 22,8 |
| Pr | 2,64 | 3,44 | 2,70 | 6,62 | 4,41 | 16,1 | 7,89 | 3,04 | 3,08 | 2,40 | 1,94 | 3,84 | 6,34 | 3,47 | 3,63 | 1,93 | 0,89 | 3,35 |
| Nd | 12,3 | 16,6 | 12,3 | 30,1 | 21,0 | 70,1 | 34,4 | 12,1 | 14,9 | 11,6 | 9,72 | 17,2 | 28,0 | 17,2 | 17,9 | 9,20 | 4,34 | 16,3 |
| Sm | 2,97 | 4,28 | 2,95 | 6,93 | 5,34 | 15,6 | 7,64 | 2,22 | 3,90 | 3,08 | 2,72 | 4,09 | 6,42 | 4,93 | 5,09 | 2,42 | 1,17 | 4,41 |
| Eu | 1,21 | 1,66 | 1,20 | 2,27 | 1,75 | 3,40 | 2,3 | 1,58 | 1,33 | 1,30 | 1,03 | 1,32 | 1,81 | 1,78 | 1,79 | 0,89 | 0,40 | 1,22 |
| Gd | 3,09 | 4,43 | 3,07 | 7,09 | 6,42 | 15,1 | 7,72 | 1,96 | 5,00 | 3,91 | 3,71 | 4,07 | 7,91 | 6,61 | 6,92 | 3,15 | 1,57 | 5,66 |
| Tb | 0,59 | 0,82 | 0,57 | 1,29 | 1,01 | 2,63 | 1,25 | 0,28 | 0,70 | 0,55 | 0,54 | 0,67 | 1,08 | 0,95 | 0,99 | 0,44 | 0,23 | 0,83 |
| Dy | 3,83 | 5,22 | 3,75 | 8,10 | 6,45 | 15,4 | 7,93 | 1,70 | 4,50 | 3,63 | 3,68 | 4,11 | 6,99 | 6,12 | 6,43 | 2,88 | 1,49 | 5,57 |
| Ho | 0,74 | 1,02 | 0,75 | 1,63 | 1,27 | 3,00 | 1,54 | 0,34 | 0,90 | 0,73 | 0,75 | 0,81 | 1,39 | 1,21 | 1,27 | 0,58 | 0,30 | 1,12 |
| Er | 2,24 | 3,00 | 2,34 | 4,96 | 3,75 | 8,98 | 4,71 | 1,05 | 2,69 | 2,18 | 2,26 | 2,41 | 4,22 | 3,52 | 3,69 | 1,72 | 0,87 | 3,41 |
| Tm | 0,29 | 0,40 | 0,31 | 0,65 | 0,49 | 1,15 | 0,62 | 0,13 | 0,35 | 0,29 | 0,30 | 0,31 | 0,57 | 0,46 | 0,49 | 0,23 | 0,11 | 0,46 |
| Yb | 1,87 | 2,57 | 2,15 | 4,53 | 3,23 | 7,81 | 4,18 | 0,95 | 2,42 | 1,97 | 2,08 | 2,07 | 3,85 | 3,12 | 3,32 | 1,51 | 0,78 | 3,26 |
| Lu | 0,26 | 0,38 | 0,31 | 0,65 | 0,46 | 1,11 | 0,59 | 0,14 | 0,35 | 0,29 | 0,30 | 0,29 | 0,55 | 0,44 | 0,47 | 0,22 | 0,11 | 0,46 |
| Hf | 1,11 | 1,59 | 1,20 | 3,40 | 4,20 | 7,76 | 5,73 | 0,77 | 1,44 | 1,08 | 1,28 | 1,14 | 2,32 | 1,25 | 1,17 | 1,26 | 0,56 | 1,26 |
| Ta | 0,13 | 0,33 | 0,11 | 0,29 | 0,75 | 1,37 | 0,78 | 0,27 | 0,17 | 0,14 | 0,17 | 0,37 | 0,52 | 0,36 | 0,37 | 0,09 | 0,05 | 0,21 |
| W | 0,23 | 0,38 | 0,35 | 0,46 | 0,71 | 1,05 | 0,30 | 1,22 | 1,65 | 0,49 | 0,07 | 0,66 | 0,58 | 0,24 | 0,75 | 0,10 | 0,07 | 0,35 |
| Pb | 39,8 | 17,3 | 11,4 | 9,96 | 2,49 | 1320 | 10,6 | 7,99 | 2,47 | 1,88 | 2,07 | 10,2 | 5,90 | 7,80 | 6,02 | 2,74 | 3,02 | 3,00 |
| Th | 1,06 | 0,79 | 1,19 | 2,17 | 1,52 | 11,1 | 7,41 | 1,57 | 0,49 | 0,52 | 0,43 | 2,25 | 5,06 | 0,87 | 0,89 | 0,51 | 0,39 | 1,46 |
| U | 0,21 | 0,28 | 0,23 | 0,55 | 0,39 | 2,66 | 0,88 | 0,40 | 0,17 | 0,16 | 0,15 | 0,54 | 1,03 | 0,16 | 0,18 | 0,18 | 0,12 | 0,43 |

**Table 9** (part 2). Whole rock geochemistry data of mafic rocks from HMC and KF.

| Unit | Aandgloed-N | Aandgloed-N | Aandgloed-S | Aandgloed-N | Aandgloed-S | Aandgloed-S | Aandgloed-S | Rooikop | Rooikop | Rooikop | Rooikop | Rooikop | Rooikop |
|---|---|---|---|---|---|---|---|---|---|---|---|---|---|
| **Sample ID** | 150900-9 | 170900-14 | 200900-1 | 220802-6 | 220802-7 | 220802-9 | 290709-5 | 101203-2 | 121203-2 | 210503-9a | 260406-10 | 260406-12 | 260406-4 |
| **Major element [wt.%]** | | | | | | | | | | | | | |
| $SiO_2$ | 46,8 | 59,3 | 59,3 | 48,5 | 50,2 | 49,4 | 50,7 | 48,2 | 43,1 | 50,0 | 49,2 | 46,9 | 51,5 |
| $TiO_2$ | 2,05 | 1,61 | 0,66 | 1,66 | 1,30 | 1,33 | 1,98 | 2,41 | 0,91 | 1,50 | 1,64 | 1,82 | 1,91 |
| $Al_2O_3$ | 15,6 | 10,1 | 22,3 | 14,8 | 15,4 | 14,9 | 13,2 | 15,8 | 18,4 | 14,1 | 15,7 | 15,0 | 13,3 |
| $Fe_2O_3$ | 15,2 | 14,3 | 6,30 | 14,9 | 12,9 | 14,4 | 15,6 | 15,2 | 14,5 | 12,0 | 13,9 | 16,3 | 15,8 |
| MnO | 0,30 | 0,11 | 0,10 | 0,24 | 0,21 | 0,23 | 0,15 | 0,24 | 0,30 | 0,13 | 0,14 | 0,27 | 0,23 |
| MgO | 6,37 | 0,07 | 1,49 | 6,38 | 6,16 | 6,17 | 4,82 | 4,34 | 8,90 | 7,16 | 6,78 | 6,26 | 5,72 |
| CaO | 9,24 | 12,1 | 0,49 | 8,98 | 8,44 | 7,53 | 7,73 | 8,02 | 9,27 | 11,7 | 9,20 | 8,75 | 8,98 |
| $Na_2O$ | 2,12 | 0,04 | 0,74 | 2,44 | 3,25 | 3,24 | 4,34 | 2,26 | 1,94 | 2,49 | 1,85 | 2,32 | 0,97 |
| $K_2O$ | 0,23 | 0,01 | 5,09 | 0,51 | 0,47 | 0,72 | 0,24 | 0,32 | 0,14 | 0,25 | 0,38 | 0,43 | 0,54 |
| $P_2O_5$ | 0,27 | 0,31 | 0,16 | 0,28 | 0,14 | 0,15 | 0,36 | 0,55 | 0,14 | 0,24 | 0,48 | 0,44 | 0,23 |
| LOI | 1,48 | | | 0,82 | 1,37 | | | | | | | | |
| Sum | 98,2 | 97,9 | 96,6 | 98,7 | 98,5 | 98,1 | 99,1 | 97,3 | 97,6 | 99,6 | 99,3 | 98,5 | 99,2 |
| **Trace elements [ppm]** | | | | | | | | | | | | | |
| Li | 28,3 | 0,80 | 22,6 | 8,75 | 8,39 | 11,1 | 3,10 | 16,2 | 30,2 | 7,14 | 12,2 | 13,3 | 15,2 |
| Be | 1,14 | 0,51 | 2,92 | 1,03 | 0,99 | 1,43 | | 1,10 | 0,78 | 1,09 | 1,16 | 1,12 | 1,16 |
| Sc | 27,5 | 25,9 | 15,8 | 33,3 | 40,3 | 61,3 | | 42,3 | 37,8 | 50,8 | 29,3 | 34,6 | 42,6 |
| V | 295 | 273 | 110 | 315 | 330 | 281 | | 102 | 290 | 330 | 132 | 198 | 204 |
| Co | 53,9 | 11,2 | 43,3 | 48,1 | 42,1 | 38,1 | | 43,0 | 65,8 | 59,1 | 71,8 | 57,6 | 66,6 |
| Ni | 99,2 | 20,1 | 33,6 | 83,1 | 63,4 | 48,3 | 133 | 16,9 | 112 | 45,0 | 76,4 | 36,5 | 31,1 |
| Y | 25,8 | 31,8 | 27,3 | 32,2 | 29,1 | 31,7 | 34,3 | 49,3 | 18,8 | 27,5 | 41,0 | 38,6 | 45,4 |
| Zr | 37,0 | 53,0 | 160 | 43,9 | 91,0 | 104 | 127 | 125 | 22,7 | 31,8 | 90,5 | 92,3 | 65,2 |
| Nb | 6,50 | 6,30 | 14,0 | 6,67 | 5,28 | 5,50 | 7,57 | 18,6 | 1,89 | 7,39 | 9,31 | 8,26 | 9,15 |
| Rb | 4,81 | 0,34 | 182 | 7,27 | 7,12 | 17,8 | 3,86 | 8,69 | 3,65 | 4,23 | 12,9 | 8,39 | 9,95 |
| Sr | 263 | 1030 | 193 | 97,0 | 149 | 323 | 335 | 245 | 262 | 256 | 248 | 302 | 92,8 |
| Cs | 0,37 | 0,56 | 1,97 | 0,13 | 0,14 | 0,39 | 0,08 | 0,23 | 0,44 | 0,12 | 5,64 | 0,23 | 0,53 |
| Ba | 156 | 28,4 | 1060 | 196 | 256 | 333 | 95,1 | 108 | 57,6 | 46,7 | 292 | 242 | 106 |
| La | 18,9 | 28,2 | 52,4 | 21,4 | 17,1 | 14,4 | 26,8 | 42,5 | 6,78 | 16,7 | 31,7 | 21,6 | 25,3 |
| Ce | 36,4 | 49,8 | 65,1 | 39,8 | 32,3 | 28,7 | 50,5 | 79,3 | 11,8 | 34,1 | 58,1 | 42,4 | 47,5 |
| Pr | 5,30 | 6,41 | 9,26 | 5,37 | 4,18 | 3,86 | 6,77 | 10,6 | 1,68 | 4,66 | 7,63 | 5,55 | 6,34 |
| Nd | 25,3 | 28,5 | 34,3 | 23,9 | 18,7 | 18,5 | 30,5 | 48,6 | 7,89 | 20,4 | 33,9 | 25,3 | 29,0 |
| Sm | 6,29 | 6,74 | 5,93 | 5,38 | 4,51 | 4,77 | 7,10 | 12,2 | 2,22 | 4,58 | 7,43 | 5,84 | 7,09 |
| Eu | 2,16 | 2,11 | 1,15 | 1,64 | 1,39 | 1,61 | 2,03 | 3,44 | 0,82 | 1,28 | 2,20 | 2,05 | 2,09 |
| Gd | 7,95 | 8,77 | 4,85 | 5,15 | 4,51 | 5,44 | 7,34 | 12,8 | 2,44 | 4,26 | 7,60 | 6,74 | 7,82 |
| Tb | 1,13 | 1,25 | 0,74 | 0,86 | 0,76 | 0,92 | 1,38 | 1,88 | 0,46 | 0,70 | 1,20 | 1,08 | 1,31 |
| Dy | 7,31 | 8,31 | 4,52 | 5,49 | 4,86 | 6,15 | 8,65 | 11,1 | 3,09 | 4,43 | 7,58 | 7,08 | 8,58 |
| Ho | 1,44 | 1,68 | 0,92 | 1,11 | 0,99 | 1,21 | 1,74 | 2,09 | 0,65 | 0,92 | 1,56 | 1,48 | 1,75 |
| Er | 4,24 | 4,97 | 3,01 | 3,37 | 2,98 | 3,68 | 5,39 | 6,03 | 1,97 | 2,83 | 4,67 | 4,51 | 5,19 |
| Tm | 0,55 | 0,65 | 0,42 | 0,44 | 0,40 | 0,50 | 0,73 | 0,80 | 0,26 | 0,39 | 0,62 | 0,61 | 0,69 |
| Yb | 3,72 | 4,42 | 2,91 | 3,00 | 2,65 | 3,34 | 4,95 | 5,38 | 1,79 | 2,71 | 4,22 | 4,09 | 4,66 |
| Lu | 0,52 | 0,62 | 0,42 | 0,42 | 0,38 | 0,47 | 0,73 | 0,79 | 0,26 | 0,40 | 0,62 | 0,60 | 0,67 |
| Hf | 0,89 | 1,75 | 4,80 | 1,38 | 2,61 | 2,87 | 3,49 | 3,70 | 0,87 | 1,09 | 2,50 | 2,42 | 2,24 |
| Ta | 0,40 | 0,40 | 1,27 | 0,39 | 0,35 | 0,29 | 0,44 | 1,40 | 0,15 | 0,45 | 0,53 | 0,47 | 0,49 |
| W | 0,26 | 0,68 | 325 | 0,57 | 0,62 | 0,48 | 0,62 | 58,9 | 93,8 | 225 | 140 | 154 | 133 |
| Pb | 21,1 | 16,8 | 22,3 | 5,51 | 7,33 | 6,91 | 2,72 | 12,0 | 52,5 | 1,42 | 7,00 | 11,9 | 5,94 |
| Th | 0,98 | 3,27 | 17,5 | 1,28 | 2,10 | 2,59 | 4,50 | 7,79 | 0,61 | 0,92 | 3,75 | 2,05 | 3,62 |
| U | 0,25 | 0,75 | 3,75 | 0,28 | 0,55 | 0,57 | 1,10 | 2,85 | 0,19 | 0,63 | 0,65 | 0,50 | 1,07 |

***Geochemical classification***

Various diagrams based on ratios of two or more elements allow the classification of mafic igneous rocks geochemically.

In the Q'/ANOR classification, samples of the Ehobib Domain plot in the diorite and quartz diorite fields, samples of the Aandgloed Domain mainly in the quartz-gabbro fields, and samples of the Suiderkruis and Rooikop domains in the gabbro and quartz-gabbro fields. This documents only slight fractionation from lower crustal stockworks (i.e. Rooikop-Aandgloed-Suiderkruis) to upper levels represented by the Ehobib Domain.

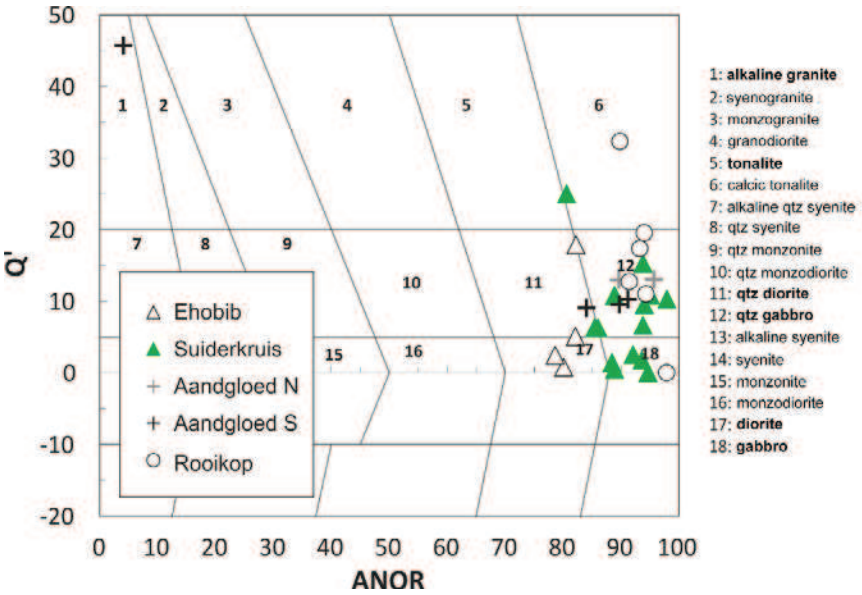


**Figure 45**. Classification of the samples is based on normative mineral abundance (calculated with the MesoNorm using the Geochemical DataKit of Janousek *et al*. (2006) and plotted in the Q-ANOR diagram of Streckeisen & Le Maître (1979)); Q′= ¼ Quartz/(Quartz + Orthoclase + Albite + Anorthite) and ANOR ¼ 100* Anorthite/(Orthoclase + Anorthite).

In the TAS diagram, the samples plot mostly in the alkaline and subalkaline basalt fields. A few samples with higher SiO2 and alkali elements plot in the basaltic trachy-andesite, trachyandesite and andesite fields and two samples with lower $SiO_2$ values in the picrobasalt field (Fig. 46). Of these, sample 290802-7 classifies as ultramafic rock, marked by low $SiO_2$ (42.6%), and elevated MgO (23.2 %), Ni (501 ppm) and Cr (4898 ppm). The diagram does not discriminate amphibolites from the various domains.

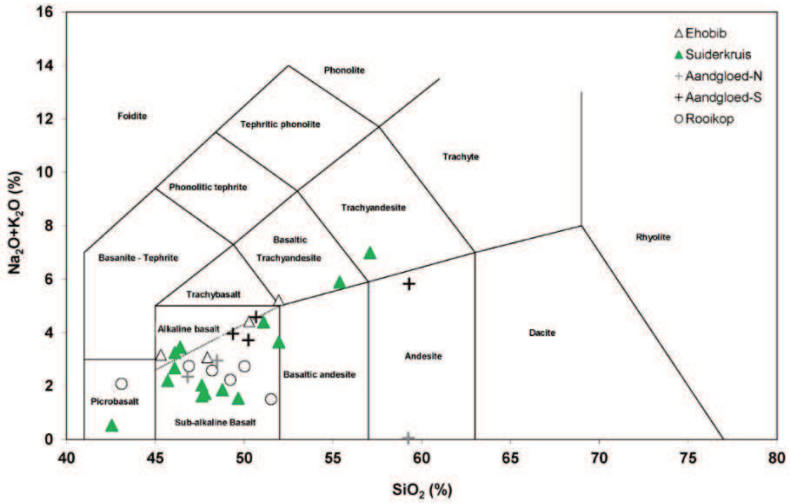


**Figure 46.** Classification of amphibolite in the In the TAS diagram; most samples plot in the subalkaline and alkaline basalt fields.

In classification diagrams of volcanic rocks by Winchester & Floyd (1977), low $Zr/TiO_2$ and Nb/Y ratios define most samples as subalkaline basalts and a few as andesitic basalt. Further distinction into tholeiitic or calc-alkaline series by trace element ratios and element concentrations (Pearce, 1996), yielded contradictory results. However, discrimination diagrams based on trace element ratios are less reliable due to generally higher relative analytical errors. In the Ce/Yb vs. Ta/Yb diagram, elevated Ce/Yb ratios classify all samples as calc-alkaline (Fig. 47a) whereas in the Zr vs Y diagram low Zr and Y concentrations define a mostly tholeiitic trend (Fig. 47c). In the latter, samples of the UMC are marked by low Zr and Y concentrations defining a tholeiitic trend, whereas samples of the Aandgloed and Rooikop SD plot at higher values in the continuation of this trend suggesting progressive fractionation of the same magma. In the Th/Yb vs. Ta/Yb and Th vs. Yb diagrams, the data of all subdomains are evenly distributed in the calc-alkaline and tholeiitic fields. The data set displays little variation in the Ta/Yb ratio but considerable changes in the Th/Yb ratio. In the $Al_2O_3$-FeO-MgO (AFM) ternary diagram the samples define a tholeiitic trend when assuming a $FeO/(FeO+Fe_2O_3)$ ratio of 0.85 (Fig. 48).

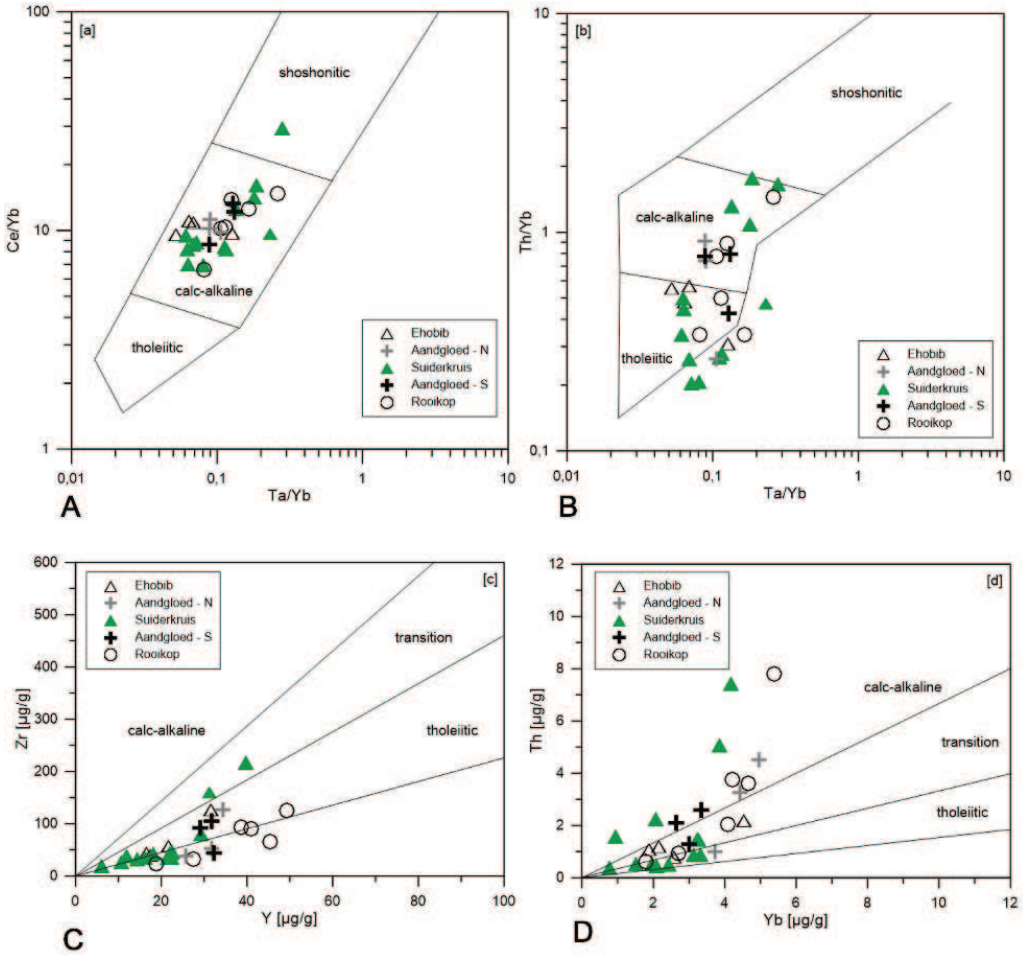


**Figure 47**. Classification diagrams used for discriminating calc-alkaline, transitional, tholeiitic, and shoshonitic trends (Pearce, 1996). A) Ce/Yb vs Ta/Yb; B) Th/Yb vsTa/Yb, C) Zr vs. Y; D) Th vs.Yb.

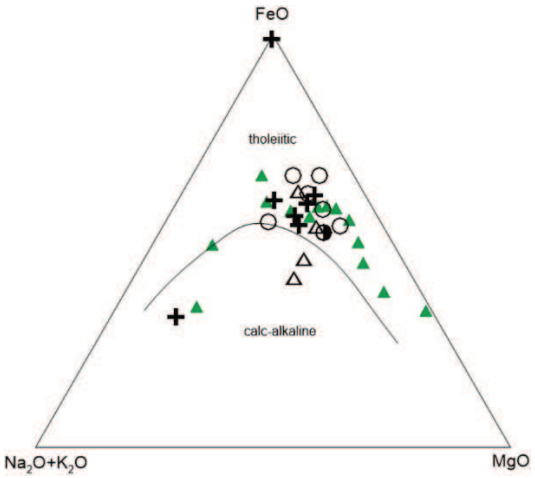


**Figure 48**. In the ternary $Al_2O_3$-FeO-MgO (AFM) diagram mafic samples lie on a tholeiitic trend.

***Plate tectonic setting***

Various major and trace element diagrams discriminate between plate tectonic settings under which modern (unmetamorphosed and unaltered) basalts evolved. Active continental margin (ACM) settings are commonly marked by low concentrations of incompatible elements, Nb/La ratios <0.5 and relatively steep REE pattern with $(La/Sm)_N$ >1. These features result from Nb fractionation into refractory phases (titanite, rutile) and the higher mobility of LREE relative to HREE during transports of fluids from the subducted plate into the overlying mantle wedge (Hawkesworth *et al*. 1993). The diagram Nb/La vs $(La/Sm)_N$ by John *et al*. (2003) shows that all samples of the HMC plot in the ACM field (Fig. 49a). Most of them display high Nb depletion being characteristic of subduction related magmas influenced by continental crust. In the Th-Hf/3-Ta ternary diagram (Wood 1980) high Th and low Ta, Hf values classify the mafic rocks as calc-alkaline basalt associated with active continental margin settings (Fig. 49b). None of diagrams discriminates individual domains of the HMC, however several samples of the UMC show a tendency towards island arc tholeiites.

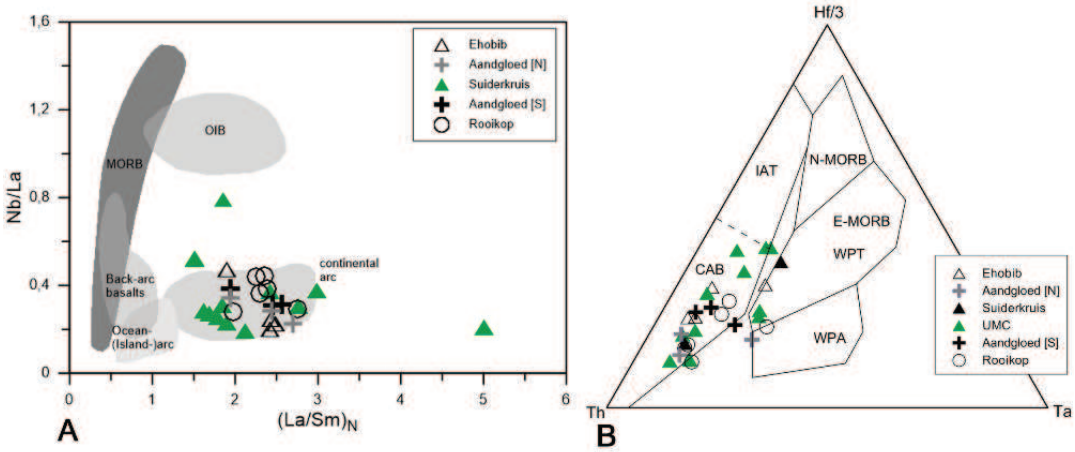


**Figure 49**. Two diagrams indicating plate tectonic settings under which the rocks evolved. A) Nb/La vs $(La/Sm)_N$ by John *et al*. (2003); B) Th-Hf/3-Ta ternary diagram by Wood (1980).

The M/Yb vs Ta/Yb ratios allow identification of mantle source(s) and evaluate the impact of crustal contamination on the magma composition (Pearce, 1982, Pearce & Peate, 1995, Pearce *et al*. 2004). Yb-normalised ratios reduce the effects of both fractional crystallisation and cumulate processes; they are useful for discriminating N-MORB (low Ta/Yb), E-MORB (medium Th/Yb) and OIB (WPB; high Th/Yb) mantle sources; M can be any incompatible element (here: Th, La). In both diagrams the samples plot above the E-MORB field, suggesting hydrothermally overprinted mantle sources above a subduction zone (i.e. predominantly E-MORB) influenced by crustal contamination (Fig. 50a-b).

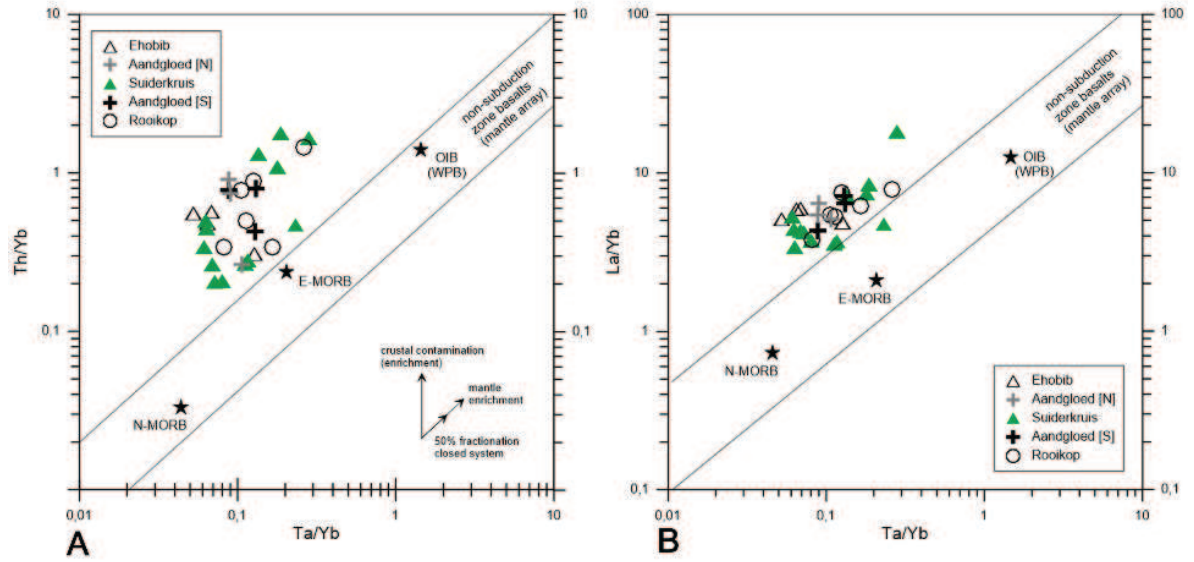


**Figure 50**. Th/Yb vs Ta/Yb and La/Yb vs Ta/Yb diagrams allow identification of the mantle source and possible crustal contamination of mafic magmas. Average composition of N-MORB, E-MORB and OIB are after Sun & McDonough, 1989.

***Normalised REE and trace element diagrams (spidergrams)***

Primitive mantle (PM)-normalised REE and E-MORB-normalised spidergrams of the mafic rocks are given in Fig. 51 for each subdomain of the HMC; the composition of N-MORB is shown for comparison in the multi-element diagrams (red squares). The diagrams demonstrate considerable REE enrichment relative to PM (5-65), some HREE fractionation ($Gd/Yb_N$ = 1.10-1.93) and LREE fractionation ($La/Sm_N$ = 1.47-4.87). Eu* anomalies vary from slightly negative to positive (Eu*/Eu = 0.75-2.25) with an average of 1. All these features typify calc-alkaline magmas.

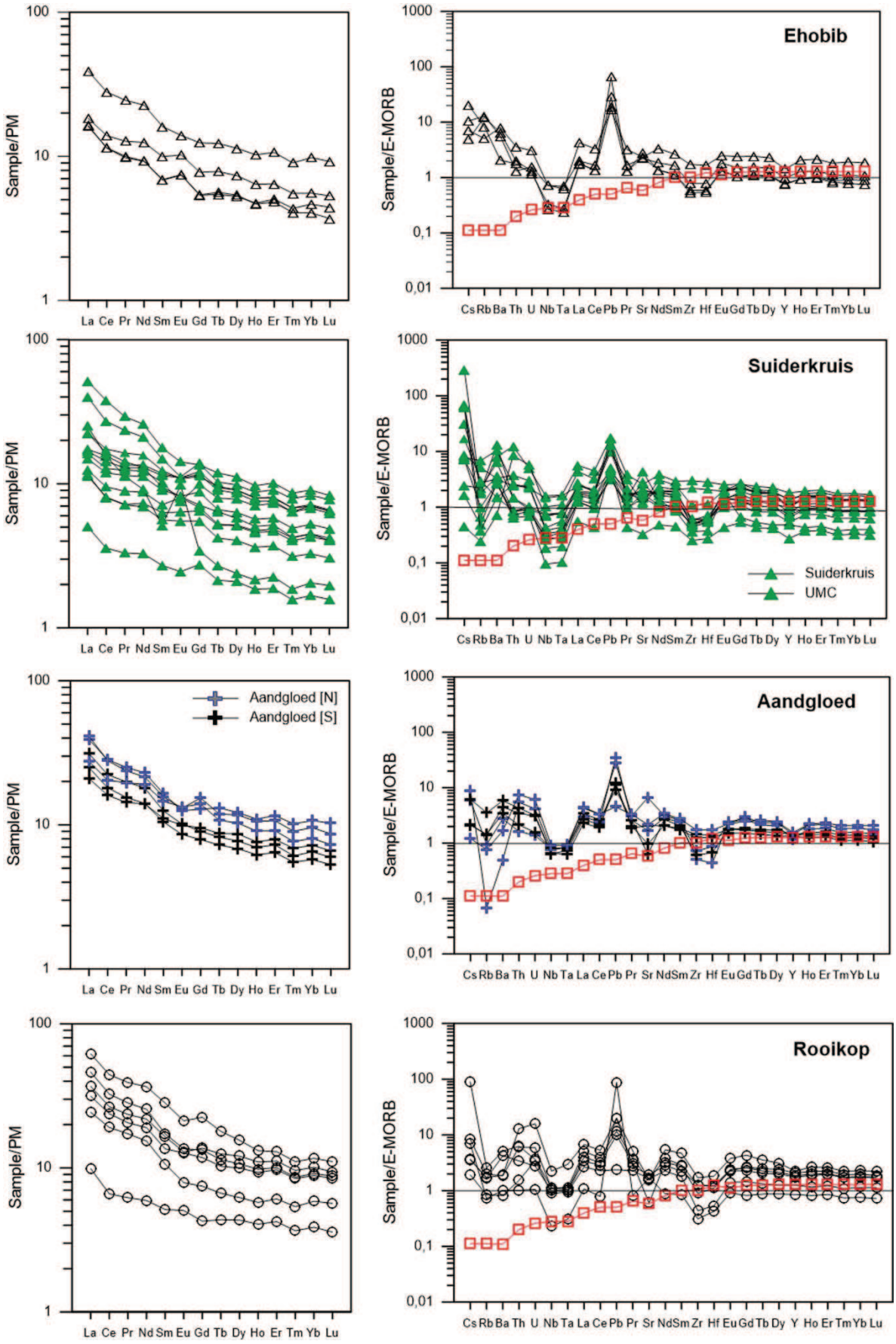


**Figure 51**. PM-normalised REE diagrams and E-MORB-normalised multi-trace-element diagrams. PM, N-MORB and E-MORB normalising factors are from Sun & McDonough (1989).

E-MORB normalised spidergrams generally show considerable enrichment of Large-ion-lithophile elements (LILE) by factors up to 300 in the left part of the abscissa (Cs-U). In combination with positive Pb-anomalies and negative Nb-Ta, Zr-Hf troughs this demonstrates crustal contamination and the influence of fluids on the magma composition. Spidergrams of samples from different domains resemble each other, however samples of the Suiderkruis SD are marked by the greatest enrichment in LILE, the lowest Pb-anomalies, and the most pronounced Nb-Ta troughs, indicating subduction derived magmas less contaminated by continental crust.

### *Sm-Nd (Rb-Sr) isotope systematics*

The results of Sm-Nd and Rb-Sr isotope analysis are given in Table 10 and Table 11. $T_{DM}$ ages were calculated using the algorithm by Nägler & Kramers (1998). Arrangement of samples in Table 10 with respect to subdomain (= crustal stock work) and $T_{DM}$ age shows the general increase of most $T_{DM}$ ages from the basal Rooikop ($T_{DM}$ 1.94-2.10 Ga) through the Aandgloed ($T_{DM}$ 1.99-2.38 Ga), and Suiderkruis ($T_{DM}$ 2.15-2.4 Ga) to the uppermost Ehobib ($T_{DM}$ 2.3-2.74 Ga) subdomains. This reflects increasing assimilation of (or contamination by) crustal host rocks during magma ascent. Assuming their common origin the age of 1.96 Ga provides the maximum emplacement age as the mafic magmas are probably derived from E-MORB yielding younger model ages. Samples 101203-2 and 260406-10 with the youngest $T_{DM}$ ages approximate the composition of their mantle source whereas $T_{DM}$ ages of ca 2.4 Ga are similar to those obtained for the granitoids and as such demonstrating the high influence of Palaeoproterozoic crust on these samples.

**Table 10.** Results of Sm-Nd isotope analyses determined on amphibolite samples of the HMC and Khoabendus Group.

| Domain | Sample ID | Rb [ppm] | Sr [ppm] | $^{87}Rb/^{86}Sr$ | $^{87}Sr/^{86}Sr$ | 2σ | $T_{[DM]}$ [Ga] | $^{87}Sr/^{86}Sr$ at 1.92 Ga |
|---|---|---|---|---|---|---|---|---|
| Ehobib | 010305-1 | 209.5 | 17 | 34.561 | 1.52541 | 0.000042 | 1.66 | 1.43105 |
| | 240709-3 | 33.5 | 359 | 0.269 | 0.71764 | 0.000023 | 4.19 | 0.71691 |
| | 260709-2 | 51.4 | 286 | 0.518 | 0.71345 | 0.000024 | 1.54 | 0.71204 |
| | 280709-1 | 48.4 | 291 | 0.479 | 0.71716 | 0.000029 | 2.22 | 0.71586 |
| | 280709-2 | 19.4 | 290 | 0.193 | 0.70819 | 0.000027 | 2.30 | 0.70766 |
| Suiderkruis | 270802-4 | 15.8 | 169 | 0.270 | 0.70719 | 0.000018 | 1.32 | 0.70645 |
| | 290802-1 | 7.8 | 260 | 0.086 | 0.71239 | 0.000024 | 10.1 | 0.71215 |
| | 290802-2 | 24.3 | 246 | 0.284 | 0.71396 | 0.000037 | 3.01 | 0.71318 |
| | 290802-3 | 1.1 | 184 | 0.018 | 0.70569 | 0.000025 | -100 | 0.70564 |
| | 290802-4 | 10.3 | 216 | 0.137 | 0.70721 | 0.000064 | 2.82 | 0.70683 |
| | 290802-5 | 9.0 | 249 | 0.103 | 0.70712 | 0.000008 | 3.88 | 0.70683 |
| | 290802-6 | 7.9 | 230 | 0.099 | 0.70551 | 0.000040 | 2.71 | 0.70524 |
| | 290802-7 | 2.3 | 53 | 0.125 | 0.70757 | 0.000024 | 3.37 | 0.70723 |
| | 290802-9 | 13.1 | 300 | 0.126 | 0.70627 | 0.000021 | 2.51 | 0.70593 |
| | 290802-10 | 33.9 | 683 | 0.143 | 0.70687 | 0.000040 | 2.50 | 0.70648 |
| | 290802-11 | 3.3 | 324 | 0.030 | 0.70354 | 0.000006 | 9.06 | 0.70346 |
| | 290802-12 | 1.8 | 421 | 0.012 | 0.70301 | 0.000025 | -3.76 | 0.70298 |
| | 290802-13 | 4.8 | 261 | 0.053 | 0.70410 | 0.000006 | 3.57 | 0.70396 |
| | 290709-8 | 21.1 | 156 | 0.390 | 0.72516 | 0.000015 | 4.21 | 0.72409 |
| Aandgloed | 150900-9 | 4.6 | 254 | 0.053 | 0.70875 | 0.000023 | 13.09 | 0.70860 |
| | 170900-14 | 0.4 | 1045 | 0.001 | 0.70425 | 0.000013 | -6.12 | 0.70425 |
| | 200900-1 | 182.3 | 201 | 2.611 | 0.76737 | 0.000009 | 1.74 | 0.76025 |
| | 220802-3 | 38.6 | 244 | 0.455 | 0.72035 | 0.000025 | 2.85 | 0.71910 |
| | 220802-6 | 7.9 | 88 | 0.517 | 0.71115 | 0.000004 | 1.22 | 0.70974 |
| | 220802-7 | 6.4 | 138 | 0.134 | 0.70842 | 0.000009 | 3.62 | 0.70805 |
| | 220802-9 | 14.7 | 212 | 0.199 | 0.71111 | 0.000073 | 3.35 | 0.71057 |
| | 260406-14 | 113.9 | 97 | 3.390 | 0.78487 | 0.000052 | 1.70 | 0.77561 |
| | 290709-5 | 2.9 | 264 | 0.031 | 0.70607 | 0.000020 | 22.50 | 0.70599 |
| | 290709-6 | na | na | na | na | na | na | na |
| Rooikop | 210503-9a | 4.0 | 254 | 0.045 | 0.70476 | 0.000814 | 6.50 | 0.70464 |
| | 101203-1 | 91.4 | 150 | 1.753 | 0.73946 | 0.000010 | 1.49 | 0.73467 |
| | 101203-2 | 7.9 | 212 | 0.108 | 0.71520 | 0.000006 | 9.70 | 0.71490 |
| | 101203-5 | 31.0 | 251 | 0.355 | 0.71991 | 0.000017 | 3.59 | 0.71894 |
| | 121203-2 | 3.4 | 256 | 0.038 | 0.71211 | 0.000840 | 32.58 | 0.712004 |
| | 260406-4 | 9.8 | 96 | 0.296 | 0.71760 | 0.000011 | 3.78 | 0.716792 |
| | 260406-10 | na | 236 | na | 0.70852 | 0.000006 | -22.50 | 0.708516 |
| | 260406-12 | 7.5 | 248 | 0.087 | 0.71071 | 0.000033 | 8.43 | 0.710478 |

The increasing influence of continental crust on mafic magma composition at higher crustal stockwork is confirmed by epsilon values calculated at time of their emplacement at 1.92 Ga. The $\varepsilon Nd_{(1.92\ Ga)}$ vs. $T_{DM}$ diagram shows high negative correlation between epsilon values and $T_{DM}$ age (Fig. 52). Higher positive values, characterising magmas little affected by lithospheric contamination, have been determined mainly in the Rooikop and Aandgloed subdomains. The Suiderkruis and Ehobib subdomains are characterised by systematically decreasing epsilon values and increasing $T_{DM}$ ages documenting the increase of assimilated country rock of Palaeo-proterozoic to Archaean provenance in higher crustal stockworks.

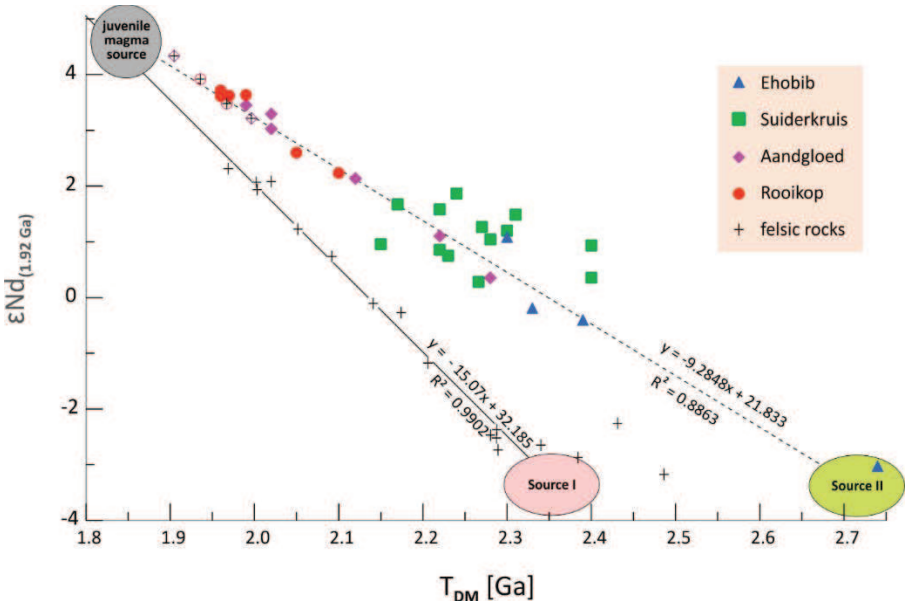


**Figure 52**. The $\varepsilon Nd_{(1.92\ Ga)}$ vs. $T_{DM}$ diagram illustrates the high negative correlation of the two parameters and increasing contamination of the mantle magmas during their ascent by two sources of country rock of Palaeoproterozoic and Neo-Archaean provenance.

Assuming a common mantle source for mafic and felsic magmas of the HMC and FFG the intersection of the two regression lines should yield the epsilon value and age of that source. The intercept age of 1.79 Ga approximates the emplacement age of the igneous rocks and therefore supports this hypothesis constraining a juvenile, depleted mantle source with an Nd-epsilon value of 25 (Fig. 52). The diagram further illustrates that the lithospheric components for mafic and felsic magmas differed considerably. Most felsic magmas lie on a mixing line between juvenile depleted mantle and a lithospheric crust of predominantly Palaeoproterozoic provenance (source I), whereas mafic magmas comprise a component of Archaean to Palaeoproterozoic provenance (source II). Unfortunately, no Sm-Nd isotope are presently available from paragneiss of the HMC, which is considered as possible Source II for the mafic rocks (as indicated by their increasing contamination in higher crustal stockworks).

Four samples of felsic rocks from the Aandgloed and Rooikop subdomains scatter around the trendline of mafic rocks suggesting that they possibly represent highly fractionated members of the mafic suite.

The same arrangement for Rb-Sr isotope analyses yielded meaningless $T_{DM}$ ages between -6.12 and 32.6 Ga demonstrating major disturbance of this system by subsequent metamorphism/hydrothermal alteration (Table 11). The increasing influence of assimilated crust in higher crustal strockworks is reflected by Rb concentrations, which increase from the basal Rooikop (3.41-9.83 ppm), through the Aandgloed (0.37-14.7 ppm), Suiderkruis (1.14-33.9 ppm) to the top Ehobib (19.4-51.4 ppm) subdomains. The system has not been consid-ered for further discussion.

**Table 11.** Results of Rb-Sr isotope analyses determined on amphibolite samples.

| Domain | Sample ID | Rb [ppm] | Sr [ppm] | $^{87}Rb/^{86}Sr$ | $^{87}Sr/^{86}Sr$ | 2σ | $T_{[DM]}$ [Ga] | $^{87}Sr/^{86}Sr$ at 1.92 Ga |
|---|---|---|---|---|---|---|---|---|
| Ehobib | 010305-1 | 209,5 | 17 | 34,561 | 1,52541 | 0,000042 | 1,66 | 1,43105 |
| | 240709-3 | 33,5 | 359 | 0,269 | 0,71764 | 0,000023 | 4,19 | 0,71691 |
| | 260709-2 | 51,4 | 286 | 0,518 | 0,71345 | 0,000024 | 1,54 | 0,71204 |
| | 280709-1 | 48,4 | 291 | 0,479 | 0,71716 | 0,000029 | 2,22 | 0,71586 |
| | 280709-2 | 19,4 | 290 | 0,193 | 0,70819 | 0,000027 | 2,30 | 0,70766 |
| Suiderkruis | 270802-4 | 15,8 | 169 | 0,270 | 0,70719 | 0,000018 | 1,32 | 0,70645 |
| | 290802-1 | 7,8 | 260 | 0,086 | 0,71239 | 0,000024 | 10,1 | 0,71215 |
| | 290802-2 | 24,3 | 246 | 0,284 | 0,71396 | 0,000037 | 3,01 | 0,71318 |
| | 290802-3 | 1,1 | 184 | 0,018 | 0,70569 | 0,000025 | -100 | 0,70564 |
| | 290802-4 | 10,3 | 216 | 0,137 | 0,70721 | 0,000064 | 2,82 | 0,70683 |
| | 290802-5 | 9,0 | 249 | 0,103 | 0,70712 | 0,000008 | 3,88 | 0,70683 |
| | 290802-6 | 7,9 | 230 | 0,099 | 0,70551 | 0,000040 | 2,71 | 0,70524 |
| | 290802-7 | 2,3 | 53 | 0,125 | 0,70757 | 0,000024 | 3,37 | 0,70723 |
| | 290802-9 | 13,1 | 300 | 0,126 | 0,70627 | 0,000021 | 2,51 | 0,70593 |
| | 290802-10 | 33,9 | 683 | 0,143 | 0,70687 | 0,000040 | 2,50 | 0,70648 |
| | 290802-11 | 3,3 | 324 | 0,030 | 0,70354 | 0,000006 | 9,06 | 0,70346 |
| | 290802-12 | 1,8 | 421 | 0,012 | 0,70301 | 0,000025 | -3,76 | 0,70298 |
| | 290802-13 | 4,8 | 261 | 0,053 | 0,70410 | 0,000006 | 3,57 | 0,70396 |
| | 290709-8 | 21,1 | 156 | 0,390 | 0,72516 | 0,000015 | 4,21 | 0,72409 |
| Aandgloed | 150900-9 | 4,6 | 254 | 0,053 | 0,70875 | 0,000023 | 13,09 | 0,70860 |
| | 170900-14 | 0,4 | 1045 | 0,001 | 0,70425 | 0,000013 | -6,12 | 0,70425 |
| | 200900-1 | 182,3 | 201 | 2,611 | 0,76737 | 0,000009 | 1,74 | 0,76025 |
| | 220802-3 | 38,6 | 244 | 0,455 | 0,72035 | 0,000025 | 2,85 | 0,71910 |
| | 220802-6 | 7,9 | 88 | 0,517 | 0,71115 | 0,000004 | 1,22 | 0,70974 |
| | 220802-7 | 6,4 | 138 | 0,134 | 0,70842 | 0,000009 | 3,62 | 0,70805 |
| | 220802-9 | 14,7 | 212 | 0,199 | 0,71111 | 0,000073 | 3,35 | 0,71057 |
| | 260406-14 | 113,9 | 97 | 3,390 | 0,78487 | 0,000052 | 1,70 | 0,77561 |
| | 290709-5 | 2,9 | 264 | 0,031 | 0,70607 | 0,000020 | 22,50 | 0,70599 |
| | 290709-6 | na | na | na | na | na | na | na |
| Rooikop | 210503-9a | 4,0 | 254 | 0,045 | 0,70476 | 0,000814 | 6,50 | 0,70464 |
| | 101203-1 | 91,4 | 150 | 1,753 | 0,73946 | 0,000010 | 1,49 | 0,73467 |
| | 101203-2 | 7,9 | 212 | 0,108 | 0,71520 | 0,000006 | 9,70 | 0,71490 |
| | 101203-5 | 31,0 | 251 | 0,355 | 0,71991 | 0,000017 | 3,59 | 0,71894 |
| | 121203-2 | 3,4 | 256 | 0,038 | 0,71211 | 0,000840 | 32,58 | 0,712004 |
| | 260406-4 | 9,8 | 96 | 0,296 | 0,71760 | 0,000011 | 3,78 | 0,716792 |
| | 260406-10 | na | 236 | na | 0,70852 | 0,000006 | -22,50 | 0,708516 |
| | 260406-12 | 7,5 | 248 | 0,087 | 0,71071 | 0,000033 | 8,43 | 0,710478 |

## Metamorphism

Field observations reveal subdivision of the HMC into the NE low-grade Ehobib, the central medium-grade Suiderkruis-Aandgloed and the southern medium to high-grade Rooikop-Lofdal subdomains. Ehobib SD is juxtaposed with underlying Suiderkruis gneisses along a folded crustal-scale shear zone and there is a significant jump in metamorphic conditions between the two subdomains. In contrast, M1 metamorphic conditions change from the Aandgloed into the Rooikop subdomains progressively to higher grades as shown by the increasing proportion of migmatite. Table 12 summarises the characteristic mineral parageneses and their host rocks in each subdomain. It shows that the same mineral associations occur in all subdomains except the Ehobib SD.

Emplacement of two regional non-migmatitic sheet-like intrusions (ROG, POGD) postdates the first regional metamorphic event described before. However, the granodioritic and granitic rocks are often mylonitic and refolded into the large scale folds that characterise the geological map of the HMC; the megasills represent marker horizons illustrating large scale D2 interference folding. D1 gneissic fabrics were transposed during D2

mostly into the new foliation and partly transformed into schist. Petrography reveals lower grade M2 conditions or a late retrograde event by chloritised garnet and muscovite crystallising in the interstices of fractured garnet grains (Fig. 53).

**Table 12.** Structural pile and characteristic metamorphic mineral parageneses of the HMC.

| Level | Subdomain | Metamophic mineral paragenesis | rocks |
|---|---|---|---|
| Top | **Ehobib** | chlorite-epidote | volcanic rocks |
| | thrust | | |
| | **Suiderkruis** | garnet-muscovite-biotite-quartz-feldspar | semipelitic paragneiss |
| | | garnet-hornblende-plagioclase-quartz | mafic rocks |
| | unconformity enhanced by thrusting | | |
| | **Aandgloed** | garnet-muscovite-biotite-quartz-feldspar | semipelitic paragneiss |
| | | garnet-hornblende-plagioclase-quartz | mafic rocks |
| | | anatectic melt (migmatite ) | in lowest part |
| | transition | | |
| | **Rooikop-Lofdal** | garnet-muscovite-biotite-quartz-feldspar | semipelitic paragneiss |
| | | garnet-hornblende-plagioclase-quartz | mafic rocks |
| Base | | pervasive anatectic melt (migmatite) | everywhere |

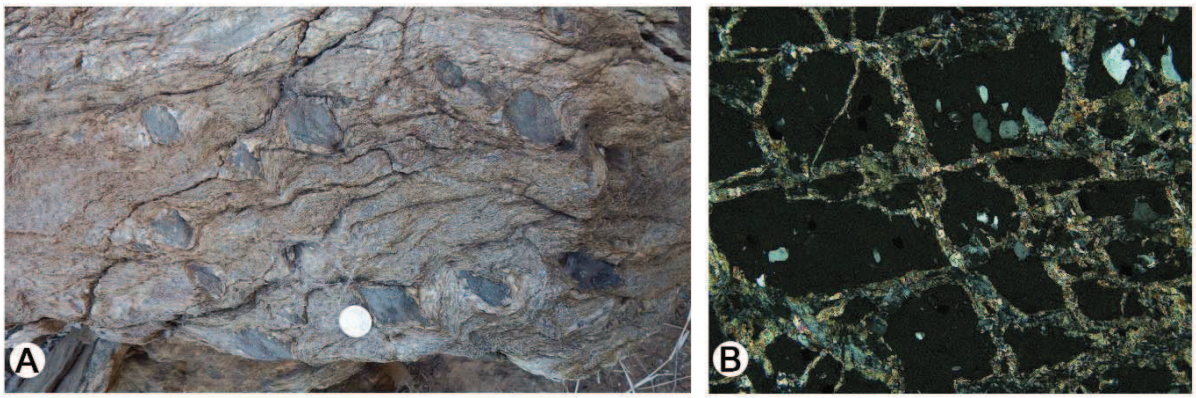


**Figure 53**. a) Very coarse-grained chloritised garnet porphyroblasts set in muscovite schist; b) muscovite growth in the interstices of fractured garnet (sample 070900-1). (Suiderkruis 668).

Petrography, microprobe analysis and P/T modelling were carried out in two studies on 13 samples from the higher grade subdomains of the HMC to constrain the metamorphic conditions M1 and M2 (Depiné, 2008; Nolte, 2012; Fig. 54, Table 13).

**Table 13.** Samples for metamorphic studies.

| Subdomain | Sample | Rock | Reference | Easting | Northing |
|---|---|---|---|---|---|
| Suiderkruis | 231104-1 | gt-bt-ms-pl-qz paragneiss (semipelite) | Depiné, 2008 | 448500 | 7775160 |
| | 260406-14 | gt-hb-bt-qz-pl gneiss (metagreywacke) | Depiné, 2008 | 475892 | 7757681 |
| | 290709-3 | banded gt leucogneiss (metaarkose?) | Nolte, 2012 | 444154 | 7785048 |
| | 290709-8 | gt-bt-hb-pl gneiss (amphibolite) | Nolte, 2012 | 449836 | 7777322 |
| Aandgloed | 200900-1 | gt-mica schist (metapelite) | Depiné, 2008 | 444154 | 7785048 |
| | 260406-10 | gt amphibolite | Depiné, 2008 | 439356 | 7759622 |
| Transition R - A | 101203-2 | gt amphibolite | Depiné, 2008 | 434867 | 7756759 |
| Rooikop | 101203-1 | gt-bt-hb-qz-pl gneiss | Depiné, 2008 | 435101 | 7757086 |
| | 260406-4 | gt amphibolite | Depiné, 2008 | 437157 | 7750078 |
| Lofdal | 020809-3 | gt amphibolite | Nolte, 2012 | 477268 | 7758050 |
| | 020809-4 | gt-hb-bt-qz-pl gneiss (metagreywacke) | Nolte, 2012 | 477088 | 7758047 |

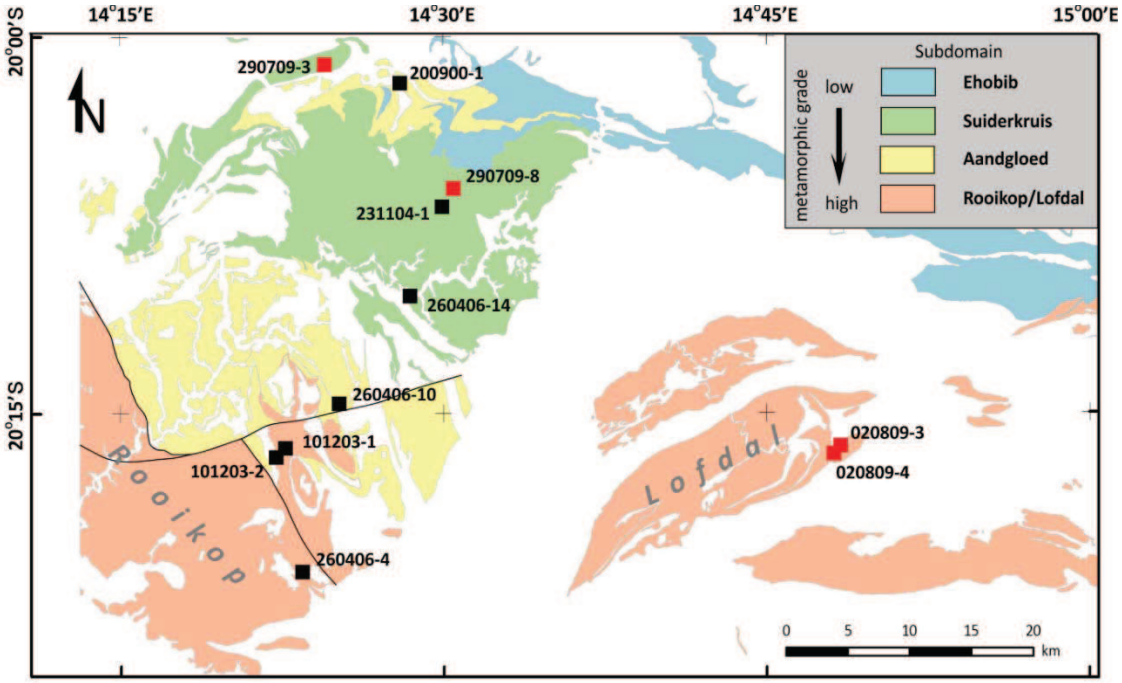


**Figure 54**. Positions of samples for metamorphic studies (black square: Depiné, 2008; red square: Nolte, 2012).

## Petrography

### *231104-1 (Suiderkruis SD)*

The texture of the garnet-biotite paragneiss is characterised by isometric porphyroblastic garnet up to cm size which is disseminated in the medium-grained, equigranular biotite-muscovite-quartz-feldspar matrix. The garnet displays dark reaction rims of garnet partly transformed into retrograde chlorite while the bleached surrounding matrix is composed mostly of fine-grained quartz (Fig. 55). Pre- to synkinematic garnet growth is suggested by asymmetric pressure shadows and deformation of the bleached matrix. The retrograde event took place under static conditions as indicated by the concentric, undeformed shape of the chlorite-garnet corona. Oriented olive biotite and flattened quartz-feldspar aggregates define the gneissic foliation, accessories are muscovite and epidote.

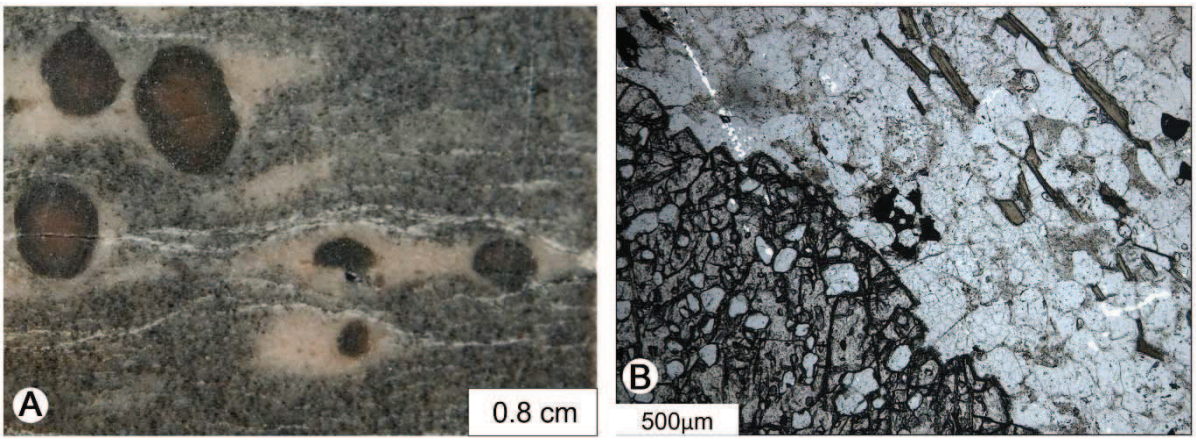


**Figure 55**. Sample 231104-1; a) hand specimen b) plane polarised light section.

### *260406-14 (Suiderkruis SD)*

The felsic paragneiss displays a medium-grained equigranular granoblastic fabric with abundant high angle boundaries indicating textural equilibrium (Fig. 57). In decreasing amounts the main components are quartz, K-feldspar (microcline), plagioclase, garnet, green hornblende and olive biotite; minor components include epidote, allanite and opaques.

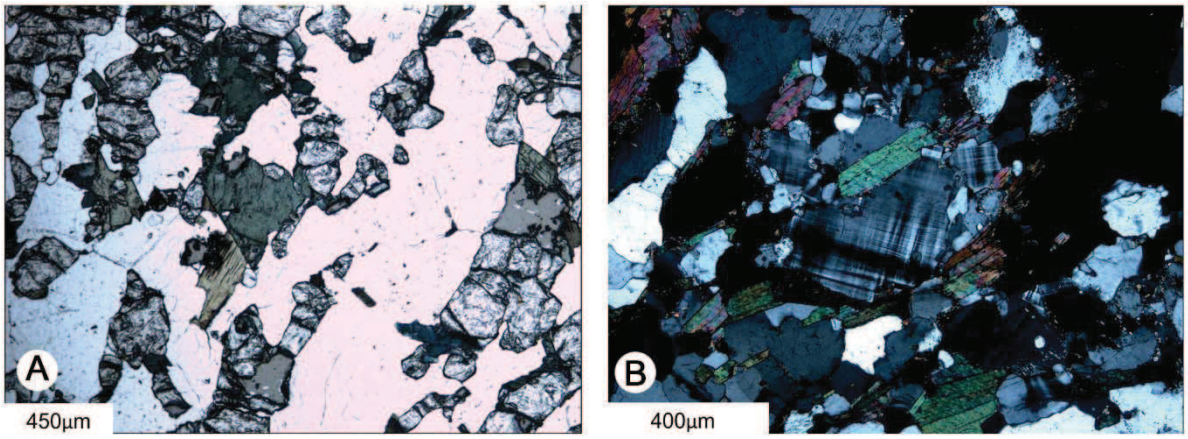


**Figure 56**. Sample 260406-14; a) plane polarised light, b) crossed nicols.

***290709-3 (Suiderkruis SD)***

The weakly-foliated gneiss is composed of very fine to medium-grained, inequigranular quartz, plagioclase, biotite, garnet, hornblende, with very minor epidote and apatite. Compositional layering at cm-scale with straight contacts is characterised by the variation of the main components (Fig. 57a). The section shows three layers enriched in (i) fine-grained chlorite-sericite; (ii) epidote-biotite, and (iii) garnet-hornblende. Undulose quartz is often associated with polytwinned partly saussuritic plagioclase forming flattened aggregates that together with oriented mica define the metamorphic foliation. Anhedral round garnet commonly displays poikiloblastic growth thus engulfing the other minerals (Fig. 57b). Flattened inclusions of quartz show the same orientation as grains outside the garnet implying flattening prior to garnet growth. Reaction rims of fine-grained biotite record subsequent retrograde metamorphism. Hornblende often forms inclusions within plagioclase and, as with the garnet, displays fine-grained reaction rims of biotite.

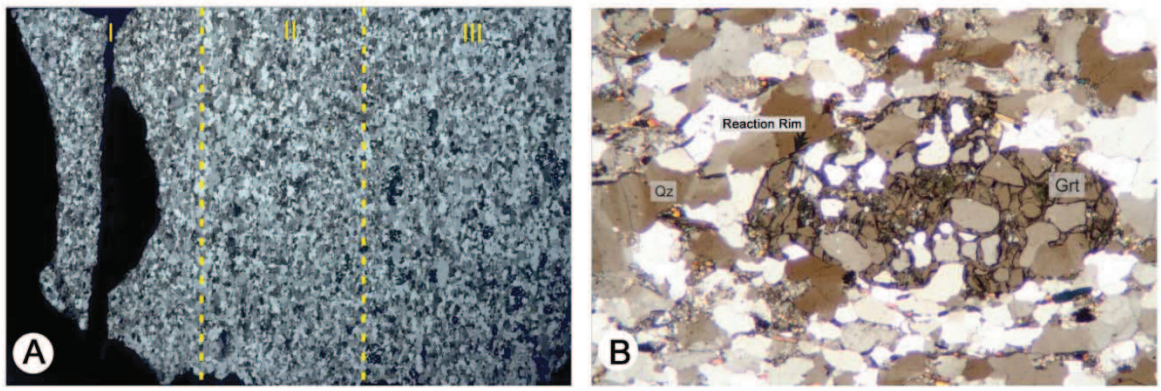


**Figure 57**. Sample 290709-3. A) hand specimen displaying faint compositional layering B) plane polarised light.

***290709-8 (Suiderkruis SD)***

The metamorphic texture is characterised by coarse-grained porphyroblastic garnet set in an inequigranular very fine-grained to medium-grained matrix comprised of biotite-hornblende-quartz-epidote-plagioclase opaques (Fig. 58). Fine metamorphic layering at sub-mm scale is defined by alternations of discontinuous flattened medium-grained quartz-feldspar aggregates and oriented green biotite. Metamorphic segregation quartz veinlets are transposed into the foliation. Minute zircon inclusions are revealed by pleochroic haloes in biotite. Disseminated poikilitic idioblastic garnet up to cm size is often fractured with very fine-grained mica and quartz crystallising in the fractures. It is often associated with medium-grained olive biotite. Anhedral green hornblende tends to form flattened aggregates and is often associated with biotite. The rim of individual crystals is sometimes transformed into biotite, as well. Ubiquitous opaques with bipyramidal (magnetite?) and rounded shapes often form inclusions in the mafic minerals.

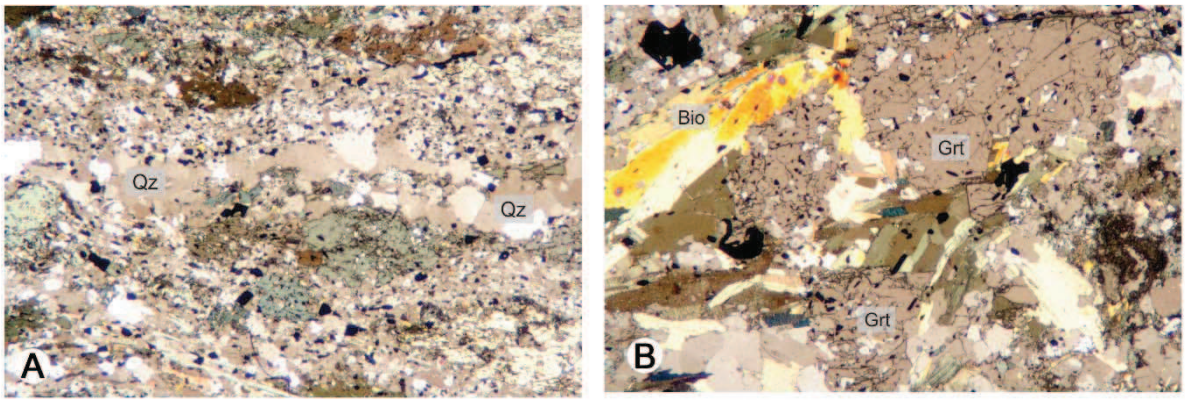


**Figure 58**. Sample 290709-8. A) vein of metamorphic segregation quartz and poikiloblastic hornblende in medium-grained, equigranular biotite-quartz-feldspar matrix (crossed nicols) B) porphyroclastic garnet associated with olive-green biotite (crossed nicols).

***200900-1 (Aandgloed SD)***

The garnet-mica schist displays compositional layering at mm-scale marked by alternating garnet and muscovite enriched laminae. Well-oriented muscovite and flattened quartz are the principal components and define a pronounced schistosity (Fig. 59). Idioblastic, partly euhedral, garnet porphyroblasts up to cm-size are set in a medium-grained equigranular quartz-muscovite matrix with minor chlorite, sericitised k-feldspar, and an opaque phase. Asymmetric pressure shadows around the garnet grains are filled by quartz and minor muscovite. Retrograde metamorphic overprint is recorded by thin reaction rims of chlorite, which are affected by shearing around the garnet grains, as well.

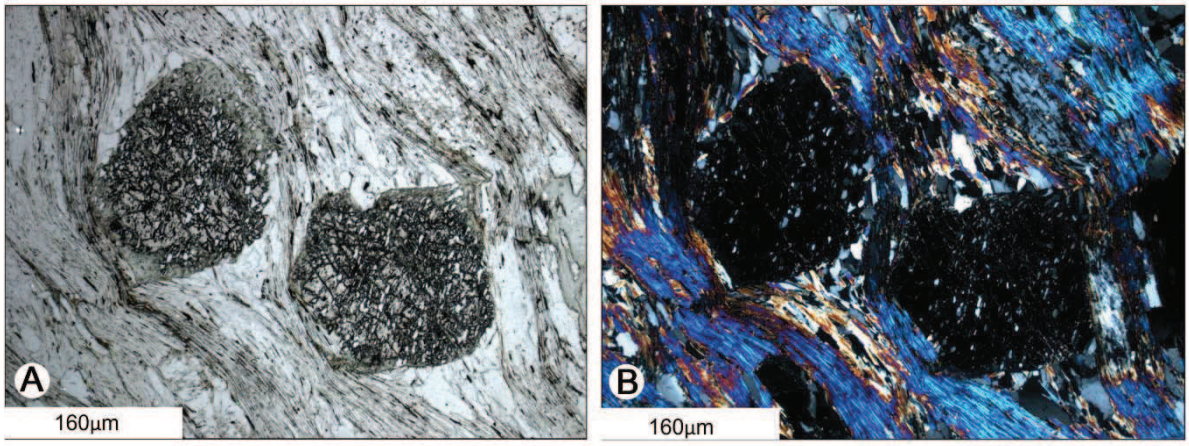


**Figure 59**. Sample 200900-1. A) plane polarised light, B) crossed nicols.

***260406-10 (Aandgloed)***

The sample is a garnet amphibolite marked by very coarse-grained granoporphyroblastic texture with idioblastic garnet porphyroblasts up to cm size set in a medium- to coarse-grained inequigranular quartz hornblende plagioclase matrix all of which are major components. Green hornblende often forms aggregates and is altered along cleavage cracks to chlorite, whereas the feldspars display saussuritisation indicating retrograde metamorphism (Fig. 60). Poikiloblastic garnet of irregular rounded outline contains abundant inclusions of quartz. Allanite and anhedral rounded opaques occur in very minor to minor amounts.

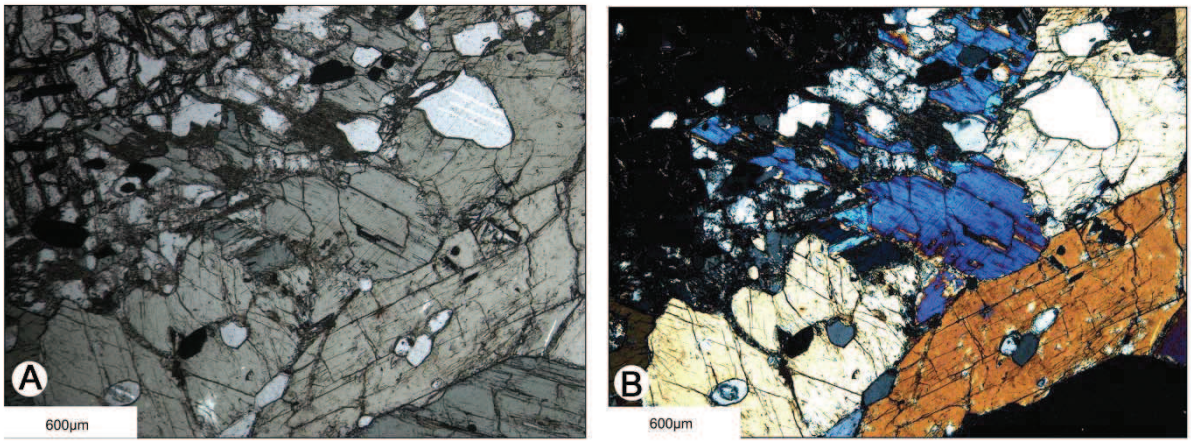


**Figure 60**. Sample 260406-10. A) plane polarised light, B) crossed nicols.

***101203-2 (Transition Aandgloed-Rooikop SD)***

Sample 101203-2 is a grano-porphyroblastic garnet-bearing orthoamphibolite derived from a mafic sill or dyke. Idioblastic garnet porphyroblasts up to several mm in size are set in a coarse-grained equigranular quartz-plagioclase-hornblende matrix without any layering or foliation (Fig. 61). Opaque minerals occur in minor amounts. Retrograde metamorphism is recorded by partly chloritised hornblende and saussuritised plagioclase.

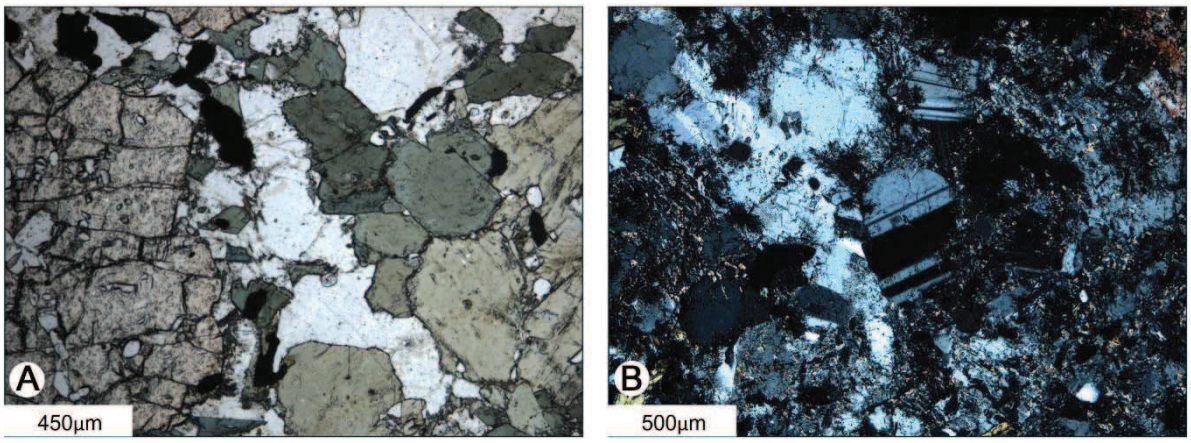


**Figure 61**. Sample 101203-2. A) porphyroblastic garnet in a coarse-grained hornblende-feldspar matrix (plane polarised light); B) polytwinned, partly saussuritised medium- to coarse-grained feldspar (crossed nicols).

***101203-1 (Rooikop SD)***

Sample 101203-1 is a biotite-hornblende-garnet gneiss characterised by a porphyro-granoblastic texture without any marked compositional layering, grain-flattening or metamorphic foliation. Pre- to syntectonic isometric, subhedral to euhedral reddish poikiloblastic garnet up to cm size with inclusions of quartz and green hornblende is set in the coarse-grained matrix of plagioclase, quartz, hornblende, garnet, and brown biotite with abundant pleochroic haloes (Fig. 62). Quartz aggregates concentrated around garnet correspond to the bleached diffusion haloes observed macroscopically.

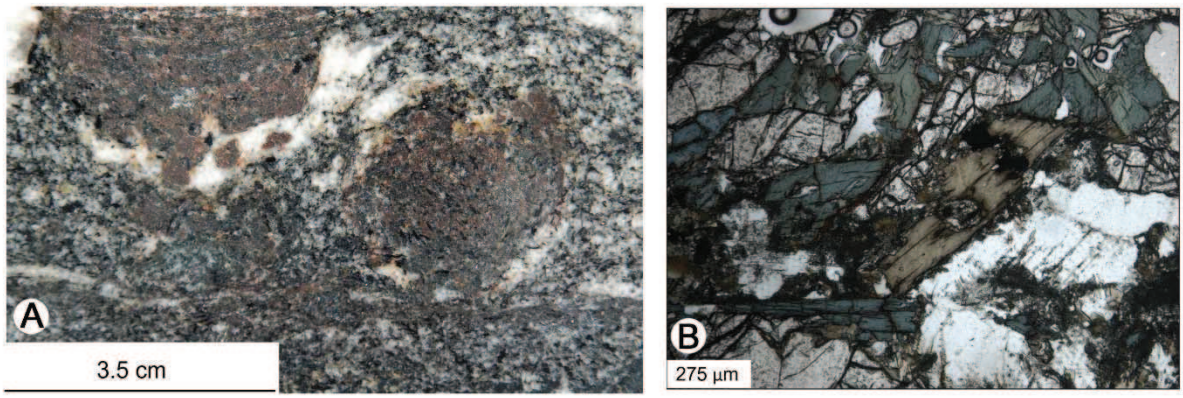


**Figure 62**. Sample101203-1. A) 0verview illustrating rotated garnet porphyroblast in medium-grained biotite-quartz-feldspar matrix; B) matrix of the rock with coarse grained green hornblende, brown biotite, garnet and feldspar as major components.

***260406-4 (Rooikop SD)***

The sample is composed of garnet amphibolite marked by grano-porphyroblastic texture with porphyroblastic idioblastic garnet up to cm size set in a medium to coarse-grained inequigranular quartz-hornblende-plagioclase matrix all of which are major components (Fig. 63). Green hornblende often form aggregates and is altered along cleavage cracks to chlorite whereas the feldspars are affected by saussuritisation indicating retrograde metamorphism. Poikiloblastic garnets with irregular rounded outlines contain abundant inclusions of quartz. Epidote and anhedral rounded opaques are minor components.

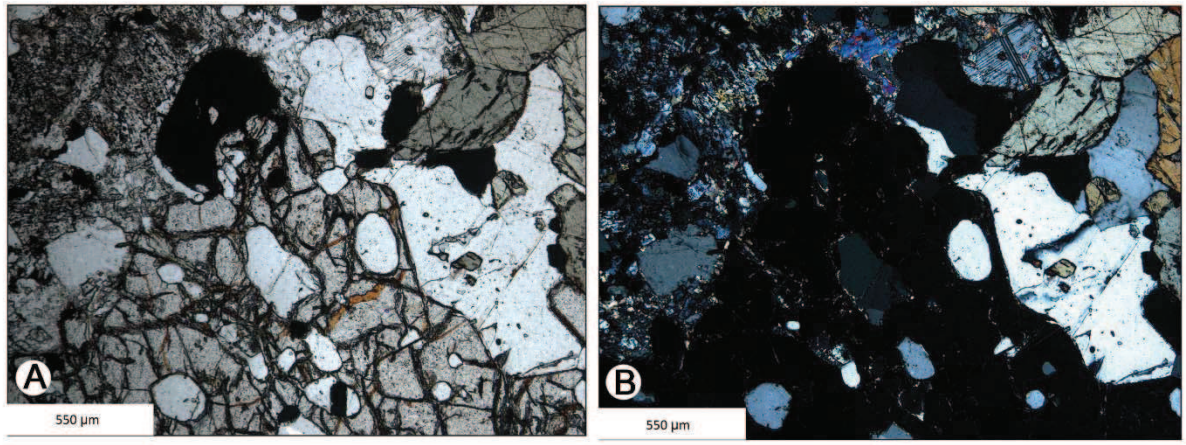


**Figure 63**. Sample260406-4 characteristic mineral assemblage green hornblende, poikilitic garnet, albite, opaques; A) plane polarised light; B) crossed nicols.

***020809-3 (Lofdal SD)***

The mesocratic garnet-amphibole gneiss displays a medium to coarse-grained, equigranular, granoblastic texture and weak metamorphic foliation defined by grain flattening and oriented biotite. The main minerals are, in decreasing amount, plagioclase, hornblende, quartz and garnet whereas epidote, titanite, rutile and hematite are accessory minerals (Fig. 64). Plagioclase is often saussuritised, garnet is cataclastic and rutile is replaced by titanite indicating retrograde metamorphism and brittle deformation.

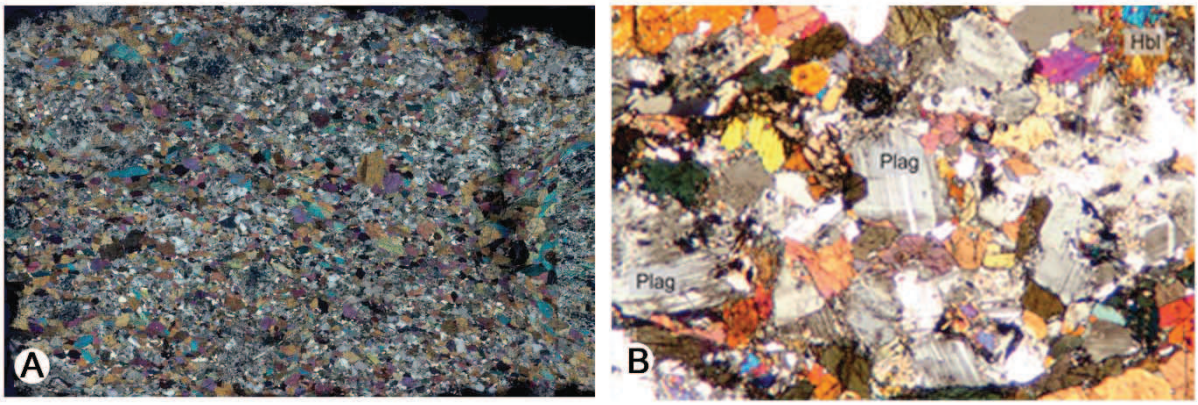


**Figure 64**. Sample 020809-3. A) Overview illustrating the oriented fabric of the medium- to coarse-grained gneiss (length of section = 2.5 cm; crossed nicols); B) close-up view showing the main components plagioclase and hornblende.

***020809-4 (Lofdal SD)***

The mesocratic hornblende-garnet gneiss is characterised by the unoriented medium- to coarse-grained, equigranular, granoblastic texture without any compositional layering (Fig. 65). The main components are, in decreasing amount, plagioclase, quartz, garnet, green hornblende with accessory epidote, titanite and hematite. Plagioclase associated with quartz is often strongly saussuritised and polytwins are only rarely preserved. Idioblastic poikilitic garnet with abundant quartz inclusions is partly altered to chlorite.

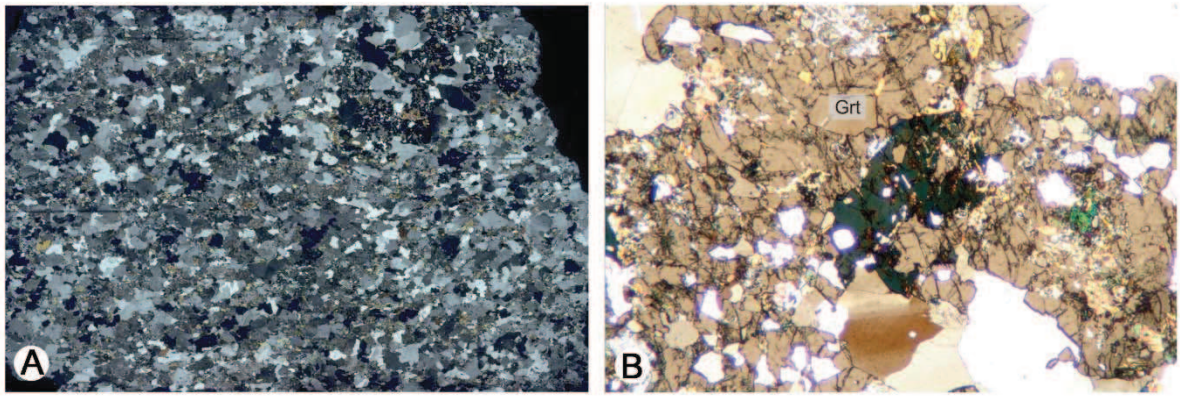


**Figure 65**. Sample 020809-4. A) Overview illustrating the unoriented fabric of the medium- to coarse-grained gneiss (length of section = 2.5 cm; crossed nicols); B) close-up view showing the poikiloblastic garnet with abundant quartz inclusions associated with green hornblende and epidote. The garnet is partly altered to chlorite.

**Mineral chemistry**

Microprobe mineral analyses of 11 samples selected for metamorphic geology are given in Table 14 indicating the minerals that were analysed in each sample. The analytical data are presented in Annex I.

***Garnet***

The garnet end member (almandine, spessartine, grossular and pyrope) compositions are given in Table 15 and in the ternary diagram of Fig. 66 (Nolte, 2012); mineral profiles of 3 to 84 points were measured across several grains to identify and characterise possible chemical zoning (Fig. 67; Depiné 2008; Nolte, 2012). The diagrams demonstrate that almandine is the predominant phase (60-80 vol.%), commonly followed by grossular (10-30 vol. %), pyrope (5-15 vol.%) and spessartine (5-15 vol.%). Most element profiles show only a little variation over most of the grain documenting principally chemically unzoned garnets (samples, 200900-1, 260406-4, 10, 14, 290709-3, 020809-3, 4). However, often the rim domains display slight or significant increases (samples 231104-1, 100203-29) of the almandine content at an almost constant or decreasing pyrope content, associated with a decrease of spessartine components, indicating volume and/or interdiffusive Fe-Mg re-equilibration during

post-peak conditions; these trends are independent of the sample locality in the subdomains (Table 15). A few exceptions are:

- One profile in sample 290709-3 (Suiderkruis) shows significant increase in the grossular and slight decrease in the other components from the core to the rim domains, all of which increase in the outermost rim domain, consistent with garnet resorption.
- Sample 020809-3 (Lofdal) shows from core to rim domains significant increase in pyrope, and decrease in spessartine, while almandine is almost constant. This is consistent with prograde growth zoning.

**Table 14.** Analysed minerals in samples studied here.

| Subdomain | Sample | Reference | Amphibole | Plagioclase | Garnet | Epidote | Chlorite | Biotite | Muscovite | Ilmenite |
|---|---|---|---|---|---|---|---|---|---|---|
| Suiderkruis | 231104-1 | Depiné, 2008 | | + | + | | | + | + | |
| | 260406-14 | Depiné, 2008 | + | + | + | + | | + | | |
| | 290709-3 | Nolte, 2012 | + | + | + | + | | + | | |
| | 290709-8 | Nolte, 2012 | + | | + | | | + | | |
| Aandgloed | 200900-1 | Depiné, 2008 | | + | + | | + | | + | |
| | 260406-10 | Depiné, 2008 | + | + | + | | | | | + |
| Transition R - A | 101203-2 | Depiné, 2008 | + | + | + | | | | | |
| Rooikop | 260406-4 | Depiné, 2008 | + | + | + | + | | | | + |
| | 101203-1 | Depiné, 2008 | + | + | + | | | + | | |
| Lofdal | 020809-3 | Nolte, 2012 | + | + | + | | | | | |
| | 020809-4 | Nolte, 2012 | + | + | + | | | + | | |

**Table 15.** Proportion of garnet end member in the core and rims of analysed garnet grains; red: increase in proportion, green: no change, blue: decrease from core to rim.

| Subdomain | sample | Almandine | | Pyrope | | Grossular | | Spessartine | |
|---|---|---|---|---|---|---|---|---|---|
| | mol% | core | rim | core | rim | core | rim | core | rim |
| Suiderkruis | 231104-1 | 64 | 80 | 3 | 3 | 19 | 10 | 14 | 7 |
| | 290709-8 | 51 | 52 | 7 | 8 | 20 | 19 | 20 | 20 |
| | 290709-3 | 65 | 65 | 4 | 5 | 22 | 23 | 4 | 1 |
| | 290709-3 | 65 | 66 | 5 | 5 | 22 | 23 | 3 | 2 |
| | 290709-3 | 62 | 66 | 4 | 5 | 21 | 22 | 8 | 3 |
| | 290709-3 | 65 | 65 | 5 | 5 | 24 | 23 | 2 | 2 |
| | 290709-3 | 66 | 64 | 5 | 4 | 21 | 25 | 3 | 2 |
| | 260406-14 | 61 | 62 | 1 | 2 | 33 | 33 | 5 | 3 |
| Aandgloed | 200900-1 | 75 | 76 | 10 | 11 | 8 | 10 | 6 | 3 |
| | 260406-10 | 64 | 66 | 17 | 15 | 15 | 16 | 3 | 4 |
| Transition R-A | 101203-2 | 61 | 65 | 9 | 9 | 26 | 23 | 4 | 3 |
| Rooikop | 260406-4 | 65 | 66 | 15 | 15 | 15 | 15 | 4 | 4 |
| | 101203-1 | 60 | 61 | 11 | 14 | 22 | 21 | 6 | 4 |
| Lofdal | 020809-3 | 53 | 53 | 7 | 10 | 23 | 25 | 12 | 8 |
| | 020809-3 | 55 | 55 | 8 | 11 | 22 | 23 | 11 | 8 |
| | 020809-4 | 46 | 46 | 3 | 2 | 45 | 47 | 3 | 1 |
| | 020809-4 | 45 | 46 | 3 | 2 | 44 | 46 | 4 | 2 |

| R > C | R = C | R< C |
|---|---|---|

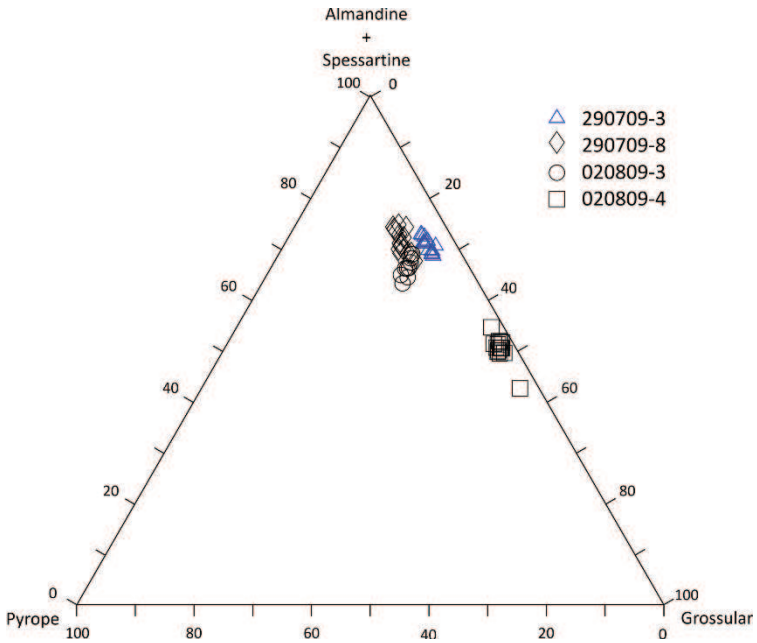


**Figure 66**. Ternary diagram with the end members pyrope, grossular and [almandine+spessartine]. Garnets of the HMC are mainly composed of almandine and grossular (data from Nolte, 2012).

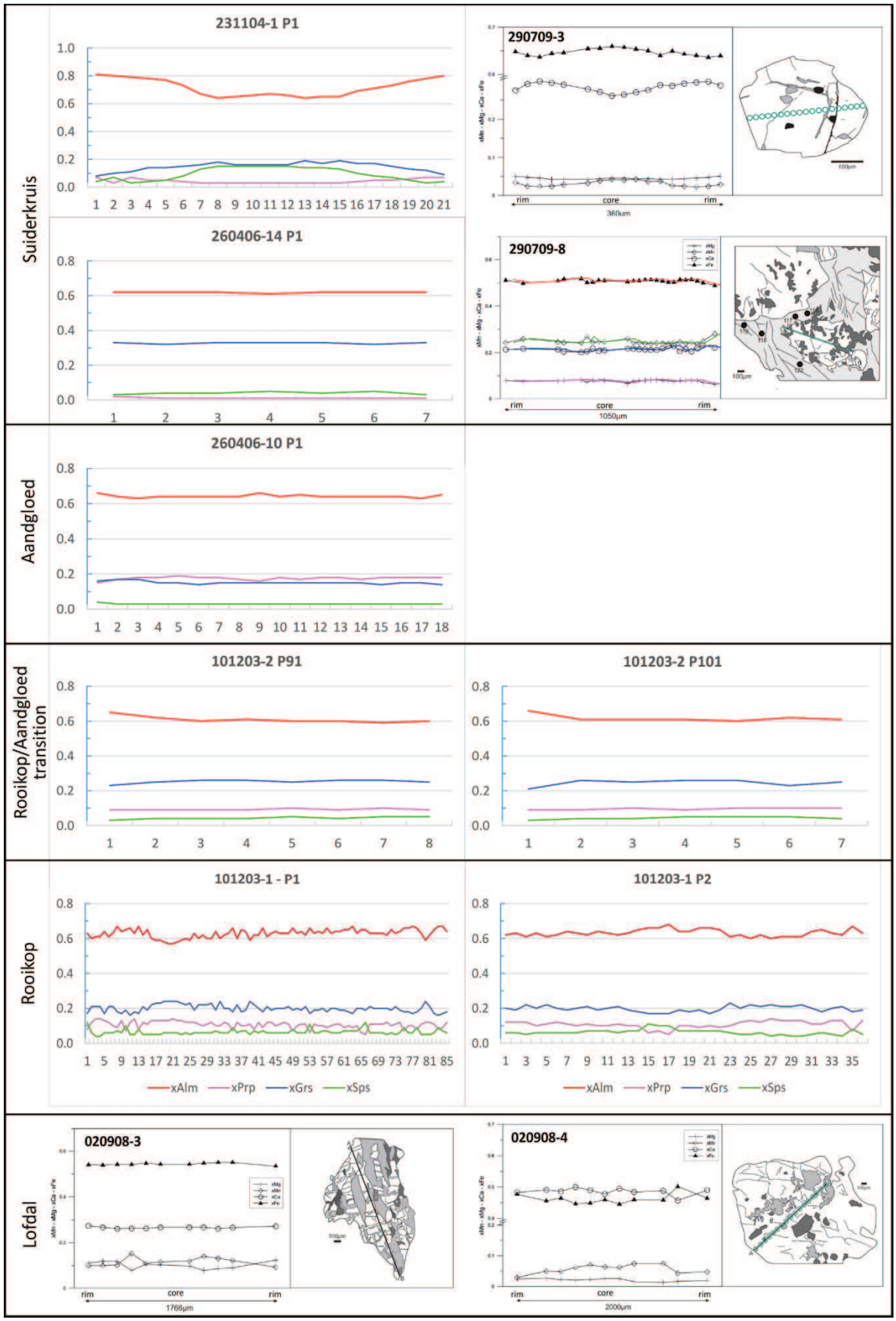


**Figure 67**. Mineral profiles through garnet show little evidence of zoning in most samples, except for 231104-1, 290709-3, and 290709-8 in the Suiderkruis Subdomain.

***Amphibole***

Amphiboles of the study area are of metamorphic origin and for their classification the criteria of Leake *et al.* (1997) were applied with cations calculated on the basis of 23 O atoms. The Si vs. Na+K diagram allows classification of amphiboles as edenite, pargasite, hornblende and tschermakite whereas the Si vs Mg/(Mg+Fe) diagram distinguishes between magnesium- and iron-rich varieties (Fig. 68).

Most amphibole analyses are marked by $T_{Si}$ values < 6.5 and $(Na+K)_A$ < 0.5 classifying them as tschermakite; the remaining analyses plot in the pargasite field (Fig. 68a). In the $Mg/(Mg+Fe^{2+})$ vs TSi diagram most data plot around the line between the tschermakite and ferro-tschermakite fields. Samples 290709-3 and 020809-4 that in Fig. 68a plot in the pargasite field are marked by $(Mg/Mg+Fe^{2+})$ <0.5 classifying them as ferro-pargasite. Sample 260406-14 that in Fig. 68a forms a separate group in the pargasite field due to low alumina ($Al^{VI}<Fe^{3+}$). The combination of the two diagrams indicates three groups (Table 16):

- G1: tschermakite to ferro-tschermakite: 290709-8, 101203-2, 260406-4, 260406-10, 101203-1, 020809-3)
- G2: ferro-pargasite: 290709-3, 020809-4
- G3: hastingsite: 260406-14

The grouping does not discriminate with regard to the subdomains, all of which comprise G1 amphiboles. G2 samples occur in the Suiderkruis and Lofdal subdomains and the G3 sample in the Aandgloed subdomain. The data suggest, however, higher variation of amphibole compositions in the Suiderkruis SD, whereas the Aandgloed and Rooikop SD comprise only tschermakite and ferro-tschermakite.

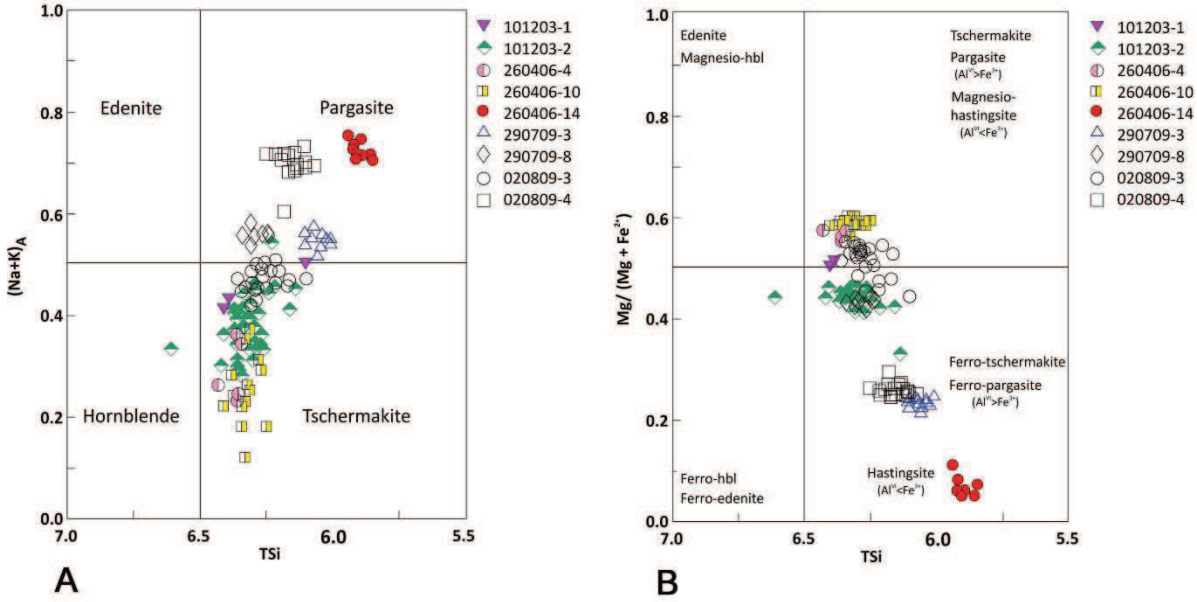


**Figure 68**. Classification diagrams of amphibole (Leake *et al*. 1997). A) $(Na+K)_A$ vs TSi; B) $Mg/(Mg+Fe^{2+})$ vs TSi.

**Table 16.** The amphiboles can be classified into three groups (1 - tschermakite to Fe-tschermakite, 2 - ferro-pargasite, and 3 - hastingsite) without any obvious correlation to the subdomains.

| Subdomain | Sample | Group |
|---|---|---|
| Suiderkruis | 231104-1 | |
| | 260406-14 | G3 |
| | 290709-3 | G2 |
| | 290709-8 | G1 |
| Aandgloed | 200900-1 | |
| | 260406-10 | G1 |
| Transition R-A | 101203-2 | G1 |
| Rooikop | 101203-1 | G1 |
| | 260406-4 | G1 |
| Lofdal | 020809-3 | |
| | 020809-3 | G1 |
| | 020809-4 | G2 |

***Biotite***

The biotite compositions of seven samples were calculated on 22 O and a $H_2O$ free basis and the method by Foster (1960) was applied for their classification. The biotites are rather low in Al/Ti/Cr with most of the analyses being in or below the lepidomelane field with a tendency towards siderophyllite. Biotite compositions of samples 260406-14 and 290709-3 of the Suiderkruis SD differ from the remaining data set being more iron / manganese-rich.

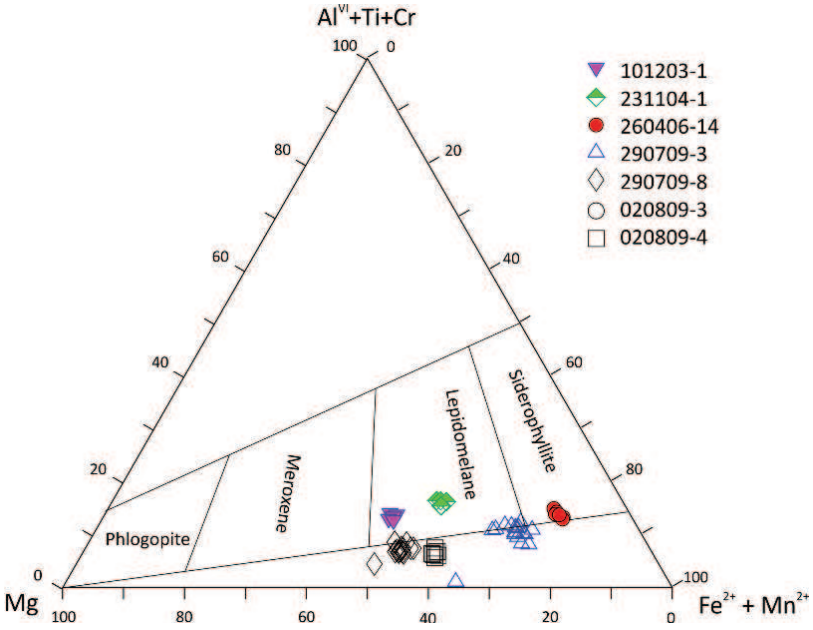


**Figure 69**. Ternary classification diagrams for biotite (Foster, 1960).

***Feldspar***

Feldspar compositions were calculated on the basis of 8 O (Annex). Most of the analyses classify as plagioclase with few K-feldspars identified in sample 260406-14. Plagioclase compositions vary widely from albite to bytownite, with the majority being andesine. Table 17 illustrates the variation of feldspar composition in individual samples. Again, there is no obvious relationship between the locality (subdomain) and mineral composition, however, feldspars from individual samples are rather homogeneous in composition.

**Table 17.** Composition of feldspars in samples for metamorphic petrology.

| Subdomain | Sample | Albite | Oligoclase | Andesine | Labradorite | Bytownite | Anorthite | K-feldspar |
|---|---|---|---|---|---|---|---|---|
| Suiderkruis | 260406-14 | | + | | | | | + |
| | 290709-3 | | | + | | | | |
| Aandgloed | 260406-10 | | | o | + | | | |
| Transition R-A | 101203-2 | | o | + | | | | |
| Rooikop | 101203-1 | o | o | + | | | | |
| | 260406-4 | | | | | + | | |
| Lofdal | 020809-3 | | | + | + | | | |
| | 020809-4 | | + | + | | | | |

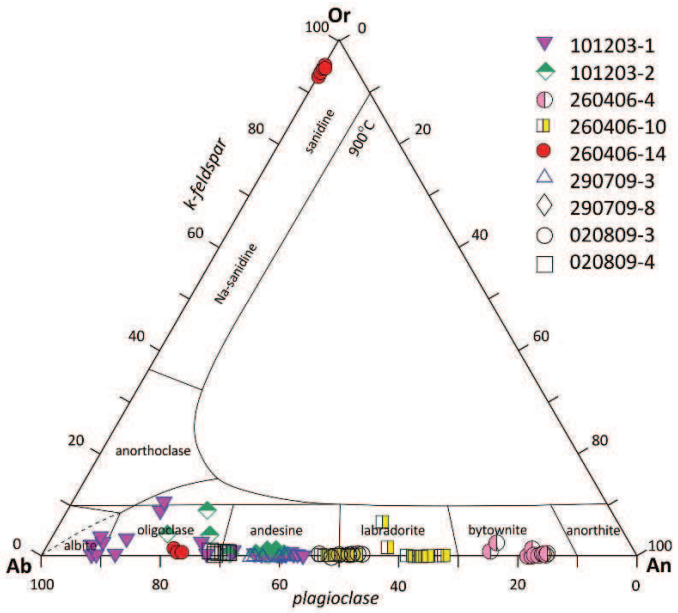


**Figure 70**. Ternary classification diagrams for feldspars.

## Geothermobarometry

P–T conditions of metamorphism were constrained through conventional thermo-barometry using ion exchange and net transfer reactions as well as from pseudosection analysis using isopleth thermobarometry.

### *Conventional thermometry*

Geothermometers are mostly based on ion exchange of mineral pairs. The following thermometers were applied (Table 20):

- gt-pl-bt-qz: Hoisch, 1990; 2 reactions; Ferry & Spear, 1978; Krogh & Raheim, 1978; Hodges & Spear, 1982; Perchuk & Lavrent'eva, 1983; Hoinkes, 1986, Hynes & Forest, 1988; Dasgupta *et al*. 1991; Kleeman & Reinhardt, 1994; Holdaway *et al*. 1997; Holdaway, 2000.
- gt-hb: Graham & Powell, 1984; Perchuk *et al.* 1985; Powell, 1985; Dale *et al*. 2000; Ravna, 2000.
- hb-pl: Holland & Blundy, 1994.
- gt-phe: Hynes & Forest, 1988; Krogh & Raheim, 1978.

(gt = garnet, pl = plagioclase, bt = biotite, hb = hornblende, phe = phengite)

Several calibrations for the gt-bt geo-thermometer (Ferry & Spear, 1978; Krogh & Raheim, 1978; Hodges & Spear, 1982; Perchuk & Lavrent'eva, 1983; Hoinkes, 1986; Hynes & Forest, 1988; Dasgupta *et al*. 1991; Kleemann & Reinhardt, 1994; Holdaway *et al*. 1997; Holdaway, 2000) were reviewed by Wu & Cheng (2006) for reproducibility and exactness. The Holdaway (2000) thermometer was considered by the authors as the most reliable

yielding the best results for garnets with low grossular and spessartine components. However, most samples comprise a significant grossular component implying the lower reliability of this method.

***Suiderkruis SD***

Gt-bt: The thermodynamic equation given by Holdaway (2000) yielded for 3 out of 4 samples temperatures between 675±25 $^{O}$C and 697±16 $^{O}$C. A significantly higher temperature of 759±29 $^{O}$C was determined in sample 290709-3 by using rim compositions of garnet indicating prograde metamorphism and implying that the other bt-gt pairs are in disequilibrium or interdiffusionally re-equilibrated during retrogression. Alternatively the possibility of two garnet generations has been discussed by Nolte (2012) with large 1$^{st}$ prograde and smaller 2$^{nd}$ retrograde phases. The other bt-gt thermometers yield widely varying results, with the majority of the temperatures between 602-688 $^{O}$C, in agreement with the presence of non-migmatitic gneisses and schist characterising the subdomain. In sample 290709-3, all thermometers indicate rising temperature from the core to the rim of zoned garnet.

Gt-hb: 2 out of 3 samples yielded lower temperatures between 526-673 $^{O}$C, more or less in agreement with field observation whereas the rim composition of sample 290709-3 constrains again unrealistic high temperatures between 687-994$^{O}$C.

Hb-pl: 3 out of 4 temperatures were calculated between 650-691 $^{O}$C, similar to the results of the gt-bt thermometer.

Gt-phe: one muscovite-bearing sample yielded a temperature of 575 $^{O}$C.

***Aandgloed SD***

Gt-hb: this mineral pair constrained in sample 260406-10 retrograde low temperatures between 550-565$^{O}$C, in conflict with field observations showing the presence of migmatisation in the area.

Hb-pl: the calculated temperatures between 600-640$^{O}$C with high errors of 50 degrees are again considered too low probably due to retrogression.

Gt-phe: garnet-muscovite schist yielded a poorly constrained temperature of 650±100 $^{O}$C. The presence of chlorite indicates re-equilibration during retrograde metamorphism.

*Transition Aandgloed – Rooikop subdomains*

Gt-hb: garnet-amphibolite records temperatures between 575-650 $^{O}$C, again in disagreement with the development of migmatitic paragneiss in this area.

Hb-plagioclase: The calculated higher temperatures (625-700 $^{O}$C) are in line with associated migmatisation Rooikop SD

Gt-hb thermometers indicate low temperatures of 555-625 $^{O}$C, implying inter- and/or volume diffusion during subsequent M2 metamorphism. Therefore, the temperatures either reflect M2 conditions or are disequilibrium conditions.

Hb-pl thermometers yielded temperatures between 625-785 $^{O}$C, which is more in line with field observations. However, it appears unlikely that this mineral pair preserved M1 conditions while garnet and/or hornblende compositions were disturbed by the M2 event.

***Lofdal SD***

The gt-bt thermometers yielded low temperatures between 410-560 $^{O}$C, in disagreement with the ubiquitous presence of diatexite. This indicates major disturbance of the mineral pair by subsequent retrograde M2 metamorphism. The same applies to gt-hb thermometers where only a few calculated temperatures lie above 560°C. Two hb-pl thermometers yield temperatures between 648-686 $^{O}$C, similar to those determined in the Rooikop SD by hb-bt thermometers. However, as before it appears unlikely that the hb-pl pair remained a closed system during the M2 event while the gt-bt system re-equilibrated.

In conclusion, the calculated conventional thermometric data show that only in the Suiderkruis SD temperatures are in accordance with field observations; the structurally lower (migmatitic) Aandgloed, Lofdal and Rooikop SD record mostly temperatures, which are too low and in conflict with the observed migmatism. Here, garnet appears to be in disequilibrium with both hornblende and biotite. Equilibrium between hornblende and plagioclase is suggested by the rather narrow interval of temperatures mostly between 625-700 $^{O}$C calculated for migmatitic subdomains. They suggest a positive gradient from the transition zone (3/4 samples = 600- 640 $^{O}$C) through the Lofdal (2/2 samples = 648-683 $^{O}$C) into the Rooikop SD (3/4 samples = 700-785 $^{O}$C).

**Table 18.** Results of conventional geothermometry (Depiné, 2008, Nolte, 2012). Most of the calculated temperatures are in conflict with the presence of migmatisation.

| **Reference** | | Depiné, 2008 | Depiné, 2008 | Nolte, 2012 | Nolte, 2012 | Nolte, 2012 | Depiné, 2008 | Depiné, 2008 | Depiné, 2008 | Depiné, 2008 | Depiné, 2008 | Nolte, 2012 | Nolte, 2012 |
|---|---|---|---|---|---|---|---|---|---|---|---|---|---|
| **Sample** | | **231104-1** | **260406-14** | **290709-3 core** | **290709-3 rim** | **290709-8** | **200900-1** | **260406-10** | **101203-2** | **101203-1** | **260406-4** | **020809-3** | **020809-4** |
| **Easting (WGS84, 33S)** | | 448500 | 475892 | 438161 | 438161 | 450321 | 444154 | 439356 | 434867 | 435101 | 437157 | 477268 | 477088 |
| **Northing (WGS84, 33S)** | | 7775160 | 7757681 | 7785741 | 7785741 | 7777111 | 7785048 | 7759622 | 7756759 | 7757086 | 7750078 | 7758050 | 7758047 |
| **Rock** | | paragneiss | paragneiss | paragneiss | paragneiss | gt-bt-amphibolite | schist | gt-amphibolite | gt-amphibolite | paragneiss | gt-amphibolite | gt-amphibolite | paragneiss |
| **Probable precursor** | | pelitic / semipelitic | semipelitic sediment | semipelitic sediment | semipelitic sediment | pelitic? sediment | pelitic sediment | mafic igneous | mafic igneous | semipelitic sediment | mafic igneous | mafic igneous | semipelitic sediment |
| **Mineral assemblage** | | ms-gt-bt-pl | hb-gt-bt-qz-pl | gt-hb-bt-pl-qz | | gt-bt-hb-qz-fsp | gt-ms-chl-qz-fs | gt-hb-gt-qz-epi | (chl)-gt-hb-pl | hb-gt-bt-qz-pl | gt-hb-gt-qz-epi | gt-hb-gt-qz-epi | gt-hb-bt-pl |
| **Authors of specific thermometers / Subdomain** | | **Suiderkruis** | | | | | **Aandgloed** | | **Transition R-A** | **Rooikop** | | **Lofdal** | |
| Holdaway, 2000 | **gt-bt** | | 675 ± 25 | 695 ± 70 | 759 ± 29 | 697 ± 16 | | | | | | | 543 ± 35 |
| Holdaway *et al*. 1997 | | | | 662 ± 67 | 707 ± 81 | 645 ± 14 | | | | | | | 520 ± 32 |
| Kleemann & Reinhardt, 1994 | | 500 ± 25 | 450 ± 25 | | | | | | | 575 ± 30 | | | |
| Dasgupta *et al*. 1991 | | | | 655 ± 96 | 745 ± 44 | 688 ± 17 | | | | | | | 560 ± 45 |
| Hoinkes, 1986 | | | | 848 ± 197 | 994 ± 66 | 755 ± 29 | | | | | | | 426 ± 50 |
| Perchuk & Lavrent'eva, 1983 | | | | 636 ±69 | 687 ± 21 | 604 ± 15 | | | | | | | 485 ± 26 |
| Hodges & Spear, 1982 | | | | 769 ± 136 | 872 ± 46 | 686 ± 17 | | | | | | | 565 ± 39 |
| Ferry & Spear, 1978 | | | | 666 ± 137 | 768 ± 45 | 602 ± 28 | | | | | | | 410 ± 39 |
| Ravna, 2000 | **gt-hb** | | | 655 ± 70 | | 673 ± 50 | | | | | | 598 ± 90 | 692 ± 68 |
| Dale *et al*. 2000 | | | | 589 ± 38 | | 579 ± 31 | | | | | | 551 ± 104 | 567 ± 29 |
| Powell, 1985 | | | | 628 ± 41 | | 539 ± 19 | | | | | | 557 ± 90 | 733 ± 24 |
| Perchuk, 1985 | | | 660 | 562 ± 26 | | 526 ± 25 | | 565 | 575 | 625 | 560 | 484 ± 72 | 504 ± 25 |
| Graham & Powell, 1984 | | | | 648 ± 39 | | 563 ± 18 | | 550 | 650 | 625 | 555 | 578 ± 88 | 743 ± 23 |
| Holland & Blundy, 1994a | **hb-pl** | | 790 ± 35 | | 691 ± 29 | | | 640 ± 50 | 700 ± 50 | 700 ± 75 | 785 ± 25 | 683 ± 36 | 658 ± 11 |
| Holland & Blundy, 1994b | | | 650 ± 25 | | 675 ± 27 | | | 600 ± 50 | 625 ± 75 | 625 ± 75 | 750 ± 60 | 686 ± 16 | 648 ± 14 |
| Hynes & Forest, 1988 | **gt-phe** | 575 | | | | | 650 | | | | | | |
| Krogh & Raheim, 1978 | | | | | | | 650 ± 100 | | | | | | |

**Table 19**. Results of conventional geobarometry (Depiné, 2008, Nolte, 2012).

| **Reference** | | Depiné, 2008 | Depiné, 2008 | Nolte, 2012 | Nolte, 2012 | Nolte, 2012 | Depiné, 2008 | Depiné, 2008 | Depiné, 2008 | Depiné, 2008 | Depiné, 2008 | Nolte, 2012 | Nolte, 2012 |
|---|---|---|---|---|---|---|---|---|---|---|---|---|---|
| **Sample** | | **231104-1** | **260406-14** | **290709-3 core** | **290709-3 rim** | **290709-8** | **200900-1** | **260406-10** | **101203-2** | **101203-1** | **260406-4** | **020809-3** | **020809-4** |
| **Easting (WGS84, 33S)** | | 448500 | 475892 | 438161 | 438161 | 450321 | 444154 | 439356 | 434867 | 435101 | 437157 | 477268 | 477088 |
| **Northing (WGS84, 33S)** | | 7775160 | 7757681 | 7785741 | 7785741 | 7777111 | 7785048 | 7759622 | 7756759 | 7757086 | 7750078 | 7758050 | 7758047 |
| **Rock** | | paragneiss | paragneiss | paragneiss | paragneiss | gt-bt-amphibolite | schist | gt-amphibolite | gt-amphibolite | paragneiss | gt-amphibolite | gt-amphibolite | paragneiss |
| **Probable precursor** | | pelitic / semipelitic | semipelitic sediment | semipelitic sediment | semipelitic sediment | pelitic? sediment | pelitic sediment | mafic igneous | mafic igneous | semipelitic sediment | mafic igneous | mafic igneous | semipelitic sediment |
| **Mineral assemblage** | | ms-gt-bt-pl | hb-gt-bt-qz-pl | gt-hb-bt-pl-qz | | gt-bt-hb-qz-fsp | gt-ms-chl-qz-fs | gt-hb-gt-qz-epi | (chl)-gt-hb-pl | hb-gt-bt-qz-pl | gt-hb-gt-qz-epi | gt-hb-gt-qz-epi | gt-hb-bt-pl |
| **Authors of specific barometers / Subdomain** | | **Suiderkruis** | | | | | **Aandgloed** | | **Transition R-A** | **Rooikop** | | **Lofdal** | |
| Hoisch, 1990 R1 | **gt-pl-bt-qz** | 5.5 ± 1 | 13.5 ± 0.5 | 12.6 ± 0.8 | | | | | | 9 ± 1 | | | 9.8 ± 0.2 |
| Hoisch, 1990 R2 | | 4.5 ± 0.25 | | 11.8 ± 0.2 | | | 8.0 | | | | | | 9.3 ± 0.2 |
| Dale *et al*. 2000, R1 | **gt-hb-pl** | | | 7.9 ± 0.5 | | | | | | | | 7.4 ± 2.4 | 7.3 ± 0.4 |
| Dale *et al*. 2000, R2 | | | | 8.5 ± 0.5 | | | | | | | | 8.6 ± 1.7 | 8.4 ± 0.3 |
| Dale *et al*. 2000, R3 | | | | 8.9 ± 0.5 | | | | | | | | 8.5 ± 2 | 8.7 ± 0.3 |
| Kohn & Spear, 1990, R1 | | | 11 ± 1 | 8.8 ± 0.4 | | | | 7.5 ± 1.5 | 8.0 ± 1 | 9.0 ± 0.5 | 4.5 ± 1 | 7.3 ± 1.7 | 10.6 ± 0.3 |
| Kohn & Spear, 1990, R2 | | | | 9.2 ± 0.3 | | | | | | | | 7.3 ± 0.3 | 10.1 ± 0.2 |
| Anderson & Smith, 1995 | **al-in-hb** | | 11.2 | 11.8 ± 0.4 (660°C) | | 9.1 ± 0.3 (650°C) | | 10.0 | 9.2 | 9.6 | 8.7 | 12.1 ± 1.6 (550°C) | 7.4 ± 0.8 (550°C) |
| Schmidt, 1992 | | | | 11.5 ± 0.4 | | 8.7 ± 0.3 | | | | | | 10.8 ± 1.4 | 10.5 ± 0.7 |
| Johnson & Rutherford, 1989 | | | | 9.5 ± 0.4 | | 7.0 ± 0.3 | | | | | | 8.8 ± 1.2 | 8.5 ± 0.6 |
| Hollister *et al*. 1987 | | | 12.0 | 12.5 ± 0.5 | | 9.1 ± 0.3 | | 9.5 | 8.8 | 9.2 | 8.1 | 11.6 ± 1.6 | 11.2 ± 0.9 |
| Hammerstrom & Zen, 1986 | | | | 11.4 ± 0.5 | | 8.5 ± 0.3 | | | | | | 10.6 ± 1.4 | 10.3 ± 0.8 |
| Hoisch, 1990 | **gt-pl-ms-qz** | 5.0 ± 0.3 | | | | | | | | | | | |
| Hodges & Crowley, 1985 | | 4.5 ± 0.3 | | | | | 7.5 | | | | | | |
| Powell & Holland, 1988 | **gt-pl-bt-ms** | 5.5 | | | | | | | | | | | |

***Conventional barometry***

Geobarometers use continuous transfer reactions resulting in progressive changes in the proportion of the involved mineral phases causing significant volume changes in the rock. The applied barometers were (Table 19, Table 20):

- gt-pl-bt-qz (Hoisch, 1990; 2 reactions).
- gt-hb-pl (Dale *et al*. 2000; 3 reactions; Kohn & Spear, 1989).
- alumina in hb (Hammerstrom & Zen, 1986; Hollister *et al*. 1987; Johnson & Rutherford, 1989; Schmidt, 1992; Anderson & Smith, 1995).
- gt-pl-ms-qz (Hodges & Crowley, 1985; Hoisch, 1990).
- gt-pl-bt-ms (Powell & Holland, 1988).

For the calculation of the pressures only samples were selected whose mineral chemistry fulfills the conditions given by the authors of the respective barometer. The table illustrates that the gt-pl-bt-qz and al-in-hb barometers yield similar results, whereas generally lower pressures are given by the gt-hb-pl barometer.

***Suiderkruis SD***

The gt-pl-bt-qz and al-in-hb barometers yielded pressures between 11 and 12 kb for samples 290709-3 (core) and 260406-14. Lower pressures between 7-9 kb and 4.5-5.5 kb were calculated for samples 290709-8 and 231104-1, respectively. The consistent results in sample 231104-1 by using different systems possibly constrain pressure conditions or disequilibrium conditions of a subsequent retrograde event.

***Aandgloed SD***

Gt-pl-bt-qz and gt-pl-ms-qz barometers yielded in sample 200900-1 s pressures between 7.5 and 8 kb, whereas two Al-in-hb barometers applied to sample 260406-10 resulted in higher pressures of 9.5-10 kb.

***Rooikop-Aandgloed Transition***

The Al-in-hb barometers yielded pressures between 8.8-9.2 kb in sample 1001203-2, where retrograde reactions are indicated by chlorite. Application of the gt-hb-pl barometer by Kohn & Spear (1990) resulted in a pressure of 8.0±1 kb.

***Rooikop SD***

6 out of 7 pressure estimates were calculated between 8.1-9.6 kb applying four different barometers.

***Lofdal SD***

The Al-in-hb barometer yielded mostly pressures between 10.3-12.1 kb. The other two applied barometers (gt-hb-pl; gt-pl-bt-qz) indicated consistently lower pressures between 7.3-10.6 kb.

The data summarised in Table 19 show altogether that gt-pl-bt-qz and al-in-hb barometers yield similar pressures of 11-13 kb in the Suiderkruis and Lofdal subdomains and slightly lower ones of 8-10 kb in the Rooikop-(Aandgloed) subdomains. Gt-hb-pl, gt-pl-ms-qz and gt-pl-bt-ms barometers yielded in all subdomains lower pressures between mostly 4.5-9 kb.

***P/T diagrams***

Pressure and temperature-sensitive reactions have been combined into P-T diagrams that indicate the stability fields for the observed mineral assemblages and their chemical composition (Fig. 71). The boundaries of these fields are defined by those geothermometers and barometers yielding minimum and maximum values. The preselection of the thermometers and barometers for each diagram is based on whole rock and mineral composition and the assumed metamorphic degree but to a certain degree it is arbitrary. Diagrams 71a-b and Fig. 71j-k have been adapted from Nolte (2012), the other ones from Depiné (2008).

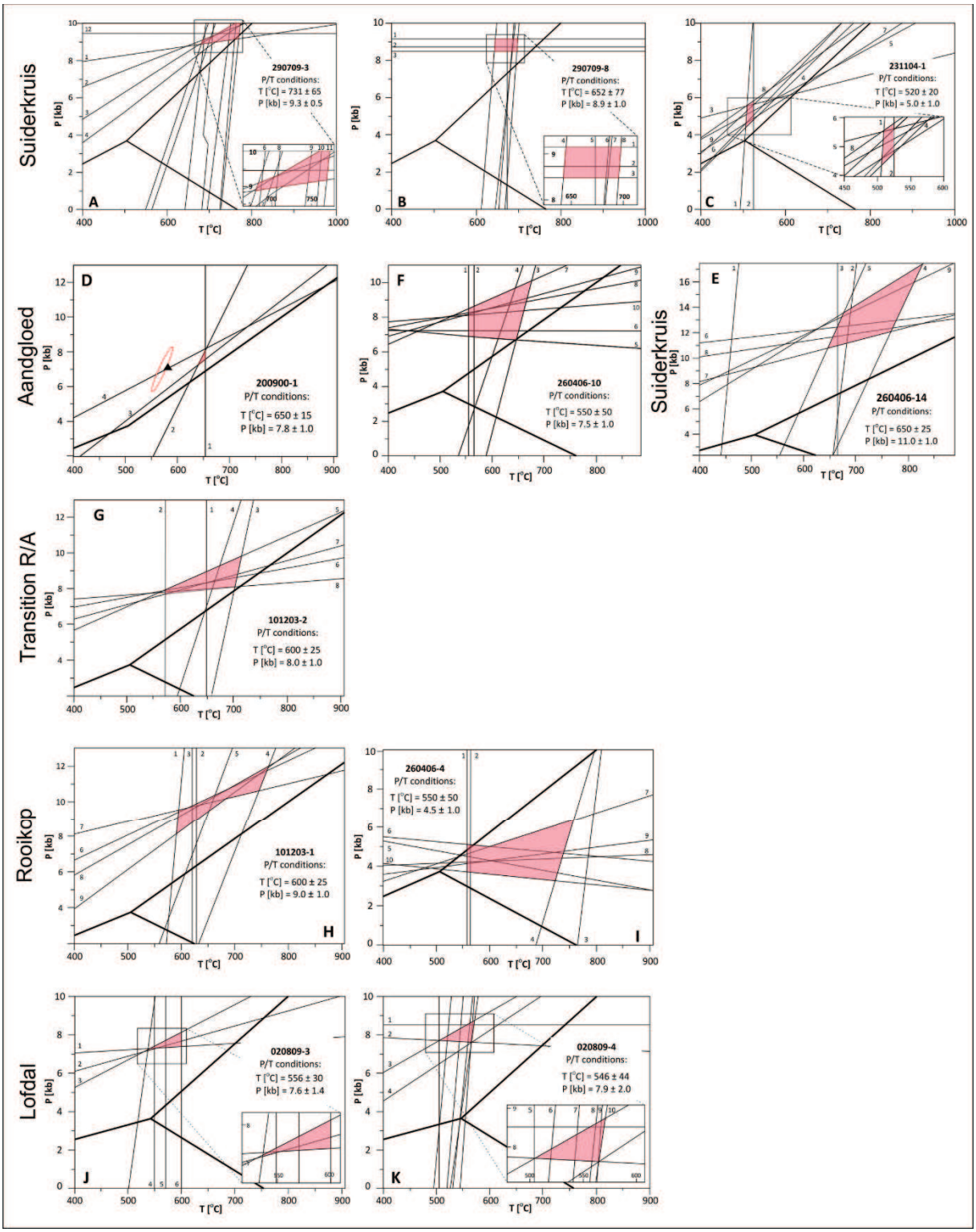


**Figure 71**. P-T diagrams of samples studied herein (A-B, J-K: Nolte, 2012; C-I: Depiné, 2008). The numbers at the reaction curves refer to the references indicated in Table 20.

***Suiderkruis SD***

Four samples show high variation in estimated P/T conditions of this subdomain. The lowest P/T conditions are recorded by sample 231104-1 (520±20$^{O}$C, 5.0±1.0 kb); the highest temperatures in sample 290709-3 (731±65$^{O}$C) and the highest pressures in sample 260406-14 (11.0±1.0 kb)

***Aandgloed SD***

Two samples yielded well-constrained pressures conditions of 7.5-7.8±1.0 kb with widely varying temperatures of 650±15$^{O}$C (200900-1) and 550±50$^{O}$C (260406-10). Conditions in sample 200900-1 are more in line with the field observations, whereas the calculated temperatures in sample 260406-10 are far below those required to account for the migmatites in the southern part of the Aandgloed SD.

***Transition Zone Aandlgoed/Rooikop***

Sample 101203-2 records P/T conditions of 8.0±1.0 kb and 600±25 $^{O}$C. The temperature is again much too low to explain the abundant migmatites in that area.

***Rooikop SD***

Two samples yielded almost identical results as in the transition zone and the temperatures are again too low to explain the anataxis that in this subdomain affected even mafic rocks.

***Lofdal***

Two samples indicate P-T conditions of 7.6-7.9±2.0 kb and 546-556±44 $^{O}$C, in line with the results from the Rooikop SD but far below the temperatures required for the observed anataxis of rocks in many localities.

***P-T pseudosection modeling***

One P-T phase diagram was calculated by Depiné (2008): for sample 231104-1 (garnet paragneiss) using the system MnCNKFMASH, which adequately covers the composition of the paragneiss. The calculations were undertaken with the TheriakDomino software (De Capitani & Brown, 1987). The calculation method was performed with the internally consistent thermodynamic data set of Holland & Powell (1998b; data set filename tc321p2.txt). The whole rock composition of the rocks for the calculation of samples preselected for P/T pseudosection modelling is given in Table 21. The calculations were generally performed for fully hydrated conditions.

The P-T path in sample 231104-1 from the Suiderkruis SD was reconstructed by Depiné (2008) using mineral reactions and the isopleths of the garnet components almandine and grossular. The P-T conditions for peak metamorphic conditions (M1) are much higher than those of the conventional P-T geo-thermobarometry, the latter of which re-equilibrated during the subsequent M2 event (Fig. 72).

**Table 20**. References for thermometers and barometers used in Fig. 71. The stability fields limiting reaction curves are given in red (max) and blue (min).

| | Sample | 290709-3 | 290709-8 | 231104-1 | 200900-1 | 260406-14 | 260406-10 | 101203-2 | 101203-1 | 260406-4 | 020809-3 | 020809-4 |
|---|---|---|---|---|---|---|---|---|---|---|---|---|
| | Reference/diagram | A | B | C | D | E | F | G | H | I | J | K |
| Barometer | Dale *et al*. 2000 | 1, 3, 4 | | | | | | | | | 3, 4 | 3, 4 |
| | Hammerstrom & Zen, 1986 | | 3 | | | | | | | | | |
| | Hodges & Crowley, 1985 | | | 6 | 3 | | | | | | | |
| | Hoisch, 1990 | | | 4, 5, 7, 8, 9 | 4 | 9, 10 | | | 8-9 | | | |
| | Hollister *et al*. 1987 | | 1 | | | | | | | | | |
| | Johnson & Rutherford, 1989 | 12 | | | | | | | | | | 1 |
| | Kohn & Spear, 1990 | 2 | | | | 6, 7, 8 | 5, 6, 7, 8, 9, 10 | 5, 6, 7, 8 | 6-7 | 5, 6, 7, 8, 9, 10 | 1, 2 | 2 |
| | Powell & Holland, 1988 | | | 3 | | | | | | | | |
| | Schmidt, 1992 | | 2 | | | | | | | | | |
| Thermometer | Dale *et al*. 2000 | | | | | | | | | | | 10 |
| | Dasgupta *et al*. 1991 | 9 | 7 | | | | | | | | | 8 |
| | Ferry & Spear, 1978 | 11 | | | | | | | | | | |
| | Graham & Powell, 1984 | | | | | | 1 | 1 | 2 | 1 | 6 | |
| | Hodges & Spear, 1982 | | 6 | | | | | | | | | 9 |
| | Holdaway *et al*. 1997 | 8 | 4 | | | | | | | | | 6 |
| | Holdaway, 2000 | 10 | 8 | | | 2 | | | | | | 7 |
| | Holland & Blundy, 1994a | 5 | | | | 4 | 3 | 3 | 4 | 3 | | |
| | Holland & Blundy, 1994b | 7 | | | | 5 | 4 | 4 | 5 | 4 | | |
| | Hynes & Forest, 1988 | | | 2 | 1 | | | | | | | |
| | Kleemann & Reinhardt, 1994 | | | 1 | | 1 | | | 1 | | | |
| | Krogh & Raheim, 1978 | | | | 2 | | | | | | | |
| | Perchuk & Lavrent'eva, 1983 | 6 | | | | | | | | | | |
| | Perchuk *et al.* 1985 | | | | | 3 | 2 | 2 | 3 | 2 | | 5 |
| | Powell, 1985 | | | | | | | | | | 5 | |
| | Ravna, 2000 | | 5 | | | | | | | | 7 | |

**Table 21.** Major element composition of samples pre-selected for P/T pseudosection.

| Sample | | 101203-1 | 101203-2 | 200900-1 | 231104-1 | 260406-4 | 260406-10 | 260406-14 | 260406-14b | 290802-11 | 290802-12 |
|---|---|---|---|---|---|---|---|---|---|---|---|
| Major elements [wt%] | $SiO_2$ | 62,0 | 48,2 | 59,3 | 68,8 | 51,5 | 49,2 | 70,7 | 70,6 | 47,6 | 47,8 |
| | $TiO_2$ | 0,65 | 2,41 | 0,66 | 0,34 | 1,91 | 1,64 | 0,49 | 0,49 | 1,18 | 1,35 |
| | $Al_2O_3$ | 14,4 | 15,8 | 22,3 | 16,2 | 13,3 | 15,7 | 12,5 | 12,2 | 14,6 | 16,8 |
| | $Fe_2O_3$ | 9,70 | 15,2 | 6,30 | 3,66 | 15,81 | 13,9 | 6,36 | 6,35 | 14,8 | 13,9 |
| | MnO | 0,26 | 0,24 | 0,10 | 0,10 | 0,23 | 0,14 | 0,10 | 0,10 | 0,38 | 0,36 |
| | MgO | 3,39 | 4,34 | 1,49 | 0,73 | 5,72 | 6,78 | 0,36 | 0,36 | 9,58 | 7,62 |
| | CaO | 4,79 | 8,02 | 0,49 | 2,96 | 8,98 | 9,20 | 2,48 | 2,48 | 11,2 | 11,8 |
| | $Na_2O$ | 2,24 | 2,26 | 0,74 | 4,95 | 0,97 | 1,85 | 2,47 | 2,38 | 1,36 | 1,60 |
| | $K_2O$ | 1,47 | 0,32 | 5,09 | 0,93 | 0,54 | 0,38 | 3,46 | 3,45 | 0,27 | 0,13 |
| | $P_2O_5$ | 0,09 | 0,55 | 0,16 | 0,14 | 0,23 | 0,48 | 0,16 | 0,16 | 0,11 | 0,14 |
| | S | <0.10 | <0.10 | <0.10 | <0.10 | <0.10 | <0.10 | <0.10 | <0.10 | <0.10 | <0.10 |
| | LOI | 1,30 | 3,26 | 3,42 | 1,03 | 1,07 | 1,22 | 0,41 | 0,39 | 0,06 | 0,15 |
| | Sum | 100,4 | 100,6 | 100,0 | 99,9 | 100,3 | 100,5 | 99,5 | 99,0 | 101,1 | 101,4 |
| Trace elements [ppm] | V | 111 | 178 | 89 | 15 | 351 | 242 | 21 | 22 | 277 | 309 |
| | Cr | 47 | 14 | 71 | <10 | 86 | 200 | <10 | <10 | 420 | 125 |
| | Co | 75 | 41 | 47 | 50 | 74 | 84 | 73 | 69 | 96 | 81 |
| | Ni | 30 | 17 | 24 | <5 | 25 | 74 | <5 | <5 | 77 | 52 |
| | Zn | 53 | 172 | 107 | 22 | 147 | 339 | 22 | 22 | 129 | 132 |
| | Ga | 19 | 32 | 29 | 20 | 29 | 30 | 24 | 23 | 18 | 24 |
| | Rb | 102 | 13 | 189 | 71 | 18 | 23 | 129 | 127 | 10 | 9 |
| | Sr | 158 | 230 | 200 | 231 | 100 | 235 | 109 | 107 | 321 | 434 |
| | Y | 120 | 54 | 30 | 37 | 45 | 42 | 129 | 126 | 21 | 16 |
| | Zr | 228 | 274 | 163 | 272 | 168 | 155 | 438 | 433 | 47 | 33 |
| | Nb | 16 | 20 | 14 | 10 | 10 | 11 | 32 | 33 | <5 | <5 |
| | Ba | 484 | 138 | 1114 | 362 | 131 | 319 | 931 | 943 | 248 | 118 |

Furthermore, the P-T diagram shows the position of analyses P6-P21 together with the calculated mineral reaction curves (Fig. 72). The intersection from the garnet core end member isopleths define a first metamorphic event at higher amphibolite grade (11 kb, 675°C), straddling the solidus of the rock.The end member isopleths from the outer part of the garnet profile record growth under systematically lower pressures and temperatures from 9.5 kb / 600°C (P17) through 7.9 kb / 575°C (P7, P19) to 6.5 kb / 550°C (P20), largely in line with results of conventional thermobarometry (Fig. 71). Retrograde garnet re-equilibration under epidote-amphibolite facies is interpreted to record M2 conditions during exhumation of the rocks whereby it is uncertain whether M1 and M2 are part of one protracted or two discrete metamorphic events. Therefore, the inferred P–T path, which is based on the observed textural relationships and the isopleth constraints, suggest simultaneous decompression and cooling during relatively slow exhumation of the high-grade rocks to higher crustal levels.

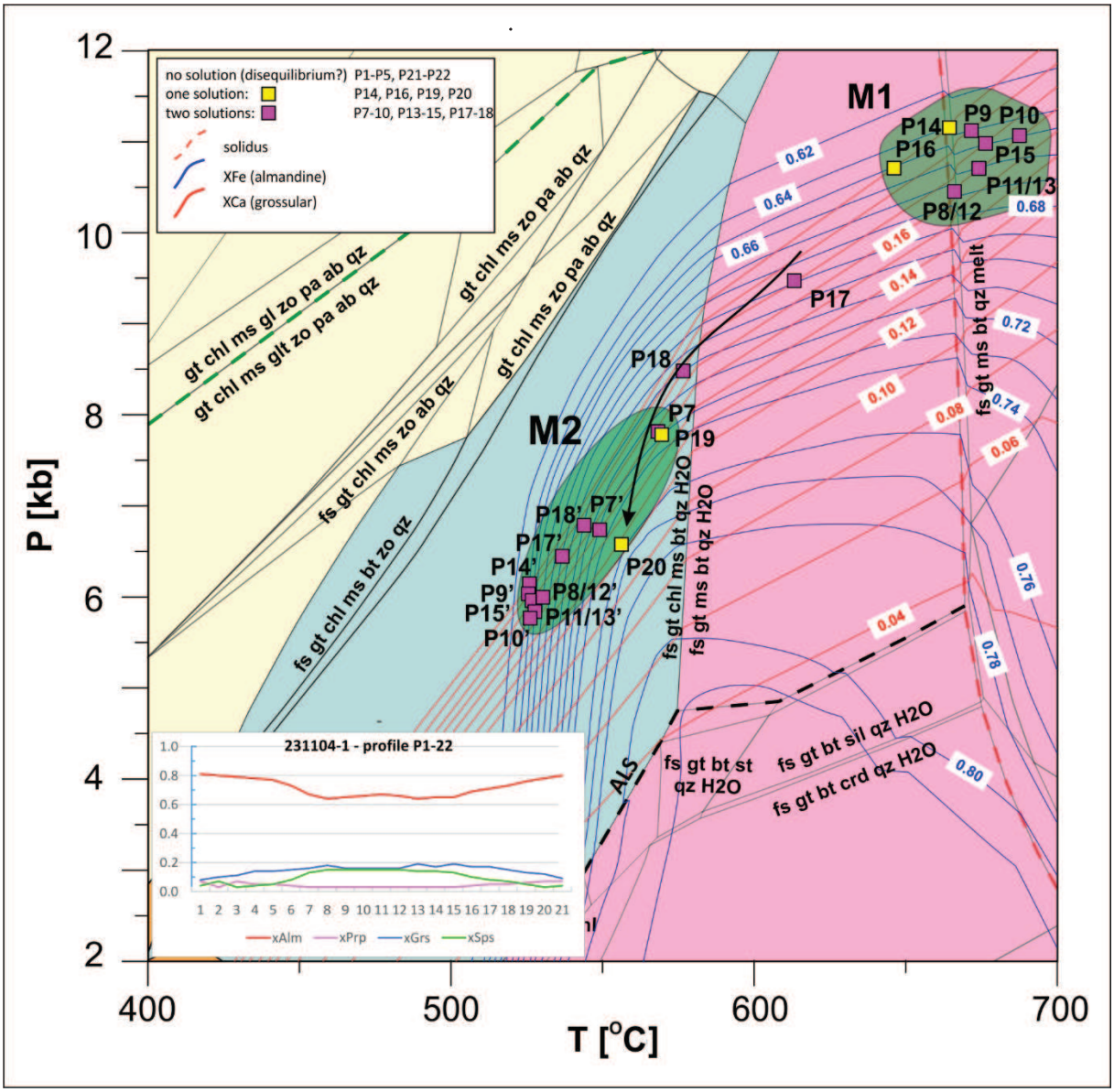


**Figure 72**. Pseudosection of sample 231104-1 indicates a first metamorphic event under P/T conditions of about 11 kb and 675°C (M1) followed by retrograde garnet growth during decompression and cooling (M2) at about 525-550$^{O}$C and 5.5-6.5 kb.

## Geochronology

U-Pb age single zircon geochronology was carried out by the working group using LA-ICP-MS (six samples; Wilsky, 2010; Kleinhanns *et al*. 2013) and SHRIMP method (three samples; this study; Table 24).

### LA-ICP-MS U-Pb single zircon analysis

Samples described and analysed by Wilsky (2010) and summarised by Kleinhanns *et al*. (2013) comprise weakly deformed granite types of the FFG Suite (170405-6 = Kaross granite; 260205-4 = Kamdescha granite; 280205-6 = Franken granodiorite), gneissic quartz-feldspar porphyry (130503-1), mylonitic red orthogneiss (210900-2/HU01), intrusive into the Upper Sequence of the Suiderkruis SD and granodioritic augengneiss (HU03) forming a regional-scale sheet-like intrusion at the boundary between the Suiderkruis and Ehobib subdomains to undifferentiated basement rocks further north and east (Fig. 16, Fig. 24, Fig. 73). The data are given in Table 22 (FFG) and Table 23 (HMC).

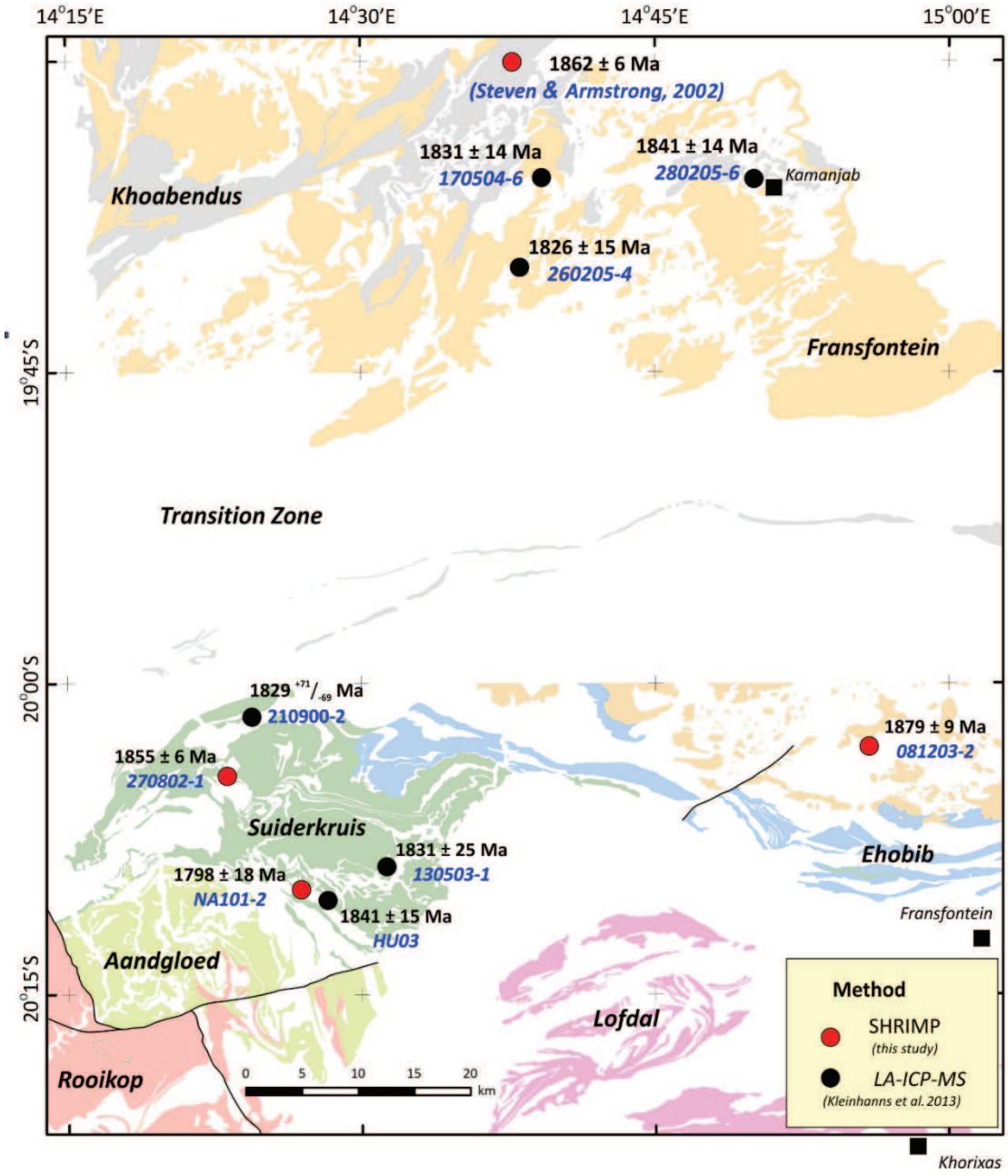


**Figure 73**. U-Pb single zircon ages of the HMC, FFG and Khoabendus Group.

**Table 22**. U-Pb single zircon ages by LA-ICP-MS method. Samples of FFG Suite. Discordances > 10% are marked in red.

| Sample | Pos | spot | Isotopic ratios | | | | | | | Ages [Ma] | | | | | | |
|---|---|---|---|---|---|---|---|---|---|---|---|---|---|---|---|---|
| | | | 206/238 | ±1σ | 207/235 | ±1σ | rho | 207/206 | ±1σ | 6/8 age | ±1σ | 7/5 age | ±1σ | 7/6 age | ±1σ | disc % |
| 260205-4 | core | 2_21 | 0.3290 | 0.01128 | 5.197 | 0.1984 | 0.45 | 0.11197 | 0.002548 | 1834 | 55 | 1852 | 33 | 1832 | 41 | -0.12 |
| | | 2_28 | 0.3326 | 0.01293 | 5.147 | 0.2032 | 0.49 | 0.11328 | 0.003778 | 1851 | 63 | 1844 | 34 | 1853 | 60 | 0.09 |
| | | 2_33 | 0.3233 | 0.00994 | 5.092 | 0.1848 | 0.42 | 0.11336 | 0.001857 | 1806 | 48 | 1835 | 31 | 1854 | 30 | 2.66 |
| | | 2_12 | 0.3241 | 0.00852 | 5.054 | 0.1676 | 0.40 | 0.11433 | 0.002667 | 1810 | 41 | 1828 | 28 | 1869 | 42 | 3.29 |
| | | 2_15 | 0.3317 | 0.02458 | 5.130 | 0.3724 | 0.51 | 0.11445 | 0.004158 | 1847 | 119 | 1841 | 62 | 1871 | 66 | 1.34 |
| | | 2_29 | 0.3029 | 0.01512 | 4.746 | 0.2360 | 0.50 | 0.11454 | 0.002280 | 1706 | 75 | 1775 | 42 | 1873 | 36 | 9.78 |
| | | 2_27 | 0.3027 | 0.01652 | 4.783 | 0.2661 | 0.49 | 0.11455 | 0.002954 | 1704 | 82 | 1782 | 47 | 1873 | 46 | 9.88 |
| | intermediate | 2_20 | 0.3339 | 0.01124 | 5.097 | 0.1409 | 0.61 | 0.11129 | 0.005435 | 1857 | 54 | 1836 | 23 | 1821 | 89 | -1.96 |
| | | 2_30 | 0.3169 | 0.01048 | 4.841 | 0.2002 | 0.40 | 0.11195 | 0.002321 | 1775 | 51 | 1792 | 35 | 1831 | 38 | 3.19 |
| | | 2_22 | 0.3226 | 0.01120 | 5.056 | 0.2164 | 0.41 | 0.11228 | 0.002280 | 1803 | 55 | 1829 | 36 | 1837 | 37 | 1.89 |
| | | 2_34 | 0.3211 | 0.01073 | 5.003 | 0.2246 | 0.37 | 0.11434 | 0.002972 | 1795 | 52 | 1820 | 38 | 1870 | 47 | 4.14 |
| | | 2_11 | 0.3303 | 0.02619 | 5.186 | 0.4385 | 0.47 | 0.11444 | 0.004124 | 1840 | 127 | 1850 | 72 | 1871 | 65 | 1.70 |
| | | 2_19 | 0.3291 | 0.00959 | 5.159 | 0.1909 | 0.39 | 0.11475 | 0.003065 | 1834 | 47 | 1846 | 31 | 1876 | 48 | 2.30 |
| | | 2_18 | 0.3211 | 0.01334 | 5.110 | 0.2120 | 0.50 | 0.11530 | 0.002481 | 1795 | 65 | 1838 | 35 | 1885 | 39 | 4.99 |
| | rim | 2_17 | 0.3493 | 0.02061 | 5.245 | 0.2534 | 0.61 | 0.10673 | 0.009994 | 1931 | 98 | 1860 | 41 | 1744 | 172 | -9.68 |
| | | 2_10 | 0.2867 | 0.01696 | 4.203 | 0.3513 | 0.35 | 0.10741 | 0.003030 | 1625 | 85 | 1675 | 69 | 1756 | 52 | 8.07 |
| | | 2_09 | 0.3291 | 0.00749 | 5.149 | 0.1357 | 0.43 | 0.11518 | 0.002260 | 1834 | 36 | 1844 | 22 | 1883 | 35 | 2.65 |
| | | 2_14 | 0.3053 | 0.02376 | 4.824 | 0.3617 | 0.52 | 0.11528 | 0.005001 | 1718 | 117 | 1789 | 63 | 1884 | 78 | 9.70 |
| | | 2_08 | 0.3036 | 0.01758 | 4.829 | 0.2976 | 0.47 | 0.11695 | 0.002371 | 1709 | 87 | 1790 | 52 | 1910 | 36 | 11.8 |
| | | 2_16 | 0.3314 | 0.01764 | 5.547 | 0.2525 | 0.58 | 0.11883 | 0.003686 | 1845 | 85 | 1908 | 39 | 1939 | 55 | 5.08 |
| | | 2_13 | 0.2870 | 0.02031 | 4.749 | 0.2408 | 0.70 | 0.11942 | 0.004834 | 1627 | 102 | 1776 | 43 | 1947 | 72 | 19.7 |
| 280205-6 | core | 1_12 | 0.3176 | 0.01958 | 4.816 | 0.3517 | 0.42 | 0.10950 | 0.004190 | 1778 | 96 | 1788 | 61 | 1791 | 70 | 0.74 |
| | | 1_30 | 0.3411 | 0.03351 | 5.512 | 0.4943 | 0.55 | 0.11340 | 0.011803 | 1892 | 161 | 1902 | 77 | 1855 | 188 | -1.98 |
| | | 1_10 | 0.3210 | 0.01470 | 5.068 | 0.2699 | 0.43 | 0.11519 | 0.004857 | 1795 | 72 | 1831 | 45 | 1883 | 76 | 4.90 |
| | | 1_08 | 0.3243 | 0.01131 | 5.106 | 0.2657 | 0.34 | 0.11686 | 0.004658 | 1811 | 55 | 1837 | 44 | 1909 | 72 | 5.41 |
| | | 1_28 | 0.3285 | 0.01691 | 5.224 | 0.2621 | 0.51 | 0.11785 | 0.003587 | 1831 | 82 | 1856 | 43 | 1924 | 55 | 5.07 |
| | | 1_09 | 0.3280 | 0.02207 | 5.405 | 0.4360 | 0.42 | 0.11958 | 0.010086 | 1828 | 107 | 1886 | 69 | 1950 | 151 | 6.65 |
| | | 1_27 | 0.3213 | 0.01246 | 5.321 | 0.3828 | 0.27 | 0.12196 | 0.011986 | 1796 | 61 | 1872 | 61 | 1985 | 175 | 10.5 |
| | intermediate | 1_16 | 0.3286 | 0.00898 | 5.164 | 0.1760 | 0.40 | 0.11394 | 0.004170 | 1832 | 44 | 1847 | 29 | 1863 | 42 | 1.73 |
| | | 1_13 | 0.3175 | 0.01885 | 4.983 | 0.3446 | 0.43 | 0.11397 | 0.003775 | 1777 | 92 | 1816 | 58 | 1864 | 78 | 4.85 |
| | | 1_32 | 0.3301 | 0.00721 | 5.180 | 0.1510 | 0.37 | 0.11429 | 0.006784 | 1839 | 35 | 1849 | 25 | 1869 | 39 | 1.63 |
| | | 1_18 | 0.3178 | 0.00771 | 5.071 | 0.1715 | 0.36 | 0.11490 | 0.005204 | 1779 | 38 | 1831 | 29 | 1878 | 41 | 5.58 |
| | | 1_17 | 0.3264 | 0.00859 | 5.146 | 0.1969 | 0.34 | 0.11567 | 0.003511 | 1821 | 42 | 1844 | 33 | 1890 | 44 | 3.83 |
| | | 1_35 | 0.3247 | 0.01638 | 5.338 | 0.2642 | 0.51 | 0.11711 | 0.002890 | 1813 | 80 | 1875 | 42 | 1913 | 44 | 5.50 |
| | | 1_29 | 0.3167 | 0.01398 | 5.155 | 0.2160 | 0.53 | 0.11837 | 0.003374 | 1774 | 68 | 1845 | 36 | 1932 | 41 | 8.92 |
| | rim | 1_14 | 0.3305 | 0.01672 | 5.151 | 0.2724 | 0.48 | 0.11161 | 0.003920 | 1841 | 81 | 1845 | 45 | 1826 | 68 | -0.81 |
| | | 1_31 | 0.3317 | 0.01026 | 5.070 | 0.2792 | 0.28 | 0.11173 | 0.005811 | 1847 | 50 | 1831 | 47 | 1828 | 61 | -1.03 |
| | | 1_38 | 0.3235 | 0.01170 | 5.036 | 0.3526 | 0.26 | 0.11281 | 0.003790 | 1807 | 57 | 1825 | 59 | 1845 | 109 | 2.13 |
| | | 1_40 | 0.3202 | 0.01010 | 4.957 | 0.3157 | 0.25 | 0.11351 | 0.004165 | 1791 | 49 | 1812 | 54 | 1856 | 83 | 3.66 |
| | | 1_36 | 0.3342 | 0.01071 | 5.285 | 0.2277 | 0.37 | 0.11381 | 0.004029 | 1859 | 52 | 1866 | 37 | 1861 | 56 | 0.13 |
| | | 1_37 | 0.3239 | 0.00860 | 5.160 | 0.1786 | 0.38 | 0.11409 | 0.003848 | 1809 | 42 | 1846 | 29 | 1866 | 46 | 3.14 |
| | | 1_41 | 0.3237 | 0.01056 | 5.111 | 0.2459 | 0.34 | 0.11479 | 0.004639 | 1808 | 51 | 1838 | 41 | 1877 | 53 | 3.82 |
| | | 1_39 | 0.3086 | 0.02051 | 4.920 | 0.3522 | 0.46 | 0.11543 | 0.006043 | 1734 | 101 | 1806 | 60 | 1887 | 61 | 8.80 |
| | | 1_15 | 0.3335 | 0.02356 | 5.397 | 0.3604 | 0.53 | 0.11578 | 0.005218 | 1855 | 114 | 1884 | 57 | 1892 | 90 | 1.99 |
| | | 1_20 | 0.3221 | 0.01453 | 5.130 | 0.2658 | 0.44 | 0.11596 | 0.002623 | 1800 | 71 | 1841 | 44 | 1895 | 59 | 5.28 |
| | | 1_33 | 0.3291 | 0.01258 | 5.167 | 0.2534 | 0.39 | 0.11598 | 0.004940 | 1834 | 61 | 1847 | 42 | 1895 | 65 | 3.34 |
| | | 1_22 | 0.3211 | 0.01383 | 5.176 | 0.2099 | 0.53 | 0.11690 | 0.002458 | 1795 | 67 | 1849 | 35 | 1909 | 62 | 6.36 |
| | | 1_21 | 0.3206 | 0.01304 | 5.131 | 0.2059 | 0.51 | 0.11732 | 0.002607 | 1793 | 64 | 1841 | 34 | 1916 | 59 | 6.86 |
| | | 1_34 | 0.3327 | 0.00804 | 5.379 | 0.2076 | 0.31 | 0.11776 | 0.002853 | 1851 | 39 | 1882 | 33 | 1923 | 71 | 3.85 |
| | | 1_19 | 0.3303 | 0.01118 | 5.369 | 0.2658 | 0.34 | 0.11821 | 0.002878 | 1840 | 54 | 1880 | 42 | 1929 | 92 | 4.86 |
| | | 1_11 | 0.3210 | 0.01198 | 5.254 | 0.2390 | 0.41 | 0.11837 | 0.002688 | 1795 | 58 | 1861 | 39 | 1932 | 79 | 7.64 |
| 170405-6 | core | 3_12 | 0.3351 | 0.01326 | 4.894 | 0.1800 | 0.54 | 0.10541 | 0.005807 | 1863 | 64 | 1801 | 31 | 1722 | 101 | -7.59 |
| | | 3_16 | 0.3338 | 0.00870 | 5.006 | 0.2193 | 0.30 | 0.10779 | 0.004615 | 1857 | 42 | 1820 | 37 | 1762 | 78 | -5.08 |
| | | 3_29 | 0.3228 | 0.01535 | 4.970 | 0.1916 | 0.62 | 0.11342 | 0.002135 | 1803 | 75 | 1814 | 33 | 1855 | 34 | 2.86 |
| | | 3_30 | 0.3159 | 0.01275 | 4.954 | 0.2082 | 0.48 | 0.11425 | 0.002087 | 1770 | 62 | 1812 | 35 | 1868 | 33 | 5.57 |
| | | 3_37 | 0.3304 | 0.01480 | 5.323 | 0.2526 | 0.47 | 0.11827 | 0.003595 | 1840 | 72 | 1873 | 41 | 1930 | 54 | 4.90 |
| | intermediate | 3_08 | 0.3409 | 0.01309 | 4.896 | 0.3325 | 0.28 | 0.10585 | 0.007622 | 1891 | 63 | 1802 | 57 | 1729 | 132 | -8.55 |
| | | 3_32 | 0.3291 | 0.01077 | 5.027 | 0.2553 | 0.32 | 0.11167 | 0.003837 | 1834 | 52 | 1824 | 43 | 1827 | 62 | -0.39 |
| | | 3_35 | 0.3307 | 0.01274 | 5.132 | 0.2462 | 0.40 | 0.11218 | 0.002742 | 1842 | 62 | 1841 | 41 | 1835 | 44 | -0.36 |
| | | 3_20 | 0.3273 | 0.00947 | 5.110 | 0.1759 | 0.42 | 0.11267 | 0.002032 | 1825 | 46 | 1838 | 29 | 1843 | 33 | 0.97 |
| | | 3_09 | 0.3141 | 0.01677 | 4.926 | 0.2767 | 0.48 | 0.11394 | 0.002505 | 1761 | 82 | 1807 | 47 | 1863 | 40 | 5.82 |
| | | 3_11 | 0.3201 | 0.00982 | 5.056 | 0.1778 | 0.44 | 0.11522 | 0.002510 | 1790 | 48 | 1829 | 30 | 1883 | 39 | 5.20 |
| | | 3_13 | 0.2825 | 0.03180 | 4.469 | 0.4908 | 0.51 | 0.11544 | 0.002534 | 1604 | 160 | 1725 | 91 | 1887 | 40 | 17.6 |
| | | 3_22 | 0.3251 | 0.00969 | 5.297 | 0.1562 | 0.51 | 0.11779 | 0.002536 | 1815 | 47 | 1868 | 25 | 1923 | 39 | 5.97 |
| | | 3_27 | 0.2686 | 0.01926 | 4.243 | 0.3393 | 0.45 | 0.11910 | 0.002688 | 1533 | 98 | 1682 | 66 | 1943 | 40 | 26.7 |
| | rim | 3_19 | 0.3382 | 0.00748 | 5.066 | 0.1941 | 0.29 | 0.10828 | 0.003569 | 1878 | 36 | 1830 | 32 | 1771 | 60 | -5.72 |
| | | 3_17 | 0.3180 | 0.01065 | 4.946 | 0.1800 | 0.46 | 0.11234 | 0.003320 | 1780 | 52 | 1810 | 31 | 1838 | 54 | 3.24 |
| | | 3_14 | 0.3186 | 0.01261 | 4.945 | 0.2284 | 0.43 | 0.11245 | 0.002089 | 1783 | 62 | 1810 | 39 | 1839 | 34 | 3.15 |
| | | 3_36 | 0.3249 | 0.01470 | 5.055 | 0.2461 | 0.46 | 0.11282 | 0.002258 | 1813 | 72 | 1829 | 41 | 1845 | 36 | 1.75 |
| | | 3_28 | 0.3200 | 0.01814 | 5.077 | 0.2489 | 0.58 | 0.11446 | 0.003035 | 1790 | 89 | 1832 | 42 | 1871 | 48 | 4.57 |
| | | 3_34 | 0.3261 | 0.01212 | 5.137 | 0.2217 | 0.43 | 0.11449 | 0.001800 | 1819 | 59 | 1842 | 37 | 1872 | 28 | 2.88 |
| | | 3_33 | 0.3296 | 0.01377 | 5.210 | 0.2404 | 0.45 | 0.11452 | 0.002282 | 1837 | 67 | 1854 | 39 | 1872 | 36 | 1.95 |
| | | 3_15 | 0.3211 | 0.00892 | 5.055 | 0.1688 | 0.42 | 0.11491 | 0.002471 | 1795 | 44 | 1829 | 28 | 1878 | 39 | 4.64 |
| | | 3_31 | 0.3350 | 0.01167 | 5.241 | 0.1983 | 0.46 | 0.11507 | 0.002391 | 1863 | 56 | 1859 | 32 | 1881 | 37 | 0.99 |
| | | 3_10 | 0.3195 | 0.01117 | 5.200 | 0.1546 | 0.59 | 0.11751 | 0.002485 | 1787 | 55 | 1853 | 25 | 1919 | 38 | 7.36 |

***Fransfontein Suite***

***<u>Kamdescha granite (sample 260205-4)</u>***

The euhedral to subhedral, short prismatic to isometric, often tabular zircons are mostly semitransluscent greyish-pink and rarely translucent, rose. The crystals are unaffected by subsequent alteration and deformation and generally only a few cracks are developed in individual grains. Back scattered electron (BSE) and cathodoluminiscene (CL) imagery reveals in most grains oscillatory igneous zoning and dark inclusions (Fig. 74) and only few are amorphic. Zoning results from compositional changes; lighter shades of grey in the BSE (correlating with darker shades in the CL) correspond to higher concentrations of heavy trace elements. Similarly, the core of many grains shows heavy trace element enrichment. Metamorphic overgrowth is indicated in a few grains by metamict rims (Fig. 74g-h).

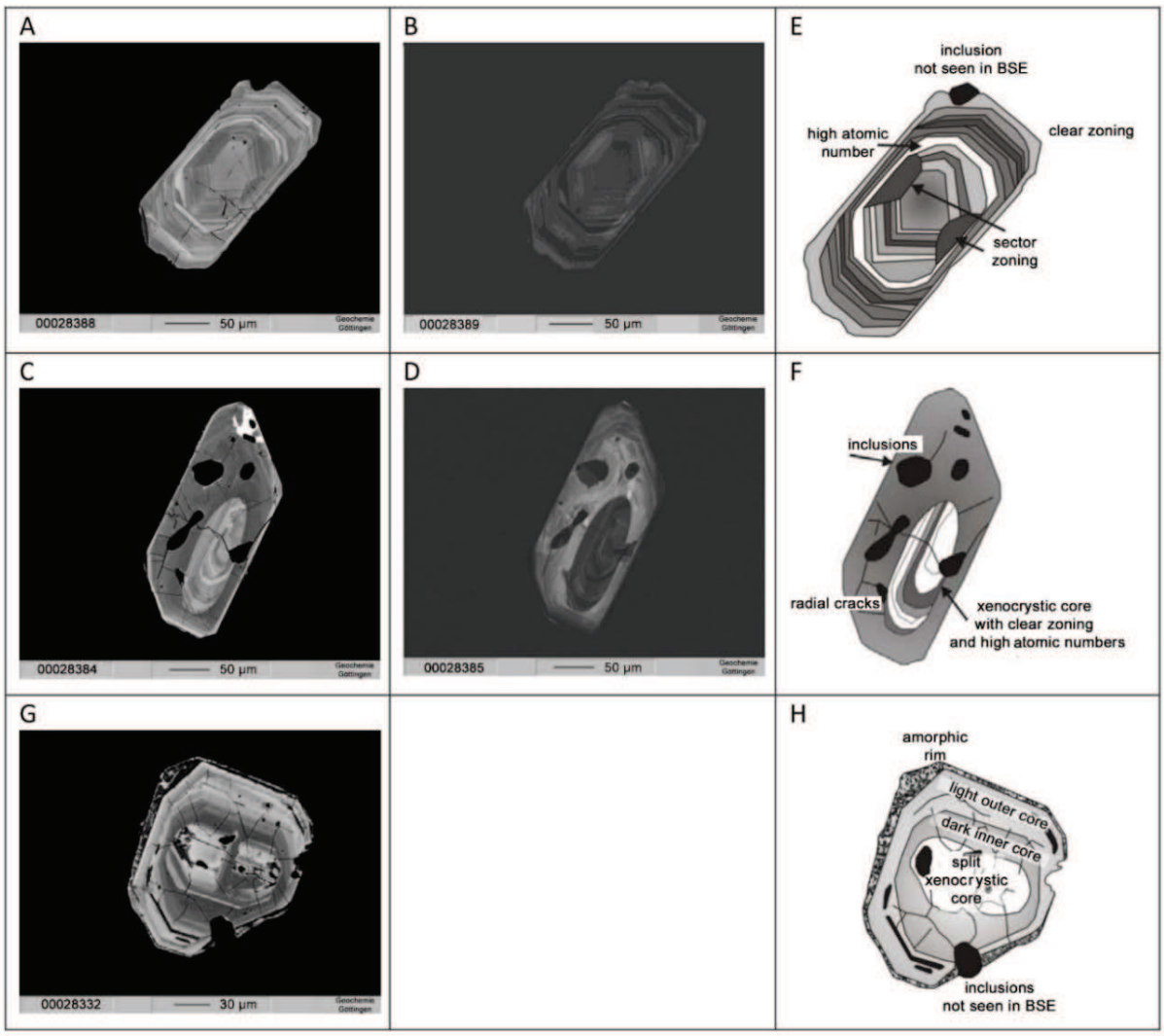


**Figure 74**. Zircons of sample 260205-4 (Kamdescha granite). A, C, G) Back-scattered electron image (BSE); B, D) cathodoluminiscence image (CL); E, F, H) sketches illustrating the characteristic features of the grains.

The results of 21 spot analyses from the cores, intermediate and outer parts of several zircon grains are presented in Table 22. The analyses are arranged in each group from younger to older $Pb^{207}/Pb^{206}$ ages; discordances higher than 10% are marked in red indicating that the age is less reliable. The groups display similar ages ranging from 1823-1873 Ma (core), 1821-1885 Ma (intermediate) and 1744-1974 (outer part). Two younger rim ages of 1744±174 Ma and 1756±52 Ma indicate possibly metamorphic overgrowth. Calculation of concordia ages based on the method by Wetherill (1956) yielded similar ages of 1824±27 Ma (core), 1826±25 Ma (intermediate) and 1827±41 Ma (rim). The combined age of

1826±15 Ma is considered as very reliable and is interpreted to date the emplacement of the Kamdescha pluton.

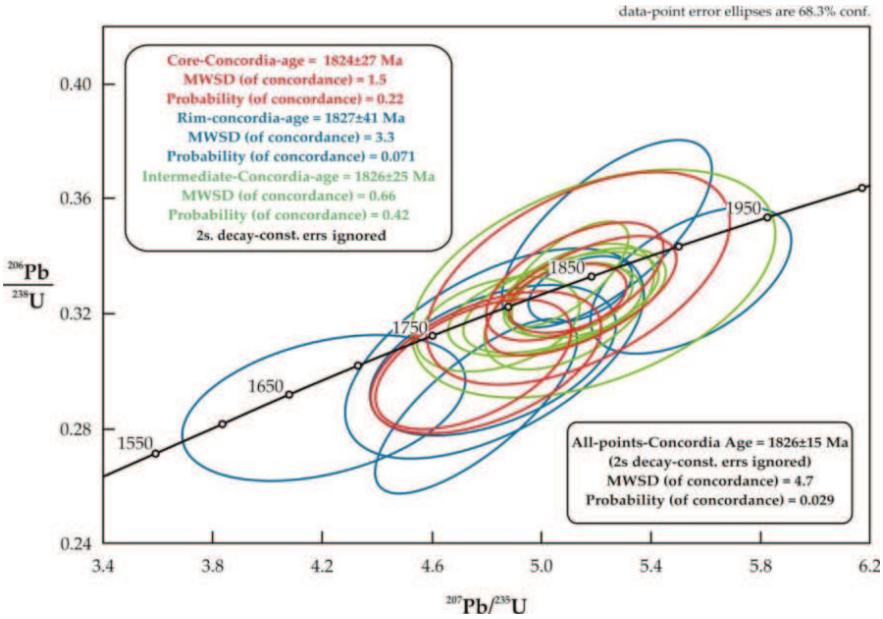


**Figure 75**. Concordia diagram of analyses from sample 260205-4 (Kamdescha granite). The data have been grouped by their position to core, intermediate and rim.

***Franken granodiorite (sample 280205-6)***

The transluscent, light pink, euhedral, zircons are generally short to long prismatic with few having isometric shapes. The crystals are unaffected by deformation and alteration and are devoid of any cracks. BSE and CL imagery reveal igneous, sometimes convolute and sector zoning and in some grains minute inclusions. As in the Kamdescha sample a first phase of magmatic growth is indicated by subhedral cores with subrounded crystal faces overgrown by the second zircon generation marked by fine oscillation zoning (Fig. 76).

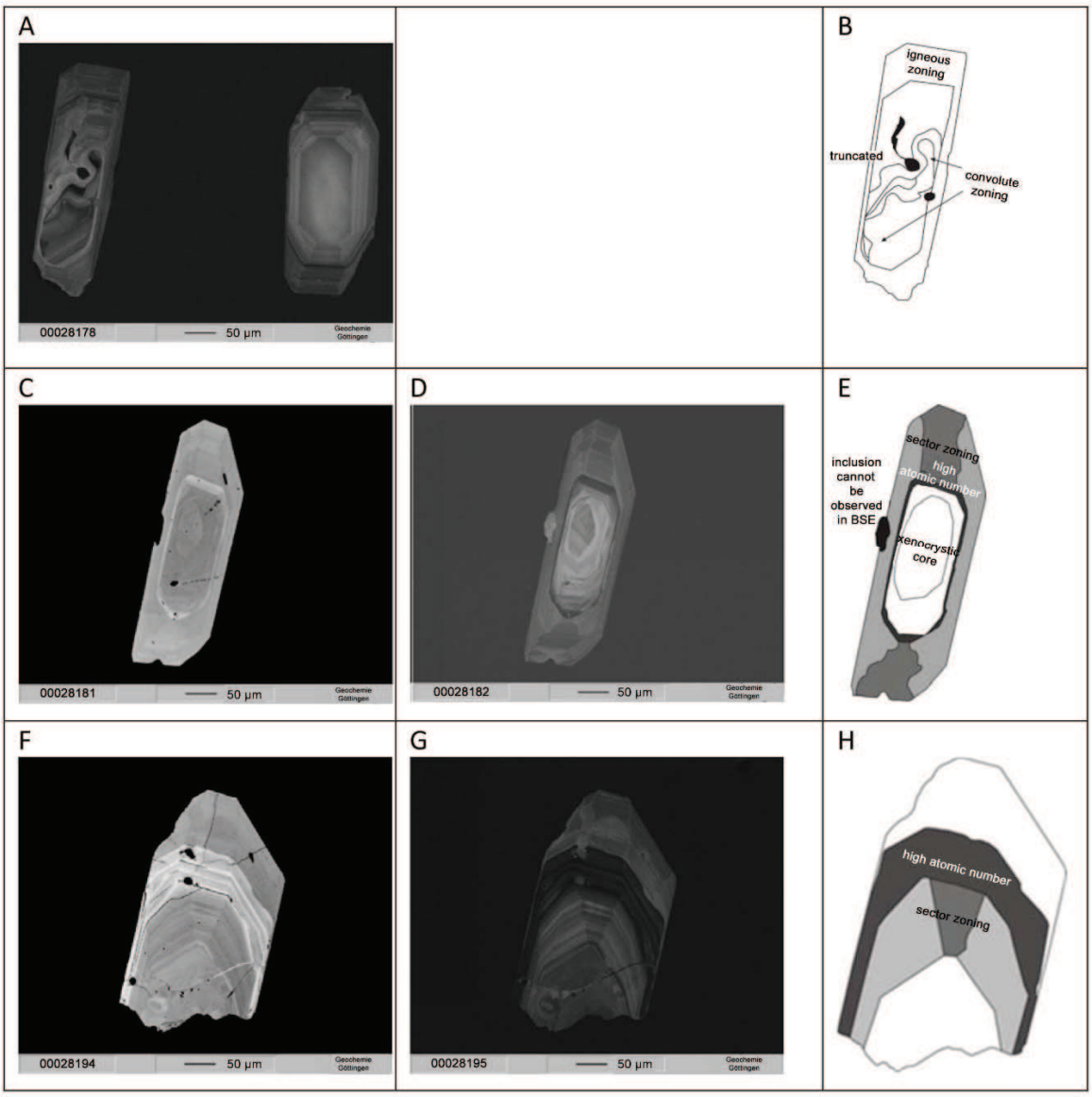


**Figure 76**. Zircons of sample 280205-6 (Franken granite). A, C, F) Back-scattered electron image (BSE); D, G) cathodoluminiscence image (CL); B, E, H) sketches illustrating the characteristic features of the grains.

The results of 30 spot analyses from the cores, intermediate and outer parts of several zircon grains are given in Table 22; the data are arranged in each group by increasing $Pb^{207}/Pb^{206}$ age and discordances higher than 10% are marked in red. Only one analysis (1-27) yielded an increased discordance of 10.5% indicating high reliability of the other data. The groups display similar $Pb^{207}/Pb^{206}$ ages ranging from 1791-1985 Ma (core), 1863-1932 Ma (intermediate) and 1826-1932 (outer part). No metamorphic overprint has been identified despite numerous analyses in the zircons rims.

Calculation of concordia ages after Wetherill (1956) yielded for all domains similar ages of 1837±38 Ma (core), 1839±19 Ma (intermediate) and 1843±19 Ma (rim). The combined age of 1841±14 Ma is considered to be very reliable and is interpreted to date the emplacement of the Franken pluton ca 15 myr prior the Kamdescha pluton.

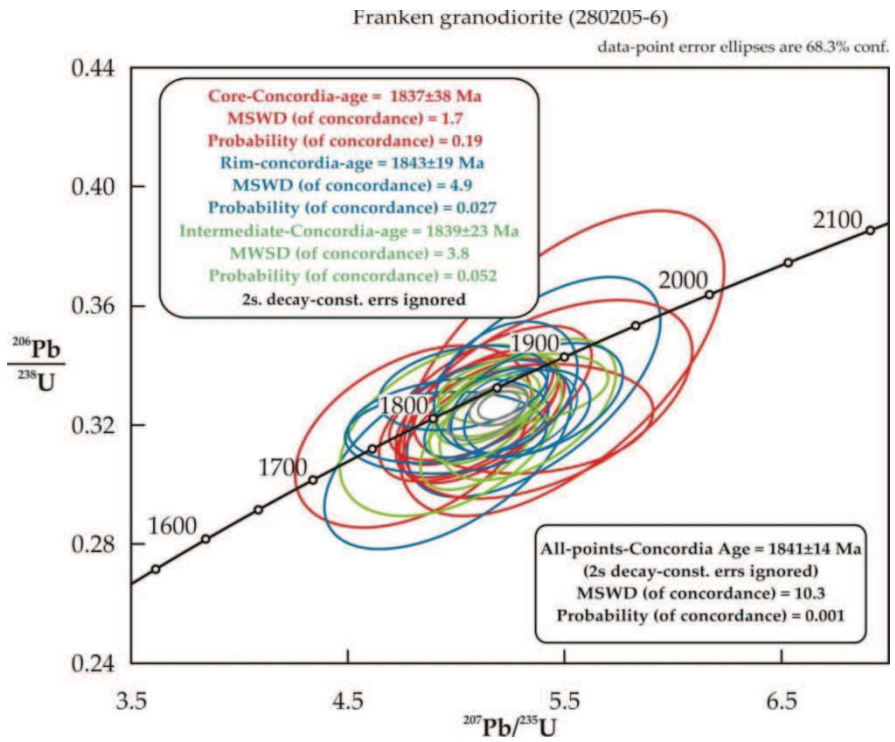


**Figure 77**. Concordia diagram of analyses from sample 280205-6 (Franken granite).

***Kaross granite (170405-6)***

The zircons are translucent light pink to semitranslucent greyish-pink in colour and of short prismatic euhedral to subhedral shape with slightly rounded edges (Fig. 78). Many grains display cracks documenting brittle deformation. Most CL-images have only low optical resolution and are not shown. BSE and CL imagery reveal oscillatory magmatic zoning. Unzoned cores in some grains witness an older phase of magmatism; they are often rounded and sometimes truncated during subsequent crystallisation, which probably resulted from partial digestion by the younger magma. Metamict rims in some grains illustrate zonal possibly metamorphic overgrowth. Higher U-concentrations resulted in the destruction of the crystal lattice by radioactive decay.

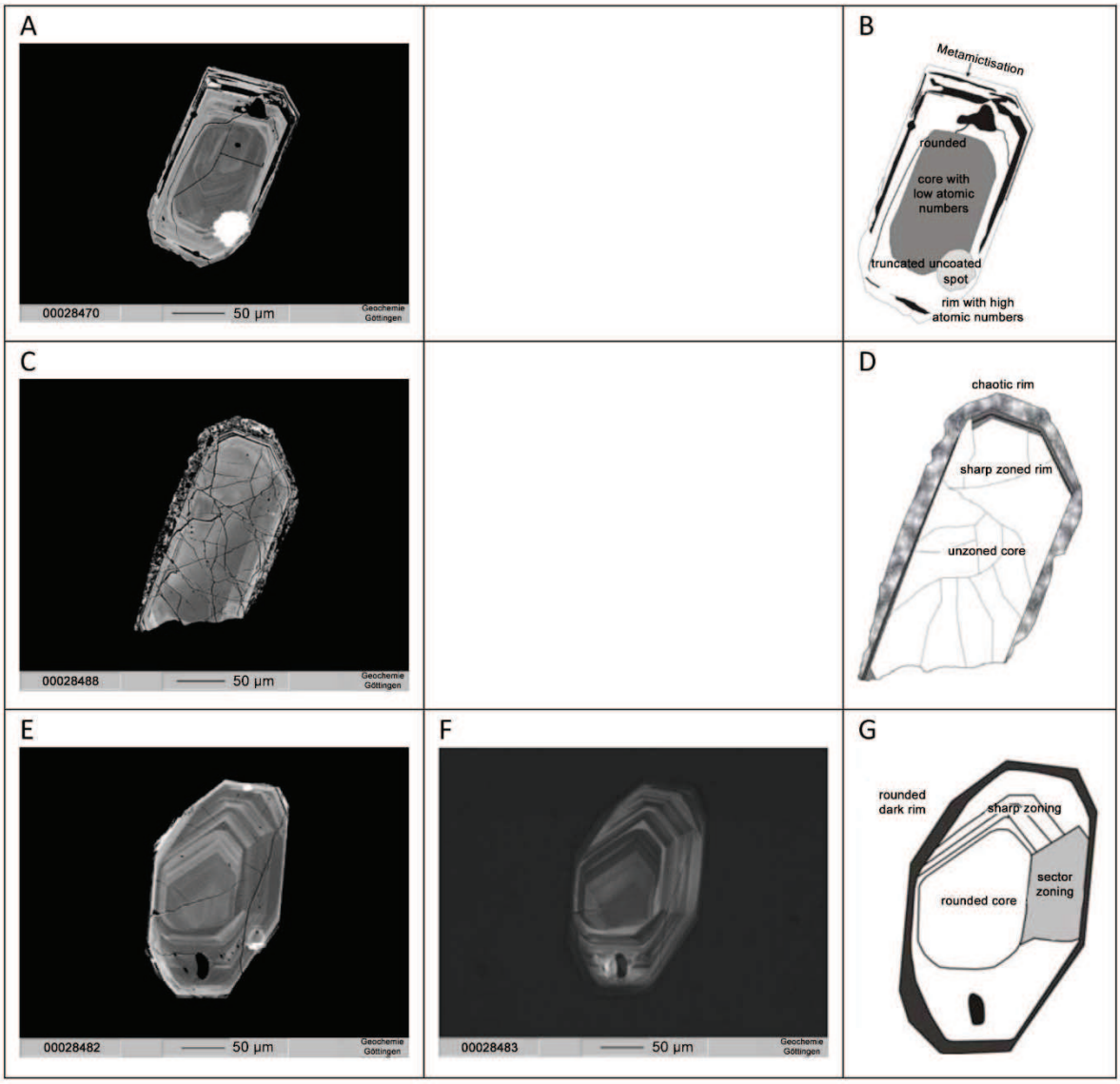


**Figure 78**. Zircons of sample 170405-6 (Kaross granite). A, C, E) Back-scattered electron image (BSE); F) cathodoluminiscence image (CL); B, D, G) sketches illustrating the characteristic features of the grains.

The results of 24 spot analyses from the cores, intermediate and outer parts of several zircon grains are given in Table 22. Two analyses (3-13, 3-27) yielded discordances above 10% indicating high reliability of the other data. The groups display similar $Pb^{207}/Pb^{206}$ ages ranging from 1722-1930 Ma (core), 1729-1943 Ma (intermediate) and 1771-1919 Ma (rim). No distinct metamorphic overprint has been identified despite numerous analyses in the outer part of the zircons.

Similar concordia ages were calculated for all domains of the grain yielding 1822±30 Ma (core), 1828±25 Ma (intermediate) and 1837±20 Ma (outer part). The combined age of 1831±14 Ma is considered to be very reliable and is interpreted to date the emplacement of the Kaross pluton in the period between the older Franken and younger Kamdescha plutons (Fig. 79).

$^{207}Pb/^{206}Pb$ ages up to ca 1940 Ma in all samples of the FFG reveal the presence of an older assimilated component of sedimentary (detrital zircons) or magmatic origin and corroborating the results of Sm-Nd studies. A magmatic origin of the inclusions would imply an older (Eburnian) underlying basement from which the magmas originated or which they traversed during their ascent. A detrital origin would constrain the maximum deposition age of the country rock.

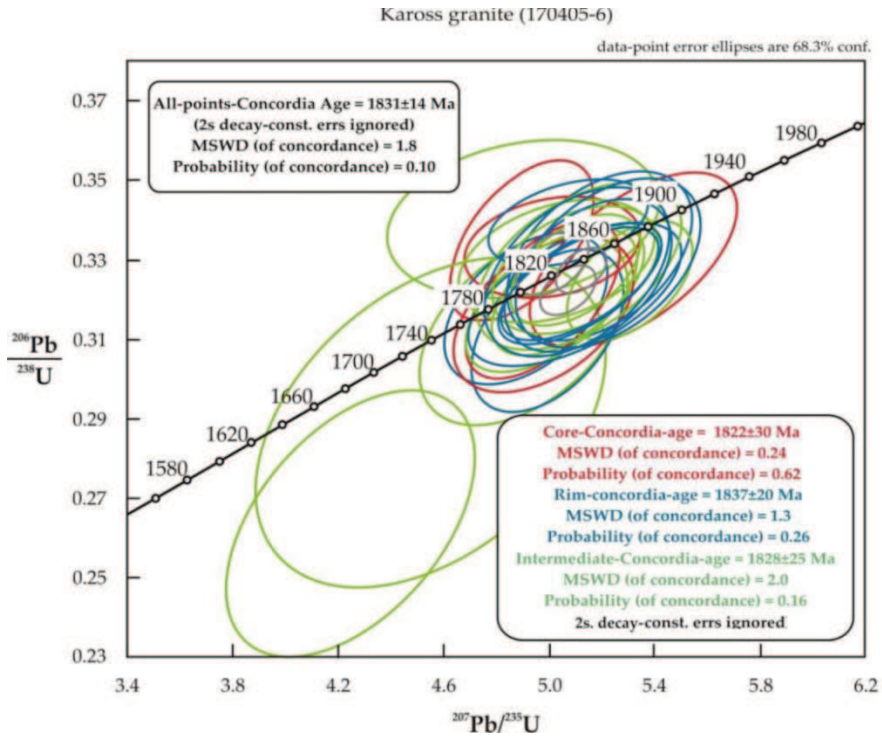


**Figure 79**. Concordia diagram of analyses from sample 170405-6 (Kaross granite).

***Huab Metamorphic Complex***

The results of LA-ICP-MS U-Pb single zircon analysis of three igneous samples from the HMC are given in Table 23. The data often show discordances above 10% indicating partial reset of the U-Pb isotope system by metamorphic or hydrothermal alteration that did not affect the granites of the FFG. The calculated $Pb^{207}/Pb^{206}$ ages are often older than 1900 Ma and up to 2200 Ma suggesting significant assimilation of an older crustal component.

***Mylonitic Red Granite Orthogneiss (ROG, sample 210900-2/HU01)***

The sample has been taken from a regional folded sheet-like intrusion (megasill) of non-migmatitic ROG emplaced into a series of quartzite and garnet-muscovite-quartz-feldspar paragneiss and subsequently transposed into parallelism with the regional gneissic fabric. All rocks are mylonitic and display prominent stretching lineations. The ROG resembles in hand specimen and intrusion mode the Kaross granite of the FFG Suite of which it may represent a higher metamorphic grade equivalent.

The translucent pale pink zircons are mostly euhedral and prismatic; columnar and isometric rounded anhedral shapes were also observed. Most zircons are broken into angular fragments, which may result from mylonitic overprint affecting the rocks pervasively. Low CL signals resulting in dark images without any information are not shown. BSE imagery reveal complex internal structures that vary widely between individual zircon grains; three examples are shown in Fig 80. A typical zircon is shown in Fig. 80a-d. The subhedral, long prismatic crystal is composed of an older rounded xenocrystic core that is truncated and surrounded by an intermediate domain marked by widely spaced oscillation growth forming a euhedral crystal with slightly rounded edges. A second stage of subsequent magmatic growth in the outer segment is characterised by faint oscillation zoning. Fig. 80b-e shows a highly altered zircon comprising an unzoned core, an intermediate domain with magmatic oscillation zoning and a metamict rim. The grain is traversed by cracks that are partly filled with secondary microcrystalline minerals. The third crystal (Fig. 80c/f) has a euhedral, long prismatic, tabular shape and comprises abundant inclusions of both zircon xenocryst fragments and other minerals. Two phases of magmatic growth are recorded by the sudden change in the oscillation pattern from the intermediate to outer part of the grain.

The results of 15 spot analyses from the cores, intermediate and outer parts of several zircon grains are given in Table 23. 8 out of 15

analyses are marked by discordances above 10 % indicating significant reset of the U-Pb isotope system after zircon crystallisation. The different domains show widely varying $Pb^{207}/Pb^{206}$ ages in the intervals [1856-2096 Ma] (core), [1729-1928 Ma] (intermediate) and [1828-2201] (rim). The significantly higher rim ages are interpreted to reflect recrystallisation and Pb-isotope exchange with the host rock during deformation.

Calculation of the discordia ages yielded 1931±67 Ma (core), $1829^{+71}/_{-69}$ Ma (intermediate) and $1887^{+97}/_{-100}$ Ma (outer part) whereas the combined age was calculated at 1883 +44/-45 Ma (MSWD = 0.93; Fig. 81). The elevated discordia age of the core domain probably dates a mixture of older xenocrysts with newly grown magmatic zircon of the intermediate domain. The rim and combined ages have no geological meaning. The intermediate age of $1829^{+71}/_{-69}$ Ma is therefore considered as a best estimate for the emplacement of the ROG and close to the age of the Kaross granite (1831±14 Ma). It constrains the minimum age of M2 gneissic recrystallisation, regional transposition and mylonitic overprint.

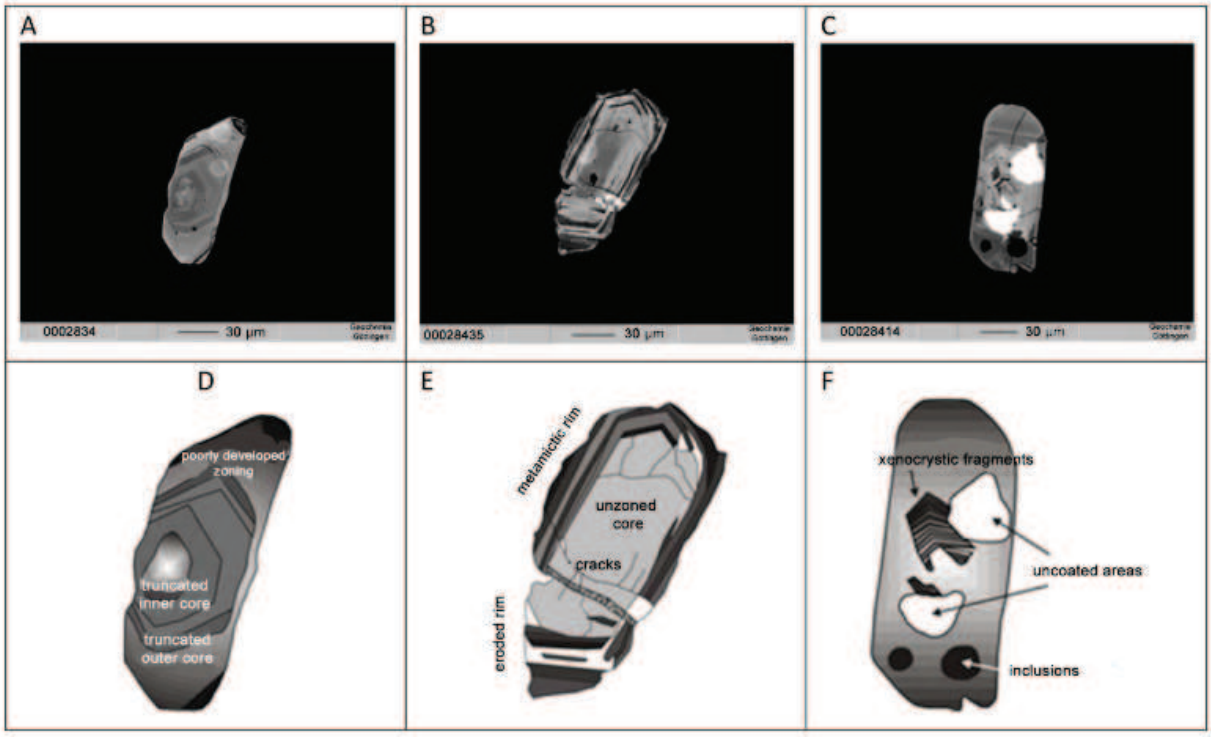


**Figure 80**. Zircons of sample 210900-2 (Red orthogneiss). A-C) Back-scattered electron image (BSE); D-F) sketches illustrating the characteristic features of the grains.

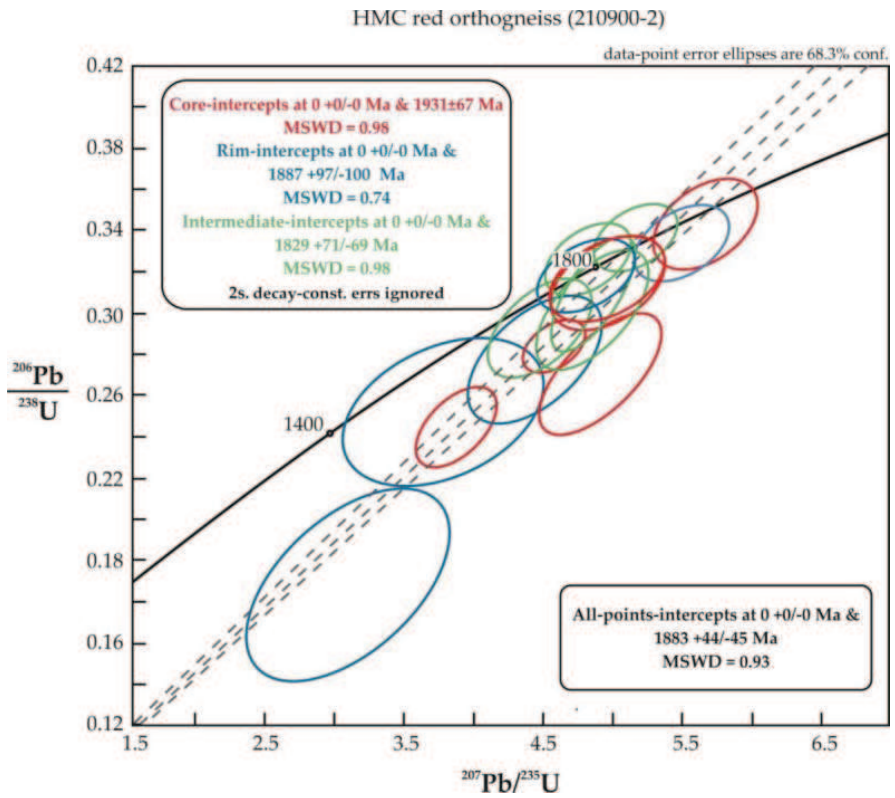


**Figure 81**. Concordia diagram with analyses of sample 210900-2 (Red Orthogneiss, ROG).

***Gneissic K-feldspar-porphyry (sample 130503-1)***

The non-migmatitic massive orthogneissic rock from the Upper Sequence of the Suiderkruis SD shows in hand specimen K-feldspar-porphyries up to cm-size in a medium-grained equigranular biotite-quartz-feldspar matrix. An intrusive or a volcanic origin is possible. Similar rocks nearby are intercalated into a series of muscovite-quartz-feldspar gneiss, alternating with quartzite, amphibolite and garnet-leucogneiss; one of the layers is interpreted to be a mylonitic sill granite whereas in other localities the rocks were interpreted as metarhyolite/ignimbrite.

Most zircons of sample 130503-1 are fragmented or otherwise damaged by mylonitic deformation. A few well-preserved crystals display euhedral long-prismatic and, less abundant, isometric shapes with well-rounded, irregular rims indicating magmatic corrosion. BSE and CL images reveal complex internal patterns (oscillatory and sector zoning) indicating several phases of magmatic growth, however, inclusions of xenocrysts are rather rare (Fig. 83). A narrow light rim around many grains is revealed by CL and possibly records a stage of metamorphic overgrowth. Internal irregular cavities are due to magmatic corrosion or other post-crystallisation alteration processes

**Table 23.** U-Pb single zircon ages by LA-ICP-MS method. Samples of HMC orthogneiss. Discordancies > 10% are marked in red.

| Sample | Pos | spot | Isotopic ratios | | | | | | | Ages [Ma] | | | | | | |
|---|---|---|---|---|---|---|---|---|---|---|---|---|---|---|---|---|
| | | | 206/238 | ±1σ | 207/235 | ±1σ | rho | 207/206 | ±1σ | 6/8 age | ±1σ | 7/5 age | ±1σ | 7/6 age | ±1σ | disc % |
| 210900-2 | core | 2_57 | 0.3148 | 0.01503 | 4.983 | 0.2734 | 0.44 | 0.11349 | 0.003817 | 1764 | 74 | 1816 | 46 | 1856 | 61 | 5.19 |
| | | 2_58 | 0.2451 | 0.01312 | 3.891 | 0.1913 | 0.54 | 0.11443 | 0.004588 | 1413 | 68 | 1612 | 40 | 1871 | 72 | 32.4 |
| | | 2_62 | 0.3161 | 0.01228 | 4.952 | 0.2888 | 0.33 | 0.11488 | 0.003702 | 1771 | 60 | 1811 | 49 | 1878 | 58 | 6.07 |
| | | 2_59 | 0.2841 | 0.00816 | 4.593 | 0.1522 | 0.43 | 0.11864 | 0.002825 | 1612 | 41 | 1748 | 28 | 1936 | 43 | 20.1 |
| | | 2_55 | 0.3433 | 0.01421 | 5.683 | 0.2509 | 0.47 | 0.11899 | 0.003158 | 1902 | 68 | 1929 | 38 | 1941 | 47 | 2.03 |
| | | 2_61 | 0.2708 | 0.01917 | 4.922 | 0.2847 | 0.61 | 0.12989 | 0.008868 | 1545 | 97 | 1806 | 49 | 2096 | 120 | 35.7 |
| | intermediate | 2_63 | 0.3264 | 0.01190 | 4.842 | 0.1995 | 0.44 | 0.10957 | 0.002107 | 1821 | 58 | 1792 | 35 | 1792 | 35 | -1.57 |
| | | 2_67 | 0.3368 | 0.01086 | 5.174 | 0.1981 | 0.42 | 0.11112 | 0.003514 | 1871 | 52 | 1848 | 33 | 1818 | 57 | -2.87 |
| | | 2_56 | 0.2928 | 0.01572 | 4.494 | 0.2395 | 0.50 | 0.11174 | 0.002284 | 1655 | 78 | 1730 | 44 | 1828 | 37 | 10.4 |
| | | 2_60 | 0.3099 | 0.01840 | 4.877 | 0.2059 | 0.70 | 0.11413 | 0.003105 | 1740 | 91 | 1798 | 36 | 1866 | 49 | 7.24 |
| | | 2_65 | 0.3017 | 0.01929 | 4.866 | 0.2653 | 0.59 | 0.11809 | 0.004469 | 1700 | 96 | 1796 | 46 | 1928 | 68 | 13.4 |
| | rim | 2_64 | 0.2777 | 0.02020 | 4.456 | 0.3157 | 0.51 | 0.11174 | 0.003064 | 1580 | 102 | 1723 | 59 | 1828 | 50 | 15.7 |
| | | 2_54 | 0.3192 | 0.01168 | 4.816 | 0.2337 | 0.38 | 0.11181 | 0.002661 | 1786 | 57 | 1788 | 41 | 1829 | 43 | 2.42 |
| | | 2_53 | 0.3343 | 0.01207 | 5.509 | 0.2291 | 0.43 | 0.12071 | 0.002617 | 1859 | 58 | 1902 | 36 | 1967 | 39 | 5.77 |
| | | 2_68 | 0.2525 | 0.02343 | 3.790 | 0.4807 | 0.37 | 0.13194 | 0.022101 | 1451 | 121 | 1591 | 102 | 2124 | 293 | 46.3 |
| | | 2_66 | 0.1696 | 0.03038 | 3.108 | 0.4875 | 0.57 | 0.13789 | 0.007184 | 1010 | 167 | 1435 | 120 | 2201 | 90 | 118 |
| 130503-1 | core | 2_46 | 0.3286 | 0.00960 | 4.944 | 0.2190 | 0.33 | 0.11059 | 0.003505 | 1832 | 47 | 1810 | 37 | 1809 | 58 | -1.23 |
| | int | 2_41 | 0.3162 | 0.01306 | 4.798 | 0.2539 | 0.39 | 0.10999 | 0.003046 | 1771 | 64 | 1785 | 44 | 1799 | 50 | 1.58 |
| | | 2_47 | 0.3407 | 0.01770 | 6.156 | 0.3288 | 0.49 | 0.13195 | 0.002784 | 1890 | 85 | 1998 | 47 | 2124 | 37 | 12.4 |
| | rim | 2_43 | 0.3365 | 0.00804 | 4.987 | 0.3214 | 0.19 | 0.10672 | 0.007334 | 1870 | 39 | 1817 | 55 | 1744 | 126 | -6.71 |
| | | 2_39 | 0.3324 | 0.01072 | 4.929 | 0.2367 | 0.34 | 0.10826 | 0.004354 | 1850 | 52 | 1807 | 41 | 1770 | 73 | -4.30 |
| | | 2_48 | 0.3335 | 0.01356 | 5.173 | 0.2391 | 0.44 | 0.11411 | 0.002335 | 1855 | 66 | 1848 | 39 | 1866 | 37 | 0.56 |
| | | 2_45 | 0.2960 | 0.01136 | 4.543 | 0.1961 | 0.44 | 0.11584 | 0.003143 | 1672 | 56 | 1739 | 36 | 1893 | 49 | 13.2 |
| | | 2_42 | 0.3282 | 0.01681 | 5.037 | 0.2398 | 0.54 | 0.11745 | 0.005560 | 1830 | 82 | 1826 | 40 | 1918 | 85 | 4.80 |
| | | 2_40 | 0.3274 | 0.01287 | 5.468 | 0.2054 | 0.52 | 0.12062 | 0.005203 | 1826 | 63 | 1896 | 32 | 1965 | 77 | 7.66 |
| HU-3 | core | 1_73 | 0.3248 | 0.00905 | 5.066 | 0.2011 | 0.35 | 0.11297 | 0.002970 | 1813 | 44 | 1830 | 34 | 1848 | 48 | 1.91 |
| | | 1_70 | 0.3009 | 0.01484 | 4.774 | 0.2445 | 0.48 | 0.11372 | 0.002590 | 1696 | 74 | 1780 | 43 | 1860 | 41 | 9.67 |
| | | 1_50 | 0.3082 | 0.01010 | 4.842 | 0.1510 | 0.53 | 0.11380 | 0.001570 | 1732 | 50 | 1792 | 26 | 1861 | 25 | 7.46 |
| | | 1_46 | 0.3127 | 0.02524 | 4.968 | 0.4326 | 0.46 | 0.11482 | 0.004963 | 1754 | 124 | 1814 | 74 | 1877 | 78 | 7.03 |
| | | 1_67 | 0.3201 | 0.01339 | 5.106 | 0.2083 | 0.51 | 0.11549 | 0.002389 | 1790 | 65 | 1837 | 35 | 1888 | 37 | 5.44 |
| | | 1_60 | 0.3167 | 0.01321 | 5.069 | 0.2769 | 0.38 | 0.11615 | 0.003982 | 1774 | 65 | 1831 | 46 | 1898 | 62 | 7.00 |
| | | 1_49 | 0.3172 | 0.01586 | 5.487 | 0.3979 | 0.34 | 0.12026 | 0.007639 | 1776 | 78 | 1898 | 62 | 1960 | 113 | 10.4 |
| | | 1_52 | 0.3006 | 0.01678 | 5.011 | 0.3234 | 0.43 | 0.12299 | 0.006381 | 1694 | 83 | 1821 | 55 | 2000 | 92 | 18.0 |
| | | 1_65 | 0.2865 | 0.01931 | 4.952 | 0.2234 | 0.75 | 0.12380 | 0.003750 | 1624 | 97 | 1811 | 38 | 2012 | 54 | 23.9 |
| | intermediate | 1_69 | 0.3314 | 0.00808 | 5.113 | 0.2023 | 0.31 | 0.11265 | 0.003258 | 1845 | 39 | 1838 | 34 | 1843 | 52 | -0.13 |
| | | 1_59 | 0.3268 | 0.00753 | 5.142 | 0.1479 | 0.40 | 0.11287 | 0.002438 | 1823 | 37 | 1843 | 24 | 1846 | 39 | 1.29 |
| | | 1_53 | 0.3277 | 0.02177 | 5.227 | 0.2192 | 0.79 | 0.11344 | 0.009800 | 1827 | 106 | 1857 | 36 | 1855 | 156 | 1.54 |
| | | 1_57 | 0.2942 | 0.01614 | 4.800 | 0.2201 | 0.60 | 0.11755 | 0.002554 | 1663 | 80 | 1785 | 39 | 1919 | 39 | 15.4 |
| | | 1_48 | 0.3133 | 0.01349 | 5.242 | 0.2202 | 0.51 | 0.11886 | 0.003458 | 1757 | 66 | 1859 | 36 | 1939 | 52 | 10.4 |
| | | 1_51 | 0.3559 | 0.01308 | 6.283 | 0.2783 | 0.41 | 0.12665 | 0.003169 | 1963 | 62 | 2016 | 39 | 2052 | 44 | 4.56 |
| | | 1_54 | 0.2809 | 0.05368 | 4.992 | 0.4964 | 0.96 | 0.12755 | 0.009566 | 1596 | 270 | 1818 | 84 | 2064 | 132 | 29.4 |
| | | 1_74 | 0.3106 | 0.01391 | 5.231 | 0.2450 | 0.48 | 0.12952 | 0.007318 | 1744 | 68 | 1858 | 40 | 2091 | 99 | 19.9 |
| | rim | 1_58 | 0.3296 | 0.01071 | 5.176 | 0.1859 | 0.45 | 0.11274 | 0.002366 | 1837 | 52 | 1849 | 31 | 1844 | 38 | 0.41 |
| | | 1_66 | 0.3371 | 0.00875 | 5.188 | 0.2013 | 0.33 | 0.11312 | 0.002566 | 1873 | 42 | 1851 | 33 | 1850 | 41 | -1.20 |
| | | 1_68 | 0.3170 | 0.02253 | 5.130 | 0.3414 | 0.53 | 0.11510 | 0.008450 | 1775 | 110 | 1841 | 57 | 1881 | 132 | 6.00 |
| | | 1_72 | 0.3219 | 0.01129 | 5.241 | 0.1912 | 0.48 | 0.11577 | 0.002758 | 1799 | 55 | 1859 | 31 | 1892 | 43 | 5.17 |
| | | 1_71 | 0.3092 | 0.01045 | 4.874 | 0.1980 | 0.42 | 0.11631 | 0.002697 | 1737 | 51 | 1798 | 34 | 1900 | 42 | 9.42 |

.

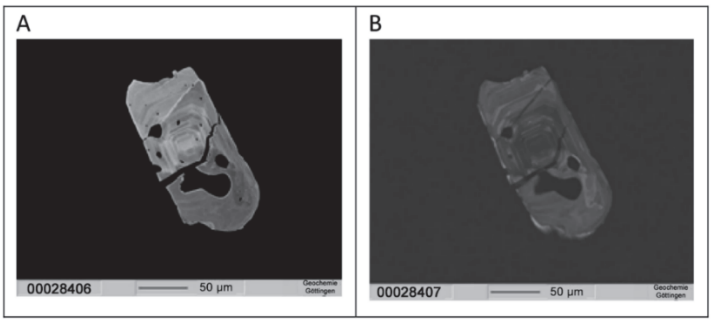


**Figure 82**. A) BSE and B) CL imagery of a well-preserved zircon from sample 130503-1.

The results of 9 spot analyses from the core (1), intermediate (2) and outer (6) parts of several zircons are given in Table 23. 2 analyses are marked by discordances above 10% indicating significant reset of the U-Pb isotope system after zircon crystallisation. $Pb^{207}/Pb^{206}$ ages have been calculated at 1809±58 Ma (core), and with large errors in the intervals [1799-2124 Ma] (intermediate) and [1744-1965 Ma] (margin).

The concordia ages were calculated at 1817±67 Ma (core), at 1860±210 Ma (intermediate) and at 1827±29 Ma (outer part). The combined age was calculated at 1831±25 Ma (MSWD = 0.43) and is considered to be a good estimate for the timing of magmatic crystallisation (Fig. 83). It coincides within errors with the emplacement ages of the FFG granites, the ROG and the POGD (see below) in the period between 1840-1820 Ma.

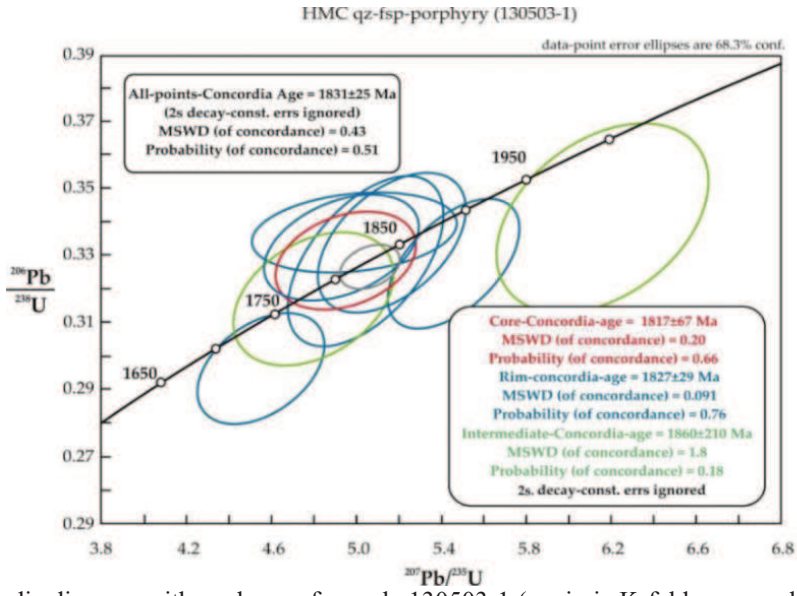


**Figure 83**. Concordia diagram with analyses of sample 130503-1 (gneissic K-feldspar porphyry) from the Upper Sequence of the HMC.

***K-feldspar porpyhritic granodiorite (augen) gneiss (POGD, sample 100900/HU-03)***

The POGD forms deca-kilometric intrusions of folded sheet-like geometry similar to that of the ROG to which it is sometimes subparallel. The massive, dark grey rock is characterised in hand specimen by cm-size K-feldspar set in a coarse-grained, equigranular biotite-quartz-feldspar matrix. In different parts of the HMC it is variously overprinted by one or several processes (i) grain flattening, (ii) simple shearing and mylonitisation and (iii) recrystallisation resulting in grain-size reduction. In the Rooikop SD, migmatitic orthogneiss of similar appearance has been observed, however, it is unclear whether this facies belongs to the POGD, which is elsewhere non-migmatitic.

Sample 100900 (HU-03) is from a blasted outcrop along the Mesepotamie-Huab Valley road. Two zircon populations of translucent rosy and cloudy brown zircons can be distinguished by binocular. Very dark CL-images provide no information on internal structures and are not presented in Fig. 84.

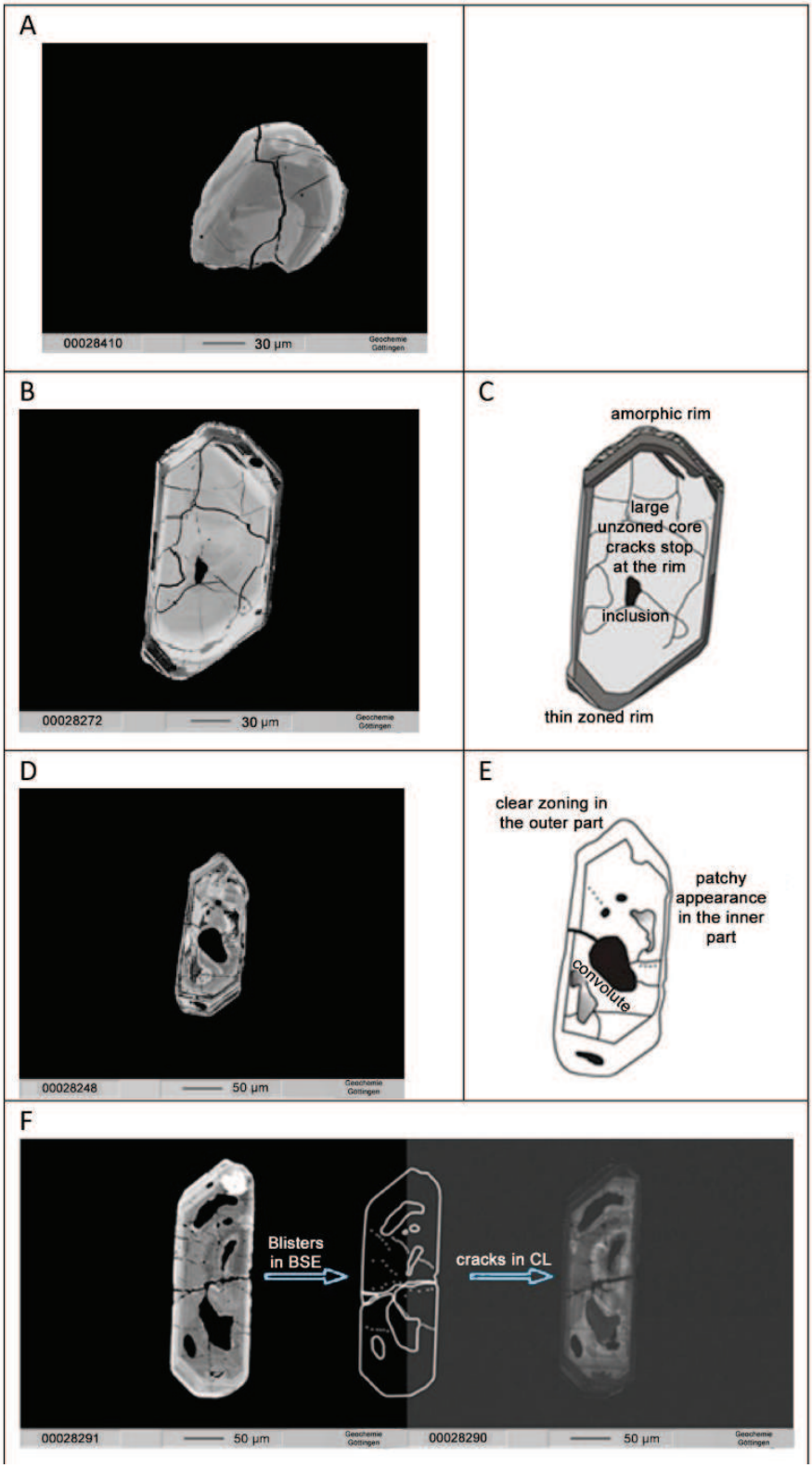


**Figure 84**. Zircons of sample 100900 (K-feldspar augengneiss POGD); left: Back-scattered electron image; right: sketches illustrating the characteristic features of the grains. CL images were dark and therefore are not shown.

In BSE imagery many crystals are fragmented, show numerous cracks (which may result partly from the road blast) and form again two populations. Zircons of the first group display faint internal zoning, which can be also absent. The often well-rounded grains show generally few cracks, inclusions or cavities (Fig. 84a). Group 2 zircons are euhedral to subhedral, short to long prismatic and display chaotic, sometimes highly damaged, internal structures.

Several grains are traversed by numerous cracks that stop, however, at the zoned rims excluding their origin by mechanical fracturing during sample preparation or by blasting (Fig. 84b). Other, highly metamict grains exhibit a blurry, patchy, sometimes convolute zoning while oscillatory magmatic zoning is absent in the central and intermediate part (Fig. 84b-e). Few zircon crystals contain fluid inclusion trails (Fig. 84d-f).

The results of 22 spot isotope analyses from the core, intermediate and outer parts of zircons are given in Table 23. Six analyses have discordances above 10% indicating generally moderate post-emplacement alteration of the mineral. The core and intermediate domains display a similar spread of $Pb^{207}/Pb^{206}$ ages ranging from 1848-2012 Ma (core) and 1843-2019 Ma (intermediate). Ages from the outer parts have similar minimum and significantly lower maximum ages (1844-1900 Ma). No distinct metamorphic overprint has been identified. The abundance of ages older than 1880 Ma is taken as evidence for the presence of multiple xenocryst inclusions giving some insight in the age of the host or source rocks

Calculation of concordia ages yielded similar ages of 1817±25 Ma (core), 1862±35 Ma (intermediate) and 1838±30 Ma (outer part) for all domains (Fig. 85). The data do not therefore show any indications of polyphase magmatic crystallisation or metamorphic overgrowth. The combined age of 1841±15 Ma (MSWD =7.0) is considered to be very reliable and is interpreted to date the emplacement of the POGD sill. It further suggests that the orthogneiss is a deep-level equivalent of the FFG Suite, dated in this study between 1879±8.9 and 1826±15 Ma. This is supported by similar zircon crystal shapes in samples of the Franken and Kaross granites.

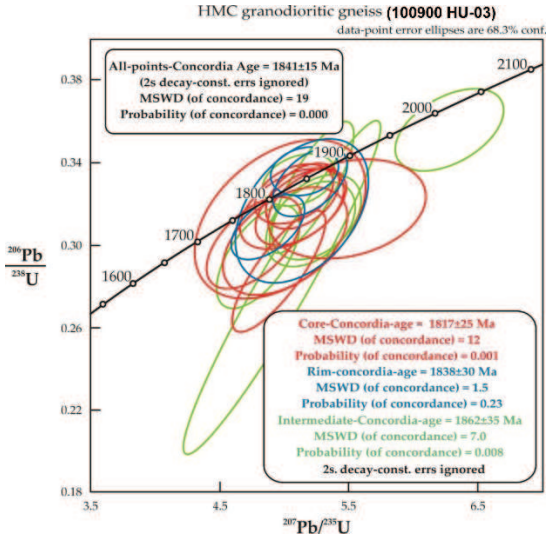


**Figure 85**. Concordia diagram with analyses of sample 100900 (HU03/ Porphyritic granodiorite K-feldspar (augen) gneiss = POGD).

In summary, the LA-ICP-MS zircon U-Pb ages demonstrate that FFG Suite granites near Kamanjab were emplaced over a rather short period of seven million years from 1831±14 Ma (Kaross Granite), 1826±15 Ma (Kamdescha Granite) and 1841±14 Ma (Franken Granodiorite). In the HMC, granodioritic augengneiss and supercrustal gneissic quartz-feldspar porphyry yield similar ages of 1841±15 Ma and 1831±25 Ma, respectively. They demonstrate the continuation of the FFG into the HMC, but with an additional pervasive tectonic overprint.

**Table 24.** U-Pb single zircon age determinations by SHRIMP method. Samples 270802, 081203: Stanford University; sample NA101-2: St Petersburg. Analysis 15.2 (in red) with high errors, is excluded from discussion.

| Sample | Spot | $^{206}Pb_c$ [%] | U [ppm] | Th [ppm] | $^{232}Th/^{238}U$ | $^{206}Pb^*$ [ppm] | (1) $^{206}Pb/^{238}U$ [Ma] | | (1) $^{207}Pb/^{206}Pb$ [Ma] | | Discord. [%] | (1) $^{238}U/^{206}Pb^*$ | ±% | (1) $^{207}Pb^*/^{206}Pb^*$ | ±% | (1) $^{207}Pb^*/^{235}U$ | ±% | (1) $^{206}Pb^*/^{238}U$ | ±% | error corr |
|---|---|---|---|---|---|---|---|---|---|---|---|---|---|---|---|---|---|---|---|---|
| 270802-1 | 21-1 | 0,13 | 87 | 54 | 0,64 | 25.7 | 1911 | ±29 | 1787 | ±39 | -7 | 2.898 | 1.7 | 0.1092 | 2.1 | 5.2 | 2.7 | 0.3451 | 1.7 | ,628 |
| | 21-7 | 0,21 | 105 | 72 | 0,71 | 29.5 | 1827 | ±23 | 1805 | ±37 | -1 | 3.052 | 1.4 | 0.1104 | 2 | 4.99 | 2.5 | 0.3276 | 1.4 | ,577 |
| | 21-12 | 0,13 | 149 | 112 | 0,78 | 41.6 | 1814 | ±19 | 1828 | ±28 | 1 | 3.077 | 1.2 | 0.1118 | 1.6 | 5.009 | 2 | 0.325 | 1.2 | ,616 |
| | 21-11 | 0,00 | 111 | 74 | 0,69 | 31.3 | 1835 | ±23 | 1841 | ±30 | 0 | 3.038 | 1.4 | 0.1125 | 1.7 | 5.11 | 2.2 | 0.3292 | 1.4 | ,644 |
| | 21-9 | 0,17 | 89 | 65 | 0,75 | 25.8 | 1868 | ±25 | 1851 | ±35 | -1 | 2.975 | 1.5 | 0.1132 | 2 | 5.24 | 2.5 | 0.3361 | 1.5 | ,616 |
| | 21-4 | 0,12 | 137 | 112 | 0,84 | 39.1 | 1843 | ±22 | 1858 | ±30 | 1 | 3.022 | 1.4 | 0.1136 | 1.6 | 5.18 | 2.1 | 0.3309 | 1.4 | ,641 |
| | 21-8 | 0,14 | 201 | 150 | 0,77 | 58.3 | 1872 | ±18 | 1869 | ±26 | 0 | 2.969 | 1.1 | 0.1143 | 1.5 | 5.308 | 1.8 | 0.3369 | 1.1 | ,598 |
| | 21-3 | 0,00 | 114 | 80 | 0,73 | 33.3 | 1892 | ±25 | 1869 | ±31 | -1 | 2.931 | 1.5 | 0.1143 | 1.7 | 5.38 | 2.3 | 0.3412 | 1.5 | ,655 |
| | 21-10 | 0,07 | 193 | 147 | 0,79 | 55.9 | 1868 | ±18 | 1875 | ±24 | 0 | 2.976 | 1.1 | 0.1147 | 1.3 | 5.313 | 1.7 | 0.336 | 1.1 | ,640 |
| | 21-5 | 0,00 | 96 | 59 | 0,64 | 27.7 | 1875 | ±28 | 1886 | ±35 | 1 | 2.963 | 1.7 | 0.1154 | 2 | 5.37 | 2.6 | 0.3375 | 1.7 | ,656 |
| | 21-2 | 0,00 | 149 | 122 | 0,84 | 42.7 | 1858 | ±22 | 1888 | ±28 | 2 | 2.994 | 1.4 | 0.1155 | 1.6 | 5.32 | 2.1 | 0.334 | 1.4 | ,656 |
| 081203-2 | 22-12 | 0,35 | 194 | 268 | 1,42 | 54.4 | 1812 | ±15 | 1833 | ±23 | 1 | 3.08 | 0.94 | 0.1121 | 1.3 | 5.015 | 1.6 | 0.3246 | 0.94 | ,600 |
| | 22-2 | 0,15 | 106 | 108 | 1,06 | 30.7 | 1874 | ±16 | 1838 | ±30 | -2 | 2.964 | 1 | 0.1123 | 1.7 | 5.23 | 2 | 0.3374 | 1 | ,513 |
| | 22-3 | 0,26 | 89 | 81 | 0,93 | 26 | 1877 | ±18 | 1839 | ±28 | -2 | 2.958 | 1.1 | 0.1125 | 1.6 | 5.24 | 1.9 | 0.338 | 1.1 | ,581 |
| | 22-5 | 0,46 | 224 | 173 | 0,80 | 64.4 | 1854 | ±11 | 1846 | ±24 | 0 | 2.999 | 0.71 | 0.1129 | 1.3 | 5.187 | 1.5 | 0.3333 | 0.71 | ,475 |
| | 22-7 | 0,11 | 395 | 652 | 1,70 | 116 | 1891 | ± 8.8 | 1852 | ±12 | -2 | 2.933 | 0.54 | 0.11322 | 0.68 | 5.322 | 0.87 | 0.3409 | 0.54 | ,616 |
| | 22-8 | 0,14 | 240 | 144 | 0,62 | 70.2 | 1887 | ±11 | 1858 | ±16 | -2 | 2.941 | 0.7 | 0.1136 | 0.9 | 5.327 | 1.1 | 0.34 | 0.7 | ,613 |
| | 22-11 | 0,22 | 96 | 132 | 1,43 | 27.8 | 1872 | ±19 | 1860 | ±26 | -1 | 2.967 | 1.1 | 0.1137 | 1.4 | 5.286 | 1.8 | 0.337 | 1.1 | ,621 |
| | 22-4 | 0,30 | 88 | 88 | 1,03 | 26.5 | 1928 | ±19 | 1867 | ±28 | -3 | 2.867 | 1.1 | 0.1142 | 1.5 | 5.49 | 1.9 | 0.3487 | 1.1 | ,591 |
| | 22-9 | 0,42 | 82 | 79 | 0,99 | 24.1 | 1893 | ±20 | 1868 | ±34 | -1 | 2.93 | 1.2 | 0.1142 | 1.9 | 5.37 | 2.2 | 0.3413 | 1.2 | ,540 |
| | 22-10 | 0,00 | 221 | 136 | 0,63 | 64.4 | 1885 | ±12 | 1880 | ±15 | 0 | 2.944 | 0.75 | 0.11498 | 0.82 | 5.385 | 1.1 | 0.3397 | 0.75 | ,676 |
| | 22-1 | -- | 276 | 228 | 0,85 | 81.6 | 1906.9 | ±10 | 1881 | ±13 | -1 | 2.905 | 0.6 | 0.11505 | 0.72 | 5.46 | 0.94 | 0.3442 | 0.6 | ,640 |
| | 22-6 | 0,06 | 182 | 207 | 1,17 | 52.7 | 1871 | ±13 | 1887 | ±17 | 1 | 2.969 | 0.8 | 0.1155 | 0.95 | 5.362 | 1.2 | 0.3368 | 0.8 | ,645 |
| NA101-2 | 15,2 | 16,69 | 2983 | 319 | 0,11 | 307 | 591 | ±7.2 | 1751 | 130 | 196 | 10,010 | 1,3 | 0.1072 | 6,9 | 1,418 | 7,0 | 0,096 | 1,3 | ,183 |
| | 11,2 | 0,36 | 726 | 57 | 0,08 | 205 | 1828 | ±18 | 1786 | 21 | -2 | 3,048 | 1,1 | 0.1092 | 1,1 | 4,937 | 1,6 | 0,328 | 1,1 | ,709 |
| | 3,2 | 0,21 | 2045 | 108 | 0,05 | 469 | 1523 | ±14 | 1796 | 13 | 18 | 3,750 | 1,1 | 0.1098 | 0,7 | 4,035 | 1,3 | 0,267 | 1,1 | ,822 |
| | 7,1 | 0,27 | 153 | 124 | 0,84 | 42,2 | 1790 | ±13 | 1801 | 27 | 1 | 3,122 | 0,8 | 0.1101 | 1,5 | 4,859 | 1,7 | 0,320 | 0,8 | ,483 |
| | 16,1 | 0,16 | 282 | 238 | 0,87 | 77,4 | 1787 | ±15 | 1808 | 18 | 1 | 3,130 | 1,0 | 0.1106 | 1,0 | 4,869 | 1,4 | 0,319 | 1,0 | ,690 |
| | 8,2 | 0,20 | 353 | 92 | 0,27 | 101 | 1855 | ±14 | 1890 | 32 | 2 | 2,999 | 0,9 | 0.1156 | 1,8 | 5,310 | 2,0 | 0,333 | 0,9 | ,437 |
| | 8,1 | 0,80 | 240 | 127 | 0,55 | 70,9 | 1891 | ±14 | 1912 | 33 | 1 | 2,928 | 0,8 | 0.1171 | 1,8 | 5,500 | 2,0 | 0,341 | 0,8 | ,413 |
| | 4,1 | 0,08 | 160 | 171 | 1,11 | 50,9 | 2034 | ±20 | 1994 | 22 | -2 | 2,696 | 1,2 | 0.1226 | 1,3 | 6,270 | 1,7 | 0,371 | 1,2 | ,676 |
| | 6,1 | 0,11 | 239 | 200 | 0,86 | 76,5 | 2042 | ±14 | 2016 | 19 | -1 | 2,683 | 0,8 | 0.1241 | 1,1 | 6,375 | 1,3 | 0,373 | 0,8 | ,588 |
| | 5,1 | 0,04 | 296 | 309 | 1,08 | 95 | 2048 | ±15 | 2017 | 17 | -2 | 2,673 | 0,9 | 0.1242 | 0,9 | 6,404 | 1,3 | 0,374 | 0,9 | ,674 |
| | 13,1 | 0,17 | 165 | 106 | 0,66 | 52,3 | 2018 | ±19 | 2023 | 22 | 0 | 2,719 | 1,1 | 0.1246 | 1,3 | 6,320 | 1,7 | 0,368 | 1,1 | ,652 |
| | 2,1 | 0,19 | 289 | 137 | 0,49 | 93,1 | 2048 | ±13 | 2038 | 18 | 0 | 2,673 | 0,7 | 0.1257 | 1,0 | 6,479 | 1,3 | 0,374 | 0,7 | ,577 |
| | 12,1 | 0,31 | 465 | 381 | 0,85 | 150 | 2052 | ±18 | 2046 | 15 | 0 | 2,667 | 1,0 | 0.1263 | 0,9 | 6,523 | 1,3 | 0,375 | 1,0 | ,767 |
| | 9,1 | 0,08 | 588 | 225 | 0,39 | 192 | 2075 | ±15 | 2047 | 13 | -1 | 2,632 | 0,9 | 0.1263 | 0,8 | 6,615 | 1,2 | 0,380 | 0,9 | ,752 |
| | 1,1 | 0,20 | 399 | 331 | 0,86 | 131 | 2087 | ±15 | 2050 | 14 | -2 | 2,615 | 0,8 | 0.1265 | 0,8 | 6,666 | 1,2 | 0,382 | 0,8 | ,716 |
| | 10,1 | 0,59 | 95 | 114 | 1,25 | 30,3 | 2032 | ±23 | 2060 | 40 | 1 | 2,694 | 1,3 | 0.1273 | 2,3 | 6,500 | 2,6 | 0,371 | 1,3 | ,504 |
| | 14,1 | 0,03 | 419 | 248 | 0,61 | 136 | 2064 | ±13 | 2064 | 12 | 0 | 2,649 | 0,7 | 0.1275 | 0,7 | 6,635 | 1,0 | 0,377 | 0,7 | ,724 |
| | 15,1 | 0,10 | 186 | 140 | 0,78 | 60,1 | 2058 | ±15 | 2068 | 18 | 0 | 2,659 | 0,9 | 0.1278 | 1,0 | 6,626 | 1,4 | 0,376 | 0,9 | ,637 |
| | 3,1 | 1,79 | 288 | 89 | 0,32 | 82,7 | 1818 | ±14 | 2450 | 27 | 35 | 3,051 | 0,9 | 0.1595 | 1,6 | 7,160 | 1,8 | 0,326 | 0,9 | ,480 |
| | 11,1 | 0,23 | 234 | 46 | 0,20 | 94,6 | 2482 | ±20 | 2461 | 15 | -1 | 2,128 | 1,0 | 0.1605 | 0,9 | 10,390 | 1,3 | 0,470 | 1,0 | ,743 |

Errors are 1-sigma; $Pb_c$ and $Pb^*$ indicate the common and radiogenic portions, respectively.
Error in Standard calibration was 0.44% (Stanford) and 0.4% (St Petersburg) ( not included in above errors but required when comparing data from different mounts).
(1) Common Pb corrected using measured $^{204}Pb$.

| WGS84/UTM33S | Easting | Northing |
|---|---|---|
| 270802-1 | 435785 | 7780095 |
| 081203-2 | 492927 | 7782815 |
| NA101-2 | 442376 | 7770033 |

Zircons of the ROG were altered by post-emplacement processes and the ages are partly reset. The best estimate for the emplacement was calculated at $1829^{+71}/_{-69}$ Ma and falls into the same time slot as the other samples. It further constrains the maximum age of the D2 folding and mylonitisation, whereas the oldest ages constrain the minimum age for the M1/D1 event recorded only in the HMC. The multitude of older $^{207}Pb/^{206}Pb$ ages indicates major contribution of Orosirian to Rhyacian source rocks in the magma evolution of the FFG and HMC orthogneiss either by crustal anataxis or assimilation. The timing of the M2 event could not be determined so far, either because metamorphic overgrowth rims are very small (if at all present), or highly metamict and therefore cannot be used for geochronological analysis.

**SHRIMP U-Pb zircon analysis**

Three samples were analysed by the SHRIMP method. They are from metarhyolite of the Suiderkruis SD (270802-1), from undeformed granite of the Fransfontein Suite east of the Ehobib SD (081203-2) and from late- to post-tectonic garnet-bearing granite which intruded a NW-SE striking crustal scale fault near the Suiderkruis-Aandgloed boundary (NA101-2).

***Fransfontein Suite***

***Kamdescha Granite (sample 081203-2)***

The sample has been taken from macroscopically undeformed granite of the FFG Suite ca 5 km north of the Ehobib SD (Fig. 73). The massive, homogeneous hornblende-biotite-bearing coarse-grained equigranular rock comprises equal proportions of slightly saussuritised greenish plagioclase, rose zoned K-feldspar and grey quartz (Fig. 86) corresponding to the Kamdescha variety in the Kamanjab area (Fig. 15).

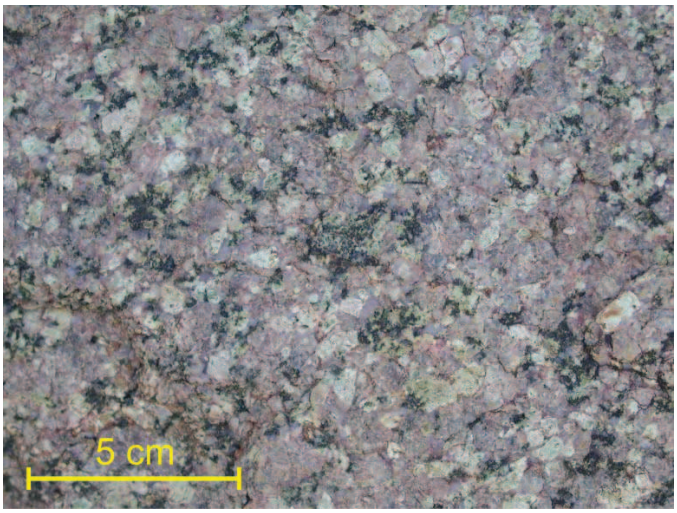


**Figure 86**. Sample 081203-2 (FFG Suite, Kamdescha variety).

12 zircon analyses yield mostly concordant $Pb^{207/206}$ ages (discordance < 3%) from 1883 to 1887 Ma (Table 24). In the Wetherill diagram, they define a nearly concordant age of 1879±9 Ma, which is interpreted to date emplacement and crystallisation of the granite (Fig. 88a). Any structural model must take into account the presence of older undeformed granite close to younger, highly deformed orthogneiss in the HMC (HU03).

***Huab Metamorphic Complex***

***Metarhyolite (sample 270802-1)***

Sample 270802-1 is from a metarhyolite or ignimbrite intercalated in a series of folded metamorphic monomict and polymict conglomerate, quartzite, sandstone, biotite-muscovite schist, chert, amygaloidal metabasalts and garnet-bearing amphibolite. The rocks are often overprinted by hydro-thermal epidote, which in places forms massive, up to 1 m thick, horizons. A few, up to 5 m thick, granite sills intruded the series and are transposed into the principal foliation.

The rather homogeneous massive but foliated rhyolite body extends laterally for less than 100 m. In hand specimen the unaltered rock shows K-feldspar porphyries in a pinkish fine- to medium-grained equigranular quartz-feldspar matrix. Welding structures weather out as irregular laminae indicating the volcanic or subvolcanic origin (Fig. 87). It is uncertain whether the rhyolite is a remnant of Khoabendus Group volcanics of the Ehobib SD or part of the Suiderkruis SD. Similar rhyolite bodies up to km size have been mapped in several places in that area.

**Figure 87**. Metarhyolite of Farm Suiderkruis 668. The rock was dated by U-Pb zircon SHRIMP method at 1855±6 Ma indicating its affiliation with the Khoabendus Group.

12 zircon analyses yield mostly concordant $Pb^{207}/^{206}$ ages (discordance < 7%) from 1805 to 1888 Ma (Table 24). In the Wetherill diagram, they define a near concordant age of 1855±6 Ma, which is interpreted to date crystallisation of the metavolcanic rock, arguing for its affiliation with the Khoabendus Group of the Ehobib SD nearby (Fig. 88b).

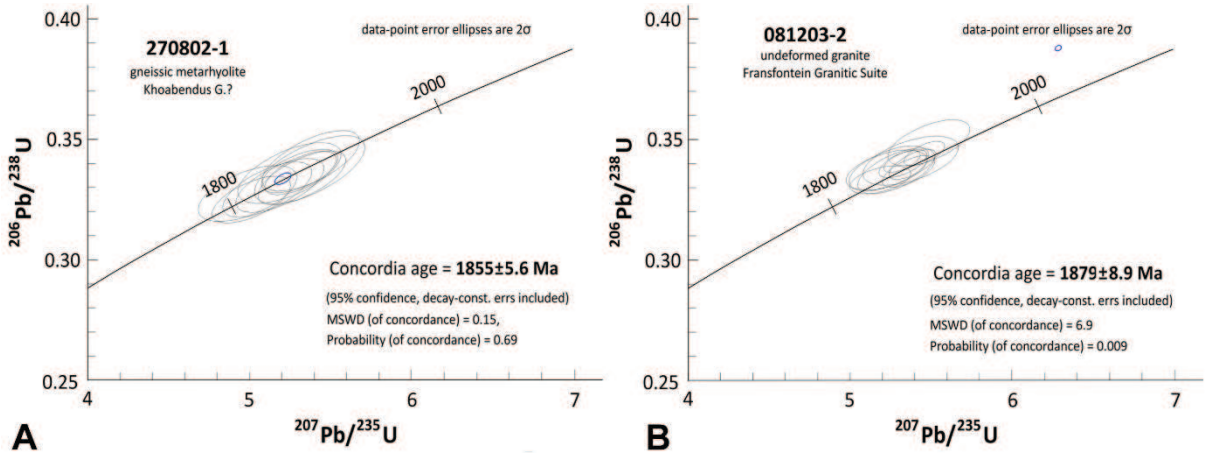


**Figure 88.** Wetherill plots of samples 270802-1 (A) and 081203-2 (B).

***Fault breccia (Sample NA101-2)***

Sample NA101-2 was taken from fault injected granite, which is illustrated in Fig. 33 and described in the respective paragraph of the tectonics chapter. The results of U-Pb single zircon SHRIMP analysis are presented in Fig. 89.

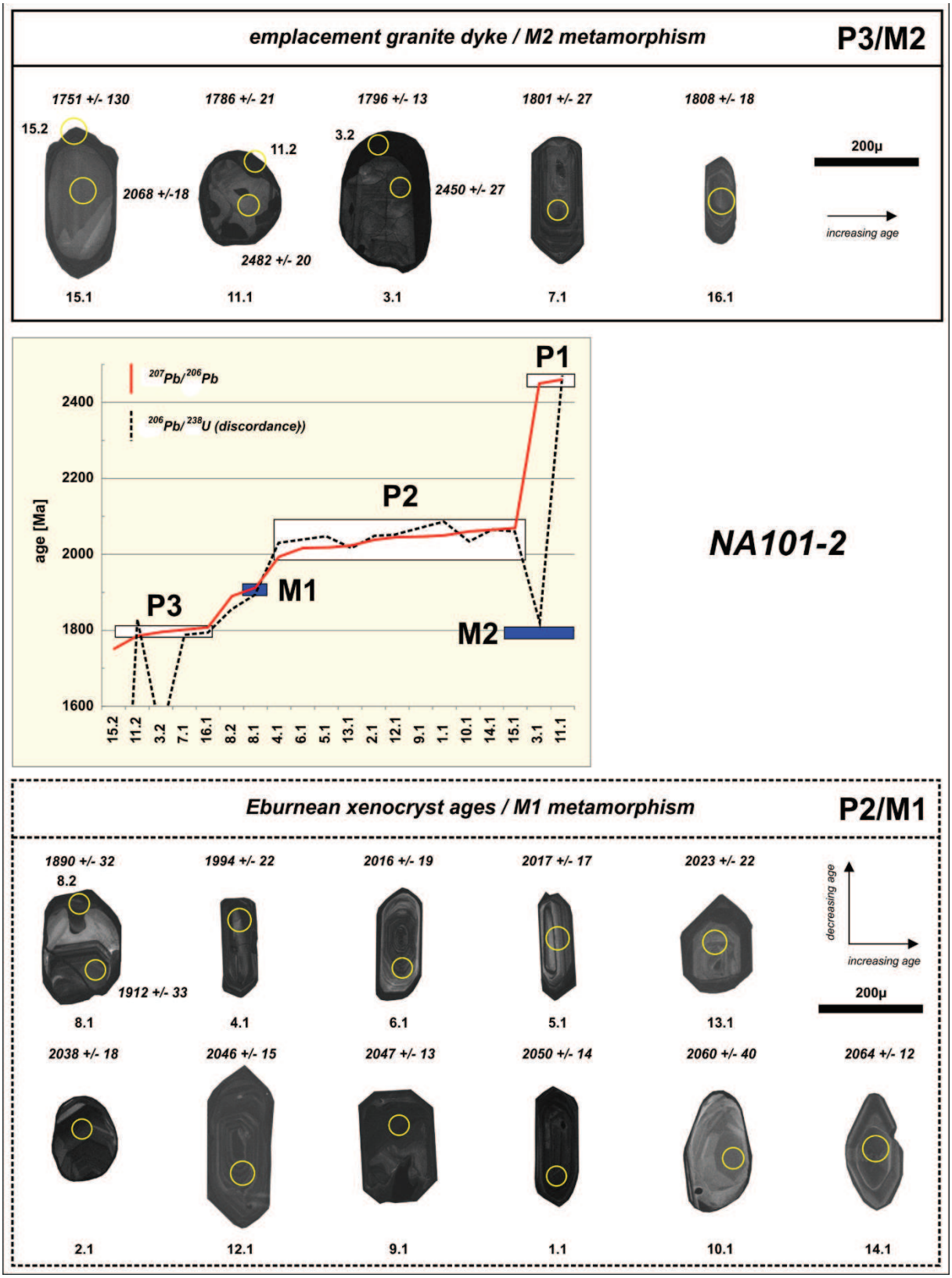


**Figure 89**. Zircons of sample NA101-2 on which geochronology was carried out. Most of the zircons are xenocrysts of Eburnean provenance (2064-2016 Ma, P2); metamorphic overgrowth in grain 8.1 was dated at ca 1890 Ma. P3 zircons date emplacement of the granite at ca 1801-1808 Ma (grains 7.1, 16.1) coinciding with metamorphic overgrowth at 1786-1796 Ma (grains 3.1, 11.1 and 1).

14 out of 16 analysed zircon grains are xenocrysts with widely varying ages recording two magmatic (P1-P2) and two metamorphic events (M1+M2).

Three analysed xenocrysts are well-rounded (2.1, 3.1, 11.1) constraining clearly their sedimentary origin from a distant provenance area. Two out of these yielded the oldest ages of 2482±20 Ma and 2450±27 Ma (P1) corresponding in Gabon to the onset of Eburnean magmatism in western Central Africa (Thiéblemont *et al*. 2009)

The other xenocrysts are subhedral to euhedral and isometric, tabular or long prismatic in shape; their ages between 2064±12 Ma and 1912±12 Ma define magmatic pulse P2 and correspond in central Africa to widespread magmatism at the end of Eburnean orogeny (Thiéblemont *et al*. 2009). Partly rounded zircons of the lower row are clearly of detrital origin constraining the minimum deposition age of HMC sediments at 2038±18 Ma. Sub- to euhedral shapes of zircons in the upper row indicate their transport from a more proximal provenance area, or assimilated magmatic rocks which are not exposed in the KI. Considering the detrital origin more likely, the youngest age 1912±33 Ma provides the maximum deposition age of the precursor sediments and subsequent D1 deformation and metamorphism.

The probable emplacement age of the magmatic breccia has been dated by two analyses in the core of magmatic euhedral zircon grains (7.1, 16.1) at 1801±27 Ma and 1808±18 Ma. Alternatively, these grains are also xenocrysts constraining the maximum age of the granite.

Metamorphic overgrowths, marked by dark rims and low Th/U ratios, have been identified in four zircon grains. They were dated at 1890±32 Ma (8.2), 1751±130 Ma (15.2), 1786±21 Ma (11.2) and 1796±13 Ma (3.2) as such indicating two metamorphic events at 1890 Ma (M1) and at 1795 Ma (M2). M2 coincides within error with the youngest magmatic ages.

**K-Ar muscovite geochronology**

The ages of muscovite concentrates (4) of samples from the Aandgloed, Suiderkruis and Rooikop subdomains have been determined by using conventional gas mass spectrometry combined with AAS-Analysis (Table 25).

Four samples from the Aandgloed SD have been taken over a distance of about 200 m to evaluate age scatter related to local alteration. Their ages vary from 1270±25 Ma to 1401±15 Ma and are interpreted to document Mesoproterozoic thermal overprint and/or uplift and cooling of the rocks (Fig. 90a). Muscovite flakes of several cm size from thick, poorly deformed second generation pegmatite (see above) yielded an age of 1356±14 Ma (231104-5), whereas muscovite concentrates from quartz-feldspar-muscovite schist yielded both the youngest and oldest ages (samples 210802-1, 310104-2 and 310104-3, 231104-6). Quartz-feldspar-muscovite schist from the Rooikop SD 20 km southwest of the first sample group yielded an age of 869±5 Ma (050605-1), interpreted as partial reset of the Mesoproterozoic ages by Pan-African over-print.

**Table 25.** Analytical parameters of K-Ar muscovite isotope analysis and resulting ages.

| Ar - Isotopic Abundance | | Spike-Isotopic Comp. | | Decay Constants [1/a]: | | Potassium | |
|---|---|---|---|---|---|---|---|
| $^{40}$Ar : | 99,6000% | $^{40}$Ar : | 0,0099980% | λ ε : | 5,810E-11 | $^{40}$K : | 0,011670% |
| $^{38}$Ar : | 0,0630% | $^{38}$Ar : | 99,9890000% | λ β : | 4,962E-10 | $K_2O$/K : | 0,8302 |
| $^{36}$Ar : | 0,3370% | $^{36}$Ar : | 0,0009998% | | | Atomic Weight [g/mol]: | |
| Standard Temperature Pressure (STP) | | | | λ tot: | 5,543E-10 | tot Ar : | 39,9477 |
| 0° C; 760 mm Hg | | | | Molar Volume | | $^{40}$Ar : | 39,9624 |
| Normal Atmosphere (DIN 1343) | | | | [ml] : | 22413,8 | tot K : | 39,1027 |
| 273,15K; 1013,25 mbar | | | | | | | |

| Sample | Spike [ No. ] | $K_2O$ [ Wt. % ] | $^{40}$Ar * [ nl/g ] STP | $^{40}$Ar * [ % ] | Age [ Ma ] | 2σ-Error [ Ma ] | 2σ-Error [%] |
|---|---|---|---|---|---|---|---|
| **210802 - 1** | 3515 | 10,39 | 701,37 | 99,76 | **1389,5** | 16,5 | 1,2 |
| **310104 - 2** | 3513 | 10,63 | 726,30 | 99,44 | **1401,3** | 14,7 | 1,0 |
| **310104 - 3** | 3511 | 10,69 | 635,48 | 99,70 | **1270,0** | 25,2 | 2,0 |
| **231104 - 5** | 3510 | 10,70 | 697,27 | 99,59 | **1355,6** | 14,3 | 1,1 |
| **231104 - 6** | 3509 | 10,91 | 648,81 | 99,83 | **1270,4** | 17,7 | 1,4 |
| **050605 - 1** | 3508 | 10,60 | 381,60 | 98,94 | **868,9** | 5,3 | 0,6 |

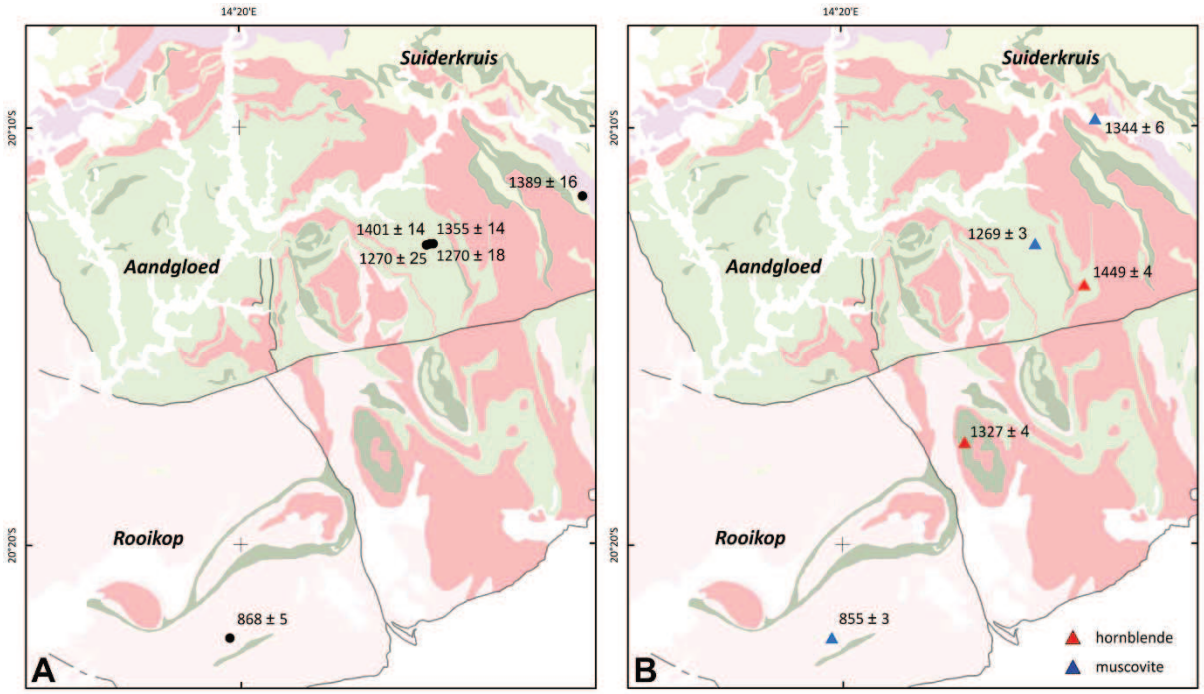


**Figure 90**. K-Ar muscovite ages in the Suiderkruis, Aandgloed and Rooikop subdomains (A); $^{40}Ar/^{39}Ar$ muscovite and hornblende ages (B).

### $^{40}Ar/^{39}Ar$ hornblende geochronology

$^{40}Ar/^{39}Ar$ geochronology has been applied to reveal possibly polyphase metamorphic histories by stepwise heating. 5 out of 6 samples were taken from localities close to those for the K-Ar samples; the analysed mineral concentrates are hornblende (2) and muscovite (4) (Fig. 90b). Muscovite-bearing mylonite from an E-W trending shear zone 20 km north of the Huab area was sampled to date the age of mylonitisation (not shown). The results of step wise heating are given in Table 26 and illustrated in Fig. 12; the samples localities with the resulting age estimate are shown in Fig. 90b.

Two hornblende concentrates (090606-3C; 090606-2) from amphibolite of the Aandgloed SD yielded well-defined plateau ages of 1327±4 and 1449±4 Ma. Two muscovite concentrates from the Suiderkruis and Aandgloed SD yield non-plateau ages of 1344±6 and 1269±3 Ma. The third sample in the Rooikop SD yield an age of 855±4 Ma and is significantly younger. These three muscovite ages were obtained from the steps which are secondarily equivalent to the plateau, in which a condition of the definition for the plateau lacks (Fleck *et al*. 1977). In samples C16041 and C16043 the range covers more than 50% of total $^{39}Ar$, but consists of only a single step. In sample C17015 the range consists of two steps whose ages agree within 2 sigma error, but their $^{39}Ar$ fraction (41%) is less than 50%. The sample from the shear zone (260709-4) yielded no plateau, therefore, the total gas age of 637±2 Ma was concluded.

The $^{40}Ar/^{39}Ar$ and K-Ar methods therefore produced similar ages and the $^{40}Ar/^{39}Ar$ method provides no additional information with respect to polyphase metamorphism. The greatest age of 1449±4 Ma has been determined in sample 090606-2. Regional thermal overprint is bracketed by several samples from various localities between 1401-1327 Ma; a second peak at 1270±25 Ma is indicated by three samples taken at one locality in the Kuiper Valley (Fig. 90).

**Table 26.** Results of stepwise heating $^{40}Ar/^{39}Ar$ method applied on hornblende and muscovite.

| Mineral | Sample | Laser output | $^{40}Ar/^{39}Ar$ (Ma) | $^{37}Ar/^{39}Ar$ | $^{36}Ar/^{39}Ar$ ($x10^{-3}$) | K/Ca | $^{40}Ar^*$ (%) | $^{39}ArK$ frac (%) | $^{40}Ar^*/^{39}ArK$ (Ma) | Age(±1s) (Ma) |
|---|---|---|---|---|---|---|---|---|---|---|
| Hornblende | 090606-2 | 1,8% | 6366 ± 100 | 2,43 ± 0,08 | 2644 ± 42,9 | 0,241 | 87,7 | 1,16 | 5594 ± 88 | 3403 ± 25 |
| | | 2,2% | 1073 ± 12 | 3,29 ± 0,06 | 247 ± 5,00 | 0,178 | 93,2 | 3,52 | 1002 ± 11 | 1252 ± 11 |
| | | 2,4% | 1082 ± 4 | 6,98 ± 0,03 | 40,9 ± 0,79 | 0,084 | 98,9 | 12,3 | 1076 ± 4 | 1317 ± 5 |
| | | 2,5% | 1235 ± 7 | 7,97 ± 0,09 | 41,7 ± 1,83 | 0,073 | 99,1 | 15,1 | 1229 ± 7 | 1446 ± 7 |
| | | 2,6% | 1247 ± 10 | 8,01 ± 0,08 | 31,6 ± 1,25 | 0,073 | 99,3 | 20,1 | 1245 ± 10 | 1459 ± 9 |
| | | 2,7% | 1240 ± 6 | 8,00 ± 0,07 | 30,7 ± 0,61 | 0,073 | 99,3 | 26 | 1238 ± 6 | 1454 ± 6 |
| | | 2,8% | 1225 ± 17 | 7,79 ± 0,16 | 52,5 ± 3,12 | 0,075 | 98,8 | 9,86 | 1217 ± 17 | 1436 ± 15 |
| | | 2,9% | 1209 ± 12 | 8,21 ± 0,11 | 55,8 ± 2,24 | 0,071 | 98,7 | 3,34 | 1200 ± 12 | 1422 ± 11 |
| | | 3,1% | 1243 ± 12 | 8,41 ± 0,09 | 31,6 ± 1,06 | 0,07 | 99,3 | 8,54 | 1241 ± 12 | 1456 ± 10 |
| | 090606-3C | 1,8% | 2342 ± 27 | 2,08 ± 0,06 | 1418 ± 19,7 | 0,282 | 82,1 | 1,08 | 1926 ± 22 | 1939 ± 15 |
| | | 2,2% | 849 ± 7 | 3,34 ± 0,05 | 187 ± 2,06 | 0,176 | 93,5 | 2,48 | 796 ± 7 | 1058 ± 8 |
| | | 2,6% | 1093 ± 6 | 4,39 ± 0,04 | 31,6 ± 0,76 | 0,134 | 99,2 | 55,6 | 1087 ± 6 | 1329 ± 6 |
| | | 2,7% | 1087 ± 4 | 4,66 ± 0,05 | 26,6 ± 0,46 | 0,126 | 99,3 | 16,9 | 1083 ± 4 | 1325 ± 5 |
| | | 2,8% | 1084 ± 12 | 4,47 ± 0,05 | 27 ± 0,57 | 0,131 | 99,3 | 13,3 | 1079 ± 12 | 1323 ± 11 |
| | | 2,9% | 1128 ± 8 | 4,47 ± 0,07 | 36,9 ± 1,62 | 0,131 | 99,1 | 6,63 | 1121 ± 8 | 1358 ± 8 |
| | | 3,0% | 1092 ± 6 | 5,08 ± 0,06 | 27,8 ± 1,27 | 0,115 | 99,3 | 2,98 | 1088 ± 6 | 1330 ± 6 |
| | | 3,2% | 1125 ± 18 | 4,91 ± 0,11 | 62,3 ± 2,81 | 0,119 | 98,4 | 1,01 | 1111 ± 18 | 1350 ± 15 |
| Muscovite | 231104-6 | 1,4% | 1112 ± 3 | 0,084 ± 0,02 | 44,9 ± 0,59 | 7,02 | 98,8 | 10,3 | 1099 ± 3 | 1343 ± 5 |
| | | 1,5% | 1087 ± 2 | 0,069 ± 0,01 | 19,9 ± 0,25 | 8,54 | 99,5 | 18,9 | 1081 ± 2 | 1328 ± 4 |
| | | 1,6% | 1016 ± 3 | 0,065 ± 0,01 | 15,1 ± 0,29 | 8,99 | 99,6 | 21,4 | 1011 ± 3 | 1266 ± 4 |
| | | 1,7% | 1020 ± 2 | 0,071 ± 0,01 | 10,4 ± 0,31 | 8,32 | 99,7 | 19,7 | 1017 ± 2 | 1271 ± 4 |
| | | 1,8% | 939 ± 2 | 0,096 ± 0,02 | 10,8 ± 0,44 | 6,14 | 99,7 | 12,2 | 936 ± 2 | 1197 ± 4 |
| | | 1,9% | 897 ± 8 | 0,016 ± 0,04 | 12,1 ± 0,97 | 36,6 | 99,6 | 5,87 | 894 ± 8 | 1157 ± 8 |
| | | 2,1% | 1026 ± 9 | 0,049 ± 0,09 | 38,8 ± 2,55 | 11,9 | 98,9 | 1,91 | 1015 ± 9 | 1269 ± 9 |
| | | 6,1% | 1009 ± 5 | 0,037 ± 0,02 | 20,1 ± 0,76 | 16,0 | 99,4 | 9,63 | 1003 ± 5 | 1259 ± 6 |
| | 050605-1 | 1,4% | 713 ± 8 | 0,008 ± 0,02 | 153 ± 3,13 | 72,4 | 93,6 | 13,1 | 668 ± 7 | 927 ± 8 |
| | | 1,5% | 606 ± 2 | 0,006 ± 0 | 12,5 ± 0,41 | 97,6 | 99,4 | 65,1 | 602 ± 2 | 855 ± 4 |
| | | 1,6% | 628 ± 4 | 0,033 ± 0,02 | 31,2 ± 1,62 | 17,8 | 98,5 | 14,6 | 619 ± 4 | 873 ± 5 |
| | | 1,7% | 627 ± 6 | 0,053 ± 0,06 | 38,6 ± 6,44 | 11,1 | 98,2 | 3,95 | 615 ± 6 | 869 ± 8 |
| | | 1,9% | 631 ± 18 | 0,090 ± 0,12 | 73,1 ± 11,4 | 6,52 | 96,6 | 2,05 | 610 ± 18 | 863 ± 20 |
| | | 3,6% | 654 ± 19 | 0,075 ± 0,25 | 110 ± 22,2 | 7,85 | 95 | 1,12 | 622 ± 19 | 876 ± 22 |
| | 260709-4 | 1,3% | 290 ± 8 | 0,063 ± 0,18 | 228 ± 20,1 | 9,29 | 76,8 | 0,33 | 223 ± 8 | 364 ± 13 |
| | | 1,4% | 360 ± 7 | 0,057 ± 0,13 | 80,8 ± 7,26 | 10,2 | 93,4 | 0,50 | 336 ± 7 | 525 ± 10 |
| | | 1,5% | 407 ± 6 | 0,019 ± 0,04 | 68,8 ± 5,23 | 30,6 | 95 | 1,49 | 387 ± 6 | 592 ± 8 |
| | | 1,6% | 455 ± 3 | 0,012 ± 0 | 15,8 ± 0,62 | 47,8 | 99 | 16,2 | 450 ± 3 | 672 ± 4 |
| | | 1,7% | 436 ± 3 | 0,052 ± 0,01 | 13 ± 0,61 | 11,3 | 99,1 | 34,8 | 432 ± 3 | 650 ± 4 |
| | | 1,8% | 399 ± 1 | 0,012 ± 0 | 8,3 ± 0,29 | 50,9 | 99,4 | 20,2 | 397 ± 1 | 605 ± 3 |
| | | 1,9% | 409 ± 3 | 0,017 ± 0,01 | 11,1 ± 0,59 | 35,4 | 99,2 | 10,3 | 406 ± 3 | 617 ± 4 |
| | | 2,3% | 424 ± 3 | 0,015 ± 0,01 | 7,2 ± 0,52 | 38,8 | 99,5 | 15,0 | 421 ± 3 | 637 ± 4 |
| | | 3,1% | 473 ± 5 | 0,086 ± 0,06 | 131 ± 5,86 | 6,82 | 91,8 | 1,21 | 434 ± 5 | 652 ± 7 |
| | 300709-4 | 1,3% | 480 ± 24 | 0,815 ± 0,73 | 453 ± 0,72 | 0,721 | 72,1 | 0,19 | 346 ± 24 | 539 ± 33 |
| | | 1,4% | 954 ± 40 | 0,154 ± 0,38 | 308 ± 3,81 | 3,814 | 90,5 | 0,35 | 863 ± 38 | 1127 ± 37 |
| | | 1,5% | 1173 ± 20 | 0,128 ± 0,06 | 84,5 ± 4,61 | 4,609 | 97,9 | 1,68 | 1148 ± 19 | 1384 ± 17 |
| | | 1,6% | 1104 ± 5 | 0,039 ± 0,01 | 11,1 ± 15,1 | 15,14 | 99,7 | 70,3 | 1101 ± 5 | 1344 ± 6 |
| | | 1,7% | 979 ± 8 | 0,023 ± 0,02 | 23,5 ± 26 | 25,99 | 99,3 | 7,60 | 972 ± 8 | 1230 ± 8 |
| | | 2,1% | 1002 ± 7 | 0,009 ± 0,01 | 11,8 ± 66,6 | 66,57 | 99,7 | 11,6 | 998 ± 7 | 1253 ± 7 |
| | | 2,7% | 1144 ± 10 | 0,033 ± 0,01 | 29 ± 17,6 | 17,65 | 99,3 | 8,20 | 1135 ± 10 | 1373 ± 9 |

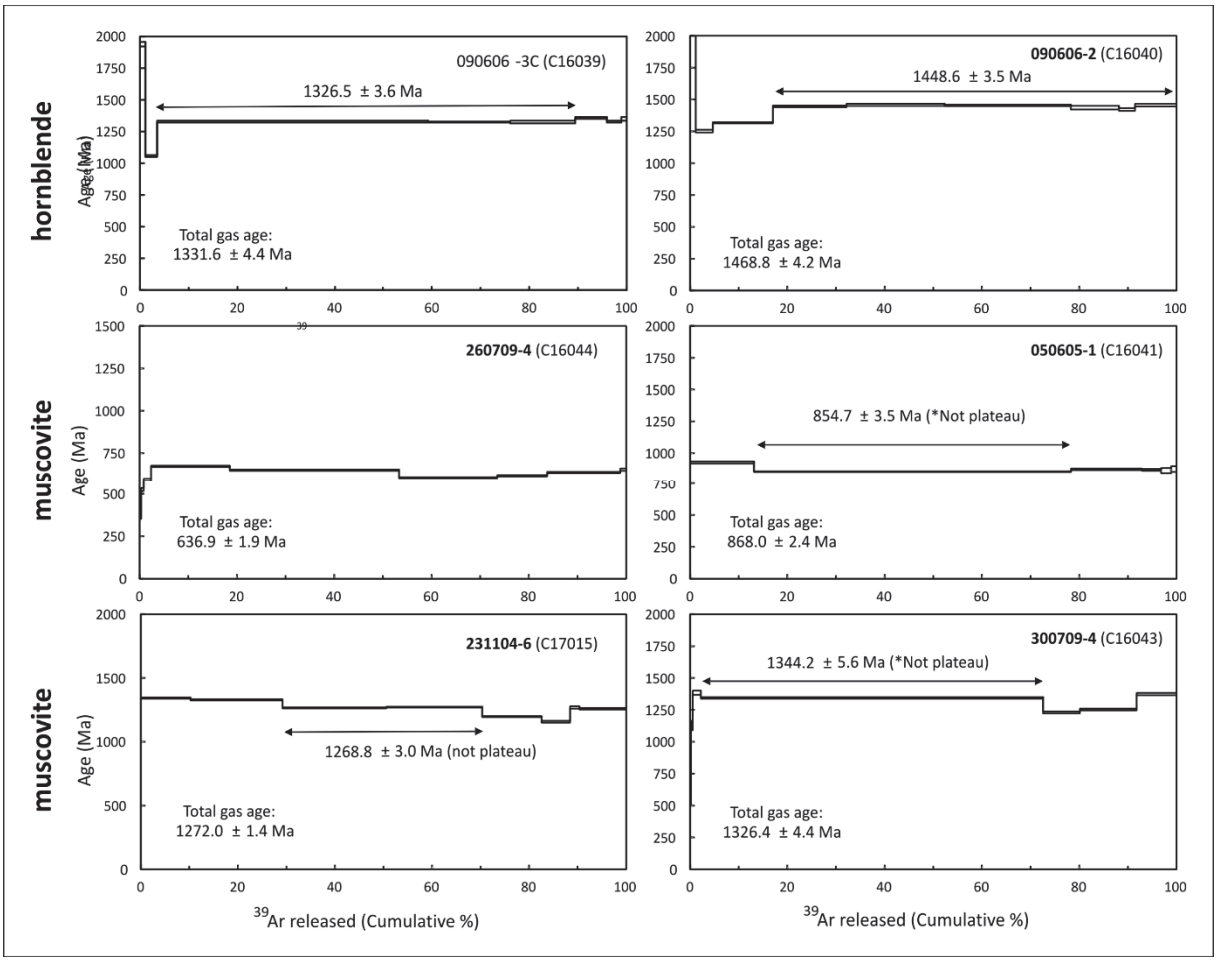


**Figure 91**. Stepwise heating method yields Ar-Ar plateau ages of 1332 and 1449 Ma for hornblende and non-plateau ages between 637-1344 Ma for muscovite.

## Discussion

### Depositional environment, magmatism, plate tectonic setting

#### *Huab Metamorphic Complex*

Geological mapping of the HMC shows that the basal part (Lofdal and Rooikop subdomains) is chiefly comprised of medium- to coarse-grained paragneiss derived from immature psammitic to semipelitic precursors such as greywacke. Quartzite and muscovite schist are minor constituents and carbonate rocks are absent. Sedimentary structures were almost completely overprinted by subsequent deformation and metamorphism. Intercalated finely banded leucogneiss is of volcanic or sedimentary (arkose) origin and abundant amphibolite was probably mostly intrusive. The absence of pre-Fransfontein granitoids is noteworthy. The overlying Aandgloed SD records in the lower part similar rock types derived from mainly silicoclastic coarse-grained sediments. In the upper part, increasing amounts of muscovite schist alternating with metapsammitic paragneiss are interpreted as former turbidite sequences. Finely banded leucogneiss alternating locally with thin layers of amphibolite possibly records bimodal volcanic sequences. The Suiderkruis SD, which forms the upper part of the HMC, starts with massive white quartzite documenting a major change in sedimentation. Rare cross-bedding and oscillation ripples document shallow water fluviatile or marine deposition. The quartzite is in thrust contact with an overlying mixed series of muscovite schist, quartzite, garnet-biotite leucogneiss, semipelitic paragneiss and amphibolite. The rocks in the (extensional) thrust comprise chlorite phyllonite derived from pelitic precursors that possibly record marine transgression, whereas the overlying rocks may constitute metaturbidite sequences with intercalated volcanic rocks. Increasing input of volcanic rocks is documented in the rocks above the mixed series by amygdaloidal metabasalts, metachert and metarhyolite alternating with the

metapsammitic and semipelitic gneisses. A few horizons of monomict metaconglomerate suggest shallow water deposition under fluvial or marine conditions. Alternatively, these rocks were already part of the Khoabendus Fm, which were folded tightly with the gneisses of the HMC. The uppermost part of the Suiderkruis SD is composed of quartz-feldspar-muscovite schist alternating with paragneiss overlain by graphite-bearing schist indicating the return to deep marine sedimentation.

In the absence of detrital zircon studies, the youngest of few rounded xenocrysts in late stage granodiorite emplaced in a fault (sample NA101-2) constrains the maximum age of HMC sedimentation, regional metamorphism and deformation at 1994±22 Ma. The youngest euhedral xenocryst yielded an age of 1912±33 Ma but it may be derived from an orthogneiss. However, so far magmatic rocks of this age have not been identified in the KI suggesting detrital origin of this grain, which implies even younger ages of sedimentation, metamorphism and deformation. The other xenocrysts indicate the chiefly Eburnean provenance of the sediments. They define an older (minor) magmatic pulse P1 at 2450-2482 Ma, dating the onset of Eburnean magmatism in Gabon (Thiéblemont *et al*. 2009). The main magmatic pulse P2 at 1994-2064 Ma marks in Gabon, Congo Brazzaville and Angola, regional late stage plutonism of the Eburnean orogeny (Thiéblemont *et al*. 2009; Hanson, 2003). The predominantly Eburnean age of the source area is further indicated by Sm-Nd $T_{DM}$ model ages of HMC gneisses (2.1-2.2 Ga), FFG granite (2.3-2.7 Ga) and amphibolite (1.96-2.4 Ga). This suggests the interpretation of the HMC as a molasse basin of the Eburnean orogen at the passive southern margin of the Congo (Kasai) Craton / Angola Shield.

***Khoabendus Group***

The Khoabendus Group postdates the first regional medium to high-grade tectono-metamorphism recorded in the HMC. However, all observed contacts in the Huab area were overprinted by subsequent shearing under lower grade conditions whereas in the Kamanjab area, the group is intruded in its lower part by FFG granites obscuring the contact with a hypothetical basement in this area (Fig. 5). Miller (2008) suggested a depositional environment comprising a gradually subsiding terrain made up of one large or several smaller depositional basins with a large proportion of the volcanic rocks deposited under subaqueous conditions. The sediments indicate relatively quiet, shallow water depositional conditions with occasional transgressions or regressions. Abundant intermediate volcanic rocks (andesite) are taken as indicators for an active continental margin setting.

The stratigraphic profile through the Bruno syncline illustrates the change in the West End Fm from lower coarse silicoclastic rocks into a series of epiclastic rocks interbedded with pyroclastic rocks and rare basalt flows that are now separated as the Ombonde Member. Planar- and cross-bedding in the sandstones indicate deposition under fluviatile conditions. Felsic volcanism culminates at the top of the West End Fm with a massive ignimbrite more than 500 m thick, most probably deposited under subaerial conditions. In the revised stratigraphy these rocks are formalised as the Bruno Member

A second volcaniclastic depositional cycle is distinguished as the Blyerus Fm, which could represent, however, just a lateral facies change of the West End Fm. The ca 500 m thick series starts with polymict small-pebble conglomerate overlain by planar-bedded sandstone that higher up alternates with beds of andesitic tuff/ite. The top of the formation comprises conglomerate and arkosic sandstone laterally grading into small-pebble conglomerate. More massive andesite beds in the NW corner of the Khoabendus area probably correspond to the Smalruggens Member in the south and have been classified as such.

The overlying Otjovazandu Formation records the change from bimodal volcanism and volcaniclastic series into chiefly sedimentary deposition. It starts with massive white quartzite with occasional cross-bedding and oscillation ripple structures indicating fluviatile or shallow marine deposition and the origin of the sediments from a mature source (sandstone). Contemporaneous felsic volcanism is recorded by andesitic and rhyolitic rocks SE of Kamanjab and in the NW-most part of the Khoabendus mapping area. A few kilometres further SE, new field observations reveal local deposition of calc-silicate and carbonate rocks on top of the massive white quartzite. The transitional nature of the contact is shown by intercalated grey quartzite layers in the lower part of the carbonate sequence. Higher up, horizons of microbial mats document very shallow water

conditions in a lagoon; the partly organic-rich metasediments form potential source rocks for hydrocarbons. In the revised stratigraphy the series is formalised as the Dorslaan Member. Deposition of the overlying Arendnes Member (AM) marks a phase of regional transgression with sudden change to deep water deposition. The lower part of the member comprises chlorite phyllite with lenses of Mn/Fe-rich dark carbonate rocks that higher up grade into a succession of phyllite with intercalated thin beds of dark quartzite interpreted as distal turbidite sequences. Miller (2008) described lateral variations with intercalated quartzite, pebbly quartzite and oolite indicating intermittent shallow water conditions, however, these facies were not observed in the study area. An iron-rich horizon 10-15 m thick at the base of the AM is interpreted to result from hydrothermal alteration of the chlorite phyllite by stratiform fluids. Similar iron formation has been reported by Porada (1974) at the base of the overlying Dinteri Member that, however, was observed in the Honib Syncline. Here, the unit is represented by massive dolomite overlying the chlorite phyllite along a sharp sedimentary contact, forming the top of the stratigraphic profile in the study area (Fig. 5) and documenting the sudden return to shallow water deposition. The absence of the regression cycle between the phyllite and dolomite suggests a period of emersion during which these rocks were eroded.

We consider back-arc basins behind the volcanic chain as the most probable tectonic setting allowing preservation of the volcanic and sedimentary rocks in an environment that was only little affected by subsequent deformation and low-grade metamorphism.

***Mafic magmatism***

Field observation reveals a marked difference between the HMC where mafic rocks are ubiquitous and the Khoabendus Group recording only a few basalt flows but major intermediate (andesite, dacite) to felsic (rhyolite) volcanism. Most of the mafic rocks in the HMC are probably of intrusive origin although, locally, a volcanic origin cannot be excluded for thin layers of amphibolite alternating with leucogneiss. The rocks precede regional tectono-metamorphism by which they are overprinted whereas the Khoabendus Group and the FFG postdate this event. The interpretation of the mafic rocks as less differentiated intrusive correlates of the Khoabendus volcanic rocks can therefore be excluded. Geochemical data classify the rocks as subalkaline gabbros with tholeiitic to calc-alkaline affinity, and combined with Sm-Nd isotope systematics characterise them as subduction-related magmas influenced by assimilated continental crust. Increasing Nd $T_{DM}$ ages document progressive contamination of the magmas by country rocks of mainly Neoarchaean provenance towards higher crustal levels, i.e. from the basal Rooikop / Lofdal subdomains through the Aandgloed SD into the Suiderkruis SD. The mafic magmatism is bracketed in time between the youngest Nd $T_{DM}$ age of 1960 Ma and the oldest FFG granitoids dated at 1880±9 Ma (this study). The youngest xenocrysts in sample NA101-2 possibly further narrow the age of HMC sedimentation, mafic magmatism and regional tectono-metamorphism to younger than 1912±33 Ma.

***Fransfontein Granite Suite – HMC orthogneiss- Felsic volcanism Khoabendus Group.***

The Fransfontein granitoids, the HMC granodioritic augengneiss and the HMC rhyolites are thought to have evolved in a similar geodynamic setting with active continental margin characteristics. The major element signatures define met- and peraluminous compositions with A/NK ratios >1, A/CNK ratios < 1.1 and relatively low $FeO^T/(FeO^T+MgO)$ ratios being characteristic of I-type igneous rocks with a magnesian ("Cordilleran") signature. Trace element patterns show a strong subduction zone signature, which is, however, more pronounced within the FFG suite with higher LILE/HFSE ratios. This can be explained by continuous fractionation of hornblende and plagioclase during ascent of the FFG magmas into the upper crust. Increasing contamination of the subduction-derived magmas is indicated by the $NdT_{DM}$ ages, which are significantly higher in the FFG granitoids (2.3-2.7 Ga) than in the HMC orthogneisses (2.1-2.2 Ga). The oldest $NdT_{DM}$ ages suggest Archaean source rocks for the Palaeoproterozoic sediments constituting most of the KI. U-Pb single zircon ages indicate igneous activity between 1880±9 Ma (this study) and 1826±30 Ma (Kleinhanns *et al.* 2013)

Non-migmatitic red orthogneiss (ROG) forming large sheet-like bodies in the HMC

could be the mid-crust equivalent of the Kaross-type granite of the FFG. However, currently missing geochemical data from the latter group prevent the hypothesis from being tested. Geochemical data classify the ROG as metaluminous syenogranite with a ferroan ("A-type") signature. Trace element distributions are similar to the other felsic igneous rocks of the HMC and FFG but are enriched in Zr, Hf and HREE resulting in lower LILE/HFSE ratios. They display the lowest $T_{DM}$ ages of 2.0 Ga and high $\varepsilon(Nd)_{1.85Ga}$ values of 2.3 and 2.6 Ga classifying them as juvenile A-type granitoids evolving in a subduction setting.

The augengneiss and ROG are important time markers constraining the minimum age of the first regional tectono-metamorphic event M1, which is recorded in migmatitic paragneiss and amphibolite of the HMC. Furthermore, they provide the maximum age of the second stage of regional tectono-metamorphism and mylonitic deformation M2 affecting the HMC and Khoabendus Group. The minimum age of M2 is constrained by undeformed granite emplaced in a late stage fault dated at 1801±27 Ma.

**Tectonics and metamorphism**

Field observation, metamorphic petrology and geochronology document two tectono-thermal and one thermal event in the HMC prior to the Damara orogenic cycle. In the Khoabendus Group and FFG only the second event is recorded.

***M1 tectono-metamorphic event***

The M1 event is bracketed between a pulse of voluminous mafic magmatism and deposition of the Khoabendus Group accompanied by emplacement of the coeval FFG. Geochronology constrains the timing between 1994±22 (or 1912±33 Ma), the probable maximum age of HMC sedimentation, and 1880±9 Ma (emplacement of the oldest FFG granite). Metamorphic overgrowth, was dated in one zircon grain of sample NA101-2 at 1890±32 Ma.

The present lithodemic pile of the HMC was created during this event comprising the basal medium to high-grade (migmatitic) Lofdal-Rooikop, the central Aandgloed and the upper Suiderkruis subdomains. Transition from non-migmatitic to migmatitic gneisses is recorded in the lower part of the Aandgloed Subdomain that in turn appears to grade into the Lofdal-Rooikop subdomains marked by pervasive migmatisation and abundant pegmatite veins. At a later stage (post-M2), east-directed thrusting of the Rooikop over the Aandgloed SD along the Soutput Thrust enhanced the metamorphic gradient between the two units.

M1 small scale structures comprise stromatic layering transposed into the planar fabrics and overprinted by isoclinal folding. Asymmetric pressure shadows around pre- to synkinematic garnets indicate in several localities top to the E to ESE movements. However, due to subsequent overfolding, these indicators are not particularly reliable. A second generation of post-tectonic, sometimes megacrystic garnet displays undeformed reaction rims but may be related to M2.

Metamorphic petrology has yielded preliminary data only; the most likely M1 peak conditions in the northern, non-migmatitic part of the HMC were calculated at 10.5-11.3 kb and 650-700 $^{o}$C corresponding to upper amphibolite facies and Barrovian type metamorphism. Uplift of the HMC, involving simultaneous decompression and cooling, into the upper crust took place prior to the deposition of Khoabendus Group sediments and volcanic rocks.

Geochemical signatures of the mafic rocks and the FFG demonstrate that, overall, a geodynamic subduction zone setting prevailed during the entire period from 1920-1800 Ma and therefore excludes models involving continent collision to explain the M1 event. Accretionary orogeny by amalgamation of island arcs or exotic terranes can be excluded, too, since the typical features of this scenario are HP/LT metamorphic assemblages and ophiolite mélanges associated with arc metamorphic–magmatic complexes (Zhang *et al*. 2019), none of which occur in the KI. Instead, emplacement of voluminous mafic magmas in the HMC may have triggered metamorphism and deformation. This process adds heat to the continental crust and can cause regional-scale granulite- to amphibolite-facies metamorphism, anatexis, and surface uplift (Huppert & Sparks, 1988; Fountain, 1989; Mareschal & Bergantz, 1990). The high volume of mafic rocks in the Lofdal SD contributes field evidence for such a scenario.

Migmatisation related to mafic magmatic underplating and intra- or back-arc spreading above a subduction boundary has

been described in the Palaeoproterozoic orogenic belt of the Fennoscandian Shield of SE Sweden (Stephens & Andersson, 2015). Polyphase tectonothermal evolution with anatexis under low-P metamorphic conditions around 1.86 Ga (M1) and 1.84–1.81 Ga (M2) is inferred for migmatitic gneisses of the Bergslagen unit. 1.86–1.85 Ga ductile D1 deformation under medium-grade metamorphic conditions is recorded in the adjacent lithotectonic unit to the south (Småland unit). Anatexis in the Bergslagen lithotectonic unit is related by the authors to pulses of mafic underplating, during the early stages of two separate, magmatic episodes related to intra- or back-arc spreading above a subduction boundary, which had entered a retreating mode with separate, long periods (20–50 Ma) of extension or transtension. Similar timing and mechanisms under higher P/T conditions can be assumed for the early evolution of the HMC

Another example of granulite to amphibolite metamorphism induced by mafic magmatic underplating has been described from the Ivrea Zone of the Alps exposing a continuous rock section through the lower to middle crust (Henk *et al*. 1997; Klötzli *et al*. 2014). Magmatic underplating (gabbro) at the base of the Moho was accompanied by important crustal attenuation resulting in crustal thinning and uplift. Assuming a similar mechanism in the KI, magmatic underplating may have caused the formation of subsequent (continental) back arc basin into which the Khoabendus rocks were deposited. The gabbros of the HMC would have been deformed and metamorphosed during M1 soon after their emplacement.

***M2 tectono-metamorphic event***

The M2 event is of lower grade and overprinted the HMC, the FFG and the Khoabendus Group geochronology constrains M2 between $1829^{+71}/_{-69}$ Ma, the age of red sill granite transformed into mylonitic red orthogneiss, and 1798±18 Ma, the age of undeformed late to post-M2 granite and gabbro emplaced into a fault. Alternatively the youngest zircons in the granite are xenocrysts, constraining only the maximum age of magmatic emplacement and metamorphism. Metamorphic overgrowth was dated in three zircon grains of sample NA101-2 at 1751±130 Ma, 1786 ±21 Ma and 1796±13 Ma.

In the northern part of the HMC (Ehobib, Suiderkruis, Aandgloed subdomains), M2 is marked by complex interference folding and folded mylonitic low- to high-angle thrusts that left, however, the existing lithodemic pile mostly unaffected. More specifically, the event is marked by the following features:

- Most of the pre-Panafrican structures (thrusts, folds) on the geological map are associated with the M2/D2 event, while older structures were transposed.
- Metamorphic petrology has yielded only preliminary data but the most likely peak conditions are of lower amphibolite facies and medium pressure (525-600 $^{o}$C, 5.5-8 kb).
- The low-grade Ehobib SD (Khoabendus Group) is juxtaposed along steep to shallow mylonite zones with the Aandgloed-Suiderkruis SD and mainly preserved in a tectonic graben as fault-bound, tight, upright synforms. In the northern part of the HMC the mylonite changes from a steeply into a shallowly dipping structure separating overlying Ehobib rocks from underlying HMC gneisses, suggesting the interpretation as a detachment.
- M2 extensional tectonics are recorded on the northern flank of the Eersbegin Dome by (i) the development of a phyllonite and tectonic breccia at the interface between underlying quartzite and overlying schist and gneiss, (ii) abundant boudins up to several tens of metres diameter concentrated in one horizon and (iii) kinematic indicators around the structure suggesting movements away from the central part of the dome (Fig. 16).
- Mylonitic quartzite marks the contact between the Aandgloed and the overlying Suiderkruis SD.
- Granitic and granodioritic sheet-like bodies, considered to be deep-level equivalents of the FFG, are transformed into (augen) ortho-gneiss and overprinted by folding and mylonitisation.

- Foliations in the Suiderkruis and Ehobib SD dip mainly moderately to steeply in northerly directions. In the Suiderkruis SD large scale interference folding around NNW-SSE axes is illustrated by curved axial traces on the geological map and the wide scatter of foliations in stereograms.
- Axial planes of the Kuyper and Eersbegin synforms dip moderately in northernly directions, away from the HMC.
- Stretching lineations are principally down-dip with small lateral components.
- Kinematic indicators record mainly north-directed down-dip movements, away from the HMC.

In the southern part of the HMC, M2 structural style is characterised by vertical sheath-folds (Rooikop SD) and complex interference folding (Lofdal-Rooikop subdomains) affecting orthogneiss attributed to the FFG. Further characteristics are:

- Mylonitic gneiss and schist is limited to post-M2 structures (e.g. Soutpoort Shear Belt, Soutput Thrust).
- Moderate to steep foliations dip mainly in easterly and SE directions
- Down-dip lineations vary widely in plunge and plunge direction, however steep plunges predominate.

In the Transition Zone remnants of the Khoabendus Group are preserved in a tight, upright NE-SW striking synform more than 50 km in length, bound by subvertical shear zones. Further characteristics are:

- Foliations are steeply SE dipping
- Lineations show main down-dip and minor horizontal components documenting vertical movements with a minor left-lateral component.
- Kinematic indicators suggest mainly top to the N movements.

In the Kamanjab-Grootberg area, the following tectonothermal features are observed:

- FFG and Khoabendus Group record metamorphism below greenschist facies conditions.
- NE-SW foliations are mainly steep and associated with steep to moderately plunging lineations suggesting principally vertical movements.
- Folds are marked by subvertical fold axial planes and vary from tight to gentle. The fold axis plunges generally at a low angle but varies considerably in direction. This is especially evident in the NE of the study area where regional folds envelop the Oortrek intrusion (Fig. 16)
- FFG granite bodies are generally weakly deformed and overprinted at various degrees by subvertical NE-SW foliation.
- Contact metamorphism transformed the country rock around the Oortrek intrusion partly into hornfels and tremolite fels.
- Two hydrothermal events comprise pervasive epidote-chert altering the former rocks SW of the Oortrek pluton into epidosite and hydrothermal epidote crystallising in discrete vertical shear zones.

All features suggest that M2 deformation was related to an extensional setting leading to the formation of a mantled gneiss dome (Eskola, 1949) with a core of migmatite and gneisses (HMC) overlain by layered metasediments and volcanic rocks (Khoabendus Fm). Gneiss domes are large scale structures that can be formed by multiple mechanisms associated with compressive, strike-slip or extensional tectonics (Yin, 2004; Baldim & Oliveira, 2016). They include (1) diapiric flow induced by density inversion, (2) buckling under horizontal constriction (i.e. extension perpendicular to compression), (3) coeval orthogonal contraction or superposition of multiple phases of folding in different orientations, (4) instability induced by vertical variation of viscosity, (5) arching of corrugated detachment faults by extension-induced isostatic rebound and (6) formation of doubly plunging antiforms induced by thrust-duplex development (Yin, 2004; Fig. 92).

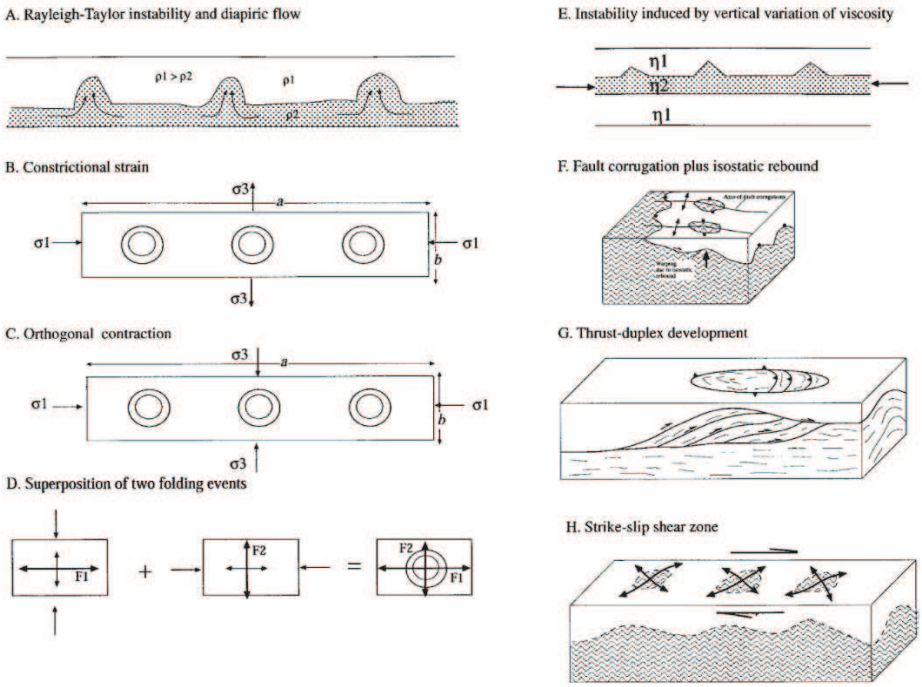


**Figure 92**. Major geological processes and mechanical models for the formation of gneiss domes. (A) Rayleigh-Taylor instability and diapric flow; ρ is crustal density. (B) Constrictional strain field under horizontal loads; σ1 and σ3 are the maximum and minimum principal stresses; '*a*' and '*b*' are the length and width of the extensional belt. Ratio a/b defines the aspect ratio of the system. (C) Orthogonal contraction. (D) Superposition of two folding events. (E) Instability induced by vertical variation of viscosity (η). (F) Arching of corrugated detachment fault by isostatic rebound. (G) Development of thrust duplex. (H) Broad folds in strike-slip shear zone (Yin, 2004).

Structural features in the study area suggest that formation of the HMC gneiss dome is the product of fault-related processes, of which the three principle types are (i) arching of corrugated detachment faults by extension-induced isostatic rebound = metamorphic core complex (Fig. 92f), (ii) thrust-duplex development (Fig. 92g), and (iii) development of broad folds in strike-slip zones (Fig. 92h).

Applying the classification scheme by Yin (2004) thrust duplex development and passive-roof fault models can be excluded because of the absence of thrusted stacks with inverse metamorphic gradients in the HMC (Fig. 93). Strike-slip shear zones associated gneiss domes are also very unlikely because these structures were not observed in the transition zone between HMC and the Kamanjab-Grootberg area.

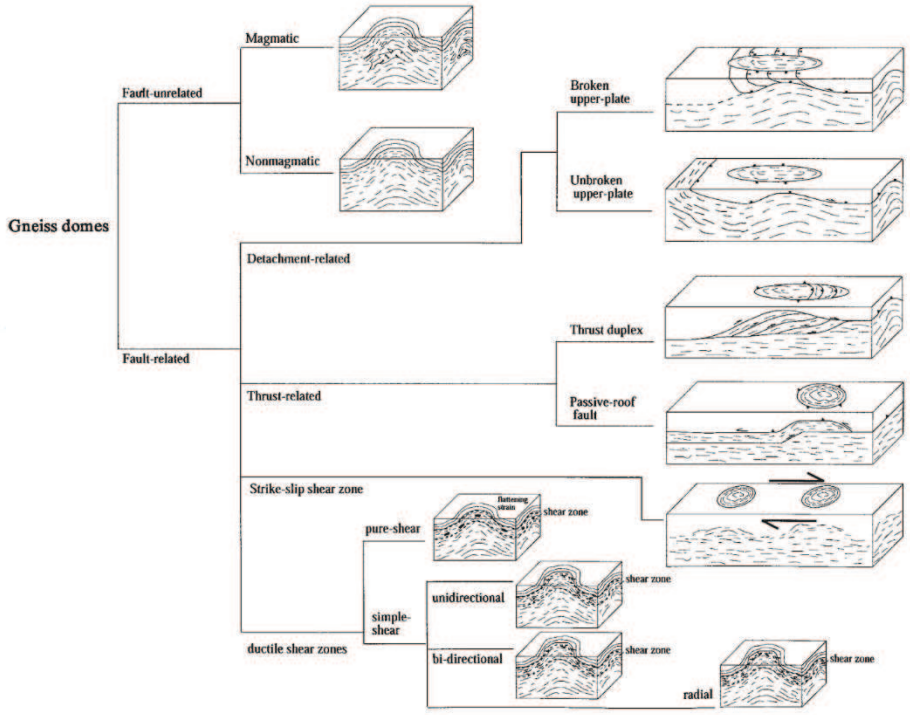


**Figure 93**. Classification of individual gneiss domes (Yin, 2004).

M2 structures (steep foliations, down-dip lineations, normal geothermal gradient, and absence of reverse thrusts) document predominantly vertical tectonics in the KI suggesting an extensional geodynamic setting. Uplift of the HMC during this stage was accompanied by folding and the development of extensional mylonitic thrusts along which low-grade Khoabendus rocks were transported downdip in northerly directions, away from the HMC. Juxtaposition of the low-grade Ehobib SD with the northern flank of the HMC took place along steep normal faults in which the rocks were transformed into mylonite. Highly ductile conditions and vertical movements are indicated in the Rooikop SD by vertical sheath folds, steep to vertical lineations and widely varying steep to moderate foliation directions. In the Transition Zone and the Kamanjab Grootberg area, rocks of the Khoabendus Group and FFG underwent low to very low-grade metamorphism and deformation is character-ised by steep foliations, and lineations major NE-SW normal faults and upright tight folds, some of which are clearly associated with the faults. These observations indicate detachment-related gneiss broken upper plate domes as most likely description of the HMC.

The structural data bear resemblance with Metamorphic Core Complex (MCC) models (Fig. 94). The term has been defined in the Basin and Range Province (Davis & Coney, 1979; Crittenden *et al*. 1980; Wernicke, 1981; Lister & Davis, 1989). MCC mainly develop in continental crust, especially where it has been previously thickened by collision (Ring, 2014). Radioactive decay within the thickened crust introduces heat, thereby lowering rock viscosity and ultimately causing failure of the lower crust. The rise of MCC results from strong tectonic denudation in a continental lithospheric extension setting, leading to exhumation and deformation of middle to lower crustal rocks. The driving force for the development of MCC is therefore a hot, weak, low viscosity lower crust (Gessner *et al*. 2007).

MCC are classically divided into two units: (1) a lower unit composed of high-grade metamorphic and migmatitic rocks, sometimes associated with plutonic bodies that are created within the evolution of the MCC, (2) an upper unit consisting of unmetamorphosed or previously metamorphosed rocks associated with syntectonic basin infill (Fig. 94). The two units are separated by a master detachment fault zone comprising mylonitic to ultramylonitic rocks.

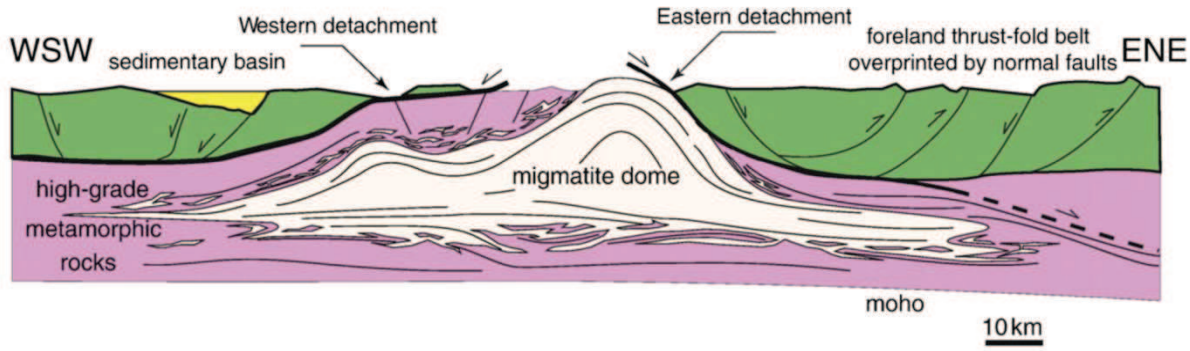


**Figure 94.** Classic model of a metamorphic core complex. Synthetic cross-section through the Shuswap MCC (British Columbia, Canada, after Vanderhaeghe *et al*. (1999).

In this model the HMC forms the core of the MCC (even though the observed migmatitic rocks are clearly older) overlain by the Khoabendus Group and FFG as the upper unit (Fig. 95). The model explains well (i) the strong gradient in deformation between coeval magmatic rocks across the contact (e.g. weakly foliated FFG granite and mylonitic HMC orthogneiss, (ii) the undisturbed crustal stack, (iii) important mylonites in the northern part of the HMC at the contact between Ehobib and Aandgloed/Suiderkruis subdomains, (iv) extensional structures in the Transition Zone and Kamanjab-Grootberg area recording N-directed movements, away from the HMC, and (v) formation of structural domes within the HMC recording radial movements away from the apex.

Synsedimentary basins which may have existed, were subsequently eroded as were any vestiges of contemporaneous volcanism. However, igneous activity during the formation of the MCC is documented by the sill granite and local gabbro and granite emplaced within a fault.

So far, the preliminary P/T estimates do not allow definition of the normal or reverse M2 gradient in the HMC, which is an important parameter for MCC models requiring normal gradients from the margin to the centre of the structure. Other problems are (i) the predominantly steep lineations in the Lofdal and Rooikop SD suggesting highly ductile conditions and diapir-style tectonics (in the core of classical MCC the lineations are commonly subhorizontal and foliations are shallow dipping), (ii) the absence of M2 migmatite and associated plutonic rocks, (iii) MCC mostly evolve in late to post-orogenic collisional settings. However, development of MCC in back arc environments were described in northern China (Li *et al*. 2019) and in a non-over-thickened crust at Liaoding Peninsula, East Asia (Wang *et al*. 2015).

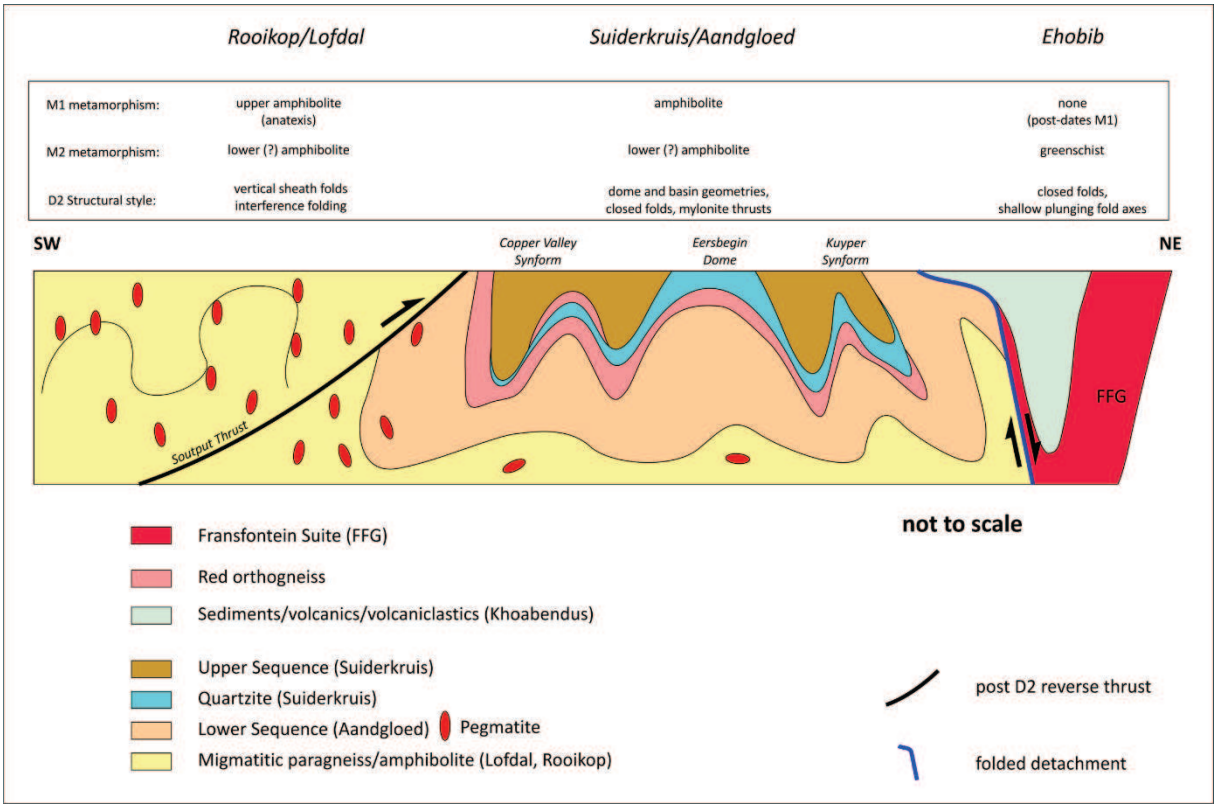


**Figure 95**. Schematic SW-NE cross section through the HMC gneisses (Rooikop/Lofdal-Suiderkruis/Aandgloed subdomains) and Khoabendus Group rocks (Ehobib SD). The Soutput Thrust postdates M2.

***Mesoproterozoic thermal event***

K-Ar and Ar-Ar geochronology reveal, in the HMC, complete reset of the hornblende and muscovite clocks between 1.28-1.45 Ga requiring temperatures above the highest closure temperatures between 480-550$^{O}$C for these minerals. In the Epupa Complex NW of the KI, the emplacement of the Kunene Anorthosite Complex and contemporaneous granulite metamorphism falls into this time span and has been associated with the Kibaran Rift in eastern Congo, Tanzania (Seth *et al*. 1998, 2003, 2005; Brandt & Klemd, 2008). The connection with the M2/D2 event in the KI, described in the foregoing section, is excluded solely on the basis of U-Pb single zircon ages in sample NA101-2 from post-tectonic granite yielding an age of 1798±18 Ma (3 zircon grains!). If these zircons are xenocrysts, any younger age is permitted for the M2/D2 event whose structural inventory fits well with a rift setting.

***Post-M2 / pre-Damara deformation***

The geometric relations between Post-M2 / pre-Damara shear zones and thrusts and their host rocks indicate the following succession of events:

- Soutput Thrust: the thrust is characterised by east-directed thrusting of the Rooikop over the Aandgloed SD, rocks in the thrust turned into mylonite and schist,
- Huab Fault: the oblique fault offsets the Soutput Thrust about 7 km indicating a major left-lateral component. In the eastern part of the study area it affects Otavi Goup carbonates but is overlain by folded Mulden Group sedimentary rocks,
- Soutpoort Shear Belt: the steep shear zone runs parallel to the Huab fault and may be part of the same deformation event. It is overlain by folded Mulden Group sedimentary rocks.

***Pan-African deformation***

The deformation overprinting Damara rocks displays widely varying geometry, orientation and plunge of different folds, which have been described in detail by Frets (1974). Based on geometric considerations the author subdivided four fold phases of (1) gentle to open E-W trending folds with a wavelength of several km, (2) refolding of F1 folds into NNW-SSE to WNW-ESE trending similar-style folds

associated with a penetrative cleavage, (3) local folding into N-S trending subvertical folds and (4) local WSW-ESE open to closed SW-verging (back)folding.

**Regional context**

The KI belongs to a group of Palaeoproterozoic inliers located at the margins of the Congo and Tanzania cratons (Fig. 97). These cratons were amalgamated during the Orosirian (2.1-1.9 Ga) period along the Ubendian/Usagaran belt. The Zimbabwe-Kalahari nuclei are surrounded by similar Palaeoproterozoic terranes (Magondi/Limpopo Belt, Kheis Belt, Rehoboth Inlier, Namaqua Belt and Natal Belt), however, collision of this assemblage with the Congo-Tanzania continent probably happened much later during the Stenian period within the Irumide orogeny (ca 1.1-1.0 Ga). Various attempts over the past 20 years to reconstruct the Palaeoproterozoic so-called Columbia Supercontinent show the Kalahari and Congo cratons in widely varying areas from each other, both adjacent to each other (Ernst & Youbi, 2017; Salminen *et al.* 2019; Chaves & Rezende, 2019; Chaves, 2021, Fig. 96a) and at opposite sides (Zhao *et al.* 2002, 2004; Evans & Mitchell, 2011; Zhang *et al.* 2012; Wu *et al*. 2020; Fig. 96b) of Columbia. Therefore, these terranes are not discussed further.

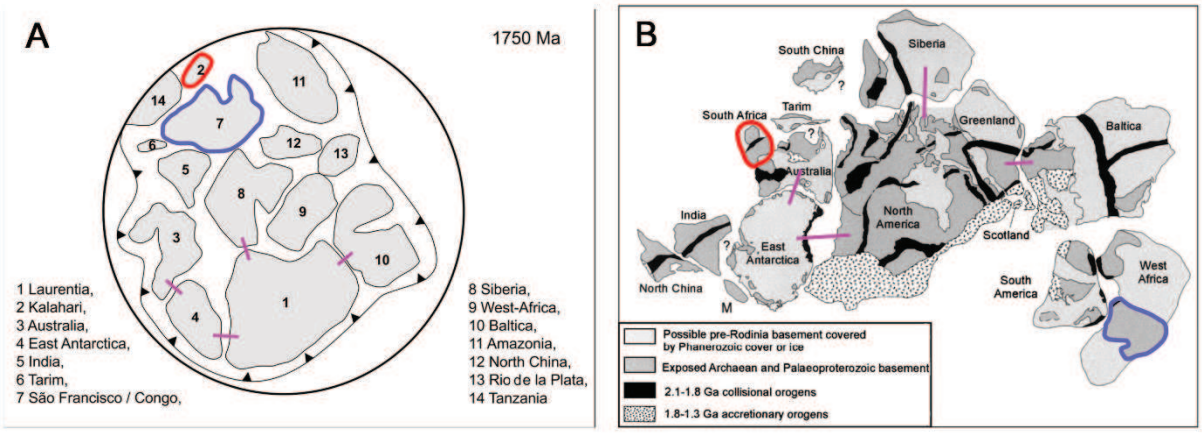


**Figure 96**. Two examples of reconstructions of the Columbia Supercontinent. A) simplified from Chaves (2021) and rotated 180° allowing better comparison between the two reconstructions; B) the "classical model" (Zhao *et al*. 2002, 2004). Red outline = Kalahari Craton; blue outline = Congo Craton. The diagrams illustrate the great uncertainty in reconstructing Columbia. Pink lines indicate similar connections in the two configurations (Baltica-North America-East Antarctica-Siberia).

Modern geochronological data determined in various studies of the Palaeoproterozoic inliers are shown in Table 27 building on a compilation by Mapeo *et al*. (2019). The data are organised for each unit into three columns (magmatic emplacement (red), metamorphism (blue) and sedimentation/ volcanism (green) to monitor the Archaean to Mesoproterozoic crustal evolution along the cratonic margin. They demonstrate considerable variation even between adjacent inliers, resulting from incomplete or poorly-constrained data (e.g. periods of sedimentation/ volcanism and metamorphism) but also indicating lateral changes in coeval plate-tectonic settings.

**Table 27**. Timing of magmatic (red), metamorphic (green) and sedimentary (blue) events in basement inliers and orogenic belts around the southern part of the Congo-Kasai Craton.
The respective references are shown below each inlier and are arranged in chronological order.

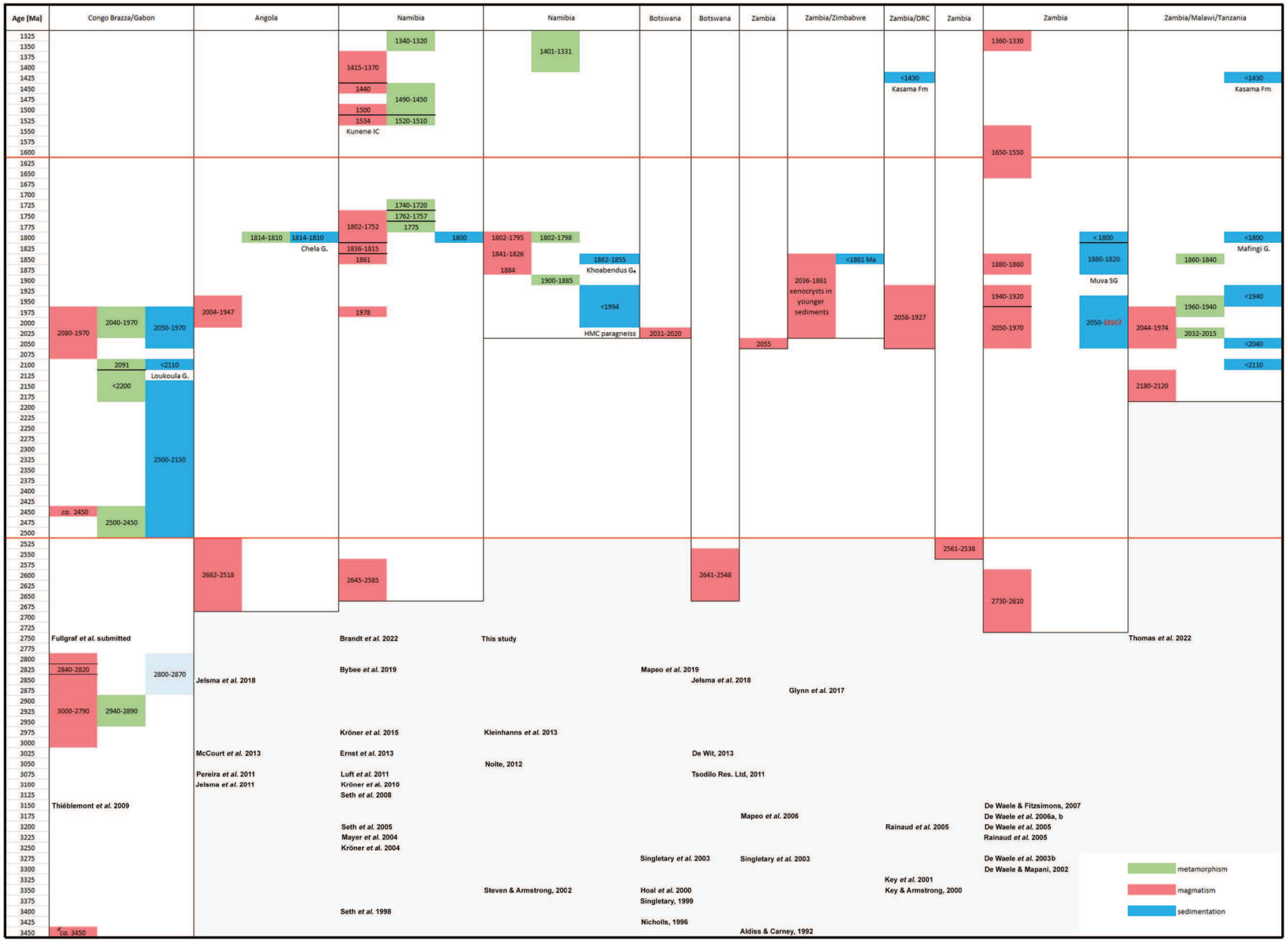

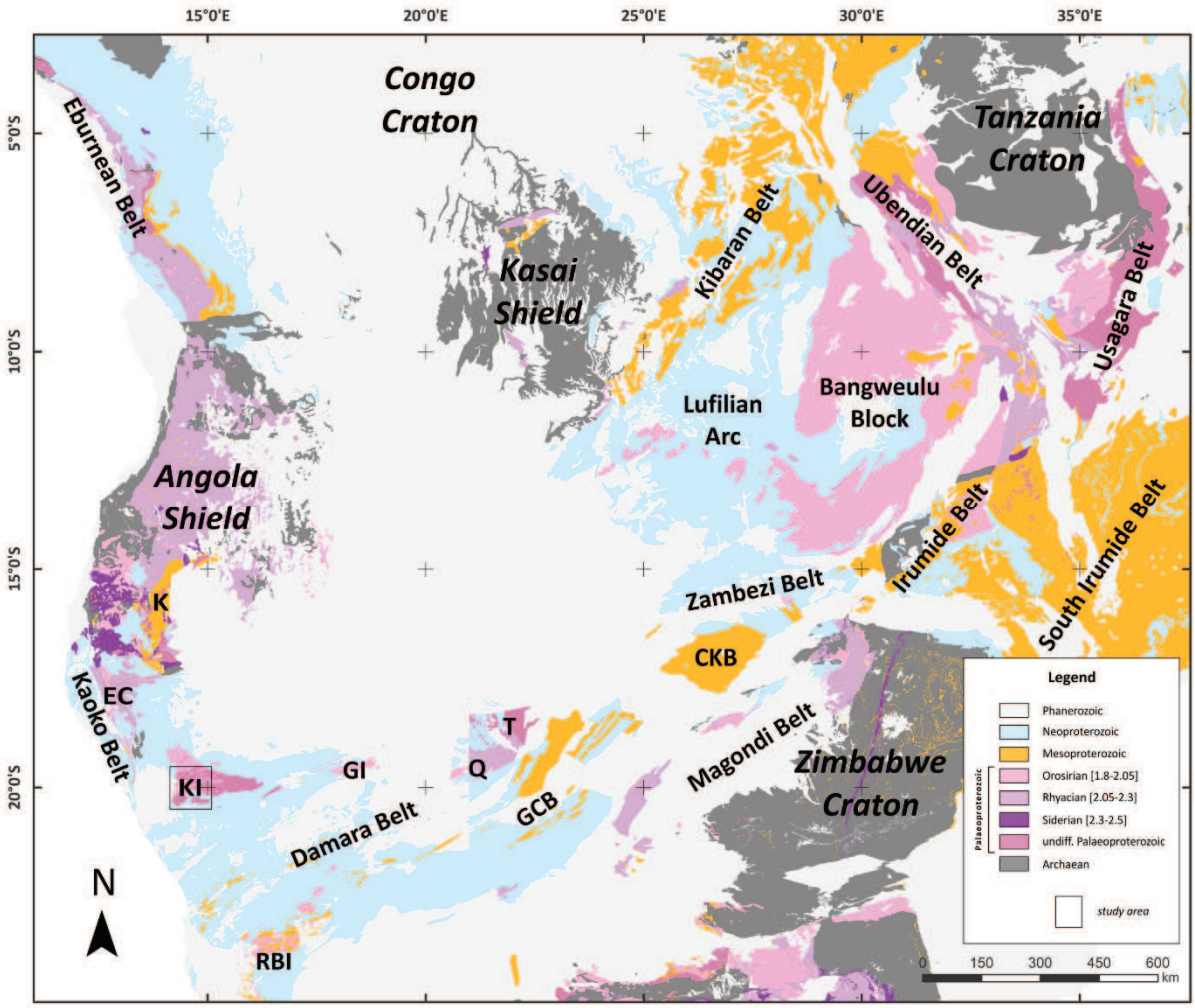


**Figure 97**. Precambrian geology of central to southern Africa. Simplified extract from BRGM SIG-Afrique (unpublished). CKB = Choma-Kalomo Block, EC = Epupa Complex, GCB = Ghanzi-Chobe Belt, GI = Grootfontein Inlier, K = Kunene Igneous Complex, KI = Kamanjab Inlier, RBI = Rehoboth Basement Inlier, Q = Quangwadum Valley, T = Tsodilo Hills.

***Palaeoproterozoic Era***

***<u>Magmatism and sedimentation</u>***

The SW edge of the Tanzania Craton was an active continental, Andean-type margin during the Neoarchaean (~2.7 Ga), with subduction eastwards, beneath the craton and the generation and emplacement of voluminous calc-alkaline granitoids into the upper (cratonic) plate. At 2.64 Ga subduction ceased and the SW Tanzania Craton became passive during the long ca 500 Ma interval up to ~2.05 Ga. Subsequent voluminous arc and collision-related magmatism between 2080-1970 Ma is recorded along the entire margin in the West Congo (Eburnean) and Ubendian/Usangara belts, the Bangwuela Block and several other inliers in Zambia (Table 27).

A passive margin setting is proposed for the western part of the Congo craton during the Eburnean orogeny between 2.2-2.0 Ga (Thiéblemont *et al.* 2009 and references therein). Sediments in the Foreland of the Eburnean orogeny are combined into the ca 2.1-1.95 Ga Francevillean SG. The lower part (Francevillean A-B) was deposited in graben structures interpreted as pull-apart basins (Weber *et al.* 2016). The upper part (Francevillean C-D) was deposited in broad basins. Sedimentation was accompanied by felsic, partly alkaline magmatism dated at 2072±29 Ma.

Voluminous plutonism between 2.08-2.0 Ga in the West-Gabon/São Francisco plate is associated with an active margin setting. The magmatism ceased after continental collision at ca 2 Ga.

In Namibia, only post-Eburnean 1.98 Ga magmatism has been reported in the EC (Kröner *et al.* 2010) and possibly marks the onset of a renewed active margin setting.

Subsequent pulses of arc-related felsic magmatism in the intervals 1940-1920, 1880-1860, 1841-1815 Ma are localised in northern Namibia and the Bangweulu block but are absent in the Eburnean and Ubendian domains, where Palaeoproterozoic orogeny was largely completed. Missing records of these pulses in the inliers between northern Malawi and eastern Zambia may be attributed to poor outcrop. Diachronic evolution from old to young is suggested by the present geochronological data from east to west: the Bangweulu block records arc magmatism from 1940-1860 Ma, the KI from 1880-1820 Ma and the EC from 1860-1750 Ma (Table 27). Subduction in the Bangwuela block was probably terminated after the collision of the Congo and Tanzania Cratons at ca 1840 Ma.

***Metamorphism***

The geochronological data set of metamorphic events is currently incomplete and is partly based on indirect arguments such as geometric relationships, often only loosely constraining the time intervals. This applies especially to terranes subjected to subsequent tectonothermal events overprinting mostly older vestiges. So far, few studies have been dedicated to metamorphic geochronology and petrology in the Palaeoproterozoic inliers around the Congo Craton (Thiéblemont *et al*. 2009; Seth *et al*. 2008).

On the western side of the Congo Craton, two early Eburnean highT and highP-mediumT orogenic phases are recorded in the (Pan-African) West Congo Belt between 2200 and 2100 Ma, followed by a third, poorly constrained, low-grade event in the interval 2040-1970 Ma, the collision stage of the Eburnean orogeny (Thiéblemont *et al*. 2009). Eastward subduction of the oceanic lithosphere produced eclogites at 2120±38 Ma marked by P/T conditions of 8-10 kb and 700-550 $^{O}$C (Feybesse *et al*. 1998; Weber *et al*. 2016). The blocking of the subduction by continent collision between 2040-2000 Ma was accompanied by voluminous granite magmatism, however, only thrust tectonics under low to medium-grade metamorphism has been reported in western Gabon, which therefore represents the eastern external zone of the orogen (Thiéblemont *et al*. 2009).

Metamorphic ages from southern Angola and northern Namibia suggest several short-lived local events in the intervals [1900-1885 Ma; KI], [1814-1810 Ma; AS], [1802-1798 Ma; KI], [1775 ma; EC], and [1762-1757 Ma; EC] concomitant to arc magmatism in this area. This argues for input of heat into the crust by magmatic underplating and subduction-related magmas rising into mid- to upper crustal levels. The absence of a regional late-Palaeoproterozoic metamorphic and deformation event shows that cessation of the active arc setting around 1750 Ma was not caused by continent collision.

In the Ubendian Belt modern studies demonstrate the extremely complex collision history resulting in an array of micro-terranes marked by widely varying P/T conditions. The first phase of Ubendian tectonothermal activity occurred between ~2093 and 2048 Ma with syntectonic magmatic intrusions and accompanied by eclogite (in the Upende and Upifa terranes) and high pressure granulite facies metamorphism in the others (Lenoir *et al*. 1994; Ring *et al*. 1997). Following the ~1960 Ma event, to about 1817 Ma (Boniface *et al*. 2012) several episodes of tectonism, metamorphism and magmatism have been recorded in the Ubendian terranes. In essence, however, the Palaeoproterozoic history of the Ubendian belt is seen in terms of renewed Andean-type subduction of the passive margin beneath the Tanzania Craton, with the production of eclogite in the downgoing slab and high-grade metamorphism of the Late Neoarchaean to Palaeoproterozoic passive margin sediments,

***Mesoproterozoic Era***

***Magmatism***

Intraplate magmatism associated with continental rifting related to the Kibaran event and break-up of Columbia supercontinent is represented in NW Namibia and SW Angola by the oval Kunene Igneous Complex (KIC) ca 45,000 km$^2$ in area. The western part of the 18,000 km$^2$ surface is exposed in a N-S trending 350 km long, 25-50 km wide strip whereas the larger eastern part is obscured beneath Kalahari sands (Rey-Moral *et al*. 2022). The layered intrusion comprises mainly anorthosite with minor gabbro, troctolite, and norite. The earliest stage of KIC magmatism has been dated at 1503±6.7 Ma (Bybee *et al*. 2019), the main phase at 1438-1375 Ma (Baxe, 2007; Drüppel *et al*. 2007; Brower, 2017; Bybee *et al*. 2019) and late stage mangerite at 1371±2.5 Ma (Mayer *et al*. 2004). Slightly older to coeval and younger

felsic magmatism in this area comprises "Red granite", leucogranite, quartz monzonite, syenite, and rhyolite spanning the period from 1534-1176 Ma (Mayer *et al*. 2004; Baxe, 2007; McCourt *et al*. 2013; Kröner & Rojas-Agramonte, 2017; Brower, 2017).

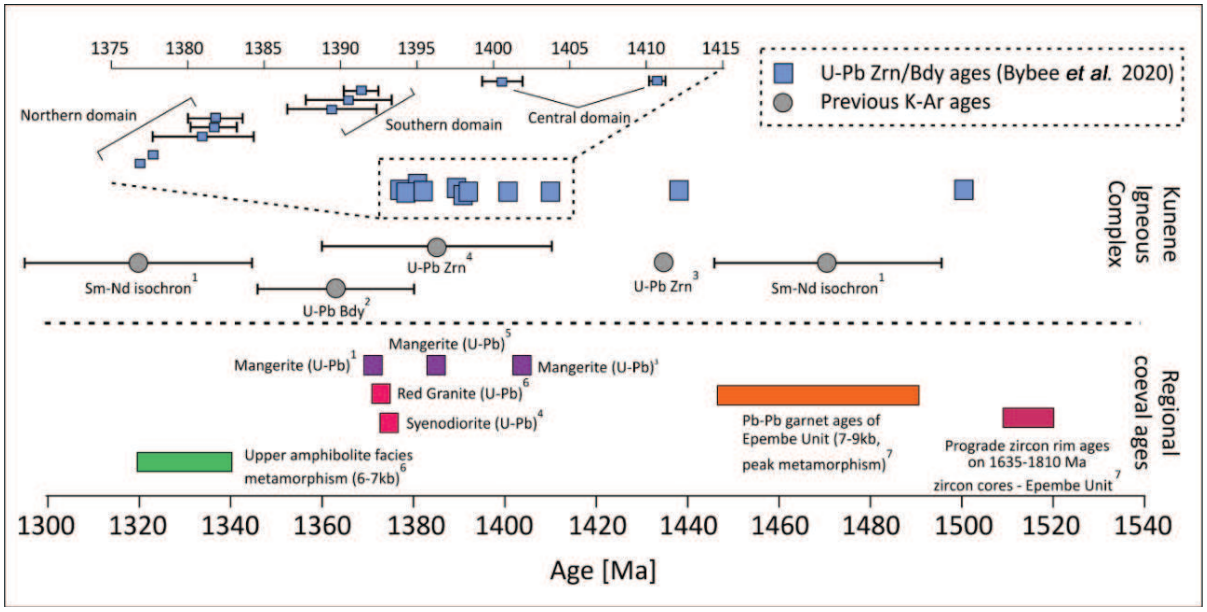


**Figure 98**. Summary of geochronological data obtained for the KIC and broadly coeval granitoid intrusions (Bybee *et al*. 2019). Regional metamorphic ages of EC paragneisses coincide with the onset of KIC magmatism at ~1500 Ma, signifying an earlier initiation of magmatism compared to previous estimates. Ages are extracted from the following references: 1 – Mayer *et al*. 2004; 2 – Maier *et al*. 2013; 3 – Baxe, 2007; 4 – Drüppel *et al*. 2007; 5 – McCourt *et al*. 2013; 6 – Seth *et al*. 2005; 7 –Seth *et al*. 2003. Rb–Sr ages have been omitted as errors are large. Error bars for regional ages are not shown for clarity (bdy = baddeleyite, zrn = zircon).

The proposed geodynamic settings for the magmatism are (i) emplacement as large igneous province associated with intraplate extension within the Kibaran rift event (Mayer *et al*. 2004; Tack *et al*. 2010; Ernst *et al*. 2013) or (ii) associated with crustal thickening through E-W shortening in a convergent environment that commonly occurs in subduction and/or rift-related crustal hot zones (Brower, 2017; Bybee *et al*. 2019). The KIC intrusion follows a NE-SW to NNE-SSW Palaeoproterozoic trend that probably constitutes a wide zone of lithospheric weakness through which the intrusion of the mantle-derived melts was harnessed (Rey-Moral *et al*. 2022). Deposition of the 1320 Ma Okapuka Fm in this area was suggested in an extensional intracontinental setting (Kröner & Rojas-Agramonte, 2017) supporting such an assumption. The connection with the coeval Kibaran Belt is probable but remains unclear since the structure was modified by Pan-African deformation in the Lufilian Arc and its continuation further SW is obscured by Kalahari sediments.

In Zambia, a large group of anorogenic alkaline granites (DeWaele *et al*. 2003b, 2006b) at the deformed SW margin of the Bangweulu Block was emplaced in two pulses between 1664-1627 Ma and 1610-1551 Ma, thereby straddling the boundary between the Palaeo- and Mesoproterozoic eras. It possibly heralds Mesoproterozoic extension and rifting settings characterising the 1600-1200 Ma Calymmian and Ectasian periods on the Congo-Kasai craton. A minor suite of 1.36-1.33 Ga anorogenic plutons (nepheline syenite and biotite granite) in the north-eastern part of the Bangweulu margin can be associated probably with the Kibaran Rift (Table 27; De Waele *et al*. 2006b).

### ***Metamorphism***

The most recent version of the metamorphic history of the KIC and its hosting gneisses of the EC is given by Bybee *et al*. (2019) see Brandt *et al*. (2021). The emplacement depth of the KIC is not well constrained. Ti-in-amphibole thermobarometry for anorthositic rocks of the Zebra Mountains in Namibia indicates pressures of 7–9 kb for the

late stages of crystallisation, suggesting emplacement at lower crustal depths (Drüppel *et al*. 2001). However, in apparent contradiction, two-pyroxene thermobarometry analyses on a single sample from the northern domain of the Angolan portion of the complex yielded crystallisation conditions of ~880°C at 3–5 kb, i.e. emplacement at shallow crustal levels (Slejko *et al*. 2002). Further evidence comes from the hosting high-grade paragneisses. In the Epembe Unit south of the Zebra Mountains, zircon overgrowths record initial prograde metamorphism (5–7 kb) at 1520–1510 Ma (Seth *et al*. 2003), to reach peak granulite-facies conditions (1000°C and 9.5 kb) recorded in garnet at 1490–1447 Ma (Brandt *et al*. 2003, 2007). Brandt *et al*. (2007) have attributed ultrahigh-temperature metamorphism to initial emplacement of the KIC magmas at ~20 km and subsidence due to magmatic loading to a depth of ~30 km, however, the currently published age range for the KIC does not support this hypothesis (Bybee *et al*. 2019). The Orue Unit, which abuts Kunene anorthosites south of the Zebra Mountains, preserves peak upper amphibolite facies metamorphism (6–7 kb) at 1340–1320 Ma (Brandt & Klemd, 2008; Seth *et al*. 2005), post-dating the recognised emplacement age of the KIC. Relationships between the shear-zone-bounded Epembe and Orue units are unclear and additional work is required to understand how the disparate P–T conditions relate to each other and to the KIC. However, geochronology by Bybee *et al*. (2019) allows the magmatic loading hypothesis of Brandt *et al*. (2007) to be discarded.

K-Ar and Ar-Ar hornblende and muscovite cooling ages between 1401-1331 Ma determined in the HMC (this study) document the far-reaching thermal impact of the Kunene IC or reset of the isotope system by high geothermal gradient in a continental rift setting. The continuation into the Kibaran rift has been proposed by various authors (Nolte, 2012; Bybee *et al*. 2019; Lehmann *et al*. 2020; Rey-Moral *et al*. 2022) associated with the breakup of Columbia and prior the amalgamation of Rodinia (Ernst *et al*. 2013). It is even possible that the entire tectonic-thermal M2 event of the HMC is associated with Kibaran rifting.

## Conclusions

The multidisciplinary study of the Huab Metamorphic Complex and the Khoabendus Group combined with the review of Palaeo- to Mesoproterozoic terranes at the southern margin of the Congo Craton contributes to the reconstruction of their complex polyphase history from ca 2.2-1.3 Ga at both continental and regional scales marked by four major phases (Fig. 99).

### 2200-2100 Ma

The Congo and Tanzania cratons record passive margin settings during this period, whereas oceanic lithosphere was subducted towards the west beneath the West Gabon/São Francisco plate producing eclogites at 2120±38 Ma (Fig. 99a). The absence of arc-related magmatism at the active margin suggests shallow subduction of young, hot oceanic lithosphere (Zheng *et al*. 2022).

### 2100-1950 Ma

Continued subduction along the eastern active margin of the West-Gabon/ São Francisco plate was accompanied by voluminous arc-related magmatism at 2.08-2.04 Ga indicating steepening of the subducting slab. Subsequent continent collision at 2.04-1.98 Ga (Eburnean event) resulted in welding of the São Francisco with the Congo (SF-Congo) plate and termination of arc magmatism (Fig. 99b). On the Congo Craton, the Francevillean SG was deposited between 2.05-1.95 Ga in broad foreland basins of the Eburnean orogen. Initial sedimentation associated with felsic magmatism took place in tectonic grabens, interpreted as pull-apart structures (Weber *et al*. 2016). Subsequent sedimentation records the molasse stage of Eburnean orogeny. Deposition of HMC sediments may have taken place during this period in such an environment, too.

The western side of the Tanzania Craton turned into an active margin along which microterranes were accreted marked by individual tectono-thermal histories. The first phase of Ubendian orogeny at 2.09-2.05 Ga is marked by eclogite and high pressure granulite facies metamorphism accompanied by syntectonic magmatic intrusions.

### 1950-1750 Ma

The onset of a new E-W trending magmatic arc at the southern margin of the SF-Congo plate is documented by voluminous

mafic magmatism in the HMC, probably post-dating 1.92 Ga (Fig. 99c). Several pulses of arc-related felsic magmatism in the intervals 1940-1920, 1880-1860, and 1841-1815 are localised in northern Namibia and the Bangweulu block but are absent from the Eburnean domain, where Palaeoproterozoic orogeny was largely completed.

Diachronic arc evolution from old to young is suggested from east to west: the Bangweulu block records the first pulse of arc magmatism but not the last. In the KI, deposition of the Khoabendus Group and emplacement of the coeval FFG took place at 1880-1815 Ma whereas in the Epupa Complex adjacent to the NW Palaeoproterozoic arc activity ceased at ca 1750 Ma without any terminal continent collision.

In the Ubendian terranes several episodes of tectonism, metamorphism and magmatism are recorded between 1960 Ma and 1817 Ma. Collision between the Tanzania Craton and the Bangweulu Block of the Congo Craton at ca 1840 Ma was accompanied by differential exhumation in a predominantly dextral strike-slip transpressional setting in the Ubendian part whereas the Usangara belt formed the frontal ramp during collision.

**1650-1300 Ma**

The Kibaran event is heralded in NE Zambia by anorogenic, partly alkaline granite magmatism between 1650-1550 Ma (DeWaele *et al*. 2003b, 2006b). The main period of rifting, deformation and metamorphism is bracketed in time from ca 1500-1300 Ma and recorded within the Kibaran-Karagwe-Ankole belt stretching from NE Congo, Rwanda and Burundi, to SW Uganda and NW Tanzania. Voluminous bimodal magmatism occurred in the period between 1380-1370 Ma (Tack *et al*. 2010). In Namibia and Angola, Kibaran-age magmatism between 1500-1340 Ma is represented by the Kunene IC with the main pulse taking place at 1410-1380 Ma. Polyphase metamorphism up to granulite facies in the host rocks may or may not be associated with the magmatic emplacement. Thermal impact of the Kibaran event in the HMC is recorded by K-Ar and Ar-Ar mineral ages between 1440-1330 Ma.

The history of the Kamanjab Inlier within this regional framework can be subdivided into four phases (Fig. 100). In the first stage from ca 2.0-1.92 Ga the KI formed a Francevillean type molasse basin in the foreland of the Eburnean orogen, which was filled by the debris of the mountain belt (Fig. 100a).

A new ENE-WSW trending arc system was initiated south of the KI soon after termination of the Eburnean orogeny, extending for more than 1700 km into Zambia (not shown). Asthenospheric convection behind the arc caused lateral extension and lithospheric thinning resulting in the initiation of a back-arc basin. Mantle-derived magmas overprinted by metasomatism above the subducting slab intruded the attenuated lithospheric crust in dyke swarms serving as feeders for mafic and felsic volcanism. Subsequent magmatic under-plating at the mantle-crust boundary triggered regional medium to high-grade M1 metamorphism and D1 deformation, trans-forming the highly ductile rocks into isoclinally folded gneisses and anataxis in the lower part of the structural pile (Rooikop/Lofdal SD). M1 conditions in the upper outer part of the HMC are estimated at 675-700°C and 10.5-12 kb, whereas in the lower, central part subsequent M2 metamorphic mineral reactions obscured the older event. Preliminary thermobarometric modelling suggests a relatively slow exhum-ation, involving simultaneous decompression and cooling from M1 to M2 conditions, of the outer part of the HMC to higher crustal levels.

In the following period (1.88-1.82 Ga) the back-arc basin evolved into a (failed?) rift, into which the Khoabendus rocks were deposited. Voluminous felsic volcanism in the lower part of the group is associated with the emplacement of the FFG suite. Geochemistry and Nd-isotopes demonstrate the volcanic arc-related origin of the magmas, which during their ascent were increasingly modified by AFC processes (assimilation + fractional crystallis-ation). Sediments and volcanics of the Khoabendus Group were deposited under mostly subaqueous conditions. Strong lateral variations over short distances in sediment type and thickness argue for the development of small basins in the basal part with regressions and transgressions. A major transgression phase is recorded in the upper part of the Otjovasandu Fm by a 300 m thick distal turbidite sequence of phyllite alternating with thin layers of psammite. The return to very shallow deposition in the restricted milieu of a lagoon is demonstrated by overlying dolomite rocks of the Dinteri M. Pyroclastic rocks throughout the Khoabendus Group document show the

presence of active volcanoes over the entire period.

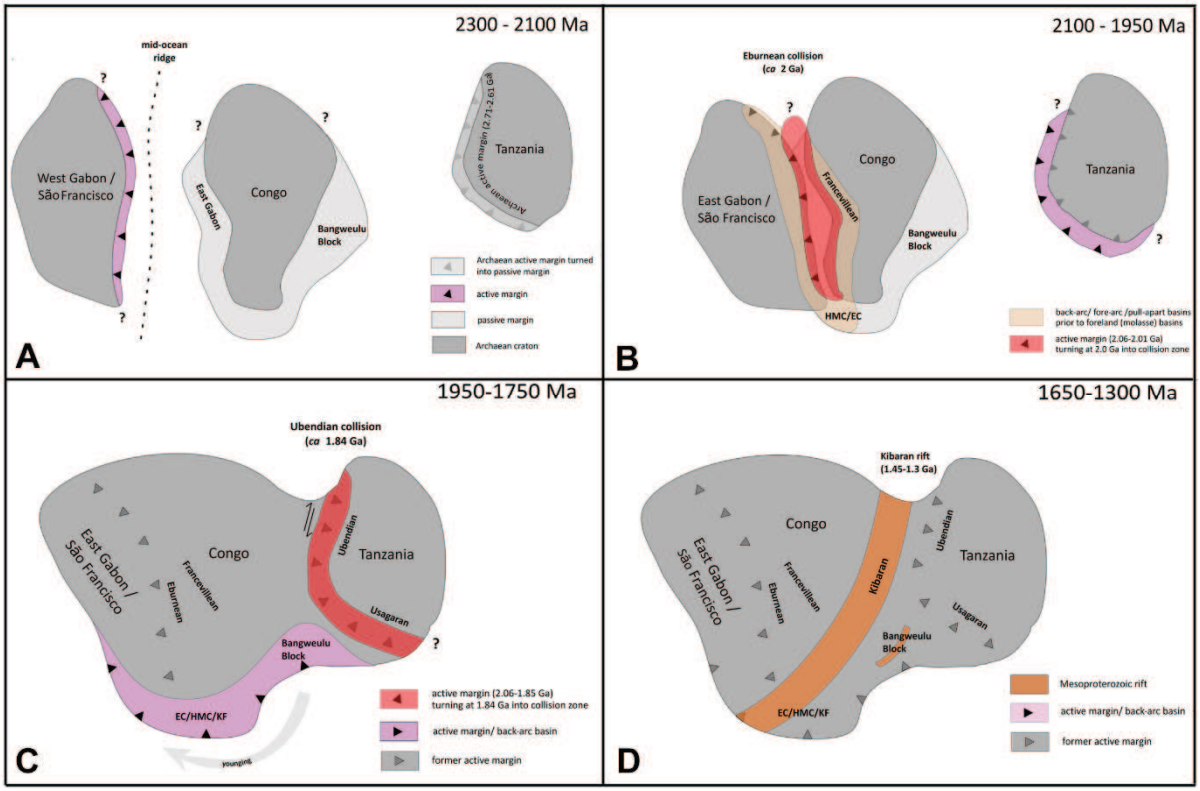


**Figure 99**. Plate tectonic evolution of central Africa from Palaeoproterozoic to Mesoproterozoic times.

The final stage in the evolution of the KI at ca 1800 Ma is characterised by the development of a mantled gneissic dome or metamorphic core complex. Extensional thrusting during exhumation juxtaposed low-grade, variably deformed Khoabendus and FFG rocks with the HMC comprising gneissic equivalents of the FFG. The present day geometry of the KI was achieved mainly during this event. M2 metamorphic conditions are estimated at 525-550°C, 5.5-7.0 kb. Alternatively, M2 extension and metamorphism are associated with Kibaran rifting in the interval 1.45-1.3 Ga.

The youngest arc-related orthogneisses aged 1.75 Ga have been identified in the EC NW of the KI. It coincides with 1.74-1.70 Ga juvenile arc magmatism in the Rehoboth Inlier in central Namibia (Becker *et al.* 2004). Cessation and start of active arcs on opposite sides of a hypothetical basin may be related, however, the palaeogeography of the Congo/Tanzania and Kalahari cratons at this time is currently poorly constrained and this may be just a coincidence.

In conclusion, the present study argues for the evolution of the Kamanjab Inlier under mostly extensional conditions in a continental arc setting that was active between 1.92-1.8 Ga. Sedimentation, magmatism and both tectono-thermal events can be associated with a back-arc setting, which also allowed preservation of supracrustal Khoabendus rocks in the troughs of a failed rift. This deformation style may be much more frequent in Precambrian rocks, but can only rarely be demonstrated because the supracrustal series are commonly eroded obscuring the relationship between the upper plate and the underlying gneissic domes.

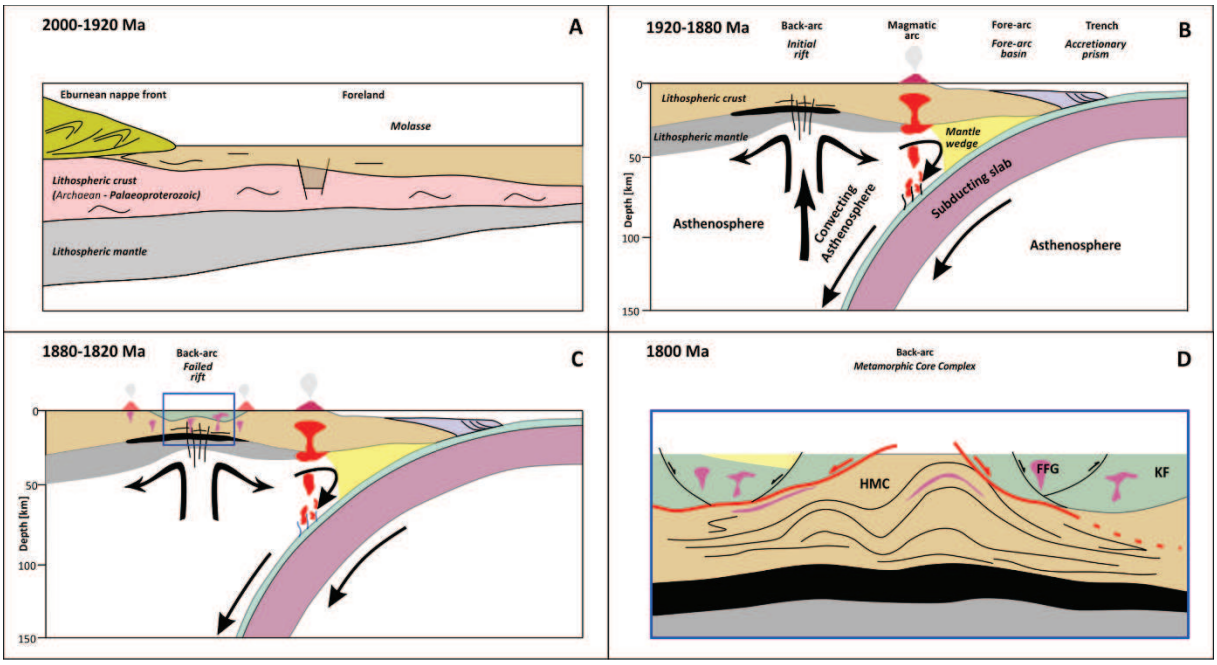


**Figure 100**. Geological history of the Kamanjab Inlier.

## Open Questions

Insufficient geochronological data poorly constrain the sedimentary and metamorphic history of the HMC and Khoabendus Fm, and this has implications for understanding the geodynamic settings through time and the application of structural models. The following subjects are of major interest:

**Khoabendus Group:**

- Detrital zircon studies of clastic rocks to identify ages and changes of source areas and constrain maximum deposition ages.
- Detailed mapping by applying principles of modern sequence stratigraphy.
- U-Pb zircon geochronology of felsic volcanic rocks constraining magmatic pulses and establish the age range of Khoabendus deposition.

**Huab Metamorphic Complex**

- Detrital zircon geochronology of paragneisses and quartzite to identify ages and changes of source areas and constrain maximum depositional ages.
- Sm-Nd studies of paragneissic rocks to characterise the mean crustal age of provenance areas.
- U-Pb geochronology and geochemistry of banded amphibolite-leucogneiss sequences of the Rooikop/Aandgloed SD, which could represent metavolcanic rocks.
- U-Pb zircon geochronology of migmatitic leucosome(s) and pegmatite to determine the age of M1 anataxis.
- U-Pb monazite (titanite, rutile) geochronology to determine the age of M2 metamorphism and the possible relationship with Kibaran rifting.
- Detailed U-Pb zircon study of late- to post-tectonic granite/gabbro/granodiorite emplaced in a fault. The data from sample NA101-2 are inconclusive and allow for late Palaeoproterozoic or much younger (Mesoproterozoic?) ages. The fault represents an important time marker post-dating D2 deformation.
- U-Pb zircon geochronology of migmatitic orthogneiss of the Rooikop SD. Both, palaeosome and leucocratic neosome should be analysed to constrain the age of emplacement and metamorphism.
- Further petrographic and P/T studies involving thermobarometric modeling combined with geochronology to

improve reconstruction of M1 and M2 P/T conditions and P/T/t paths,
- Correlation of HMC gneisses with those of the Epupa Complex (where similar studies should be carried out).
- Establish mineral potential in KI.
- Refinement of structural model by detailed structural analysis to test alternative models for gneissic domes.

## Acknowledgements

The manuscript was reviewed by Masafumi Sudo and Klaus Wemmer (Ar-Ar and K-Ar isotope part), by Reiner Klemd (metamorphic part), and by Patrick Ledru (structural part). Many thanks to Ute Schreiber and Martin Pickford for their meticulous editorial work and map production. We thank all the farmers in the Kamanjab area who permitted us to survey the rocks on their land. Finally, we acknowledge the administrative and logistic support of the Geological Survey of Namibia (Ministry of Mines and Energy).

## References

Ahrend H., Behr H.J., Clauer N., Hunziker J.C., Porada H. & Weber K. 1983b.The Northern Branch: depositional development and timing of the structural and metamorphic evolution within the framework of the Damara Orogen, 723-743. *In*: Martin H. & Eder F.W. (Eds), *Intracontinental Fold Belts*. Springer, Berlin, 945 pp.

Ahrend H., Behr H.J., Clauer N., Porada H. & Weber K. 1983a. K/Ar age determinations of the northern Damara branch and their implications for the structural and metamorphic evolution of the Damara Orogen, South West Africa/Namibia, 299-306. *In*: Miller R.McG. (Ed.) Evolution of the Damara Orogen of South West Africa/ Namibia. *Special Publication Geological Society South Africa*, **11**, 515 pp.

Aldiss, D.T. & Carney, J.N. 1992. The geology and regional correlation of the Proterozoic Okwa Inlier, western Botswana. *Precambrian Research*, **56**, 255–274.

Anderson, J.L. & Smith, D.R. 1995. The effects of temperature and $fO_2$ on the Al-in-Hornblende barometer. *American Mineralogist*, **80**, 549-559.

Anonymous, 2005. Namibia. *Mining Journal Special Publication* **2**, 1-16. London, November 2005.

Baldim, M.R. & Oliveira, E.P. 2016. Anatomy of the Alto Alegre gneiss dome, São Francisco Craton, Brazil: A geological record of transpression along a Paleoproterozoic arc-continent collision zone. *Precambrian Research*, **286**, 250-268.

Barbarin, B. 1999. A review of the relationships between granitoid types, their origins and their geodynamic environments. *Lithos*, **46**, 605-626.

Batchelor, R.A. & Bowden, P. 1985. Petrogenetic interpretation of granitoid rock series using multicationic parameters. *Chemical Geology*, **48**, 43-55.

Baxe, O. 2007. *Geocronologia de complexos máfico-ultramáficos: exemplo da série superior do complexo de Niquelándia, Brasil, e do complexo Kunene, Angola*. Unpublished PhD Thesis, Universidade de Brasília, Instituto de Geociências, Brazil. 77 pp.

Becker, T. 2004a. *Geological map of Namibia; 1:50,000 Geological Series; Sheet 2014BA Welcom*. Ministry of Mines and Energy, Geological Survey of Namibia.

Becker, T. 2004b. *Geological map of Namibia; 1:50,000 Geological Series; Sheet 2014AD Bethanis*. Ministry of Mines and Energy, Geological Survey of Namibia.

Becker, T. 2004c. *Geological map of Namibia; 1:50,000 Geological Series; Sheet 2014AB Suiderkruis*. Ministry of Mines and Energy, Geological Survey of Namibia.

Becker, T. 2005a. *Geological map of Namibia; 1:50,000 Geological Series; Sheet 2014BD Khorixas.* Ministry of Mines and Energy, Geological Survey of Namibia.

Becker, T. 2005b. *Geological map of Namibia; 1:50,000 Geological Series; Sheet 2014BC Petrified Forest*. Ministry of Mines and Energy, Geological Survey of Namibia.

Becker, T. 2005c. *Geological map of Namibia; 1:50,000 Geological Series; Sheet 2014BB Rockeys*. Ministry of Mines and Energy, Geological Survey of Namibia.

Becker, T. 2006a. *Geological map of Namibia; 1:50,000 Geological Series; Sheet 1914DA Bruno*. Ministry of Mines and Energy, Geological Survey of Namibia.

Becker, T. 2006b. *Geological map of Namibia; 1:50,000 Geological Series; Sheet 1914DB Kamanjab*. Ministry of Mines and Energy, Geological Survey of Namibia.

Becker, T. 2006c. *Geological map of Namibia; 1:50,000 Geological Series; Sheet 1914CB Atlanta*. Ministry of Mines and Energy, Geological Survey of Namibia.

Becker, T., Hansen, B.T, Weber K. & Wiegand, B. 2004. Isotope systematics (Sm/Nd, Rb/Sr, U/Pb) of the Elim Fm, the Alberta Complex, and the Weener Igneous Complex – probable genetic links between magmatic rocks of the Paleoproterozoic Rehoboth Basement Inlier/ Namibia. *Communications of the Geological Survey Namibia*, **13**, 75-84.

Black, L.P. & Kamo, S.L. 2003. TEMORA 1: a new zircon standard for U–Pb geochronology. *Chemical Geology*, **200**, 155-170.

Black, L.P., Kamo, S.L., Allen, C.M., Davis, D.W., Aleinikoff, J.N. & Valley, J.W. 2004. Improved $^{206}Pb/^{238}U$ microprobe geochronology by the monitoring of a trace-element-related matrix effect; SHRIMP, ID–TIMS, ELA–ICP–MS and oxygen isotope documentation for a series of zircon standards. *Chemical Geology*, **205** (**1-2**), 115-140.

Boniface, N., Schenk, V. & Appel, P. 2012. Paleoproterozoic eclogites of MORB-type chemistry and three Proterozoic orogenic cycles in the Ubendian belt (Tanzania): evidence from monazite and zircon geochronology, and geochemistry. *Precambrian Research*, **192-195**, 16-33.

Brandt, S. & Klemd, R. 2008. Upper-amphibolite facies partial melting of paragneisses from the Epupa Complex, NW Namibia, and relations to Mesoproterozoic anorthosite magmatism. *Journal of Metamorphic Geology*, **26** (**9**), 871-893.

Brandt, S., Klemd, R. & Okrusch, M. 2003. Ultrahigh-temperature metamorphism and multistage evolution of garnet–orthopyroxene granulites from the Proterozoic Epupa Complex, NW Namibia. *Journal of Petrology*, **44** (**6**), 1121-1144.

Brandt, S., Klemd, K., Xie, H. & Bobek, P. 2021. Unravelling the P-T-t history of three high-grade metamorphic events in the Epupa complex, NW Namibia: implications for the Paleoproterozoic to Mesoproterozoic evolution of the Congo Craton. *American Journal of Science*, **321**, 235-296.

Brandt, S., Will, T.M. & Klemd, R. 2007. Magmatic loading in the Proterozoic Epupa Complex, NW Namibia, as evidenced by ultrahigh-temperature sapphirine-bearing ortho-pyroxene-sillimanite-quartz granulites. *Precambrian Research*, **153** (**3-4**), 143-178.

Brower, A.M. 2017. *Understanding Magmatic Timescales and Magma Dynamics in Proterozoic Anorthosites: a Geochronological and Remote Sensing Investigation of the Kunene Complex (Angola)*. Unpublished PhD Thesis, University of Witwatersrand, Johannesubrg, South Africa, 86 pp.

Burger, A.J., Clifford, T.N. & Miller, R. McG. 1976. Zircon U-Pb ages of the Franzfontein granitic suite, northern South West Africa. *Precambrian Research*, **3** (**5**), 415–431.

Burger, A.J. & Coertze, F.J. 1973. *Radiometric Age Measurements on Rocks from Southern Africa to the End of 1971*. Pretoria: Govt. Printer.

Burger, A.J. & Coertze, F.J. 1975. Age determinations - April 1972 to March 1974. *Annals of the Geological Survey South Africa*, **10**, 135-141.

Bybee, G.M., Hayes, B., Owen-Smith, T.M., Lehmann, J., Ashwal, L.D., Brower, A.M., Hill, C.M., Corfu, F. & Manga, M. 2019. Proterozoic massif-type anorthosites as the archetypes of long-lived (2100 Myr) magmatic systems - New evidence from the Kunene Anorthosite Complex (Angola). *Precambrian Research*, **332,** 105393.

Chaves A.O. 2021. Columbia (Nuna) supercontinent with external subduction girdle and concentric accretionary, collisional and intracontinental orogens permeated by large igneous provinces and rifts. *Precambrian Research*, **352**, 106017.

Chaves, A.O. & Rezende, C.R. 2019. Fragments of 1.79-1.75 Ga Large Igneous Provinces in reconstructing Columbia (Nuna): a Statherian supercontinent-superplume coupling? *Episodes*, **42**, 55-67.

Clifford, T.N., Nicolaysen, L.O. & Burger, A.J. 1962. Petrology and Age of the Pre-Otavi Basement Granite at Franzfontein, Northern South-West Africa. *Journal of Petrology*, **3** (**2**), 244-279.

Clifford, T.N., Rooke, J.M. & Allsopp, H.L. 1969. Petrochemistry and age of the Franzfontein granitic rocks of northern

South-West Africa. *Geochimica Cosmochimica Acta*, **33** (**8**), 973-986.

Coble, M.A., Vazquez, J.A., Barth, A.P., Wooden, J., Burns, D. & Kylander-Clark, A. 2018. Trace element characterization of MAD-559 Zircon reference material for ion microprobe analysis. *Geostandards and Geoanalytical Research*, **42**, 481-497.

Condie, K.C. 2000. Episodic continental growth models: afterthoughts and extensions. *Tectonophysics*, **322** (**1-2**), 153-162.

Condie, K.C., Belousova, E., Griffin, W.L. & Sircombe, K.N. 2009. Granitoid events in space and time: Constraints from igneous and detrital zircon age spectra. *Gondwana Research*, **15** (**3-4**), 228-242.

Crittenden, M.D., Coney, P.J. & Davis, G.H. (Eds) 1980. Tectonic significance of metamorphic core complexes of the North American Cordillera. *Memoir of the Geological Society of America*, **153**, 490 pp.

Dale, J., Holland, T. & Powell, R. 2000. Hornblende-garnet-plagioclase thermobarometry: a natural assemblage calibration of the thermodynamics of hornblende. *Contributions to Mineralogy and Petrology*, **140** (**3**), 353-362.

Dasgupta, S., Sengupta, P., Guha, D. & Fukuoka, M. 1991. A refined garnet - biotite Fe-Mg exchange geothermometer and its application in amphibolites and granulites. *Contributions to Mineralogy and Petrology*, **109** (**1**), 130-137.

Davis, G.H. & Coney, P.J. 1979. Geologic development of the Cordilleran metamorphic core complexes. *Geology*, **7**, 120-124.

De Capitani, C. & Brown, T.H. 1987. The computation of chemical equilibrium in complex systems containing non-ideal solutions: *Geochimica Cosmochimica Acta*, **51**, 2639-2652.

Depiné, M. 2008. *Petrologisch-geochemische Untersuchung der metamorphen Gesteine des Huab Komplex, NW Namibia*. Diplomarbeit, Julius-Maximilians Universität Würzburg (unpublished).

De Waele, B. & Fitzsimons, I.C.W. 2007. The nature and timing of Paleoproterozoic sedimentation at the southeastern margin of the Congo Craton. *Precambrian Research*, **159**, 95-116.

De Waele, B., Fitzsimons, I.C.W., Wingate, M.T.D. & Mapani, B. 2003a.The tectonothermal history of the Irumide belt of Zambia. Regional significance of new geochronological constraints. *In*: Li, H. & Zhang, S. (Eds), *Assembly and Breakup of Rodinia, South China Field Symposium, Chengdu Institute of Geology and Mineral Resources*, China Geological Survey, Hangzhou, China, pp. 16-19.

De Waele, B., Kampunzu, A.B., Mapani, B.S.E. & Tembo, F. 2006a. The Mesoproterozoic Irumide belt of Zambia. *Journal of African Earth Sciences*, **46**, 36-70.

De Waele, B., Liègeois, J. P., Nemchin, A.A. & Tembo, F. 2006b. Isotopic and geochemical evidence of Proterozoic episodic crustal reworking within the Irumide Belt of south-central Africa, the southern metacratonic boundary of an Archaean Bangweulu Craton. *Precambrian Research*, **148**, 225-256.

De Waele, B. & Mapani, B. 2002. Geology and correlation of the central Irumide belt. *Journal of African Earth Sciences*, **35** (**3**), 385-397.

De Waele, B., Wingate, M.T.D., Mapani, B. & Fitzsimons, I.C.W. 2003b Untying the Kibaran knot: a reassessment of Mesoproterozoic correlations in southern Africa based on SHRIMP U–Pb data from the Irumide belt. *Geology*, **31** (**6**), 509-512.

De Wit, M.C.J. 2013. The Xaudum kimberlite province straddling the southern margin of the Angolan craton. *In*: *24th Colloquium of African Geology, January 8-14, Addis Ababa*, Ethiopia.

Drüppel, K., Littmann, S., Romer, R.L. & Okrusch, M. 2007. Petrology and isotope geochemistry of the Mesoproterozoic anorthosite and related rocks of the Kunene. Intrusive Complex, NW Namibia. *Precambrian Research*, **156** (**1-2**), 1-31.

Drüppel, K., von Seckendorff, V. & Okrusch, M. 2001. Subsolidus reaction textures in anorthosites of the Kunene Intrusive Complex, NW Namibia. *European Journal of Mineralogy*, **13**, 289-309.

Ernst, R., Pereira, E., Hamilton, M.A., Pisarevsky, S., Rodriques, J., Tassinari, C.C.G., Teixeira, W. & Van Dunem, V. 2013. Mesoproterozoic intraplate magmatic "barcode" record of the Angola portion of the Congo Craton: newly dated magmatic events at 1505 and 1110 Ma and implications for Nuna (Columbia) supercontinent reconstructions. *Precambrian Research*, **230**, 103-118.

Ernst, R.E. & Youbi, N. 2017. How Large Igneous Provinces affect global climate,

sometimes cause mass extinctions and represent natural markers in the geological record. *Palaeogeography, Palaeoclimatology, Palaeoecology*, **478**, 30-52.

Eskola, P.E. 1949. The problem of mantled gneiss domes. *Quarterly Journal of the Geological Society of London*, **104**, 461-476.

Evans, D.A.D. & Mitchel, R.N. 2011. Assembly and breakup of the core of Paleo-Mesoproterozoic supercontinent Nuna. *Geology*, **39** (**5**), 443-446.

Ferry, J.M. & Spear, F.S. 1978. Experimental calibration of the partitioning of Fe and Mg between biotite and garnet. *Contributions to Mineralogy and Petrology*, **66** (**2**), 113-117.

Feybesse, J.-L., Johan, V., Triboulet, C., Guerrot, C., Mayaga-Mikolo, F., Bouchot, V. & Eko N'dong, J. 1998. The West Central African belt: a model of 2.5–2.0 Ga accretion and two-phase orogenic evolution. *Precambrian Research*, **87**, 161-216.

Fleck, R.J., Sutter, J.F. & Elliot, D.H. 1977. Interpretation of discordant $^{40}Ar/^{39}Ar$ age-spectra of Mesozoic tholeiites from Antarctica. *Geochimica et Cosmochimica Acta*, **41**, 15-32.

Foster, M.D. 1960. Interpretation of the composition of trioctahedral micas. *US Geological Survey Professional Paper*, **354 (B5)**, 11-48.

Fountain, D.M. 1989. Growth and modification of lower continental crust in extended terrains: The role of extension and magmatic underplating. *In*: Mereu, R.F., Mueller, S. & Fountain, D.M. (Eds). Properties and processes of earth's lower crust. *American Geophysical Union Monograph*. **51**, 287-299.

Frets, D.C. 1969. Geology and structure of the Huab-Welwitschia area, South West Africa. *University of Cape Town Bulletin*, **5**, 235 pp.

Frost, B.R., Barnes, C.G., Collins, W.J., Arculus, R.J., Ellis, D.J. & Frost, C.D. 2001. A geochemical classification for granitic rocks. *Journal of Petrology*, **42** (**11**), 2033-2048.

Fuhrmann, U., Lippolt, H.J. & Hess J.C. 1987. Examination of some proposed K–Ar standards: 40Ar/39Ar analyses and conventional K-Ar data. *Chemical Geology (Isotope Geoscience Section)*, **66**, 41-51.

Gessner, K., Wijns, C. & Moresi, L. 2007. Significance of strain localization in the lower crust for structural evolution and thermal history of metamorphic core complexes. *Tectonics*, **26**, TC2012, 13 pp.

Glynn, S.M., Master, S., Wiedenbeck, M., Davis, S.W., Kramers, J.D., Belyanin, G.A., Frei, D. & Obertür, T. 2017. The Proterozoic Choma-Kalomo block, SE Zambia: exotic terrane or a reworked segment of the Zimbabwe craton? *Precambrian Research*, **298**, 421-438.

Goldstein, S.L., O'Nions, R.K. & Hamilton, P.J. 1984. A Sm-Nd isotopic study of atmospheric dusts and particulates from major river systems. *Earth and Planetary Science Letters*, **70**, 221-236.

Graham, C.M. & Powell, R. 1984. A garnet-hornblende geothermometer: calibration, testing, and application to the Pelona Schist, Southern California. *Journal of Metamorphic Geology*, **2** (**1**), 13-31.

Guj, P. 1970. The relationships between the "Fransfontein Granite" and the Huab and Khoabendus Formations northwest of Fransfontein, South West Africa. *Annals of the Geological Survey of South Africa*, **8**, 49-51.

Halama, R., Konrad-Schmolke, M., Sudo, M., Marschall, H. & Wiedenbeck, M. 2014. Effects of fluid-rock interaction on $^{40}Ar/^{39}Ar$ geochronology in high-pressure rocks (Sesia-Lanzo Zone, Western Alps). *Geochimica et Cosmochimica Acta*, **126**, 475-494.

Hammerstrom, J.M. & Zen, E. 1986. Aluminium in hornblende: an empirical igneous barometer. *American Mineralogist*, **71**, 1297-1313.

Hanson, R. 2003. Proterozoic geochronology and tectonic evolution of southern Africa. *In*: Yoshida, M., Windley, B.F. & Dasgupta, S. (Eds) Proterozoic East Gondwana: Supercontinent Assembly and Breakup. *Geological Society, London, Special Publications*, **206**, 427-463.

Hards, V.L. 1995. *The Evolution of the Snaefell Volcanic Centre, Eastern Iceland*. Durham University. Retrieved from http://etheses.dur.ac.uk/1452/.

Hawkesworth, C.J., Gledhill, A.R., Roddick, J.C., Miller, R.McG. & Kröner, A. 1983. Rb/Sr and 40Ar/39Ar studies bearing on models for the thermal evolution of the Damara belt. *In*: Miller, R.McG. (Ed.) Evolution of the Damara Orogen, South West Africa/Namibia, *Geological Society of South Africa, Special Publication*, **11**, 323-338.

Hawkesworth, C., Gallagher, K., Herget, J.M. & McDermott, F. 1993. Mantle and Slab Contribution in Arc Magmas. *Annual Review of Earth and Planetary Sciences*, **21** (**1**), 175-204.

Henk. A., Leander, F., Teufel, S. & Oncken, O. 1997. Magmatic underplating, extension, and crustal reequilibration: Insights from a cross-section through the Ivrea Zone and Strona-Ceneri Zone, Northern Italy. *Journal of Geology*, **105**, 367-377.

Hoal, K.O, Hoal, B.G, Griffin, W.L. & Armstrong, R.A. 2000. Characterisation of the age and nature of the lithosphere in the Tsumkwe region, Namibia. *Communications of the Geological Survey of Namibia*, **12**, 21-28.

Hodges, K.V. & Crowley, P.D. 1985. Error estimation and empirical geothermobarometry for pelitic systems. *American Mineralogist,* **70** (**7-8**), 702-709.

Hodges, K.V. & Spear, F.S. 1982. Geothermometry, geobarometry and the Al2 SiO5 triple point at Mt. Moosilauke, New Hampshire. *American Mineralogist*, **67** (**11-12**), 1118-1134.

Hoinkes, G. 1986. Effect of grossular-content in garnet on the partitioning of Fe and Mg between garnet and biotite. *Contributions to Mineralogy and Petrology*, **92** (**3**), 393-399.

Hoisch, D. 1990. Empirical calibration of six geobarometers for the mineral assemblage quartz + muscovite + biotite + garnet + plagioclase. *Contributions to Mineralogy and Petrology*, **104**, 225-234.

Holdaway, M.J. 2000. Application of new experimental and garnet Margules data to the garnet-biotite geothermometer. *American Mineralogist*, **85** (**7-8**), 881-892.

Holdaway, M.J, Mukhopadhyay, B., Dyar, M.D, Guidotti, C.V. & Dutrow, B.L. 1997. Garnet-biotite geothermometry revised: New Margules parameters and a natural specimen data set from Maine. *American Mineralogist*, **82**, 582-595.

Holland, T. & Blundy, J. 1994. Non-ideal interactions in calcic amphiboles and their bearing on amphibole-plagioclase thermometry. *Contributions to Mineralogy and Petrology*, **116** (**4**), 433-447.

Hollister, L.S, Grissmo, G.C, Peters, E.K, Stowell, H.H. & Sisson, V.B. 1987. Confirmation of the empirical correlation of Al in hornblende with pressure of solidification of calcalkaline plutons. *American Mineralogist*, **72**, 231-239.

Hugo, P.J. & Schalk, K.E.L. 1974. The isotopic ages of certain granites and acid lavas in the Rehoboth and Maltahöhe Districts, South West Africa. *Annals of the Geological Survey of South Africa*, **9**, 103-105.

Huppert, H.E. & Sparks, S.J. 1988. The generation of granitic magmas by intrusion of basalt into continental crust. *Journal of Petrology*, **29**, 599-624.

Hynes, A. & Forest, R.C. 1988. Empirical garnet-muscovite geothermometry in low-grade metapelites, Selwyn Range (Canadian Rockies). *Journal of Metamorphic Geolo*gy, **6**, (**3**), 297-309.

Irvine, T.N. & Baragar, W.R.A. 1971. A guide to the chemical classification of the common volcanic rocks. *Canadian Journal of Earth Sciences*, **8**, 523-548.

Ishizuka, O. 1998. Vertical and horizontal variation of the fast neutron flux in a single irradiation capsule and their significance in the laser-heating $^{40}Ar/^{39}Ar$ analysis: Case study for the hydraulic rabbit facility of the JMTR reactor, Japan. *Geochemical Journal*, **32**, 243-252.

Jackson, S.E., Pearson, N.J., Griffin, W.L. & Belousova, E.A. 2004. The application of laser ablation-inductively coupled plasma-mass spectrometry to in situ U–Pb zircon geochronology. *Chemical Geology*, **211**, 47-69.

Janoušek, V., Farrow, C.M., & Erban, V. 2006. Interpretation of whole-rock geochemical data in igneous geochemistry: introducing Geochemical Data Toolkit (GCDkit). *Journal of Petrology*, **47** (**6**), 1255-1259.

Jelsma, H.A., McCourt, S., Perritt, S.H. & Armstrong, R.A. 2018. The geology and evolution of the Angolan Shield, Congo craton. *In*: Siegesmund, S., Basei, M.A.S., Oyhantçabal, P. & Oriolo, S. (Eds), *Geology of Southwest Gondwana, Regional Geology Reviews*. Springer International Publishing, pp. 217-239.

Jelsma, H.A., Perrit, S.H., Armstrong, R.A. & Ferreira, H.H. 2011. SHRIMP U-Pb zircon geochronology of basement rocks of the Angolan Shield, western Angola. *In*: *Proceedings of the 23rd Colloquium of African Geology, Johannesburg, South Africa*. Council for Geoscience, Pretoria, 203 pp.

John, T., Schenk, V., Haase, K., Scherer, E. & Tembo, F. 2003. Evidence for a Neoproterozoic ocean in south-central Africa from mid-oceanic-ridge-type geochemical signatures and pressure-temperature estimates of Zambian eclogites. *Geology*, **31** (**3**), 243-246.

Johnson, M.C. & Rutherford, M.J. 1989. Experimental calibration of the aluminum-in-hornblende geobarometer with application to Long Valley caldera (California) volcanic rocks. *Geology*, **17** (**9**), 837-841.

Key, R.M. & Armstrong, R.A. 2000. Geology and geochronology of pre-Katangan igneous and meta-igneous rocks north of the Lufilian Arc in northwest Zambia. *Journal of African Earth Sciences*, **31**, 36-37.

Key, R.M., Liyungu, A.K., Njamu, F.M., Somwe, V., Banda, J., Mosley, P.N. & Armstrong, R.A. 2001. The western arm of the Lufilian Arc in NW Zambia and its potential for copper mineralization. *Journal of African Earth Sciences*, **33**, 503-528.

Kleemann, U. & Reinhardt, J. 1994. Garnet-biotite thermometry revisited; the effect of $Al^{VI}$ and Ti in biotite. *European Journal of Mineralogy*, **6** (**6**), 925-941.

Kleinhanns, I.C., Füllgraf, T., Wilsky, F., Nolte, N., Fliegel, D., Klemd, R. & Hansen, B.T. 2013. U-Pb zircon age and (isotope) geochemical signatures of the Kamanjab Inlier (NW Namibia): constraints on crustal evolution along the southern Congo Craton. Continent Formation through Time. *Special Publication Series of the Geological Society of London*, **389**, 165-195.

Klötzli, U.S., Sinigo, S., Quick, J.E., Demarchi, G., Tassinari, C.C.G., Sato, K. & Günes, Z. 2014. Duration of igneous activity in the Sesia Magmatic System and implications for high-temperature metamorphism in the Ivrea–Verbano deep crust. *Lithos*. **206-207**, 19-33.

Kohn, M. J. & Spear, F.S. 1989. Empirical calibration of geobarometers for the assemblage garnet + hornblende + plagioclase + quartz. *American Mineralogist*, **74**, 77-84.

Kohn, M.J. & Spear, F.S. 1990. Two new geobarometers for garnet amphibolites, with applications to southeastern Vermont. *American Mineralogist*, **75**, 89-96.

Košler, J., Fonneland, H., Sylvester, P., Tubrett, M. & Pedersen, R.-B. 2002. U–Pb dating of detrital zircons for sediment provenance studies - a comparison of laser ablation ICPMS and SIMS techniques. *Chemical Geology*, **182**, 605-618.

Krogh, E.J. & Raheim, A. 1978. Temperature and pressure dependence of Fe-Mg partitioning between garnet and phengite, with particular reference to eclogites. *Contributions to Mineralogy and Petrology*, **66** (**1**), 75-80.

Kröner, S., Konopasek, J., Kröner, A., Passchier, C.W., Poller, U., Wingate, M.T.D. & Hofmann, K.H. 2004. U-Pb and Pb-Pb zircon ages for metamorphic rocks in the Kaoko Belt of northwestern Namibia: a Paleo- to Mesoproterozoic basement reworked during Pan-African orogeny. *South African Journal of Geology*, **107**, 455-476.

Kröner, A. & Rojas-Agramonte, Y. 2017. Mesoproterozoic (Grenville-age) granitoids and supracrustal rocks in Kaokoland, northwestern Namibia. *Precambrian Research*, **298**, 572-592.

Kröner, A., Rojas-Agramonte, Y., Hegner, E., Hoffmann, K.-H. & Wingate, M.T.D. 2010. SHRIMP zircon dating and Nd isotopic systematics of Paleoproterozoic migmatitic orthogneisses in the Epupa Metamorphic Complex of northwestern Namibia: The Impact of SHRIMP on Understanding the Precambrian. *Precambrian Research*, **183** (**1**), 50-69.

Kröner, A., Rojas-Agramonte, Y., Wong, J. & Wilde, S.A. 2015. Zircon reconnaissance dating of Proterozoic gneisses along the Kunene River of northwestern Namibia. *Tectonophysics*, **662**, 125-139.

Lanphere, M.A. & Baadsgaard, H. 2001. Precise K-Ar, $^{40}Ar/^{39}Ar$, Rb-Sr and U/Pb mineral ages from the 27.5 Ma Fish Canyon Tuff reference standard. *Chemical Geology*, **175**, 653-671.

Leake, B.E, Woolley, A.R., Arps, C.E.S., Birch, W.D., Gilbert, M.C., Grice, J.D., Hawthorne, F.C., Kato, A., Kisch, H.J., Krivovichev, V.G., Linthout, K., Laird, J., Mandarino, J.A., Maresch, W.V., Nickel, E.H., Rock, N.M.S., Schumacher, J.C., Smith, D.C., Stephenson, N.C.N., Ungaretti, L., Whittaker, E.J.W. & Youzhi, G. 1997. Nomenclature of amphiboles: Report of the Subcommittee on Amphiboles of the International Mineralogical Association, Commission on New Minerals and Mineral Names. *Canadian Mineralogy*, **35**, 219-246.

Lehmann, J., Bybee, G.M., Hayes, B., Owen-Smith, T.M. & Belyanin, B. 2020.

Emplacement of the giant Kunene AMCG complex into a contractional ductile shear zone and implications for the Mesoproterozoic tectonic evolution of SW Angola. *International Journal of Earth Sciences*, **109**, 1463–1485.

Lenoir, J.L., Liegeas, J.P. & Klerkx, J. 1994. The Paleoproterozoic Ubendian shear Belt in Tanzania: geochronology and structure. *Journal of African Earth Sciences*, **19**, 169-184.

Li, Y, Zhu, G., Su, N., Xiao, S., Zhang, S., Liu, C., Xie, C., Yin, H. & Wu, X. 2019. The Xiaoqinling metamorphic core complex: A record of Early Cretaceous backarc extension along the southern part of the North China Craton. *Geological Society of America Bulletin*, **132**, 617-637.

Lister, G.S. & Davis, G.A. 1989. The origin of metamorphic core complexes and detachment faults formed during Tertiary continental extension in the northern Colorado River region, U.S.A. *Journal of Structural Geology*, **11** (**1/2**) 65-94.

Ludwig, K.R. 2000. SQUID 1.00: a user's manual. *Berkeley Geochronological Centre, Special Publications*, **2**, 1-19.

Ludwig, K.R. 2009. *In*: SQUID 2, A User's Manual (Vol. 100). *Berkeley Geochronology Center Special Publication*.

Ludwig, K.R. 2012. *In*: Isoplot 3.75 - A geochronological Toolkit for Excel (Vol. 75). *Berkeley Geochronology Center Special Publication*.

Luft, J.L., Chemale Jr., F. & Armstrong, R.A. 2011. Evidence of 1.7 to 1.8 Ga collisional Arc in the Kaoko belt, NW Namibia. *International Journal of Earth Sciences*, **100**, 305-321.

Maier, W.D., Rasmussen, B., Fletcher, I.R., Li, C., Barnes, S.-J. & Huhma, H. 2013. *Society of Economic Geologists*, **108**, 953-986.

Maniar, P.D. & Piccoli, P.M. 1989. Tectonic discrimination of granitoids. *Geological Society of America Bulletin*, **101**, 635-643.

Mapeo, R.B.M., Ramokate, L.V., Corfu, F., Davis, D.W. & Kampunzu, A.B. 2006. The Okwa basement complex, western Botswana: U-Pb zircon geochronology and implications for Eburnean processes in southern Africa. *Journal of African Earth Sciences*, **46**, 253-262.

Mapeo, R.B.M, Wendorff, M., Ramokate, L.V., Armstrong, R.A., Mphinyanea, T. & Koobokile, M. 2019. Zircon geochronology of basement granitoid gneisses and sedimentary rocks of the Tsodilo Hills Group in the Pan-African Damara Belt, western Botswana: age constraints, provenance, and tectonic significance. *Journal of African Earth Sciences* **159**, 103576.

Mareschal, J.C. & Bergantz, J. 1990. Constraints on thermal models of the Basin and Range province. *Tectonophysics*, **174**, 137-146.

Martin, H. 1965. *The Precambrian Geology of South West Africa and Namaqualand*. Precambrian Research Unit, University of Cape Town, 159 pp

Mayer, A., Hofmann, A., Sinigoi, S. & Morais, E. 2004. Mesoproterozoic Sm-Nd and U-Pb ages for the Kunene anorthosite complex of SW Angola. *Precambrian Research*, **133**, 187-206.

McCourt, S., Armstrong, R.A., Jelsma, H. & Mapeo, R.B.M. 2013. New U-Pb SHRIMP ages from Lubango region, SW Angola: insights into the Paleoproterozoic evolution of the Angolan Shield, southern Congo craton, Africa. *Journal of the Geological Society of London*, **170**, 353-363.

Mhopjeni, K. 2006. *Mineralisation in the Northern Part of the Khoabendus Group, NW Namibia*. B.Sc. Thesis, Geology Department, Rhodes University, Grahamstown, South Africa, (unpubl.), 40 pp.

Miller, R.McG. 2008. *The Geology of Namibia*. Volume 1: *Archaean to Mesoproterozoic*. Windhoek Namibia: Ministry of Mines and Energy, Geological Survey, 690 pp.

Geological Survey of Namibia. 1992. *Mineral Resources of Namibia*. Special Publications of the Geological Survey of Namibia, Windhoek, 598 pp.

Muvangua, E. 2006. *Petrology and Geochemistry of the Khoabendus Group and the Fransfontein Suite in the Kamanjab Area, Northwestern Namibia*. B.Sc. Thesis, Department of Geology, University of Stellenbosch, South Africa, (unpubl.), 52 pp.

Nägler, Th.F. & Kramers, J.D. 1998. Nd isotopic evolution of the upper mantle during the Precambrian: models, data and the uncertainty of both. *Precambrian Research*, **91** (**3-4**), 233-252.

Nicholls, J. 1996. *Tsumkwe/Gam Diamond Project Final Report*. Rio Tinto Namibia (Pty) Ltd.

Nolte, N. 2012. *Paläoproterozoisches Krustenwachstum (2.0 - 1.8 Ga) am Beispiel der*

*Västervik-Region in SE-Schweden und dem Kamanjab Inlier in NW-Namibia*. Ph.D. Thesis, University Göttingen, Germany, 218 pp, 7 appendices.

Pearce, J.A. 1982. Trace element characteristics of lavas from destructive plate boundaries. *In*: Thorpe, R.S. (Ed.) *Orogenic Andesites and Related Rocks*, pp. 528-548. Chichester, England: John Wiley and Sons.

Pearce, J.A. 1996. Source and settings of granitic rocks. *Episodes*, **19**, 120-125.

Pearce, J.A. & Peate, D.W. 1995. Tectonic Implications of the Composition of Volcanic Arc Magmas. *Annual Review of Earth and Planetary Sciences*, **23** (**1**), 251-285.

Pearce, J., Stern, R.J., Bloomer, S.H. & Fryer, P. 2004. Geochemical mapping of the Mariana arc-basin system: Implications for the nature and distribution of subduction components. *Geochemistry, Geophysics, Geosystems* (*G3*), **6**, 1-27.

Perchuk, L., Aranovich, L. Y., Podlesskii, K.K., Lavrent'eva, I.V., Gerasimov, V., Fed'kin, V., Kitsul, V.I., Karsakov, L.P. & Berdnikov, N.V. 1985. Precambrian granulites of the Aldan shield, eastern Siberia, USSR. *Journal of Metamorphic Geology*, **3** (**3**), 265-310.

Perchuk, L. & Lavrent'eva, I.V. 1983. Experimental investigation of exchange equilibria in the system cordierite-garnet-biotite. *In*: Saxena, S.K. (Ed.) *Kinetics and Equilibrium in Mineral Reactions*, pp. 199-239. Advances in Physical Geochemistry, Volume. 3. New York: Springer.

Pereira, E., Tassinari, C.C.G., Rodrigues, J.F. & Van-Dunen, M.V. 2011. New data on the deposition of the volcano sedimentary Chela Group and its Eburnean basement: implications to post Eburnean crustal evolution of the SW of Angola. *Comunicacões Geologicas*, **98**, 29-40.

Porada, H. 1974. The Khoabendus Formation in the Area Northwest of Kamanjab and in the Southeastern Kaokoveld, South West Africa. *Memoirs of the Geological Survey of South Africa, South West Africa Series*, **4**, 23 pp.

Powell, R. 1985. Regression diagnostics and robust regression in geothermometer/ geobarometer calibration: the garnet-clinopyroxene geothermometer revisited. *Journal of Metamorphic Geology*, **3** (**3**), 231-243.

Powell, R. & Holland, T.J.B. 1988. An internally consistent dataset with uncertainties and correlations; 3, Applications to geobarometry, worked examples and a computer program. *Journal of Metamorphic Geology*, **6** (**2**), 173-204.

Rainaud, C., Master, S., Armstrong, R.A. & Robb, L.J. 2005. Geochronology and nature of the Paleoproterozoic basement in the Central African Copperbelt (Zambia and the Democratic Republic of Congo), with regional implications: Recent Advances in the Geology and Mineralization of the Central African Copperbelt Dedicated to the memory and work of Henri Ali Basira Kampunzu Joint IAGOD Symposium - GSSA Geocongress. *Journal of African Earth Sciences*, **42** (**1-5**), 1-31.

Ravna, E. & Krogh, E.J. 2000. Distribution of Fe2+ and Mg between coexisting garnet and hornblende in synthetic and natural systems: an empirical calibration of the garnet-hornblende Fe-Mg geothermometer. *Lithos*, **53** (**3-4**), 265-277.

Rey-Moral, C., Machales, T., Merino Martinez, E., Lobón J.L.G., López Bahut M.T., Martin-Banda, R. Feria, M.C., Ballesteros, D., Machadinho, A. & Alves, D. 2022. Recording the largest gabbro-anorthositic complex worldwide: The Kunene Camplex (KC), SW Angola. *Precambrian Research*, **379**, 106790.

Ring. U. 2014. Metamorphic Core Complexes. *Encyclopedia of Marine Geosciences* DOI 10.1007/978-94-007-6644-0_104-4

Ring, U., Kröner, A. & Toulkeridis, T. 1997. Paleoproterozoic granulite-facies metamorphism and granitoid intrusions in the Ubendian-Usagaran Orogen of northern Malawi, east-central Africa. *Precambrian Research*, **85**, 27-51.

Rogers, J.J.W. & Santosh, M. 2002. Mesoproterozoic Supercontinent: Introduction. *Gondwana Research*, **5** (**1**), 3-4.

SACS, 1980. (South African Committee for Stratigraphy). Lithostratigraphy of the Republic of South Africa, South West Africa/Namibia and the Republics of Bophuthatswana, Transkei and Venda. Part 1. *Handbook Geological Survey South Africa*, **8**, 690 pp.

Salminen, J.M., Evans, D.A.D., Trindade, R.I.F., Oliveira, E.P., Piispa, E.J. & Smirnov, A.V. 2016. Paleogeography of the Congo/ São Francisco craton at 1.5 Ga: expanding the core of Nuna supercontinent. *Precambrian Research*, **286**, 195-212

Schärer, U. 1984. The effect of initial 230Th disequilibrium on young U-Pb ages: The

Makalu case, Himalaya. *Earth and Planetary Science Letters*, **67** (**2**), 191-204.

Schmidt, M.W. 1992. Amphibole composition in tonalite as a function of pressure: an experimental calibration of the Al-in-hornblende barometer. *Contributions to Mineralogy and Petrology*, **110** (**2**), 304-310.

Schumacher, E. 1975. Herstellung von > 99.9997 % 38Ar für die 40K/40Ar Geochronologie. *Geochronologica Chimica*, **29**, 441-442.

Seth, B., Armstrong, R.A., Brandt, S., Villa, I.M. & Kramers, J.D. 2003. Mesoproterozoic U-Pb and Pb-Pb ages of granulites in NW Namibia: reconstructing a complete orogenic cycle. *Precambrian Research*, **126**, 147-168.

Seth, B., Armstrong, R.A., Büttner, A. & Villa, I.M. 2005. Time constraints for Mesoproterozoic upper amphibolite facies metamorphism in NW Namibia: a multi-isotopic approach. *Earth and Planetary Science Letters*, **230** (**3-4**), 355-378.

Seth, B., Jung, S. & Gruner, B. 2008. Deciphering polymetamorphic episodes in high-grade metamorphic orogens: Constraints from PbSL, Sm/Nd and Lu/Hf garnet dating of low to high-grade metasedimentary rocks from the Kaoko belt (Namibia). *Lithos*, **104** (**1-4**), 131-146.

Seth, B., Kröner, A., Mezger, K., Nemchin, A.A., Pidgeon, R.T. & Okrusch, M. 1998. Archaean to Neoproterozoic magmatic events in the Kaoko belt of NW Namibia and their geodynamic significance. *Precambrian Research*, **92** (**4**), 341-363.

Singletary, S.J. 1999. *Geochronology and Regional Tectonic Significance of Isolated Proterozoic Basement Outcrops and Drill Cores in the Kalahari Desert. Botswana*. Unpublished M.Sc. Thesis, Texas Christian University, USA, 99 pp.

Singletary, S.J., Hanson, R.E., Martin, M., Bowring, S.A., Key, R.M., Ramokate, L.V., Direng, B.B. & Krol, M.A. 2003. Geochronology of basement rocks in the Kalahari Desert, Botswana, and implications for regional tectonics. *Precambrian Research*, **121**, 47-71.

Sláma, J., Košler, J., Condon, D.J., Crowley, J.L., Gerdes, A., Hanchar, J.M., Horstwood, M.S.A., Morris, G.A., Nasdala, L., Norberg, N., Schaltegger, U., Schoene, B., Tubrett, M.N. & Whitehouse, M.J. 2008. Plešovice zircon - A new natural reference material for U-Pb and Hf isotopic microanalysis *Chemical Geology*, **249** (**1-2**), 1-35.

Slejko, F.F., Demarchi, G. & Morais, E. 2002. Mineral chemistry and Nd isotopic composition of two anorthositic rocks from the Kunene complex (South Western Angola). *Journal of African Earth Sciences*, **35**, 77-88.

Stacey, J.S. & Kramers, J.D. 1975. Approximation of terrestrial lead isotope evolution by a two-stage model. *Earth and Planetary Science Letters*, **26** (**2**), 207-221.

Stahl, A., 1940. Die Otaviformation des Etoschabogens (Südwest-Afrika). *Beitraege Geologischer Erforschung Deutscher Schutzgebiete*, **22**, 66.

Steiger R.H. & Jäger, E. 1977. Subcommission on Geochronology: Convention to the use of decay constants in geo- and cosmochronology. *Earth and Planetary Science Letters*, **36**, 358-362.

Stephens, M.B. & Andersson, J. 2015. Migmatization related to mafic underplating and intra- or back-arc spreading above a subduction boundary in a 2.0–1.8 Ga accretionary orogen, Sweden. *Precambrian Research*, **264**, 235-257.

Steven, N.M. 2000. Exploration for volcanogenic massive sulphide (VMS) deposits in the Khoabendus Group, near Kamanjab, northwestern Namibia: The wrong tectonic setting and an alternative exploration model. *Economic Geology Research Unit Information Circular*, University of the Witwatersrand, Johannesburg, Issue **341**.

Steven, N.M. & Armstrong, R. 2002. The potential for clastic-hosted zinc deposits in the upper Khoabendus Group near Kamanjab, N.W. Namibia. *11th IAGOD Quadrennial Symposium and Geocongress, Windhoek*, Namibia, Extended Abstracts.

Streckeisen, A.L. & Le Maître, R.W. 1979. A chemical approximation to the modal QAPF classification of igneous rocks. *Neues Jahrbuch für Mineralogie*, **136**, 169-206.

Sun, S.S. & McDonough, W.F. 1989. Chemical and Isotopic Systematics of Oceanic Basalts: Implications for Mantle Composition and Processes: Magmatism in Oceanic Basins. *Geological Society Special Publication*, **42**, 313-345.

Tack, L., Wingate, M.T.D., De Waele, B., Meert, J., Belousova, E., Griffin, B., Tahon, A. & Fernandez-Alonso, M. 2010. The 1375

Ma Kibaran event in Central Africa: prominent emplacement of bimodal magmatism under extensional regime. *Precambrian Research*, **180**, 63-84.

Tegtmeyer, A. & Kröner, A. 1985. U-Pb zircon ages for granitoid gneisses in northern Namibia and their significance for Proterozoic crustal evolution of southwestern Africa. *Precambrian Research*, **28** (**3-4**), 311-326.

Thiéblemont, D., Castaing, C., Billa, M., Bouton, A. & Préat, A. 2009. *Notice explicative de la carte géologique et des ressources minérales de la République gabonaise à 1 : 1,000,000*. Programme Sysmin 8 ACP GA 017, Ministère des Mines, du Pétrole, des Hydrocarbures. Direction Générale des Mines et de la Géologie, 384 pp.

Thomas, R.J., Boger, S.D., Fullgraf, T., Bracciali, L., Frey, D., Le Roux, P., Lach, P., Lahay, Y., Ruffet, G. 2022. Geological Mapping and Mineral Assessment Project of Malawi (GEMMAP). Geochronology and radiogenic isotopes (U-Pb single zircon, Sm-Nd whole rock, Ar-Ar muscovite). *Geological Survey Department, Zomba, Malawi, Memoir*, 116 pp.

Tsodilo Resources Ltd. 2011. June 2011 News Release of Completion of Phase 1 of Exploration.

Uto, K., Ishizuka, O., Matsumoto, A., Kamioka, H. & Togashi, S. 1997. Laser-heating $^{40}Ar/^{39}Ar$ dating system of the Geological Survey of Japan: System outline and preliminary results. *Bulletin of the Geological Survey of Japan*, **48**, 23-46.

Vanderhaeghe, O., Teyssier, C. & Wysoczanski, R. 1999. Structural and geochronological constraints on the role of partial melting during the formation of the Shuswap metamorphic core complex at the latitude of the Thor-Odin dome, British Columbia. *Canadian Journal of Earth Sciences*, **36** (**6**), 917-943.

Wang, K., Burov, E., Gumiaux, C., Chen, Y., Lu, G., Mezri, L. & Zhao, L. 2015. Formation of Metamorphic Core Complexes in non-over-thickened continental crust: A case study of Liaodong Peninsula (East Asia), *Lithos*, **238**, 86-100.

Weber, F., Gauthier-Lafaye, F., Whitechurch, H., Ulrich, M. & El Albani, A. 2016. The 2-Ga Eburnean Orogeny in Gabon and the opening of the Francevillian intracratonic basins: A review. *Comptes Rendus Geoscience*, **348**, 572-586.

Wernicke, B. 1981. Low-angle faults in the Basin and Range Province: nappe tectonics in an extending orogen. *Nature*, **291**, 645-648.

Wetherill, G.W. 1956, Discordant uranium-lead ages: I. EOS, *Transactions American Geophysical Union*, **37** (**3**), 320-326.

Wiedenbeck, M., Allen, P., Corfu, F., Griffin, W.L., Meier, M., Oberli, F., Von Quadt, A., Roddick, J.C. & Spiegel, W. 1995. Three natural zircon standards for U–Th–Pb, Lu–Hf, trace element and REE analyses. *Geostandards Newsletters*, **19**, 1-23.

Wilke, F.D.H., O'Brien, P.J., Gerdes, A., Timmerman, M.J., Sudo, M. & Khan, M.A. 2010. The multistage exhumation history of the Kaghan Valley UHP series, NW Himalaya, Pakistan from U-Pb and $^{40}Ar/^{39}Ar$ ages. *European Journal of Mineralogy*, **22**, 703-719.

Williams, I.S. 1998. U-Th-Pb Geochronology by Ion Microprobe. *Reviews in Economic Geology*, **7**, 1-35.

Wilsky, F. 2010. *Geochemische Charakterisierung einer metasomatischen Überprägung granitoider Gesteine der Västervik-Region (SE-Schweden)*. Diploma thesis, Geowissenschaftliches Zentrum Georg-August Universität Göttingen, Germany (unpublished), 129 pp.

Winchester, J.A. & Floyd, P.A. 1977. Geochemical discrimination of different magma series and their differentiation products using immobile elements. *Chemical Geology*, **20**, 325-343.

Wood, D.A. 1980. The application of a Th-Hf-Ta diagram to problems of tectonomagmatic classification and to establishing the nature of crustal contamination of basaltic lavas of the British Tertiary Volcanic Province. *Earth and Planetary Science Letters*, **50** (**1**), 11-30.

Wu, C.M. & Cheng, B.H. 2006. Valid garnet–biotite (GB) geothermometry and garnet aluminum silicate - plagioclase - quartz (GASP) geobarometry in metapelitic rocks. *Lithos*, **89** (**1-2**), 1-23.

Yin, A. 2004. Gneiss domes and gneiss dome systems. *In*: Whitney, D.L., Teyssier, C. & Siddoway, C.S. (Eds), Gneiss domes in orogeny Boulder, Colorado, *Geological Society of America Special Paper*, **380**, 1-14.

York, D. 1969. Least squares fitting of a straight line with correlated errors. *Earth and Planetary Science Letters*, **5**, 320-324.

Zhang, S.H., Li, Z.X., Evans, D.A.D., Wu, H., Li, H. & Dong, J. 2012. Pre-Rodinia supercontinent Nuna shaping up: A global synthesis with new paleomagnetic results from North China. *Earth and Planetary Science Letters*, **353-354**, 145-155.

Zhang, J., Mattinson, C., Yu, S., Li, Y., Yu, Mao, X., Lu, Z. & Peng, Y. 2019. Two contrasting accretion v. collision orogenies: insights from Early Paleozoic polyphase metamorphism in the Altun–Qilian–North Qaidam orogenic system, NW China. *Geological Society of London, Special Publications*, **474**, 153–181.

Zhao, G., Cawood, P.A., Wilde, S.A. & Sun, M. 2002. Review of global 2.1-1.8 Ga orogens: implications for a pre-Rodinia supercontinent. *Earth-Science Reviews*, **59** (**1-4**), 125-162.

Zhao, G., Sun, M., Wilde, S A. & Li, S. 2004. A Paleo-Mesoproterozoic supercontinent: assembly, growth and breakup. *Earth-Science Reviews*, **67**, 91-123.

Zheng, Y., Chen, Y., Chen, R. & Dai, L. 2022. Tectonic evolution of convergent plate margins and its geological effects. *Science China Earth Sciences*, **65**, 1247-1276.

## Annexes

I - Kamanjab Inlier - sample locations, geochemistry and isotope analyses
II - Mineral analyses, Depiné (2008)
III - Mineral analyses Nolte (2012)
IV - 1: 100 000 Geological Map of the Khoabendus Area
V - 1: 100 000 Geological Map of the Huab Metamorphic Complex
VI - Abbreviations
VII - Toponymics

**Annex I** – Kamanjab Inlier - sample locations, geochemistry and isotope analyses.

| Sample | Easting | Northing | Field Des. | Met. Pet. | Geochemistry | Isotope analysis |
|---|---|---|---|---|---|---|
| 010305-1 | 444064 | 7785051 | | | mafic whole rock | Sm-Nd, Rb-Sr WR mafic |
| 020809-3 | 477268 | 7758050 | | x | | |
| 020809-4 | 477088 | 7758047 | | x | | |
| 050605-1 | 429931 | 7747375 | | | | K-Ar musovite |
| 050605-1 | 429931 | 7747375 | | | | Ar-Ar muscovite |
| 070900-1 | 439137 | 7770851 | x | | | |
| 081203-2 | 492927 | 7782815 | | | felsic whole rock | Sm-Nd, Rb-Sr WR felsic |
| 081203-2 | 492927 | 7782815 | | | | SHRIMP single zircon |
| 090606-1 | 441110 | 7762987 | | | felsic whole rock | Sm-Nd, Rb-Sr WR felsic |
| 090606-2 | 441103 | 7762991 | | | | Ar-Ar hornblende |
| 090606-3C | 435810 | 7755991 | | | | Ar-Ar hornblende |
| 090606-5 | 432703 | 7753249 | | | felsic whole rock | Sm-Nd, Rb-Sr WR felsic |
| 101203-1 | 435101 | 7757086 | | x | mafic whole rock | Sm-Nd, Rb-Sr WR mafic |
| 101203-2 | 434867 | 7756759 | | x | mafic whole rock | Sm-Nd, Rb-Sr WR mafic |
| 101203-5 | 435111 | 7756525 | | | | Sm-Nd, Rb-Sr WR mafic |
| 110503-1 | 433548 | 7763416 | | | | Sm-Nd, Rb-Sr WR felsic |
| 121203-2 | 443610 | 7753027 | | | mafic whole rock | Sm-Nd, Rb-Sr WR mafic |
| 130503-1 | 450066 | 7772045 | | | felsic whole rock | Sm-Nd WR felsic |
| 130503-1 | 450066 | 7772045 | | | | LA-ICP-MS single zircon |
| 150900-9 | 442040 | 7780206 | | | mafic whole rock | Sm-Nd, Rb-Sr WR mafic |
| 151104-1 | 432560 | 7832943 | | | felsic whole rock | Sm-Nd, Rb-Sr WR felsic |
| 170405-6 | 463749 | 7833403 | | | felsic whole rock | Sm-Nd, Rb-Sr WR felsic |
| 170405-6 | 463749 | 7833403 | | | | |
| 170405-6 | 463749 | 7833403 | | | | LA-ICP-MS single zircon |
| 170900-14 | 442262 | 7778202 | | | mafic whole rock | Sm-Nd, Rb-Sr WR mafic |
| 200900-1 | 444154 | 7785048 | | x | mafic whole rock | Sm-Nd, Rb-Sr WR mafic |
| 210503-9a | 477610 | 7758294 | | | mafic whole rock | Sm-Nd, Rb-Sr WR mafic |
| 210802 - 1 | 445530 | 7766900 | | | | K-Ar musovite |
| 210900-2 | 437903 | 7785386 | | | felsic whole rock | Sm-Nd, Rb-Sr WR felsic |
| 210900-2 | 437903 | 7785386 | | | | LA-ICP-MS single zircon |
| 220802-12 | 440033 | 7761035 | | | felsic whole rock | Sm-Nd, Rb-Sr WR felsic |
| 220802-13 | 483306 | 7776759 | | | felsic whole rock | Sm-Nd, Rb-Sr WR felsic |
| 220802-3 | 439178 | 7764856 | | | mafic whole rock | Sm-Nd, Rb-Sr WR mafic |
| 220802-6 | 439178 | 7764856 | | | mafic whole rock | Sm-Nd, Rb-Sr WR mafic |
| 220802-7 | 439178 | 7764856 | | | mafic whole rock | Sm-Nd, Rb-Sr WR mafic |
| 220802-9 | 440447 | 7763816 | | | mafic whole rock | Sm-Nd, Rb-Sr WR mafic |
| 231104-1 | 448500 | 7775160 | | x | | |
| 231104-5 | 438778 | 7764787 | | | | K-Ar musovite |
| 231104-6 | 438923 | 7764797 | | | | K-Ar musovite |
| 231104-6 | 438923 | 7764797 | | | | Ar-Ar muscovite |
| 240709-3 | 453533 | 7832755 | | | mafic whole rock | Sm-Nd, Rb-Sr WR mafic |
| 260205-4 | 461861 | 7825462 | | | felsic whole rock | Sm-Nd, Rb-Sr WR felsic |
| 260205-4 | 461861 | 7825462 | | | | LA-ICP-MS single zircon |
| 260205-4 | 461861 | 7825462 | | | felsic whole rock | |
| 260406-10 | 439356 | 7759622 | | x | mafic whole rock | Sm-Nd, Rb-Sr WR mafic |
| 260406-12 | 439309 | 7759668 | | | mafic whole rock | Sm-Nd, Rb-Sr WR mafic |
| 260406-14 | 475892 | 7757681 | | x | mafic whole rock | Sm-Nd, Rb-Sr WR mafic |
| 260406-4 | 437157 | 7750078 | | x | mafic whole rock | Sm-Nd, Rb-Sr WR mafic |
| 260709-2 | 453684 | 7805166 | | | mafic whole rock | Sm-Nd, Rb-Sr WR mafic |
| 260709-4 | 441580 | 7797132 | | | | Ar-Ar muscovite |
| 270802-1 | 435785 | 7780095 | | | felsic whole rock | Rb-Sr WR felsic |
| 270802-1 | 435785 | 7780095 | | | | SHRIMP single zircon |
| 270802-4 | 436570 | 7778821 | | | mafic whole rock | Sm-Nd, Rb-Sr WR mafic |
| 280205-3 | 473389 | 7843283 | | | felsic whole rock | Sm-Nd, Rb-Sr WR felsic |
| 280205-6 | 482717 | 7833268 | | | felsic whole rock | Sm-Nd, Rb-Sr WR felsic |
| 280205-6 | 482717 | 7833268 | | | | LA-ICP-MS single zircon |
| 280205-7 | 482717 | 7833268 | | | felsic whole rock | Sm-Nd, Rb-Sr WR felsic |
| 280709-1 | 436731 | 7778567 | | | mafic whole rock | Sm-Nd, Rb-Sr WR mafic |
| 280709-2 | 436825 | 7778436 | | | mafic whole rock | Sm-Nd, Rb-Sr WR mafic |

| | | | | | | |
|---|---|---|---|---|---|---|
| 280802-2 | 432863 | 7779958 | | | felsic whole rock | Sm-Nd, Rb-Sr WR felsic |
| 290709-5 | 438129 | 7785781 | | | mafic whole rock | Sm-Nd, Rb-Sr WR mafic |
| 290709-8 | 449836 | 7777322 | | x | mafic whole rock | Sm-Nd, Rb-Sr WR mafic |
| 290802-1 | 435735 | 7780980 | | | mafic whole rock | Sm-Nd, Rb-Sr WR mafic |
| 290802-10 | 436839 | 7778506 | | | mafic whole rock | Sm-Nd, Rb-Sr WR mafic |
| 290802-11 | 436839 | 7778506 | | | mafic whole rock | Sm-Nd, Rb-Sr WR mafic |
| 290802-12 | 436839 | 7778506 | | | mafic whole rock | Sm-Nd, Rb-Sr WR mafic |
| 290802-13 | 436470 | 7778523 | | | mafic whole rock | Sm-Nd, Rb-Sr WR mafic |
| 290802-2 | 435735 | 7780980 | | | mafic whole rock | Sm-Nd, Rb-Sr WR mafic |
| 290802-3 | 435878 | 7780682 | | | mafic whole rock | Sm-Nd, Rb-Sr WR mafic |
| 290802-4 | 435923 | 7780544 | | | mafic whole rock | Sm-Nd, Rb-Sr WR mafic |
| 290802-5 | 435922 | 7780544 | | | mafic whole rock | Sm-Nd, Rb-Sr WR mafic |
| 290802-6 | 436274 | 7778846 | | | mafic whole rock | Sm-Nd, Rb-Sr WR mafic |
| 290802-7 | 437213 | 7777699 | | | mafic whole rock | Sm-Nd, Rb-Sr WR mafic |
| 290802-9 | 436840 | 7778205 | | | mafic whole rock | Sm-Nd, Rb-Sr WR mafic |
| 300709-4 | 441580 | 7770324 | | | | Ar-Ar muscovite |
| 310104-2 | 438627 | 7764738 | | | | K-Ar musovite |
| 310104-3 | 438627 | 7764738 | | | | K-Ar musovite |
| Beatrice | | | | | felsic whole rock | |
| Cypress | | | | | felsic whole rock | |
| Dante | | | | | felsic whole rock | |
| Eduardsfelde | | | | | felsic whole rock | |
| ETM5 | | | | | felsic whole rock | |
| ETM8 | | | | | felsic whole rock | |
| Franzfontein I | | | | | felsic whole rock | |
| Franzfontein II | | | | | felsic whole rock | |
| HU03 | 442645 | 7762399 | | | | LA-ICP-MS single zircon |
| HU03 | 442645 | 7762399 | | | felsic whole rock | |
| HU03 | 442645 | 7762399 | | | | Sm-Nd, Rb-Sr WR felsic |
| JM01-CC10 | | | | | felsic whole rock | |
| JM01-CC11 | | | | | felsic whole rock | |
| JM01-CC12 | | | | | felsic whole rock | |
| JM01-CC16 | | | | | felsic whole rock | |
| JM01-CC18 | | | | | felsic whole rock | |
| Kranzpoort | | | | | felsic whole rock | |
| NA037 | 438139 | 7785792 | x | | | |
| NA038 | 443648 | 7780638 | x | | | |
| NA040 | 450284 | 7772952 | x | | | |
| NA044 | 438990 | 7764828 | x | | | |
| NA045 | 441109 | 7763072 | x | | | |
| NA049 | 433655 | 7763413 | x | | | |
| NA052-58 | | | x | | | |
| NA075 | 448434 | 7775833 | x | | | |
| NA078 | | | x | | | |
| NA101 | 442376 | 7770033 | x | | | U-Pb zircon |
| NA101-2 | 442376 | 7770033 | | | | SHRIMP single zircon |
| NA112 | | | x | | | |
| NA124 | | | | | | |
| NA125 | | | | | | |
| NA131 | | | | | | |
| Persephone | | | | | felsic whole rock | |
| Schönau | | | | | felsic whole rock | |
| Schönau | | | | | felsic whole rock | |
| Schönau | | | | | felsic whole rock | |
| TBE1 | | | | | felsic whole rock | |
| TBE3 | | | | | felsic whole rock | |
| TBE4 | | | | | felsic whole rock | |

**Annex II** – Whole rock analyses, Depiné (2008).

| | Sample | 101203-1 | 101203-2 | 101203-2b | 200900-1 | 231104-1 | 260406-4 | 260406-4b | 260406-10 | 260406-14 | 260406-14b | 290802-11 | 290802-12 |
|---|---|---|---|---|---|---|---|---|---|---|---|---|---|
| Whole rock | **Major elements [wt%]** | | | | | | | | | | | | |
| | $SiO_2$ | 62,04 | 48,20 | 47,49 | 59,29 | 68,83 | 51,52 | 51,18 | 49,23 | 70,74 | 70,62 | 47,63 | 47,80 |
| | $TiO_2$ | 0,65 | 2,41 | 2,43 | 0,66 | 0,34 | 1,91 | 1,92 | 1,64 | 0,49 | 0,49 | 1,18 | 1,35 |
| | $Al_2O_3$ | 14,42 | 15,79 | 15,35 | 22,28 | 16,20 | 13,30 | 13,30 | 15,66 | 12,49 | 12,24 | 14,57 | 16,82 |
| | $Fe_2O_3$tot | 9,70 | 15,21 | 15,11 | 6,30 | 3,66 | 15,81 | 15,67 | 13,91 | 6,36 | 6,35 | 14,77 | 13,89 |
| | MnO | 0,26 | 0,24 | 0,24 | 0,10 | 0,10 | 0,23 | 0,23 | 0,14 | 0,10 | 0,10 | 0,38 | 0,36 |
| | MgO | 3,39 | 4,34 | 4,10 | 1,49 | 0,73 | 5,72 | 5,49 | 6,78 | 0,36 | 0,36 | 9,58 | 7,62 |
| | CaO | 4,79 | 8,02 | 8,01 | 0,49 | 2,96 | 8,98 | 8,96 | 9,20 | 2,48 | 2,48 | 11,20 | 11,84 |
| | $Na_2O$ | 2,24 | 2,26 | 2,28 | 0,74 | 4,95 | 0,97 | 0,95 | 1,85 | 2,47 | 2,38 | 1,36 | 1,60 |
| | $K_2O$ | 1,47 | 0,32 | 0,29 | 5,09 | 0,93 | 0,54 | 0,50 | 0,38 | 3,46 | 3,45 | 0,27 | 0,13 |
| | $P_2O_5$ | 0,09 | 0,55 | 0,53 | 0,16 | 0,14 | 0,23 | 0,23 | 0,48 | 0,16 | 0,16 | 0,11 | 0,14 |
| | S | <0.10 | <0.10 | <0.10 | <0.10 | <0.10 | <0.10 | <0.10 | <0.10 | <0.10 | <0.10 | <0.10 | <0.10 |
| | LOI | 1,30 | 3,26 | 3,22 | 3,42 | 1,03 | 1,07 | 1,05 | 1,22 | 0,41 | 0,39 | 0,06 | 0,15 |
| | Sum | 100,35 | 100,60 | 99,05 | 100,02 | 99,87 | 100,28 | 99,48 | 100,49 | 99,52 | 99,02 | 101,11 | 101,40 |
| | **Trace elements [ppm]** | | | | | | | | | | | | |
| | V | 111 | 178 | 182 | 89 | 15 | 351 | 346 | 242 | 21 | 22 | 277 | 309 |
| | Cr | 47 | 14 | 17 | 71 | <10 | 86 | 93 | 200 | <10 | <10 | 420 | 125 |
| | Co | 75 | 41 | 46 | 47 | 50 | 74 | 57 | 84 | 73 | 69 | 96 | 81 |
| | Ni | 30 | 17 | 12 | 24 | <5 | 25 | 25 | 74 | <5 | <5 | 77 | 52 |
| | Zn | 53 | 172 | 168 | 107 | 22 | 147 | 145 | 339 | 22 | 22 | 129 | 132 |
| | Ga | 19 | 32 | 37 | 29 | 20 | 29 | 26 | 30 | 24 | 23 | 18 | 24 |
| | Rb | 102 | 13 | 17 | 189 | 71 | 18 | 17 | 23 | 129 | 127 | 10 | 9 |
| | Sr | 158 | 230 | 222 | 200 | 231 | 100 | 96 | 235 | 109 | 107 | 321 | 434 |
| | Y | 120 | 54 | 50 | 30 | 37 | 45 | 45 | 42 | 129 | 126 | 21 | 16 |
| | Zr | 228 | 274 | 290 | 163 | 272 | 168 | 167 | 155 | 438 | 433 | 47 | 33 |
| | Nb | 16 | 20 | 18 | 14 | 10 | 10 | 11 | 11 | 32 | 33 | <5 | <5 |
| | Mo | <5 | <5 | 5 | <5 | <5 | <5 | <5 | <5 | <5 | <5 | <5 | <5 |
| | Sn | <15 | <15 | <15 | <15 | <15 | <15 | <15 | <15 | <15 | 19 | <15 | <15 |
| | Ba | 484 | 138 | 145 | 1114 | 362 | 131 | 133 | 319 | 931 | 943 | 248 | 118 |
| | Pb | <5 | 15 | <5 | 17 | 13 | <5 | <5 | <5 | <5 | <5 | <5 | <5 |
| | Th | 15 | 9 | 8 | 20 | 14 | <5 | <5 | 8 | 20 | 19 | <5 | <5 |
| | U | <5 | <5 | <5 | <5 | <5 | <5 | <5 | <5 | <5 | <5 | <5 | <5 |

**Annex II** – Mineral analyses, Depiné (2008).

| | Sample | 101203-1 | | | | | | | | | | | | | | | | | | |
|---|---|---|---|---|---|---|---|---|---|---|---|---|---|---|---|---|---|---|---|---|
| | **Ox. wt%** | **P1** | **P3** | **P4** | **P5** | **P8** | **P10** | **P11** | **P13** | **P14** | **P15** | **P18** | **P19** | **P20** | **P21** | **P22** | **P23** | **P24** | **P25** | **P26** | **P28** |
| **Garnet** | $SiO_2$ | 36,74 | 37,18 | 37,24 | 37,22 | 37,05 | 37,20 | 36,74 | 37,02 | 36,80 | 36,60 | 37,21 | 36,91 | 36,76 | 37,26 | 37,05 | 37,08 | 37,43 | 37,02 | 37,17 | 36,97 |
| | $TiO_2$ | 0,00 | 0,00 | 0,03 | 0,04 | 0,02 | 0,00 | 0,01 | 0,01 | 0,00 | 0,03 | 0,00 | 0,01 | 0,00 | 0,05 | 0,02 | 0,04 | 0,04 | 0,02 | 0,04 | 0,01 |
| | $Al_2O_3$ | 20,71 | 21,03 | 21,04 | 21,29 | 21,07 | 20,96 | 20,95 | 20,72 | 20,97 | 20,69 | 20,90 | 20,91 | 20,84 | 20,94 | 21,11 | 21,23 | 21,16 | 21,07 | 20,83 | 21,02 |
| | $Cr_2O_3$ | 0,00 | 0,00 | 0,03 | 0,06 | 0,04 | 0,03 | 0,01 | 0,00 | 0,01 | 0,00 | 0,00 | 0,02 | 0,00 | 0,00 | 0,03 | 0,02 | 0,00 | 0,00 | 0,00 | 0,01 |
| | $Fe_2O_3$ | 0,63 | 0,57 | 0,67 | 0,67 | 1,05 | 0,45 | 0,88 | 0,07 | 1,10 | 0,89 | 0,25 | 1,29 | 0,36 | 0,59 | 0,82 | 0,88 | 0,57 | 1,11 | 1,16 | 1,27 |
| | FeO | 27,71 | 26,88 | 26,97 | 27,32 | 28,18 | 27,09 | 27,76 | 29,61 | 28,12 | 28,38 | 29,45 | 27,72 | 29,57 | 27,77 | 28,80 | 26,50 | 26,58 | 25,97 | 25,59 | 25,32 |
| | MnO | 5,08 | 2,85 | 1,97 | 1,76 | 2,67 | 2,61 | 2,76 | 2,92 | 2,75 | 4,25 | 2,31 | 2,27 | 3,34 | 1,98 | 2,17 | 2,15 | 2,16 | 2,31 | 2,55 | 2,54 |
| | MgO | 1,99 | 2,90 | 3,41 | 3,41 | 3,24 | 2,94 | 2,37 | 2,20 | 3,09 | 1,60 | 3,04 | 3,35 | 1,97 | 3,11 | 2,77 | 3,32 | 3,27 | 3,25 | 3,28 | 3,25 |
| | CaO | 5,87 | 7,43 | 7,42 | 7,32 | 5,99 | 7,43 | 7,16 | 6,09 | 5,92 | 6,45 | 5,69 | 6,35 | 5,86 | 7,24 | 6,55 | 7,63 | 7,96 | 7,95 | 8,18 | 8,23 |
| | sum | 98,72 | 98,86 | 98,77 | 99,08 | 99,30 | 98,70 | 98,63 | 98,50 | 98,75 | 98,89 | 98,85 | 98,84 | 98,70 | 98,94 | 99,32 | 98,85 | 99,16 | 98,70 | 98,80 | 98,61 |
| | **Cations** | | | | | | | | | | | | | | | | | | | | |
| | Si | 2,99 | 2,99 | 2,98 | 2,97 | 2,97 | 2,99 | 2,97 | 3,01 | 2,97 | 2,98 | 3,00 | 2,97 | 2,99 | 2,99 | 2,97 | 2,97 | 2,99 | 2,97 | 2,98 | 2,97 |
| | Ti | 0,00 | 0,00 | 0,00 | 0,00 | 0,00 | 0,00 | 0,00 | 0,00 | 0,00 | 0,00 | 0,00 | 0,00 | 0,00 | 0,00 | 0,00 | 0,00 | 0,00 | 0,00 | 0,00 | 0,00 |
| | Al | 1,98 | 1,99 | 1,99 | 2,00 | 1,99 | 1,99 | 2,00 | 1,98 | 1,99 | 1,98 | 1,99 | 1,98 | 2,00 | 1,98 | 2,00 | 2,00 | 1,99 | 1,99 | 1,97 | 1,99 |
| | Cr | 0,00 | 0,00 | 0,00 | 0,00 | 0,00 | 0,00 | 0,00 | 0,00 | 0,00 | 0,00 | 0,00 | 0,00 | 0,00 | 0,00 | 0,00 | 0,00 | 0,00 | 0,00 | 0,00 | 0,00 |
| | $Fe^{3+}$ | 0,04 | 0,03 | 0,04 | 0,04 | 0,06 | 0,03 | 0,05 | 0,00 | 0,07 | 0,05 | 0,02 | 0,08 | 0,02 | 0,04 | 0,05 | 0,05 | 0,03 | 0,07 | 0,07 | 0,08 |
| | $Fe^{2+}$ | 1,88 | 1,81 | 1,81 | 1,82 | 1,89 | 1,82 | 1,88 | 2,01 | 1,90 | 1,93 | 1,99 | 1,86 | 2,01 | 1,86 | 1,93 | 1,77 | 1,77 | 1,74 | 1,71 | 1,70 |
| | Mn | 0,35 | 0,19 | 0,13 | 0,12 | 0,18 | 0,18 | 0,19 | 0,20 | 0,19 | 0,29 | 0,16 | 0,15 | 0,23 | 0,13 | 0,15 | 0,15 | 0,15 | 0,16 | 0,17 | 0,17 |
| | Mg | 0,24 | 0,35 | 0,41 | 0,41 | 0,39 | 0,35 | 0,29 | 0,27 | 0,37 | 0,19 | 0,36 | 0,40 | 0,24 | 0,37 | 0,33 | 0,40 | 0,39 | 0,39 | 0,39 | 0,39 |
| | Ca | 0,51 | 0,64 | 0,64 | 0,63 | 0,51 | 0,64 | 0,62 | 0,53 | 0,51 | 0,56 | 0,49 | 0,55 | 0,51 | 0,62 | 0,56 | 0,65 | 0,68 | 0,68 | 0,70 | 0,71 |
| | sum | 8,00 | 8,00 | 8,00 | 8,00 | 8,00 | 8,00 | 8,00 | 8,00 | 8,00 | 8,00 | 8,00 | 8,00 | 8,00 | 8,00 | 8,00 | 8,00 | 8,00 | 8,00 | 8,00 | 8,00 |
| | norm. coeff. | 0,20 | 0,21 | 0,21 | 0,21 | 0,21 | 0,21 | 0,21 | 0,20 | 0,21 | 0,20 | 0,21 | 0,21 | 0,20 | 0,21 | 0,21 | 0,21 | 0,21 | 0,21 | 0,21 | 0,21 |
| | xFe | 0,89 | 0,84 | 0,82 | 0,82 | 0,83 | 0,84 | 0,87 | 0,88 | 0,84 | 0,91 | 0,85 | 0,83 | 0,90 | 0,84 | 0,86 | 0,82 | 0,82 | 0,82 | 0,82 | 0,82 |
| | xAlm | 0,63 | 0,60 | 0,61 | 0,61 | 0,64 | 0,61 | 0,63 | 0,67 | 0,64 | 0,65 | 0,66 | 0,63 | 0,67 | 0,62 | 0,65 | 0,60 | 0,59 | 0,59 | 0,58 | 0,57 |
| | xPrp | 0,08 | 0,12 | 0,14 | 0,14 | 0,13 | 0,12 | 0,10 | 0,09 | 0,13 | 0,07 | 0,12 | 0,14 | 0,08 | 0,12 | 0,11 | 0,13 | 0,13 | 0,13 | 0,13 | 0,13 |
| | xGrs | 0,17 | 0,21 | 0,21 | 0,21 | 0,17 | 0,21 | 0,21 | 0,18 | 0,17 | 0,19 | 0,16 | 0,18 | 0,17 | 0,21 | 0,19 | 0,22 | 0,23 | 0,23 | 0,24 | 0,24 |
| | xSps | 0,12 | 0,06 | 0,04 | 0,04 | 0,06 | 0,06 | 0,06 | 0,07 | 0,06 | 0,10 | 0,05 | 0,05 | 0,08 | 0,05 | 0,05 | 0,05 | 0,05 | 0,05 | 0,06 | 0,06 |

**Annex II** – Mineral analyses, Depiné (2008).

| | Sample | 101203-1 | | | | | | | | | | | | | | | | | | |
|---|---|---|---|---|---|---|---|---|---|---|---|---|---|---|---|---|---|---|---|---|
| | **Ox. wt%** | **P59** | **P60** | **P61** | **P62** | **P63** | **P64** | **P66** | **P68** | **P70** | **P74** | **P75** | **P76** | **P77** | **P78** | **P80** | **P81** | **P84** | **P86** | **P87** | **P89** |
| **Garnet** | $SiO_2$ | 37,05 | 36,28 | 36,77 | 36,69 | 36,71 | 37,09 | 36,76 | 36,87 | 36,60 | 36,84 | 37,05 | 36,63 | 36,71 | 36,71 | 37,22 | 36,08 | 36,82 | 36,95 | 37,05 | 36,65 |
| | $TiO_2$ | 0,00 | 0,00 | 0,05 | 0,03 | 0,03 | 0,00 | 0,01 | 0,03 | 0,00 | 0,03 | 0,03 | 0,06 | 0,01 | 0,05 | 0,07 | 0,00 | 0,00 | 0,01 | 0,02 | 0,03 |
| | $Al_2O_3$ | 20,94 | 20,88 | 21,05 | 20,86 | 21,01 | 20,68 | 20,82 | 20,95 | 20,81 | 21,00 | 20,90 | 20,93 | 20,47 | 20,87 | 21,01 | 20,75 | 20,89 | 20,77 | 20,70 | 20,87 |
| | $Cr_2O_3$ | 0,01 | 0,00 | 0,01 | 0,00 | 0,00 | 0,00 | 0,02 | 0,00 | 0,01 | 0,02 | 0,03 | 0,00 | 0,05 | 0,02 | 0,00 | 0,01 | 0,00 | 0,00 | 0,02 | 0,01 |
| | $Fe_2O_3$ | 0,78 | 1,55 | 1,83 | 1,47 | 1,43 | 0,64 | 1,32 | 1,03 | 1,10 | 1,34 | 0,79 | 1,76 | 0,45 | 1,25 | 0,50 | 2,73 | 0,82 | 0,87 | 0,69 | 0,99 |
| | FeO | 27,63 | 28,62 | 26,92 | 27,87 | 28,05 | 28,06 | 27,56 | 27,62 | 28,92 | 27,96 | 28,42 | 27,16 | 28,89 | 27,80 | 28,73 | 27,25 | 29,21 | 27,85 | 28,23 | 28,15 |
| | MnO | 2,44 | 3,13 | 2,74 | 2,68 | 2,52 | 2,60 | 2,70 | 2,73 | 3,43 | 2,58 | 2,74 | 2,58 | 4,66 | 2,82 | 2,72 | 2,89 | 2,85 | 2,81 | 2,56 | 2,76 |
| | MgO | 2,94 | 2,15 | 2,86 | 2,91 | 2,47 | 2,72 | 2,86 | 2,60 | 1,76 | 2,58 | 2,63 | 2,79 | 1,52 | 2,66 | 2,51 | 2,47 | 2,14 | 2,57 | 2,70 | 2,59 |
| | CaO | 6,99 | 6,06 | 7,21 | 6,34 | 6,96 | 6,88 | 6,70 | 7,09 | 6,44 | 6,95 | 6,60 | 7,11 | 5,92 | 6,67 | 6,72 | 6,70 | 6,34 | 6,97 | 6,78 | 6,48 |
| | sum | 98,78 | 98,67 | 99,43 | 98,86 | 99,18 | 98,67 | 98,74 | 98,92 | 99,06 | 99,30 | 99,17 | 99,03 | 98,69 | 98,84 | 99,49 | 98,87 | 99,07 | 98,79 | 98,75 | 98,52 |
| | **Cations** | | | | | | | | | | | | | | | | | | | | |
| | Si | 2,98 | 2,95 | 2,95 | 2,96 | 2,96 | 3,00 | 2,97 | 2,97 | 2,97 | 2,96 | 2,98 | 2,95 | 3,00 | 2,97 | 2,99 | 2,93 | 2,98 | 2,98 | 2,99 | 2,97 |
| | Ti | 0,00 | 0,00 | 0,00 | 0,00 | 0,00 | 0,00 | 0,00 | 0,00 | 0,00 | 0,00 | 0,00 | 0,00 | 0,00 | 0,00 | 0,00 | 0,00 | 0,00 | 0,00 | 0,00 | 0,00 |
| | Al | 1,99 | 2,00 | 1,99 | 1,98 | 2,00 | 1,97 | 1,98 | 1,99 | 1,99 | 1,99 | 1,98 | 1,99 | 1,97 | 1,99 | 1,99 | 1,98 | 1,99 | 1,98 | 1,97 | 1,99 |
| | Cr | 0,00 | 0,00 | 0,00 | 0,00 | 0,00 | 0,00 | 0,00 | 0,00 | 0,00 | 0,00 | 0,00 | 0,00 | 0,00 | 0,00 | 0,00 | 0,00 | 0,00 | 0,00 | 0,00 | 0,00 |
| | $Fe^{3+}$ | 0,05 | 0,09 | 0,11 | 0,09 | 0,09 | 0,04 | 0,08 | 0,06 | 0,07 | 0,08 | 0,05 | 0,11 | 0,03 | 0,08 | 0,03 | 0,17 | 0,05 | 0,05 | 0,04 | 0,06 |
| | $Fe^{2+}$ | 1,86 | 1,95 | 1,80 | 1,88 | 1,89 | 1,90 | 1,86 | 1,86 | 1,96 | 1,88 | 1,91 | 1,83 | 1,97 | 1,88 | 1,93 | 1,85 | 1,98 | 1,88 | 1,91 | 1,91 |
| | Mn | 0,17 | 0,22 | 0,19 | 0,18 | 0,17 | 0,18 | 0,18 | 0,19 | 0,24 | 0,18 | 0,19 | 0,18 | 0,32 | 0,19 | 0,19 | 0,20 | 0,20 | 0,19 | 0,18 | 0,19 |
| | Mg | 0,35 | 0,26 | 0,34 | 0,35 | 0,30 | 0,33 | 0,34 | 0,31 | 0,21 | 0,31 | 0,32 | 0,34 | 0,19 | 0,32 | 0,30 | 0,30 | 0,26 | 0,31 | 0,33 | 0,31 |
| | Ca | 0,60 | 0,53 | 0,62 | 0,55 | 0,60 | 0,60 | 0,58 | 0,61 | 0,56 | 0,60 | 0,57 | 0,61 | 0,52 | 0,58 | 0,58 | 0,58 | 0,55 | 0,60 | 0,59 | 0,56 |
| | sum | 8,00 | 8,00 | 8,00 | 8,00 | 8,00 | 8,00 | 8,00 | 8,00 | 8,00 | 8,00 | 8,00 | 8,00 | 8,00 | 8,00 | 8,00 | 8,00 | 8,00 | 8,00 | 8,00 | 8,00 |
| | norm. coeff. | 0,21 | 0,20 | 0,21 | 0,21 | 0,21 | 0,21 | 0,21 | 0,21 | 0,21 | 0,21 | 0,21 | 0,21 | 0,20 | 0,21 | 0,21 | 0,21 | 0,21 | 0,21 | 0,21 | 0,21 |
| | xFe | 0,84 | 0,89 | 0,85 | 0,85 | 0,87 | 0,86 | 0,85 | 0,86 | 0,91 | 0,86 | 0,86 | 0,85 | 0,92 | 0,86 | 0,87 | 0,87 | 0,89 | 0,86 | 0,86 | 0,86 |
| | xAlm | 0,62 | 0,66 | 0,61 | 0,63 | 0,64 | 0,63 | 0,63 | 0,63 | 0,66 | 0,63 | 0,64 | 0,62 | 0,66 | 0,63 | 0,64 | 0,63 | 0,66 | 0,63 | 0,64 | 0,64 |
| | xPrp | 0,12 | 0,09 | 0,12 | 0,12 | 0,10 | 0,11 | 0,12 | 0,11 | 0,07 | 0,10 | 0,11 | 0,11 | 0,06 | 0,11 | 0,10 | 0,10 | 0,09 | 0,10 | 0,11 | 0,11 |
| | xGrs | 0,20 | 0,18 | 0,21 | 0,19 | 0,20 | 0,20 | 0,20 | 0,21 | 0,19 | 0,20 | 0,19 | 0,21 | 0,17 | 0,19 | 0,19 | 0,20 | 0,18 | 0,20 | 0,20 | 0,19 |
| | xSps | 0,06 | 0,07 | 0,06 | 0,06 | 0,06 | 0,06 | 0,06 | 0,06 | 0,08 | 0,06 | 0,06 | 0,06 | 0,11 | 0,06 | 0,06 | 0,07 | 0,07 | 0,06 | 0,06 | 0,06 |

**Annex II** – Mineral analyses, Depiné (2008).

| | Sample | 101203-1 | | | | | | | | | | | | | | | | | | |
|---|---|---|---|---|---|---|---|---|---|---|---|---|---|---|---|---|---|---|---|---|
| | **Ox. wt%** | **P90** | **P91** | **P92** | **P94** | **P95** | **P96** | **P97** | **P98** | **P99** | **P103** | **P106** | **P107** | **P109** | **P110** | **P111** | **P112** | **P114** | **P116** | **P117** | **P118** |
| | $SiO_2$ | 36,40 | 36,80 | 36,93 | 36,63 | 36,48 | 36,34 | 36,71 | 36,72 | 36,64 | 36,30 | 36,63 | 36,30 | 37,00 | 36,55 | 35,98 | 36,65 | 36,84 | 36,60 | 36,88 | 36,62 |
| | $TiO_2$ | 0,05 | 0,02 | 0,00 | 0,01 | 0,00 | 0,00 | 0,05 | 0,03 | 0,01 | 0,01 | 0,04 | 0,00 | 0,03 | 0,00 | 0,07 | 0,04 | 0,00 | 0,05 | 0,01 | 0,04 |
| | $Al_2O_3$ | 20,87 | 20,88 | 20,62 | 20,64 | 20,77 | 20,90 | 20,78 | 20,81 | 21,05 | 20,85 | 20,75 | 20,68 | 21,06 | 20,89 | 20,60 | 20,83 | 20,61 | 20,70 | 21,22 | 20,88 |
| | $Cr_2O_3$ | 0,00 | 0,03 | 0,02 | 0,00 | 0,00 | 0,00 | 0,00 | 0,02 | 0,01 | 0,02 | 0,00 | 0,01 | 0,00 | 0,05 | 0,00 | 0,01 | 0,03 | 0,01 | 0,03 | 0,00 |
| | $Fe_2O_3$ | 1,82 | 1,45 | 0,45 | 1,95 | 1,02 | 1,23 | 1,45 | 1,64 | 1,68 | 1,99 | 1,77 | 2,11 | 1,03 | 1,55 | 2,00 | 0,98 | 0,61 | 0,85 | 1,55 | 1,80 |
| | FeO | 28,49 | 28,51 | 29,56 | 27,76 | 28,30 | 28,04 | 27,53 | 27,54 | 27,47 | 27,37 | 27,19 | 28,24 | 27,91 | 27,94 | 28,63 | 28,79 | 29,68 | 28,83 | 27,73 | 26,02 |
| | MnO | 2,81 | 2,88 | 2,99 | 2,92 | 3,94 | 4,98 | 2,55 | 2,58 | 2,57 | 2,60 | 2,28 | 2,55 | 2,28 | 2,40 | 3,63 | 2,59 | 2,58 | 3,86 | 2,36 | 2,00 |
| | MgO | 2,31 | 2,59 | 2,19 | 2,53 | 1,35 | 1,27 | 2,67 | 2,69 | 2,74 | 2,72 | 3,04 | 2,55 | 2,77 | 2,87 | 1,80 | 2,57 | 2,45 | 1,85 | 2,81 | 2,99 |
| | CaO | 6,34 | 6,24 | 5,98 | 6,70 | 6,97 | 6,33 | 7,08 | 7,01 | 6,93 | 6,69 | 6,95 | 6,28 | 7,11 | 6,43 | 5,91 | 6,15 | 5,78 | 6,08 | 7,01 | 8,16 |
| | sum | 99,10 | 99,39 | 98,73 | 99,13 | 98,83 | 99,09 | 98,83 | 99,04 | 99,09 | 98,54 | 98,64 | 98,70 | 99,20 | 98,68 | 98,63 | 98,60 | 98,58 | 98,81 | 99,59 | 98,51 |
| | **Cations** | | | | | | | | | | | | | | | | | | | | |
| **Garnet** | Si | 2,95 | 2,96 | 3,00 | 2,96 | 2,97 | 2,96 | 2,96 | 2,96 | 2,95 | 2,94 | 2,96 | 2,95 | 2,97 | 2,96 | 2,94 | 2,97 | 2,99 | 2,98 | 2,95 | 2,95 |
| | Ti | 0,00 | 0,00 | 0,00 | 0,00 | 0,00 | 0,00 | 0,00 | 0,00 | 0,00 | 0,00 | 0,00 | 0,00 | 0,00 | 0,00 | 0,00 | 0,00 | 0,00 | 0,00 | 0,00 | 0,00 |
| | Al | 1,99 | 1,98 | 1,97 | 1,96 | 1,99 | 2,01 | 1,98 | 1,98 | 2,00 | 1,99 | 1,97 | 1,98 | 1,99 | 1,99 | 1,99 | 1,99 | 1,97 | 1,98 | 2,00 | 1,98 |
| | Cr | 0,00 | 0,00 | 0,00 | 0,00 | 0,00 | 0,00 | 0,00 | 0,00 | 0,00 | 0,00 | 0,00 | 0,00 | 0,00 | 0,00 | 0,00 | 0,00 | 0,00 | 0,00 | 0,00 | 0,00 |
| | $Fe^{3+}$ | 0,11 | 0,09 | 0,03 | 0,12 | 0,06 | 0,08 | 0,09 | 0,10 | 0,10 | 0,12 | 0,11 | 0,13 | 0,06 | 0,09 | 0,12 | 0,06 | 0,04 | 0,05 | 0,09 | 0,11 |
| | $Fe^{2+}$ | 1,93 | 1,92 | 2,01 | 1,87 | 1,93 | 1,91 | 1,86 | 1,86 | 1,85 | 1,86 | 1,84 | 1,92 | 1,87 | 1,89 | 1,96 | 1,95 | 2,02 | 1,96 | 1,86 | 1,75 |
| | Mn | 0,19 | 0,20 | 0,21 | 0,20 | 0,27 | 0,34 | 0,17 | 0,18 | 0,18 | 0,18 | 0,16 | 0,17 | 0,15 | 0,16 | 0,25 | 0,18 | 0,18 | 0,27 | 0,16 | 0,14 |
| | Mg | 0,28 | 0,31 | 0,27 | 0,30 | 0,16 | 0,15 | 0,32 | 0,32 | 0,33 | 0,33 | 0,37 | 0,31 | 0,33 | 0,35 | 0,22 | 0,31 | 0,30 | 0,22 | 0,33 | 0,36 |
| | Ca | 0,55 | 0,54 | 0,52 | 0,58 | 0,61 | 0,55 | 0,61 | 0,61 | 0,60 | 0,58 | 0,60 | 0,55 | 0,61 | 0,56 | 0,52 | 0,53 | 0,50 | 0,53 | 0,60 | 0,70 |
| | sum | 8,00 | 8,00 | 8,00 | 8,00 | 8,00 | 8,00 | 8,00 | 8,00 | 8,00 | 8,00 | 8,00 | 8,00 | 8,00 | 8,00 | 8,00 | 8,00 | 8,00 | 8,00 | 8,00 | 8,00 |
| | norm. coeff. | 0,21 | 0,21 | 0,20 | 0,21 | 0,20 | 0,20 | 0,21 | 0,21 | 0,21 | 0,21 | 0,21 | 0,21 | 0,21 | 0,21 | 0,20 | 0,21 | 0,20 | 0,20 | 0,21 | 0,21 |
| | xFe | 0,88 | 0,87 | 0,88 | 0,87 | 0,92 | 0,93 | 0,86 | 0,86 | 0,86 | 0,86 | 0,84 | 0,87 | 0,85 | 0,85 | 0,90 | 0,87 | 0,87 | 0,90 | 0,85 | 0,84 |
| | xAlm | 0,65 | 0,65 | 0,67 | 0,63 | 0,65 | 0,65 | 0,63 | 0,63 | 0,63 | 0,63 | 0,62 | 0,65 | 0,63 | 0,64 | 0,66 | 0,66 | 0,67 | 0,66 | 0,63 | 0,59 |
| | xPrp | 0,09 | 0,10 | 0,09 | 0,10 | 0,06 | 0,05 | 0,11 | 0,11 | 0,11 | 0,11 | 0,12 | 0,10 | 0,11 | 0,12 | 0,07 | 0,10 | 0,10 | 0,08 | 0,11 | 0,12 |
| | xGrs | 0,19 | 0,18 | 0,17 | 0,20 | 0,20 | 0,19 | 0,21 | 0,20 | 0,20 | 0,20 | 0,20 | 0,19 | 0,21 | 0,19 | 0,18 | 0,18 | 0,17 | 0,18 | 0,20 | 0,24 |
| | xSps | 0,07 | 0,07 | 0,07 | 0,07 | 0,09 | 0,12 | 0,06 | 0,06 | 0,06 | 0,06 | 0,05 | 0,06 | 0,05 | 0,06 | 0,09 | 0,06 | 0,06 | 0,09 | 0,05 | 0,05 |

**Annex II** – Mineral analyses, Depiné (2008).

| | Sample | 101203-1 | | | | | | | | | | | | | | | | | | |
|---|---|---|---|---|---|---|---|---|---|---|---|---|---|---|---|---|---|---|---|---|
| | **Ox. wt%** | **P119** | **P120** | **P121** | **P122** | **P124** | **P1** | **P2** | **P3** | **P4** | **P5** | **P6** | **P7** | **P8** | **P9** | **P10** | **P11** | **P12** | **P13** | **P14** | **P15** |
| **Garnet** | $SiO_2$ | 36,47 | 36,32 | 36,12 | 36,54 | 36,63 | 36,64 | 37,05 | 37,07 | 37,00 | 36,95 | 37,31 | 36,80 | 36,66 | 36,43 | 36,76 | 36,61 | 36,95 | 36,70 | 36,84 | 36,37 |
| | $TiO_2$ | 0,03 | 0,01 | 0,03 | 0,01 | 0,00 | 0,00 | 0,00 | 0,06 | 0,02 | 0,00 | 0,07 | 0,03 | 0,00 | 0,07 | 0,05 | 0,01 | 0,00 | 0,02 | 0,04 | 0,00 |
| | $Al_2O_3$ | 21,35 | 20,93 | 20,74 | 20,84 | 20,93 | 20,91 | 20,81 | 20,87 | 20,80 | 20,83 | 21,12 | 20,71 | 20,95 | 20,99 | 20,78 | 20,97 | 20,99 | 20,58 | 20,73 | 20,63 |
| | $Cr_2O_3$ | 0,00 | 0,00 | 0,04 | 0,01 | 0,03 | 0,00 | 0,04 | 0,00 | 0,04 | 0,00 | 0,04 | 0,01 | 0,04 | 0,01 | 0,01 | 0,00 | 0,00 | 0,00 | 0,01 | 0,00 |
| | $Fe_2O_3$ | 1,74 | 2,17 | 1,94 | 1,25 | 1,30 | 1,51 | 0,84 | 1,12 | 1,16 | 1,17 | 0,81 | 1,06 | 1,45 | 2,03 | 0,91 | 1,84 | 1,26 | 1,52 | 0,91 | 1,55 |
| | FeO | 27,14 | 28,38 | 28,75 | 29,23 | 27,90 | 27,29 | 28,10 | 27,15 | 27,92 | 26,91 | 27,67 | 28,22 | 27,54 | 27,08 | 28,30 | 27,73 | 27,59 | 27,79 | 28,62 | 28,55 |
| | MnO | 2,32 | 2,58 | 3,80 | 3,22 | 2,67 | 2,68 | 2,44 | 2,36 | 2,72 | 2,66 | 2,67 | 2,82 | 2,71 | 2,81 | 2,87 | 2,84 | 2,77 | 3,08 | 2,93 | 4,59 |
| | MgO | 2,83 | 2,75 | 2,00 | 2,22 | 2,87 | 2,88 | 3,03 | 2,97 | 2,58 | 2,82 | 3,01 | 2,63 | 2,57 | 2,62 | 2,51 | 2,50 | 2,63 | 2,55 | 2,45 | 1,52 |
| | CaO | 7,12 | 5,88 | 5,52 | 5,67 | 6,31 | 6,77 | 6,51 | 7,45 | 7,02 | 7,45 | 6,98 | 6,45 | 7,00 | 7,05 | 6,49 | 6,81 | 7,11 | 6,59 | 6,36 | 5,92 |
| | sum | 98,98 | 99,02 | 98,93 | 98,99 | 98,64 | 98,67 | 98,81 | 99,06 | 99,24 | 98,79 | 99,68 | 98,75 | 98,92 | 99,09 | 98,68 | 99,30 | 99,30 | 98,84 | 98,89 | 99,13 |
| | **Cations** | | | | | | | | | | | | | | | | | | | | |
| | Si | 2,93 | 2,94 | 2,94 | 2,96 | 2,96 | 2,96 | 2,99 | 2,98 | 2,98 | 2,98 | 2,98 | 2,98 | 2,96 | 2,94 | 2,98 | 2,95 | 2,97 | 2,97 | 2,98 | 2,96 |
| | Ti | 0,00 | 0,00 | 0,00 | 0,00 | 0,00 | 0,00 | 0,00 | 0,00 | 0,00 | 0,00 | 0,00 | 0,00 | 0,00 | 0,00 | 0,00 | 0,00 | 0,00 | 0,00 | 0,00 | 0,00 |
| | Al | 2,02 | 1,99 | 1,99 | 1,99 | 1,99 | 1,99 | 1,98 | 1,97 | 1,97 | 1,98 | 1,99 | 1,97 | 1,99 | 1,99 | 1,98 | 1,99 | 1,99 | 1,96 | 1,98 | 1,98 |
| | Cr | 0,00 | 0,00 | 0,00 | 0,00 | 0,00 | 0,00 | 0,00 | 0,00 | 0,00 | 0,00 | 0,00 | 0,00 | 0,00 | 0,00 | 0,00 | 0,00 | 0,00 | 0,00 | 0,00 | 0,00 |
| | $Fe^{3+}$ | 0,11 | 0,13 | 0,12 | 0,08 | 0,08 | 0,09 | 0,05 | 0,07 | 0,07 | 0,07 | 0,05 | 0,06 | 0,09 | 0,12 | 0,06 | 0,11 | 0,08 | 0,09 | 0,06 | 0,10 |
| | $Fe^{2+}$ | 1,83 | 1,92 | 1,96 | 1,98 | 1,89 | 1,84 | 1,89 | 1,82 | 1,88 | 1,81 | 1,85 | 1,91 | 1,86 | 1,83 | 1,92 | 1,87 | 1,85 | 1,88 | 1,94 | 1,94 |
| | Mn | 0,16 | 0,18 | 0,26 | 0,22 | 0,18 | 0,18 | 0,17 | 0,16 | 0,19 | 0,18 | 0,18 | 0,19 | 0,19 | 0,19 | 0,20 | 0,19 | 0,19 | 0,21 | 0,20 | 0,32 |
| | Mg | 0,34 | 0,33 | 0,24 | 0,27 | 0,35 | 0,35 | 0,36 | 0,36 | 0,31 | 0,34 | 0,36 | 0,32 | 0,31 | 0,31 | 0,30 | 0,30 | 0,32 | 0,31 | 0,29 | 0,18 |
| | Ca | 0,61 | 0,51 | 0,48 | 0,49 | 0,55 | 0,59 | 0,56 | 0,64 | 0,61 | 0,64 | 0,60 | 0,56 | 0,61 | 0,61 | 0,56 | 0,59 | 0,61 | 0,57 | 0,55 | 0,52 |
| | sum | 8,00 | 8,00 | 8,00 | 8,00 | 8,00 | 8,00 | 8,00 | 8,00 | 8,00 | 8,00 | 8,00 | 8,00 | 8,00 | 8,00 | 8,00 | 8,00 | 8,00 | 8,00 | 8,00 | 8,00 |
| | norm. coeff. | 0,21 | 0,21 | 0,20 | 0,21 | 0,21 | 0,21 | 0,21 | 0,21 | 0,21 | 0,21 | 0,21 | 0,21 | 0,21 | 0,21 | 0,21 | 0,21 | 0,21 | 0,21 | 0,21 | 0,20 |
| | xFe | 0,85 | 0,86 | 0,90 | 0,88 | 0,85 | 0,85 | 0,84 | 0,84 | 0,86 | 0,85 | 0,84 | 0,86 | 0,86 | 0,86 | 0,87 | 0,87 | 0,86 | 0,86 | 0,87 | 0,92 |
| | xAlm | 0,62 | 0,65 | 0,67 | 0,67 | 0,64 | 0,62 | 0,63 | 0,61 | 0,63 | 0,61 | 0,62 | 0,64 | 0,63 | 0,62 | 0,64 | 0,63 | 0,62 | 0,63 | 0,65 | 0,66 |
| | xPrp | 0,12 | 0,11 | 0,08 | 0,09 | 0,12 | 0,12 | 0,12 | 0,12 | 0,10 | 0,11 | 0,12 | 0,11 | 0,10 | 0,11 | 0,10 | 0,10 | 0,11 | 0,10 | 0,10 | 0,06 |
| | xGrs | 0,21 | 0,17 | 0,16 | 0,17 | 0,18 | 0,20 | 0,19 | 0,22 | 0,20 | 0,22 | 0,20 | 0,19 | 0,20 | 0,21 | 0,19 | 0,20 | 0,21 | 0,19 | 0,18 | 0,17 |
| | xSps | 0,05 | 0,06 | 0,09 | 0,07 | 0,06 | 0,06 | 0,06 | 0,05 | 0,06 | 0,06 | 0,06 | 0,06 | 0,06 | 0,07 | 0,07 | 0,07 | 0,06 | 0,07 | 0,07 | 0,11 |

**Annex II** – Mineral analyses, Depiné (2008).

| | Sample | 101203-1 | | | | | | | | | | | | | | | | | | |
|---|---|---|---|---|---|---|---|---|---|---|---|---|---|---|---|---|---|---|---|---|
| | **Ox. wt%** | **P17** | **P18** | **P19** | **P20** | **P21** | **P22** | **P24** | **P26** | **P34** | **P35** | **P38** | **P42** | **P43** | **P45** | **P46** | **P49** | **P53** | **P56** | **P57** | **P59** |
| **Garnet** | $SiO_2$ | 36,32 | 36,28 | 36,63 | 36,97 | 35,94 | 36,77 | 36,79 | 36,79 | 37,02 | 36,83 | 36,89 | 37,29 | 36,79 | 37,10 | 37,19 | 36,87 | 36,71 | 37,21 | 37,30 | 36,52 |
| | $TiO_2$ | 0,01 | 0,02 | 0,00 | 0,04 | 0,00 | 0,05 | 0,02 | 0,03 | 0,05 | 0,03 | 0,04 | 0,00 | 0,00 | 0,06 | 0,00 | 0,01 | 0,05 | 0,05 | 0,03 | 0,06 |
| | $Al_2O_3$ | 20,70 | 20,52 | 20,91 | 20,96 | 20,85 | 20,74 | 21,15 | 21,18 | 20,96 | 21,06 | 21,06 | 21,36 | 21,08 | 21,14 | 21,10 | 21,13 | 21,05 | 21,11 | 21,00 | 20,83 |
| | $Cr_2O_3$ | 0,00 | 0,00 | 0,00 | 0,00 | 0,00 | 0,00 | 0,06 | 0,00 | 0,01 | 0,03 | 0,00 | 0,03 | 0,00 | 0,00 | 0,01 | 0,02 | 0,03 | 0,01 | 0,02 | 0,06 |
| | $Fe_2O_3$ | 1,21 | 1,40 | 1,67 | 1,46 | 2,50 | 0,83 | 1,62 | 1,89 | 1,15 | 1,98 | 1,34 | 1,07 | 1,86 | 1,08 | 1,09 | 0,93 | 1,39 | 0,76 | 1,07 | 0,98 |
| | FeO | 28,87 | 29,40 | 28,15 | 28,48 | 28,16 | 29,09 | 28,55 | 26,73 | 27,67 | 26,40 | 27,16 | 26,89 | 27,03 | 27,31 | 27,06 | 28,07 | 28,70 | 27,84 | 27,67 | 29,14 |
| | MnO | 4,22 | 4,32 | 2,99 | 3,00 | 2,89 | 2,90 | 2,97 | 2,73 | 2,34 | 2,21 | 2,41 | 1,72 | 2,10 | 1,84 | 1,86 | 2,36 | 2,42 | 1,98 | 1,72 | 3,62 |
| | MgO | 1,69 | 1,33 | 2,46 | 2,56 | 2,20 | 2,43 | 2,28 | 2,37 | 3,02 | 3,17 | 2,93 | 3,40 | 3,14 | 3,26 | 3,28 | 2,60 | 2,67 | 3,19 | 3,34 | 1,82 |
| | CaO | 5,69 | 5,66 | 6,43 | 6,37 | 6,22 | 5,98 | 6,54 | 8,04 | 6,95 | 7,64 | 7,27 | 7,72 | 7,21 | 7,37 | 7,55 | 7,02 | 6,27 | 7,03 | 7,23 | 5,99 |
| | sum | 98,71 | 98,92 | 99,23 | 99,83 | 98,76 | 98,78 | 99,99 | 99,74 | 99,16 | 99,34 | 99,10 | 99,49 | 99,22 | 99,15 | 99,14 | 99,01 | 99,29 | 99,18 | 99,39 | 99,02 |
| | **Cations** | | | | | | | | | | | | | | | | | | | | |
| | Si | 2,97 | 2,97 | 2,96 | 2,96 | 2,92 | 2,98 | 2,95 | 2,94 | 2,97 | 2,95 | 2,96 | 2,97 | 2,95 | 2,97 | 2,97 | 2,97 | 2,96 | 2,98 | 2,98 | 2,97 |
| | Ti | 0,00 | 0,00 | 0,00 | 0,00 | 0,00 | 0,00 | 0,00 | 0,00 | 0,00 | 0,00 | 0,00 | 0,00 | 0,00 | 0,00 | 0,00 | 0,00 | 0,00 | 0,00 | 0,00 | 0,00 |
| | Al | 1,99 | 1,98 | 1,99 | 1,98 | 2,00 | 1,98 | 2,00 | 2,00 | 1,98 | 1,98 | 1,99 | 2,00 | 1,99 | 1,99 | 1,99 | 2,00 | 2,00 | 1,99 | 1,98 | 1,99 |
| | Cr | 0,00 | 0,00 | 0,00 | 0,00 | 0,00 | 0,00 | 0,00 | 0,00 | 0,00 | 0,00 | 0,00 | 0,00 | 0,00 | 0,00 | 0,00 | 0,00 | 0,00 | 0,00 | 0,00 | 0,00 |
| | $Fe^{3+}$ | 0,07 | 0,09 | 0,10 | 0,09 | 0,15 | 0,05 | 0,10 | 0,11 | 0,07 | 0,12 | 0,08 | 0,06 | 0,11 | 0,07 | 0,07 | 0,06 | 0,08 | 0,05 | 0,06 | 0,06 |
| | $Fe^{2+}$ | 1,97 | 2,01 | 1,90 | 1,91 | 1,92 | 1,97 | 1,91 | 1,79 | 1,86 | 1,77 | 1,82 | 1,79 | 1,81 | 1,83 | 1,81 | 1,89 | 1,93 | 1,86 | 1,85 | 1,98 |
| | Mn | 0,29 | 0,30 | 0,20 | 0,20 | 0,20 | 0,20 | 0,20 | 0,18 | 0,16 | 0,15 | 0,16 | 0,12 | 0,14 | 0,12 | 0,13 | 0,16 | 0,17 | 0,13 | 0,12 | 0,25 |
| | Mg | 0,21 | 0,16 | 0,30 | 0,31 | 0,27 | 0,29 | 0,27 | 0,28 | 0,36 | 0,38 | 0,35 | 0,40 | 0,38 | 0,39 | 0,39 | 0,31 | 0,32 | 0,38 | 0,40 | 0,22 |
| | Ca | 0,50 | 0,50 | 0,56 | 0,55 | 0,54 | 0,52 | 0,56 | 0,69 | 0,60 | 0,65 | 0,63 | 0,66 | 0,62 | 0,63 | 0,65 | 0,61 | 0,54 | 0,60 | 0,62 | 0,52 |
| | sum | 8,00 | 8,00 | 8,00 | 8,00 | 8,00 | 8,00 | 8,00 | 8,00 | 8,00 | 8,00 | 8,00 | 8,00 | 8,00 | 8,00 | 8,00 | 8,00 | 8,00 | 8,00 | 8,00 | 8,00 |
| | norm. coeff. | 0,20 | 0,20 | 0,21 | 0,21 | 0,20 | 0,21 | 0,21 | 0,21 | 0,21 | 0,21 | 0,21 | 0,21 | 0,21 | 0,21 | 0,21 | 0,21 | 0,21 | 0,21 | 0,21 | 0,20 |
| | xFe | 0,91 | 0,93 | 0,87 | 0,87 | 0,89 | 0,87 | 0,88 | 0,87 | 0,84 | 0,83 | 0,84 | 0,82 | 0,84 | 0,83 | 0,83 | 0,86 | 0,86 | 0,83 | 0,83 | 0,90 |
| | xAlm | 0,66 | 0,68 | 0,64 | 0,64 | 0,66 | 0,66 | 0,65 | 0,61 | 0,62 | 0,60 | 0,62 | 0,60 | 0,61 | 0,61 | 0,61 | 0,64 | 0,65 | 0,63 | 0,62 | 0,67 |
| | xPrp | 0,07 | 0,05 | 0,10 | 0,10 | 0,09 | 0,10 | 0,09 | 0,10 | 0,12 | 0,13 | 0,12 | 0,14 | 0,13 | 0,13 | 0,13 | 0,11 | 0,11 | 0,13 | 0,13 | 0,07 |
| | xGrs | 0,17 | 0,17 | 0,19 | 0,18 | 0,19 | 0,17 | 0,19 | 0,23 | 0,20 | 0,22 | 0,21 | 0,22 | 0,21 | 0,21 | 0,22 | 0,20 | 0,18 | 0,20 | 0,21 | 0,18 |
| | xSps | 0,10 | 0,10 | 0,07 | 0,07 | 0,07 | 0,07 | 0,07 | 0,06 | 0,05 | 0,05 | 0,06 | 0,04 | 0,05 | 0,04 | 0,04 | 0,05 | 0,06 | 0,05 | 0,04 | 0,08 |

**Annex II** – Mineral analyses, Depiné (2008).

| | Sample | 101203-1 | 101203-2 | | | | | | | | | | | | | | | | | |
|---|---|---|---|---|---|---|---|---|---|---|---|---|---|---|---|---|---|---|---|---|
| | **Ox. wt%** | **P 64** | **P 2** | **P 3** | **P 4** | **P 5** | **P 6** | **P 7** | **P 8** | **P 9** | **P 3** | **P 5** | **P 7** | **P 8** | **P 9** | **P 1** | **P 2** | **P 3** | **P 4** | **P 5** | **P 7** |
| **Garnet** | $SiO_2$ | 37,31 | 37,86 | 37,57 | 37,55 | 37,73 | 37,84 | 37,24 | 36,99 | 37,34 | 37,26 | 37,37 | 37,91 | 37,61 | 37,38 | 37,05 | 37,31 | 37,56 | 37,64 | 37,37 | 37,43 |
| | $TiO_2$ | 0,04 | 0,04 | 0,03 | 0,05 | 0,03 | 0,00 | 0,05 | 0,10 | 0,01 | 0,05 | 0,02 | 0,07 | 0,03 | 0,09 | 0,03 | 0,01 | 0,06 | 0,00 | 0,04 | 0,10 |
| | $Al_2O_3$ | 3,00 | 20,94 | 20,94 | 20,67 | 20,71 | 20,95 | 21,01 | 20,61 | 20,54 | 20,51 | 20,25 | 20,89 | 20,90 | 21,00 | 20,70 | 20,40 | 20,78 | 20,76 | 20,87 | 20,78 |
| | $Cr_2O_3$ | 0,03 | 0,00 | 0,00 | 0,02 | 0,00 | 0,02 | 0,06 | 0,01 | 0,00 | 0,00 | 0,02 | 0,00 | 0,00 | 0,00 | 0,01 | 0,00 | 0,00 | 0,00 | 0,01 | 0,01 |
| | $Fe_2O_3$ | 0,68 | 0,16 | 0,42 | 0,34 | 0,55 | 0,37 | 0,75 | 1,16 | 0,99 | 0,67 | 1,13 | 0,02 | 0,91 | 0,52 | 1,11 | 1,10 | 0,14 | 0,19 | 1,32 | 0,59 |
| | FeO | 28,15 | 29,41 | 27,94 | 27,19 | 27,35 | 27,36 | 26,88 | 26,34 | 26,93 | 26,70 | 26,57 | 27,29 | 27,06 | 27,29 | 29,31 | 27,16 | 27,27 | 27,28 | 26,70 | 27,93 |
| | MnO | 2,08 | 1,44 | 1,56 | 1,83 | 1,97 | 2,13 | 1,91 | 2,10 | 2,18 | 1,43 | 1,73 | 1,88 | 1,94 | 1,94 | 1,53 | 1,74 | 1,87 | 2,14 | 2,07 | 2,03 |
| | MgO | 3,24 | 2,33 | 2,31 | 2,30 | 2,38 | 2,43 | 2,35 | 2,47 | 2,38 | 2,26 | 2,50 | 2,46 | 2,57 | 2,39 | 2,27 | 2,36 | 2,53 | 2,22 | 2,49 | 2,46 |
| | CaO | 6,72 | 8,02 | 8,85 | 9,22 | 9,03 | 8,91 | 9,04 | 8,93 | 8,82 | 9,69 | 9,32 | 9,23 | 8,89 | 8,80 | 7,35 | 8,98 | 8,81 | 9,07 | 8,98 | 8,19 |
| | sum | 99,20 | 100,20 | 99,35 | 99,21 | 99,99 | 100,06 | 98,89 | 98,63 | 99,15 | 98,32 | 99,54 | 99,75 | 100,01 | 99,11 | 99,06 | 99,43 | 99,01 | 99,41 | 99,76 | 99,54 |
| | **Cations** | | | | | | | | | | | | | | | | | | | | |
| | Si | 2,99 | 3,01 | 3,01 | 3,01 | 3,00 | 3,01 | 3,00 | 2,98 | 3,00 | 3,01 | 2,98 | 3,02 | 2,99 | 3,00 | 2,99 | 2,99 | 3,01 | 3,01 | 2,98 | 3,00 |
| | Ti | 0,00 | 0,00 | 0,00 | 0,00 | 0,00 | 0,00 | 0,00 | 0,01 | 0,00 | 0,00 | 0,00 | 0,00 | 0,00 | 0,01 | 0,00 | 0,00 | 0,00 | 0,00 | 0,00 | 0,01 |
| | Al | 1,98 | 1,96 | 1,95 | 1,96 | 1,96 | 1,97 | 1,95 | 1,95 | 1,94 | 1,93 | 1,96 | 1,96 | 1,97 | 1,96 | 1,94 | 1,96 | 1,96 | 1,97 | 1,95 | 1,96 |
| | Cr | 0,00 | 0,00 | 0,00 | 0,00 | 0,00 | 0,00 | 0,00 | 0,00 | 0,00 | 0,00 | 0,00 | 0,00 | 0,00 | 0,00 | 0,00 | 0,00 | 0,00 | 0,00 | 0,00 | 0,00 |
| | $Fe^{3+}$ | 0,04 | 0,01 | 0,03 | 0,02 | 0,03 | 0,02 | 0,05 | 0,07 | 0,06 | 0,04 | 0,07 | 0,00 | 0,05 | 0,03 | 0,07 | 0,07 | 0,01 | 0,01 | 0,08 | 0,04 |
| | $Fe^{2+}$ | 1,89 | 1,96 | 1,87 | 1,82 | 1,82 | 1,82 | 1,81 | 1,78 | 1,81 | 1,80 | 1,77 | 1,82 | 1,80 | 1,83 | 1,98 | 1,82 | 1,83 | 1,82 | 1,78 | 1,87 |
| | Mn | 0,14 | 0,10 | 0,11 | 0,12 | 0,13 | 0,14 | 0,13 | 0,14 | 0,15 | 0,10 | 0,12 | 0,13 | 0,13 | 0,13 | 0,10 | 0,12 | 0,13 | 0,15 | 0,14 | 0,14 |
| | Mg | 0,39 | 0,28 | 0,28 | 0,27 | 0,28 | 0,29 | 0,28 | 0,30 | 0,28 | 0,27 | 0,30 | 0,29 | 0,30 | 0,29 | 0,27 | 0,28 | 0,30 | 0,26 | 0,30 | 0,29 |
| | Ca | 0,58 | 0,68 | 0,76 | 0,79 | 0,77 | 0,76 | 0,78 | 0,77 | 0,76 | 0,84 | 0,80 | 0,79 | 0,76 | 0,76 | 0,64 | 0,77 | 0,76 | 0,78 | 0,77 | 0,70 |
| | sum | 8,00 | 8,00 | 8,00 | 8,00 | 8,00 | 8,00 | 8,00 | 8,00 | 8,00 | 8,00 | 8,00 | 8,00 | 8,00 | 8,00 | 8,00 | 8,00 | 8,00 | 8,00 | 8,00 | 8,00 |
| | norm. coeff. | 0,21 | 0,21 | 0,21 | 0,21 | 0,21 | 0,21 | 0,21 | 0,21 | 0,21 | 0,21 | 0,21 | 0,21 | 0,21 | 0,21 | 0,21 | 0,21 | 0,21 | 0,21 | 0,21 | 0,21 |
| | xFe | 0,83 | 0,88 | 0,87 | 0,87 | 0,87 | 0,86 | 0,87 | 0,86 | 0,87 | 0,87 | 0,86 | 0,86 | 0,86 | 0,87 | 0,88 | 0,87 | 0,86 | 0,87 | 0,86 | 0,87 |
| | xAlm | 0,63 | 0,65 | 0,62 | 0,60 | 0,61 | 0,60 | 0,60 | 0,59 | 0,60 | 0,60 | 0,59 | 0,60 | 0,60 | 0,61 | 0,66 | 0,61 | 0,61 | 0,61 | 0,60 | 0,62 |
| | xPrp | 0,13 | 0,09 | 0,09 | 0,09 | 0,09 | 0,10 | 0,09 | 0,10 | 0,09 | 0,09 | 0,10 | 0,10 | 0,10 | 0,10 | 0,09 | 0,09 | 0,10 | 0,09 | 0,10 | 0,10 |
| | xGrs | 0,19 | 0,23 | 0,25 | 0,26 | 0,26 | 0,25 | 0,26 | 0,26 | 0,25 | 0,28 | 0,27 | 0,26 | 0,25 | 0,25 | 0,21 | 0,26 | 0,25 | 0,26 | 0,26 | 0,23 |
| | xSps | 0,05 | 0,03 | 0,04 | 0,04 | 0,04 | 0,05 | 0,04 | 0,05 | 0,05 | 0,03 | 0,04 | 0,04 | 0,04 | 0,04 | 0,03 | 0,04 | 0,04 | 0,05 | 0,05 | 0,05 |

**Annex II** – Mineral analyses, Depiné (2008).

| | Sample | 101203-2 | | | | | | | 200900-1 | | | | | | | | | | | | | |
|---|---|---|---|---|---|---|---|---|---|---|---|---|---|---|---|---|---|---|---|---|---|---|
| | **Ox. wt%** | **P8** | **P1** | **P4** | **P5** | **P6** | **P9** | **P10** | **P2** | **P3** | **P4** | **P5** | **P7** | **P8** | **P1** | **P2** | **P3** | **P5** | **P6** | **P7** | **P8** |
| **Garnet** | $SiO_2$ | 37,23 | 37,05 | 36,85 | 37,56 | 37,46 | 37,37 | 37,35 | 37,43 | 36,92 | 36,97 | 37,22 | 37,15 | 36,70 | 37,29 | 37,10 | 37,39 | 37,08 | 37,00 | 37,23 | 37,09 |
| | $TiO_2$ | 0,03 | 0,02 | 0,07 | 0,04 | 0,04 | 0,05 | 0,05 | 0,00 | 0,05 | 0,05 | 0,04 | 0,05 | 0,01 | 0,01 | 0,00 | 0,07 | 0,04 | 0,04 | 0,02 | 0,02 |
| | $Al_2O_3$ | 21,07 | 20,83 | 20,71 | 20,79 | 21,17 | 20,52 | 20,52 | 21,05 | 20,69 | 20,64 | 20,88 | 20,91 | 20,60 | 20,91 | 20,81 | 20,82 | 20,59 | 20,63 | 20,86 | 20,77 |
| | $Cr_2O_3$ | 0,00 | 0,00 | 0,01 | 0,00 | 0,00 | 0,00 | 0,00 | 0,02 | 0,00 | 0,00 | 0,02 | 0,03 | 0,02 | 0,02 | 0,00 | 0,00 | 0,00 | 0,02 | 0,02 | 0,01 |
| | $Fe_2O_3$ | 1,37 | 1,78 | 1,75 | 0,15 | 1,17 | 0,97 | 0,67 | 0,31 | 0,81 | 0,86 | 0,35 | 0,71 | 1,69 | 0,17 | 0,42 | 0,42 | 0,56 | 0,35 | 0,68 | 0,73 |
| | FeO | 27,18 | 27,81 | 26,33 | 27,07 | 27,02 | 27,37 | 29,83 | 33,56 | 33,01 | 32,07 | 32,84 | 32,52 | 32,41 | 33,82 | 34,13 | 33,90 | 33,21 | 33,26 | 33,33 | 33,19 |
| | MnO | 1,67 | 1,58 | 1,84 | 1,76 | 1,61 | 1,46 | 1,50 | 1,83 | 2,38 | 2,98 | 2,86 | 2,61 | 2,03 | 1,42 | 1,60 | 1,83 | 2,38 | 2,81 | 2,17 | 1,89 |
| | MgO | 2,47 | 2,32 | 2,47 | 2,23 | 2,39 | 2,27 | 2,40 | 2,87 | 2,73 | 2,46 | 2,35 | 2,44 | 2,75 | 2,80 | 2,71 | 3,02 | 2,92 | 2,57 | 3,26 | 3,32 |
| | CaO | 8,79 | 8,43 | 9,00 | 9,46 | 9,31 | 9,23 | 7,10 | 3,31 | 3,05 | 3,73 | 3,61 | 3,86 | 3,54 | 3,40 | 2,97 | 2,85 | 2,77 | 2,81 | 2,50 | 2,62 |
| | sum | 99,81 | 99,81 | 99,01 | 99,06 | 100,17 | 99,25 | 99,41 | 100,38 | 99,63 | 99,76 | 100,18 | 100,29 | 99,73 | 99,85 | 99,73 | 100,31 | 99,54 | 99,48 | 100,07 | 99,64 |
| | **Cations** | | | | | | | | | | | | | | | | | | | | |
| | Si | 2,97 | 2,96 | 2,96 | 3,01 | 2,97 | 3,00 | 3,00 | 3,00 | 2,99 | 2,99 | 3,00 | 2,98 | 2,97 | 3,00 | 3,00 | 3,00 | 3,00 | 3,00 | 2,99 | 2,99 |
| | Ti | 0,00 | 0,00 | 0,00 | 0,00 | 0,00 | 0,00 | 0,00 | 0,00 | 0,00 | 0,00 | 0,00 | 0,00 | 0,00 | 0,00 | 0,00 | 0,00 | 0,00 | 0,00 | 0,00 | 0,00 |
| | Al | 1,98 | 1,96 | 1,96 | 1,96 | 1,98 | 1,94 | 1,95 | 1,99 | 1,97 | 1,97 | 1,98 | 1,98 | 1,96 | 1,98 | 1,98 | 1,97 | 1,96 | 1,97 | 1,97 | 1,97 |
| | Cr | 0,00 | 0,00 | 0,00 | 0,00 | 0,00 | 0,00 | 0,00 | 0,00 | 0,00 | 0,00 | 0,00 | 0,00 | 0,00 | 0,00 | 0,00 | 0,00 | 0,00 | 0,00 | 0,00 | 0,00 |
| | $Fe^{3+}$ | 0,08 | 0,11 | 0,11 | 0,01 | 0,07 | 0,06 | 0,04 | 0,02 | 0,05 | 0,05 | 0,02 | 0,04 | 0,10 | 0,01 | 0,03 | 0,03 | 0,03 | 0,02 | 0,04 | 0,04 |
| | $Fe^{2+}$ | 1,81 | 1,86 | 1,77 | 1,81 | 1,79 | 1,84 | 2,01 | 2,25 | 2,23 | 2,17 | 2,21 | 2,18 | 2,19 | 2,28 | 2,30 | 2,27 | 2,25 | 2,26 | 2,24 | 2,24 |
| | Mn | 0,11 | 0,11 | 0,12 | 0,12 | 0,11 | 0,10 | 0,10 | 0,12 | 0,16 | 0,20 | 0,20 | 0,18 | 0,14 | 0,10 | 0,11 | 0,12 | 0,16 | 0,19 | 0,15 | 0,13 |
| | Mg | 0,29 | 0,28 | 0,30 | 0,27 | 0,28 | 0,27 | 0,29 | 0,34 | 0,33 | 0,30 | 0,28 | 0,29 | 0,33 | 0,34 | 0,33 | 0,36 | 0,35 | 0,31 | 0,39 | 0,40 |
| | Ca | 0,75 | 0,72 | 0,77 | 0,81 | 0,79 | 0,79 | 0,61 | 0,28 | 0,26 | 0,32 | 0,31 | 0,33 | 0,31 | 0,29 | 0,26 | 0,24 | 0,24 | 0,24 | 0,21 | 0,23 |
| | sum | 8,00 | 8,00 | 8,00 | 8,00 | 8,00 | 8,00 | 8,00 | 8,00 | 8,00 | 8,00 | 8,00 | 8,00 | 8,00 | 8,00 | 8,00 | 8,00 | 8,00 | 8,00 | 8,00 | 8,00 |
| | norm. coeff. | 0,21 | 0,21 | 0,21 | 0,21 | 0,21 | 0,21 | 0,21 | 0,21 | 0,21 | 0,21 | 0,21 | 0,21 | 0,21 | 0,21 | 0,21 | 0,21 | 0,21 | 0,21 | 0,21 | 0,21 |
| | xFe | 0,87 | 0,88 | 0,86 | 0,87 | 0,87 | 0,87 | 0,88 | 0,87 | 0,87 | 0,88 | 0,89 | 0,88 | 0,87 | 0,87 | 0,88 | 0,86 | 0,87 | 0,88 | 0,85 | 0,85 |
| | xAlm | 0,61 | 0,63 | 0,60 | 0,60 | 0,60 | 0,61 | 0,67 | 0,75 | 0,75 | 0,72 | 0,74 | 0,73 | 0,74 | 0,76 | 0,77 | 0,76 | 0,75 | 0,75 | 0,75 | 0,75 |
| | xPrp | 0,10 | 0,09 | 0,10 | 0,09 | 0,09 | 0,09 | 0,10 | 0,11 | 0,11 | 0,10 | 0,09 | 0,10 | 0,11 | 0,11 | 0,11 | 0,12 | 0,12 | 0,10 | 0,13 | 0,13 |
| | xGrs | 0,25 | 0,24 | 0,26 | 0,27 | 0,27 | 0,26 | 0,20 | 0,09 | 0,09 | 0,11 | 0,10 | 0,11 | 0,10 | 0,10 | 0,09 | 0,08 | 0,08 | 0,08 | 0,07 | 0,08 |
| | xSps | 0,04 | 0,04 | 0,04 | 0,04 | 0,04 | 0,03 | 0,03 | 0,04 | 0,05 | 0,07 | 0,07 | 0,06 | 0,05 | 0,03 | 0,04 | 0,04 | 0,05 | 0,06 | 0,05 | 0,04 |

**Annex II** – Mineral analyses, Depiné (2008).

| | Sample | 200900-1 | | | | | 231104-1 | | | | | | | | | | | | | | |
|---|---|---|---|---|---|---|---|---|---|---|---|---|---|---|---|---|---|---|---|---|---|
| | **Ox. wt%** | **P9** | **P 10** | **P 1** | **P 2** | **P 3** | **P1** | **P 2** | **P 3** | **P 4** | **P 5** | **P 7** | **P 8** | **P 9** | **P 10** | **P 11** | **P 12** | **P 13** | **P 14** | **P 15** | **P 16** |
| **Garnet** | $SiO_2$ | 37,19 | 37,35 | 36,96 | 36,84 | 37,24 | 36,43 | 36,40 | 36,73 | 36,60 | 36,90 | 36,62 | 36,62 | 36,76 | 36,35 | 36,74 | 36,80 | 36,57 | 36,88 | 36,68 | 36,87 |
| | $TiO_2$ | 0,04 | 0,00 | 0,06 | 0,03 | 0,03 | 0,00 | 0,02 | 0,04 | 0,07 | 0,02 | 0,07 | 0,00 | 0,03 | 0,08 | 0,05 | 0,02 | 0,08 | 0,07 | 0,07 | 0,07 |
| | $Al_2O_3$ | 20,77 | 20,98 | 20,90 | 21,00 | 20,99 | 20,69 | 20,55 | 20,86 | 20,77 | 20,88 | 20,66 | 20,58 | 20,76 | 20,44 | 20,58 | 20,72 | 20,46 | 20,87 | 20,59 | 20,71 |
| | $Cr_2O_3$ | 0,03 | 0,00 | 0,00 | 0,04 | 0,02 | 0,02 | 0,00 | 0,03 | 0,00 | 0,00 | 0,00 | 0,00 | 0,00 | 0,02 | 0,02 | 0,02 | 0,00 | 0,03 | 0,01 | 0,00 |
| | $Fe_2O_3$ | 0,13 | 0,91 | 1,07 | 0,90 | 0,46 | 1,35 | 0,34 | 1,11 | 0,90 | 0,88 | 1,20 | 0,64 | 0,77 | 1,22 | 0,70 | 0,61 | 0,72 | 0,96 | 0,87 | 0,43 |
| | FeO | 33,74 | 33,24 | 32,79 | 32,42 | 32,98 | 35,48 | 34,65 | 34,72 | 34,10 | 33,89 | 31,87 | 29,52 | 28,25 | 28,39 | 29,20 | 29,49 | 28,81 | 28,33 | 28,77 | 28,82 |
| | MnO | 1,78 | 1,55 | 1,51 | 2,50 | 2,08 | 1,61 | 2,99 | 1,20 | 1,66 | 2,14 | 3,53 | 5,71 | 6,51 | 6,54 | 6,54 | 6,31 | 6,42 | 6,15 | 6,06 | 5,58 |
| | MgO | 2,93 | 3,12 | 3,00 | 2,93 | 2,96 | 1,69 | 0,82 | 1,70 | 1,14 | 1,18 | 1,01 | 0,82 | 0,80 | 0,82 | 0,73 | 0,63 | 0,79 | 0,79 | 0,78 | 0,85 |
| | CaO | 2,91 | 3,35 | 3,58 | 3,06 | 3,28 | 2,68 | 3,44 | 3,91 | 4,69 | 4,66 | 5,16 | 5,49 | 6,02 | 5,51 | 5,36 | 5,47 | 5,54 | 6,39 | 5,96 | 6,39 |
| | sum | 99,52 | 100,52 | 99,85 | 99,70 | 100,03 | 99,94 | 99,22 | 100,30 | 99,93 | 100,55 | 100,11 | 99,37 | 99,89 | 99,36 | 99,91 | 100,08 | 99,38 | 100,46 | 99,78 | 99,71 |
| | **Cations** | | | | | | | | | | | | | | | | | | | | |
| | Si | 3,00 | 2,98 | 2,97 | 2,97 | 2,99 | 2,97 | 2,99 | 2,97 | 2,97 | 2,98 | 2,97 | 2,99 | 2,98 | 2,97 | 2,99 | 2,99 | 2,99 | 2,97 | 2,98 | 2,99 |
| | Ti | 0,00 | 0,00 | 0,00 | 0,00 | 0,00 | 0,00 | 0,00 | 0,00 | 0,00 | 0,00 | 0,00 | 0,00 | 0,00 | 0,00 | 0,00 | 0,00 | 0,01 | 0,00 | 0,00 | 0,00 |
| | Al | 1,98 | 1,98 | 1,98 | 2,00 | 1,99 | 1,99 | 1,99 | 1,99 | 1,99 | 1,99 | 1,98 | 1,98 | 1,98 | 1,97 | 1,97 | 1,98 | 1,97 | 1,98 | 1,97 | 1,98 |
| | Cr | 0,00 | 0,00 | 0,00 | 0,00 | 0,00 | 0,00 | 0,00 | 0,00 | 0,00 | 0,00 | 0,00 | 0,00 | 0,00 | 0,00 | 0,00 | 0,00 | 0,00 | 0,00 | 0,00 | 0,00 |
| | $Fe^{3+}$ | 0,01 | 0,05 | 0,06 | 0,05 | 0,03 | 0,08 | 0,02 | 0,07 | 0,05 | 0,05 | 0,07 | 0,04 | 0,05 | 0,08 | 0,04 | 0,04 | 0,04 | 0,06 | 0,05 | 0,03 |
| | $Fe^{2+}$ | 2,28 | 2,22 | 2,21 | 2,19 | 2,21 | 2,42 | 2,38 | 2,35 | 2,32 | 2,29 | 2,16 | 2,02 | 1,92 | 1,94 | 1,99 | 2,00 | 1,97 | 1,91 | 1,96 | 1,96 |
| | Mn | 0,12 | 0,10 | 0,10 | 0,17 | 0,14 | 0,11 | 0,21 | 0,08 | 0,11 | 0,15 | 0,24 | 0,39 | 0,45 | 0,45 | 0,45 | 0,43 | 0,44 | 0,42 | 0,42 | 0,38 |
| | Mg | 0,35 | 0,37 | 0,36 | 0,35 | 0,35 | 0,21 | 0,10 | 0,20 | 0,14 | 0,14 | 0,12 | 0,10 | 0,10 | 0,10 | 0,09 | 0,08 | 0,10 | 0,10 | 0,09 | 0,10 |
| | Ca | 0,25 | 0,29 | 0,31 | 0,26 | 0,28 | 0,23 | 0,30 | 0,34 | 0,41 | 0,40 | 0,45 | 0,48 | 0,52 | 0,48 | 0,47 | 0,48 | 0,48 | 0,55 | 0,52 | 0,56 |
| | sum | 8,00 | 8,00 | 8,00 | 8,00 | 8,00 | 8,00 | 8,00 | 8,00 | 8,00 | 8,00 | 8,00 | 8,00 | 8,00 | 8,00 | 8,00 | 8,00 | 8,00 | 8,00 | 8,00 | 8,00 |
| | norm. coeff. | 0,21 | 0,21 | 0,21 | 0,21 | 0,21 | 0,20 | 0,20 | 0,21 | 0,20 | 0,21 | 0,21 | 0,20 | 0,21 | 0,20 | 0,20 | 0,20 | 0,20 | 0,21 | 0,20 | 0,21 |
| | xFe | 0,87 | 0,86 | 0,86 | 0,86 | 0,86 | 0,92 | 0,96 | 0,92 | 0,94 | 0,94 | 0,95 | 0,95 | 0,95 | 0,95 | 0,96 | 0,96 | 0,95 | 0,95 | 0,95 | 0,95 |
| | xAlm | 0,76 | 0,74 | 0,74 | 0,74 | 0,74 | 0,81 | 0,80 | 0,79 | 0,78 | 0,77 | 0,73 | 0,67 | 0,64 | 0,65 | 0,66 | 0,67 | 0,66 | 0,64 | 0,65 | 0,65 |
| | xPrp | 0,12 | 0,12 | 0,12 | 0,12 | 0,12 | 0,07 | 0,03 | 0,07 | 0,05 | 0,05 | 0,04 | 0,03 | 0,03 | 0,03 | 0,03 | 0,03 | 0,03 | 0,03 | 0,03 | 0,03 |
| | xGrs | 0,08 | 0,10 | 0,10 | 0,09 | 0,09 | 0,08 | 0,10 | 0,11 | 0,14 | 0,14 | 0,15 | 0,16 | 0,18 | 0,16 | 0,16 | 0,16 | 0,16 | 0,19 | 0,17 | 0,19 |
| | xSps | 0,04 | 0,04 | 0,03 | 0,06 | 0,05 | 0,04 | 0,07 | 0,03 | 0,04 | 0,05 | 0,08 | 0,13 | 0,15 | 0,15 | 0,15 | 0,15 | 0,15 | 0,14 | 0,14 | 0,13 |

**Annex II** – Mineral analyses, Depiné (2008).

| | Sample | 231104-1 | | | | | | 260406-4 | | | | | | | | | | | 260406-10 | | |
|---|---|---|---|---|---|---|---|---|---|---|---|---|---|---|---|---|---|---|---|---|---|
| | Ox. wt% | P17 | P 18 | P 19 | P 20 | P 21 | P 22 | P1 | P 2 | P 3 | P 4 | P 5 | P 6 | P 7 | P 8 | P 9 | P 10 | P 12 | P1 | P 2 | P 3 |
| Garnet | $SiO_2$ | 36,67 | 36,98 | 36,86 | 36,75 | 36,87 | 36,55 | 37,40 | 37,75 | 37,59 | 37,46 | 37,66 | 37,69 | 37,07 | 37,61 | 37,56 | 37,56 | 37,54 | 37,31 | 37,71 | 37,67 |
| | $TiO_2$ | 0,02 | 0,04 | 0,00 | 0,06 | 0,00 | 0,02 | 0,04 | 0,02 | 0,03 | 0,03 | 0,02 | 0,06 | 0,05 | 0,04 | 0,01 | 0,03 | 0,03 | 0,01 | 0,01 | 0,01 |
| | $Al_2O_3$ | 20,65 | 20,78 | 21,03 | 20,94 | 20,85 | 20,78 | 21,30 | 21,07 | 20,90 | 20,85 | 21,05 | 21,05 | 20,92 | 20,86 | 21,06 | 21,16 | 21,25 | 21,14 | 21,30 | 21,43 |
| | $Cr_2O_3$ | 0,03 | 0,00 | 0,00 | 0,00 | 0,00 | 0,04 | 0,00 | 0,00 | 0,02 | 0,00 | 0,01 | 0,03 | 0,03 | 0,02 | 0,00 | 0,02 | 0,01 | 0,02 | 0,02 | 0,05 |
| | $Fe_2O_3$ | 0,65 | 0,51 | 0,97 | 1,16 | 1,27 | 0,99 | 1,00 | 0,32 | 0,37 | 0,66 | 0,57 | 0,62 | 1,76 | 0,00 | 0,92 | 0,05 | 1,06 | 1,55 | 1,02 | 1,18 |
| | FeO | 30,24 | 31,22 | 32,27 | 33,24 | 34,24 | 34,79 | 29,47 | 29,67 | 29,63 | 29,67 | 28,89 | 29,42 | 28,33 | 30,04 | 29,18 | 30,01 | 29,46 | 29,44 | 28,87 | 28,43 |
| | MnO | 4,54 | 3,62 | 3,01 | 2,16 | 1,48 | 1,73 | 1,87 | 1,81 | 1,91 | 1,85 | 1,81 | 1,77 | 1,85 | 1,93 | 1,77 | 1,96 | 1,86 | 1,64 | 1,17 | 1,14 |
| | MgO | 0,95 | 1,13 | 1,30 | 1,54 | 1,83 | 1,75 | 3,76 | 3,93 | 3,74 | 3,63 | 3,94 | 3,88 | 3,89 | 3,47 | 3,95 | 3,36 | 3,96 | 3,65 | 4,25 | 4,46 |
| | CaO | 5,72 | 5,75 | 5,03 | 4,55 | 3,98 | 3,17 | 5,23 | 5,20 | 5,27 | 5,32 | 5,71 | 5,45 | 5,65 | 5,34 | 5,40 | 5,44 | 5,09 | 5,48 | 5,83 | 5,87 |
| | sum | 99,47 | 100,03 | 100,47 | 100,40 | 100,51 | 99,82 | 100,07 | 99,75 | 99,46 | 99,47 | 99,65 | 99,96 | 99,54 | 99,31 | 99,84 | 99,58 | 100,26 | 100,24 | 100,18 | 100,24 |
| | **Cations** | | | | | | | | | | | | | | | | | | | | |
| | **Si** | 2,99 | 2,99 | 2,97 | 2,97 | 2,97 | 2,97 | 2,97 | 3,00 | 3,00 | 3,00 | 3,00 | 2,99 | 2,96 | 3,01 | 2,99 | 3,00 | 2,97 | 2,96 | 2,98 | 2,97 |
| | Ti | 0,00 | 0,00 | 0,00 | 0,00 | 0,00 | 0,00 | 0,00 | 0,00 | 0,00 | 0,00 | 0,00 | 0,00 | 0,00 | 0,00 | 0,00 | 0,00 | 0,00 | 0,00 | 0,00 | 0,00 |
| | Al | 1,98 | 1,98 | 2,00 | 1,99 | 1,98 | 1,99 | 1,99 | 1,97 | 1,97 | 1,97 | 1,97 | 1,97 | 1,97 | 1,97 | 1,97 | 1,99 | 1,98 | 1,98 | 1,98 | 1,99 |
| | Cr | 0,00 | 0,00 | 0,00 | 0,00 | 0,00 | 0,00 | 0,00 | 0,00 | 0,00 | 0,00 | 0,00 | 0,00 | 0,00 | 0,00 | 0,00 | 0,00 | 0,00 | 0,00 | 0,00 | 0,00 |
| | $Fe^{3+}$ | 0,04 | 0,03 | 0,06 | 0,07 | 0,08 | 0,06 | 0,06 | 0,02 | 0,02 | 0,04 | 0,03 | 0,04 | 0,11 | 0,00 | 0,05 | 0,00 | 0,06 | 0,09 | 0,06 | 0,07 |
| | $Fe^{2+}$ | 2,06 | 2,11 | 2,18 | 2,24 | 2,31 | 2,37 | 1,96 | 1,97 | 1,98 | 1,98 | 1,92 | 1,95 | 1,89 | 2,01 | 1,94 | 2,00 | 1,95 | 1,96 | 1,91 | 1,87 |
| | Mn | 0,31 | 0,25 | 0,21 | 0,15 | 0,10 | 0,12 | 0,13 | 0,12 | 0,13 | 0,13 | 0,12 | 0,12 | 0,13 | 0,13 | 0,12 | 0,13 | 0,12 | 0,11 | 0,08 | 0,08 |
| | Mg | 0,12 | 0,14 | 0,16 | 0,19 | 0,22 | 0,21 | 0,44 | 0,47 | 0,45 | 0,43 | 0,47 | 0,46 | 0,46 | 0,41 | 0,47 | 0,40 | 0,47 | 0,43 | 0,50 | 0,52 |
| | Ca | 0,50 | 0,50 | 0,43 | 0,39 | 0,34 | 0,28 | 0,45 | 0,44 | 0,45 | 0,46 | 0,49 | 0,46 | 0,48 | 0,46 | 0,46 | 0,47 | 0,43 | 0,47 | 0,49 | 0,50 |
| | sum | 8,00 | 8,00 | 8,00 | 8,00 | 8,00 | 8,00 | 8,00 | 8,00 | 8,00 | 8,00 | 8,00 | 8,00 | 8,00 | 8,00 | 8,00 | 8,00 | 8,00 | 8,00 | 8,00 | 8,00 |
| | norm. coeff. | 0,20 | 0,21 | 0,21 | 0,21 | 0,21 | 0,20 | 0,21 | 0,21 | 0,21 | 0,21 | 0,21 | 0,21 | 0,21 | 0,21 | 0,21 | 0,21 | 0,21 | 0,21 | 0,21 | 0,21 |
| | xFe | 0,95 | 0,94 | 0,93 | 0,93 | 0,92 | 0,92 | 0,82 | 0,81 | 0,82 | 0,82 | 0,81 | 0,81 | 0,81 | 0,83 | 0,81 | 0,83 | 0,81 | 0,83 | 0,80 | 0,79 |
| | xAlm | 0,69 | 0,71 | 0,73 | 0,76 | 0,78 | 0,80 | 0,66 | 0,66 | 0,66 | 0,66 | 0,64 | 0,65 | 0,64 | 0,67 | 0,65 | 0,67 | 0,66 | 0,66 | 0,64 | 0,63 |
| | xPrp | 0,04 | 0,05 | 0,05 | 0,06 | 0,07 | 0,07 | 0,15 | 0,16 | 0,15 | 0,14 | 0,16 | 0,15 | 0,16 | 0,14 | 0,16 | 0,13 | 0,16 | 0,15 | 0,17 | 0,18 |
| | xGrs | 0,17 | 0,17 | 0,15 | 0,13 | 0,12 | 0,09 | 0,15 | 0,15 | 0,15 | 0,15 | 0,16 | 0,15 | 0,16 | 0,15 | 0,15 | 0,16 | 0,15 | 0,16 | 0,17 | 0,17 |
| | xSps | 0,10 | 0,08 | 0,07 | 0,05 | 0,03 | 0,04 | 0,04 | 0,04 | 0,04 | 0,04 | 0,04 | 0,04 | 0,04 | 0,04 | 0,04 | 0,04 | 0,04 | 0,04 | 0,03 | 0,03 |

**Annex II** – Mineral analyses, Depiné (2008).

| | Sample | 260406-10 | | | | | | | | | | | | | | | 260406-14 | | | | |
|---|---|---|---|---|---|---|---|---|---|---|---|---|---|---|---|---|---|---|---|---|---|
| | **Ox. wt%** | **P4** | **P5** | **P6** | **P8** | **P9** | **P10** | **P11** | **P12** | **P13** | **P14** | **P15** | **P16** | **P17** | **P18** | **P19** | **P1** | **P2** | **P3** | **P5** | **P6** |
| **Garnet** | $SiO_2$ | 37,61 | 37,77 | 37,77 | 37,39 | 37,77 | 37,43 | 37,66 | 37,56 | 37,78 | 37,65 | 37,70 | 37,53 | 37,61 | 37,38 | 37,63 | 36,86 | 37,11 | 36,75 | 36,77 | 36,68 |
| | $TiO_2$ | 0,00 | 0,03 | 0,02 | 0,00 | 0,03 | 0,00 | 0,01 | 0,04 | 0,02 | 0,00 | 0,03 | 0,00 | 0,00 | 0,00 | 0,02 | 0,16 | 0,16 | 0,04 | 0,13 | 0,15 |
| | $Al_2O_3$ | 21,12 | 21,27 | 21,49 | 21,21 | 21,20 | 21,28 | 21,32 | 21,44 | 21,30 | 21,41 | 21,37 | 21,25 | 21,28 | 21,35 | 21,43 | 20,53 | 20,57 | 20,71 | 20,57 | 20,42 |
| | $Cr_2O_3$ | 0,02 | 0,04 | 0,05 | 0,04 | 0,01 | 0,04 | 0,04 | 0,03 | 0,02 | 0,03 | 0,07 | 0,03 | 0,05 | 0,05 | 0,01 | 0,00 | 0,00 | 0,00 | 0,00 | 0,01 |
| | $Fe_2O_3$ | 0,36 | 1,10 | 0,79 | 1,11 | 1,10 | 1,28 | 1,28 | 0,84 | 0,72 | 1,12 | 1,07 | 1,43 | 1,12 | 1,70 | 1,64 | 0,67 | 0,08 | 0,85 | 0,54 | 0,69 |
| | FeO | 28,98 | 28,78 | 29,12 | 28,60 | 28,84 | 29,45 | 28,72 | 29,24 | 29,15 | 28,92 | 29,08 | 28,74 | 28,75 | 28,36 | 29,28 | 27,35 | 27,71 | 27,28 | 27,03 | 27,24 |
| | MnO | 1,18 | 1,29 | 1,31 | 1,36 | 1,55 | 1,54 | 1,38 | 1,40 | 1,29 | 1,34 | 1,52 | 1,43 | 1,36 | 1,39 | 1,40 | 1,48 | 1,76 | 1,78 | 2,04 | 1,78 |
| | MgO | 4,56 | 4,72 | 4,67 | 4,49 | 4,44 | 3,91 | 4,49 | 4,21 | 4,47 | 4,59 | 4,37 | 4,59 | 4,56 | 4,59 | 4,45 | 0,38 | 0,36 | 0,32 | 0,31 | 0,31 |
| | CaO | 5,21 | 5,23 | 5,01 | 5,26 | 5,37 | 5,29 | 5,40 | 5,29 | 5,29 | 5,13 | 5,23 | 5,08 | 5,25 | 5,27 | 4,98 | 11,47 | 11,23 | 11,19 | 11,27 | 11,23 |
| | sum | 99,04 | 100,21 | 100,23 | 99,45 | 100,31 | 100,23 | 100,29 | 100,05 | 100,05 | 100,19 | 100,44 | 100,06 | 99,97 | 100,09 | 100,83 | 98,89 | 98,99 | 98,92 | 98,66 | 98,52 |
| | **Cations** | | | | | | | | | | | | | | | | | | | | |
| | **Si** | 3,00 | 2,98 | 2,98 | 2,97 | 2,98 | 2,97 | 2,97 | 2,97 | 2,99 | 2,97 | 2,97 | 2,97 | 2,97 | 2,95 | 2,96 | 2,99 | 3,01 | 2,98 | 2,99 | 2,99 |
| | Ti | 0,00 | 0,00 | 0,00 | 0,00 | 0,00 | 0,00 | 0,00 | 0,00 | 0,00 | 0,00 | 0,00 | 0,00 | 0,00 | 0,00 | 0,00 | 0,01 | 0,01 | 0,00 | 0,01 | 0,01 |
| | Al | 1,98 | 1,98 | 2,00 | 1,99 | 1,97 | 1,99 | 1,98 | 2,00 | 1,98 | 1,99 | 1,99 | 1,98 | 1,98 | 1,99 | 1,99 | 1,96 | 1,96 | 1,98 | 1,97 | 1,96 |
| | Cr | 0,00 | 0,00 | 0,00 | 0,00 | 0,00 | 0,00 | 0,00 | 0,00 | 0,00 | 0,00 | 0,00 | 0,00 | 0,00 | 0,00 | 0,00 | 0,00 | 0,00 | 0,00 | 0,00 | 0,00 |
| | $Fe^{3+}$ | 0,02 | 0,07 | 0,05 | 0,07 | 0,07 | 0,08 | 0,08 | 0,05 | 0,04 | 0,07 | 0,06 | 0,08 | 0,07 | 0,10 | 0,10 | 0,04 | 0,00 | 0,05 | 0,03 | 0,04 |
| | $Fe^{2+}$ | 1,93 | 1,90 | 1,92 | 1,90 | 1,90 | 1,95 | 1,89 | 1,94 | 1,93 | 1,91 | 1,92 | 1,90 | 1,90 | 1,87 | 1,92 | 1,85 | 1,88 | 1,85 | 1,84 | 1,86 |
| | Mn | 0,08 | 0,09 | 0,09 | 0,09 | 0,10 | 0,10 | 0,09 | 0,09 | 0,09 | 0,09 | 0,10 | 0,10 | 0,09 | 0,09 | 0,09 | 0,10 | 0,12 | 0,12 | 0,14 | 0,12 |
| | Mg | 0,54 | 0,55 | 0,55 | 0,53 | 0,52 | 0,46 | 0,53 | 0,50 | 0,53 | 0,54 | 0,51 | 0,54 | 0,54 | 0,54 | 0,52 | 0,05 | 0,04 | 0,04 | 0,04 | 0,04 |
| | Ca | 0,44 | 0,44 | 0,42 | 0,45 | 0,45 | 0,45 | 0,46 | 0,45 | 0,45 | 0,43 | 0,44 | 0,43 | 0,44 | 0,45 | 0,42 | 1,00 | 0,97 | 0,97 | 0,98 | 0,98 |
| | sum | 8,00 | 8,00 | 8,00 | 8,00 | 8,00 | 8,00 | 8,00 | 8,00 | 8,00 | 8,00 | 8,00 | 8,00 | 8,00 | 8,00 | 8,00 | 8,00 | 8,00 | 8,00 | 8,00 | 8,00 |
| | norm. coeff. | 0,21 | 0,21 | 0,21 | 0,21 | 0,21 | 0,21 | 0,21 | 0,21 | 0,21 | 0,21 | 0,21 | 0,21 | 0,21 | 0,21 | 0,21 | 0,21 | 0,21 | 0,21 | 0,20 | 0,20 |
| | xFe | 0,78 | 0,78 | 0,78 | 0,79 | 0,79 | 0,81 | 0,79 | 0,80 | 0,79 | 0,79 | 0,79 | 0,79 | 0,79 | 0,79 | 0,79 | 0,98 | 0,98 | 0,98 | 0,98 | 0,98 |
| | xAlm | 0,64 | 0,64 | 0,64 | 0,64 | 0,64 | 0,66 | 0,64 | 0,65 | 0,64 | 0,64 | 0,64 | 0,64 | 0,64 | 0,63 | 0,65 | 0,62 | 0,62 | 0,62 | 0,61 | 0,62 |
| | xPrp | 0,18 | 0,19 | 0,18 | 0,18 | 0,17 | 0,16 | 0,18 | 0,17 | 0,18 | 0,18 | 0,17 | 0,18 | 0,18 | 0,18 | 0,18 | 0,02 | 0,01 | 0,01 | 0,01 | 0,01 |
| | xGrs | 0,15 | 0,15 | 0,14 | 0,15 | 0,15 | 0,15 | 0,15 | 0,15 | 0,15 | 0,15 | 0,15 | 0,14 | 0,15 | 0,15 | 0,14 | 0,33 | 0,32 | 0,33 | 0,33 | 0,33 |
| | xSps | 0,03 | 0,03 | 0,03 | 0,03 | 0,03 | 0,03 | 0,03 | 0,03 | 0,03 | 0,03 | 0,03 | 0,03 | 0,03 | 0,03 | 0,03 | 0,03 | 0,04 | 0,04 | 0,05 | 0,04 |

**Annex II** – Mineral analyses, Depiné (2008).

| | Sample | 101203-1 | | | | | | | | | | | | | | | | | | |
|---|---|---|---|---|---|---|---|---|---|---|---|---|---|---|---|---|---|---|---|---|
| | **Ox. wt%** | **P1** | **P2** | **P3** | **P4** | **P5** | **P6** | **P7** | **P8** | **P9** | **P10** | **P1** | **P2** | **P3** | **P4** | **P5** | **P6** | **P7** | **P8** | **P1** | **P2** |
| **Feldspar** | $SiO_2$ | 56,84 | 57,85 | 57,99 | 58,05 | 57,66 | 57,95 | 57,56 | 57,66 | 56,69 | 57,01 | 57,38 | 57,10 | 57,59 | 57,20 | 57,13 | 57,10 | 57,26 | 57,32 | 57,27 | 57,86 |
| | $Al_2O_3$ | 25,87 | 25,10 | 25,13 | 25,11 | 25,18 | 25,55 | 25,07 | 25,52 | 25,99 | 26,36 | 25,75 | 25,65 | 25,59 | 26,18 | 25,98 | 26,02 | 25,74 | 25,75 | 25,71 | 25,58 |
| | FeO | 0,00 | 0,01 | 0,01 | 0,00 | 0,03 | 0,02 | 0,00 | 0,00 | 0,02 | 0,09 | 0,13 | 0,03 | 0,05 | 0,02 | 0,00 | 0,09 | 0,00 | 0,07 | 0,07 | 0,06 |
| | $Fe_2O_3$ | 0,00 | 0,02 | 0,02 | 0,00 | 0,03 | 0,02 | 0,00 | 0,00 | 0,02 | 0,09 | 0,14 | 0,03 | 0,05 | 0,03 | 0,00 | 0,10 | 0,00 | 0,08 | 0,07 | 0,07 |
| | MgO | 0,00 | 0,00 | 0,00 | 0,00 | 0,00 | 0,00 | 0,00 | 0,00 | 0,00 | 0,00 | 0,00 | 0,00 | 0,00 | 0,00 | 0,00 | 0,00 | 0,00 | 0,00 | 0,00 | 0,00 |
| | BaO | 0,00 | 0,02 | 0,04 | 0,03 | 0,04 | 0,05 | 0,00 | 0,01 | 0,04 | 0,08 | 0,14 | 0,04 | 0,00 | 0,05 | 0,00 | 0,01 | 0,02 | 0,00 | 0,00 | 0,01 |
| | CaO | 8,34 | 7,61 | 7,66 | 7,40 | 7,72 | 7,77 | 7,54 | 7,60 | 8,34 | 8,47 | 8,04 | 8,01 | 8,26 | 8,28 | 8,08 | 8,07 | 8,18 | 8,31 | 8,09 | 8,03 |
| | $Na_2O$ | 6,70 | 7,27 | 7,36 | 7,21 | 7,09 | 7,25 | 7,07 | 7,13 | 6,75 | 6,73 | 6,86 | 6,81 | 6,75 | 6,62 | 6,91 | 6,59 | 6,78 | 6,83 | 6,77 | 7,03 |
| | $K_2O$ | 0,07 | 0,11 | 0,08 | 0,08 | 0,07 | 0,07 | 0,06 | 0,09 | 0,08 | 0,06 | 0,12 | 0,13 | 0,11 | 0,11 | 0,08 | 0,08 | 0,08 | 0,09 | 0,06 | 0,08 |
| | sum | 97,81 | 97,97 | 98,28 | 97,88 | 97,77 | 98,64 | 97,30 | 98,00 | 97,91 | 98,79 | 98,42 | 97,77 | 98,33 | 98,47 | 98,17 | 97,96 | 98,05 | 98,37 | 97,97 | 98,64 |
| | **Cations** | | | | | | | | | | | | | | | | | | | | |
| | Si | 2,60 | 2,64 | 2,64 | 2,65 | 2,63 | 2,63 | 2,64 | 2,63 | 2,59 | 2,59 | 2,61 | 2,61 | 2,62 | 2,60 | 2,60 | 2,60 | 2,61 | 2,61 | 2,61 | 2,62 |
| | Al | 1,39 | 1,35 | 1,35 | 1,35 | 1,36 | 1,36 | 1,36 | 1,37 | 1,40 | 1,41 | 1,38 | 1,38 | 1,37 | 1,40 | 1,39 | 1,40 | 1,38 | 1,38 | 1,38 | 1,37 |
| | $Fe^{3+}$ | 0,00 | 0,00 | 0,00 | 0,00 | 0,00 | 0,00 | 0,00 | 0,00 | 0,00 | 0,00 | 0,00 | 0,00 | 0,00 | 0,00 | 0,00 | 0,00 | 0,00 | 0,00 | 0,00 | 0,00 |
| | Mg | 0,00 | 0,00 | 0,00 | 0,00 | 0,00 | 0,00 | 0,00 | 0,00 | 0,00 | 0,00 | 0,00 | 0,00 | 0,00 | 0,00 | 0,00 | 0,00 | 0,00 | 0,00 | 0,00 | 0,00 |
| | Ba | 0,00 | 0,00 | 0,00 | 0,00 | 0,00 | 0,00 | 0,00 | 0,00 | 0,00 | 0,00 | 0,00 | 0,00 | 0,00 | 0,00 | 0,00 | 0,00 | 0,00 | 0,00 | 0,00 | 0,00 |
| | Ca | 0,41 | 0,37 | 0,37 | 0,36 | 0,38 | 0,38 | 0,37 | 0,37 | 0,41 | 0,41 | 0,39 | 0,39 | 0,40 | 0,40 | 0,39 | 0,39 | 0,40 | 0,40 | 0,40 | 0,39 |
| | Na | 0,59 | 0,64 | 0,65 | 0,64 | 0,63 | 0,64 | 0,63 | 0,63 | 0,60 | 0,59 | 0,61 | 0,60 | 0,59 | 0,58 | 0,61 | 0,58 | 0,60 | 0,60 | 0,60 | 0,62 |
| | K | 0,00 | 0,01 | 0,00 | 0,00 | 0,00 | 0,00 | 0,00 | 0,01 | 0,00 | 0,00 | 0,01 | 0,01 | 0,01 | 0,01 | 0,00 | 0,00 | 0,00 | 0,01 | 0,00 | 0,00 |
| | sum | 5,00 | 5,01 | 5,01 | 5,00 | 5,00 | 5,01 | 5,00 | 5,00 | 5,01 | 5,01 | 5,00 | 5,00 | 5,00 | 4,99 | 5,01 | 4,99 | 5,00 | 5,00 | 5,00 | 5,00 |
| | xAn | 40,60 | 36,43 | 36,35 | 36,02 | 37,42 | 37,07 | 36,93 | 36,88 | 40,36 | 40,89 | 39,02 | 39,12 | 40,09 | 40,61 | 39,06 | 40,19 | 39,82 | 39,99 | 39,61 | 38,52 |
| | xOr | 0,41 | 0,60 | 0,47 | 0,48 | 0,38 | 0,39 | 0,35 | 0,51 | 0,46 | 0,36 | 0,68 | 0,73 | 0,61 | 0,61 | 0,45 | 0,47 | 0,45 | 0,53 | 0,36 | 0,43 |
| | xAb | 58,99 | 62,97 | 63,18 | 63,50 | 62,20 | 62,54 | 62,72 | 62,60 | 59,18 | 58,75 | 60,30 | 60,14 | 59,30 | 58,78 | 60,49 | 59,34 | 59,74 | 59,48 | 60,03 | 61,05 |
| | sum | 100,00 | 100,00 | 100,00 | 100,00 | 100,00 | 100,00 | 100,00 | 100,00 | 100,00 | 100,00 | 100,00 | 100,00 | 100,00 | 100,00 | 100,00 | 100,00 | 100,00 | 100,00 | 100,00 | 100,00 |

**Annex II** – Mineral analyses, Depiné (2008).

| | Sample | 101203-1 | | | | | | | | | | | | | | | | | | |
|---|---|---|---|---|---|---|---|---|---|---|---|---|---|---|---|---|---|---|---|---|
| | **Ox. wt%** | **P3** | **P4** | **P5** | **P6** | **P8** | **P9** | **P1** | **P2** | **P3** | **P4** | **P5** | **P6** | **P7** | **P8** | **P11** | **P12** | **P13** | **P14** | **P15** | **P16** |
| **Feldspar** | $SiO_2$ | 57,75 | 57,56 | 57,82 | 58,00 | 57,75 | 57,25 | 57,27 | 57,45 | 57,56 | 57,79 | 57,10 | 59,50 | 60,78 | 63,72 | 61,39 | 57,14 | 58,17 | 56,90 | 57,32 | 57,41 |
| | Al | 25,50 | 25,61 | 25,50 | 25,28 | 25,83 | 25,80 | 25,40 | 25,84 | 25,39 | 25,06 | 25,11 | 24,48 | 23,91 | 21,90 | 24,79 | 25,68 | 25,31 | 25,87 | 25,91 | 25,45 |
| | FeO | 0,03 | 0,03 | 0,04 | 0,03 | 0,05 | 0,05 | 0,00 | 0,04 | 0,01 | 0,03 | 0,00 | 0,06 | 0,00 | 0,05 | 0,04 | 0,00 | 0,00 | 0,01 | 0,01 | 0,00 |
| | $Fe_2O_3$ | 0,04 | 0,03 | 0,05 | 0,03 | 0,06 | 0,06 | 0,00 | 0,04 | 0,02 | 0,03 | 0,00 | 0,06 | 0,00 | 0,05 | 0,04 | 0,00 | 0,00 | 0,01 | 0,01 | 0,00 |
| | MgO | 0,00 | 0,00 | 0,00 | 0,00 | 0,00 | 0,00 | 0,00 | 0,00 | 0,00 | 0,00 | 0,00 | 0,00 | 0,00 | 0,01 | 0,05 | 0,00 | 0,00 | 0,00 | 0,00 | 0,00 |
| | BaO | 0,00 | 0,01 | 0,03 | 0,00 | 0,05 | 0,02 | 0,00 | 0,04 | 0,00 | 0,03 | 0,07 | 0,00 | 0,03 | 0,05 | 0,06 | 0,03 | 0,00 | 0,00 | 0,00 | 0,00 |
| | CaO | 8,12 | 7,87 | 7,82 | 7,84 | 8,03 | 8,13 | 8,00 | 8,20 | 7,94 | 7,62 | 7,73 | 6,43 | 5,68 | 2,49 | 3,00 | 8,09 | 7,58 | 8,21 | 8,14 | 8,08 |
| | $Na_2O$ | 7,04 | 7,05 | 6,98 | 7,10 | 7,02 | 6,85 | 6,92 | 6,91 | 7,05 | 7,28 | 7,02 | 7,77 | 8,37 | 9,58 | 8,36 | 6,72 | 7,17 | 6,70 | 6,79 | 7,08 |
| | $K_2O$ | 0,07 | 0,10 | 0,09 | 0,05 | 0,10 | 0,05 | 0,08 | 0,06 | 0,11 | 0,07 | 0,15 | 0,10 | 0,10 | 0,56 | 1,51 | 0,14 | 0,10 | 0,06 | 0,08 | 0,06 |
| | sum | 98,51 | 98,22 | 98,28 | 98,29 | 98,82 | 98,14 | 97,66 | 98,53 | 98,07 | 97,88 | 97,19 | 98,33 | 98,87 | 98,36 | 99,18 | 97,80 | 98,34 | 97,74 | 98,26 | 98,07 |
| | **Cations** | | | | | | | | | | | | | | | | | | | | |
| | Si | 2,62 | 2,62 | 2,63 | 2,64 | 2,61 | 2,61 | 2,62 | 2,61 | 2,62 | 2,64 | 2,63 | 2,69 | 2,73 | 2,85 | 2,74 | 2,61 | 2,64 | 2,60 | 2,61 | 2,62 |
| | Al | 1,36 | 1,37 | 1,37 | 1,35 | 1,38 | 1,39 | 1,37 | 1,38 | 1,36 | 1,35 | 1,36 | 1,31 | 1,27 | 1,16 | 1,31 | 1,38 | 1,35 | 1,39 | 1,39 | 1,37 |
| | $Fe^{3+}$ | 0,00 | 0,00 | 0,00 | 0,00 | 0,00 | 0,00 | 0,00 | 0,00 | 0,00 | 0,00 | 0,00 | 0,00 | 0,00 | 0,00 | 0,00 | 0,00 | 0,00 | 0,00 | 0,00 | 0,00 |
| | Mg | 0,00 | 0,00 | 0,00 | 0,00 | 0,00 | 0,00 | 0,00 | 0,00 | 0,00 | 0,00 | 0,00 | 0,00 | 0,00 | 0,00 | 0,00 | 0,00 | 0,00 | 0,00 | 0,00 | 0,00 |
| | Ba | 0,00 | 0,00 | 0,00 | 0,00 | 0,00 | 0,00 | 0,00 | 0,00 | 0,00 | 0,00 | 0,00 | 0,00 | 0,00 | 0,00 | 0,00 | 0,00 | 0,00 | 0,00 | 0,00 | 0,00 |
| | Ca | 0,39 | 0,38 | 0,38 | 0,38 | 0,39 | 0,40 | 0,39 | 0,40 | 0,39 | 0,37 | 0,38 | 0,31 | 0,27 | 0,12 | 0,14 | 0,40 | 0,37 | 0,40 | 0,40 | 0,39 |
| | Na | 0,62 | 0,62 | 0,62 | 0,63 | 0,62 | 0,61 | 0,61 | 0,61 | 0,62 | 0,64 | 0,63 | 0,68 | 0,73 | 0,83 | 0,72 | 0,60 | 0,63 | 0,59 | 0,60 | 0,63 |
| | K | 0,00 | 0,01 | 0,00 | 0,00 | 0,01 | 0,00 | 0,00 | 0,00 | 0,01 | 0,00 | 0,01 | 0,01 | 0,01 | 0,03 | 0,09 | 0,01 | 0,01 | 0,00 | 0,00 | 0,00 |
| | sum | 5,01 | 5,01 | 5,00 | 5,00 | 5,01 | 5,00 | 5,00 | 5,00 | 5,01 | 5,01 | 5,01 | 5,00 | 5,00 | 5,00 | 5,01 | 5,00 | 5,00 | 5,00 | 5,00 | 5,01 |
| | xAn | 38,78 | 37,95 | 38,04 | 37,80 | 38,53 | 39,50 | 38,82 | 39,48 | 38,14 | 36,50 | 37,50 | 31,20 | 27,09 | 12,14 | 15,05 | 39,65 | 36,65 | 40,24 | 39,66 | 38,55 |
| | xAb | 60,83 | 61,47 | 61,47 | 61,94 | 60,93 | 60,21 | 60,74 | 60,18 | 61,24 | 63,09 | 61,61 | 68,24 | 72,32 | 84,59 | 75,92 | 59,53 | 62,78 | 59,41 | 59,85 | 61,10 |
| | xOr | 0,39 | 0,57 | 0,49 | 0,26 | 0,54 | 0,29 | 0,44 | 0,34 | 0,62 | 0,40 | 0,89 | 0,55 | 0,59 | 3,27 | 9,03 | 0,82 | 0,58 | 0,35 | 0,49 | 0,35 |
| | sum | 100,00 | 100,00 | 100,00 | 100,00 | 100,00 | 100,00 | 100,00 | 100,00 | 100,00 | 100,00 | 100,00 | 100,00 | 100,00 | 100,00 | 100,00 | 100,00 | 100,00 | 100,00 | 100,00 | 100,00 |

**Annex II** – Mineral analyses, Depiné (2008).

| | Sample | 101203-1 | | | | | | | | | | | | | | | | | | |
|---|---|---|---|---|---|---|---|---|---|---|---|---|---|---|---|---|---|---|---|---|
| | **Ox. wt%** | **P17** | **P18** | **P1** | **P3** | **P4** | **P10** | **P12** | **P14** | **P15** | **P1** | **P2** | **P3** | **P4** | **P5** | **P6** | **P7** | **P8** | **P11** | **P14** | **P15** |
| **Feldspar** | $SiO_2$ | 56,83 | 57,04 | 65,33 | 64,86 | 65,40 | 64,42 | 64,14 | 64,37 | 65,11 | 58,11 | 57,68 | 57,49 | 57,78 | 57,85 | 57,65 | 57,64 | 57,62 | 57,16 | 57,28 | 58,02 |
| | $Al_2O_3$ | 25,49 | 25,40 | 20,47 | 20,70 | 20,07 | 20,85 | 21,00 | 20,96 | 20,29 | 25,13 | 24,97 | 25,20 | 25,51 | 25,54 | 25,47 | 25,56 | 24,85 | 25,08 | 25,37 | 24,74 |
| | FeO | 0,04 | 0,08 | 0,15 | 0,17 | 0,06 | 0,07 | 0,09 | 0,03 | 0,07 | 0,05 | 0,04 | 0,00 | 0,01 | 0,00 | 0,06 | 0,01 | 0,04 | 0,01 | 0,06 | 0,00 |
| | $Fe_2O_3$ | 0,05 | 0,09 | 0,17 | 0,19 | 0,06 | 0,08 | 0,10 | 0,03 | 0,07 | 0,05 | 0,04 | 0,00 | 0,01 | 0,00 | 0,07 | 0,01 | 0,05 | 0,02 | 0,06 | 0,00 |
| | MgO | 0,00 | 0,00 | 0,07 | 0,03 | 0,00 | 0,07 | 0,12 | 0,00 | 0,00 | 0,00 | 0,08 | 0,00 | 0,28 | 0,00 | 0,00 | 0,00 | 0,02 | 0,00 | 0,18 | 0,00 |
| | BaO | 0,00 | 0,00 | 0,04 | 0,05 | 0,01 | 0,03 | 0,04 | 0,02 | 0,02 | 0,00 | 0,10 | 0,01 | 0,06 | 0,01 | 0,01 | 0,03 | 0,07 | 0,03 | 0,08 | 0,06 |
| | CaO | 8,13 | 8,30 | 1,45 | 1,70 | 1,59 | 2,48 | 1,61 | 2,50 | 1,77 | 7,83 | 7,81 | 7,67 | 7,82 | 8,02 | 7,93 | 7,83 | 7,64 | 7,85 | 7,97 | 7,34 |
| | $Na_2O$ | 6,96 | 6,75 | 10,48 | 10,11 | 10,50 | 10,10 | 10,26 | 10,24 | 10,43 | 7,34 | 7,04 | 7,16 | 7,27 | 7,19 | 7,00 | 7,20 | 7,09 | 6,95 | 7,15 | 7,41 |
| | $K_2O$ | 0,09 | 0,07 | 0,38 | 0,52 | 0,08 | 0,09 | 0,67 | 0,12 | 0,14 | 0,10 | 0,06 | 0,06 | 0,08 | 0,10 | 0,09 | 0,06 | 0,12 | 0,09 | 0,06 | 0,08 |
| | sum | 97,55 | 97,64 | 98,39 | 98,14 | 97,70 | 98,11 | 97,92 | 98,23 | 97,82 | 98,54 | 97,78 | 97,58 | 98,80 | 98,70 | 98,19 | 98,31 | 97,44 | 97,17 | 98,13 | 97,65 |
| | **Cations** | | | | | | | | | | | | | | | | | | | | |
| | Si | 2,61 | 2,61 | 2,92 | 2,91 | 2,93 | 2,89 | 2,89 | 2,88 | 2,92 | 2,64 | 2,64 | 2,63 | 2,62 | 2,62 | 2,62 | 2,62 | 2,64 | 2,63 | 2,61 | 2,65 |
| | Al | 1,38 | 1,37 | 1,08 | 1,09 | 1,06 | 1,10 | 1,11 | 1,11 | 1,07 | 1,34 | 1,35 | 1,36 | 1,36 | 1,36 | 1,37 | 1,37 | 1,34 | 1,36 | 1,36 | 1,33 |
| | $Fe^{3+}$ | 0,00 | 0,00 | 0,01 | 0,01 | 0,00 | 0,00 | 0,00 | 0,00 | 0,00 | 0,00 | 0,00 | 0,00 | 0,00 | 0,00 | 0,00 | 0,00 | 0,00 | 0,00 | 0,00 | 0,00 |
| | Mg | 0,00 | 0,00 | 0,00 | 0,00 | 0,00 | 0,00 | 0,01 | 0,00 | 0,00 | 0,00 | 0,01 | 0,00 | 0,02 | 0,00 | 0,00 | 0,00 | 0,00 | 0,00 | 0,01 | 0,00 |
| | Ba | 0,00 | 0,00 | 0,00 | 0,00 | 0,00 | 0,00 | 0,00 | 0,00 | 0,00 | 0,00 | 0,00 | 0,00 | 0,00 | 0,00 | 0,00 | 0,00 | 0,00 | 0,00 | 0,00 | 0,00 |
| | Ca | 0,40 | 0,41 | 0,07 | 0,08 | 0,08 | 0,12 | 0,08 | 0,12 | 0,09 | 0,38 | 0,38 | 0,38 | 0,38 | 0,39 | 0,39 | 0,38 | 0,38 | 0,39 | 0,39 | 0,36 |
| | Na | 0,62 | 0,60 | 0,91 | 0,88 | 0,91 | 0,88 | 0,89 | 0,89 | 0,91 | 0,65 | 0,62 | 0,64 | 0,64 | 0,63 | 0,62 | 0,64 | 0,63 | 0,62 | 0,63 | 0,66 |
| | K | 0,01 | 0,00 | 0,02 | 0,03 | 0,00 | 0,01 | 0,04 | 0,01 | 0,01 | 0,01 | 0,00 | 0,00 | 0,00 | 0,01 | 0,00 | 0,00 | 0,01 | 0,01 | 0,00 | 0,00 |
| | sum | 5,01 | 5,00 | 5,01 | 5,00 | 4,99 | 5,00 | 5,02 | 5,01 | 5,00 | 5,02 | 5,00 | 5,01 | 5,02 | 5,01 | 5,00 | 5,01 | 5,00 | 5,00 | 5,02 | 5,01 |
| | xAn | 39,03 | 40,27 | 6,96 | 8,26 | 7,69 | 11,88 | 7,67 | 11,80 | 8,50 | 36,89 | 37,90 | 37,06 | 37,13 | 37,90 | 38,31 | 37,41 | 37,06 | 38,25 | 38,00 | 35,20 |
| | xAb | 60,45 | 59,32 | 90,85 | 88,75 | 91,85 | 87,58 | 88,52 | 87,54 | 90,71 | 62,56 | 61,78 | 62,59 | 62,42 | 61,52 | 61,19 | 62,28 | 62,24 | 61,21 | 61,69 | 64,35 |
| | xOr | 0,52 | 0,42 | 2,19 | 2,99 | 0,46 | 0,54 | 3,81 | 0,65 | 0,79 | 0,54 | 0,32 | 0,35 | 0,45 | 0,57 | 0,49 | 0,31 | 0,69 | 0,53 | 0,31 | 0,45 |
| | sum | 100,00 | 100,00 | 100,00 | 100,00 | 100,00 | 100,00 | 100,00 | 100,00 | 100,00 | 100,00 | 100,00 | 100,00 | 100,00 | 100,00 | 100,00 | 100,00 | 100,00 | 100,00 | 100,00 | 100,00 |

**Annex II** – Mineral analyses, Depiné (2008).

| | Sample | 101203-1 | | | | | | | | | | | | | | | | | | |
|---|---|---|---|---|---|---|---|---|---|---|---|---|---|---|---|---|---|---|---|---|
| | **Ox. wt%** | **P16** | **P17** | **P18** | **P19** | **P2** | **P4** | **P5** | **P6** | **P7** | **P8** | **P9** | **P11** | **P12** | **P13** | **P14** | **P15** | **P18** | **P19** | **P1** | **P10** |
| | $SiO_2$ | 60,32 | 60,55 | 56,09 | 55,73 | 56,63 | 56,34 | 56,20 | 56,34 | 56,24 | 56,38 | 56,46 | 56,37 | 56,88 | 56,19 | 56,30 | 56,32 | 57,03 | 56,22 | 57,07 | 56,99 |
| | $Al_2O_3$ | 24,04 | 24,33 | 26,21 | 26,13 | 26,04 | 26,35 | 26,59 | 26,37 | 26,35 | 26,18 | 26,20 | 26,34 | 26,07 | 26,40 | 26,30 | 26,11 | 26,06 | 26,43 | 25,46 | 25,64 |
| | FeO | 0,17 | 0,05 | 0,04 | 0,00 | 0,15 | 0,08 | 0,03 | 0,05 | 0,09 | 0,07 | 0,05 | 0,06 | 0,10 | 0,05 | 0,06 | 0,10 | 0,09 | 0,09 | 0,09 | 0,05 |
| | $Fe_2O_3$ | 0,19 | 0,05 | 0,04 | 0,00 | 0,17 | 0,08 | 0,04 | 0,06 | 0,10 | 0,08 | 0,06 | 0,07 | 0,11 | 0,05 | 0,06 | 0,11 | 0,10 | 0,10 | 0,10 | 0,05 |
| | MgO | 0,09 | 0,05 | 0,03 | 0,00 | 0,01 | 0,00 | 0,00 | 0,00 | 0,02 | 0,00 | 0,00 | 0,00 | 0,00 | 0,00 | 0,00 | 0,00 | 0,00 | 0,00 | 0,00 | 0,00 |
| | BaO | 0,10 | 0,00 | 0,01 | 0,06 | 0,06 | 0,01 | 0,05 | 0,04 | 0,07 | 0,00 | 0,00 | 0,00 | 0,02 | 0,06 | 0,00 | 0,00 | 0,05 | 0,06 | 0,00 | 0,00 |
| | CaO | 3,06 | 5,41 | 8,41 | 8,89 | 8,71 | 8,73 | 8,73 | 8,86 | 8,69 | 8,81 | 8,96 | 8,87 | 8,85 | 8,64 | 9,08 | 8,72 | 8,37 | 8,77 | 7,95 | 8,09 |
| | $Na_2O$ | 8,48 | 8,45 | 6,85 | 6,33 | 6,49 | 6,50 | 6,46 | 6,56 | 6,46 | 6,51 | 6,67 | 6,53 | 6,64 | 6,50 | 6,45 | 6,49 | 6,81 | 6,77 | 6,95 | 6,94 |
| | $K_2O$ | 1,85 | 0,46 | 0,08 | 0,06 | 0,08 | 0,08 | 0,06 | 0,06 | 0,22 | 0,07 | 0,06 | 0,09 | 0,09 | 0,04 | 0,07 | 0,08 | 0,09 | 0,06 | 0,05 | 0,07 |
| **Feldspar** | sum | 98,11 | 99,30 | 97,72 | 97,20 | 98,17 | 98,08 | 98,11 | 98,28 | 98,13 | 98,02 | 98,41 | 98,25 | 98,64 | 97,88 | 98,26 | 97,82 | 98,50 | 98,40 | 97,56 | 97,78 |
| | **Cations** | | | | | | | | | | | | | | | | | | | | |
| | Si | 2,74 | 2,71 | 2,57 | 2,57 | 2,59 | 2,57 | 2,57 | 2,57 | 2,57 | 2,58 | 2,57 | 2,57 | 2,59 | 2,57 | 2,57 | 2,58 | 2,59 | 2,57 | 2,62 | 2,61 |
| | Al | 1,29 | 1,29 | 1,42 | 1,42 | 1,40 | 1,42 | 1,43 | 1,42 | 1,42 | 1,41 | 1,41 | 1,42 | 1,40 | 1,42 | 1,42 | 1,41 | 1,40 | 1,42 | 1,38 | 1,38 |
| | $Fe^{3+}$ | 0,01 | 0,00 | 0,00 | 0,00 | 0,01 | 0,00 | 0,00 | 0,00 | 0,00 | 0,00 | 0,00 | 0,00 | 0,00 | 0,00 | 0,00 | 0,00 | 0,00 | 0,00 | 0,00 | 0,00 |
| | Mg | 0,01 | 0,00 | 0,00 | 0,00 | 0,00 | 0,00 | 0,00 | 0,00 | 0,00 | 0,00 | 0,00 | 0,00 | 0,00 | 0,00 | 0,00 | 0,00 | 0,00 | 0,00 | 0,00 | 0,00 |
| | Ba | 0,00 | 0,00 | 0,00 | 0,00 | 0,00 | 0,00 | 0,00 | 0,00 | 0,00 | 0,00 | 0,00 | 0,00 | 0,00 | 0,00 | 0,00 | 0,00 | 0,00 | 0,00 | 0,00 | 0,00 |
| | Ca | 0,15 | 0,26 | 0,41 | 0,44 | 0,43 | 0,43 | 0,43 | 0,43 | 0,43 | 0,43 | 0,44 | 0,43 | 0,43 | 0,42 | 0,44 | 0,43 | 0,41 | 0,43 | 0,39 | 0,40 |
| | Na | 0,75 | 0,73 | 0,61 | 0,57 | 0,57 | 0,58 | 0,57 | 0,58 | 0,57 | 0,58 | 0,59 | 0,58 | 0,59 | 0,58 | 0,57 | 0,58 | 0,60 | 0,60 | 0,62 | 0,62 |
| | K | 0,11 | 0,03 | 0,00 | 0,00 | 0,00 | 0,00 | 0,00 | 0,00 | 0,01 | 0,00 | 0,00 | 0,00 | 0,00 | 0,00 | 0,00 | 0,00 | 0,01 | 0,00 | 0,00 | 0,00 |
| | sum | 5,04 | 5,02 | 5,02 | 5,00 | 5,00 | 5,00 | 5,00 | 5,01 | 5,01 | 5,01 | 5,02 | 5,01 | 5,01 | 5,00 | 5,01 | 5,00 | 5,01 | 5,02 | 5,01 | 5,01 |
| | xAn | 14,83 | 25,48 | 40,24 | 43,55 | 42,37 | 42,43 | 42,60 | 42,58 | 42,07 | 42,62 | 42,45 | 42,66 | 42,19 | 42,25 | 43,57 | 42,43 | 40,24 | 41,57 | 38,61 | 39,01 |
| | xAb | 74,47 | 71,95 | 59,34 | 56,12 | 57,15 | 57,14 | 57,07 | 57,06 | 56,65 | 57,00 | 57,20 | 56,85 | 57,32 | 57,50 | 56,03 | 57,13 | 59,26 | 58,10 | 61,11 | 60,57 |
| | xOr | 10,70 | 2,58 | 0,43 | 0,33 | 0,47 | 0,43 | 0,34 | 0,36 | 1,28 | 0,38 | 0,36 | 0,49 | 0,49 | 0,25 | 0,41 | 0,44 | 0,50 | 0,33 | 0,28 | 0,41 |
| | sum | 100,00 | 100,00 | 100,00 | 100,00 | 100,00 | 100,00 | 100,00 | 100,00 | 100,00 | 100,00 | 100,00 | 100,00 | 100,00 | 100,00 | 100,00 | 100,00 | 100,00 | 100,00 | 100,00 | 100,00 |

**Annex II** – Mineral analyses, Depiné (2008).

| | Sample | 101203-1 | | | | | | | | | | 101203-2 | | | | | | | | | |
|---|---|---|---|---|---|---|---|---|---|---|---|---|---|---|---|---|---|---|---|---|---|
| | **Ox. wt%** | **P11** | **P12** | **P13** | **P14** | **P15** | **P16** | **P18** | **P19** | **P20** | **P2** | **P1** | **P2** | **P3** | **P4** | **P5** | **P6** | **P7** | **P8** | **P10** | **P2** |
| | $SiO_2$ | 56,56 | 56,67 | 56,31 | 56,82 | 57,05 | 58,90 | 56,91 | 57,30 | 56,58 | 58,24 | 58,81 | 58,75 | 58,29 | 58,63 | 58,48 | 58,24 | 58,08 | 61,89 | 58,53 | 57,97 |
| | $Al_2O_3$ | 25,84 | 25,94 | 26,03 | 25,85 | 26,48 | 25,39 | 26,03 | 26,02 | 26,03 | 25,81 | 25,72 | 25,79 | 26,15 | 26,26 | 25,78 | 26,15 | 25,90 | 24,13 | 26,10 | 26,33 |
| | FeO | 0,00 | 0,04 | 0,03 | 0,02 | 0,05 | 0,11 | 0,07 | 0,06 | 0,08 | 0,00 | 0,00 | 0,02 | 0,01 | 0,08 | 0,10 | 0,02 | 0,06 | 0,08 | 0,04 | 0,00 |
| | $Fe_2O_3$ | 0,00 | 0,04 | 0,04 | 0,02 | 0,06 | 0,13 | 0,07 | 0,07 | 0,09 | 0,00 | 0,00 | 0,02 | 0,01 | 0,09 | 0,11 | 0,02 | 0,07 | 0,09 | 0,04 | 0,00 |
| | MgO | 0,12 | 0,03 | 0,00 | 0,00 | 0,06 | 0,00 | 0,02 | 0,00 | 0,01 | 0,00 | 0,00 | 0,00 | 0,00 | 0,00 | 0,00 | 0,00 | 0,00 | 0,00 | 0,00 | 0,00 |
| | BaO | 0,00 | 0,07 | 0,06 | 0,05 | 0,00 | 0,01 | 0,02 | 0,05 | 0,00 | 0,00 | 0,00 | 0,00 | 0,00 | 0,02 | 0,00 | 0,00 | 0,00 | 0,01 | 0,00 | 0,08 |
| | CaO | 8,24 | 8,34 | 8,22 | 8,32 | 8,47 | 5,34 | 8,56 | 8,51 | 8,51 | 7,60 | 7,81 | 7,31 | 7,70 | 7,69 | 7,96 | 7,81 | 7,85 | 5,30 | 7,98 | 8,27 |
| | $Na_2O$ | 6,77 | 6,80 | 6,85 | 6,91 | 6,91 | 7,33 | 6,54 | 6,75 | 6,48 | 7,12 | 7,24 | 7,26 | 7,15 | 7,21 | 7,05 | 7,05 | 6,96 | 8,85 | 6,92 | 7,12 |
| | $K_2O$ | 0,09 | 0,07 | 0,05 | 0,07 | 0,10 | 1,33 | 0,08 | 0,05 | 0,10 | 0,08 | 0,09 | 0,11 | 0,09 | 0,10 | 0,08 | 0,09 | 0,12 | 0,08 | 0,08 | 0,05 |
| | sum | 97,62 | 97,97 | 97,55 | 98,04 | 99,12 | 98,41 | 98,22 | 98,73 | 97,79 | 98,85 | 99,67 | 99,24 | 99,38 | 99,98 | 99,44 | 99,36 | 98,96 | 100,33 | 99,66 | 99,81 |
| **Feldspar** | **Cations** | | | | | | | | | | | | | | | | | | | | |
| | Si | 2,59 | 2,59 | 2,59 | 2,60 | 2,58 | 2,67 | 2,59 | 2,60 | 2,59 | 2,63 | 2,64 | 2,64 | 2,62 | 2,62 | 2,63 | 2,62 | 2,62 | 2,74 | 2,62 | 2,60 |
| | Al | 1,40 | 1,40 | 1,41 | 1,39 | 1,41 | 1,36 | 1,40 | 1,39 | 1,40 | 1,37 | 1,36 | 1,37 | 1,38 | 1,38 | 1,36 | 1,39 | 1,38 | 1,26 | 1,38 | 1,39 |
| | $Fe^{3+}$ | 0,00 | 0,00 | 0,00 | 0,00 | 0,00 | 0,00 | 0,00 | 0,00 | 0,00 | 0,00 | 0,00 | 0,00 | 0,00 | 0,00 | 0,00 | 0,00 | 0,00 | 0,00 | 0,00 | 0,00 |
| | Mg | 0,01 | 0,00 | 0,00 | 0,00 | 0,00 | 0,00 | 0,00 | 0,00 | 0,00 | 0,00 | 0,00 | 0,00 | 0,00 | 0,00 | 0,00 | 0,00 | 0,00 | 0,00 | 0,00 | 0,00 |
| | Ba | 0,00 | 0,00 | 0,00 | 0,00 | 0,00 | 0,00 | 0,00 | 0,00 | 0,00 | 0,00 | 0,00 | 0,00 | 0,00 | 0,00 | 0,00 | 0,00 | 0,00 | 0,00 | 0,00 | 0,00 |
| | Ca | 0,41 | 0,41 | 0,40 | 0,41 | 0,41 | 0,26 | 0,42 | 0,41 | 0,42 | 0,37 | 0,37 | 0,35 | 0,37 | 0,37 | 0,38 | 0,38 | 0,38 | 0,25 | 0,38 | 0,40 |
| | Na | 0,60 | 0,60 | 0,61 | 0,61 | 0,61 | 0,64 | 0,58 | 0,59 | 0,58 | 0,62 | 0,63 | 0,63 | 0,62 | 0,62 | 0,61 | 0,61 | 0,61 | 0,76 | 0,60 | 0,62 |
| | K | 0,01 | 0,00 | 0,00 | 0,00 | 0,01 | 0,08 | 0,00 | 0,00 | 0,01 | 0,00 | 0,01 | 0,01 | 0,01 | 0,01 | 0,00 | 0,01 | 0,01 | 0,00 | 0,00 | 0,00 |
| | sum | 5,01 | 5,01 | 5,02 | 5,01 | 5,02 | 5,01 | 5,00 | 5,00 | 5,00 | 5,00 | 5,00 | 5,00 | 5,00 | 5,00 | 5,00 | 5,00 | 5,00 | 5,01 | 4,99 | 5,01 |
| | xAn | 40,02 | 40,24 | 39,75 | 39,77 | 40,15 | 26,44 | 41,79 | 40,95 | 41,79 | 37,15 | 35,53 | 37,11 | 36,86 | 38,26 | 37,77 | 38,13 | 23,48 | 38,71 | 39,01 | 39,42 |
| | xAb | 59,46 | 59,36 | 59,96 | 59,84 | 59,28 | 65,70 | 57,77 | 58,78 | 57,62 | 62,34 | 63,87 | 62,38 | 62,59 | 61,29 | 61,72 | 61,19 | 67,65 | 60,82 | 60,74 | 60,14 |
| | xOr | 0,52 | 0,41 | 0,29 | 0,39 | 0,57 | 7,86 | 0,44 | 0,27 | 0,59 | 0,50 | 0,61 | 0,52 | 0,55 | 0,45 | 0,52 | 0,68 | 8,87 | 0,47 | 0,25 | 0,44 |
| | sum | 100,00 | 100,00 | 100,00 | 100,00 | 100,00 | 100,00 | 100,00 | 100,00 | 100,00 | 100,00 | 100,00 | 100,00 | 100,00 | 100,00 | 100,00 | 100,00 | 100,00 | 100,00 | 100,00 | 100,00 |

**Annex II** – Mineral analyses, Depiné (2008).

| | Sample | 101203-2 | | | | | | | | | | | | | | | | | | |
|---|---|---|---|---|---|---|---|---|---|---|---|---|---|---|---|---|---|---|---|---|
| | **Ox. wt%** | **P4** | **P5** | **P6** | **P1** | **P2** | **P4** | **P5** | **P1** | **P2** | **P3** | **P4** | **P5** | **P6** | **P1** | **P2** | **P3** | **P4** | **P5** | **P6** | **P8** |
| | $SiO_2$ | 58,17 | 58,09 | 59,04 | 57,91 | 61,09 | 57,77 | 60,42 | 60,52 | 58,92 | 57,81 | 57,79 | 58,31 | 62,19 | 58,61 | 58,08 | 57,69 | 58,09 | 58,57 | 57,98 | 58,51 |
| | $Al_2O_3$ | 26,17 | 26,44 | 26,04 | 26,33 | 25,02 | 26,50 | 25,03 | 24,97 | 26,04 | 26,48 | 26,41 | 26,44 | 23,27 | 25,70 | 26,61 | 26,45 | 26,39 | 26,40 | 26,43 | 25,91 |
| | FeO | 0,02 | 0,06 | 0,01 | 0,08 | 0,20 | 0,05 | 0,13 | 0,18 | 0,03 | 0,04 | 0,05 | 0,06 | 0,16 | 0,27 | 0,11 | 0,00 | 0,01 | 0,11 | 0,04 | 0,00 |
| | $Fe_2O_3$ | 0,02 | 0,06 | 0,01 | 0,09 | 0,22 | 0,06 | 0,14 | 0,20 | 0,03 | 0,04 | 0,05 | 0,07 | 0,18 | 0,29 | 0,12 | 0,00 | 0,01 | 0,12 | 0,05 | 0,00 |
| | MgO | 0,00 | 0,00 | 0,00 | 0,00 | 0,05 | 0,00 | 0,00 | 0,00 | 0,00 | 0,00 | 0,00 | 0,00 | 0,06 | 0,00 | 0,00 | 0,00 | 0,00 | 0,00 | 0,00 | 0,00 |
| | BaO | 0,00 | 0,01 | 0,09 | 0,00 | 0,01 | 0,01 | 0,00 | 0,06 | 0,03 | 0,00 | 0,08 | 0,06 | 0,00 | 0,06 | 0,01 | 0,01 | 0,03 | 0,00 | 0,00 | 0,00 |
| | CaO | 8,15 | 8,06 | 7,90 | 8,19 | 5,42 | 8,17 | 6,37 | 6,39 | 7,61 | 8,26 | 8,05 | 8,34 | 3,88 | 7,67 | 8,31 | 8,33 | 8,40 | 8,43 | 8,09 | 7,74 |
| | $Na_2O$ | 7,01 | 6,94 | 7,09 | 6,76 | 8,01 | 6,85 | 7,74 | 7,75 | 7,07 | 6,94 | 6,91 | 6,82 | 8,83 | 7,02 | 6,81 | 6,77 | 6,81 | 6,71 | 7,00 | 7,13 |
| | $K_2O$ | 0,09 | 0,09 | 0,13 | 0,08 | 0,72 | 0,08 | 0,08 | 0,09 | 0,12 | 0,07 | 0,22 | 0,11 | 0,74 | 0,24 | 0,10 | 0,06 | 0,09 | 0,08 | 0,07 | 0,08 |
| **Feldspar** | sum | 99,61 | 99,68 | 100,30 | 99,35 | 100,53 | 99,43 | 99,77 | 99,96 | 99,82 | 99,59 | 99,50 | 100,13 | 99,12 | 99,56 | 100,02 | 99,31 | 99,81 | 100,29 | 99,62 | 99,37 |
| | **Cations** | | | | | | | | | | | | | | | | | | | | |
| | Si | 2,61 | 2,60 | 2,63 | 2,60 | 2,70 | 2,60 | 2,69 | 2,69 | 2,63 | 2,60 | 2,60 | 2,61 | 2,78 | 2,63 | 2,60 | 2,60 | 2,60 | 2,61 | 2,60 | 2,63 |
| | Al | 1,38 | 1,40 | 1,37 | 1,40 | 1,31 | 1,40 | 1,31 | 1,31 | 1,37 | 1,40 | 1,40 | 1,39 | 1,23 | 1,36 | 1,40 | 1,40 | 1,39 | 1,39 | 1,40 | 1,37 |
| | $Fe^{3+}$ | 0,00 | 0,00 | 0,00 | 0,00 | 0,01 | 0,00 | 0,00 | 0,01 | 0,00 | 0,00 | 0,00 | 0,00 | 0,01 | 0,01 | 0,00 | 0,00 | 0,00 | 0,00 | 0,00 | 0,00 |
| | Mg | 0,00 | 0,00 | 0,00 | 0,00 | 0,00 | 0,00 | 0,00 | 0,00 | 0,00 | 0,00 | 0,00 | 0,00 | 0,00 | 0,00 | 0,00 | 0,00 | 0,00 | 0,00 | 0,00 | 0,00 |
| | Ba | 0,00 | 0,00 | 0,00 | 0,00 | 0,00 | 0,00 | 0,00 | 0,00 | 0,00 | 0,00 | 0,00 | 0,00 | 0,00 | 0,00 | 0,00 | 0,00 | 0,00 | 0,00 | 0,00 | 0,00 |
| | Ca | 0,39 | 0,39 | 0,38 | 0,39 | 0,26 | 0,39 | 0,30 | 0,30 | 0,36 | 0,40 | 0,39 | 0,40 | 0,19 | 0,37 | 0,40 | 0,40 | 0,40 | 0,40 | 0,39 | 0,37 |
| | Na | 0,61 | 0,60 | 0,61 | 0,59 | 0,69 | 0,60 | 0,67 | 0,67 | 0,61 | 0,60 | 0,60 | 0,59 | 0,76 | 0,61 | 0,59 | 0,59 | 0,59 | 0,58 | 0,61 | 0,62 |
| | K | 0,01 | 0,01 | 0,01 | 0,00 | 0,04 | 0,00 | 0,00 | 0,01 | 0,01 | 0,00 | 0,01 | 0,01 | 0,04 | 0,01 | 0,01 | 0,00 | 0,01 | 0,00 | 0,00 | 0,00 |
| | sum | 5,00 | 5,00 | 5,00 | 4,99 | 5,00 | 5,00 | 4,99 | 4,99 | 4,99 | 5,00 | 5,01 | 5,00 | 5,01 | 5,00 | 5,00 | 5,00 | 5,00 | 4,99 | 5,00 | 5,00 |
| | xAn | 38,90 | 37,82 | 39,92 | 26,11 | 39,04 | 31,11 | 31,14 | 37,05 | 39,54 | 38,68 | 40,10 | 18,70 | 37,14 | 40,03 | 40,33 | 40,32 | 40,77 | 38,82 | 34,19 | 38,05 |
| | xAb | 60,57 | 61,42 | 59,64 | 69,75 | 60,63 | 68,40 | 68,33 | 62,25 | 60,08 | 60,07 | 59,27 | 77,06 | 61,47 | 59,42 | 59,30 | 59,16 | 58,75 | 60,77 | 52,10 | 61,53 |
| | xOr | 0,52 | 0,76 | 0,44 | 4,14 | 0,33 | 0,49 | 0,52 | 0,71 | 0,38 | 1,26 | 0,62 | 4,23 | 1,40 | 0,55 | 0,37 | 0,52 | 0,48 | 0,41 | 13,72 | 0,42 |
| | sum | 100,00 | 100,00 | 100,00 | 100,00 | 100,00 | 100,00 | 100,00 | 100,00 | 100,00 | 100,00 | 100,00 | 100,00 | 100,00 | 100,00 | 100,00 | 100,00 | 100,00 | 100,00 | 100,00 | 100,00 |

**Annex II** – Mineral analyses, Depiné (2008).

| | Sample | 101203-2 | | 200900-1 | | | | | | | | | | | | | 231104-1 | | | |
|---|---|---|---|---|---|---|---|---|---|---|---|---|---|---|---|---|---|---|---|---|
| | Ox. wt% | P9 | P10 | P2 | P3 | P4 | P5 | P6 | P8 | P9 | P10 | P4 | P5 | P7 | P8 | P9 | P10 | P3 | P4 | P5 | P6 |
| Feldspar | $SiO_2$ | 58,63 | 58,43 | 61,16 | 61,01 | 61,68 | 61,53 | 64,92 | 60,82 | 60,72 | 60,83 | 61,96 | 62,89 | 60,09 | 60,59 | 62,80 | 67,24 | 61,91 | 61,66 | 61,39 | 61,78 |
| | $Al_2O_3$ | 26,00 | 26,08 | 24,40 | 24,27 | 24,79 | 24,40 | 21,95 | 24,89 | 24,58 | 24,02 | 24,06 | 23,12 | 24,97 | 25,25 | 23,45 | 21,02 | 23,40 | 23,60 | 23,62 | 23,48 |
| | FeO | 0,01 | 0,10 | 0,00 | 0,08 | 0,10 | 0,02 | 0,07 | 0,05 | 0,04 | 0,02 | 0,00 | 0,02 | 0,01 | 0,06 | 0,00 | 0,00 | 0,03 | 0,03 | 0,04 | 0,05 |
| | $Fe_2O_3$ | 0,01 | 0,11 | 0,00 | 0,09 | 0,11 | 0,02 | 0,08 | 0,05 | 0,04 | 0,02 | 0,00 | 0,03 | 0,01 | 0,06 | 0,00 | 0,00 | 0,03 | 0,04 | 0,04 | 0,05 |
| | MgO | 0,00 | 0,00 | 0,00 | 0,00 | 0,00 | 0,00 | 0,04 | 0,00 | 0,00 | 0,00 | 0,00 | 0,04 | 0,00 | 0,00 | 0,00 | 0,01 | 0,00 | 0,00 | 0,00 | 0,00 |
| | BaO | 0,00 | 0,01 | 0,00 | 0,00 | 0,00 | 0,04 | 0,00 | 0,05 | 0,04 | 0,00 | 0,04 | 0,00 | 0,06 | 0,06 | 0,07 | 0,01 | 0,03 | 0,00 | 0,04 | 0,00 |
| | CaO | 7,98 | 7,99 | 5,86 | 5,76 | 5,73 | 5,56 | 1,64 | 5,66 | 5,89 | 5,38 | 5,15 | 4,09 | 6,28 | 6,15 | 4,84 | 1,33 | 4,94 | 5,01 | 5,05 | 5,02 |
| | $Na_2O$ | 7,13 | 7,05 | 8,40 | 8,33 | 8,34 | 8,44 | 10,26 | 8,10 | 8,10 | 8,70 | 8,56 | 9,13 | 8,20 | 8,02 | 8,87 | 10,73 | 8,80 | 8,70 | 8,76 | 8,69 |
| | $K_2O$ | 0,07 | 0,08 | 0,02 | 0,05 | 0,06 | 0,06 | 0,47 | 0,03 | 0,03 | 0,02 | 0,05 | 0,18 | 0,05 | 0,07 | 0,06 | 0,07 | 0,11 | 0,07 | 0,07 | 0,09 |
| | sum | 99,83 | 99,85 | 99,84 | 99,59 | 100,81 | 100,07 | 99,43 | 99,65 | 99,44 | 98,99 | 99,82 | 99,50 | 99,67 | 100,26 | 100,09 | 100,41 | 99,25 | 99,11 | 99,01 | 99,16 |
| | **Cations** | | | | | | | | | | | | | | | | | | | | |
| | Si | 2,62 | 2,62 | 2,72 | 2,72 | 2,72 | 2,73 | 2,87 | 2,71 | 2,71 | 2,73 | 2,75 | 2,79 | 2,68 | 2,69 | 2,78 | 2,93 | 2,76 | 2,76 | 2,75 | 2,76 |
| | Al | 1,37 | 1,38 | 1,28 | 1,28 | 1,29 | 1,28 | 1,14 | 1,31 | 1,29 | 1,27 | 1,26 | 1,21 | 1,31 | 1,32 | 1,22 | 1,08 | 1,23 | 1,24 | 1,25 | 1,24 |
| | $Fe^{3+}$ | 0,00 | 0,00 | 0,00 | 0,00 | 0,00 | 0,00 | 0,00 | 0,00 | 0,00 | 0,00 | 0,00 | 0,00 | 0,00 | 0,00 | 0,00 | 0,00 | 0,00 | 0,00 | 0,00 | 0,00 |
| | Mg | 0,00 | 0,00 | 0,00 | 0,00 | 0,00 | 0,00 | 0,00 | 0,00 | 0,00 | 0,00 | 0,00 | 0,00 | 0,00 | 0,00 | 0,00 | 0,00 | 0,00 | 0,00 | 0,00 | 0,00 |
| | Ba | 0,00 | 0,00 | 0,00 | 0,00 | 0,00 | 0,00 | 0,00 | 0,00 | 0,00 | 0,00 | 0,00 | 0,00 | 0,00 | 0,00 | 0,00 | 0,00 | 0,00 | 0,00 | 0,00 | 0,00 |
| | Ca | 0,38 | 0,38 | 0,28 | 0,28 | 0,27 | 0,26 | 0,08 | 0,27 | 0,28 | 0,26 | 0,24 | 0,19 | 0,30 | 0,29 | 0,23 | 0,06 | 0,24 | 0,24 | 0,24 | 0,24 |
| | Na | 0,62 | 0,61 | 0,72 | 0,72 | 0,71 | 0,73 | 0,88 | 0,70 | 0,70 | 0,76 | 0,74 | 0,79 | 0,71 | 0,69 | 0,76 | 0,91 | 0,76 | 0,75 | 0,76 | 0,75 |
| | K | 0,00 | 0,00 | 0,00 | 0,00 | 0,00 | 0,00 | 0,03 | 0,00 | 0,00 | 0,00 | 0,00 | 0,01 | 0,00 | 0,00 | 0,00 | 0,00 | 0,01 | 0,00 | 0,00 | 0,01 |
| | sum | 5,00 | 5,00 | 5,00 | 5,00 | 4,99 | 5,00 | 5,00 | 4,99 | 4,99 | 5,02 | 4,99 | 5,00 | 5,01 | 5,00 | 4,99 | 4,98 | 5,00 | 5,00 | 5,01 | 5,00 |
| | xAn | 38,34 | 38,34 | 27,78 | 27,56 | 27,44 | 26,60 | 7,88 | 27,81 | 28,60 | 25,44 | 24,88 | 19,62 | 29,65 | 29,62 | 23,09 | 6,37 | 23,52 | 24,04 | 24,08 | 24,08 |
| | xAb | 61,21 | 61,21 | 72,10 | 72,14 | 72,24 | 73,08 | 89,45 | 72,01 | 71,22 | 74,46 | 74,84 | 79,33 | 70,06 | 69,96 | 76,56 | 93,20 | 75,84 | 75,55 | 75,55 | 75,40 |
| | xOr | 0,45 | 0,45 | 0,11 | 0,30 | 0,32 | 0,32 | 2,67 | 0,18 | 0,19 | 0,10 | 0,28 | 1,05 | 0,29 | 0,41 | 0,35 | 0,42 | 0,65 | 0,41 | 0,37 | 0,52 |
| | sum | 100,00 | 100,00 | 100,00 | 100,00 | 100,00 | 100,00 | 100,00 | 100,00 | 100,00 | 100,00 | 100,00 | 100,00 | 100,00 | 100,00 | 100,00 | 100,00 | 100,00 | 100,00 | 100,00 | 100,00 |

**Annex II** – Mineral analyses, Depiné (2008).

| | Sample | 231104-1 | | | | | | | | | 260406-4 | | | | | | | | | | |
|---|---|---|---|---|---|---|---|---|---|---|---|---|---|---|---|---|---|---|---|---|---|
| | **Ox. wt%** | **P7** | **P8** | **P3** | **P4** | **P5** | **P7** | **P8** | **P9** | **P10** | **P3** | **P4** | **P5** | **P6** | **P7** | **P1** | **P2** | **P3** | **P4** | **P5** | **P6** |
| **Feldspar** | $SiO_2$ | 61,64 | 61,70 | 62,11 | 62,29 | 64,51 | 61,73 | 62,03 | 61,58 | 62,76 | 46,89 | 46,97 | 47,56 | 47,10 | 46,73 | 46,61 | 47,01 | 47,22 | 47,02 | 47,12 | 45,99 |
| | $Al_2O_3$ | 23,47 | 23,80 | 23,58 | 23,22 | 23,46 | 23,72 | 23,96 | 23,82 | 23,58 | 33,92 | 33,79 | 33,54 | 33,76 | 33,99 | 33,73 | 33,60 | 33,86 | 33,30 | 33,64 | 32,25 |
| | FeO | 0,01 | 0,02 | 0,02 | 0,03 | 0,03 | 0,04 | 0,00 | 0,03 | 0,02 | 0,12 | 0,13 | 0,03 | 0,10 | 0,08 | 0,22 | 0,06 | 0,05 | 0,07 | 0,07 | 1,70 |
| | $Fe_2O_3$ | 0,01 | 0,02 | 0,03 | 0,03 | 0,03 | 0,04 | 0,00 | 0,04 | 0,02 | 0,13 | 0,14 | 0,04 | 0,11 | 0,09 | 0,25 | 0,07 | 0,05 | 0,07 | 0,08 | 1,89 |
| | MgO | 0,00 | 0,00 | 0,00 | 0,00 | 0,01 | 0,00 | 0,00 | 0,00 | 0,00 | 0,00 | 0,00 | 0,00 | 0,00 | 0,00 | 0,00 | 0,00 | 0,00 | 0,00 | 0,00 | 0,00 |
| | BaO | 0,00 | 0,05 | 0,03 | 0,02 | 0,00 | 0,03 | 0,00 | 0,00 | 0,00 | 0,00 | 0,00 | 0,04 | 0,03 | 0,09 | 0,01 | 0,09 | 0,00 | 0,00 | 0,00 | 0,01 |
| | CaO | 5,06 | 4,78 | 4,75 | 4,71 | 3,65 | 4,91 | 5,08 | 5,06 | 4,64 | 16,96 | 17,30 | 16,52 | 17,24 | 17,34 | 16,91 | 17,15 | 17,02 | 16,75 | 16,84 | 17,46 |
| | $Na_2O$ | 8,68 | 8,60 | 8,84 | 8,80 | 9,11 | 8,88 | 8,69 | 8,57 | 8,93 | 1,83 | 1,81 | 1,88 | 1,82 | 1,84 | 1,91 | 1,84 | 1,96 | 2,04 | 1,85 | 1,70 |
| | $K_2O$ | 0,08 | 0,07 | 0,06 | 0,11 | 0,17 | 0,07 | 0,09 | 0,11 | 0,10 | 0,00 | 0,02 | 0,29 | 0,00 | 0,04 | 0,07 | 0,01 | 0,03 | 0,03 | 0,02 | 0,06 |
| | sum | 98,94 | 99,02 | 99,39 | 99,18 | 100,93 | 99,38 | 99,83 | 99,18 | 100,03 | 99,73 | 100,02 | 99,86 | 100,04 | 100,11 | 99,46 | 99,76 | 100,13 | 99,21 | 99,53 | 99,18 |
| | **Cations** | | | | | | | | | | | | | | | | | | | | |
| | Si | 2,76 | 2,76 | 2,77 | 2,78 | 2,81 | 2,75 | 2,75 | 2,75 | 2,78 | 2,16 | 2,16 | 2,18 | 2,16 | 2,15 | 2,15 | 2,17 | 2,16 | 2,18 | 2,17 | 2,14 |
| | Al | 1,24 | 1,25 | 1,24 | 1,22 | 1,21 | 1,25 | 1,25 | 1,25 | 1,23 | 1,84 | 1,83 | 1,82 | 1,83 | 1,84 | 1,84 | 1,82 | 1,83 | 1,82 | 1,83 | 1,77 |
| | $Fe^{3+}$ | 0,00 | 0,00 | 0,00 | 0,00 | 0,00 | 0,00 | 0,00 | 0,00 | 0,00 | 0,00 | 0,00 | 0,00 | 0,00 | 0,00 | 0,01 | 0,00 | 0,00 | 0,00 | 0,00 | 0,07 |
| | Mg | 0,00 | 0,00 | 0,00 | 0,00 | 0,00 | 0,00 | 0,00 | 0,00 | 0,00 | 0,00 | 0,00 | 0,00 | 0,00 | 0,00 | 0,00 | 0,00 | 0,00 | 0,00 | 0,00 | 0,00 |
| | Ba | 0,00 | 0,00 | 0,00 | 0,00 | 0,00 | 0,00 | 0,00 | 0,00 | 0,00 | 0,00 | 0,00 | 0,00 | 0,00 | 0,00 | 0,00 | 0,00 | 0,00 | 0,00 | 0,00 | 0,00 |
| | Ca | 0,24 | 0,23 | 0,23 | 0,23 | 0,17 | 0,23 | 0,24 | 0,24 | 0,22 | 0,84 | 0,85 | 0,81 | 0,85 | 0,85 | 0,84 | 0,85 | 0,84 | 0,83 | 0,83 | 0,87 |
| | Na | 0,75 | 0,75 | 0,76 | 0,76 | 0,77 | 0,77 | 0,75 | 0,74 | 0,77 | 0,16 | 0,16 | 0,17 | 0,16 | 0,16 | 0,17 | 0,16 | 0,17 | 0,18 | 0,17 | 0,15 |
| | K | 0,00 | 0,00 | 0,00 | 0,01 | 0,01 | 0,00 | 0,00 | 0,01 | 0,01 | 0,00 | 0,00 | 0,02 | 0,00 | 0,00 | 0,00 | 0,00 | 0,00 | 0,00 | 0,00 | 0,00 |
| | sum | 5,00 | 4,99 | 5,00 | 4,99 | 4,97 | 5,01 | 5,00 | 5,00 | 5,00 | 5,00 | 5,01 | 5,00 | 5,00 | 5,01 | 5,01 | 5,00 | 5,01 | 5,01 | 5,00 | 5,01 |
| | xAn | 24,24 | 23,40 | 22,80 | 22,69 | 17,93 | 23,29 | 24,30 | 24,44 | 22,19 | 83,63 | 84,00 | 81,51 | 83,99 | 83,70 | 82,69 | 83,71 | 82,57 | 81,77 | 83,32 | 84,69 |
| | xAb | 75,28 | 76,17 | 76,84 | 76,70 | 81,10 | 76,30 | 75,21 | 74,91 | 77,27 | 16,34 | 15,87 | 16,78 | 16,00 | 16,10 | 16,92 | 16,22 | 17,25 | 18,06 | 16,58 | 14,95 |
| | xOr | 0,47 | 0,43 | 0,36 | 0,61 | 0,97 | 0,41 | 0,50 | 0,65 | 0,54 | 0,02 | 0,13 | 1,71 | 0,01 | 0,21 | 0,40 | 0,08 | 0,18 | 0,17 | 0,10 | 0,36 |
| | sum | 100,00 | 100,00 | 100,00 | 100,00 | 100,00 | 100,00 | 100,00 | 100,00 | 100,00 | 100,00 | 100,00 | 100,00 | 100,00 | 100,00 | 100,00 | 100,00 | 100,00 | 100,00 | 100,00 | 100,00 |

**Annex II** – Mineral analyses, Depiné (2008).

| | Sample | 260406-4 | | | | | 260406-10 | | | | | | | | | | | | | | |
|---|---|---|---|---|---|---|---|---|---|---|---|---|---|---|---|---|---|---|---|---|---|
| | **Ox. wt%** | **P1** | **P3** | **P4** | **P2** | **P3** | **P2** | **P4** | **P5** | **P7** | **P8** | **P1** | **P3** | **P4** | **P5** | **P6** | **P7** | **P8** | **P9** | **P10** | **P3** |
| | $SiO_2$ | 49,61 | 48,06 | 46,90 | 46,99 | 46,91 | 52,22 | 52,16 | 51,34 | 51,82 | 50,88 | 52,87 | 55,20 | 51,43 | 51,45 | 52,11 | 51,87 | 62,22 | 51,95 | 52,68 | 51,91 |
| | $Al_2O_3$ | 31,77 | 32,31 | 33,39 | 33,74 | 33,61 | 30,25 | 29,85 | 30,38 | 30,41 | 31,14 | 29,74 | 29,39 | 30,86 | 30,74 | 30,37 | 30,50 | 23,50 | 30,55 | 30,05 | 30,20 |
| | FeO | 0,04 | 0,04 | 0,08 | 0,03 | 0,01 | 0,08 | 0,29 | 0,24 | 0,15 | 0,33 | 0,38 | 0,52 | 0,10 | 0,02 | 0,02 | 0,05 | 0,11 | 0,10 | 0,16 | 0,03 |
| | $Fe_2O_3$ | 0,04 | 0,05 | 0,08 | 0,04 | 0,01 | 0,09 | 0,33 | 0,27 | 0,17 | 0,37 | 0,42 | 0,58 | 0,11 | 0,03 | 0,02 | 0,06 | 0,12 | 0,11 | 0,18 | 0,03 |
| | MgO | 0,00 | 0,00 | 0,00 | 0,00 | 0,00 | 0,00 | 0,00 | 0,00 | 0,00 | 0,00 | 0,13 | 0,41 | 0,00 | 0,00 | 0,00 | 0,01 | 0,06 | 0,00 | 0,00 | 0,00 |
| | BaO | 0,01 | 0,01 | 0,01 | 0,00 | 0,00 | 0,00 | 0,02 | 0,06 | 0,02 | 0,00 | 0,07 | 0,09 | 0,02 | 0,08 | 0,05 | 0,00 | 0,00 | 0,00 | 0,07 | 0,00 |
| | CaO | 15,12 | 15,36 | 17,01 | 16,91 | 17,07 | 12,84 | 12,65 | 13,27 | 13,20 | 13,89 | 10,20 | 5,89 | 13,47 | 13,50 | 12,94 | 13,01 | 4,61 | 13,37 | 12,48 | 13,02 |
| | $Na_2O$ | 2,49 | 2,76 | 1,94 | 1,87 | 1,98 | 4,18 | 4,38 | 3,89 | 4,15 | 3,75 | 4,59 | 4,89 | 3,94 | 3,84 | 4,21 | 4,07 | 9,05 | 4,09 | 4,51 | 4,20 |
| | $K_2O$ | 0,46 | 0,18 | 0,03 | 0,02 | 0,01 | 0,04 | 0,05 | 0,03 | 0,05 | 0,01 | 1,32 | 2,66 | 0,03 | 0,03 | 0,05 | 0,09 | 0,11 | 0,03 | 0,05 | 0,03 |
| | sum | 99,49 | 98,71 | 99,35 | 99,56 | 99,59 | 99,61 | 99,39 | 99,21 | 99,80 | 100,00 | 99,28 | 99,04 | 99,85 | 99,66 | 99,74 | 99,59 | 99,67 | 100,09 | 100,01 | 99,39 |
| **Feldspar** | **Cations** | | | | | | | | | | | | | | | | | | | | |
| | Si | 2,28 | 2,23 | 2,17 | 2,17 | 2,16 | 2,38 | 2,38 | 2,35 | 2,36 | 2,32 | 2,41 | 2,50 | 2,34 | 2,35 | 2,37 | 2,36 | 2,77 | 2,36 | 2,39 | 2,37 |
| | Al | 1,72 | 1,77 | 1,82 | 1,83 | 1,83 | 1,62 | 1,61 | 1,64 | 1,63 | 1,67 | 1,60 | 1,57 | 1,65 | 1,65 | 1,63 | 1,64 | 1,23 | 1,63 | 1,61 | 1,62 |
| | $Fe^{3+}$ | 0,00 | 0,00 | 0,00 | 0,00 | 0,00 | 0,00 | 0,01 | 0,01 | 0,01 | 0,01 | 0,01 | 0,02 | 0,00 | 0,00 | 0,00 | 0,00 | 0,00 | 0,00 | 0,01 | 0,00 |
| | Mg | 0,00 | 0,00 | 0,00 | 0,00 | 0,00 | 0,00 | 0,00 | 0,00 | 0,00 | 0,00 | 0,01 | 0,03 | 0,00 | 0,00 | 0,00 | 0,00 | 0,00 | 0,00 | 0,00 | 0,00 |
| | Ba | 0,00 | 0,00 | 0,00 | 0,00 | 0,00 | 0,00 | 0,00 | 0,00 | 0,00 | 0,00 | 0,00 | 0,00 | 0,00 | 0,00 | 0,00 | 0,00 | 0,00 | 0,00 | 0,00 | 0,00 |
| | Ca | 0,74 | 0,76 | 0,84 | 0,84 | 0,84 | 0,63 | 0,62 | 0,65 | 0,64 | 0,68 | 0,50 | 0,29 | 0,66 | 0,66 | 0,63 | 0,63 | 0,22 | 0,65 | 0,61 | 0,64 |
| | Na | 0,22 | 0,25 | 0,17 | 0,17 | 0,18 | 0,37 | 0,39 | 0,35 | 0,37 | 0,33 | 0,41 | 0,43 | 0,35 | 0,34 | 0,37 | 0,36 | 0,78 | 0,36 | 0,40 | 0,37 |
| | K | 0,03 | 0,01 | 0,00 | 0,00 | 0,00 | 0,00 | 0,00 | 0,00 | 0,00 | 0,00 | 0,08 | 0,15 | 0,00 | 0,00 | 0,00 | 0,01 | 0,01 | 0,00 | 0,00 | 0,00 |
| | sum | 4,99 | 5,02 | 5,01 | 5,00 | 5,01 | 5,00 | 5,01 | 5,00 | 5,01 | 5,01 | 5,02 | 4,99 | 5,00 | 5,00 | 5,00 | 5,00 | 5,01 | 5,01 | 5,01 | 5,00 |
| | xAn | 74,95 | 74,71 | 82,74 | 83,26 | 82,62 | 62,81 | 61,32 | 65,24 | 63,53 | 67,16 | 50,81 | 32,92 | 65,32 | 65,88 | 62,75 | 63,50 | 21,84 | 64,25 | 60,27 | 63,02 |
| | xAb | 22,31 | 24,26 | 17,09 | 16,63 | 17,31 | 36,97 | 38,41 | 34,61 | 36,17 | 32,77 | 41,37 | 49,41 | 34,52 | 33,95 | 36,99 | 35,97 | 77,55 | 35,57 | 39,42 | 36,79 |
| | xOr | 2,73 | 1,03 | 0,18 | 0,11 | 0,07 | 0,22 | 0,28 | 0,16 | 0,30 | 0,07 | 7,82 | 17,68 | 0,16 | 0,17 | 0,26 | 0,53 | 0,61 | 0,18 | 0,31 | 0,19 |
| | sum | 100,00 | 100,00 | 100,00 | 100,00 | 100,00 | 100,00 | 100,00 | 100,00 | 100,00 | 100,00 | 100,00 | 100,00 | 100,00 | 100,00 | 100,00 | 100,00 | 100,00 | 100,00 | 100,00 | 100,00 |

**Annex II** – Mineral analyses, Depiné (2008).

| | Sample | 260406-10 | | | | | | | | | | | | | | 260406-14 | | | | | |
|---|---|---|---|---|---|---|---|---|---|---|---|---|---|---|---|---|---|---|---|---|---|
| | **Ox. wt%** | **P4** | **P5** | **P6** | **P7** | **P9** | **P10** | **P1** | **P3** | **P5** | **P6** | **P7** | **P8** | **P9** | **P1** | **P1** | **P2** | **P3** | **P4** | **P5** | **P6** |
| **Feldspar** | $SiO_2$ | 52,53 | 55,23 | 55,46 | 52,73 | 51,53 | 50,71 | 51,56 | 54,72 | 56,09 | 56,01 | 55,74 | 55,71 | 55,10 | 51,19 | 63,51 | 63,43 | 63,78 | 64,04 | 63,25 | 63,66 |
| | $Al_2O_3$ | 29,45 | 28,51 | 27,93 | 29,52 | 30,14 | 31,13 | 30,39 | 28,70 | 27,81 | 27,81 | 27,71 | 27,75 | 28,48 | 30,71 | 18,33 | 18,52 | 18,29 | 18,40 | 18,34 | 18,36 |
| | FeO | 0,02 | 0,07 | 0,13 | 0,36 | 0,06 | 0,39 | 0,06 | 0,03 | 0,01 | 0,00 | 0,01 | 0,01 | 0,02 | 0,18 | 0,01 | 0,02 | 0,00 | 0,00 | 0,02 | 0,00 |
| | $Fe_2O_3$ | 0,02 | 0,07 | 0,14 | 0,40 | 0,06 | 0,43 | 0,07 | 0,04 | 0,01 | 0,00 | 0,01 | 0,01 | 0,02 | 0,20 | 0,01 | 0,02 | 0,00 | 0,00 | 0,02 | 0,00 |
| | MgO | 0,00 | 0,00 | 0,00 | 0,18 | 0,00 | 0,00 | 0,00 | 0,00 | 0,00 | 0,00 | 0,00 | 0,00 | 0,00 | 0,00 | 0,00 | 0,00 | 0,00 | 0,00 | 0,01 | 0,02 |
| | BaO | 0,00 | 0,02 | 0,00 | 0,04 | 0,00 | 0,05 | 0,00 | 0,00 | 0,05 | 0,02 | 0,00 | 0,00 | 0,00 | 0,01 | 0,58 | 0,56 | 0,59 | 0,58 | 0,55 | 0,61 |
| | CaO | 11,45 | 10,40 | 10,40 | 10,61 | 13,21 | 13,88 | 13,48 | 10,99 | 9,89 | 9,94 | 9,76 | 9,99 | 10,72 | 13,38 | 0,00 | 0,00 | 0,00 | 0,00 | 0,01 | 0,00 |
| | $Na_2O$ | 4,52 | 5,63 | 5,75 | 4,24 | 4,04 | 3,68 | 3,96 | 5,35 | 5,97 | 5,96 | 6,03 | 5,87 | 5,44 | 3,97 | 0,50 | 0,72 | 0,56 | 0,62 | 0,69 | 0,64 |
| | $K_2O$ | 0,29 | 0,06 | 0,06 | 1,12 | 0,02 | 0,03 | 0,05 | 0,05 | 0,07 | 0,02 | 0,04 | 0,02 | 0,06 | 0,02 | 15,41 | 14,94 | 15,19 | 15,23 | 15,09 | 15,06 |
| | sum | 98,25 | 99,93 | 99,73 | 98,81 | 99,00 | 99,87 | 99,50 | 99,84 | 99,88 | 99,76 | 99,29 | 99,34 | 99,82 | 99,47 | 98,35 | 98,19 | 98,41 | 98,86 | 97,96 | 98,34 |
| | **Cations** | | | | | | | | | | | | | | | | | | | | |
| | Si | 2,42 | 2,49 | 2,50 | 2,42 | 2,36 | 2,31 | 2,35 | 2,47 | 2,52 | 2,52 | 2,52 | 2,52 | 2,49 | 2,34 | 2,99 | 2,98 | 3,00 | 2,99 | 2,99 | 2,99 |
| | Al | 1,60 | 1,51 | 1,49 | 1,59 | 1,63 | 1,67 | 1,64 | 1,53 | 1,47 | 1,48 | 1,48 | 1,48 | 1,51 | 1,65 | 1,02 | 1,03 | 1,01 | 1,01 | 1,02 | 1,02 |
| | $Fe^{3+}$ | 0,00 | 0,00 | 0,00 | 0,01 | 0,00 | 0,01 | 0,00 | 0,00 | 0,00 | 0,00 | 0,00 | 0,00 | 0,00 | 0,01 | 0,00 | 0,00 | 0,00 | 0,00 | 0,00 | 0,00 |
| | Mg | 0,00 | 0,00 | 0,00 | 0,01 | 0,00 | 0,00 | 0,00 | 0,00 | 0,00 | 0,00 | 0,00 | 0,00 | 0,00 | 0,00 | 0,00 | 0,00 | 0,00 | 0,00 | 0,00 | 0,00 |
| | Ba | 0,00 | 0,00 | 0,00 | 0,00 | 0,00 | 0,00 | 0,00 | 0,00 | 0,00 | 0,00 | 0,00 | 0,00 | 0,00 | 0,00 | 0,01 | 0,01 | 0,01 | 0,01 | 0,01 | 0,01 |
| | Ca | 0,56 | 0,50 | 0,50 | 0,52 | 0,65 | 0,68 | 0,66 | 0,53 | 0,48 | 0,48 | 0,47 | 0,48 | 0,52 | 0,66 | 0,00 | 0,00 | 0,00 | 0,00 | 0,00 | 0,00 |
| | Na | 0,40 | 0,49 | 0,50 | 0,38 | 0,36 | 0,33 | 0,35 | 0,47 | 0,52 | 0,52 | 0,53 | 0,51 | 0,48 | 0,35 | 0,05 | 0,07 | 0,05 | 0,06 | 0,06 | 0,06 |
| | K | 0,02 | 0,00 | 0,00 | 0,07 | 0,00 | 0,00 | 0,00 | 0,00 | 0,00 | 0,00 | 0,00 | 0,00 | 0,00 | 0,00 | 0,93 | 0,90 | 0,91 | 0,91 | 0,91 | 0,90 |
| | sum | 5,00 | 5,00 | 5,00 | 5,00 | 5,00 | 5,01 | 5,00 | 5,00 | 5,00 | 5,00 | 5,00 | 5,00 | 5,00 | 5,01 | 4,99 | 4,98 | 4,98 | 4,98 | 4,99 | 4,98 |
| | xAn | 57,31 | 50,35 | 49,82 | 54,06 | 64,29 | 67,46 | 65,14 | 53,01 | 47,62 | 47,88 | 47,13 | 48,40 | 51,93 | 64,98 | 0,00 | 0,00 | 0,00 | 0,00 | 0,07 | 0,00 |
| | xAb | 40,97 | 49,32 | 49,87 | 39,13 | 35,58 | 32,37 | 34,59 | 46,71 | 52,01 | 52,00 | 52,66 | 51,49 | 47,75 | 34,90 | 4,69 | 6,84 | 5,30 | 5,81 | 6,49 | 6,07 |
| | xOr | 1,72 | 0,32 | 0,31 | 6,81 | 0,14 | 0,16 | 0,28 | 0,28 | 0,37 | 0,13 | 0,21 | 0,11 | 0,32 | 0,13 | 95,31 | 93,16 | 94,70 | 94,19 | 93,44 | 93,93 |
| | sum | 100,00 | 100,00 | 100,00 | 100,00 | 100,00 | 100,00 | 100,00 | 100,00 | 100,00 | 100,00 | 100,00 | 100,00 | 100,00 | 100,00 | 100,00 | 100,00 | 100,00 | 100,00 | 100,00 | 100,00 |

**Annex II** – Mineral analyses, Depiné (2008).

| | Sample | 260406-14 | | | | | | | | | |
|---|---|---|---|---|---|---|---|---|---|---|---|
| | **Ox. wt%** | **P7** | **P8** | **P9** | **P1** | **P2** | **P3** | **P4** | **P5** | **P6** | **P7** |
| **Feldspar** | $SiO_2$ | 63,75 | 63,68 | 63,80 | 62,47 | 63,79 | 62,19 | 63,59 | 63,41 | 62,20 | 63,73 |
| | $Al_2O_3$ | 18,54 | 18,45 | 18,52 | 23,34 | 18,59 | 23,53 | 18,42 | 18,52 | 23,63 | 18,74 |
| | FeO | 0,03 | 0,01 | 0,00 | 0,00 | 0,00 | 0,00 | 0,00 | 0,03 | 0,07 | 0,01 |
| | $Fe_2O_3$ | 0,04 | 0,01 | 0,00 | 0,00 | 0,00 | 0,00 | 0,00 | 0,04 | 0,08 | 0,01 |
| | MgO | 0,01 | 0,00 | 0,00 | 0,00 | 0,00 | 0,00 | 0,02 | 0,00 | 0,00 | 0,00 |
| | BaO | 0,61 | 0,63 | 0,50 | 0,00 | 0,56 | 0,03 | 0,55 | 0,58 | 0,00 | 0,61 |
| | CaO | 0,00 | 0,00 | 0,00 | 4,56 | 0,00 | 4,69 | 0,00 | 0,00 | 4,88 | 0,00 |
| | $Na_2O$ | 0,62 | 0,66 | 0,57 | 8,83 | 0,58 | 8,81 | 0,61 | 0,58 | 8,70 | 0,50 |
| | $K_2O$ | 15,11 | 15,13 | 15,20 | 0,24 | 15,26 | 0,16 | 15,42 | 15,30 | 0,12 | 15,52 |
| | sum | 98,67 | 98,55 | 98,60 | 99,44 | 98,79 | 99,42 | 98,59 | 98,42 | 99,60 | 99,10 |
| | **Cations** | | | | | | | | | | |
| | Si | 2,99 | 2,99 | 2,99 | 2,78 | 2,98 | 2,77 | 2,99 | 2,98 | 2,76 | 2,98 |
| | Al | 1,02 | 1,02 | 1,02 | 1,22 | 1,03 | 1,23 | 1,02 | 1,03 | 1,24 | 1,03 |
| | $Fe^{3+}$ | 0,00 | 0,00 | 0,00 | 0,00 | 0,00 | 0,00 | 0,00 | 0,00 | 0,00 | 0,00 |
| | Mg | 0,00 | 0,00 | 0,00 | 0,00 | 0,00 | 0,00 | 0,00 | 0,00 | 0,00 | 0,00 |
| | Ba | 0,01 | 0,01 | 0,01 | 0,00 | 0,01 | 0,00 | 0,01 | 0,01 | 0,00 | 0,01 |
| | Ca | 0,00 | 0,00 | 0,00 | 0,22 | 0,00 | 0,22 | 0,00 | 0,00 | 0,23 | 0,00 |
| | Na | 0,06 | 0,06 | 0,05 | 0,76 | 0,05 | 0,76 | 0,06 | 0,05 | 0,75 | 0,05 |
| | K | 0,90 | 0,91 | 0,91 | 0,01 | 0,91 | 0,01 | 0,92 | 0,92 | 0,01 | 0,93 |
| | sum | 4,98 | 4,98 | 4,98 | 5,00 | 4,98 | 5,00 | 4,99 | 4,99 | 4,99 | 4,99 |
| | xAn | 0,00 | 0,00 | 0,00 | 21,88 | 0,00 | 22,51 | 0,00 | 0,00 | 23,52 | 0,00 |
| | xAb | 5,83 | 6,17 | 5,39 | 76,74 | 5,50 | 76,55 | 5,65 | 5,40 | 75,81 | 4,65 |
| | xOr | 94,17 | 93,83 | 94,61 | 1,38 | 94,50 | 0,93 | 94,35 | 94,60 | 0,67 | 95,35 |
| | sum | 100,00 | 100,00 | 100,00 | 100,00 | 100,00 | 100,00 | 100,00 | 100,00 | 100,00 | 100,00 |

**Annex II** – Mineral analyses, Depiné (2008).

| | Sample | 101203-1 | | | 101203-2 | | | | | | | | | | | | | | | |
|---|---|---|---|---|---|---|---|---|---|---|---|---|---|---|---|---|---|---|---|---|
| | **Ox. wt%** | **P1** | **P2** | **P3** | **P1** | **P12** | **P21** | **P22** | **P31** | **P32** | **P41** | **P42** | **P1** | **P2** | **P3** | **P4** | **P5** | **P6** | **P7** | **P8** | **P9** |
| | $SiO_2$ | 41,88 | 41,64 | 39,35 | 40,56 | 40,98 | 41,56 | 41,45 | 40,37 | 41,25 | 41,75 | 41,53 | 41,47 | 41,22 | 40,99 | 40,68 | 41,1 | 41,17 | 42,16 | 41,62 | 41,41 |
| | $TiO_2$ | 0,94 | 0,96 | 0,34 | 1,04 | 1,08 | 0,81 | 1,11 | 0,53 | 1,01 | 0,77 | 1,11 | 0,94 | 1,07 | 1,18 | 1,1 | 1,1 | 1,09 | 1,02 | 1,13 | 1,14 |
| | $Al_2O_3$ | 12,70 | 12,58 | 15,58 | 13,09 | 13,12 | 14,18 | 12,81 | 15,16 | 13,03 | 13,81 | 12,75 | 12,94 | 12,88 | 13,40 | 12,96 | 12,99 | 12,97 | 12,56 | 12,90 | 12,59 |
| | $Cr_2O_3$ | 0,06 | 0,08 | 0,00 | 0,01 | 0,00 | 0,00 | 0,00 | 0,00 | 0,03 | 0,00 | 0,00 | 0,03 | 0,00 | 0,00 | 0,04 | 0,01 | 0,00 | 0,03 | 0,05 | 0,00 |
| | $Fe_2O_3$ | 5,86 | 6,09 | 7,40 | 7,15 | 7,65 | 5,84 | 7,04 | 5,82 | 6,61 | 5,24 | 7,26 | 5,99 | 6,60 | 6,48 | 7,01 | 6,22 | 6,27 | 5,97 | 6,83 | 6,47 |
| | FeO | 13,77 | 13,32 | 13,28 | 14,56 | 14,90 | 15,16 | 15,29 | 14,90 | 14,84 | 15,60 | 15,32 | 15,61 | 15,55 | 15,85 | 15,33 | 15,43 | 15,12 | 15,09 | 15,57 | 15,59 |
| | MgO | 7,74 | 7,87 | 6,18 | 6,85 | 6,85 | 6,70 | 6,94 | 5,98 | 6,94 | 6,54 | 6,86 | 6,58 | 6,62 | 6,29 | 6,51 | 6,56 | 6,71 | 7,19 | 6,69 | 6,83 |
| | MnO | 0,34 | 0,37 | 0,23 | 0,22 | 0,23 | 0,25 | 0,18 | 0,23 | 0,36 | 0,25 | 0,21 | 0,30 | 0,29 | 0,29 | 0,29 | 0,26 | 0,35 | 0,33 | 0,29 | 0,21 |
| | CaO | 11,47 | 11,46 | 11,56 | 10,81 | 10,77 | 11,34 | 10,90 | 11,59 | 10,93 | 11,54 | 11,12 | 11,22 | 10,90 | 11,04 | 10,73 | 11,23 | 11,22 | 11,44 | 11,27 | 10,82 |
| | $Na_2O$ | 1,34 | 1,42 | 1,38 | 1,42 | 1,50 | 1,39 | 1,45 | 1,48 | 1,46 | 1,39 | 1,58 | 1,35 | 1,46 | 1,51 | 1,40 | 1,40 | 1,55 | 1,35 | 1,36 | 1,35 |
| | $K_2O$ | 0,68 | 0,62 | 0,84 | 0,63 | 0,66 | 0,62 | 0,65 | 0,50 | 0,62 | 0,55 | 0,73 | 0,62 | 0,61 | 0,74 | 0,72 | 0,65 | 0,64 | 0,53 | 0,63 | 0,65 |
| | sum | 96,77 | 96,39 | 96,13 | 96,33 | 97,74 | 97,85 | 97,81 | 96,55 | 97,09 | 97,42 | 98,46 | 97,05 | 97,20 | 97,77 | 96,77 | 96,94 | 97,09 | 97,66 | 98,33 | 97,06 |
| | **Tetrahedral position** | | | | | | | | | | | | | | | | | | | | |
| | Si.T1 | 5,00 | 5,00 | 5,00 | 5,00 | 5,00 | 5,00 | 5,00 | 5,00 | 5,00 | 5,00 | 5,00 | 5,00 | 5,00 | 5,00 | 5,00 | 5,00 | 5,00 | 5,00 | 5,00 | 5,00 |
| | Si.T2 | 1,41 | 1,39 | 1,10 | 1,27 | 1,26 | 1,31 | 1,32 | 1,22 | 1,32 | 1,37 | 1,31 | 1,37 | 1,33 | 1,28 | 1,28 | 1,33 | 1,33 | 1,41 | 1,32 | 1,36 |
| | Al.T2 | 1,59 | 1,61 | 1,90 | 1,73 | 1,74 | 1,69 | 1,68 | 1,78 | 1,68 | 1,63 | 1,69 | 1,63 | 1,67 | 1,72 | 1,72 | 1,67 | 1,67 | 1,59 | 1,68 | 1,64 |
| | sum | 8,00 | 8,00 | 8,00 | 8,00 | 8,00 | 8,00 | 8,00 | 8,00 | 8,00 | 8,00 | 8,00 | 8,00 | 8,00 | 8,00 | 8,00 | 8,00 | 8,00 | 8,00 | 8,00 | 8,00 |
| | **M1-5** | **(Octahedral)** | | | | | | | | | | | | | | | | | | | |
| | Al.M | 0,70 | 0,67 | 0,95 | 0,66 | 0,62 | 0,84 | 0,62 | 0,98 | 0,68 | 0,85 | 0,60 | 0,72 | 0,66 | 0,70 | 0,64 | 0,69 | 0,69 | 0,67 | 0,63 | 0,63 |
| | Cr | 0,01 | 0,01 | 0,00 | 0,00 | 0,00 | 0,00 | 0,00 | 0,00 | 0,00 | 0,00 | 0,00 | 0,00 | 0,00 | 0,00 | 0,00 | 0,00 | 0,00 | 0,00 | 0,01 | 0,00 |
| | Ti | 0,11 | 0,11 | 0,04 | 0,12 | 0,12 | 0,09 | 0,13 | 0,06 | 0,12 | 0,09 | 0,13 | 0,11 | 0,12 | 0,14 | 0,13 | 0,13 | 0,13 | 0,12 | 0,13 | 0,13 |
| | $Fe^{3+}$ | 0,67 | 0,70 | 0,86 | 0,83 | 0,88 | 0,67 | 0,81 | 0,68 | 0,76 | 0,60 | 0,83 | 0,69 | 0,76 | 0,75 | 0,81 | 0,72 | 0,73 | 0,68 | 0,78 | 0,75 |
| | $Fe^{2+}$ | 1,76 | 1,71 | 1,72 | 1,88 | 1,90 | 1,92 | 1,95 | 1,92 | 1,90 | 1,99 | 1,95 | 2,01 | 2,00 | 2,03 | 1,98 | 1,99 | 1,95 | 1,92 | 1,98 | 2,00 |
| | Mg | 1,77 | 1,80 | 1,43 | 1,58 | 1,56 | 1,52 | 1,58 | 1,37 | 1,59 | 1,49 | 1,55 | 1,51 | 1,51 | 1,44 | 1,50 | 1,51 | 1,54 | 1,63 | 1,51 | 1,56 |
| | Mn | 0,04 | 0,05 | 0,03 | 0,03 | 0,03 | 0,03 | 0,02 | 0,03 | 0,05 | 0,03 | 0,03 | 0,04 | 0,04 | 0,04 | 0,04 | 0,03 | 0,05 | 0,04 | 0,04 | 0,03 |
| | sum | 5,06 | 5,05 | 5,04 | 5,10 | 5,11 | 5,07 | 5,10 | 5,04 | 5,10 | 5,05 | 5,09 | 5,07 | 5,10 | 5,09 | 5,10 | 5,07 | 5,07 | 5,06 | 5,08 | 5,10 |
| | **B-Position** | **(Hexahedral)** | | | | | | | | | | | | | | | | | | | |
| | Ca | 1,88 | 1,89 | 1,92 | 1,79 | 1,76 | 1,84 | 1,78 | 1,91 | 1,80 | 1,89 | 1,81 | 1,85 | 1,79 | 1,81 | 1,78 | 1,85 | 1,85 | 1,87 | 1,83 | 1,78 |
| | Na | 0,12 | 0,11 | 0,08 | 0,21 | 0,24 | 0,16 | 0,22 | 0,09 | 0,20 | 0,11 | 0,19 | 0,15 | 0,21 | 0,19 | 0,22 | 0,15 | 0,15 | 0,13 | 0,17 | 0,22 |
| | sum | 2,00 | 2,00 | 2,00 | 2,00 | 2,00 | 2,00 | 2,00 | 2,00 | 2,00 | 2,00 | 2,00 | 2,00 | 2,00 | 2,00 | 2,00 | 2,00 | 2,00 | 2,00 | 2,00 | 2,00 |
| | **A-Position** | | | | | | | | | | | | | | | | | | | | |
| | Na | 0,28 | 0,31 | 0,34 | 0,22 | 0,20 | 0,25 | 0,21 | 0,36 | 0,23 | 0,30 | 0,28 | 0,25 | 0,23 | 0,26 | 0,19 | 0,27 | 0,31 | 0,26 | 0,23 | 0,18 |
| | K | 0,13 | 0,12 | 0,16 | 0,12 | 0,13 | 0,12 | 0,12 | 0,10 | 0,12 | 0,11 | 0,14 | 0,12 | 0,12 | 0,14 | 0,14 | 0,13 | 0,12 | 0,10 | 0,12 | 0,13 |
| | sum | 0,41 | 0,43 | 0,50 | 0,34 | 0,33 | 0,37 | 0,33 | 0,45 | 0,35 | 0,40 | 0,42 | 0,37 | 0,35 | 0,40 | 0,33 | 0,40 | 0,44 | 0,36 | 0,36 | 0,31 |
| | xMg | 0,50 | 0,51 | 0,45 | 0,46 | 0,45 | 0,44 | 0,45 | 0,42 | 0,45 | 0,43 | 0,44 | 0,43 | 0,43 | 0,41 | 0,43 | 0,43 | 0,44 | 0,46 | 0,43 | 0,44 |
| | $xFe^{3+}$ | 0,28 | 0,29 | 0,33 | 0,31 | 0,32 | 0,26 | 0,29 | 0,26 | 0,29 | 0,23 | 0,30 | 0,26 | 0,28 | 0,27 | 0,29 | 0,27 | 0,27 | 0,26 | 0,28 | 0,27 |
| | SiTetra | 6,41 | 6,39 | 6,10 | 6,27 | 6,26 | 6,31 | 6,32 | 6,22 | 6,32 | 6,37 | 6,31 | 6,37 | 6,33 | 6,28 | 6,28 | 6,33 | 6,33 | 6,41 | 6,32 | 6,36 |
| | (Na+K)A | 0,41 | 0,43 | 0,50 | 0,34 | 0,33 | 0,37 | 0,33 | 0,45 | 0,35 | 0,40 | 0,42 | 0,37 | 0,35 | 0,40 | 0,33 | 0,40 | 0,44 | 0,36 | 0,36 | 0,31 |

Amphibole

**Annex II** – Mineral analyses, Depiné (2008).

| | Sample | 101203-3 | | | | | | | | | | | | | | | | | | |
|---|---|---|---|---|---|---|---|---|---|---|---|---|---|---|---|---|---|---|---|---|
| | **Ox. wt%** | **P10** | **P11** | **P12** | **P13** | **P14** | **P15** | **P1** | **P2** | **P3** | **P4** | **P5** | **P6** | **P7** | **P8** | **P9** | **P10** | **P11** | **P12** | **P13** | **P14** |
| | $SiO_2$ | 41,67 | 41,13 | 41,2 | 40,95 | 41,37 | 40,99 | 39,52 | 39,99 | 40,98 | 41,15 | 40,99 | 41,21 | 41,51 | 41,49 | 40,87 | 41,09 | 41,7 | 41,51 | 41,42 | 40,47 |
| | $TiO_2$ | 1,1 | 1,17 | 1,06 | 1,18 | 1,1 | 1,09 | 0,42 | 0,45 | 0,87 | 0,88 | 0,93 | 1,02 | 1,01 | 0,98 | 1,02 | 0,96 | 0,96 | 1,01 | 0,79 | 0,36 |
| | $Al_2O_3$ | 12,98 | 13,22 | 12,88 | 12,93 | 12,75 | 13,47 | 16,07 | 15,53 | 13,34 | 13,44 | 13,33 | 13,12 | 13,17 | 13,22 | 13,03 | 13,36 | 13,49 | 13,10 | 13,56 | 17,27 |
| | $Cr_2O_3$ | 0,04 | 0,00 | 0,02 | 0,00 | 0,03 | 0,04 | 0,01 | 0,01 | 0,00 | 0,00 | 0,02 | 0,00 | 0,00 | 0,00 | 0,02 | 0,03 | 0,05 | 0,00 | 0,03 | 0,00 |
| | $Fe_2O_3$ | 5,99 | 7,19 | 7,16 | 5,83 | 6,79 | 5,82 | 5,71 | 6,48 | 6,17 | 6,02 | 6,76 | 5,70 | 6,51 | 5,63 | 6,60 | 7,20 | 6,08 | 6,38 | 5,94 | 2,76 |
| | FeO | | 14,78 | 15,22 | 15,36 | 14,73 | 14,76 | 16,46 | 14,60 | 14,64 | 14,88 | 14,56 | 15,04 | 15,06 | 15,15 | 14,57 | 14,53 | 15,25 | 15,06 | 15,22 | 17,54 |
| | MgO | 6,92 | 6,88 | 6,81 | 6,74 | 6,98 | 6,83 | 4,63 | 5,88 | 6,77 | 6,77 | 6,85 | 6,82 | 6,85 | 6,83 | 6,89 | 6,91 | 6,80 | 6,95 | 6,59 | 4,67 |
| | MnO | 0,22 | 0,27 | 0,23 | 0,30 | 0,32 | 0,28 | 0,24 | 0,25 | 0,31 | 0,30 | 0,24 | 0,28 | 0,28 | 0,27 | 0,31 | 0,28 | 0,36 | 0,27 | 0,31 | 0,21 |
| | CaO | 10,95 | 11,21 | 10,83 | 10,71 | 11,40 | 11,24 | 11,33 | 11,45 | 11,29 | 11,17 | 11,27 | 11,23 | 11,32 | 11,34 | 11,09 | 11,16 | 11,23 | 11,11 | 11,40 | 11,06 |
| | $Na_2O$ | 1,45 | 1,40 | 1,36 | 1,51 | 1,39 | 1,32 | 1,43 | 1,42 | 1,33 | 1,32 | 1,26 | 1,39 | 1,37 | 1,44 | 1,40 | 1,33 | 1,36 | 1,46 | 1,42 | 2,00 |
| | $K_2O$ | 0,64 | 0,64 | 0,68 | 0,64 | 0,60 | 0,61 | 0,67 | 0,51 | 0,61 | 0,61 | 0,61 | 0,61 | 0,59 | 0,61 | 0,62 | 0,66 | 0,60 | 0,58 | 0,60 | 0,61 |
| | sum | 97,48 | 97,88 | 97,45 | 96,14 | 97,46 | 96,45 | 96,49 | 96,59 | 96,30 | 96,54 | 96,82 | 96,41 | 97,67 | 96,97 | 96,43 | 97,49 | 97,88 | 97,41 | 97,27 | 96,93 |
| | **Tetrahedral position** | | | | | | | | | | | | | | | | | | | | |
| | Si.T1 | 5,00 | 5,00 | 5,00 | 5,00 | 5,00 | 5,00 | 5,00 | 5,00 | 5,00 | 5,00 | 5,00 | 5,00 | 5,00 | 5,00 | 5,00 | 5,00 | 5,00 | 5,00 | 5,00 | 5,00 |
| | Si.T2 | 1,36 | 1,27 | 1,30 | 1,34 | 1,33 | 1,31 | 1,14 | 1,16 | 1,33 | 1,33 | 1,30 | 1,36 | 1,33 | 1,37 | 1,31 | 1,27 | 1,33 | 1,34 | 1,34 | 1,23 |
| | Al.T2 | 1,64 | 1,73 | 1,70 | 1,66 | 1,67 | 1,69 | 1,86 | 1,84 | 1,67 | 1,67 | 1,70 | 1,64 | 1,67 | 1,63 | 1,69 | 1,73 | 1,67 | 1,66 | 1,66 | 1,77 |
| | sum | 8,00 | 8,00 | 8,00 | 8,00 | 8,00 | 8,00 | 8,00 | 8,00 | 8,00 | 8,00 | 8,00 | 8,00 | 8,00 | 8,00 | 8,00 | 8,00 | 8,00 | 8,00 | 8,00 | 8,00 |
| | **M1-5** | ` | | | | | | | | | | | | | | | | | | | |
| | Al.M | 0,69 | 0,64 | 0,63 | 0,70 | 0,63 | 0,76 | 1,09 | 0,98 | 0,75 | 0,77 | 0,71 | 0,74 | 0,69 | 0,76 | 0,68 | 0,68 | 0,75 | 0,70 | 0,79 | 1,36 |
| | Cr | 0,00 | 0,00 | 0,00 | 0,00 | 0,00 | 0,01 | 0,00 | 0,00 | 0,00 | 0,00 | 0,00 | 0,00 | 0,00 | 0,00 | 0,00 | 0,00 | 0,01 | 0,00 | 0,00 | 0,00 |
| | Ti | 0,13 | 0,13 | 0,12 | 0,14 | 0,13 | 0,13 | 0,05 | 0,05 | 0,10 | 0,10 | 0,11 | 0,12 | 0,12 | 0,11 | 0,12 | 0,11 | 0,11 | 0,12 | 0,09 | 0,04 |
| | $Fe^{3+}$ | 0,69 | 0,82 | 0,82 | 0,68 | 0,78 | 0,67 | 0,67 | 0,75 | 0,72 | 0,70 | 0,78 | 0,66 | 0,75 | 0,65 | 0,77 | 0,83 | 0,69 | 0,73 | 0,68 | 0,32 |
| | $Fe^{2+}$ | 1,98 | 1,88 | 1,95 | 1,99 | 1,89 | 1,90 | 2,14 | 1,88 | 1,89 | 1,91 | 1,87 | 1,94 | 1,92 | 1,94 | 1,88 | 1,86 | 1,94 | 1,92 | 1,95 | 2,26 |
| | Mg | 1,58 | 1,56 | 1,55 | 1,56 | 1,59 | 1,57 | 1,07 | 1,35 | 1,56 | 1,55 | 1,57 | 1,57 | 1,56 | 1,56 | 1,59 | 1,57 | 1,54 | 1,58 | 1,50 | 1,07 |
| | Mn | 0,03 | 0,03 | 0,03 | 0,04 | 0,04 | 0,04 | 0,03 | 0,03 | 0,04 | 0,04 | 0,03 | 0,04 | 0,04 | 0,04 | 0,04 | 0,04 | 0,05 | 0,03 | 0,04 | 0,03 |
| | sum | 5,10 | 5,08 | 5,10 | 5,10 | 5,06 | 5,07 | 5,05 | 5,05 | 5,06 | 5,07 | 5,07 | 5,07 | 5,07 | 5,06 | 5,08 | 5,08 | 5,08 | 5,09 | 5,06 | 5,08 |
| | **B-Position** | | | | | | | | | | | | | | | | | | | | |
| | Ca | 1,79 | 1,83 | 1,78 | 1,78 | 1,87 | 1,85 | 1,89 | 1,89 | 1,87 | 1,84 | 1,85 | 1,86 | 1,85 | 1,86 | 1,83 | 1,83 | 1,83 | 1,82 | 1,87 | 1,82 |
| | Na | 0,21 | 0,17 | 0,22 | 0,22 | 0,13 | 0,15 | 0,11 | 0,11 | 0,13 | 0,16 | 0,15 | 0,14 | 0,15 | 0,14 | 0,17 | 0,17 | 0,17 | 0,18 | 0,13 | 0,18 |
| | sum | 2,00 | 2,00 | 2,00 | 2,00 | 2,00 | 2,00 | 2,00 | 2,00 | 2,00 | 2,00 | 2,00 | 2,00 | 2,00 | 2,00 | 2,00 | 2,00 | 2,00 | 2,00 | 2,00 | 2,00 |
| | **A-Position** | | | | | | | | | | | | | | | | | | | | |
| | Na | 0,22 | 0,24 | 0,18 | 0,23 | 0,28 | 0,25 | 0,32 | 0,32 | 0,27 | 0,24 | 0,23 | 0,27 | 0,25 | 0,29 | 0,25 | 0,22 | 0,23 | 0,25 | 0,29 | 0,42 |
| | K | 0,12 | 0,12 | 0,13 | 0,13 | 0,12 | 0,12 | 0,13 | 0,10 | 0,12 | 0,12 | 0,12 | 0,12 | 0,11 | 0,12 | 0,12 | 0,13 | 0,12 | 0,11 | 0,11 | 0,12 |
| | sum | 0,34 | 0,36 | 0,31 | 0,36 | 0,40 | 0,37 | 0,45 | 0,41 | 0,39 | 0,35 | 0,35 | 0,39 | 0,37 | 0,41 | 0,38 | 0,34 | 0,34 | 0,36 | 0,41 | 0,54 |
| | xMg | 0,44 | 0,45 | 0,44 | 0,44 | 0,46 | 0,45 | 0,33 | 0,42 | 0,45 | 0,45 | 0,46 | 0,45 | 0,45 | 0,45 | 0,46 | 0,46 | 0,44 | 0,45 | 0,44 | 0,32 |
| | $xFe^{3+}$ | 0,26 | 0,30 | 0,30 | 0,25 | 0,29 | 0,26 | 0,24 | 0,29 | 0,27 | 0,27 | 0,29 | 0,25 | 0,28 | 0,25 | 0,29 | 0,31 | 0,26 | 0,28 | 0,26 | 0,12 |
| | SiTetra | 6,36 | 6,27 | 6,30 | 6,34 | 6,33 | 6,31 | 6,14 | 6,16 | 6,33 | 6,33 | 6,30 | 6,36 | 6,33 | 6,37 | 6,31 | 6,27 | 6,33 | 6,34 | 6,34 | 6,23 |
| | (Na+K)A | 0,34 | 0,36 | 0,31 | 0,36 | 0,40 | 0,37 | 0,45 | 0,41 | 0,39 | 0,35 | 0,35 | 0,39 | 0,37 | 0,41 | 0,38 | 0,34 | 0,34 | 0,36 | 0,41 | 0,54 |

**Amphibole**

**Annex II** – Mineral analyses, Depiné (2008).

| | Sample | 101203-3 | | | | | | | | | | | | | | | | 260406-4 | | |
|---|---|---|---|---|---|---|---|---|---|---|---|---|---|---|---|---|---|---|---|---|
| | **Ox. wt%** | **P1** | **P2** | **P4** | **P5** | **P6** | **P7** | **P8** | **P9** | **P10** | **P3** | **P11** | **P12** | **P13** | **P14** | **P15** | **P16** | **P17** | **K4-P 1** | **K4-P 2** | **P 4-CNTR** |
| Amphibole | $SiO_2$ | 41,47 | 41,22 | 41,01 | 41,66 | 41,6 | 41,3 | 41,4 | 40,96 | 41,21 | 43,29 | 40,78 | 42,43 | 41,5 | 42,08 | 41,7 | 40,94 | 41,46 | 41,97 | 42,08 | 42,47 |
| | $TiO_2$ | 1,06 | 1,11 | 1,14 | 1,09 | 1,07 | 1,12 | 1,12 | 1,07 | 1,08 | 0,99 | 1,06 | 1,09 | 1,14 | 1,07 | 1,01 | 0,68 | 0,43 | 1,28 | 1,36 | 1,15 |
| | $Al_2O_3$ | 13,16 | 12,75 | 13,24 | 12,56 | 12,92 | 12,71 | 13,33 | 13,06 | 13,31 | 11,23 | 12,65 | 12,27 | 13,19 | 12,81 | 13,32 | 14,57 | 15,28 | 12,92 | 13,04 | 12,87 |
| | $Cr_2O_3$ | 0,02 | 0,00 | 0,00 | 0,02 | 0,00 | 0,00 | 0,00 | 0,03 | 0,00 | 0,00 | 0,00 | 0,00 | 0,00 | 0,02 | 0,01 | 0,00 | 0,02 | 0,04 | 0,01 | 0,00 |
| | $Fe_2O_3$ | 6,02 | 6,18 | 6,72 | 7,02 | 6,39 | 6,21 | 6,75 | 6,81 | 6,12 | 4,58 | 7,31 | 6,27 | 6,45 | 6,54 | 6,23 | 6,42 | 4,78 | 6,33 | 5,70 | 6,75 |
| | FeO | 15,80 | 15,44 | 15,54 | 15,76 | 16,00 | 15,46 | 15,26 | 15,11 | 15,63 | 16,42 | 14,48 | 15,93 | 15,34 | 16,09 | 15,52 | 15,01 | 15,66 | 12,00 | 12,75 | 12,56 |
| | MgO | 6,57 | 6,70 | 6,47 | 6,90 | 6,68 | 6,79 | 6,84 | 6,66 | 6,68 | 7,34 | 6,81 | 7,15 | 6,87 | 6,80 | 6,76 | 6,27 | 6,22 | 9,05 | 8,81 | 9,07 |
| | MnO | 0,18 | 0,21 | 0,22 | 0,23 | 0,21 | 0,15 | 0,18 | 0,27 | 0,21 | 0,20 | 0,22 | 0,25 | 0,25 | 0,28 | 0,29 | 0,24 | 0,19 | 0,17 | 0,13 | 0,19 |
| | CaO | 11,19 | 11,16 | 11,10 | 10,50 | 10,71 | 11,09 | 11,08 | 11,08 | 10,70 | 11,32 | 11,52 | 10,83 | 11,00 | 10,78 | 11,12 | 11,59 | 11,33 | 11,20 | 11,06 | 10,69 |
| | $Na_2O$ | 1,40 | 1,45 | 1,69 | 1,49 | 1,41 | 1,47 | 1,36 | 1,42 | 1,55 | 1,25 | 1,37 | 1,43 | 1,50 | 1,51 | 1,48 | 1,50 | 1,51 | 1,36 | 1,42 | 1,33 |
| | $K_2O$ | 0,63 | 0,63 | 0,71 | 0,65 | 0,62 | 0,62 | 0,68 | 0,63 | 0,66 | 0,56 | 0,67 | 0,62 | 0,64 | 0,58 | 0,63 | 0,51 | 0,50 | 0,70 | 0,80 | 0,75 |
| | sum | 97,49 | 96,84 | 97,84 | 97,90 | 97,61 | 96,92 | 97,99 | 97,08 | 97,15 | 97,19 | 96,87 | 98,27 | 97,87 | 98,57 | 98,07 | 97,72 | 97,36 | 97,01 | 97,15 | 97,82 |
| | **Tetrahedral position** | | | | | | | | | | | | | | | | | | | | |
| | Si.T1 | 5,00 | 5,00 | 5,00 | 5,00 | 5,00 | 5,00 | 5,00 | 5,00 | 5,00 | 5,00 | 5,00 | 5,00 | 5,00 | 5,00 | 5,00 | 5,00 | 5,00 | 5,00 | 5,00 | 5,00 |
| | Si.T2 | 1,34 | 1,35 | 1,29 | 1,34 | 1,35 | 1,36 | 1,29 | 1,30 | 1,32 | 1,61 | 1,30 | 1,42 | 1,32 | 1,36 | 1,34 | 1,24 | 1,31 | 1,34 | 1,36 | 1,36 |
| | Al.T2 | 1,66 | 1,65 | 1,71 | 1,66 | 1,65 | 1,64 | 1,71 | 1,70 | 1,68 | 1,39 | 1,70 | 1,58 | 1,68 | 1,64 | 1,66 | 1,76 | 1,69 | 1,66 | 1,64 | 1,64 |
| | sum | 8,00 | 8,00 | 8,00 | 8,00 | 8,00 | 8,00 | 8,00 | 8,00 | 8,00 | 8,00 | 8,00 | 8,00 | 8,00 | 8,00 | 8,00 | 8,00 | 8,00 | 8,00 | 8,00 | 8,00 |
| | **M1-5** | **(Octahedral)** | | | | | | | | | | | | | | | | | | | |
| | Al.M | 0,72 | 0,67 | 0,68 | 0,60 | 0,67 | 0,66 | 0,68 | 0,66 | 0,73 | 0,63 | 0,60 | 0,61 | 0,68 | 0,65 | 0,72 | 0,86 | 1,05 | 0,64 | 0,68 | 0,63 |
| | Cr | 0,00 | 0,00 | 0,00 | 0,00 | 0,00 | 0,00 | 0,00 | 0,00 | 0,00 | 0,00 | 0,00 | 0,00 | 0,00 | 0,00 | 0,00 | 0,00 | 0,00 | 0,00 | 0,00 | 0,00 |
| | Ti | 0,12 | 0,13 | 0,13 | 0,12 | 0,12 | 0,13 | 0,13 | 0,12 | 0,12 | 0,11 | 0,12 | 0,12 | 0,13 | 0,12 | 0,12 | 0,08 | 0,05 | 0,15 | 0,15 | 0,13 |
| | $Fe^{3+}$ | 0,69 | 0,72 | 0,78 | 0,80 | 0,73 | 0,72 | 0,77 | 0,79 | 0,71 | 0,53 | 0,85 | 0,71 | 0,74 | 0,74 | 0,71 | 0,74 | 0,55 | 0,72 | 0,65 | 0,76 |
| | $Fe^{2+}$ | 2,02 | 1,99 | 1,99 | 2,01 | 2,04 | 1,99 | 1,94 | 1,94 | 2,00 | 2,10 | 1,87 | 2,02 | 1,95 | 2,03 | 1,97 | 1,91 | 1,99 | 1,52 | 1,61 | 1,57 |
| | Mg | 1,50 | 1,54 | 1,48 | 1,57 | 1,52 | 1,56 | 1,55 | 1,53 | 1,53 | 1,67 | 1,57 | 1,61 | 1,56 | 1,53 | 1,53 | 1,43 | 1,41 | 2,04 | 1,98 | 2,02 |
| | Mn | 0,02 | 0,03 | 0,03 | 0,03 | 0,03 | 0,02 | 0,02 | 0,03 | 0,03 | 0,03 | 0,03 | 0,03 | 0,03 | 0,04 | 0,04 | 0,03 | 0,02 | 0,02 | 0,02 | 0,02 |
| | sum | 5,08 | 5,07 | 5,08 | 5,13 | 5,12 | 5,08 | 5,09 | 5,08 | 5,11 | 5,07 | 5,04 | 5,11 | 5,10 | 5,12 | 5,09 | 5,05 | 5,07 | 5,09 | 5,10 | 5,13 |
| | **B-Position** | **(Hexahedral)** | | | | | | | | | | | | | | | | | | | |
| | Ca | 1,83 | 1,84 | 1,82 | 1,71 | 1,75 | 1,83 | 1,80 | 1,82 | 1,76 | 1,85 | 1,91 | 1,76 | 1,79 | 1,75 | 1,81 | 1,89 | 1,85 | 1,81 | 1,79 | 1,71 |
| | Na | 0,17 | 0,16 | 0,18 | 0,29 | 0,25 | 0,17 | 0,20 | 0,18 | 0,24 | 0,15 | 0,09 | 0,24 | 0,21 | 0,25 | 0,19 | 0,11 | 0,15 | 0,19 | 0,21 | 0,29 |
| | sum | 2,00 | 2,00 | 2,00 | 2,00 | 2,00 | 2,00 | 2,00 | 2,00 | 2,00 | 2,00 | 2,00 | 2,00 | 2,00 | 2,00 | 2,00 | 2,00 | 2,00 | 2,00 | 2,00 | 2,00 |
| | **A-Position** | | | | | | | | | | | | | | | | | | | | |
| | Na | 0,25 | 0,28 | 0,32 | 0,15 | 0,17 | 0,27 | 0,20 | 0,25 | 0,22 | 0,22 | 0,32 | 0,18 | 0,24 | 0,19 | 0,25 | 0,34 | 0,29 | 0,21 | 0,21 | 0,10 |
| | K | 0,12 | 0,12 | 0,14 | 0,13 | 0,12 | 0,12 | 0,13 | 0,12 | 0,13 | 0,11 | 0,13 | 0,12 | 0,12 | 0,11 | 0,12 | 0,10 | 0,10 | 0,13 | 0,15 | 0,14 |
| | sum | 0,37 | 0,40 | 0,46 | 0,28 | 0,29 | 0,39 | 0,33 | 0,37 | 0,35 | 0,33 | 0,45 | 0,30 | 0,36 | 0,30 | 0,37 | 0,44 | 0,39 | 0,34 | 0,36 | 0,24 |
| | xMg | 0,43 | 0,44 | 0,43 | 0,44 | 0,43 | 0,44 | 0,44 | 0,44 | 0,43 | 0,44 | 0,46 | 0,44 | 0,44 | 0,43 | 0,44 | 0,43 | 0,41 | 0,57 | 0,55 | 0,56 |
| | $xFe^{3+}$ | 0,26 | 0,26 | 0,28 | 0,29 | 0,26 | 0,27 | 0,28 | 0,29 | 0,26 | 0,20 | 0,31 | 0,26 | 0,27 | 0,27 | 0,27 | 0,28 | 0,22 | 0,32 | 0,29 | 0,33 |
| | SiTetra | 6,34 | 6,35 | 6,29 | 6,34 | 6,35 | 6,36 | 6,29 | 6,30 | 6,32 | 6,61 | 6,30 | 6,42 | 6,32 | 6,36 | 6,34 | 6,24 | 6,31 | 6,34 | 6,36 | 6,36 |
| | (Na+K)A | 0,37 | 0,40 | 0,46 | 0,28 | 0,29 | 0,39 | 0,33 | 0,37 | 0,35 | 0,33 | 0,45 | 0,30 | 0,36 | 0,30 | 0,37 | 0,44 | 0,39 | 0,34 | 0,36 | 0,24 |

**Annex II** – Mineral analyses, Depiné (2008).

| | Sample | 260406-4 | | 260406-10 | | | | | | | | | | | | | | | 260406-14 | | |
|---|---|---|---|---|---|---|---|---|---|---|---|---|---|---|---|---|---|---|---|---|---|
| | **Ox. wt%** | P 4-RIM | P 5 | P1 | P2 | P3 | P4 | P5 | P6 | P7 | P8 | P9 | P10 | P11 | P1 | P2 | P3 | P4 | P1 | P 2 | P 3 |
| | $SiO_2$ | 43,06 | 42,37 | 42,78 | 42,19 | 42,31 | 42,24 | 42,51 | 42,96 | 42,46 | 41,91 | 42,35 | 42,46 | 42,39 | 42,45 | 43,02 | 42,25 | 42,57 | 36,45 | 36,60 | 35,85 |
| | $TiO_2$ | 0,99 | 1,31 | 0,63 | 0,65 | 0,68 | 0,7 | 0,77 | 0,69 | 0,67 | 0,89 | 0,86 | 0,88 | 0,72 | 0,79 | 0,61 | 0,8 | 0,7 | 0,41 | 0,15 | 0,24 |
| | $Al_2O_3$ | 13,04 | 12,58 | 14,15 | 14,65 | 14,09 | 14,36 | 14,63 | 14,40 | 14,02 | 14,77 | 15,08 | 14,67 | 14,18 | 14,31 | 13,90 | 14,50 | 13,88 | 15,15 | 15,77 | 15,58 |
| | $Cr_2O_3$ | 0,05 | 0,00 | 0,13 | 0,06 | 0,03 | 0,06 | 0,07 | 0,05 | 0,06 | 0,02 | 0,06 | 0,09 | 0,07 | 0,04 | 0,13 | 0,04 | 0,03 | 0,00 | 0,00 | 0,00 |
| | $Fe_2O_3$ | 5,48 | 6,61 | 6,42 | 7,19 | 6,13 | 6,08 | 5,41 | 5,28 | 6,20 | 5,85 | 5,16 | 6,07 | 4,91 | 6,00 | 5,30 | 5,81 | 6,53 | 9,13 | 9,34 | 9,81 |
| | FeO | 12,54 | 12,62 | 12,14 | 11,45 | 11,24 | 11,13 | 12,44 | 11,82 | 11,68 | 11,52 | 11,81 | 11,59 | 11,93 | 11,69 | 11,97 | 11,51 | 11,35 | 19,65 | 20,59 | 20,15 |
| | MgO | 9,27 | 9,10 | 9,30 | 9,28 | 9,41 | 9,35 | 8,78 | 9,41 | 9,33 | 9,05 | 9,11 | 9,27 | 9,11 | 9,24 | 9,43 | 9,27 | 9,52 | 1,34 | 0,64 | 0,63 |
| | MnO | 0,12 | 0,20 | 0,16 | 0,19 | 0,16 | 0,15 | 0,16 | 0,10 | 0,14 | 0,18 | 0,13 | 0,17 | 0,10 | 0,12 | 0,15 | 0,13 | 0,14 | 0,17 | 0,25 | 0,24 |
| | CaO | 11,13 | 10,65 | 10,32 | 10,34 | 10,94 | 11,12 | 11,16 | 11,07 | 10,66 | 10,98 | 11,05 | 11,00 | 11,12 | 11,01 | 10,83 | 10,91 | 10,83 | 11,01 | 11,07 | 10,82 |
| | $Na_2O$ | 1,25 | 1,29 | 1,43 | 1,64 | 1,43 | 1,79 | 1,75 | 1,46 | 1,43 | 1,58 | 1,63 | 1,72 | 1,44 | 1,52 | 1,48 | 1,53 | 1,48 | 1,14 | 1,07 | 1,09 |
| | $K_2O$ | 0,61 | 0,76 | 0,38 | 0,40 | 0,33 | 0,38 | 0,36 | 0,34 | 0,34 | 0,36 | 0,41 | 0,39 | 0,37 | 0,37 | 0,36 | 0,36 | 0,35 | 2,29 | 2,20 | 2,27 |
| | sum | 97,54 | 97,48 | 97,83 | 98,02 | 96,73 | 97,38 | 98,02 | 97,58 | 96,99 | 97,10 | 97,63 | 98,30 | 96,34 | 97,52 | 97,18 | 97,12 | 97,37 | 96,73 | 97,68 | 96,67 |
| | **Tetrahedral position** | | | | | | | | | | | | | | | | | | | | |
| | Si.T1 | 5,00 | 5,00 | 5,00 | 5,00 | 5,00 | 5,00 | 5,00 | 5,00 | 5,00 | 5,00 | 5,00 | 5,00 | 5,00 | 5,00 | 5,00 | 5,00 | 5,00 | 5,00 | 5,00 | 5,00 |
| | Si.T2 | 1,43 | 1,36 | 1,33 | 1,25 | 1,33 | 1,31 | 1,33 | 1,37 | 1,34 | 1,27 | 1,29 | 1,28 | 1,38 | 1,32 | 1,41 | 1,31 | 1,34 | 0,94 | 0,91 | 0,86 |
| | Al.T2 | 1,57 | 1,64 | 1,67 | 1,75 | 1,67 | 1,69 | 1,67 | 1,63 | 1,66 | 1,73 | 1,71 | 1,72 | 1,62 | 1,68 | 1,59 | 1,69 | 1,66 | 2,06 | 2,09 | 2,14 |
| | sum | 8,00 | 8,00 | 8,00 | 8,00 | 8,00 | 8,00 | 8,00 | 8,00 | 8,00 | 8,00 | 8,00 | 8,00 | 8,00 | 8,00 | 8,00 | 8,00 | 8,00 | 8,00 | 8,00 | 8,00 |
| | **M1-5** | **(Octahedral)** | | | | | | | | | | | | | | | | | | | |
| | Al.M | 0,72 | 0,59 | 0,80 | 0,80 | 0,82 | 0,84 | 0,89 | 0,88 | 0,81 | 0,87 | 0,93 | 0,84 | 0,89 | 0,83 | 0,85 | 0,86 | 0,77 | 0,84 | 0,92 | 0,87 |
| | Cr | 0,01 | 0,00 | 0,01 | 0,01 | 0,00 | 0,01 | 0,01 | 0,01 | 0,01 | 0,00 | 0,01 | 0,01 | 0,01 | 0,01 | 0,02 | 0,00 | 0,00 | 0,00 | 0,00 | 0,00 |
| | Ti | 0,11 | 0,15 | 0,07 | 0,07 | 0,08 | 0,08 | 0,09 | 0,08 | 0,08 | 0,10 | 0,10 | 0,10 | 0,08 | 0,09 | 0,07 | 0,09 | 0,08 | 0,05 | 0,02 | 0,03 |
| | $Fe^{3+}$ | 0,62 | 0,75 | 0,71 | 0,80 | 0,69 | 0,68 | 0,61 | 0,59 | 0,70 | 0,66 | 0,58 | 0,68 | 0,56 | 0,67 | 0,59 | 0,65 | 0,73 | 1,12 | 1,14 | 1,21 |
| | $Fe^{2+}$ | 1,57 | 1,59 | 1,50 | 1,42 | 1,41 | 1,39 | 1,55 | 1,47 | 1,46 | 1,44 | 1,47 | 1,43 | 1,50 | 1,46 | 1,49 | 1,44 | 1,41 | 2,68 | 2,78 | 2,76 |
| | Mg | 2,06 | 2,04 | 2,05 | 2,05 | 2,10 | 2,08 | 1,95 | 2,08 | 2,08 | 2,02 | 2,02 | 2,04 | 2,04 | 2,05 | 2,09 | 2,06 | 2,11 | 0,32 | 0,15 | 0,15 |
| | Mn | 0,02 | 0,02 | 0,02 | 0,02 | 0,02 | 0,02 | 0,02 | 0,01 | 0,02 | 0,02 | 0,02 | 0,02 | 0,01 | 0,01 | 0,02 | 0,02 | 0,02 | 0,02 | 0,03 | 0,03 |
| | sum | 5,10 | 5,13 | 5,10 | 5,10 | 5,04 | 5,02 | 5,02 | 5,04 | 5,06 | 5,01 | 5,02 | 5,02 | 5,02 | 5,03 | 5,06 | 5,03 | 5,05 | 4,99 | 5,02 | 5,02 |
| | **B-Position** | **(Hexahedral)** | | | | | | | | | | | | | | | | | | | |
| | Ca | 1,78 | 1,71 | 1,64 | 1,64 | 1,75 | 1,78 | 1,78 | 1,76 | 1,71 | 1,76 | 1,76 | 1,74 | 1,79 | 1,76 | 1,73 | 1,74 | 1,73 | 1,92 | 1,92 | 1,90 |
| | Na | 0,22 | 0,29 | 0,36 | 0,36 | 0,25 | 0,22 | 0,22 | 0,24 | 0,29 | 0,24 | 0,24 | 0,26 | 0,21 | 0,24 | 0,27 | 0,26 | 0,27 | 0,08 | 0,08 | 0,10 |
| | sum | 2,00 | 2,00 | 2,00 | 2,00 | 2,00 | 2,00 | 2,00 | 2,00 | 2,00 | 2,00 | 2,00 | 2,00 | 2,00 | 2,00 | 2,00 | 2,00 | 2,00 | 2,00 | 2,00 | 2,00 |
| | **A-Position** | | | | | | | | | | | | | | | | | | | | |
| | Na | 0,14 | 0,09 | 0,05 | 0,11 | 0,17 | 0,30 | 0,28 | 0,18 | 0,12 | 0,22 | 0,23 | 0,24 | 0,21 | 0,19 | 0,16 | 0,19 | 0,15 | 0,28 | 0,25 | 0,24 |
| | K | 0,11 | 0,14 | 0,07 | 0,07 | 0,06 | 0,07 | 0,07 | 0,06 | 0,06 | 0,07 | 0,08 | 0,07 | 0,07 | 0,07 | 0,07 | 0,07 | 0,07 | 0,47 | 0,45 | 0,47 |
| | sum | 0,26 | 0,23 | 0,12 | 0,18 | 0,23 | 0,37 | 0,35 | 0,24 | 0,18 | 0,29 | 0,31 | 0,31 | 0,28 | 0,26 | 0,22 | 0,25 | 0,22 | 0,75 | 0,70 | 0,71 |
| | xMg | 0,57 | 0,56 | 0,58 | 0,59 | 0,60 | 0,60 | 0,56 | 0,59 | 0,59 | 0,58 | 0,58 | 0,59 | 0,58 | 0,58 | 0,58 | 0,59 | 0,60 | 0,11 | 0,05 | 0,05 |
| | $xFe^{3+}$ | 0,28 | 0,32 | 0,32 | 0,36 | 0,33 | 0,33 | 0,28 | 0,29 | 0,32 | 0,31 | 0,28 | 0,32 | 0,27 | 0,32 | 0,29 | 0,31 | 0,34 | 0,29 | 0,29 | 0,30 |
| | SiTetra | 6,43 | 6,36 | 6,33 | 6,25 | 6,33 | 6,31 | 6,33 | 6,37 | 6,34 | 6,27 | 6,29 | 6,28 | 6,38 | 6,32 | 6,41 | 6,31 | 6,34 | 5,94 | 5,91 | 5,86 |
| | (Na+K)A | 0,26 | 0,23 | 0,12 | 0,18 | 0,23 | 0,37 | 0,35 | 0,24 | 0,18 | 0,29 | 0,31 | 0,31 | 0,28 | 0,26 | 0,22 | 0,25 | 0,22 | 0,75 | 0,70 | 0,71 |

**Amphibole**

**Annex II** – Mineral analyses, Depiné (2008).

| | Sample | 260406-14 | | | | | |
|---|---|---|---|---|---|---|---|
| | **Ox. wt%** | **P 4** | **P 5** | **P 6** | **P 7** | **P 8** | **P 9** |
| Amphibole | $SiO_2$ | 36,07 | 36,38 | 35,96 | 36,54 | 36,35 | 36,65 |
| | $TiO_2$ | 0,31 | 0,31 | 0,29 | 0,36 | 0,18 | 0,12 |
| | $Al_2O_3$ | 15,40 | 15,65 | 15,19 | 15,56 | 15,78 | 15,87 |
| | $Cr_2O_3$ | 0,01 | 0,01 | 0,01 | 0,00 | 0,04 | 0,00 |
| | $Fe_2O_3$ | 9,11 | 8,92 | 9,76 | 9,66 | 10,29 | 9,06 |
| | FeO | 20,34 | 20,62 | 20,29 | 20,60 | 20,03 | 20,05 |
| | MgO | 0,68 | 0,70 | 0,66 | 0,73 | 0,82 | 1,00 |
| | MnO | 0,26 | 0,17 | 0,20 | 0,18 | 0,26 | 0,18 |
| | CaO | 10,89 | 10,97 | 10,89 | 11,04 | 10,93 | 11,07 |
| | $Na_2O$ | 1,08 | 1,11 | 1,08 | 1,19 | 1,11 | 1,16 |
| | $K_2O$ | 2,21 | 2,27 | 2,19 | 2,27 | 2,31 | 2,19 |
| | sum | 96,35 | 97,09 | 96,52 | 98,12 | 98,09 | 97,35 |
| | **Tetrahedral position** | | | | | | |
| | Si.T1 | 5,00 | 5,00 | 5,00 | 5,00 | 5,00 | 5,00 |
| | Si.T2 | 0,91 | 0,92 | 0,89 | 0,89 | 0,85 | 0,92 |
| | Al.T2 | 2,09 | 2,08 | 2,11 | 2,11 | 2,15 | 2,08 |
| | sum | 8,00 | 8,00 | 8,00 | 8,00 | 8,00 | 8,00 |
| | **M1-5** | **(Octahedral)** | | | | | |
| | Al.M | 0,89 | 0,91 | 0,83 | 0,85 | 0,85 | 0,95 |
| | Cr | 0,00 | 0,00 | 0,00 | 0,00 | 0,00 | 0,00 |
| | Ti | 0,04 | 0,04 | 0,04 | 0,04 | 0,02 | 0,01 |
| | $Fe^{3+}$ | 1,12 | 1,09 | 1,20 | 1,17 | 1,25 | 1,10 |
| | $Fe^{2+}$ | 2,79 | 2,80 | 2,78 | 2,78 | 2,70 | 2,71 |
| | Mg | 0,17 | 0,17 | 0,16 | 0,18 | 0,20 | 0,24 |
| | Mn | 0,04 | 0,02 | 0,03 | 0,03 | 0,04 | 0,02 |
| | sum | 5,00 | 5,00 | 5,01 | 5,00 | 5,03 | 5,02 |
| | **B-Position** | **(Hexahedral)** | | | | | |
| | Ca | 1,91 | 1,91 | 1,91 | 1,91 | 1,89 | 1,92 |
| | Na | 0,09 | 0,09 | 0,09 | 0,09 | 0,11 | 0,08 |
| | sum | 2,00 | 2,00 | 2,00 | 2,00 | 2,00 | 2,00 |
| | **A-Position** | | | | | | |
| | Na | 0,25 | 0,26 | 0,25 | 0,28 | 0,23 | 0,28 |
| | K | 0,46 | 0,47 | 0,45 | 0,46 | 0,47 | 0,45 |
| | sum | 0,71 | 0,72 | 0,71 | 0,74 | 0,70 | 0,73 |
| | xMg | 0,06 | 0,06 | 0,06 | 0,06 | 0,07 | 0,08 |
| | $xFe^{3+}$ | 0,29 | 0,28 | 0,30 | 0,30 | 0,32 | 0,29 |
| | SiTetra | 5,91 | 5,92 | 5,89 | 5,89 | 5,85 | 5,92 |
| | (Na+K)A | 0,71 | 0,72 | 0,71 | 0,74 | 0,70 | 0,73 |

**Annex II** – Mineral analyses, Depiné (2008).

| | Sample | 101203-1 | | | | | | | | | | | | | | | | | | 231104-1 | |
|---|---|---|---|---|---|---|---|---|---|---|---|---|---|---|---|---|---|---|---|---|---|
| | **Ox. wt%** | P 1 | P 2 | P 3 | P 4 | P 5 | P 6 | P 7 | P 10 | P 11 | P 12 | P 13 | P 14 | P 19 | P20 | P 21 | P 22 | P 23 | P 27 | P1 | P 4 |
| **Biotite** | $SiO_2$ | 35,45 | 35,01 | 35,21 | 35,43 | 35,20 | 35,14 | 35,33 | 35,18 | 35,43 | 35,09 | 35,30 | 35,78 | 35,70 | 35,64 | 35,52 | 35,30 | 35,38 | 35,57 | 33,90 | 34,09 |
| | $TiO_2$ | 1,86 | 1,97 | 1,75 | 1,85 | 1,92 | 1,53 | 1,65 | 1,95 | 2,01 | 2,01 | 1,98 | 2,02 | 2,06 | 2,08 | 2,05 | 1,86 | 1,96 | 2,05 | 2,09 | 2,21 |
| | $Al_2O_3$ | 16,56 | 16,69 | 17,08 | 17,01 | 16,82 | 17,15 | 17,06 | 16,99 | 16,88 | 16,94 | 16,84 | 16,91 | 16,77 | 16,79 | 16,81 | 16,81 | 16,71 | 16,47 | 18,00 | 18,08 |
| | $Cr_2O_3$ | 0,00 | 0,05 | 0,00 | 0,00 | 0,02 | 0,00 | 0,04 | 0,02 | 0,00 | 0,03 | 0,03 | 0,00 | 0,00 | 0,00 | 0,02 | 0,05 | 0,04 | 0,00 | 0,00 | 0,00 |
| | $Fe_2O_3$ | 20,73 | 20,98 | 20,85 | 21,09 | 20,79 | 20,74 | 20,81 | 20,79 | 20,74 | 20,78 | 20,62 | 20,39 | 20,09 | 20,08 | 20,50 | 20,86 | 20,94 | 20,68 | 23,77 | 23,50 |
| | FeO | 0,18 | 0,21 | 0,22 | 0,21 | 0,19 | 0,22 | 0,16 | 0,25 | 0,14 | 0,26 | 0,20 | 0,19 | 0,19 | 0,23 | 0,17 | 0,20 | 0,21 | 0,16 | 0,08 | 0,00 |
| | MgO | 9,56 | 9,63 | 9,88 | 9,50 | 9,65 | 9,90 | 9,60 | 9,44 | 9,38 | 9,58 | 9,62 | 9,90 | 9,83 | 9,81 | 9,75 | 9,90 | 9,51 | 9,58 | 7,37 | 7,18 |
| | BaO | 0,32 | 0,27 | 0,29 | 0,29 | 0,40 | 0,29 | 0,32 | 0,35 | 0,28 | 0,26 | 0,24 | 0,35 | 0,31 | 0,21 | 0,36 | 0,36 | 0,28 | 0,29 | 0,40 | 0,47 |
| | CaO | 0,00 | 0,03 | 0,02 | 0,00 | 0,06 | 0,00 | 0,00 | 0,00 | 0,00 | 0,00 | 0,02 | 0,00 | 0,00 | 0,00 | 0,00 | 0,00 | 0,00 | 0,00 | 0,02 | 0,00 |
| | $Na_2O$ | 0,10 | 0,07 | 0,05 | 0,06 | 0,12 | 0,04 | 0,01 | 0,08 | 0,04 | 0,04 | 0,10 | 0,07 | 0,11 | 0,09 | 0,05 | 0,07 | 0,08 | 0,06 | 0,09 | 0,09 |
| | $K_2O$ | 9,55 | 9,54 | 9,30 | 9,39 | 9,37 | 9,14 | 9,43 | 9,43 | 9,58 | 9,49 | 9,18 | 9,49 | 9,68 | 9,44 | 9,35 | 9,40 | 9,44 | 9,50 | 8,60 | 8,95 |
| | OH | 3,84 | 3,84 | 3,86 | 3,87 | 3,85 | 3,85 | 3,85 | 3,85 | 3,85 | 3,85 | 3,85 | 3,89 | 3,88 | 3,87 | 3,87 | 3,86 | 3,85 | 3,85 | 3,80 | 3,81 |
| | sum | 98,16 | 98,27 | 98,50 | 98,71 | 98,37 | 97,99 | 98,27 | 98,32 | 98,32 | 98,31 | 98,00 | 98,98 | 98,61 | 98,22 | 98,43 | 98,68 | 98,41 | 98,21 | 98,12 | 98,37 |
| | sum-$H_2O$ | 94,31 | 94,43 | 94,64 | 94,84 | 94,52 | 94,14 | 94,41 | 94,47 | 94,46 | 94,46 | 94,15 | 95,09 | 94,73 | 94,35 | 94,57 | 94,81 | 94,55 | 94,36 | 94,32 | 94,56 |
| | **Cations** | | | | | | | | | | | | | | | | | | | | |
| | Si | 5,53 | 5,47 | 5,47 | 5,49 | 5,48 | 5,48 | 5,50 | 5,48 | 5,51 | 5,47 | 5,50 | 5,52 | 5,52 | 5,53 | 5,51 | 5,48 | 5,51 | 5,54 | 5,35 | 5,37 |
| | Ti | 0,22 | 0,23 | 0,20 | 0,22 | 0,22 | 0,18 | 0,19 | 0,23 | 0,23 | 0,23 | 0,23 | 0,23 | 0,24 | 0,24 | 0,24 | 0,22 | 0,23 | 0,24 | 0,25 | 0,26 |
| | $Al^{[IV]}$ | 2,47 | 2,53 | 2,53 | 2,51 | 2,52 | 2,52 | 2,50 | 2,52 | 2,49 | 2,53 | 2,50 | 2,48 | 2,48 | 2,47 | 2,49 | 2,52 | 2,49 | 2,46 | 2,65 | 2,63 |
| | $Al^{[VI]}$ | 0,57 | 0,54 | 0,60 | 0,60 | 0,57 | 0,63 | 0,63 | 0,60 | 0,60 | 0,58 | 0,59 | 0,59 | 0,58 | 0,60 | 0,58 | 0,56 | 0,58 | 0,56 | 0,70 | 0,72 |
| | Cr | 0,00 | 0,01 | 0,00 | 0,00 | 0,00 | 0,00 | 0,00 | 0,00 | 0,00 | 0,00 | 0,00 | 0,00 | 0,00 | 0,00 | 0,00 | 0,01 | 0,00 | 0,00 | 0,00 | 0,00 |
| | Fe | 2,70 | 2,74 | 2,71 | 2,74 | 2,71 | 2,70 | 2,71 | 2,71 | 2,70 | 2,71 | 2,69 | 2,63 | 2,60 | 2,60 | 2,66 | 2,71 | 2,73 | 2,69 | 3,14 | 3,09 |
| | Mn | 0,02 | 0,03 | 0,03 | 0,03 | 0,03 | 0,03 | 0,02 | 0,03 | 0,02 | 0,03 | 0,03 | 0,03 | 0,02 | 0,03 | 0,02 | 0,03 | 0,03 | 0,02 | 0,01 | 0,00 |
| | Mg | 2,22 | 2,24 | 2,29 | 2,20 | 2,24 | 2,30 | 2,23 | 2,19 | 2,17 | 2,23 | 2,23 | 2,27 | 2,27 | 2,27 | 2,26 | 2,29 | 2,21 | 2,22 | 1,73 | 1,68 |
| | Ba | 0,02 | 0,02 | 0,02 | 0,02 | 0,02 | 0,02 | 0,02 | 0,02 | 0,02 | 0,02 | 0,01 | 0,02 | 0,02 | 0,01 | 0,02 | 0,02 | 0,02 | 0,02 | 0,02 | 0,03 |
| | Ca | 0,00 | 0,00 | 0,00 | 0,00 | 0,01 | 0,00 | 0,00 | 0,00 | 0,00 | 0,00 | 0,00 | 0,00 | 0,00 | 0,00 | 0,00 | 0,00 | 0,00 | 0,00 | 0,00 | 0,00 |
| | Na | 0,03 | 0,02 | 0,02 | 0,02 | 0,04 | 0,01 | 0,00 | 0,02 | 0,01 | 0,01 | 0,03 | 0,02 | 0,03 | 0,03 | 0,01 | 0,02 | 0,02 | 0,02 | 0,03 | 0,03 |
| | K | 1,90 | 1,90 | 1,84 | 1,86 | 1,86 | 1,82 | 1,87 | 1,87 | 1,90 | 1,89 | 1,82 | 1,87 | 1,91 | 1,87 | 1,85 | 1,86 | 1,87 | 1,89 | 1,73 | 1,80 |
| | sum | 15,69 | 15,72 | 15,70 | 15,67 | 15,70 | 15,68 | 15,68 | 15,68 | 15,66 | 15,69 | 15,65 | 15,66 | 15,68 | 15,64 | 15,65 | 15,70 | 15,68 | 15,66 | 15,61 | 15,61 |
| | xFe | 0,55 | 0,55 | 0,54 | 0,55 | 0,55 | 0,54 | 0,55 | 0,55 | 0,55 | 0,55 | 0,55 | 0,54 | 0,53 | 0,53 | 0,54 | 0,54 | 0,55 | 0,55 | 0,64 | 0,65 |
| | Fe+Mn | 2,73 | 2,77 | 2,74 | 2,76 | 2,73 | 2,73 | 2,73 | 2,74 | 2,72 | 2,74 | 2,71 | 2,65 | 2,63 | 2,63 | 2,68 | 2,73 | 2,75 | 2,71 | 3,15 | 3,09 |
| | $Al^{[VI]}$+Ti+Cr | 0,79 | 0,78 | 0,80 | 0,82 | 0,79 | 0,81 | 0,82 | 0,83 | 0,83 | 0,81 | 0,82 | 0,82 | 0,82 | 0,84 | 0,82 | 0,78 | 0,81 | 0,80 | 0,95 | 0,98 |

**Annex II** – Mineral analyses, Depiné (2008).

| | Sample | 260406-14 | | | | | | |
|---|---|---|---|---|---|---|---|---|
| | **Ox. wt%** | **P 5** | **P 6** | **P1** | **P 2** | **P 3** | **P 4** | **P5** |
| Biotite | $SiO_2$ | 34,07 | 33,99 | 33,83 | 33,76 | 33,56 | 33,99 | 33,77 |
| | $TiO_2$ | 2,38 | 2,20 | 1,62 | 1,30 | 1,78 | 1,83 | 0,61 |
| | $Al_2O_3$ | 17,79 | 18,02 | 16,47 | 16,65 | 16,74 | 16,42 | 16,22 |
| | $Cr_2O_3$ | 0,00 | 0,00 | 0,00 | 0,00 | 0,05 | 0,01 | 0,01 |
| | $Fe_2O_3$ | 23,54 | 23,73 | 31,12 | 31,03 | 30,73 | 31,46 | 32,15 |
| | FeO | 0,03 | 0,03 | 0,15 | 0,12 | 0,14 | 0,12 | 0,13 |
| | MgO | 7,20 | 7,16 | 2,85 | 2,83 | 2,85 | 2,83 | 2,72 |
| | BaO | 0,35 | 0,43 | 0,11 | 0,07 | 0,03 | 0,08 | 0,03 |
| | CaO | 0,00 | 0,00 | 0,00 | 0,00 | 0,00 | 0,00 | 0,00 |
| | $Na_2O$ | 0,08 | 0,13 | 0,07 | 0,10 | 0,05 | 0,03 | 0,02 |
| | $K_2O$ | 8,95 | 8,99 | 8,89 | 8,84 | 9,03 | 8,99 | 8,97 |
| | OH | 3,80 | 3,81 | 3,69 | 3,68 | 3,69 | 3,71 | 3,69 |
| | sum | 98,20 | 98,49 | 98,80 | 98,37 | 98,64 | 99,46 | 99,31 |
| | sum-$H_2O$ | 94,39 | 94,68 | 95,10 | 94,70 | 94,95 | 95,75 | 95,62 |
| | **Cations** | | | | | | | |
| | Si | 5,37 | 5,35 | 5,50 | 5,50 | 5,46 | 5,49 | 5,49 |
| | Ti | 0,28 | 0,26 | 0,20 | 0,16 | 0,22 | 0,22 | 0,20 |
| | $Al^{[IV]}$ | 2,63 | 2,65 | 2,50 | 2,50 | 2,54 | 2,51 | 2,51 |
| | $Al^{[VI]}$ | 0,68 | 0,69 | 0,65 | 0,70 | 0,67 | 0,62 | 0,59 |
| | Cr | 0,00 | 0,00 | 0,00 | 0,00 | 0,01 | 0,00 | 0,00 |
| | Fe | 3,10 | 3,12 | 4,23 | 4,23 | 4,18 | 4,25 | 4,37 |
| | Mn | 0,00 | 0,00 | 0,02 | 0,02 | 0,02 | 0,02 | 0,02 |
| | Mg | 1,69 | 1,68 | 0,69 | 0,69 | 0,69 | 0,68 | 0,66 |
| | Ba | 0,02 | 0,03 | 0,01 | 0,00 | 0,00 | 0,01 | 0,00 |
| | Ca | 0,00 | 0,00 | 0,00 | 0,00 | 0,00 | 0,00 | 0,00 |
| | Na | 0,02 | 0,04 | 0,02 | 0,03 | 0,02 | 0,01 | 0,00 |
| | K | 1,80 | 1,81 | 1,84 | 1,84 | 1,87 | 1,85 | 1,86 |
| | sum | 15,60 | 15,64 | 15,66 | 15,67 | 15,66 | 15,66 | 15,70 |
| | xFe | 0,65 | 0,65 | 0,86 | 0,86 | 0,86 | 0,86 | 0,87 |
| | Fe+Mn | 3,11 | 3,13 | 4,25 | 4,25 | 4,20 | 4,27 | 4,39 |
| | $Al^{[VI]}$+Ti+Cr | 0,96 | 0,95 | 0,85 | 0,86 | 0,89 | 0,84 | 0,79 |

| | sample | 200900-1 | | | | | |
|---|---|---|---|---|---|---|---|
| | **Ox. wt.%** | **P 1** | **P 2** | **P 3** | **P 4** | **P 5** | **P 6** |
| Chlorite | $SiO_2$ | 23,73 | 24,06 | 23,97 | 24,05 | 23,78 | 23,94 |
| | $TiO_2$ | 0,05 | 0,07 | 0,09 | 0,06 | 0,05 | 0,06 |
| | $Al_2O_3$ | 21,20 | 21,29 | 21,46 | 20,55 | 21,08 | 22,01 |
| | $Cr_2O_3$ | 0,00 | 0,00 | 0,03 | 0,04 | 0,00 | 0,00 |
| | $Fe_2O_3$ | 0,33 | 0,00 | 0,00 | 0,06 | 0,45 | 0,02 |
| | FeO | 30,29 | 30,19 | 30,29 | 29,88 | 30,47 | 30,41 |
| | MgO | 11,04 | 11,05 | 11,22 | 11,32 | 10,95 | 11,27 |
| | MnO | 0,15 | 0,16 | 0,21 | 0,15 | 0,18 | 0,20 |
| | CaO | 0,02 | 0,01 | 0,02 | 0,05 | 0,03 | 0,04 |
| | $Na_2O$ | 0,00 | 0,02 | 0,00 | 0,03 | 0,01 | 0,00 |
| | $K_2O$ | 0,03 | 0,03 | 0,01 | 0,11 | 0,02 | 0,03 |
| | sum | 86,83 | 86,87 | 87,31 | 86,29 | 86,99 | 87,98 |
| | **Cations** | | | | | | |
| | Si | 5,22 | 5,28 | 5,23 | 5,31 | 5,23 | 5,18 |
| | Ti | 0,01 | 0,01 | 0,02 | 0,01 | 0,01 | 0,01 |
| | $Al^{[IV]}$ | 2,78 | 2,72 | 2,77 | 2,69 | 2,77 | 2,82 |
| | $Al^{[VI]}$ | 2,71 | 2,79 | 2,75 | 2,66 | 2,69 | 2,80 |
| | Cr | 0,00 | 0,00 | 0,01 | 0,01 | 0,00 | 0,00 |
| | $Fe^{3+}$ | 0,06 | 0,00 | 0,00 | 0,01 | 0,07 | 0,00 |
| | $Fe^{2+}$ | 5,57 | 5,54 | 5,53 | 5,52 | 5,60 | 5,50 |
| | Mg | 3,62 | 3,62 | 3,65 | 3,73 | 3,59 | 3,64 |
| | Mn | 0,03 | 0,03 | 0,04 | 0,03 | 0,03 | 0,04 |
| | Ca | 0,00 | 0,00 | 0,01 | 0,01 | 0,01 | 0,01 |
| | Na | 0,00 | 0,01 | 0,00 | 0,01 | 0,00 | 0,00 |
| | K | 0,01 | 0,01 | 0,00 | 0,02 | 0,00 | 0,01 |
| | sum | 20,00 | 20,00 | 20,00 | 20,00 | 20,00 | 20,00 |
| | xFe | 0,61 | 0,61 | 0,60 | 0,60 | 0,61 | 0,60 |

**Annex II** – Mineral analyses, Depiné (2008).

| Muscovite | Sample | 200900-1 | | 231104-1 | | |
|---|---|---|---|---|---|---|
| | **Ox. wt%** | **P 2** | **P 3** | **P 1** | **P 2** | **P 4** |
| | $SiO_2$ | 45,75 | 45,84 | 45,34 | 45,65 | 44,70 |
| | $TiO_2$ | 0,29 | 0,42 | 0,26 | 0,57 | 0,47 |
| | $Al_2O_3$ | 34,88 | 35,22 | 36,20 | 35,65 | 35,60 |
| | $Cr_2O_3$ | 0,07 | 0,01 | 0,00 | 0,00 | 0,00 |
| | $Fe_2O_3$ | 2,17 | 2,31 | 1,42 | 1,45 | 1,50 |
| | FeO | 0,03 | 0,00 | 0,01 | 0,02 | 0,03 |
| | MgO | 0,53 | 0,58 | 0,54 | 0,66 | 0,55 |
| | MnO | 0,26 | 0,24 | 1,26 | 1,19 | 1,20 |
| | CaO | 0,01 | 0,00 | 0,00 | 0,00 | 0,00 |
| | $Na_2O$ | 1,68 | 1,65 | 1,13 | 0,97 | 1,10 |
| | $K_2O$ | 8,66 | 8,57 | 9,20 | 9,12 | 9,24 |
| | sum | 4,46 | 4,49 | 4,49 | 4,49 | 4,43 |
| | sum | 98,77 | 99,32 | 99,84 | 99,75 | 98,81 |
| | sum-$H_2O$ | 94,31 | 94,83 | 95,36 | 95,26 | 94,38 |
| | **Cations** | | | | | |
| | Si | 6,15 | 6,13 | 6,06 | 6,10 | 6,05 |
| | Ti | 0,03 | 0,04 | 0,03 | 0,06 | 0,05 |
| | $Al^{[IV]}$ | 1,85 | 1,87 | 1,94 | 1,90 | 1,95 |
| | $Al^{[VI]}$ | 3,68 | 3,68 | 3,77 | 3,72 | 3,73 |
| | Cr | 0,01 | 0,00 | 0,00 | 0,00 | 0,00 |
| | Fe | 0,24 | 0,26 | 0,16 | 0,16 | 0,17 |
| | Mn | 0,00 | 0,00 | 0,00 | 0,00 | 0,00 |
| | Mg | 0,11 | 0,12 | 0,11 | 0,13 | 0,11 |
| | Ba | 0,01 | 0,01 | 0,07 | 0,06 | 0,06 |
| | Ca | 0,00 | 0,00 | 0,00 | 0,00 | 0,00 |
| | Na | 0,44 | 0,43 | 0,29 | 0,25 | 0,29 |
| | K | 1,49 | 1,46 | 1,57 | 1,55 | 1,59 |
| | sum | 14,01 | 14,00 | 13,99 | 13,94 | 14,01 |
| | Muscovite | 77,20 | 77,42 | 84,26 | 86,08 | 84,68 |
| | Paragonite | 22,80 | 22,58 | 15,74 | 13,92 | 15,32 |
| | M2+ | 0,37 | 0,39 | 0,33 | 0,36 | 0,35 |
| | Altot | 5,53 | 5,55 | 5,70 | 5,62 | 5,68 |

| Ilmenite | Sample: | 260406-4 | | | 260406-10 | | |
|---|---|---|---|---|---|---|---|
| | **Ox. wt%** | **P1** | **P 2** | **P3** | **P1** | **P 2** | **P3** |
| | $SiO_2$ | 0,07 | 0,03 | 0,02 | 0,03 | 0,00 | 0,04 |
| | $TiO_2$ | 53,41 | 53,60 | 52,47 | 53,58 | 53,39 | 54,19 |
| | $Cr_2O_3$ | 0,00 | 0,00 | 0,01 | 0,00 | 0,00 | 0,00 |
| | $Al_2O_3$ | 0,05 | 0,04 | 0,05 | 0,07 | 0,08 | 0,17 |
| | $Fe_2O_3$ | 0,00 | 0,00 | 0,00 | 0,00 | 0,00 | 0,00 |
| | FeO | 44,60 | 45,97 | 45,35 | 45,89 | 46,18 | 44,83 |
| | MnO | 1,60 | 1,85 | 1,63 | 1,58 | 1,33 | 1,45 |
| | MgO | 0,10 | 0,20 | 0,12 | 0,16 | 0,10 | 0,14 |
| | sum | 99,81 | 101,69 | 99,65 | 101,32 | 101,08 | 100,82 |
| | **Cations** | | | | | | |
| | Si | 0,00 | 0,00 | 0,00 | 0,00 | 0,00 | 0,00 |
| | Ti | 1,02 | 1,00 | 1,00 | 1,00 | 1,00 | 1,02 |
| | Cr | 0,00 | 0,00 | 0,00 | 0,00 | 0,00 | 0,00 |
| | Al | 0,00 | 0,00 | 0,00 | 0,00 | 0,00 | 0,00 |
| | $Fe^{3+}$ | 0,00 | 0,00 | 0,00 | 0,00 | 0,00 | 0,00 |
| | $Fe^{2+}$ | 0,94 | 0,95 | 0,96 | 0,95 | 0,96 | 0,94 |
| | Mn | 0,03 | 0,04 | 0,03 | 0,03 | 0,03 | 0,03 |
| | Mg | 0,00 | 0,01 | 0,00 | 0,01 | 0,00 | 0,01 |
| | sum | 2,00 | 2,00 | 2,00 | 2,00 | 2,00 | 2,00 |
| | ilm | 0,96 | 0,95 | 0,96 | 0,96 | 0,97 | 0,96 |
| | hem | 0,00 | 0,00 | 0,00 | 0,00 | 0,00 | 0,00 |
| | gey(mg) | 0,00 | 0,01 | 0,00 | 0,01 | 0,00 | 0,01 |
| | pyro(mn) | 0,03 | 0,04 | 0,03 | 0,03 | 0,03 | 0,03 |
| | sum | 1,00 | 1,00 | 1,00 | 1,00 | 1,00 | 1,00 |

**Annex II** – Mineral analyses, Depiné (2008).

| | Sample | 260406-4 | | | | | | | 260406-14 | | | | | |
|---|---|---|---|---|---|---|---|---|---|---|---|---|---|---|
| | **Ox. wt%** | **P 2** | **P 3** | **P 4** | **P 5** | **P 6** | **P7** | **P8** | **P1** | **P 2** | **P 4** | **P 5** | **P 6** | **P7** |
| **Epidote** | $SiO_2$ | 38,47 | 38,23 | 38,21 | 38,24 | 38,23 | 37,93 | 37,70 | 30,78 | 37,55 | 37,34 | 31,20 | 37,72 | 37,59 |
| | $TiO_2$ | 0,01 | 0,02 | 0,01 | 0,10 | 0,01 | 0,00 | 0,00 | 27,99 | 0,10 | 0,07 | 28,70 | 0,06 | 0,05 |
| | $Al_2O_3$ | 27,50 | 27,64 | 27,37 | 27,43 | 27,80 | 28,29 | 27,08 | 8,74 | 25,44 | 23,93 | 8,23 | 26,32 | 25,51 |
| | $Cr_2O_3$ | 0,02 | 0,01 | 0,00 | 0,00 | 0,02 | 0,00 | 0,02 | 0,02 | 0,00 | 0,02 | 0,00 | 0,02 | 0,02 |
| | $Fe_2O_3$ | 7,83 | 7,60 | 8,08 | 7,89 | 7,84 | 7,39 | 8,33 | 0,68 | 10,77 | 12,62 | 0,73 | 10,02 | 10,43 |
| | FeO | 0,08 | 0,13 | 0,03 | 0,07 | 0,06 | 0,09 | 0,02 | 0,03 | 0,03 | 0,05 | 0,05 | 0,11 | 0,08 |
| | MgO | 0,00 | 0,00 | 0,00 | 0,00 | 0,00 | 0,00 | 0,00 | 0,00 | 0,00 | 0,00 | 0,00 | 0,00 | 0,00 |
| | MnO | 0,15 | 0,00 | 0,07 | 0,01 | 0,00 | 0,00 | 0,00 | 0,00 | 0,03 | 0,02 | 0,00 | 0,00 | 0,00 |
| | CaO | 23,90 | 23,46 | 24,17 | 23,73 | 23,99 | 24,06 | 24,15 | 29,10 | 23,72 | 23,43 | 29,30 | 23,16 | 23,42 |
| | $Na_2O$ | 0,02 | 0,02 | 0,04 | 0,04 | 0,02 | 0,02 | 0,00 | 0,04 | 0,03 | 0,01 | 0,00 | 0,00 | 0,03 |
| | $K_2O$ | 0,00 | 0,17 | 0,00 | 0,10 | 0,00 | 0,03 | 0,02 | 0,02 | 0,01 | 0,02 | 0,01 | 0,01 | 0,01 |
| | OH | 1,92 | 1,91 | 1,92 | 1,91 | 1,92 | 1,92 | 1,90 | 1,81 | 1,89 | 1,88 | 1,83 | 1,90 | 1,89 |
| | sum | 99,91 | 99,19 | 99,89 | 99,50 | 99,89 | 99,72 | 99,21 | 99,22 | 99,57 | 99,39 | 100,05 | 99,33 | 99,02 |
| | sum-$H_2O$ | 97,99 | 97,28 | 97,97 | 97,59 | 97,97 | 97,80 | 97,31 | 97,40 | 97,68 | 97,52 | 98,22 | 97,43 | 97,13 |
| | **Cations** | | | | | | | | | | | | | |
| | Si | 3,00 | 3,00 | 2,99 | 2,99 | 2,98 | 2,96 | 2,97 | 2,55 | 2,97 | 2,98 | 2,56 | 2,98 | 2,99 |
| | Ti | 0,00 | 0,00 | 0,00 | 0,01 | 0,00 | 0,00 | 0,00 | 1,74 | 0,01 | 0,00 | 1,77 | 0,00 | 0,00 |
| | $Al^{[IV]}$ | 0,00 | 0,00 | 0,01 | 0,01 | 0,02 | 0,04 | 0,03 | 0,45 | 0,03 | 0,02 | 0,44 | 0,02 | 0,01 |
| | $Al^{[VI]}$ | 2,53 | 2,56 | 2,51 | 2,52 | 2,54 | 2,56 | 2,49 | 0,40 | 2,34 | 2,23 | 0,36 | 2,43 | 2,38 |
| | Cr | 0,00 | 0,00 | 0,00 | 0,00 | 0,00 | 0,00 | 0,00 | 0,00 | 0,00 | 0,00 | 0,00 | 0,00 | 0,00 |
| | $Fe^{3+}$ | 0,46 | 0,45 | 0,48 | 0,47 | 0,46 | 0,43 | 0,49 | 0,04 | 0,64 | 0,76 | 0,04 | 0,60 | 0,62 |
| | Mn | 0,01 | 0,01 | 0,00 | 0,00 | 0,00 | 0,01 | 0,00 | 0,00 | 0,00 | 0,00 | 0,00 | 0,01 | 0,01 |
| | Mg | 0,00 | 0,00 | 0,00 | 0,00 | 0,00 | 0,00 | 0,00 | 0,00 | 0,00 | 0,00 | 0,00 | 0,00 | 0,00 |
| | Ba | 0,00 | 0,00 | 0,00 | 0,00 | 0,00 | 0,00 | 0,00 | 0,00 | 0,00 | 0,00 | 0,00 | 0,00 | 0,00 |
| | Ca | 2,00 | 1,97 | 2,02 | 1,99 | 2,00 | 2,01 | 2,04 | 2,58 | 2,01 | 2,00 | 2,58 | 1,96 | 1,99 |
| | Na | 0,00 | 0,00 | 0,01 | 0,01 | 0,00 | 0,00 | 0,00 | 0,01 | 0,00 | 0,00 | 0,00 | 0,00 | 0,00 |
| | K | 0,00 | 0,02 | 0,00 | 0,01 | 0,00 | 0,00 | 0,00 | 0,00 | 0,00 | 0,00 | 0,00 | 0,00 | 0,00 |
| | sum | 8,00 | 8,01 | 8,02 | 8,01 | 8,01 | 8,02 | 8,02 | 7,77 | 8,02 | 8,01 | 7,75 | 8,00 | 8,01 |
| | $Fe^{3+}/(Fe^{3+}+Al)$ | 15,38 | 14,94 | 15,86 | 15,52 | 15,26 | 14,30 | 16,42 | 4,72 | 21,28 | 25,19 | 5,32 | 19,54 | 20,70 |

**Annex III** - Mineral analyses Nolte (2012).

| | Sample | 290709-3 | | | | | | | | | | | | | | | | | |
|---|---|---|---|---|---|---|---|---|---|---|---|---|---|---|---|---|---|---|---|
| | ***Ox. wt%*** | *15-rim* | *16-core* | *17-rim* | *19-rim* | *20-core* | *21-core* | *22-rim* | *25-rim* | *26-rim* | *27-core* | *28-rim* | *29-rim* | *30-core* | *31-rim* | *40-rim* | *41-rim* | *50-rim* | *51-core* | *52-rim* |
| Garnet | $SiO_2$ | 36,9 | 38,3 | 38,2 | 37,8 | 38,7 | 38,4 | 37,2 | 38,2 | 36,9 | 38,0 | 38,3 | 38,1 | 38,0 | 38,0 | 38,7 | 38,6 | 37,8 | 37,4 | 38,1 |
| | $TiO_2$ | 0,14 | 0,03 | 0,14 | 0,17 | 0,00 | 0,11 | 0,05 | 0,01 | 0,14 | 0,08 | 0,05 | 0,02 | 0,08 | 0,02 | 0,10 | 0,09 | 0,08 | 0,06 | 0,00 |
| | $Al_2O_3$ | 21,3 | 21,7 | 21,7 | 21,5 | 21,6 | 21,5 | 21,7 | 21,6 | 21,6 | 21,5 | 21,5 | 21,9 | 21,7 | 21,8 | 21,4 | 21,6 | 21,9 | 21,7 | 21,6 |
| | $Cr_2O_3$ | 0,00 | 0,04 | 0,00 | 0,01 | 0,05 | 0,00 | 0,00 | 0,00 | 0,05 | 0,00 | 0,04 | 0,08 | 0,00 | 0,01 | 0,00 | 0,03 | 0,03 | 0,00 | 0,01 |
| | $Fe_2O_3$ | 1,68 | 1,71 | 1,68 | 1,66 | 1,66 | 1,64 | 1,66 | 1,69 | 1,66 | 1,65 | 1,69 | 1,67 | 1,57 | 1,68 | 1,66 | 1,69 | 1,68 | 1,68 | 1,68 |
| | FeO | 28,7 | 29,2 | 28,8 | 28,4 | 28,4 | 28,1 | 28,3 | 28,9 | 28,4 | 28,2 | 28,8 | 28,5 | 26,9 | 28,8 | 28,5 | 28,9 | 28,7 | 28,8 | 28,7 |
| | MnO | 0,78 | 0,79 | 0,78 | 0,74 | 1,42 | 1,88 | 1,20 | 0,75 | 1,49 | 1,06 | 0,79 | 1,24 | 3,29 | 1,14 | 0,74 | 0,78 | 0,73 | 0,69 | 0,69 |
| | MgO | 1,24 | 1,12 | 1,07 | 1,16 | 1,08 | 0,94 | 1,16 | 1,27 | 1,19 | 1,14 | 1,24 | 1,23 | 1,06 | 1,23 | 1,15 | 1,03 | 1,23 | 1,14 | 1,29 |
| | CaO | 9,43 | 9,63 | 9,59 | 9,60 | 9,37 | 9,13 | 9,54 | 9,49 | 9,30 | 9,50 | 9,72 | 9,34 | 8,73 | 9,10 | 9,94 | 9,84 | 9,81 | 9,96 | 9,75 |
| | $Na_2O$ | 0,02 | 0,00 | 0,02 | 0,02 | 0,01 | 0,04 | 0,01 | 0,00 | 0,00 | 0,01 | 0,04 | 0,02 | 0,00 | 0,00 | 0,00 | 0,02 | 0,00 | 0,02 | 0,01 |
| | sum | 100,11 | 102,53 | 101,91 | 101,16 | 102,28 | 101,72 | 100,85 | 101,89 | 100,78 | 101,10 | 102,20 | 102,15 | 101,38 | 101,79 | 102,16 | 102,59 | 102,00 | 101,39 | 101,82 |
| | ***Structural formula based on 24 O*** | | | | | | | | | | | | | | | | | | | |
| | Si | 5,90 | 5,99 | 6,01 | 5,99 | 6,07 | 6,06 | 5,92 | 6,00 | 5,88 | 6,02 | 6,00 | 5,98 | 6,02 | 5,99 | 6,08 | 6,03 | 5,93 | 5,90 | 5,98 |
| | Al | 0,10 | 0,01 | 0,00 | 0,01 | 0,00 | 0,00 | 0,09 | 0,00 | 0,12 | 0,00 | 0,00 | 0,02 | 0,00 | 0,01 | 0,00 | 0,00 | 0,07 | 0,10 | 0,02 |
| | Sum Z | 6,00 | 6,00 | 6,01 | 6,00 | 6,07 | 6,06 | 6,00 | 6,00 | 6,00 | 6,02 | 6,00 | 6,00 | 6,02 | 6,00 | 6,08 | 6,03 | 6,00 | 6,00 | 6,00 |
| | $Al^{(VI)}$ | 3,91 | 3,98 | 4,02 | 4,00 | 3,98 | 4,00 | 3,97 | 4,00 | 3,93 | 4,01 | 3,97 | 4,02 | 4,05 | 4,03 | 3,95 | 3,98 | 3,98 | 3,94 | 3,99 |
| | $Fe^{3+}$ | 0,20 | 0,20 | 0,20 | 0,20 | 0,20 | 0,20 | 0,20 | 0,20 | 0,20 | 0,20 | 0,20 | 0,20 | 0,19 | 0,20 | 0,20 | 0,20 | 0,20 | 0,20 | 0,20 |
| | Ti | 0,02 | 0,00 | 0,02 | 0,02 | 0,00 | 0,01 | 0,01 | 0,00 | 0,02 | 0,01 | 0,01 | 0,00 | 0,01 | 0,00 | 0,01 | 0,01 | 0,01 | 0,01 | 0,00 |
| | Cr | 0,00 | 0,00 | 0,00 | 0,00 | 0,01 | 0,00 | 0,00 | 0,00 | 0,01 | 0,00 | 0,01 | 0,01 | 0,00 | 0,00 | 0,00 | 0,00 | 0,00 | 0,00 | 0,00 |
| | Sum Y | 4,13 | 4,19 | 4,23 | 4,22 | 4,18 | 4,21 | 4,18 | 4,20 | 4,15 | 4,21 | 4,18 | 4,23 | 4,25 | 4,23 | 4,16 | 4,20 | 4,19 | 4,14 | 4,19 |
| | $Fe^{2+}$ | 3,85 | 3,83 | 3,78 | 3,77 | 3,73 | 3,71 | 3,76 | 3,80 | 3,78 | 3,74 | 3,78 | 3,74 | 3,56 | 3,79 | 3,73 | 3,78 | 3,77 | 3,81 | 3,77 |
| | Mg | 0,30 | 0,26 | 0,25 | 0,27 | 0,25 | 0,22 | 0,28 | 0,30 | 0,28 | 0,27 | 0,29 | 0,29 | 0,25 | 0,29 | 0,27 | 0,24 | 0,29 | 0,27 | 0,30 |
| | Mn | 0,11 | 0,11 | 0,10 | 0,10 | 0,19 | 0,25 | 0,16 | 0,10 | 0,20 | 0,14 | 0,11 | 0,17 | 0,44 | 0,15 | 0,10 | 0,10 | 0,10 | 0,09 | 0,09 |
| | Ca | 1,62 | 1,61 | 1,62 | 1,63 | 1,57 | 1,54 | 1,62 | 1,60 | 1,59 | 1,61 | 1,63 | 1,57 | 1,48 | 1,54 | 1,67 | 1,65 | 1,65 | 1,69 | 1,64 |
| | Na | 0,01 | 0,00 | 0,01 | 0,01 | 0,00 | 0,01 | 0,00 | 0,00 | 0,00 | 0,00 | 0,01 | 0,01 | 0,00 | 0,00 | 0,00 | 0,01 | 0,00 | 0,01 | 0,00 |
| | Sum X | 5,87 | 5,81 | 5,76 | 5,78 | 5,75 | 5,73 | 5,82 | 5,80 | 5,85 | 5,76 | 5,82 | 5,77 | 5,74 | 5,77 | 5,77 | 5,77 | 5,81 | 5,86 | 5,81 |
| | Total | 16,00 | 16,00 | 16,00 | 16,00 | 16,00 | 16,00 | 16,00 | 16,00 | 16,00 | 16,00 | 16,00 | 16,00 | 16,00 | 16,00 | 16,00 | 16,00 | 16,00 | 16,00 | 16,00 |
| | ***End member (Mol-%)*** | | | | | | | | | | | | | | | | | | | |
| | Almandine | 65,6 | 65,9 | 65,8 | 65,3 | 64,9 | 64,8 | 64,6 | 65,6 | 64,6 | 64,9 | 65,1 | 64,9 | 62,1 | 65,7 | 64,7 | 65,5 | 65,0 | 65,0 | 65,0 |
| | Andradite | 5,18 | 5,20 | 5,19 | 5,15 | 5,12 | 5,11 | 5,10 | 5,17 | 5,10 | 5,12 | 5,14 | 5,13 | 4,90 | 5,19 | 5,11 | 5,17 | 5,13 | 5,13 | 5,13 |
| | Grossular | 22,4 | 22,5 | 22,9 | 23,0 | 22,1 | 21,9 | 22,8 | 22,4 | 21,9 | 22,9 | 22,9 | 21,9 | 20,9 | 21,4 | 23,8 | 23,3 | 23,2 | 23,7 | 23,1 |
| | Pyrope | 5,03 | 4,51 | 4,35 | 4,75 | 4,39 | 3,85 | 4,74 | 5,14 | 4,82 | 4,68 | 4,97 | 4,98 | 4,35 | 5,01 | 4,64 | 4,16 | 4,94 | 4,60 | 5,19 |
| | Spessartine | 1,79 | 1,80 | 1,80 | 1,71 | 3,28 | 4,40 | 2,77 | 1,72 | 3,43 | 2,46 | 1,81 | 2,86 | 7,70 | 2,64 | 1,71 | 1,80 | 1,67 | 1,57 | 1,59 |
| | Uvarovite | 0,01 | 0,11 | 0,00 | 0,04 | 0,16 | 0,00 | 0,00 | 0,00 | 0,15 | 0,000 | 0,122 | 0,252 | 0,000 | 0,016 | 0,000 | 0,084 | 0,080 | 0,000 | 0,029 |
| | ***Proportion*** | | | | | | | | | | | | | | | | | | | |
| | X(Ca) | 0,276 | 0,278 | 0,281 | 0,282 | 0,274 | 0,270 | 0,279 | 0,276 | 0,271 | 0,280 | 0,281 | 0,272 | 0,258 | 0,266 | 0,289 | 0,286 | 0,284 | 0,288 | 0,283 |
| | X(Fe) | 0,656 | 0,659 | 0,658 | 0,653 | 0,649 | 0,648 | 0,646 | 0,655 | 0,646 | 0,649 | 0,651 | 0,649 | 0,621 | 0,657 | 0,647 | 0,655 | 0,650 | 0,650 | 0,650 |
| | X(Mg) | 0,050 | 0,045 | 0,043 | 0,047 | 0,044 | 0,038 | 0,047 | 0,051 | 0,048 | 0,047 | 0,050 | 0,050 | 0,043 | 0,050 | 0,046 | 0,042 | 0,049 | 0,046 | 0,052 |
| | X(Mn) | 0,024 | 0,024 | 0,024 | 0,023 | 0,043 | 0,058 | 0,037 | 0,023 | 0,045 | 0,033 | 0,024 | 0,038 | 0,099 | 0,034 | 0,023 | 0,024 | 0,022 | 0,021 | 0,021 |

**Annex III** - Mineral analyses Nolte (2012).

| | Sample | 290709-3 | | | | | | | | | | | | | | | | | |
|---|---|---|---|---|---|---|---|---|---|---|---|---|---|---|---|---|---|---|---|
| | ***Ox. wt%*** | *profile 1-2* | *profile 1-2* | *profile 1-3* | *profile 1-3* | *profile 1-4* | *profile 1-5* | *profile 1-6* | *profile 1-7* | *profile 1-8* | *profile 1-9* | *profile 1-10* | *profile 1-11* | *profile 1-12* | *profile 1-13* | *profile 1-14* | *profile 1-15* | *profile 1-16* | *profile 1-17* | *112-rim* |
| Garnet | $SiO_2$ | 37,6 | 38,3 | 37,8 | 38,0 | 37,7 | 38,1 | 38,5 | 38,6 | 38,2 | 38,5 | 38,3 | 38,0 | 38,4 | 37,8 | 37,9 | 37,2 | 37,8 | 37,5 | 38,5 |
| | $TiO_2$ | 0,08 | 0,05 | 0,05 | 0,00 | 0,06 | 0,05 | 0,07 | 0,11 | 0,01 | 0,00 | 0,07 | 0,06 | 0,13 | 0,07 | 0,05 | 0,00 | 0,08 | 0,00 | 0,20 |
| | $Al_2O_3$ | 21,5 | 21,5 | 21,8 | 21,6 | 21,4 | 21,4 | 21,4 | 21,6 | 21,7 | 21,8 | 21,5 | 21,7 | 21,4 | 21,7 | 21,7 | 21,7 | 21,8 | 21,8 | 21,5 |
| | $Cr_2O_3$ | 0,11 | 0,01 | 0,00 | 0,00 | 0,05 | 0,00 | 0,00 | 0,06 | 0,02 | 0,04 | 0,00 | 0,00 | 0,01 | 0,00 | 0,03 | 0,00 | 0,00 | 0,01 | 0,00 |
| | $Fe_2O_3$ | 1,66 | 1,62 | 1,64 | 1,67 | 1,64 | 1,55 | 1,68 | 1,69 | 1,69 | 1,68 | 1,67 | 1,66 | 1,63 | 1,65 | 1,65 | 1,65 | 1,64 | 1,64 | 1,34 |
| | FeO | 28,5 | 27,8 | 28,1 | 28,5 | 28,0 | 26,5 | 28,8 | 28,9 | 28,9 | 28,7 | 28,5 | 28,4 | 27,9 | 28,2 | 28,2 | 28,2 | 28,1 | 28,1 | 22,9 |
| | MnO | 1,13 | 0,78 | 0,77 | 0,79 | 0,91 | 1,92 | 1,08 | 1,30 | 1,42 | 1,36 | 1,42 | 1,21 | 1,21 | 0,84 | 0,79 | 0,74 | 0,79 | 0,94 | 8,78 |
| | MgO | 1,22 | 1,17 | 1,14 | 1,05 | 1,01 | 0,79 | 1,04 | 1,08 | 1,14 | 1,14 | 1,06 | 1,11 | 1,04 | 1,04 | 1,09 | 1,13 | 1,18 | 1,26 | 2,05 |
| | CaO | 9,47 | 9,92 | 10,33 | 10,23 | 9,86 | 9,72 | 9,57 | 9,37 | 8,98 | 9,05 | 9,22 | 9,47 | 9,85 | 9,76 | 10,07 | 10,25 | 10,31 | 9,91 | 6,47 |
| | $Na_2O$ | 0,03 | 0,01 | 0,00 | 0,00 | 0,03 | 0,00 | 0,02 | 0,01 | 0,00 | 0,00 | 0,01 | 0,01 | 0,02 | 0,00 | 0,00 | 0,00 | 0,00 | 0,01 | 0,02 |
| | sum | 101,30 | 101,10 | 101,60 | 102,00 | 100,70 | 100,00 | 102,10 | 102,80 | 102,10 | 102,40 | 101,78 | 101,63 | 101,52 | 101,02 | 101,46 | 100,88 | 101,67 | 101,15 | 101,77 |
| | ***Structural formula based on 24 O*** | | | | | | | | | | | | | | | | | | | |
| | Si | 5,96 | 6,06 | 5,95 | 5,98 | 5,99 | 6,11 | 6,04 | 6,03 | 6,01 | 6,04 | 6,04 | 5,99 | 6,05 | 6,00 | 5,97 | 5,90 | 5,95 | 5,93 | 6,06 |
| | Al | 0,04 | 0,00 | 0,05 | 0,03 | 0,01 | 0,00 | 0,00 | 0,00 | 0,00 | 0,00 | 0,00 | 0,01 | 0,00 | 0,01 | 0,03 | 0,11 | 0,05 | 0,07 | 0,00 |
| | Sum Z | 6,00 | 6,06 | 6,00 | 6,00 | 6,00 | 6,11 | 6,04 | 6,03 | 6,01 | 6,04 | 6,04 | 6,00 | 6,05 | 6,00 | 6,00 | 6,00 | 6,00 | 6,00 | 6,06 |
| | $Al^{(VI)}$ | 3,96 | 4,01 | 3,99 | 3,98 | 4,01 | 4,03 | 3,96 | 3,98 | 4,01 | 4,03 | 3,99 | 4,02 | 3,98 | 4,04 | 4,01 | 3,95 | 3,98 | 3,99 | 3,99 |
| | $Fe^{3+}$ | 0,20 | 0,19 | 0,19 | 0,20 | 0,20 | 0,19 | 0,20 | 0,20 | 0,20 | 0,20 | 0,20 | 0,20 | 0,19 | 0,20 | 0,20 | 0,20 | 0,19 | 0,20 | 0,16 |
| | Ti | 0,01 | 0,01 | 0,01 | 0,00 | 0,01 | 0,01 | 0,01 | 0,01 | 0,00 | 0,00 | 0,01 | 0,01 | 0,02 | 0,01 | 0,01 | 0,00 | 0,01 | 0,00 | 0,02 |
| | Cr | 0,01 | 0,00 | 0,00 | 0,00 | 0,01 | 0,00 | 0,00 | 0,01 | 0,00 | 0,01 | 0,00 | 0,00 | 0,00 | 0,00 | 0,00 | 0,00 | 0,00 | 0,00 | 0,00 |
| | Sum Y | 4,18 | 4,20 | 4,19 | 4,18 | 4,22 | 4,22 | 4,17 | 4,20 | 4,22 | 4,23 | 4,20 | 4,22 | 4,19 | 4,25 | 4,22 | 4,15 | 4,18 | 4,18 | 4,17 |
| | $Fe^{2+}$ | 3,77 | 3,67 | 3,70 | 3,75 | 3,73 | 3,55 | 3,79 | 3,78 | 3,80 | 3,77 | 3,76 | 3,75 | 3,68 | 3,74 | 3,72 | 3,75 | 3,70 | 3,71 | 3,02 |
| | Mg | 0,29 | 0,28 | 0,27 | 0,25 | 0,24 | 0,19 | 0,24 | 0,25 | 0,27 | 0,27 | 0,25 | 0,26 | 0,24 | 0,25 | 0,26 | 0,27 | 0,28 | 0,30 | 0,48 |
| | Mn | 0,15 | 0,10 | 0,10 | 0,11 | 0,12 | 0,26 | 0,14 | 0,17 | 0,19 | 0,18 | 0,19 | 0,16 | 0,16 | 0,11 | 0,11 | 0,10 | 0,11 | 0,13 | 1,17 |
| | Ca | 1,61 | 1,68 | 1,74 | 1,72 | 1,68 | 1,67 | 1,61 | 1,57 | 1,51 | 1,52 | 1,56 | 1,60 | 1,67 | 1,66 | 1,70 | 1,74 | 1,74 | 1,68 | 1,09 |
| | Na | 0,01 | 0,00 | 0,00 | 0,00 | 0,01 | 0,00 | 0,01 | 0,00 | 0,00 | 0,00 | 0,00 | 0,00 | 0,01 | 0,00 | 0,00 | 0,00 | 0,00 | 0,00 | 0,01 |
| | Sum X | 5,82 | 5,74 | 5,81 | 5,82 | 5,78 | 5,67 | 5,79 | 5,78 | 5,77 | 5,73 | 5,76 | 5,78 | 5,75 | 5,75 | 5,79 | 5,86 | 5,82 | 5,82 | 5,77 |
| | Total | 16,00 | 16,00 | 16,00 | 16,00 | 16,00 | 16,00 | 16,00 | 16,00 | 16,00 | 16,00 | 16,00 | 16,00 | 16,00 | 16,00 | 16,00 | 16,00 | 16,00 | 16,00 | 16,00 |
| | ***End member (Mol-%)*** | | | | | | | | | | | | | | | | | | | |
| | Almandine | 64,8 | 64,0 | 63,6 | 64,4 | 64,6 | 62,7 | 65,4 | 65,5 | 65,9 | 65,7 | 65,3 | 65,0 | 64,0 | 64,9 | 64,3 | 64,0 | 63,6 | 63,9 | 52,4 |
| | Andradite | 5,12 | 5,05 | 5,02 | 5,08 | 5,10 | 4,95 | 5,16 | 5,17 | 5,20 | 5,19 | 5,15 | 5,13 | 5,05 | 5,13 | 5,08 | 5,05 | 5,02 | 5,04 | 4,14 |
| | Grossular | 22,2 | 24,3 | 25,0 | 24,5 | 23,9 | 24,5 | 22,7 | 21,8 | 21,0 | 21,2 | 21,9 | 22,6 | 23,9 | 23,7 | 24,3 | 24,7 | 24,8 | 23,8 | 14,8 |
| | Pyrope | 4,97 | 4,82 | 4,61 | 4,22 | 4,15 | 3,32 | 4,22 | 4,36 | 4,64 | 4,65 | 4,35 | 4,52 | 4,25 | 4,29 | 4,44 | 4,56 | 4,77 | 5,10 | 8,34 |
| | Spessartine | 2,60 | 1,82 | 1,76 | 1,81 | 2,13 | 4,59 | 2,49 | 2,98 | 3,29 | 3,15 | 3,29 | 2,79 | 2,81 | 1,95 | 1,82 | 1,71 | 1,81 | 2,16 | 20,31 |
| | Uvarovite | 0,35 | 0,02 | 0,00 | 0,00 | 0,15 | 0,01 | 0,00 | 0,19 | 0,06 | 0,14 | 0,00 | 0,01 | 0,02 | 0,00 | 0,08 | 0,00 | 0,00 | 0,03 | 0,00 |
| | ***Proportion*** | | | | | | | | | | | | | | | | | | | |
| | X(Ca) | 0,276 | 0,293 | 0,3 | 0,296 | 0,291 | 0,294 | 0,279 | 0,272 | 0,262 | 0,265 | 0,271 | 0,277 | 0,29 | 0,288 | 0,294 | 0,297 | 0,299 | 0,289 | 0,189 |
| | X(Fe) | 0,648 | 0,64 | 0,637 | 0,644 | 0,646 | 0,627 | 0,654 | 0,655 | 0,659 | 0,657 | 0,653 | 0,65 | 0,64 | 0,649 | 0,643 | 0,64 | 0,636 | 0,639 | 0,524 |
| | X(Mg) | 0,050 | 0,048 | 0,046 | 0,042 | 0,042 | 0,033 | 0,042 | 0,044 | 0,046 | 0,046 | 0,043 | 0,045 | 0,042 | 0,043 | 0,044 | 0,046 | 0,048 | 0,051 | 0,083 |
| | X(Mn) | 0,034 | 0,024 | 0,024 | 0,024 | 0,029 | 0,062 | 0,033 | 0,039 | 0,043 | 0,041 | 0,043 | 0,037 | 0,038 | 0,026 | 0,025 | 0,023 | 0,025 | 0,029 | 0,242 |

**Annex III** - Mineral analyses Nolte (2012).

| | Sample | 290709-8 | | | | | | | | | | | | | | | | | |
|---|---|---|---|---|---|---|---|---|---|---|---|---|---|---|---|---|---|---|---|
| | ***Ox. wt%*** | *113-rim* | *114-rim* | *115-rim* | *spot-159* | *spot-160* | *spot-161* | *spot-162* | *profile 2-3* | *profile 2-4* | *profile 2-6* | *profile 2-7* | *profile 2-10* | *profile 2-11* | *profile 2-12* | *profile 2-13* | *profile 2-14* | *profile 2-15* | *profile 2-16* | *profile 2-17* |
| Garnet | $SiO_2$ | 38,6 | 37,6 | 38,5 | 38,3 | 38,0 | 38,4 | 38,3 | 37,8 | 36,8 | 36,8 | 36,3 | 36,3 | 36,7 | 36,7 | 37,5 | 36,9 | 36,4 | 37,5 | 37,1 |
| | $TiO_2$ | 0,03 | 0,12 | 0,11 | 0,08 | 0,18 | 0,21 | 0,10 | 0,20 | 0,09 | 0,28 | 0,25 | 0,12 | 0,14 | 0,13 | 0,09 | 0,21 | 0,29 | 0,20 | 0,26 |
| | $Al_2O_3$ | 21,4 | 21,4 | 21,6 | 22,0 | 21,6 | 21,1 | 21,5 | 21,5 | 21,4 | 21,3 | 21,4 | 21,7 | 21,4 | 21,5 | 21,8 | 21,4 | 21,5 | 21,5 | 21,6 |
| | $Cr_2O_3$ | 0,00 | 0,00 | 0,08 | 0,00 | 0,02 | 0,00 | 0,00 | 0,00 | 0,01 | 0,01 | 0,00 | 0,00 | 0,01 | 0,00 | 0,00 | 0,03 | 0,00 | 0,00 | 0,00 |
| | $Fe_2O_3$ | 1,34 | 1,31 | 1,31 | 1,29 | 1,27 | 1,28 | 1,32 | 1,32 | 1,31 | 1,28 | 1,29 | 1,27 | 1,32 | 1,31 | 1,33 | 1,33 | 1,31 | 1,34 | 1,30 |
| | FeO | 22,9 | 22,4 | 22,4 | 22,0 | 21,7 | 21,9 | 22,6 | 22,5 | 22,4 | 21,8 | 22,0 | 21,8 | 22,6 | 22,3 | 22,8 | 22,7 | 22,3 | 22,9 | 22,2 |
| | MnO | 8,65 | 8,63 | 8,20 | 9,22 | 9,79 | 8,61 | 8,55 | 8,54 | 8,54 | 9,06 | 9,29 | 9,48 | 9,01 | 8,66 | 8,67 | 8,56 | 8,50 | 8,73 | 9,64 |
| | MgO | 1,96 | 1,77 | 1,91 | 1,80 | 1,75 | 1,83 | 1,99 | 1,94 | 1,99 | 1,84 | 1,82 | 1,56 | 1,92 | 1,92 | 1,95 | 2,00 | 1,99 | 2,00 | 1,77 |
| | CaO | 7,11 | 7,80 | 7,84 | 6,99 | 7,02 | 7,66 | 7,29 | 7,31 | 7,72 | 7,37 | 6,97 | 7,35 | 7,16 | 7,27 | 7,02 | 7,23 | 7,27 | 6,94 | 7,07 |
| | $Na_2O$ | 0,02 | 0,01 | 0,01 | 0,03 | 0,00 | 0,03 | 0,03 | 0,04 | 0,04 | 0,03 | 0,02 | 0,03 | 0,01 | 0,03 | 0,01 | 0,07 | 0,06 | 0,05 | 0,04 |
| | sum | 101,99 | 101,06 | 101,98 | 101,75 | 101,38 | 101,11 | 101,74 | 101,10 | 100,25 | 99,76 | 99,33 | 99,53 | 100,24 | 99,84 | 101,07 | 100,50 | 99,62 | 101,15 | 101,00 |
| | ***Structural formula based on 24 O*** | | | | | | | | | | | | | | | | | | | |
| | Si | 6,06 | 5,97 | 6,04 | 6,02 | 6,01 | 6,08 | 6,03 | 5,98 | 5,87 | 5,90 | 5,86 | 5,85 | 5,87 | 5,89 | 5,94 | 5,89 | 5,84 | 5,94 | 5,90 |
| | Al | 0,00 | 0,03 | 0,00 | 0,00 | 0,00 | 0,00 | 0,00 | 0,02 | 0,13 | 0,10 | 0,14 | 0,15 | 0,13 | 0,11 | 0,07 | 0,12 | 0,16 | 0,06 | 0,10 |
| | Sum Z | 6,06 | 6,00 | 6,04 | 6,02 | 6,01 | 6,08 | 6,03 | 6,00 | 6,00 | 6,00 | 6,00 | 6,00 | 6,00 | 6,00 | 6,00 | 6,00 | 6,00 | 6,00 | 6,00 |
| | $Al^{(VI)}$ | 3,97 | 3,96 | 4,00 | 4,08 | 4,03 | 3,94 | 3,98 | 3,99 | 3,88 | 3,93 | 3,93 | 3,96 | 3,90 | 3,94 | 4,00 | 3,90 | 3,91 | 3,95 | 3,94 |
| | $Fe^{3+}$ | 0,16 | 0,16 | 0,15 | 0,15 | 0,15 | 0,15 | 0,16 | 0,16 | 0,16 | 0,15 | 0,16 | 0,15 | 0,16 | 0,16 | 0,16 | 0,16 | 0,16 | 0,16 | 0,16 |
| | Ti | 0,00 | 0,02 | 0,01 | 0,01 | 0,02 | 0,03 | 0,01 | 0,02 | 0,01 | 0,03 | 0,03 | 0,02 | 0,02 | 0,02 | 0,01 | 0,03 | 0,04 | 0,02 | 0,03 |
| | Cr | 0,00 | 0,00 | 0,01 | 0,00 | 0,00 | 0,00 | 0,00 | 0,00 | 0,00 | 0,00 | 0,00 | 0,00 | 0,00 | 0,00 | 0,00 | 0,00 | 0,00 | 0,00 | 0,00 |
| | Sum Y | 4,13 | 4,13 | 4,17 | 4,25 | 4,20 | 4,12 | 4,15 | 4,17 | 4,05 | 4,12 | 4,11 | 4,13 | 4,07 | 4,11 | 4,17 | 4,09 | 4,10 | 4,13 | 4,13 |
| | $Fe^{2+}$ | 3,01 | 2,97 | 2,94 | 2,90 | 2,88 | 2,90 | 2,98 | 2,98 | 2,99 | 2,93 | 2,97 | 2,93 | 3,02 | 2,99 | 3,02 | 3,03 | 3,00 | 3,03 | 2,94 |
| | Mg | 0,46 | 0,42 | 0,45 | 0,42 | 0,41 | 0,43 | 0,47 | 0,46 | 0,47 | 0,44 | 0,44 | 0,38 | 0,46 | 0,46 | 0,46 | 0,48 | 0,48 | 0,47 | 0,42 |
| | Mn | 1,15 | 1,16 | 1,09 | 1,23 | 1,31 | 1,16 | 1,14 | 1,15 | 1,15 | 1,23 | 1,27 | 1,29 | 1,22 | 1,18 | 1,16 | 1,16 | 1,16 | 1,17 | 1,30 |
| | Ca | 1,20 | 1,33 | 1,32 | 1,18 | 1,19 | 1,30 | 1,23 | 1,24 | 1,32 | 1,27 | 1,21 | 1,27 | 1,23 | 1,25 | 1,19 | 1,23 | 1,25 | 1,18 | 1,20 |
| | Na | 0,01 | 0,00 | 0,00 | 0,01 | 0,00 | 0,01 | 0,01 | 0,01 | 0,01 | 0,01 | 0,01 | 0,01 | 0,00 | 0,01 | 0,00 | 0,02 | 0,02 | 0,02 | 0,01 |
| | Sum X | 5,82 | 5,87 | 5,79 | 5,74 | 5,79 | 5,80 | 5,82 | 5,84 | 5,95 | 5,88 | 5,89 | 5,88 | 5,93 | 5,89 | 5,83 | 5,91 | 5,90 | 5,87 | 5,87 |
| | Total | 16,00 | 16,00 | 16,00 | 16,00 | 16,00 | 16,00 | 16,00 | 16,00 | 16,00 | 16,00 | 16,00 | 16,00 | 16,00 | 16,00 | 16,00 | 16,00 | 16,00 | 16,00 | 16,00 |
| | ***End member (Mol-%)*** | | | | | | | | | | | | | | | | | | | |
| | Almandine | 51,7 | 50,6 | 50,7 | 50,6 | 49,7 | 50,2 | 51,3 | 51,2 | 42,9 | 49,9 | 44,0 | 44,1 | 43,7 | 50,9 | 51,7 | 44,2 | 44,5 | 51,8 | 50,2 |
| | Andradite | 4,08 | 3,99 | 4,00 | 3,99 | 3,92 | 3,96 | 4,05 | 4,04 | 4,57 | 3,94 | 4,50 | 4,41 | 4,62 | 4,02 | 4,08 | 4,65 | 4,56 | 4,09 | 3,96 |
| | Grossular | 16,5 | 18,6 | 18,5 | 16,6 | 16,6 | 18,5 | 17,1 | 17,3 | 21,0 | 17,6 | 18,7 | 19,8 | 19,1 | 17,2 | 16,4 | 19,3 | 19,5 | 16,0 | 16,5 |
| | Pyrope | 7,88 | 7,10 | 7,73 | 7,37 | 7,15 | 7,47 | 8,01 | 7,88 | 9,16 | 7,49 | 8,44 | 7,15 | 8,87 | 7,80 | 7,90 | 9,26 | 9,18 | 8,08 | 7,16 |
| | Spessartine | 19,80 | 19,74 | 18,81 | 21,46 | 22,65 | 19,95 | 19,61 | 19,67 | 22,39 | 20,99 | 24,40 | 24,63 | 23,67 | 20,01 | 19,95 | 22,49 | 22,27 | 20,01 | 22,12 |
| | Uvarovite | 0,00 | 0,00 | 0,25 | 0,00 | 0,06 | 0,00 | 0,00 | 0,00 | 0,02 | 0,05 | 0,00 | 0,00 | 0,03 | 0,00 | 0,00 | 0,10 | 0,00 | 0,00 | 0,00 |
| | ***Proportion*** | | | | | | | | | | | | | | | | | | | |
| | X(Ca) | 0,206 | 0,226 | 0,228 | 0,206 | 0,205 | 0,224 | 0,211 | 0,213 | 0,222 | 0,216 | 0,205 | 0,216 | 0,207 | 0,213 | 0,204 | 0,209 | 0,213 | 0,201 | 0,205 |
| | X(Fe) | 0,517 | 0,506 | 0,507 | 0,506 | 0,497 | 0,502 | 0,512 | 0,512 | 0,504 | 0,499 | 0,505 | 0,499 | 0,51 | 0,509 | 0,517 | 0,514 | 0,51 | 0,518 | 0,502 |
| | X(Mg) | 0,079 | 0,071 | 0,077 | 0,074 | 0,072 | 0,075 | 0,080 | 0,079 | 0,080 | 0,075 | 0,075 | 0,064 | 0,077 | 0,078 | 0,079 | 0,081 | 0,081 | 0,081 | 0,072 |
| | X(Mn) | 0,241 | 0,246 | 0,235 | 0,261 | 0,276 | 0,249 | 0,240 | 0,242 | 0,242 | 0,259 | 0,263 | 0,272 | 0,251 | 0,246 | 0,242 | 0,240 | 0,241 | 0,242 | 0,269 |

**Annex III** - Mineral analyses Nolte (2012).

| | Sample | 290709-8 | | | | | | | | | | | | | | | | | | |
|---|---|---|---|---|---|---|---|---|---|---|---|---|---|---|---|---|---|---|---|---|
| | Ox. wt% | profile 2-18 | profile 2-19 | profile 2-20 | profile 2-21 | profile 2-24 | profile 2-25 | profile 2-26 | profile 2-27 | profile 2-28 | profile 2-29 | profile 2-30 | profile 2-31 | profile 2-32 | profile 2-33 | profile 2-34 | profile 2-35 | profile 2-36 | profile 2-37 | profile 2-38 |
| Garnet | $SiO_2$ | 37,9 | 36,6 | 37,2 | 36,6 | 38,1 | 37,7 | 38,5 | 38,3 | 37,9 | 37,7 | 37,6 | 37,9 | 38,3 | 38,1 | 37,3 | 36,9 | 37,4 | 37,8 | 37,0 |
| | $TiO_2$ | 0,20 | 0,14 | 0,11 | 0,14 | 0,10 | 0,08 | 0,05 | 0,25 | 0,37 | 0,29 | 0,15 | 0,09 | 0,10 | 0,11 | 0,03 | 0,00 | 0,14 | 0,18 | 0,05 |
| | $Al_2O_3$ | 21,5 | 21,4 | 21,4 | 21,1 | 21,3 | 21,5 | 21,6 | 21,5 | 21,4 | 21,6 | 21,6 | 21,2 | 21,2 | 21,7 | 21,6 | 21,6 | 21,5 | 21,5 | 21,4 |
| | $Cr_2O_3$ | 0,00 | 0,00 | 0,01 | 0,00 | 0,00 | 0,00 | 0,04 | 0,00 | 0,00 | 0,00 | 0,00 | 0,00 | 0,02 | 0,00 | 0,00 | 0,04 | 0,01 | 0,00 | 0,00 |
| | $Fe_2O_3$ | 1,30 | 1,31 | 1,31 | 1,27 | 1,30 | 1,32 | 1,32 | 1,33 | 1,32 | 1,32 | 1,31 | 1,30 | 1,29 | 1,32 | 1,33 | 1,32 | 1,31 | 1,29 | 1,31 |
| | FeO | 22,2 | 22,4 | 22,3 | 21,7 | 22,3 | 22,5 | 22,6 | 22,8 | 22,5 | 22,6 | 22,4 | 22,2 | 22,0 | 22,6 | 22,8 | 22,5 | 22,4 | 22,1 | 22,4 |
| | MnO | 8,56 | 8,75 | 8,75 | 8,60 | 9,17 | 8,62 | 8,61 | 8,49 | 8,39 | 8,56 | 8,42 | 8,29 | 8,41 | 8,70 | 8,47 | 8,63 | 8,29 | 8,63 | 8,80 |
| | MgO | 2,03 | 1,95 | 1,95 | 1,79 | 1,68 | 1,92 | 1,96 | 1,96 | 1,99 | 1,99 | 1,95 | 1,92 | 1,84 | 1,94 | 1,96 | 1,94 | 1,95 | 1,75 | 1,71 |
| | CaO | 7,51 | 7,05 | 7,14 | 8,22 | 7,46 | 7,46 | 7,40 | 7,34 | 7,20 | 7,25 | 7,50 | 7,90 | 7,79 | 7,03 | 7,46 | 7,00 | 7,62 | 7,97 | 7,84 |
| | $Na_2O$ | 0,01 | 0,04 | 0,02 | 0,01 | 0,04 | 0,01 | 0,04 | 0,03 | 0,03 | 0,06 | 0,06 | 0,04 | 0,00 | 0,04 | 0,03 | 0,05 | 0,03 | 0,06 | 0,05 |
| | sum | 101,15 | 99,69 | 100,19 | 99,46 | 101,45 | 100,99 | 102,07 | 102,01 | 101,09 | 101,38 | 100,96 | 100,86 | 100,97 | 101,48 | 100,99 | 100,01 | 100,62 | 101,25 | 100,60 |
| | ***Structural formula based on 24 O*** | | | | | | | | | | | | | | | | | | | |
| | Si | 5,99 | 5,88 | 5,95 | 5,89 | 6,02 | 5,97 | 6,04 | 6,02 | 6,00 | 5,95 | 5,96 | 6,01 | 6,08 | 6,00 | 5,91 | 5,91 | 5,94 | 5,98 | 5,89 |
| | Al | 0,01 | 0,12 | 0,05 | 0,11 | 0,00 | 0,03 | 0,00 | 0,00 | 0,00 | 0,05 | 0,04 | 0,00 | 0,00 | 0,00 | 0,09 | 0,09 | 0,06 | 0,02 | 0,11 |
| | Sum Z | 6,00 | 6,00 | 6,00 | 6,00 | 6,02 | 6,00 | 6,04 | 6,02 | 6,00 | 6,00 | 6,00 | 6,01 | 6,08 | 6,00 | 6,00 | 6,00 | 6,00 | 6,00 | 6,00 |
| | $Al^{(VI)}$ | 3,99 | 3,94 | 3,97 | 3,90 | 3,97 | 3,97 | 3,98 | 3,98 | 3,99 | 3,97 | 3,99 | 3,96 | 3,95 | 4,03 | 3,94 | 3,98 | 3,97 | 3,97 | 3,91 |
| | $Fe^{3+}$ | 0,15 | 0,16 | 0,16 | 0,15 | 0,16 | 0,16 | 0,16 | 0,16 | 0,16 | 0,16 | 0,16 | 0,16 | 0,15 | 0,16 | 0,16 | 0,16 | 0,16 | 0,15 | 0,16 |
| | Ti | 0,02 | 0,02 | 0,01 | 0,02 | 0,01 | 0,01 | 0,01 | 0,03 | 0,04 | 0,04 | 0,02 | 0,01 | 0,01 | 0,01 | 0,00 | 0,00 | 0,02 | 0,02 | 0,01 |
| | Cr | 0,00 | 0,00 | 0,00 | 0,00 | 0,00 | 0,00 | 0,01 | 0,00 | 0,00 | 0,00 | 0,00 | 0,00 | 0,00 | 0,00 | 0,00 | 0,00 | 0,00 | 0,00 | 0,00 |
| | Sum Y | 4,17 | 4,11 | 4,14 | 4,07 | 4,14 | 4,14 | 4,15 | 4,16 | 4,19 | 4,16 | 4,16 | 4,12 | 4,12 | 4,20 | 4,11 | 4,14 | 4,14 | 4,15 | 4,07 |
| | $Fe^{2+}$ | 2,93 | 3,01 | 2,99 | 2,92 | 2,94 | 2,98 | 2,96 | 2,99 | 2,98 | 2,99 | 2,96 | 2,94 | 2,92 | 2,98 | 3,02 | 3,01 | 2,97 | 2,92 | 2,98 |
| | Mg | 0,48 | 0,47 | 0,47 | 0,43 | 0,40 | 0,45 | 0,46 | 0,46 | 0,47 | 0,47 | 0,46 | 0,45 | 0,44 | 0,46 | 0,46 | 0,46 | 0,46 | 0,41 | 0,41 |
| | Mn | 1,15 | 1,19 | 1,18 | 1,17 | 1,23 | 1,16 | 1,14 | 1,13 | 1,13 | 1,15 | 1,13 | 1,11 | 1,13 | 1,16 | 1,14 | 1,17 | 1,12 | 1,16 | 1,19 |
| | Ca | 1,27 | 1,21 | 1,22 | 1,42 | 1,26 | 1,27 | 1,24 | 1,24 | 1,22 | 1,23 | 1,27 | 1,34 | 1,32 | 1,19 | 1,27 | 1,20 | 1,30 | 1,35 | 1,34 |
| | Na | 0,00 | 0,01 | 0,01 | 0,00 | 0,01 | 0,00 | 0,01 | 0,01 | 0,01 | 0,02 | 0,02 | 0,01 | 0,00 | 0,01 | 0,01 | 0,02 | 0,01 | 0,02 | 0,01 |
| | Sum X | 5,83 | 5,89 | 5,86 | 5,93 | 5,84 | 5,86 | 5,81 | 5,82 | 5,81 | 5,84 | 5,84 | 5,87 | 5,81 | 5,80 | 5,90 | 5,86 | 5,86 | 5,85 | 5,93 |
| | Total | 16,00 | 16,00 | 16,00 | 16,00 | 16,00 | 16,00 | 16,00 | 16,00 | 16,00 | 16,00 | 16,00 | 16,00 | 16,00 | 16,00 | 16,00 | 16,00 | 16,00 | 16,00 | 16,00 |
| | ***End member (Mol-%)*** | | | | | | | | | | | | | | | | | | | |
| | Almandine | 50,3 | 51,2 | 51,0 | 41,6 | 50,5 | 50,9 | 51,0 | 51,4 | 51,4 | 51,2 | 50,8 | 50,3 | 50,3 | 51,5 | 51,3 | 51,5 | 50,8 | 50,0 | 43,2 |
| | Andradite | 3,97 | 4,04 | 4,02 | 4,45 | 3,99 | 4,02 | 4,02 | 4,06 | 4,06 | 4,04 | 4,01 | 3,97 | 3,97 | 4,06 | 4,05 | 4,07 | 4,01 | 3,95 | 4,57 |
| | Grossular | 17,9 | 16,6 | 16,8 | 23,0 | 17,7 | 17,6 | 17,3 | 17,2 | 17,0 | 17,0 | 17,8 | 19,0 | 18,7 | 16,5 | 17,5 | 16,3 | 18,2 | 19,2 | 21,4 |
| | Pyrope | 8,21 | 7,96 | 7,95 | 8,29 | 6,77 | 7,74 | 7,90 | 7,90 | 8,11 | 8,05 | 7,92 | 7,76 | 7,49 | 7,89 | 7,85 | 7,93 | 7,91 | 7,05 | 7,87 |
| | Spessartine | 19,66 | 20,25 | 20,21 | 22,67 | 21,05 | 19,75 | 19,70 | 19,44 | 19,40 | 19,65 | 19,39 | 19,01 | 19,44 | 20,10 | 19,32 | 20,01 | 19,08 | 19,81 | 23,02 |
| | Uvarovite | 0,00 | 0,00 | 0,04 | 0,00 | 0,00 | 0,00 | 0,12 | 0,00 | 0,00 | 0,00 | 0,00 | 0,00 | 0,07 | 0,00 | 0,00 | 0,11 | 0,03 | 0,00 | 0,00 |
| | ***Proportion*** | | | | | | | | | | | | | | | | | | | |
| | X(Ca) | 0,218 | 0,206 | 0,209 | 0,239 | 0,217 | 0,216 | 0,214 | 0,213 | 0,211 | 0,211 | 0,218 | 0,229 | 0,228 | 0,206 | 0,215 | 0,205 | 0,222 | 0,231 | 0,226 |
| | X(Fe) | 0,503 | 0,512 | 0,51 | 0,492 | 0,505 | 0,509 | 0,51 | 0,514 | 0,514 | 0,512 | 0,508 | 0,503 | 0,503 | 0,515 | 0,513 | 0,515 | 0,508 | 0,5 | 0,504 |
| | X(Mg) | 0,082 | 0,080 | 0,079 | 0,072 | 0,068 | 0,077 | 0,079 | 0,079 | 0,081 | 0,081 | 0,079 | 0,078 | 0,075 | 0,079 | 0,079 | 0,079 | 0,079 | 0,070 | 0,069 |
| | X(Mn) | 0,243 | 0,247 | 0,247 | 0,251 | 0,260 | 0,244 | 0,242 | 0,239 | 0,237 | 0,241 | 0,240 | 0,239 | 0,243 | 0,245 | 0,238 | 0,243 | 0,237 | 0,249 | 0,251 |

**Annex III** - Mineral analyses Nolte (2012).

| | Sample | 290709-8 | 020809-3 | | | | | | | | | | | | | | | 020809-4 | |
|---|---|---|---|---|---|---|---|---|---|---|---|---|---|---|---|---|---|---|---|
| | Ox. wt% | profile 2-39 | spot-73 | spot-74 | spot-75 | spot-76 | spot-77 | spot-141 | spot-142 | spot-143 | spot-144 | spot-145 | spot-146 | spot-148 | spot-149 | spot-150 | spot-151 | spot-154 | 9-core | 10-rim |
| Garnet | $SiO_2$ | 37,2 | 37,5 | 38,3 | 37,4 | 38,6 | 37,5 | 38,2 | 38,5 | 38,5 | 38,8 | 38,6 | 38,4 | 38,9 | 38,4 | 38,5 | 38,5 | 38,9 | 38,5 | 38,5 |
| | $TiO_2$ | 0,43 | 0,04 | 0,04 | 0,08 | 0,01 | 0,04 | 0,18 | 0,11 | 0,09 | 0,05 | 0,06 | 0,08 | 0,13 | 0,07 | 0,04 | 0,00 | 0,11 | 0,13 | 0,09 |
| | $Al_2O_3$ | 21,3 | 22,1 | 22,4 | 22,2 | 22,3 | 22,1 | 21,9 | 22,3 | 22,3 | 21,6 | 22,1 | 22,1 | 22,2 | 22,0 | 22,2 | 22,4 | 22,3 | 21,2 | 21,3 |
| | $Cr_2O_3$ | 0,00 | 0,04 | 0,07 | 0,00 | 0,07 | 0,01 | 0,01 | 0,04 | 0,00 | 0,05 | 0,03 | 0,03 | 0,00 | 0,00 | 0,00 | 0,00 | 0,00 | 0,04 | 0,02 |
| | $Fe_2O_3$ | 1,25 | 1,36 | 1,37 | 1,37 | 1,36 | 1,39 | 1,40 | 1,40 | 1,41 | 1,40 | 1,42 | 1,41 | 1,41 | 1,41 | 1,43 | 1,44 | 1,40 | 1,22 | 1,21 |
| | FeO | 21,4 | 23,3 | 23,5 | 23,4 | 23,3 | 23,7 | 24,0 | 23,9 | 24,1 | 23,9 | 24,3 | 24,2 | 24,0 | 24,2 | 24,4 | 24,6 | 23,9 | 20,9 | 20,6 |
| | MnO | 9,77 | 3,29 | 3,17 | 5,33 | 2,68 | 4,36 | 3,31 | 3,32 | 3,44 | 5,08 | 3,68 | 3,85 | 4,02 | 4,64 | 4,40 | 4,12 | 3,08 | 1,20 | 1,24 |
| | MgO | 1,54 | 2,57 | 2,59 | 1,81 | 3,23 | 1,99 | 2,77 | 2,95 | 2,94 | 1,95 | 2,64 | 2,54 | 2,45 | 1,96 | 2,16 | 2,25 | 3,08 | 0,64 | 0,69 |
| | CaO | 7,55 | 10,29 | 10,42 | 9,48 | 10,27 | 10,21 | 9,50 | 9,25 | 9,07 | 8,99 | 9,12 | 9,28 | 9,23 | 9,18 | 9,01 | 9,28 | 9,49 | 17,18 | 17,23 |
| | $Na_2O$ | 0,00 | 0,00 | 0,03 | 0,03 | 0,01 | 0,03 | 0,04 | 0,03 | 0,04 | 0,01 | 0,02 | 0,02 | 0,02 | 0,01 | 0,03 | 0,00 | 0,04 | 0,01 | 0,02 |
| | sum | 100,46 | 100,48 | 101,89 | 101,10 | 101,79 | 101,27 | 101,34 | 101,81 | 101,89 | 101,73 | 102,00 | 101,88 | 102,39 | 101,93 | 102,15 | 102,54 | 102,29 | 101,02 | 100,92 |
| | ***Structural formula based on 24 O*** | | | | | | | | | | | | | | | | | | | |
| | Si | 5,95 | 5,90 | 5,94 | 5,89 | 5,96 | 5,87 | 5,97 | 5,98 | 5,97 | 6,07 | 6,00 | 5,98 | 6,03 | 6,00 | 6,00 | 5,96 | 6,00 | 6,01 | 6,02 |
| | Al | 0,05 | 0,10 | 0,06 | 0,11 | 0,04 | 0,13 | 0,03 | 0,02 | 0,03 | 0,00 | 0,00 | 0,02 | 0,00 | 0,00 | 0,00 | 0,04 | 0,01 | 0,00 | 0,00 |
| | Sum Z | 6,00 | 6,00 | 6,00 | 6,00 | 6,00 | 6,00 | 6,00 | 6,00 | 6,00 | 6,07 | 6,00 | 6,00 | 6,03 | 6,00 | 6,00 | 6,00 | 6,00 | 6,01 | 6,02 |
| | $Al^{(VI)}$ | 3,96 | 3,99 | 4,03 | 4,01 | 4,03 | 3,96 | 4,00 | 4,05 | 4,04 | 3,98 | 4,04 | 4,03 | 4,05 | 4,06 | 4,06 | 4,04 | 4,05 | 3,91 | 3,92 |
| | $Fe^{3+}$ | 0,15 | 0,16 | 0,16 | 0,16 | 0,16 | 0,16 | 0,17 | 0,16 | 0,16 | 0,16 | 0,17 | 0,17 | 0,16 | 0,17 | 0,17 | 0,17 | 0,16 | 0,14 | 0,14 |
| | Ti | 0,05 | 0,01 | 0,01 | 0,01 | 0,00 | 0,00 | 0,02 | 0,01 | 0,01 | 0,01 | 0,01 | 0,01 | 0,02 | 0,01 | 0,00 | 0,00 | 0,01 | 0,02 | 0,01 |
| | Cr | 0,00 | 0,00 | 0,01 | 0,00 | 0,01 | 0,00 | 0,00 | 0,00 | 0,00 | 0,01 | 0,00 | 0,00 | 0,00 | 0,00 | 0,00 | 0,00 | 0,00 | 0,00 | 0,00 |
| | Sum Y | 4,16 | 4,16 | 4,20 | 4,18 | 4,19 | 4,12 | 4,18 | 4,23 | 4,22 | 4,16 | 4,22 | 4,21 | 4,22 | 4,23 | 4,23 | 4,21 | 4,23 | 4,07 | 4,07 |
| | $Fe^{2+}$ | 2,86 | 3,07 | 3,04 | 3,08 | 3,01 | 3,11 | 3,13 | 3,11 | 3,13 | 3,13 | 3,16 | 3,14 | 3,11 | 3,16 | 3,18 | 3,19 | 3,09 | 2,73 | 2,69 |
| | Mg | 0,37 | 0,60 | 0,60 | 0,43 | 0,74 | 0,47 | 0,64 | 0,68 | 0,68 | 0,46 | 0,61 | 0,59 | 0,57 | 0,46 | 0,50 | 0,52 | 0,71 | 0,15 | 0,16 |
| | Mn | 1,32 | 0,44 | 0,42 | 0,71 | 0,35 | 0,58 | 0,44 | 0,44 | 0,45 | 0,67 | 0,48 | 0,51 | 0,53 | 0,61 | 0,58 | 0,54 | 0,40 | 0,16 | 0,16 |
| | Ca | 1,29 | 1,73 | 1,73 | 1,60 | 1,70 | 1,72 | 1,59 | 1,54 | 1,51 | 1,51 | 1,52 | 1,55 | 1,53 | 1,54 | 1,50 | 1,54 | 1,57 | 2,88 | 2,88 |
| | Na | 0,00 | 0,00 | 0,01 | 0,01 | 0,00 | 0,01 | 0,01 | 0,01 | 0,01 | 0,00 | 0,01 | 0,01 | 0,01 | 0,00 | 0,01 | 0,00 | 0,01 | 0,00 | 0,01 |
| | Sum X | 5,84 | 5,84 | 5,80 | 5,82 | 5,81 | 5,88 | 5,82 | 5,77 | 5,78 | 5,77 | 5,78 | 5,79 | 5,75 | 5,77 | 5,77 | 5,79 | 5,78 | 5,92 | 5,91 |
| | Total | 16,00 | 16,00 | 16,00 | 16,00 | 16,00 | 16,00 | 16,00 | 16,00 | 16,00 | 16,00 | 16,00 | 16,00 | 16,00 | 16,00 | 16,00 | 16,00 | 16,00 | 16,00 | 16,00 |
| | ***End member (Mol-%)*** | | | | | | | | | | | | | | | | | | | |
| | Almandine | 48,9 | 52,5 | 52,6 | 52,9 | 51,8 | 53,0 | 54,0 | 53,9 | 54,2 | 54,3 | 54,7 | 54,3 | 54,3 | 54,8 | 55,1 | 55,1 | 53,5 | 46,2 | 45,6 |
| | Andradite | 3,86 | 4,14 | 4,15 | 4,18 | 4,09 | 4,18 | 4,26 | 4,25 | 4,28 | 4,28 | 4,32 | 4,29 | 4,28 | 4,32 | 4,35 | 4,35 | 4,23 | 3,64 | 3,60 |
| | Grossular | 18,3 | 25,4 | 25,6 | 23,3 | 25,0 | 25,0 | 23,1 | 22,3 | 21,9 | 21,7 | 21,9 | 22,4 | 22,4 | 22,3 | 21,8 | 22,3 | 23,0 | 44,9 | 45,2 |
| | Pyrope | 6,28 | 10,33 | 10,34 | 7,31 | 12,81 | 7,92 | 11,09 | 11,83 | 11,80 | 7,91 | 10,58 | 10,19 | 9,85 | 7,92 | 8,71 | 8,96 | 12,27 | 2,51 | 2,74 |
| | Spessartine | 22,64 | 7,51 | 7,18 | 12,22 | 6,06 | 9,87 | 7,54 | 7,57 | 7,83 | 11,68 | 8,39 | 8,76 | 9,20 | 10,65 | 10,07 | 9,33 | 6,99 | 2,69 | 2,78 |
| | Uvarovite | 0,00 | 0,12 | 0,21 | 0,00 | 0,21 | 0,03 | 0,04 | 0,12 | 0,00 | 0,17 | 0,08 | 0,08 | 0,00 | 0,01 | 0,00 | 0,00 | 0,00 | 0,11 | 0,06 |
| | ***Proportion*** | | | | | | | | | | | | | | | | | | | |
| | X(Ca) | 0,221 | 0,297 | 0,299 | 0,275 | 0,293 | 0,292 | 0,274 | 0,267 | 0,261 | 0,262 | 0,263 | 0,267 | 0,267 | 0,267 | 0,261 | 0,266 | 0,272 | 0,486 | 0,488 |
| | X(Fe) | 0,489 | 0,525 | 0,526 | 0,529 | 0,518 | 0,53 | 0,54 | 0,539 | 0,542 | 0,542 | 0,547 | 0,543 | 0,543 | 0,548 | 0,551 | 0,551 | 0,535 | 0,462 | 0,456 |
| | X(Mg) | 0,063 | 0,103 | 0,103 | 0,073 | 0,128 | 0,079 | 0,111 | 0,118 | 0,118 | 0,079 | 0,106 | 0,102 | 0,098 | 0,079 | 0,087 | 0,090 | 0,123 | 0,025 | 0,027 |
| | X(Mn) | 0,281 | 0,103 | 0,099 | 0,162 | 0,082 | 0,134 | 0,100 | 0,099 | 0,102 | 0,152 | 0,110 | 0,115 | 0,121 | 0,140 | 0,131 | 0,122 | 0,092 | 0,050 | 0,052 |

**Annex III** - Mineral analyses Nolte (2012).

| | Sample | 020809-4 | | | | | | | | | | | | | | |
|---|---|---|---|---|---|---|---|---|---|---|---|---|---|---|---|---|
| | ***Ox. wt%*** | *11-rim* | *13-rim* | *14-core* | *15-rim* | *spot-124* | *spot-125* | *spot-126* | *spot-127* | *spot-128* | *spot-129* | *spot-130* | *spot-131* | *spot-134* | *spot-135* | *spot-137* |
| | $SiO_2$ | 38,3 | 38,1 | 38,9 | 38,3 | 38,3 | 38,4 | 38,5 | 38,1 | 38,3 | 38,8 | 38,8 | 39,0 | 38,7 | 38,9 | 38,9 |
| | $TiO_2$ | 0,03 | 0,08 | 0,04 | 0,07 | 0,01 | 0,03 | 0,17 | 0,06 | 0,06 | 0,12 | 0,08 | 0,00 | 0,29 | 0,15 | 0,03 |
| | $Al_2O_3$ | 21,1 | 20,8 | 22,0 | 21,7 | 21,5 | 21,4 | 21,4 | 21,5 | 21,3 | 21,6 | 21,4 | 21,6 | 21,4 | 21,7 | 21,2 |
| | $Cr_2O_3$ | 0,01 | 0,01 | 0,00 | 0,00 | 0,04 | 0,00 | 0,00 | 0,00 | 0,04 | 0,03 | 0,05 | 0,05 | 0,00 | 0,00 | 0,01 |
| | $Fe_2O_3$ | 1,22 | 1,19 | 1,20 | 1,24 | 1,27 | 1,19 | 1,21 | 1,24 | 1,18 | 1,20 | 1,22 | 1,18 | 1,23 | 1,32 | 1,25 |
| | FeO | 20,9 | 20,4 | 20,6 | 21,1 | 21,7 | 20,4 | 20,7 | 21,2 | 20,2 | 20,4 | 20,9 | 20,2 | 21,0 | 22,6 | 21,3 |
| | MnO | 0,57 | 1,60 | 1,64 | 0,69 | 0,73 | 1,87 | 1,20 | 1,21 | 1,47 | 1,68 | 1,57 | 1,49 | 1,80 | 1,11 | 1,15 |
| | MgO | 0,62 | 0,52 | 0,78 | 0,64 | 0,63 | 0,66 | 0,68 | 0,60 | 0,53 | 0,59 | 0,67 | 0,67 | 0,36 | 0,44 | 0,52 |
| | CaO | 17,90 | 17,72 | 16,92 | 17,44 | 17,18 | 17,12 | 17,44 | 17,36 | 17,69 | 17,42 | 16,95 | 17,53 | 17,45 | 16,10 | 17,57 |
| | $Na_2O$ | 0,02 | 0,00 | 0,03 | 0,01 | 0,04 | 0,00 | 0,00 | 0,00 | 0,00 | 0,00 | 0,00 | 0,02 | 0,02 | 0,02 | 0,05 |
| | sum | 100,64 | 100,38 | 102,08 | 101,22 | 101,43 | 100,98 | 101,31 | 101,21 | 100,86 | 101,80 | 101,59 | 101,72 | 102,19 | 102,27 | 102,04 |
| | ***Structural formula based on 24 O*** | | | | | | | | | | | | | | | |
| | Si | 5,99 | 5,99 | 6,01 | 5,96 | 5,96 | 6,00 | 5,99 | 5,94 | 5,99 | 6,01 | 6,02 | 6,04 | 5,99 | 6,02 | 6,02 |
| | Al | 0,01 | 0,01 | 0,00 | 0,04 | 0,04 | 0,00 | 0,01 | 0,06 | 0,01 | 0,00 | 0,00 | 0,00 | 0,01 | 0,00 | 0,00 |
| | Sum Z | 6,00 | 6,00 | 6,01 | 6,00 | 6,00 | 6,00 | 6,00 | 6,00 | 6,00 | 6,01 | 6,02 | 6,04 | 6,00 | 6,02 | 6,02 |
| | $Al^{(VI)}$ | 3,88 | 3,85 | 4,00 | 3,95 | 3,90 | 3,93 | 3,91 | 3,88 | 3,92 | 3,94 | 3,92 | 3,94 | 3,89 | 3,96 | 3,87 |
| | $Fe^{3+}$ | 0,14 | 0,14 | 0,14 | 0,15 | 0,15 | 0,14 | 0,14 | 0,15 | 0,14 | 0,14 | 0,14 | 0,14 | 0,14 | 0,15 | 0,15 |
| | Ti | 0,00 | 0,01 | 0,01 | 0,01 | 0,00 | 0,00 | 0,02 | 0,01 | 0,01 | 0,01 | 0,01 | 0,00 | 0,03 | 0,02 | 0,00 |
| | Cr | 0,00 | 0,00 | 0,00 | 0,00 | 0,01 | 0,00 | 0,00 | 0,00 | 0,01 | 0,00 | 0,01 | 0,01 | 0,00 | 0,00 | 0,00 |
| | Sum Y | 4,03 | 4,00 | 4,14 | 4,10 | 4,05 | 4,07 | 4,08 | 4,03 | 4,07 | 4,09 | 4,08 | 4,08 | 4,07 | 4,13 | 4,02 |
| | $Fe^{2+}$ | 2,74 | 2,68 | 2,65 | 2,75 | 2,83 | 2,66 | 2,70 | 2,77 | 2,65 | 2,65 | 2,71 | 2,61 | 2,71 | 2,93 | 2,76 |
| | Mg | 0,15 | 0,12 | 0,18 | 0,15 | 0,15 | 0,15 | 0,16 | 0,14 | 0,12 | 0,14 | 0,16 | 0,16 | 0,08 | 0,10 | 0,12 |
| | Mn | 0,08 | 0,21 | 0,22 | 0,09 | 0,10 | 0,25 | 0,16 | 0,16 | 0,20 | 0,22 | 0,21 | 0,20 | 0,24 | 0,15 | 0,15 |
| | Ca | 3,00 | 2,99 | 2,80 | 2,91 | 2,86 | 2,87 | 2,91 | 2,90 | 2,96 | 2,89 | 2,82 | 2,91 | 2,89 | 2,67 | 2,91 |
| | Na | 0,01 | 0,00 | 0,01 | 0,00 | 0,01 | 0,00 | 0,00 | 0,00 | 0,00 | 0,00 | 0,00 | 0,01 | 0,01 | 0,01 | 0,01 |
| | Sum X | 5,97 | 6,00 | 5,85 | 5,90 | 5,95 | 5,93 | 5,93 | 5,97 | 5,93 | 5,90 | 5,90 | 5,88 | 5,94 | 5,85 | 5,96 |
| | Total | 16,00 | 16,00 | 16,00 | 16,00 | 16,00 | 16,00 | 16,00 | 16,00 | 16,00 | 16,00 | 16,00 | 16,00 | 16,00 | 16,00 | 16,00 |
| | ***End member (Mol-%)*** | | | | | | | | | | | | | | | |
| | Almandine | 45,9 | 35,0 | 45,4 | 46,6 | 47,7 | 44,9 | 45,6 | 37,9 | 44,6 | 44,9 | 46,0 | 44,5 | 45,8 | 50,1 | 46,4 |
| | Andradite | 3,63 | 4,14 | 3,58 | 3,68 | 3,76 | 3,54 | 3,60 | 4,24 | 3,52 | 3,55 | 3,63 | 3,51 | 3,61 | 3,95 | 3,66 |
| | Grossular | 46,7 | 54,3 | 44,3 | 45,6 | 44,4 | 44,8 | 45,5 | 52,0 | 46,3 | 45,4 | 44,1 | 45,9 | 45,2 | 41,7 | 45,3 |
| | Pyrope | 2,44 | 2,40 | 3,07 | 2,53 | 2,46 | 2,61 | 2,67 | 2,71 | 2,10 | 2,30 | 2,63 | 2,63 | 1,41 | 1,72 | 2,00 |
| | Spessartine | 1,26 | 4,16 | 3,68 | 1,54 | 1,62 | 4,18 | 2,66 | 3,09 | 3,29 | 3,74 | 3,51 | 3,33 | 3,99 | 2,49 | 2,55 |
| | Uvarovite | 0,04 | 0,04 | 0,00 | 0,00 | 0,12 | 0,01 | 0,00 | 0,00 | 0,12 | 0,10 | 0,17 | 0,17 | 0,00 | 0,00 | 0,03 |
| | ***Proportion*** | | | | | | | | | | | | | | | |
| | X(Ca) | 0,504 | 0,498 | 0,479 | 0,493 | 0,483 | 0,483 | 0,491 | 0,486 | 0,5 | 0,49 | 0,478 | 0,495 | 0,488 | 0,457 | 0,49 |
| | X(Fe) | 0,459 | 0,446 | 0,454 | 0,466 | 0,477 | 0,449 | 0,456 | 0,464 | 0,446 | 0,449 | 0,46 | 0,445 | 0,458 | 0,501 | 0,464 |
| | X(Mg) | 0,024 | 0,021 | 0,031 | 0,025 | 0,025 | 0,026 | 0,027 | 0,023 | 0,021 | 0,023 | 0,026 | 0,026 | 0,014 | 0,017 | 0,020 |
| | X(Mn) | 0,024 | 0,068 | 0,067 | 0,029 | 0,030 | 0,077 | 0,050 | 0,049 | 0,063 | 0,070 | 0,064 | 0,063 | 0,075 | 0,044 | 0,048 |

Garnet

**Annex III** - Mineral analyses Nolte (2012).

| | Sample | 290709-3 | | | | | | | 020809-3 | | | | | | | | | | 020809-4 | |
|---|---|---|---|---|---|---|---|---|---|---|---|---|---|---|---|---|---|---|---|---|
| | Ox. wt% | 37-spot | 38-core | 39-core | 58-matrix | 59-matrix | 60-rim | 61-matrix | 59-matrix | 60-core | 61-matrix | 62-matrix | 63-matrix | 64-matrix | 65-matrix | 93-matrix | 94-matrix | 95-matrix | 26-matrix | 27-core |
| Plagioclase | $SiO_2$ | 58,9 | 59,4 | 60,6 | 57,0 | 58,3 | 57,5 | 59,7 | 54,2 | 55,1 | 57,2 | 55,3 | 53,7 | 55,2 | 55,1 | 56,1 | 55,5 | 55,2 | 61,6 | 60,5 |
| | $TiO_2$ | 0,00 | 0,00 | 0,00 | 0,02 | 0,00 | 0,00 | 0,02 | 0,00 | 0,03 | 0,01 | 0,00 | 0,00 | 0,00 | 0,04 | 0,04 | 0,00 | 0,05 | 0,02 | 0,00 |
| | $Al_2O_3$ | 26,8 | 25,5 | 26,0 | 26,5 | 26,8 | 26,7 | 26,1 | 28,8 | 29,5 | 28,2 | 29,0 | 28,5 | 28,2 | 28,9 | 28,3 | 28,6 | 28,9 | 25,2 | 25,0 |
| | FeO | 0,07 | 0,03 | 0,05 | 0,03 | 0,04 | 0,01 | 0,01 | 0,06 | 0,04 | 0,02 | 0,08 | 0,00 | 0,08 | 0,07 | 0,05 | 0,00 | 0,03 | 0,00 | 0,02 |
| | MnO | 0,00 | 0,00 | 0,00 | 0,02 | 0,00 | 0,00 | 0,01 | 0,01 | 0,02 | 0,05 | 0,00 | 0,00 | 0,01 | 0,00 | 0,00 | 0,00 | 0,00 | 0,02 | 0,00 |
| | MgO | 0,0 | 0,0 | 0,0 | 0,0 | 0,0 | 0,0 | 0,0 | 0,0 | 0,0 | 0,0 | 0,0 | 0,0 | 0,0 | 0,0 | 0,0 | 0,0 | 0,0 | 0,0 | 0,0 |
| | CaO | 8,68 | 7,66 | 7,82 | 8,69 | 8,62 | 8,51 | 7,45 | 10,92 | 11,32 | 9,76 | 11,13 | 11,04 | 10,43 | 10,85 | 10,51 | 10,88 | 11,18 | 6,26 | 6,21 |
| | $Na_2O$ | 6,49 | 7,56 | 7,27 | 6,78 | 6,85 | 7,05 | 7,60 | 5,49 | 5,47 | 6,16 | 5,54 | 5,54 | 6,06 | 5,60 | 5,77 | 5,47 | 5,30 | 8,33 | 8,19 |
| | $K_2O$ | 0,08 | 0,07 | 0,06 | 0,07 | 0,08 | 0,05 | 0,09 | 0,06 | 0,07 | 0,06 | 0,07 | 0,05 | 0,05 | 0,05 | 0,04 | 0,06 | 0,06 | 0,07 | 0,08 |
| | Sum | 100,97 | 100,28 | 101,78 | 99,18 | 100,65 | 99,87 | 101,00 | 99,55 | 101,50 | 101,42 | 101,13 | 98,83 | 99,99 | 100,66 | 100,78 | 100,52 | 100,75 | 101,52 | 100,03 |
| | Structural formula based on 8 O | | | | | | | | | | | | | | | | | | | |
| | Si | 2,61 | 2,65 | 2,65 | 2,58 | 2,59 | 2,58 | 2,64 | 2,46 | 2,45 | 2,53 | 2,47 | 2,45 | 2,49 | 2,47 | 2,51 | 2,49 | 2,47 | 2,70 | 2,69 |
| | Al | 1,40 | 1,34 | 1,34 | 1,41 | 1,40 | 1,41 | 1,36 | 1,54 | 1,54 | 1,47 | 1,52 | 1,54 | 1,50 | 1,53 | 1,49 | 1,51 | 1,52 | 1,30 | 1,31 |
| | Ti | 0,00 | 0,00 | 0,00 | 0,00 | 0,00 | 0,00 | 0,00 | 0,00 | 0,00 | 0,00 | 0,00 | 0,00 | 0,00 | 0,00 | 0,00 | 0,00 | 0,00 | 0,00 | 0,00 |
| | Fe | 0,00 | 0,00 | 0,00 | 0,00 | 0,00 | 0,00 | 0,00 | 0,00 | 0,00 | 0,00 | 0,00 | 0,00 | 0,00 | 0,00 | 0,00 | 0,00 | 0,00 | 0,00 | 0,00 |
| | Mn | 0,00 | 0,00 | 0,00 | 0,00 | 0,00 | 0,00 | 0,00 | 0,00 | 0,00 | 0,00 | 0,00 | 0,00 | 0,00 | 0,00 | 0,00 | 0,00 | 0,00 | 0,00 | 0,00 |
| | Mg | 0,00 | 0,00 | 0,00 | 0,00 | 0,00 | 0,00 | 0,00 | 0,00 | 0,00 | 0,00 | 0,00 | 0,00 | 0,00 | 0,00 | 0,00 | 0,00 | 0,00 | 0,00 | 0,00 |
| | Ca | 0,41 | 0,37 | 0,37 | 0,42 | 0,41 | 0,41 | 0,35 | 0,53 | 0,54 | 0,46 | 0,53 | 0,54 | 0,50 | 0,52 | 0,50 | 0,52 | 0,54 | 0,29 | 0,30 |
| | Na | 0,56 | 0,65 | 0,62 | 0,59 | 0,59 | 0,61 | 0,65 | 0,48 | 0,47 | 0,53 | 0,48 | 0,49 | 0,53 | 0,49 | 0,50 | 0,48 | 0,46 | 0,71 | 0,71 |
| | K | 0,00 | 0,00 | 0,00 | 0,00 | 0,00 | 0,00 | 0,01 | 0,00 | 0,00 | 0,00 | 0,00 | 0,00 | 0,00 | 0,00 | 0,00 | 0,00 | 0,00 | 0,00 | 0,01 |
| | Sum | 4,98 | 5,01 | 4,99 | 5,01 | 5,00 | 5,02 | 5,01 | 5,01 | 5,01 | 5,00 | 5,01 | 5,02 | 5,03 | 5,01 | 5,00 | 5,00 | 5,00 | 5,01 | 5,01 |
| | End member (Mol.-%) | | | | | | | | | | | | | | | | | | | |
| | Ab | 57,3 | 63,9 | 62,5 | 58,3 | 58,8 | 59,8 | 64,5 | 47,5 | 46,5 | 53,1 | 47,2 | 47,4 | 51,1 | 48,1 | 49,8 | 47,5 | 46 | 70,4 | 70,2 |
| | An | 42,3 | 35,7 | 37,1 | 41,3 | 40,8 | 39,9 | 35 | 52,2 | 53,1 | 46,5 | 52,4 | 52,3 | 48,6 | 51,6 | 50 | 52,2 | 53,6 | 29,2 | 29,4 |
| | Or | 0,4 | 0,4 | 0,3 | 0,4 | 0,4 | 0,3 | 0,5 | 0,4 | 0,4 | 0,4 | 0,4 | 0,3 | 0,3 | 0,3 | 0,2 | 0,3 | 0,4 | 0,4 | 0,5 |
| | Sum | 100 | 100 | 99,9 | 100 | 100 | 100 | 100 | 100,1 | 100 | 100 | 100 | 100 | 100 | 100 | 100 | 100 | 100 | 100 | 100,1 |

**Annex III** - Mineral analyses Nolte (2012).

| | Sample | 020809-4 | | | | | | |
|---|---|---|---|---|---|---|---|---|
| | ***Ox. wt%*** | *3-matrix* | *4-matrix* | *5-matrix* | *38-matrix* | *39-matrix* | *44-matrix* | *45-core* |
| **Plagioclase** | $SiO_2$ | 61,3 | 60,3 | 61,4 | 60,4 | 61,9 | 62,0 | 62,8 |
| | $TiO_2$ | 0,00 | 0,00 | 0,04 | 0,05 | 0,00 | 0,02 | 0,00 |
| | $Al_2O_3$ | 25,0 | 24,7 | 24,7 | 25,2 | 25,1 | 25,4 | 25,0 |
| | FeO | 0,01 | 0,02 | 0,03 | 0,04 | 0,02 | 0,00 | 0,05 |
| | MnO | 0,02 | 0,01 | 0,00 | 0,00 | 0,00 | 0,00 | 0,00 |
| | MgO | 0,0 | 0,0 | 0,0 | 0,0 | 0,0 | 0,0 | 0,0 |
| | CaO | 6,38 | 6,37 | 6,20 | 6,55 | 6,43 | 6,64 | 6,04 |
| | $Na_2O$ | 8,20 | 8,17 | 8,18 | 8,07 | 8,03 | 8,12 | 8,37 |
| | $K_2O$ | 0,09 | 0,09 | 0,08 | 0,08 | 0,07 | 0,09 | 0,12 |
| | Sum | 101,02 | 99,63 | 100,69 | 100,39 | 101,52 | 102,29 | 102,34 |
| | ***Structural formula based on 8 O*** | | | | | | | |
| | Si | 2,70 | 2,69 | 2,71 | 2,68 | 2,71 | 2,70 | 2,72 |
| | Al | 1,30 | 1,30 | 1,29 | 1,32 | 1,29 | 1,30 | 1,28 |
| | Ti | 0,00 | 0,00 | 0,00 | 0,00 | 0,00 | 0,00 | 0,00 |
| | Fe | 0,00 | 0,00 | 0,00 | 0,00 | 0,00 | 0,00 | 0,00 |
| | Mn | 0,00 | 0,00 | 0,00 | 0,00 | 0,00 | 0,00 | 0,00 |
| | Mg | 0,00 | 0,00 | 0,00 | 0,00 | 0,00 | 0,00 | 0,00 |
| | Ca | 0,30 | 0,31 | 0,29 | 0,31 | 0,30 | 0,31 | 0,28 |
| | Na | 0,70 | 0,71 | 0,70 | 0,69 | 0,68 | 0,68 | 0,70 |
| | K | 0,01 | 0,01 | 0,00 | 0,00 | 0,00 | 0,01 | 0,01 |
| | Sum | 5,00 | 5,01 | 4,99 | 5,01 | 4,99 | 5,00 | 4,99 |
| | ***End member (Mol.-%)*** | | | | | | | |
| | Ab | 69,6 | 69,5 | 70,2 | 68,8 | 69,1 | 68,5 | 71 |
| | An | 29,9 | 30 | 29,4 | 30,8 | 30,6 | 30,9 | 28,3 |
| | Or | 0,5 | 0,5 | 0,4 | 0,4 | 0,4 | 0,5 | 0,7 |
| | Sum | 100 | 100 | 100 | 100 | 100,1 | 99,9 | 100 |

**Annex III** - Mineral analyses Nolte (2012).

| | Sample | 290709-3 | | | | | | | | | | | | | 290709-3 | | | 290709-8 | |
|---|---|---|---|---|---|---|---|---|---|---|---|---|---|---|---|---|---|---|---|
| | ***Ox. wt%*** | *spot-23* | *spot-24* | *spot-32* | *spot-33* | *spot-34* | *spot-35* | *spot-36* | *spot-4* | *spot-42* | *spot-43* | *spot-47* | *spot-48* | *spot-53* | *spot-54* | *spot-56* | *spot-57* | *spot-62* | *spot-102* | *spot-103* |
| Biotite | $SiO_2$ | 33,2 | 31,8 | 32,8 | 32,3 | 33,7 | 32,0 | 31,9 | 26,9 | 33,8 | 33,9 | 33,3 | 32,5 | 32,2 | 33,0 | 33,2 | 33,8 | 32,6 | 36,14 | 32,1 |
| | $TiO_2$ | 2,87 | 2,79 | 2,97 | 3,24 | 2,50 | 2,64 | 2,55 | 0,85 | 2,65 | 2,60 | 2,54 | 2,44 | 2,60 | 2,70 | 2,41 | 3,00 | 3,48 | 1,922 | 0,24 |
| | $Al_2O_3$ | 17,3 | 17,1 | 16,6 | 16,5 | 16,3 | 17,1 | 17,5 | 18,6 | 17,4 | 17,3 | 17,2 | 17,5 | 16,7 | 16,8 | 17,1 | 17,1 | 17,0 | 16,606 | 19,2 |
| | $Cr_2O_3$ | 0,00 | 0,07 | 0,00 | 0,02 | 0,06 | 0,03 | 0,07 | 0,07 | 0,00 | 0,00 | 0,02 | 0,02 | 0,10 | 0,06 | 0,01 | 0,02 | 0,01 | 0,04 | 0,01 |
| | FeO | 26,7 | 26,6 | 26,3 | 27,1 | 28,8 | 27,6 | 25,6 | 30,7 | 26,1 | 25,9 | 26,8 | 26,6 | 27,9 | 27,5 | 27,1 | 26,7 | 26,7 | 21,9 | 23,4 |
| | MnO | 0,09 | 0,11 | 0,15 | 0,11 | 0,09 | 0,10 | 0,09 | 0,17 | 0,09 | 0,11 | 0,13 | 0,18 | 0,13 | 0,15 | 0,10 | 0,11 | 0,03 | 0,338 | 0,53 |
| | MgO | 4,36 | 4,38 | 4,14 | 4,07 | 4,26 | 3,71 | 4,59 | 9,34 | 5,18 | 5,3 | 4,3 | 4,3 | 4,4 | 4,4 | 4,5 | 4,5 | 4,0 | 9,096 | 12,7 |
| | CaO | 0,00 | 0,03 | 0,03 | 0,08 | 0,05 | 0,16 | 0,05 | 0,74 | 0,03 | 0,04 | 0,05 | 0,02 | 0,04 | 0,06 | 0,03 | 0,03 | 0,06 | 0,031 | 0,09 |
| | $Na_2O$ | 0,09 | 0,13 | 0,10 | 0,12 | 0,10 | 0,06 | 0,08 | 0,02 | 0,08 | 0,09 | 0,09 | 0,07 | 0,08 | 0,10 | 0,10 | 0,10 | 0,07 | 0,086 | 0,83 |
| | $K_2O$ | 8,39 | 8,42 | 8,29 | 8,36 | 8,42 | 8,02 | 8,53 | 0,74 | 8,74 | 8,66 | 8,57 | 8,51 | 8,47 | 8,20 | 8,76 | 8,54 | 8,21 | 9,099 | 1,68 |
| | Cl | 0,15 | 0,09 | 0,12 | 0,27 | 0,47 | 0,43 | 0,37 | 0,13 | 0,18 | 0,08 | 0,24 | 0,17 | 0,30 | 0,35 | 0,23 | 0,19 | 0,31 | 0,015 | 0,02 |
| | $H_2O$ | 1,90 | 1,87 | 1,87 | 1,82 | 1,82 | 1,77 | 1,80 | 1,81 | 1,92 | 1,95 | 1,87 | 1,87 | 1,83 | 1,84 | 1,88 | 1,91 | 1,84 | 2,020 | 1,98 |
| | Total | 95,0 | 93,4 | 93,4 | 94,0 | 96,6 | 93,6 | 93,2 | 90,2 | 96,1 | 96,0 | 95,2 | 94,3 | 94,6 | 95,1 | 95,4 | 96,0 | 94,3 | 97,3 | 92,8 |
| | ***Structural formula based on 22 O and water-free*** | | | | | | | | | | | | | | | | | | | |
| | Si | 5,14 | 5,04 | 5,17 | 5,09 | 5,20 | 5,08 | 5,05 | 4,38 | 5,16 | 5,17 | 5,16 | 5,09 | 5,07 | 5,13 | 5,15 | 5,18 | 5,10 | 5,32 | 4,83 |
| | $Al^{IV}$ | 2,86 | 2,96 | 2,83 | 2,91 | 2,80 | 2,92 | 2,95 | 3,57 | 2,84 | 2,83 | 2,84 | 2,91 | 2,93 | 2,87 | 2,85 | 2,82 | 2,90 | 2,68 | 3,17 |
| | Sum T | 8,00 | 8,00 | 8,00 | 8,00 | 8,00 | 8,00 | 8,00 | 7,94 | 8,00 | 8,00 | 8,00 | 8,00 | 8,00 | 8,00 | 8,00 | 8,00 | 8,00 | 8,00 | 8,00 |
| | $Al^{VI}$ | 0,30 | 0,23 | 0,26 | 0,17 | 0,17 | 0,28 | 0,32 | 0,00 | 0,29 | 0,28 | 0,31 | 0,32 | 0,16 | 0,21 | 0,28 | 0,27 | 0,24 | 0,20 | 0,24 |
| | Ti | 0,33 | 0,33 | 0,35 | 0,38 | 0,29 | 0,32 | 0,30 | 0,10 | 0,30 | 0,30 | 0,30 | 0,29 | 0,31 | 0,32 | 0,28 | 0,35 | 0,41 | 0,21 | 0,03 |
| | $Fe^{2+}$ | 3,45 | 3,53 | 3,47 | 3,58 | 3,71 | 3,67 | 3,39 | 4,18 | 3,33 | 3,31 | 3,48 | 3,49 | 3,68 | 3,58 | 3,51 | 3,42 | 3,50 | 2,69 | 2,95 |
| | Cr | 0,00 | 0,01 | 0,00 | 0,00 | 0,01 | 0,00 | 0,01 | 0,01 | 0,00 | 0,00 | 0,00 | 0,00 | 0,01 | 0,01 | 0,00 | 0,00 | 0,00 | 0,01 | 0,00 |
| | Mn | 0,01 | 0,02 | 0,02 | 0,02 | 0,01 | 0,01 | 0,01 | 0,02 | 0,01 | 0,01 | 0,02 | 0,02 | 0,02 | 0,02 | 0,01 | 0,02 | 0,00 | 0,04 | 0,07 |
| | Mg | 1,01 | 1,04 | 0,97 | 0,96 | 0,98 | 0,88 | 1,08 | 2,26 | 1,18 | 1,21 | 1,00 | 1,01 | 1,03 | 1,03 | 1,04 | 1,02 | 0,93 | 2,00 | 2,85 |
| | Sum C | 5,10 | 5,15 | 5,08 | 5,11 | 5,17 | 5,15 | 5,12 | 6,57 | 5,10 | 5,11 | 5,10 | 5,14 | 5,20 | 5,16 | 5,12 | 5,07 | 5,08 | 5,15 | 6,13 |
| | Ca | 0,00 | 0,01 | 0,01 | 0,01 | 0,01 | 0,03 | 0,01 | 0,13 | 0,00 | 0,01 | 0,01 | 0,00 | 0,01 | 0,01 | 0,01 | 0,01 | 0,01 | 0,01 | 0,01 |
| | Na | 0,03 | 0,04 | 0,03 | 0,04 | 0,03 | 0,02 | 0,02 | 0,01 | 0,02 | 0,03 | 0,03 | 0,02 | 0,02 | 0,03 | 0,03 | 0,03 | 0,02 | 0,03 | 0,24 |
| | K | 1,66 | 1,70 | 1,67 | 1,68 | 1,66 | 1,62 | 1,72 | 0,15 | 1,70 | 1,68 | 1,70 | 1,70 | 1,70 | 1,63 | 1,73 | 1,67 | 1,64 | 1,71 | 0,32 |
| | Sum A | 1,68 | 1,68 | 1,68 | 1,68 | 1,68 | 1,68 | 1,68 | 1,68 | 1,68 | 1,68 | 1,68 | 1,68 | 1,68 | 1,68 | 1,68 | 1,68 | 1,68 | 1,68 | 1,68 |
| | ***Ratios*** | | | | | | | | | | | | | | | | | | | |
| | Fe/(Fe+Mg) | 0,77 | 0,77 | 0,78 | 0,79 | 0,79 | 0,81 | 0,76 | 0,65 | 0,74 | 0,73 | 0,78 | 0,78 | 0,78 | 0,78 | 0,77 | 0,77 | 0,79 | 0,57 | 0,51 |
| | Mg/(Fe+Mg) | 0,23 | 0,23 | 0,22 | 0,21 | 0,21 | 0,19 | 0,24 | 0,35 | 0,26 | 0,27 | 0,22 | 0,22 | 0,22 | 0,22 | 0,23 | 0,23 | 0,21 | 0,43 | 0,49 |
| | $Fe^{2+} + Mn^{2+}$ | 3,46 | 3,54 | 3,49 | 3,60 | 3,72 | 3,68 | 3,41 | 4,20 | 3,34 | 3,32 | 3,49 | 3,51 | 3,70 | 3,60 | 3,53 | 3,44 | 3,50 | 2,73 | 3,02 |
| | $Al^{VI}$+Ti+Cr | 0,63 | 0,57 | 0,61 | 0,55 | 0,46 | 0,59 | 0,63 | 0,11 | 0,59 | 0,58 | 0,61 | 0,61 | 0,48 | 0,53 | 0,56 | 0,62 | 0,65 | 0,42 | 0,27 |

**Annex III** - Mineral analyses Nolte (2012).

| | Sample | 290709-8 | | | | | | | | | | | | | 020809-4 | | | |
|---|---|---|---|---|---|---|---|---|---|---|---|---|---|---|---|---|---|---|
| | ***Ox. wt%*** | *spot-104* | *spot-105* | *spot-108* | *spot-108* | *spot-110* | *spot-111* | *spot-116* | *spot-117* | *spot-118* | *spot-119* | *spot-120* | *spot-121* | *spot-122* | *spot-6* | *spot-7* | *spot-16* | *spot-17* |
| **Biotite** | $SiO_2$ | 36,2 | 35,3 | 36,4 | 35,9 | 35,9 | 36,1 | 34,5 | 35,8 | 35,9 | 35,5 | 35,9 | 36,8 | 36,2 | 35,3 | 35,2 | 35,7 | 35,5 |
| | $TiO_2$ | 1,95 | 1,75 | 1,80 | 2,14 | 1,77 | 1,86 | 1,86 | 1,89 | 1,79 | 1,54 | 1,53 | 2,22 | 1,84 | 1,12 | 1,17 | 1,27 | 0,83 |
| | $Al_2O_3$ | 16,6 | 16,2 | 16,6 | 16,3 | 16,4 | 16,0 | 16,3 | 15,7 | 16,7 | 16,1 | 16,0 | 15,7 | 16,4 | 16,5 | 16,5 | 16,6 | 16,5 |
| | $Cr_2O_3$ | 0,03 | 0,08 | 0,00 | 0,00 | 0,03 | 0,00 | 0,01 | 0,00 | 0,00 | 0,01 | 0,00 | 0,00 | 0,00 | 0,00 | 0,00 | 0,03 | 0,03 |
| | FeO | 21,6 | 21,7 | 21,6 | 21,5 | 21,4 | 21,2 | 21,7 | 21,6 | 21,3 | 21,4 | 21,8 | 21,2 | 20,6 | 23,4 | 24,1 | 24,7 | 24,7 |
| | MnO | 0,33 | 0,36 | 0,39 | 0,36 | 0,36 | 0,32 | 0,30 | 0,39 | 0,37 | 0,35 | 0,43 | 0,32 | 0,30 | 0,03 | 0,00 | 0,08 | 0,11 |
| | MgO | 9,29 | 9,04 | 9,65 | 9,76 | 9,44 | 9,75 | 8,76 | 9,43 | 9,06 | 9,62 | 9,59 | 9,32 | 9,52 | 8,06 | 8,28 | 8,68 | 8,59 |
| | CaO | 0,04 | 0,00 | 0,04 | 0,05 | 0,07 | 0,04 | 0,08 | 0,09 | 0,02 | 0,04 | 0,09 | 0,06 | 0,08 | 0,10 | 0,21 | 0,14 | 0,09 |
| | $Na_2O$ | 0,05 | 0,04 | 0,07 | 0,08 | 0,08 | 0,07 | 0,07 | 0,09 | 0,08 | 0,04 | 0,06 | 0,10 | 0,09 | 0,10 | 0,11 | 0,07 | 0,05 |
| | $K_2O$ | 8,87 | 9,08 | 9,22 | 9,06 | 9,12 | 9,07 | 9,18 | 8,81 | 9,21 | 9,11 | 8,78 | 9,09 | 9,20 | 9,01 | 8,50 | 8,05 | 8,08 |
| | Cl | 0,03 | 0,03 | 0,04 | 0,05 | 0,07 | 0,02 | 0,02 | 0,03 | 0,01 | 0,03 | 0,06 | 0,02 | 0,02 | 0,12 | 0,10 | 0,09 | 0,09 |
| | $H_2O$ | 2,03 | 1,99 | 2,03 | 2,01 | 2,01 | 2,02 | 1,96 | 2,00 | 2,02 | 1,99 | 1,99 | 2,02 | 2,01 | 1,95 | 1,96 | 1,99 | 1,98 |
| | Total | 97,1 | 95,7 | 97,9 | 97,2 | 96,6 | 96,5 | 94,8 | 95,8 | 96,4 | 95,8 | 96,2 | 96,8 | 96,2 | 95,6 | 96,1 | 97,5 | 96,5 |
| | ***Structural formula based on 22 O and water-free*** | | | | | | | | | | | | | | | | | |
| | Si | 5,33 | 5,30 | 5,32 | 5,29 | 5,32 | 5,35 | 5,25 | 5,35 | 5,32 | 5,32 | 5,35 | 5,42 | 5,36 | 5,33 | 5,29 | 5,29 | 5,31 |
| | $Al^{IV}$ | 2,67 | 2,70 | 2,68 | 2,71 | 2,68 | 2,65 | 2,75 | 2,65 | 2,68 | 2,69 | 2,66 | 2,58 | 2,64 | 2,67 | 2,71 | 2,71 | 2,69 |
| | Sum T | 8,00 | 8,00 | 8,00 | 8,00 | 8,00 | 8,00 | 8,00 | 8,00 | 8,00 | 8,00 | 8,00 | 8,00 | 8,00 | 8,00 | 8,00 | 8,00 | 8,00 |
| | $Al^{VI}$ | 0,20 | 0,18 | 0,18 | 0,12 | 0,18 | 0,15 | 0,17 | 0,12 | 0,24 | 0,16 | 0,16 | 0,15 | 0,22 | 0,26 | 0,22 | 0,19 | 0,22 |
| | Ti | 0,22 | 0,20 | 0,20 | 0,24 | 0,20 | 0,21 | 0,21 | 0,21 | 0,20 | 0,17 | 0,17 | 0,25 | 0,21 | 0,13 | 0,13 | 0,14 | 0,09 |
| | $Fe^{2+}$ | 2,66 | 2,73 | 2,65 | 2,65 | 2,65 | 2,63 | 2,76 | 2,70 | 2,64 | 2,68 | 2,71 | 2,61 | 2,55 | 2,96 | 3,03 | 3,06 | 3,09 |
| | Cr | 0,00 | 0,01 | 0,00 | 0,00 | 0,00 | 0,00 | 0,00 | 0,00 | 0,00 | 0,00 | 0,00 | 0,00 | 0,00 | 0,00 | 0,00 | 0,00 | 0,00 |
| | Mn | 0,04 | 0,05 | 0,05 | 0,05 | 0,05 | 0,04 | 0,04 | 0,05 | 0,05 | 0,04 | 0,05 | 0,04 | 0,04 | 0,00 | 0,00 | 0,01 | 0,01 |
| | Mg | 2,04 | 2,02 | 2,10 | 2,14 | 2,09 | 2,15 | 1,98 | 2,10 | 2,00 | 2,15 | 2,13 | 2,05 | 2,10 | 1,82 | 1,86 | 1,92 | 1,92 |
| | Sum C | 5,17 | 5,18 | 5,17 | 5,19 | 5,16 | 5,17 | 5,16 | 5,18 | 5,13 | 5,20 | 5,22 | 5,09 | 5,11 | 5,17 | 5,24 | 5,32 | 5,34 |
| | Ca | 0,01 | 0,00 | 0,01 | 0,01 | 0,01 | 0,01 | 0,01 | 0,01 | 0,00 | 0,01 | 0,02 | 0,01 | 0,01 | 0,02 | 0,03 | 0,02 | 0,01 |
| | Na | 0,01 | 0,01 | 0,02 | 0,02 | 0,02 | 0,02 | 0,02 | 0,03 | 0,02 | 0,01 | 0,02 | 0,03 | 0,03 | 0,03 | 0,03 | 0,02 | 0,02 |
| | K | 1,67 | 1,74 | 1,72 | 1,70 | 1,73 | 1,71 | 1,78 | 1,68 | 1,74 | 1,74 | 1,67 | 1,71 | 1,74 | 1,74 | 1,63 | 1,52 | 1,55 |
| | Sum A | 1,68 | 1,75 | 1,75 | 1,73 | 1,76 | 1,74 | 1,81 | 1,72 | 1,77 | 1,76 | 1,70 | 1,75 | 1,78 | 1,78 | 1,70 | 1,56 | 1,57 |
| | ***Ratios*** | | | | | | | | | | | | | | | | | |
| | Fe/(Fe+Mg) | 0,57 | 0,57 | 0,56 | 0,55 | 0,56 | 0,55 | 0,58 | 0,56 | 0,57 | 0,56 | 0,56 | 0,56 | 0,55 | 0,62 | 0,62 | 0,62 | 0,62 |
| | Mg/(Fe+Mg) | 0,43 | 0,43 | 0,44 | 0,45 | 0,44 | 0,45 | 0,42 | 0,44 | 0,43 | 0,44 | 0,44 | 0,44 | 0,45 | 0,38 | 0,38 | 0,38 | 0,38 |
| | $Fe^{2+} + Mn^{2+}$ | 2,71 | 2,77 | 2,69 | 2,69 | 2,70 | 2,67 | 2,80 | 2,75 | 2,68 | 2,72 | 2,76 | 2,65 | 2,58 | 2,97 | 3,03 | 3,07 | 3,10 |
| | $Al^{VI}$+Ti+Cr | 0,42 | 0,38 | 0,38 | 0,35 | 0,38 | 0,35 | 0,38 | 0,33 | 0,44 | 0,33 | 0,33 | 0,39 | 0,42 | 0,39 | 0,35 | 0,34 | 0,32 |

**Annex III** - Mineral analyses Nolte (2012).

| | Sample | 290709-3 | | | | | | | | | | | | | 290709-8 | | | | 020809-3 | |
|---|---|---|---|---|---|---|---|---|---|---|---|---|---|---|---|---|---|---|---|---|
| | **Ox. wt%** | *spot-1* | *spot-2* | *spot-3* | *spot-6* | *spot-7* | *spot-8* | *spot-9* | *spot-12* | *spot-13* | *spot-14* | *spot-97* | *spot-98* | *spot-99* | *spot-100* | *spot-101* | *spot-106* | *spot-107* | *spot-50* | *spot-51* |
| | $SiO_2$ | 39,6 | 39,5 | 39,4 | 39,8 | 39,0 | 39,1 | 39,3 | 38,9 | 39,4 | 38,5 | 41,5 | 42,0 | 41,3 | 42,0 | 41,8 | 40,8 | 41,1 | 42,8 | 43,4 |
| | $TiO_2$ | 0,43 | 0,48 | 0,43 | 0,69 | 0,42 | 0,59 | 0,42 | 0,47 | 0,52 | 0,46 | 0,63 | 0,70 | 0,69 | 0,77 | 0,54 | 0,45 | 0,49 | 0,66 | 0,77 |
| | $Al_2O_3$ | 16,7 | 16,5 | 16,8 | 16,7 | 16,9 | 16,7 | 17,2 | 17,2 | 16,9 | 16,6 | 14,0 | 13,7 | 14,0 | 13,8 | 13,9 | 13,5 | 13,9 | 16,7 | 16,4 |
| | FeO | 23,52 | 23,50 | 22,75 | 22,80 | 23,23 | 23,26 | 23,32 | 22,89 | 23,63 | 23,05 | 19,37 | 19,93 | 20,01 | 20,05 | 19,37 | 20,24 | 19,93 | 14,62 | 14,94 |
| | $Cr_2O_3$ | 0,0 | 0,0 | 0,0 | 0,0 | 0,0 | 0,1 | 0,0 | 0,0 | 0,1 | 0,1 | 0,0 | 0,1 | | 0,0 | | 0,0 | | 0,1 | 0,1 |
| | MnO | 0,15 | 0,13 | 0,17 | 0,13 | 0,07 | 0,10 | 0,10 | 0,11 | 0,09 | 0,09 | 0,50 | 0,57 | 0,55 | 0,58 | 0,54 | 0,50 | 0,48 | 0,20 | 0,24 |
| | MgO | 3,90 | 3,95 | 3,72 | 3,98 | 4,00 | 3,89 | 3,52 | 3,71 | 3,78 | 3,91 | 7,43 | 7,60 | 7,45 | 7,43 | 7,44 | 7,08 | 7,46 | 8,99 | 9,01 |
| | CaO | 11,49 | 11,23 | 11,40 | 11,40 | 11,52 | 11,24 | 11,37 | 11,36 | 11,21 | 11,31 | 11,30 | 11,12 | 11,17 | 11,10 | 11,19 | 11,52 | 11,33 | 12,12 | 12,02 |
| | $Na_2O$ | 1,55 | 1,47 | 1,45 | 1,40 | 1,38 | 1,46 | 1,33 | 1,39 | 1,41 | 1,37 | 1,66 | 1,65 | 1,68 | 1,75 | 1,69 | 1,64 | 1,69 | 1,31 | 1,47 |
| | $K_2O$ | 0,93 | 0,99 | 0,96 | 0,98 | 0,99 | 1,03 | 0,95 | 0,99 | 1,03 | 0,96 | 0,79 | 0,89 | 0,88 | 0,96 | 0,82 | 0,66 | 0,75 | 0,67 | 0,55 |
| | Total | 98,36 | 97,67 | 97,07 | 97,84 | 97,56 | 97,51 | 97,46 | 96,99 | 97,97 | 96,36 | 97,12 | 98,17 | 97,79 | 98,38 | 97,26 | 96,37 | 97,07 | 98,08 | 98,82 |
| | ***Structural formula based on 23 O*** | | | | | | | | | | | | | | | | | | | |
| | Si | 6,07 | 6,08 | 6,11 | 6,10 | 6,01 | 6,04 | 6,06 | 6,02 | 6,05 | 6,01 | 6,30 | 6,31 | 6,24 | 6,31 | 6,34 | 6,27 | 6,25 | 6,29 | 6,33 |
| | Al | 1,93 | 1,92 | 1,90 | 1,90 | 1,99 | 1,96 | 1,94 | 1,98 | 1,96 | 1,99 | 1,70 | 1,69 | 1,76 | 1,69 | 1,66 | 1,73 | 1,76 | 1,71 | 1,67 |
| | Sum T | 8,00 | 8,00 | 8,00 | 8,00 | 8,00 | 8,00 | 8,00 | 8,00 | 8,00 | 8,00 | 8,00 | 8,00 | 8,00 | 8,00 | 8,00 | 8,00 | 8,00 | 8,00 | 8,00 |
| **Amphibole** | Al | 1,08 | 1,06 | 1,17 | 1,13 | 1,08 | 1,08 | 1,18 | 1,16 | 1,09 | 1,06 | 0,80 | 0,73 | 0,74 | 0,75 | 0,82 | 0,71 | 0,73 | 1,17 | 1,15 |
| | Cr | 0,00 | | | | | 0,01 | | 0,01 | 0,01 | 0,01 | 0,00 | 0,01 | | 0,00 | | | | 0,01 | 0,01 |
| | $Fe^{3+}$ | 0,23 | 0,27 | 0,15 | 0,17 | 0,31 | 0,25 | 0,21 | 0,22 | 0,28 | 0,33 | 0,29 | 0,37 | 0,41 | 0,32 | 0,28 | 0,41 | 0,43 | 0,07 | 0,07 |
| | Ti | 0,05 | 0,06 | 0,05 | 0,08 | 0,05 | 0,07 | 0,05 | 0,06 | 0,06 | 0,05 | 0,07 | 0,08 | 0,08 | 0,09 | 0,06 | 0,05 | 0,06 | 0,07 | 0,09 |
| | Mg | 0,89 | 0,91 | 0,86 | 0,91 | 0,92 | 0,90 | 0,81 | 0,86 | 0,87 | 0,91 | 1,68 | 1,70 | 1,68 | 1,67 | 1,68 | 1,62 | 1,69 | 1,97 | 1,96 |
| | $Fe^{2+}$ | 2,74 | 2,70 | 2,76 | 2,71 | 2,64 | 2,69 | 2,75 | 2,71 | 2,69 | 2,63 | 2,12 | 2,08 | 2,06 | 2,14 | 2,13 | 2,17 | 2,06 | 1,70 | 1,71 |
| | Mn | 0,01 | 0,01 | 0,01 | 0,01 | 0,01 | 0,01 | 0,01 | 0,01 | 0,01 | 0,01 | 0,03 | 0,04 | 0,04 | 0,04 | 0,03 | 0,03 | 0,03 | 0,01 | 0,02 |
| | Sum C | 5,00 | 5,00 | 5,00 | 5,00 | 5,00 | 5,00 | 5,00 | 5,00 | 5,00 | 5,00 | 5,00 | 5,00 | 5,00 | 5,00 | 5,00 | 5,00 | 5,00 | 5,00 | 5,00 |
| | $Fe^{2+}$ | 0,05 | 0,06 | 0,04 | 0,05 | 0,04 | 0,06 | 0,05 | 0,05 | 0,07 | 0,05 | 0,04 | 0,06 | 0,06 | 0,06 | 0,05 | 0,02 | 0,04 | 0,03 | 0,04 |
| | Mn | 0,01 | 0,01 | 0,01 | 0,01 | 0,01 | 0,01 | 0,01 | 0,01 | 0,01 | 0,01 | 0,03 | 0,04 | 0,04 | 0,04 | 0,04 | 0,03 | 0,03 | 0,01 | 0,02 |
| | Ca | 1,88 | 1,85 | 1,89 | 1,88 | 1,90 | 1,86 | 1,88 | 1,89 | 1,84 | 1,89 | 1,84 | 1,79 | 1,81 | 1,79 | 1,82 | 1,90 | 1,85 | 1,91 | 1,88 |
| | Na | 0,06 | 0,08 | 0,06 | 0,07 | 0,05 | 0,08 | 0,06 | 0,06 | 0,08 | 0,06 | 0,09 | 0,11 | 0,10 | 0,11 | 0,10 | 0,06 | 0,08 | 0,05 | 0,06 |
| | SumB | 2,00 | 2,00 | 2,00 | 2,00 | 2,00 | 2,00 | 2,00 | 2,00 | 2,00 | 2,00 | 2,00 | 2,00 | 2,00 | 2,00 | 2,00 | 2,00 | 2,00 | 2,00 | 2,00 |
| | Na | 0,40 | 0,36 | 0,38 | 0,35 | 0,36 | 0,36 | 0,33 | 0,36 | 0,34 | 0,35 | 0,40 | 0,37 | 0,39 | 0,40 | 0,40 | 0,43 | 0,42 | 0,32 | 0,35 |
| | K | 0,18 | 0,20 | 0,19 | 0,19 | 0,20 | 0,20 | 0,19 | 0,20 | 0,20 | 0,19 | 0,15 | 0,17 | 0,17 | 0,18 | 0,16 | 0,13 | 0,15 | 0,13 | 0,10 |
| | (Na+K)A | 0,58 | 0,56 | 0,57 | 0,54 | 0,55 | 0,56 | 0,52 | 0,55 | 0,54 | 0,55 | 0,56 | 0,54 | 0,56 | 0,58 | 0,56 | 0,56 | 0,56 | 0,45 | 0,46 |
| | Sum A | 1,16 | 1,11 | 1,13 | 1,09 | 1,11 | 1,12 | 1,04 | 1,11 | 1,08 | 1,09 | 1,11 | 1,08 | 1,12 | 1,17 | 1,12 | 1,12 | 1,13 | 0,90 | 0,91 |
| | Total | 15,58 | 15,56 | 15,57 | 15,54 | 15,55 | 15,56 | 15,52 | 15,55 | 15,54 | 15,55 | 15,56 | 15,54 | 15,56 | 15,58 | 15,56 | 15,56 | 15,56 | 15,45 | 15,46 |
| | ***Ratios*** | | | | | | | | | | | | | | | | | | | |
| | $Mg/(Mg+Fe^{2+})$ | 0,24 | 0,25 | 0,23 | 0,25 | 0,26 | 0,25 | 0,22 | 0,24 | 0,24 | 0,25 | 0,44 | 0,44 | 0,44 | 0,43 | 0,44 | 0,43 | 0,45 | 0,53 | 0,53 |

**Annex III** - Mineral analyses Nolte (2012).

| | Sample | 020809-3 | | | | | | | | | | | | | | | | | |
|---|---|---|---|---|---|---|---|---|---|---|---|---|---|---|---|---|---|---|---|
| | Ox. wt% | spot-52 | spot-53 | spot-54 | spot-55 | spot-56 | spot-57 | spot-58 | spot-66 | spot-67 | spot-68 | spot-69 | spot-70 | spot-71 | spot-72 | spot-78 | spot-79 | spot-80 | spot-81 | spot-82 |
| Amphibole | $SiO_2$ | 43,0 | 43,1 | 42,8 | 41,6 | 42,6 | 43,0 | 42,1 | 42,7 | 42,9 | 42,9 | 42,4 | 41,4 | 43,1 | 42,8 | 41,2 | 41,1 | 41,2 | 42,3 | 42,0 |
| | $TiO_2$ | 0,75 | 0,81 | 0,65 | 0,69 | 0,80 | 0,72 | 0,73 | 0,64 | 0,78 | 0,45 | 0,43 | 0,77 | 0,50 | 0,65 | 0,17 | 0,04 | 0,53 | 0,63 | 1,03 |
| | $Al_2O_3$ | 16,4 | 16,5 | 16,7 | 16,3 | 16,7 | 16,6 | 16,5 | 16,6 | 16,5 | 16,8 | 16,1 | 16,3 | 16,2 | 16,4 | 18,9 | 18,7 | 16,8 | 16,2 | 16,1 |
| | FeO | 14,77 | 14,70 | 15,02 | 14,68 | 14,87 | 14,83 | 14,76 | 14,96 | 14,53 | 14,77 | 14,87 | 15,72 | 15,30 | 15,19 | 16,77 | 16,43 | 16,76 | 16,37 | 15,84 |
| | $Cr_2O_3$ | 0,0 | 0,1 | | 0,1 | | 0,0 | 0,0 | 0,0 | | 0,0 | 0,0 | 0,1 | 0,1 | 0,0 | | 0,0 | 0,0 | | |
| | MnO | 0,21 | 0,21 | 0,23 | 0,18 | 0,22 | 0,19 | 0,21 | 0,23 | 0,23 | 0,22 | 0,19 | 0,31 | 0,22 | 0,21 | 0,27 | 0,24 | 0,30 | 0,30 | 0,33 |
| | MgO | 9,14 | 9,14 | 8,84 | 9,12 | 9,02 | 8,93 | 8,83 | 8,84 | 9,26 | 8,84 | 9,18 | 8,69 | 8,65 | 9,06 | 6,87 | 6,94 | 7,77 | 8,02 | 8,31 |
| | CaO | 12,02 | 11,69 | 11,92 | 12,00 | 11,89 | 11,94 | 11,81 | 12,05 | 12,05 | 12,19 | 11,97 | 11,73 | 11,87 | 11,84 | 11,67 | 11,84 | 11,68 | 11,70 | 11,55 |
| | $Na_2O$ | 1,34 | 1,27 | 1,40 | 1,35 | 1,48 | 1,41 | 1,43 | 1,37 | 1,51 | 1,49 | 1,43 | 1,36 | 1,51 | 1,37 | 1,42 | 1,47 | 1,38 | 1,41 | 1,38 |
| | $K_2O$ | 0,78 | 0,80 | 0,63 | 0,73 | 0,81 | 0,75 | 0,68 | 0,63 | 0,70 | 0,58 | 0,52 | 0,76 | 0,57 | 0,79 | 0,63 | 0,62 | 0,66 | 0,67 | 0,76 |
| | Total | 98,45 | 98,23 | 98,10 | 96,70 | 98,44 | 98,39 | 97,13 | 98,07 | 98,42 | 98,30 | 97,11 | 97,12 | 97,97 | 98,36 | 97,88 | 97,45 | 97,11 | 97,58 | 97,29 |
| | ***Structural formula based on 23 O*** | | | | | | | | | | | | | | | | | | | |
| | Si | 6,30 | 6,31 | 6,29 | 6,20 | 6,26 | 6,31 | 6,26 | 6,28 | 6,29 | 6,31 | 6,29 | 6,16 | 6,36 | 6,28 | 6,11 | 6,13 | 6,17 | 6,29 | 6,27 |
| | Al | 1,70 | 1,69 | 1,71 | 1,80 | 1,74 | 1,69 | 1,74 | 1,72 | 1,71 | 1,70 | 1,71 | 1,84 | 1,64 | 1,72 | 1,89 | 1,87 | 1,83 | 1,71 | 1,73 |
| | Sum T | 8,00 | 8,00 | 8,00 | 8,00 | 8,00 | 8,00 | 8,00 | 8,00 | 8,00 | 8,00 | 8,00 | 8,00 | 8,00 | 8,00 | 8,00 | 8,00 | 8,00 | 8,00 | 8,00 |
| | Al | 1,13 | 1,16 | 1,17 | 1,07 | 1,15 | 1,18 | 1,15 | 1,17 | 1,13 | 1,21 | 1,10 | 1,03 | 1,17 | 1,12 | 1,42 | 1,42 | 1,13 | 1,14 | 1,09 |
| | Cr | 0,00 | 0,01 | | 0,01 | | 0,00 | 0,00 | 0,00 | | 0,00 | 0,00 | 0,01 | 0,01 | 0,01 | 0,00 | 0,00 | 0,00 | | |
| | $Fe^{3+}$ | 0,09 | 0,14 | 0,11 | 0,13 | 0,10 | 0,07 | 0,10 | 0,09 | 0,07 | 0,04 | 0,13 | 0,22 | 0,07 | 0,15 | 0,15 | 0,09 | 0,20 | 0,13 | 0,14 |
| | Ti | 0,08 | 0,09 | 0,07 | 0,08 | 0,09 | 0,08 | 0,08 | 0,07 | 0,09 | 0,05 | 0,05 | 0,09 | 0,06 | 0,07 | 0,02 | 0,00 | 0,06 | 0,07 | 0,12 |
| | Mg | 2,00 | 2,00 | 1,94 | 2,03 | 1,97 | 1,95 | 1,96 | 1,94 | 2,02 | 1,94 | 2,03 | 1,93 | 1,90 | 1,98 | 1,52 | 1,54 | 1,73 | 1,78 | 1,85 |
| | $Fe^{2+}$ | 1,68 | 1,59 | 1,70 | 1,68 | 1,68 | 1,70 | 1,69 | 1,72 | 1,68 | 1,75 | 1,68 | 1,70 | 1,78 | 1,67 | 1,88 | 1,92 | 1,86 | 1,86 | 1,78 |
| | Mn | 0,01 | 0,01 | 0,02 | 0,01 | 0,01 | 0,01 | 0,01 | 0,01 | 0,01 | 0,01 | 0,01 | 0,02 | 0,01 | 0,01 | 0,02 | 0,02 | 0,02 | 0,02 | 0,02 |
| | Sum C | 5,00 | 5,00 | 5,00 | 5,00 | 5,00 | 5,00 | 5,00 | 5,00 | 5,00 | 5,00 | 5,00 | 5,00 | 5,00 | 5,00 | 5,00 | 5,00 | 5,00 | 5,00 | 5,00 |
| | $Fe^{2+}$ | 0,04 | 0,06 | 0,04 | 0,03 | 0,05 | 0,05 | 0,04 | 0,03 | 0,04 | 0,03 | 0,03 | 0,04 | 0,04 | 0,05 | 0,05 | 0,04 | 0,04 | 0,04 | 0,05 |
| | Mn | 0,01 | 0,01 | 0,02 | 0,01 | 0,01 | 0,01 | 0,01 | 0,01 | 0,01 | 0,01 | 0,01 | 0,02 | 0,01 | 0,01 | 0,02 | 0,02 | 0,02 | 0,02 | 0,02 |
| | Ca | 1,89 | 1,84 | 1,88 | 1,92 | 1,87 | 1,88 | 1,88 | 1,90 | 1,89 | 1,92 | 1,90 | 1,87 | 1,88 | 1,86 | 1,86 | 1,89 | 1,87 | 1,87 | 1,85 |
| | Na | 0,06 | 0,09 | 0,07 | 0,04 | 0,07 | 0,07 | 0,06 | 0,05 | 0,06 | 0,04 | 0,05 | 0,07 | 0,07 | 0,07 | 0,08 | 0,06 | 0,07 | 0,07 | 0,08 |
| | Sum B | 2,00 | 2,00 | 2,00 | 2,00 | 2,00 | 2,00 | 2,00 | 2,00 | 2,00 | 2,00 | 2,00 | 2,00 | 2,00 | 2,00 | 2,00 | 2,00 | 2,00 | 2,00 | 2,00 |
| | Na | 0,32 | 0,27 | 0,34 | 0,35 | 0,35 | 0,34 | 0,35 | 0,34 | 0,37 | 0,38 | 0,36 | 0,33 | 0,37 | 0,32 | 0,33 | 0,37 | 0,33 | 0,34 | 0,32 |
| | K | 0,15 | 0,15 | 0,12 | 0,14 | 0,15 | 0,14 | 0,13 | 0,12 | 0,13 | 0,11 | 0,10 | 0,14 | 0,11 | 0,15 | 0,12 | 0,12 | 0,13 | 0,13 | 0,15 |
| | (Na+K)A | 0,47 | 0,42 | 0,45 | 0,49 | 0,51 | 0,48 | 0,48 | 0,45 | 0,50 | 0,49 | 0,46 | 0,47 | 0,47 | 0,46 | | | 0,46 | 0,46 | 0,46 |
| | Sum A | 0,93 | 0,84 | 0,91 | 0,97 | 1,01 | 0,95 | 0,96 | 0,91 | 1,00 | 0,97 | 0,92 | 0,94 | 0,95 | 0,93 | 0,45 | 0,49 | 0,92 | 0,92 | 0,92 |
| | Total | 15,47 | 15,42 | 15,45 | 15,49 | 15,50 | 15,48 | 15,48 | 15,46 | 15,50 | 15,49 | 15,46 | 15,47 | 15,47 | 15,47 | 15,45 | 15,49 | 15,46 | 15,46 | 15,46 |
| | ***Ratios*** | | | | | | | | | | | | | | | | | | | |
| | Mg/(Mg+$Fe^{2+}$) | 0,54 | 0,55 | 0,53 | 0,54 | 0,53 | 0,53 | 0,53 | 0,53 | 0,54 | 0,52 | 0,54 | 0,53 | 0,51 | 0,54 | | | 0,48 | 0,48 | 0,50 |

**Annex III** - Mineral analyses Nolte (2012).

| | Sample | 020809-3 | | | | | | | | | | 020809-4 | | | | | | | | |
|---|---|---|---|---|---|---|---|---|---|---|---|---|---|---|---|---|---|---|---|---|
| | Ox. wt% | spot-83 | spot-84 | spot-85 | spot-86 | spot-87 | spot-88 | spot-89 | spot-90 | spot-91 | spot-92 | spot-18 | spot-22 | spot-23 | spot-28 | spot-29 | spot-32 | spot-33 | spot-34 | spot-35 |
| Amphibole | $SiO_2$ | 41,4 | 40,9 | 41,9 | 42,0 | 41,7 | 42,0 | 42,6 | 43,9 | 42,7 | 43,2 | 39,0 | 40,2 | 40,0 | 39,7 | 40,0 | 40,0 | 39,5 | 39,7 | 39,7 |
| | $TiO_2$ | 0,74 | 0,46 | 0,91 | 0,56 | 0,53 | 0,47 | 0,43 | 0,34 | 0,82 | 0,66 | 0,35 | 0,55 | 0,49 | 0,49 | 0,38 | 0,47 | 0,53 | 0,45 | 0,55 |
| | $Al_2O_3$ | 15,9 | 18,4 | 15,8 | 16,7 | 17,2 | 17,2 | 15,7 | 15,8 | 16,2 | 15,9 | 16,0 | 15,3 | 15,1 | 15,7 | 15,3 | 15,8 | 15,7 | 16,2 | 15,7 |
| | FeO | 15,98 | 16,75 | 16,06 | 16,82 | 16,75 | 16,49 | 14,66 | 14,46 | 14,95 | 14,94 | 23,11 | 23,60 | 23,55 | 23,02 | 22,96 | 23,21 | 23,26 | 22,50 | 23,25 |
| | $Cr_2O_3$ | 0,0 | | 0,0 | 0,1 | | | 0,0 | 0,0 | 0,0 | 0,1 | 0,0 | 0,1 | | 0,0 | | 0,1 | | 0,0 | 0,0 |
| | MnO | 0,24 | 0,30 | 0,27 | 0,29 | 0,27 | 0,35 | 0,25 | 0,22 | 0,25 | 0,26 | 0,08 | 0,09 | 0,03 | 0,05 | 0,07 | 0,07 | 0,07 | 0,10 | 0,07 |
| | MgO | 8,32 | 6,95 | 8,56 | 7,86 | 7,45 | 7,31 | 9,41 | 9,47 | 9,07 | 9,34 | 4,15 | 4,59 | 4,44 | 4,32 | 4,56 | 4,31 | 4,36 | 4,27 | 4,30 |
| | CaO | 11,65 | 11,62 | 11,50 | 11,94 | 11,70 | 11,66 | 11,91 | 11,83 | 11,71 | 11,69 | 11,53 | 11,65 | 11,63 | 11,45 | 11,48 | 11,66 | 11,63 | 11,66 | 11,78 |
| | $Na_2O$ | 1,40 | 1,46 | 1,38 | 1,40 | 1,59 | 1,53 | 1,43 | 1,33 | 1,32 | 1,44 | 1,38 | 1,44 | 1,40 | 1,34 | 1,48 | 1,40 | 1,42 | 1,35 | 1,36 |
| | $K_2O$ | 0,75 | 0,67 | 0,76 | 0,63 | 0,64 | 0,64 | 0,51 | 0,52 | 0,71 | 0,66 | 1,61 | 1,74 | 1,71 | 1,90 | 1,66 | 1,64 | 1,62 | 1,65 | 1,59 |
| | Total | 96,35 | 97,52 | 97,18 | 98,17 | 97,83 | 97,71 | 96,85 | 97,84 | 97,77 | 98,12 | 97,17 | 99,19 | 98,39 | 98,08 | 97,92 | 98,62 | 98,12 | 97,83 | 98,35 |
| | ***Structural formula based on 23 O*** | | | | | | | | | | | | | | | | | | | |
| | Si | 6,23 | 6,10 | 6,25 | 6,22 | 6,22 | 6,27 | 6,33 | 6,44 | 6,29 | 6,34 | 6,07 | 6,14 | 6,17 | 6,14 | 6,18 | 6,14 | 6,11 | 6,13 | 6,12 |
| | Al | 1,77 | 1,90 | 1,75 | 1,78 | 1,78 | 1,73 | 1,68 | 1,56 | 1,71 | 1,66 | 1,93 | 1,86 | 1,83 | 1,86 | 1,82 | 1,87 | 1,90 | 1,87 | 1,88 |
| | Sum T | 8,00 | 8,00 | 8,00 | 8,00 | 8,00 | 8,00 | 8,00 | 8,00 | 8,00 | 8,00 | 8,00 | 8,00 | 8,00 | 8,00 | 8,00 | 8,00 | 8,00 | 8,00 | 8,00 |
| | Al | 1,06 | 1,34 | 1,03 | 1,12 | 1,23 | 1,29 | 1,06 | 1,16 | 1,11 | 1,09 | 1,00 | 0,90 | 0,92 | 1,01 | 0,98 | 1,00 | 0,96 | 1,07 | 0,97 |
| | Cr | 0,00 | | 0,01 | 0,01 | | | 0,00 | 0,00 | 0,00 | 0,01 | 0,00 | 0,01 | | 0,00 | | 0,01 | | 0,00 | 0,01 |
| | $Fe^{3+}$ | 0,16 | 0,15 | 0,21 | 0,15 | 0,11 | 0,07 | 0,15 | 0,12 | 0,16 | 0,16 | 0,19 | 0,16 | 0,13 | 0,12 | 0,13 | 0,12 | 0,15 | 0,07 | 0,12 |
| | Ti | 0,08 | 0,05 | 0,10 | 0,06 | 0,06 | 0,05 | 0,05 | 0,04 | 0,09 | 0,07 | 0,04 | 0,06 | 0,06 | 0,06 | 0,04 | 0,05 | 0,06 | 0,05 | 0,06 |
| | Mg | 1,87 | 1,55 | 1,90 | 1,74 | 1,65 | 1,62 | 2,08 | 2,07 | 1,99 | 2,05 | 0,97 | 1,05 | 1,02 | 1,00 | 1,05 | 0,99 | 1,00 | 0,98 | 0,99 |
| | $Fe^{2+}$ | 1,82 | 1,90 | 1,74 | 1,91 | 1,93 | 1,94 | 1,64 | 1,60 | 1,63 | 1,61 | 2,80 | 2,82 | 2,87 | 2,82 | 2,80 | 2,83 | 2,82 | 2,81 | 2,85 |
| | Mn | 0,02 | 0,02 | 0,02 | 0,02 | 0,02 | 0,02 | 0,02 | 0,01 | 0,02 | 0,02 | 0,01 | 0,01 | 0,00 | 0,00 | 0,00 | 0,01 | 0,01 | 0,01 | 0,01 |
| | Sum C | 5,00 | 5,00 | 5,00 | 5,00 | 5,00 | 5,00 | 5,00 | 5,00 | 5,00 | 5,00 | 5,00 | 5,00 | 5,00 | 5,00 | 5,00 | 5,00 | 5,00 | 5,00 | 5,00 |
| | $Fe^{2+}$ | 0,04 | 0,05 | 0,06 | 0,03 | 0,05 | 0,04 | 0,03 | 0,05 | 0,06 | 0,06 | 0,03 | 0,04 | 0,03 | 0,04 | 0,04 | 0,03 | 0,03 | 0,03 | 0,02 |
| | Mn | 0,02 | 0,02 | 0,02 | 0,02 | 0,02 | 0,02 | 0,02 | 0,01 | 0,02 | 0,02 | 0,01 | 0,01 | 0,00 | 0,00 | 0,00 | 0,01 | 0,01 | 0,01 | 0,01 |
| | Ca | 1,88 | 1,86 | 1,84 | 1,90 | 1,87 | 1,86 | 1,90 | 1,86 | 1,85 | 1,84 | 1,93 | 1,91 | 1,92 | 1,90 | 1,90 | 1,92 | 1,92 | 1,93 | 1,94 |
| | Na | 0,06 | 0,08 | 0,09 | 0,06 | 0,07 | 0,07 | 0,06 | 0,08 | 0,08 | 0,09 | 0,04 | 0,05 | 0,04 | 0,06 | 0,05 | 0,04 | 0,04 | 0,04 | 0,03 |
| | Sum B | 2,00 | 2,00 | 2,00 | 2,00 | 2,00 | 2,00 | 2,00 | 2,00 | 2,00 | 2,00 | 2,00 | 2,00 | 2,00 | 2,00 | 2,00 | 2,00 | 2,00 | 2,00 | 2,00 |
| | Na | 0,34 | 0,35 | 0,31 | 0,35 | 0,39 | 0,37 | 0,36 | 0,30 | 0,30 | 0,32 | 0,38 | 0,38 | 0,38 | 0,35 | 0,39 | 0,37 | 0,38 | 0,37 | 0,38 |
| | K | 0,15 | 0,13 | 0,14 | 0,12 | 0,12 | 0,12 | 0,10 | 0,10 | 0,13 | 0,12 | 0,32 | 0,34 | 0,34 | 0,38 | 0,33 | 0,32 | 0,32 | 0,32 | 0,31 |
| | (Na+K)A | 0,49 | 0,47 | 0,46 | 0,47 | 0,51 | 0,49 | | | 0,43 | 0,45 | 0,70 | 0,72 | 0,71 | 0,72 | 0,72 | 0,70 | 0,70 | 0,69 | 0,69 |
| | Sum A | 0,98 | 0,95 | 0,91 | 0,93 | 1,02 | 0,98 | 0,45 | 0,40 | 0,86 | 0,89 | 1,39 | 1,43 | 1,43 | 1,44 | 1,44 | 1,39 | 1,40 | 1,38 | 1,38 |
| | Total | 15,49 | 15,47 | 15,46 | 15,47 | 15,51 | 15,49 | 15,45 | 15,40 | 15,43 | 15,45 | 15,70 | 15,72 | 15,71 | 15,72 | 15,72 | 15,70 | 15,70 | 15,69 | 15,69 |
| | ***Ratios*** | | | | | | | | | | | | | | | | | | | |
| | Mg/(Mg+$Fe^{2+}$) | 0,50 | 0,44 | 0,51 | 0,47 | 0,46 | 0,45 | | | 0,54 | 0,55 | 0,25 | 0,27 | 0,26 | 0,26 | 0,27 | 0,26 | 0,26 | 0,26 | 0,26 |

**Annex III** - Mineral analyses Nolte (2012).

| | Sample | 020809-4 | | | | | | | | |
|---|---|---|---|---|---|---|---|---|---|---|
| | ***Ox. wt%*** | *spot-36* | *spot-37* | *spot-40* | *spot-41* | *spot-42* | *spot-46* | *spot-47* | *spot-48* | *spot-49* |
| **Amphibole** | $SiO_2$ | 39,5 | 39,7 | 39,5 | 40,4 | 40,1 | 39,8 | 40,4 | 40,4 | 40,3 |
| | $TiO_2$ | 0,27 | 0,57 | 0,37 | 0,48 | 0,34 | 0,46 | 0,50 | 0,52 | 0,34 |
| | $Al_2O_3$ | 16,1 | 15,3 | 16,1 | 15,5 | 16,0 | 15,7 | 14,8 | 15,1 | 15,2 |
| | FeO | 22,96 | 23,07 | 22,86 | 23,08 | 22,97 | 23,23 | 22,94 | 23,24 | 23,20 |
| | $Cr_2O_3$ | | 0,0 | | | | | 0,0 | | |
| | MnO | 0,13 | 0,09 | 0,09 | 0,08 | 0,07 | 0,12 | 0,02 | 0,11 | 0,05 |
| | MgO | 4,29 | 4,58 | 4,31 | 4,42 | 4,23 | 4,29 | 4,59 | 4,93 | 4,38 |
| | CaO | 11,72 | 11,66 | 11,66 | 11,83 | 11,50 | 11,54 | 11,66 | 11,12 | 11,74 |
| | $Na_2O$ | 1,34 | 1,45 | 1,45 | 1,43 | 1,39 | 1,41 | 1,37 | 1,10 | 1,47 |
| | $K_2O$ | 1,63 | 1,51 | 1,72 | 1,61 | 1,67 | 1,61 | 1,76 | 1,90 | 1,58 |
| | Total | 97,98 | 97,92 | 98,06 | 98,89 | 98,26 | 98,19 | 98,12 | 98,40 | 98,28 |
| | ***Structural formula based on 23 O*** | | | | | | | | | |
| | Si | 6,10 | 6,14 | 6,11 | 6,19 | 6,17 | 6,14 | 6,25 | 6,18 | 6,22 |
| | Al | 1,90 | 1,86 | 1,89 | 1,81 | 1,83 | 1,86 | 1,75 | 1,82 | 1,79 |
| | Sum T | 8,00 | 8,00 | 8,00 | 8,00 | 8,00 | 8,00 | 8,00 | 8,00 | 8,00 |
| | Al | 1,03 | 0,91 | 1,03 | 1,00 | 1,07 | 0,99 | 0,95 | 0,91 | 0,98 |
| | Cr | | 0,00 | | | | | | | |
| | $Fe^{3+}$ | 0,15 | 0,15 | 0,10 | 0,06 | 0,11 | 0,14 | 0,06 | 0,28 | 0,07 |
| | Ti | 0,03 | 0,07 | 0,04 | 0,06 | 0,04 | 0,05 | 0,06 | 0,06 | 0,04 |
| | Mg | 0,99 | 1,06 | 0,99 | 1,01 | 0,97 | 0,99 | 1,06 | 1,13 | 1,01 |
| | $Fe^{2+}$ | 2,80 | 2,80 | 2,83 | 2,88 | 2,80 | 2,82 | 2,87 | 2,62 | 2,90 |
| | Mn | 0,01 | 0,01 | 0,01 | 0,01 | 0,00 | 0,01 | 0,00 | 0,01 | 0,00 |
| | Sum C | 5,00 | 5,00 | 5,00 | 5,00 | 5,00 | 5,00 | 5,00 | 5,00 | 5,00 |
| | $Fe^{2+}$ | 0,02 | 0,03 | 0,03 | 0,02 | 0,04 | 0,04 | 0,03 | 0,08 | 0,03 |
| | Mn | 0,01 | 0,01 | 0,01 | 0,01 | 0,00 | 0,01 | 0,00 | 0,01 | 0,00 |
| | Ca | 1,94 | 1,93 | 1,93 | 1,94 | 1,90 | 1,91 | 1,93 | 1,82 | 1,94 |
| | Na | 0,03 | 0,04 | 0,04 | 0,03 | 0,06 | 0,05 | 0,04 | 0,09 | 0,03 |
| | Sum B | 2,00 | 2,00 | 2,00 | 2,00 | 2,00 | 2,00 | 2,00 | 2,00 | 2,00 |
| | Na | 0,37 | 0,40 | 0,40 | 0,39 | 0,36 | 0,37 | 0,37 | 0,23 | 0,41 |
| | K | 0,32 | 0,30 | 0,34 | 0,31 | 0,33 | 0,32 | 0,35 | 0,37 | 0,31 |
| | (Na+K)A | 0,69 | 0,70 | 0,73 | 0,71 | 0,69 | 0,69 | 0,72 | 0,61 | 0,72 |
| | Sum A | 1,38 | 1,39 | 1,47 | 1,41 | 1,37 | 1,37 | 1,44 | 1,21 | 1,43 |
| | Total | 15,69 | 15,70 | 15,73 | 15,71 | 15,69 | 15,69 | 15,72 | 15,61 | 15,72 |
| | ***Ratios*** | | | | | | | | | |
| | $Mg/(Mg+Fe^{2+})$ | 0,26 | 0,27 | 0,26 | 0,26 | 0,25 | 0,26 | 0,27 | 0,29 | 0,26 |

| | Sample | 290709-3 | | |
|---|---|---|---|---|
| | ***Ox. wt%*** | 10,0 | 11,0 | 49,0 |
| **Epidote** | $SiO_2$ | 38,38 | 37,30 | 37,49 |
| | $TiO_2$ | 0,0 | 0,1 | 0,2 |
| | $Al_2O_3$ | 26,37 | 25,00 | 25,79 |
| | $Cr_2O_3$ | 0,1 | 0,0 | 0,0 |
| | $Fe_2O_3$ | 8,83 | 9,90 | 9,69 |
| | MnO | 0,03 | 0,06 | 0,17 |
| | MgO | 0,00 | 0,00 | 0,01 |
| | CaO | 23,83 | 23,63 | 23,41 |
| | $Na_2O$ | 0,01 | 0,01 | 0,00 |
| | $K_2O$ | 0,00 | 0,00 | 0,05 |
| | Sum | 97,5 | 96,1 | 96,9 |
| | ***Structural formula*** | | | |
| | Si | 3,00 | 2,97 | 2,96 |
| | $Al^{IV}$ | 0,00 | 0,03 | 0,04 |
| | Sum T | 3,00 | 3,00 | 3,00 |
| | $Al^{VI}$ | 2,42 | 2,32 | 2,36 |
| | Ti | 0,00 | 0,01 | 0,01 |
| | Cr | 0,01 | 0,00 | 0,00 |
| | $Fe^{3}$ | 0,58 | 0,66 | 0,64 |
| | Mg | 0,00 | 0,00 | 0,00 |
| | Mn | 0,00 | 0,00 | 0,01 |
| | Na | 0,00 | 0,00 | 0,00 |
| | Ca | 1,99 | 2,02 | 1,98 |
| | K | 0,00 | 0,00 | 0,01 |
| | Sum X | 5,00 | 5,01 | 5,01 |
| | ***End member (Mol %)*** | | | |
| | Pistacite | 19,2 | 21,9 | 21 |

## Annex VI - Abbreviations

### Lithostratigraphic terms and codes

| | |
|---|---|
| **AS** | Angola Shield |
| **CKB** | Choma – Kalomo Block |
| **EC** | Epupa Complex |
| **FFG** | Fransfontein Granite Suite |
| **FM, Fm** | Formation |
| **GI** | Grootfontein Inlier |
| **GCB** | Ghanzi – Chobe Belt |
| **HMC** | Huab Metamorphic Complex |
| **K** | Kunene Igneous Complex |
| **KG** | Khoabendus Group |
| **KI** | Kamanjab Inlier |
| **POGD** | Porphyritic gneissic granodiorite |
| **RBI** | Rehoboth Basement Inlier |
| **ROG** | Red orthogneiss |
| **SD** | Subdomain |
| **SG** | Subgroup |

### Geochemistry

| | |
|---|---|
| **A/CNK** | $Al_2O_3/CaO+Na_2O+K_2O$ |
| **AFM** | $Al_2O3$ – FeO – MgO |
| **ANOR** | (Normative) anorthite/(orthoclase+anorthite) |
| **CAB** | Continental arc basalt |
| **CNK** | $CaO+Na_2O+K_2O$ |
| **E-MORB** | Enriched mid-ocean ridge basalt |
| **$FeO_T$** | Total iron oxide |
| **HFSE** | High field strength elements |
| **HREE** | Heavy rare earth elements |
| **IAT** | Island arc tholeiite |
| **LILE** | Large ion lithophile elements |
| **LREE** | Light rare earth elements |
| **N-MORB** | Normal mid-ocean ridge basalt |
| **OIB** | Ocean island basalt |
| **Ox.** | Oxide |
| **PM** | Primitive mantle |
| **Q'** | (Normative) 0.25*quartz/(quartz+orthoclase+albite+anorthite) |
| **REE** | Rare earth elements |
| **TAS** | Total alkali silica |
| **WPA** | Within plate alkaline basalt |
| **WPT** | Within plate tholeiite |
| **WR** | Whole rock |

### Metamorphism

| | |
|---|---|
| **HT** | High temperature |
| **kb** | Kilobar |
| **LP** | Low pressure |
| **P/T** | Pressure/temperature |

| | |
|---|---|
| **MOv** | Otjovasandu Formation |
| **MOvAd** | Otjovasandu Formation – Arendnes Member |
| **MOvDo** | Otjovasandu Formation – Doorslaan Member |
| **MOvVs** | Otjovasandu Formation – Voorspoed Member Member |
| **MWs** | West End Formation |
| **MWsBr** | West End Formation – Bruno Member |
| **MWsEe** | West End Formation – Eendrag Member |
| **MWsOm** | West End Formation – Ombonde Member |

### Structural terms

| | |
|---|---|
| **AC-plane** | Plane perpendicular to fold axis |
| **$D_1$** | 1st Deformation phase |
| **$D_2$** | 2nd Deformation phase |
| **$D_3$** | 3rd Deformation phase |
| **$M_1$** | 1st Metamorphic event |
| **$M_2$** | 2nd Metamorphic event |
| **MCC** | Metamorphic core complex |
| **s0** | Bedding |
| **s1** | 1st schistosity, gneissic layering |
| **s01** | Bedding-parallel schistosity |
| **s2** | 2nd schistosity |
| **sc-fabrics** | Shear fabrics |

### Geochronology

| | |
|---|---|
| **BSE** | Back scattered electron |
| **CL** | Cathodoluminescence |
| **eva** | Evaporation |
| **Ga** | Billion years |
| **Ma** | Million years |
| **MSWD** | Mean standard weighted deviation |
| **$T_{DM}$** | Nd model age depleted mantle |

**Minerals**

| | | | | | | | |
|---|---|---|---|---|---|---|---|
| **ab** | albite | **crd** | cordierite | **hb** | hornblende | **prp** | pyrope |
| **alm** | almandine | **epi** | epidote | **LIQ** | liquid (melt) | **qz** | quartz |
| **ALS** | aluminosilicates | **fs** | feldspar | **ms** | muscovite | **sps** | spessartine |
| **bdy** | baddeleyite | **glt** | glauconite | **pa** | paragonite | **st** | staurolite |
| **bt** | biotite | **grs** | grossular | **phe** | phengite | **zo** | zoisite |
| **chl** | chlorite | **gr** | garnet | **pl** | plagioclase | **zr, zrn** | zircon |

## Annex VII - Toponymics

| *Place Name* | *Language* | *Meaning* |
|---|---|---|
| Aandgloed | Afrikaans | Evening glow (or sunset) |
| Arendsnes | Afrikaans | Arend's nest |
| Avante | Afrikaans | rendering of the Italian word ‘Avanti’ meaning ‘Advance’ |
| Beulah | Afrikaans/ English | Female name (sometimes translated as ‘married’) |
| Blyerus | Afrikaans | Rest in peace |
| Boesmanpan | Afrikaans | Bushman Pan |
| Bruno | Italian | Male name, meaning Brown (also Bear) |
| Dinteri | Afrikaans | Dinner |
| Dorslaan | Afrikaans | Thirsty land |
| Eendrag | Afrikaans | Unity |
| Eersbegin | Afrikaans | First start |
| Ehobib | Khoikhoi | ‘ib’ signifies river or spring |
| Epupa | Otjiherero | Foam |
| Franken | German | Region in Germany |
| Fransfontein | Afrikaans | Spring of Frans |
| Goeiehoop | Afrikaans | Good hope |
| Grootberg | Afrikaans | High mountain |
| Honib | Khoikhoi | ‘ib’ signifies river or spring |
| Huab | Khoikhoi | ‘ab’ signifies river |
| Kaiserfontein | Afrikaans | Spring of the emperor |
| Kamanjab | Otjiherero | Okamanja - the place of big stones + *ab*: Khoikhoi signifying potable water |
| Kaross | Khoikhoi | Rug or blanket of sewn animal skins, formerly worn as a garment by African people, now used as a bed or floor covering |
| Khoabendus | Otjiherero | Elephant gathering place: incorporating Khoikhoi word *//khoa* = elephant |
| Khorixas | Himba | Toothbrush tree (*Salvadora persica*) |
| Kunene | Uncertain | Beauty within |
| Lofdal | Afrikaans | Praise |
| Mesepotamie | Afrikaans | rendering of Mesopotamia (land between two rivers) = "between rivers" in English |
| Neuland | German | Newland |
| Noute | Afrikaans | Nuts |
| Ombonde | Uncertain | Endless pain |
| Ondaura | Otjiherero | From root word *ndaura*, referring to a colour feature of certain cattle with a white stripe on the back |
| Oortrek | Afrikaans | Cover |
| Otjovazandu | Otjiherero | Place of the young men |
| Robyn | Afrikaans | Female name |
| Rooikop | Afrikaans | Redhead (Red Hill) |
| Ruspoort | Afrikaans | Rest Gateway |
| Smalruggens | Afrikaans | Narrow backs (Narrow ridges) |
| Soutpoort | Afrikaans | Salt Gateway |
| Soutput | Afrikaans | Salt well |
| Spitskop | Afrikaans | Pointed Head (Pointed Hill) |
| Suiderkruis | Afrikaans | Southern Cross |
| Tevrede | Afrikaans | Content, happy, satisfied |
| Tweelingskop | Afrikaans | Twin head (hill with two summits) |
| Voorspoed | Afrikaans | Prosperity |
| Waterbron | Afrikaans | Water source, spring |